Ferrocene as redox-functional group in *N,N'*-disubstituted (thio)ureas and sulfite oxidase mimicking molybdenum complexes

Dissertation

zur Erlangung des Grades
„Doktor der Naturwissenschaften“
im Promotionsfach Chemie

am Fachbereich Chemie, Pharmazie und Geowissenschaften
der Johannes Gutenberg-Universität in Mainz

von

Kristina Hanauer, geb. Hüttinger
geboren in Taschkent

Mainz, 2017

Die vorliegende Arbeit wurde in der Zeit von Oktober 2010 bis April 2017 am Institut für Anorganische Chemie der Johannes Gutenberg-Universität Mainz angefertigt.

Dekan:

1. Berichterstatter:

2. Berichterstatter:

Datum der mündlichen Prüfung: 18. August 2017

D77 (Dissertation Universität Mainz)

Abstract

Ferrocene is a popular building block for the synthesis of redox-active compounds because of its good solubility in organic solvents, reversible redox properties and stability. After incorporation of a ferrocene unit into a compound, oxidation turns this unit into an electron acceptor and may also induce a change of the molecular conformation. These functionalities are exploited in this work, using two classes of molecules: *N*,*N*'-disubstituted (thio)ureas and ferrocenyl-containing molybdenum complexes.

The new ferrocenyl(thio)ureas of the type Fc-NHCXNH-R (X = O: R = Me, Et, Ph, Nap, Fc; X = S: R = Ant, Fc) were synthesized and characterized with various analytical methods like single crystal X-ray diffraction, NMR and IR spectroscopy, voltammetry and density functional theory. While the sulfur atom in ferrocenylthioureas leads to a clear preference for the *cis-trans* conformation, this preference is less pronounced in ferrocenylureas, which exist in solution as a mixture of the *cis-trans* and *trans-trans* forms. The switching from the *cis-trans* to the *trans-trans* conformation of a ferrocenylurea is achieved by its involvement in bifurcated hydrogen bonds. This occurs either in coordinating solvents, through self-assembly at high concentrations or in the solid state, or through formation of contact ion pairs upon oxidation of the ferrocene unit.

Intramolecular electron transfer (IET) coupled oxygen atom transfer (OAT), which takes place in the enzyme sulfite oxidase, was mimicked with the molybdenum(VI) complex $Mo^{VI}(L^{Fc})_2O_2$ (HL^{Fc} = *N*-((pyrrolato-2-yl)methylene)ferrocenylamine), using PMe_3 as artificial substrate. The reaction of the neutral complex with an excess of PMe_3 yields the phosphane complex $Mo^{IV}(L^{Fc})_2O(PMe_3)$ and $OPMe_3$. In the oxidized form ferrocene can act as electron acceptor after the reduction of the Mo^{VI} center to Mo^{IV} with PMe_3, mimicking the heme unit in the enzyme. This IET-coupled OAT reaction of $[Mo^{VI}(L^{Fc})_2O_2]^+$ with PMe_3 yields the EPR-active phosphoryl complex $[Mo^{V}(L^{Fc})_2O(OPMe_3)]^+$. In contrast, the analogous reaction starting from the reactive doubly oxidized complex $[Mo^{VI}(L^{Fc})_2O_2]^{2+}$ with PMe_3 does not stop at the phosphoryl Mo^{V} complex and is accompanied by side reactions in which the residual ferrocenium moiety is attacked by PMe_3.

Contents

Abbreviations

ε	molar extinction coefficient (UV-Vis)
λ	wavelength (UV-Vis) / reorganization energy (Hush theory)
Λ	molar conductivity
μ_B	Bohr magneton
μ_N	nuclear magneton
ν	frequency
$\tilde{\nu}$	wavenumber
τ	half-life (EPR)
δ	chemical shift
c	concentration
A	hyperfine coupling constant (EPR)
Ar	aryl
B	magnetic field
Bn	benzyl
c	concentration
COSY	correlation spectroscopy (NMR)
Cp	cyclopentadienyl
CV	cyclic voltammetry
CW	continuous wave
d	day
D	dimer
D	diffusion coeffient (NMR)
dB	decibel
dme	dimethyl ethane
DMF	dimethylformamide
dms	dimethyl sulfide
DOSY	diffusion ordered spectroscopy (NMR)
E_p	potential (CV)
EPR	electron paramagnetic resonance
eq.	equivalent

ESI	electron spray ionization (MS)
Et	ethyl
ET	electron transfer
EXAFS	extended X-ray absorption fine structure
EXCY	exchange spectroscopy (NMR)
exp	experimental (EPR)
F	Faraday constant
FD	field desorption (MS)
G	Gauss
$\Delta G^{\ddagger}$	Gibb's energy of activation
g	Landé factor (EPR)
h	Planck's constant
h	hour
H_{ab}	electronic coupling constant between metal centers
HIV	human immunodeficiency virus
HMBC	heteronuclear multiple bond coherence (NMR)
HOMO	highest occupied molecular orbital
HSQC	heteronuclear single quantum coherence (NMR)
$\Delta H^{\ddagger}$	activation enthalpy
I	nuclear spin
IET	intramolecular electron transfer
Int.	intensity
^{i}Pr	*iso*-propyl
IR	infrared
IVCT	intervalence charge transfer
J	coupling between nuclear spins (NMR)
K	Kelvin
K_c	comproportionation constant
KHMDS	potassium bis(trimethylsilyl)amide
L	ligand
LMCT	ligand metal charge transfer
LUMO	lowest unoccupied molecular orbital

M	monomer
Me	methyl
min	minute
Moco	molybdenum cofactor
MS	mass spectroscopy
MW	microwave
Nap	naphthyl
NIR	near infrared
NMR	nuclear magnetic resonance
NOE	nuclear Overhauser effect (NMR)
NOESY	nuclear Overhauser and exchange spectroscopy (NMR)
OAT	oxygen atom transfer
P_1-^{t}Bu	*tert*-butyliminotris(dimethylamino)phosphorane
PCM	polarizable continuum model (DFT)
Ph	phenyl
R	gas constant
S	electron spin
SDH	sulfite dehydrogenase
sim	simulated (EPR)
SO	sulfite oxidase
SWV	square wave voltammetry
T	temperature
^{t}Bu	*tert*-butyl
T_c	coalescence temperature
TD	time dependent (DFT)
THF	tetrahydrofuran
TS	transition state (DFT)
UV-Vis	ultraviolet-visible
V	Volt
VC	variable concentration
VT	variable temperature
XRD	X-ray diffraction

1 Introduction

The work presented here is composed of two parts. The first part is dedicated to the investigation of the structure of *N*-ferrocenyl(thio)ureas in solution and in the solid state with an emphasis on the impact of the oxidation state of one or even two ferrocenyl substituents in these molecules. This redox switchability of ferrocene is also a focal point in the second part of the work, which presents in particular a ferrocenyl-containing molybdenum complex as model system for the enzyme sulfite oxidase and describes the influence of oxidation of the ferrocenyl moiety on the functionality of the bioinspired complex.

The urea molecule was discovered by H. M. Rouelle in human urine in 1773.[1] Today, we know that in higher organisms like mammals, amphibians and fish, urea is a nontoxic waste product from the degradation of amino acids.[2] Many soil microorganisms, plants and fungi are able to metabolize this degradation product to ammonia, which constitutes one step in the nitrogen cycle.[3] Friedrich Wöhler's synthesis of urea from silver cyanate and ammonium chloride in 1828 was the first artificial synthesis of a natural compound from inorganic components and laid the foundation for organic chemistry.[4] A new synthetic route to urea has been developed by the Russian chemist Bazarov by heating solid ammonium carbamate (NH_2COONH_4) in a sealed vessel at high pressure and temperature.[5] Today, the Bazarov reaction is used in the industrial urea production.[6] However, urea and its derivatives have been out of focus in the 20th century and rarely serve as targets in organic synthesis, largely due to their relatively low reactivity compared to more versatile functional groups such as esters or carbamates.[7] In the last two to three decades, urea has gained importance and its property to form hydrogen bonds makes it an excellent building block in the synthesis of polymers, foldamers, organocatalysts, anion receptors and pharmaceutical drugs.[7–10] In the field of anion receptors, (thio)ureas with an incorporated transition metal complex like ferrocene have become increasingly more interesting. This inorganic moiety serves as sensor for anion binding as it can be detected via optical and electrochemical methods.[11] Ferrocene is a well-suited coupling compound due to its good accessibility, high stability, and reversible

redox behavior combined with a low reorganization energy during the redox process.[12] Oxidation of the ferrocenyl moiety has an impact on the hydrogen bonding ability of the urea group and consequently on the structure in the solid and dissolved state of the compound. In this way the ferrocene moiety turns the compounds into charge controlled switches. Although ferrocenyl(thio)ureas are well-established compounds especially in the area of receptors and sensors, the conformation and aggregation behavior of the neutral and oxidized species in solution is not sufficiently explored.

In this work the structure of new ferrocenyl(thio)ureas of the type Fc-NHCXNH-R (with X = O, S) in the solid state and in solution is investigated by several methods like single crystal X-ray diffraction, NMR, IR, UV-Vis spectroscopy, cyclic voltammetry and density functional theory (DFT). Key questions of this work are the influence of different factors like substituents, solvent and charge on the intramolecular and intermolecular hydrogen bonding interaction and crystal packing, and the difference between ureas and thioureas.

The second part of this thesis deals with dioxido molybdenum(VI) complexes as model complexes for the enzyme sulfite oxidase. This enzyme converts toxic sulfite to nontoxic sulfate by the transfer of one oxygen atom and in this way fulfills an essential reaction in many living beings like bacteria, animals and plants.[13] Oxygen atom transfer (OAT) is a fundamental reaction which is catalyzed by a variety of molybdenum-containing enzymes. These enzymes contain the so-called molybdenum cofactor (Moco), which is composed of a pyranopterin-based ligand equipped with a dithiolene group that coordinates molybdenum.[14] In case of the sulfite oxidase a cysteinato ligand and two oxido ligands are additionally coordinated by molybdenum. During the catalysis, one oxygen atom is transferred to the substrate and the free coordination site is replaced by an oxygen atom from a water molecule. Molybdenum is so far the only 4d metal atom found in biological systems, probably due to its good solubility as MoO_4^{2-} ion at pH 7 and a high bioavailability in sea water compared to other elements of the 4d row.[15] From a biochemical perspective molybdenum is suited for oxygen atom transfer processes because of its affinity to O-, S- and N-containing ligands and its ability to switch between the oxidation states VI, V and IV under physiological conditions. This ability to vary oxidation states in steps of single electrons is required because the OAT is coupled to intramolecular electron transfer (IET). Oxidation of sulfite goes along with the reduction

of molybdenum from oxidation state VI to IV. The regeneration to the Mo^{VI} state occurs in two proton-coupled single electron transfer steps to heme units. In the last decades numerous studies on enzymes have been performed to understand the catalytic mechanism of molybdenum-containing enzymes. The investigations are strongly supported by studies on a variety of model complexes containing molybdenum that is generally coordinated by bi-, tri- or tetradentate ligands and one or two oxido ligands. With these model systems an OAT reaction is successfully imitated, although phosphanes are frequently used as artificial substrates because of their high oxophilicity. However, none of the model systems reported prior to this work show spontaneous IET-coupled OAT.

The aim of this second part of the work is, in a first step, to investigate the OAT reaction employing the dioxido and imido oxido molybdenum(VI) complexes $Mo^{VI}(L^{tBu})_2O_2$ and $Mo^{VI}(L^{tBu})_2O(N^tBu)$ (HL^{tBu} = 4-*tert*-butyl phenyl(pyrrolato-2-ylmethylene)amine). The OAT reaction to phosphane molecules and the influence of the imido group on the reactivity, stability and structure of the complex are in the focus of the investigation, which has started in this author's diploma thesis. In a second step, the function of the model system is extended in order to imitate IET-coupled OAT. For this purpose the dioxido molybdenum complex $Mo^{VI}(L^{Fc})_2O_2$ based on the ferrocenyl-containing ligand *N*-((pyrrolato-2-yl)methylene)ferrocenylamine (HL^{Fc}) is synthesized. In this model complex the ferrocenyl moieties imitate the heme units in the sulfite oxidase, as they can function in their oxidized form as internal electron acceptors for electrons transferred from molybdenum. Therefore the influence of ferrocenyl-substituted ligands in different oxidation states on the OAT is studied. A detailed spectroscopic and electrochemical characterization of these complexes and their neutral and oxidized reaction products such as dimers and phosphane complexes is also in the center of the investigation. These studies aim at a better understanding of the enzymatic reaction in SOs, especially the IET step between Moco and heme.

2 (Thio)ureas and ferrocenyl(thio)ureas

2.1 Applications of (thio)ureas and ferrocenyl(thio)ureas

(Thio)ureas are able to form one hydrogen bond more than amides to the same proton acceptor (Scheme 1). This leads to the formation of more stable intermolecular $(NH)_2\cdots O{=}C$ hydrogen bonds, making the urea function a useful component in many areas of application like organocatalysis, supramolecular chemistry (nanotubes, foldamers or organogels), receptors and bioactive substances. Selected examples for (thio)urea compounds are shown in Scheme 2 and are discussed in the following.

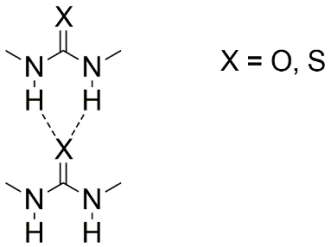

Scheme 1. Linear dimer of a (thio)urea compound, as example for a bifurcated hydrogen bonding motif.

2.1.1 Organocatalysts

In 1988 Etter has observed that *N*,*N*'-1,3-bis(*m*-nitrophenylurea) co-crystallizes with a wide variety of proton acceptors.[16,17] Due to the electron withdrawing nitro groups this urea compound behaves only as a good proton donor but not as proton acceptor. Curran and Kuo have developed the first example of an organocatalyst, the *N*,*N*'-diphenylurea derivative **A** (Scheme 2), achieving very small rate accelerations but improving the cis/trans diastereoselectivity of the radical allylation reaction of several sulfoxides.[18] Because of the in general bad solubility of ureas, **A** is equipped with octyl groups.

In some cases thioureas are preferred compared to the oxo compounds because of better solubility, easier preparation and a much weaker hydrogen bond acceptance of the thiocarbonyl group due to the lower electronegativity of the sulfur atom compared to the oxygen atom.[19,20] Schreiner et al. have designed several new thiourea catalysts for the Diels–Alder reaction. They observed the highest turnover number (up to 1000) for

thiourea **B** (Scheme 2) which experiences a strong electron withdrawing effect due to the two trifluoromethyl groups at the phenyl substituent.[19,20] The thiourea derivatives show less product inhibition which makes them attractive compared to metal-based catalysts. Jacobsen et al. have developed enantioselective (thio)ureas for the Strecker and Mannich reaction.[21–23] The Strecker reaction follows Michaelis–Menten kinetics, which is typical for enzymes.[22] The structure of the catalyst, the hydrogen bonding interaction and the reaction kinetics make these organocatalysts enzyme-like. Thus the study of catalysts with the (thio)urea functionality helps to understand the reaction mechanisms operating in enzymes.

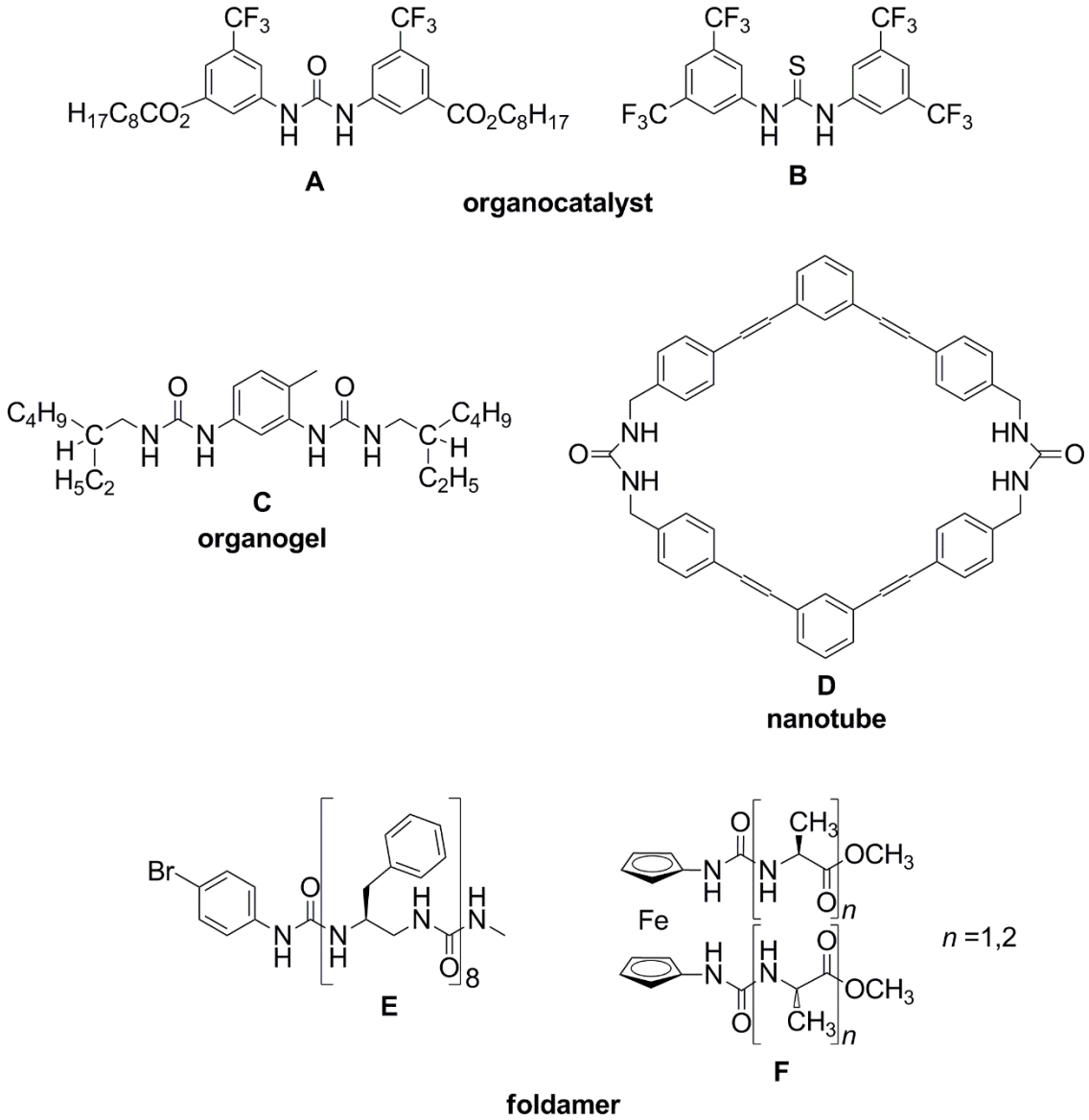

Scheme 2. Examples for (thio)urea compounds in different fields of application.

2.1.2 Supramolecular structures

In the solid state as well as in solution, ureas are able to form linear supramolecular structures. These self-assembled structures are applied for instance in the synthesis of polymers,[24–29] gel-like materials (organogelators),[9,30–34] foldamers[35–37] and nanocapsules.[38–40] In these compounds the urea group is often linked to cyclic units and/or long hydrogen carbon chains and the structure is determined especially by hydrogen bonds, van der Waals interaction and π-π stacking. The self-assembly of low molecular weight compounds to aggregates through bifurcated hydrogen bonds is a reversible process that brings some advantages compared to usual polymers, namely self-healing behavior and stimuli-responsiveness.[27]

Typically an organogel is composed of 99% solvent and 1% of a viscosity-enhancing additive.[26] An example for a typical urea-based gelator compound (**C**), shown in Scheme 2, has been designed by Bouteiller et al.[25,28] This urea derivative associates to supramolecular structures in nonpolar solvents like toluene or *n*-dodecane. The aggregation of the molecules is promoted by the two urea groups in the center of the molecule which form hydrogen bonds to two adjacent molecules resulting in long fibers. Within a fiber the hydrogen bonds run antiparallel as proven by dielectric measurements. The attachment of the long hydrocarbon chains to the urea core enhances the solubility in organic solvents and promotes also the association through van der Waals interactions between the fibers. On the other hand, the asymmetrical spacer between the two urea units and the branched alkyl chains prevent the crystallization of the fibers. Instead, the self-assembly of fibers into tubular structures has been proposed.[28]

Tube shaped structures formed by the self-association of urea compounds through hydrogen bonding can also be used as container for sensitive reactions, as ion transporters or small molecule transporters. In 2011 Shimizu et al. reported a bis-urea macrocycle **D** (Scheme 2) suitable as container for the photochemical dimerization of coumarin (55% conversion and 97% selectivity under inert conditions). X-ray diffraction data reveals the formation of hydrogen bonded chains with antiparallel orientation to each other within the tubular container, probably to minimize the dipole moment of the macrocycle.[39]

Foldamers are biomimetic oligomers mimicking naturally occurring helices, turns and linear strands. Urea compounds are suited as peptidomimetic compounds in biomedical applications because of their resistance to enzymatic degradation. Guichard et al. have

crystallized oligomers composed of five to nine *N*,*N*'-disubstituted ureas and artificial side chains (Me, ^{i}Pr, ^{i}Bu an Bn).[36] In Scheme 2, **E** represents one of these oligomers. X-ray diffraction data shows that all atoms of the urea group are involved in intramolecular and intermolecular hydrogen bonding and that the urea units are able to assemble into a helical structure. Rapić et al. have studied the secondary structure of ferrocene-based bis(ureido) peptides **F** (Scheme 2). The alanyl-substituted peptide (n = 1) forms two NH···OC$_{ester}$ intramolecular hydrogen bonds (IHBs) which result in a stable secondary structure with positive helical ferrocene units. In the bis(alanyl)-substituted peptide (n = 2), NH···OC$_{amide}$ IHBs have been found, which lead to a more stable structure because amide carbonyl groups are better hydrogen acceptors than ester carbonyl groups.[41]

2.1.3 Receptors and sensors

One very broad area of application for urea compounds is that of receptors and sensors. Wilcox and Hamilton were the first to observe the interaction of anions with *N*,*N*'-disubstituted urea derivatives.[42,43] The interest in the synthesis of receptors has increased with the discovery of ion receptors in biological systems (ion transporters).[44] Today a great number of organic as well as organometallic receptors is known, most of which contain proton donor units like amide[45,46] and (thio)urea groups for the complexation of anions. Synthetic anion receptors can for instance be used in the treatment of defects in natural anion channels.[47] Advanced receptors are able to recognize anions combined with cations.[11,48,49] In general, synthetic receptors consist of a unit which binds the ion and a second unit that functions as sensor. Typically a fluorophore or a redox-active unit is used as sensor, in some cases such sensors are applied in combination.[50] Coordination of ions causes shifts in the detected emission spectra and redox potentials of the sensors. Ferrocene has proven to be a suitable redox sensor because of its stability, good solubility in less polar solvents and easy substitution at the cyclopentadienyl ring.[44] Redox-active sensors based on ferrocene have been intensively studied by Molina, Beer and Tucker.[11,48,49,51–56] Selected examples of these ferrocene-based receptors are presented in Scheme 3.

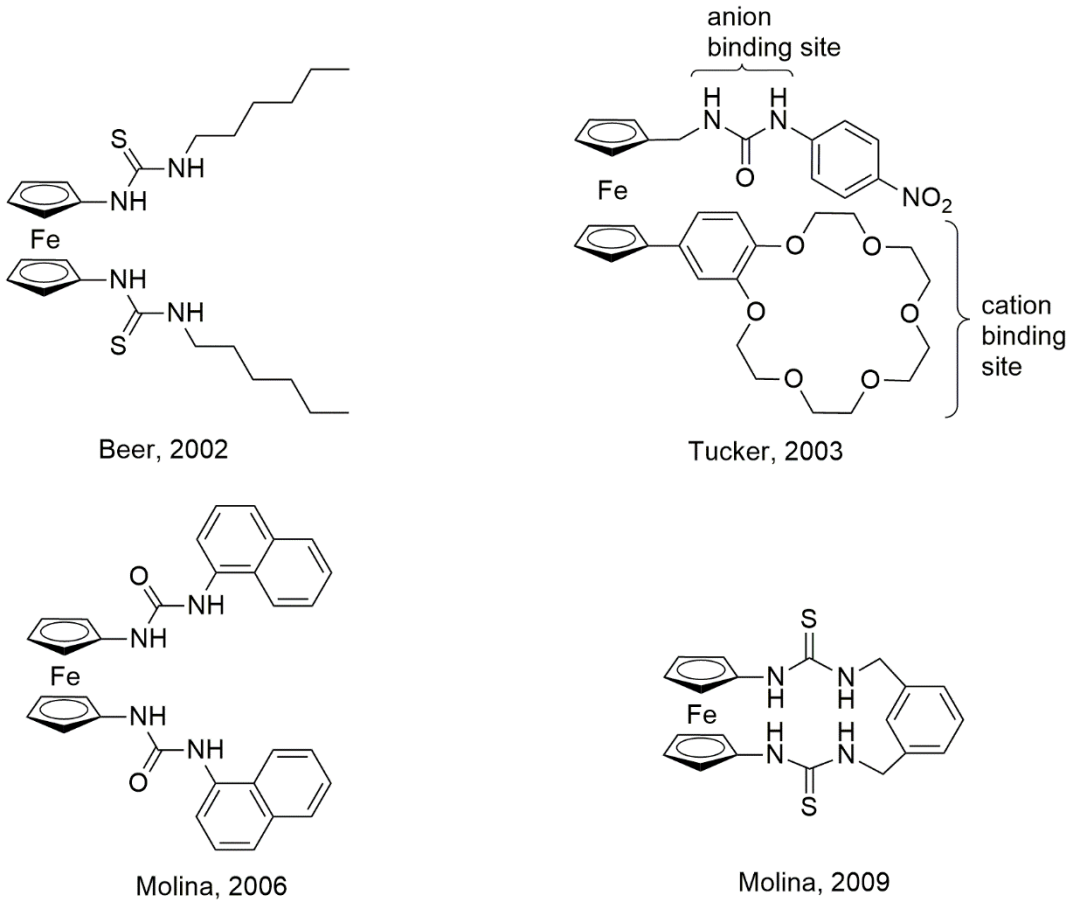

Scheme 3. Selected ferrocene-based ion receptors.[50,51,53,55]

2.1.4 Biomedical applications

Ferrocenyl compounds are known to show antitumor and antibacterial activity in biological systems.[57–61] The most prominent representative, ferrocifen, is applied against some types of cancer.[58] (Thio)urea compounds have also been studied with respect to their activity in living systems. The investigations have shown positive effects against HIV,[62] bacteria[10] and cancer.[63] Liu et al. have combined these bioactive organic and inorganic functionalities to *N*,*N*'-arylferrocenylurea compounds and have identified two compounds with potential to inhibit the HIV-1 protease which is necessary for the augmentation of HIV.[64]

2.2 Conformation of (thio)ureas

In the following section the possible conformations of mono- and disubstituted urea and thiourea molecules are discussed. The existing experimental conformational studies on

N,*N*'-disubstituted (thio)urea compounds are mainly based on IR spectroscopy.[65–76] For the investigation of the aggregation behavior of the molecules additional methods like rheometry, osmometry (for average molecular weights determination) and dipole moment measurements have been used.[77–83]

2.2.1 Conformational preferences and electronic properties of unsubstituted urea and thiourea

Theoretical calculations using second order Møller–Plesset perturbation theory (MP2) show that unsubstituted urea and thiourea molecules do not exist in the planar form, but with the NH_2 groups in a pyramidal conformation. Experimentally, the nonplanar structure of $CO(NH_2)_2$ is also confirmed by microwave experiments.[84] Scheme 4 shows the possible conformations of urea and thiourea. Hay et al. have found in the case of urea two minima corresponding to the *anti* (C_2) and the *syn* (C_s) conformation, with both NH_2 groups pyramidalized on the opposite (*anti*) or on the same side of the molecular plane (*syn*).[85]

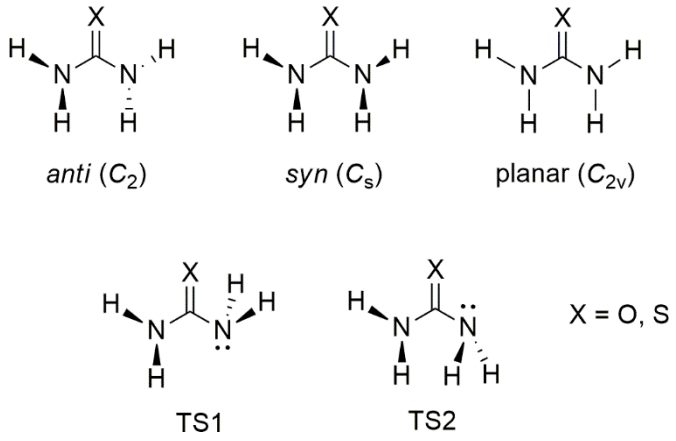

Scheme 4. Stationary points for urea and thiourea.

As reason for the nonplanar structure of urea the orbital interaction of the nitrogen lone pair with the π* orbital of the carbonyl group is discussed.[86] In the planar structure, electron density from both nitrogen atoms should be equally transferred to the CO π* orbital. However, this orbital cannot accommodate all charges and therefore the planar structure becomes instable. For unsubstituted thiourea, Hay et al. have found only one minimum structure corresponding to the *anti* (C_2) conformation. In contrast to urea, the *syn* structure with C_s symmetry represents a transition state. Isomerizations by inversion

of the nitrogen centers are possible through energetically low-lying transition states, namely TS3 in urea (4.5 kJ mol^{-1}) and the *syn* (C_s) structure in case of thiourea (2.1 kJ mol^{-1}). However, this inversion does not switch the positions of hydrogen atoms and cannot account for isomerizations between *cis* and *trans* forms in case of substituted (thio)ureas. The latter requires a rotation about the C-N bond through either of the transition states TS1 or TS2.

In TS2 the lone pair of the nitrogen atom points towards the carbonyl group, leading to a higher energy (urea: 56 kJ mol^{-1}, thiourea: 64 kJ mol^{-1}) than for TS1 where the lone pair of the nitrogen atom points into the opposite direction (urea: 34 kJ mol^{-1}, thiourea: 36 kJ mol^{-1}). These calculated values for the transitions states indicate that the rotation barrier of urea is lower than for thiourea. Experimentally determined rotation barriers confirm this energetic difference between urea and thiourea ($\Delta G^{\ddagger}$ = 46 – 49 kJ mol^{-1} for $CO(NH_2)_2$ and $\Delta G^{\ddagger}$ = 56 – 60 kJ mol^{-1} for $CS(NH_2)_2$).[87] This is analogous to the observed difference between amides and thioamides for which a detailed explanation is provided by a study on the acidity and oxidation behavior of carboxamides and thiocarboxamides by Bordwell et al. from 1988.[88] According to their findings, the thiocarboxamide group is by about 40 kJ mol^{-1} more acidic and more readily oxidized by about 210 kJ mol^{-1}. This higher acidity is explained with the greater ability of sulfur to stabilize the anionic and radical forms due to a decreased lone pair-lone pair interaction in the larger S^- ion and $S^{\bullet}$ radical, compared to their oxygen analogues. For example, PhSH is by about 45 kJ mol^{-1} more acidic than PhOH in DMSO.[88] The greater ability of sulfur to stabilize charge also leads to a weaker C=S bond compared to the C=O bond in thiocarboxamides and carboxamides, respectively, by about 125 kJ mol^{-1}.[88] Scheme 5 shows the possible resonance structures of carboxamides and thiocarboxamides. In the case of thiocarboxamides, structure **c** has a higher contribution to the electronic ground state, leading to a higher C-N rotation barrier for thiocarboxamides than for carboxamides. Theoretical studies on the electronic structure of formamide and thioformamide by Wiberg et al. are in agreement with the results of Bordwell and show that charge polarization in C=S bonds is much weaker than in the C=O bond. Therefore the contribution of structure **b** is reduced in thioformamide compared to formamide.[89]

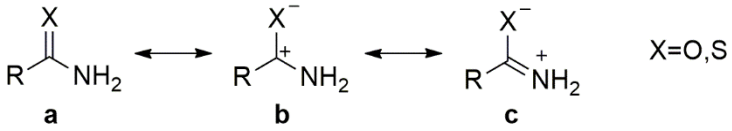

Scheme 5. Resonance structures of (thio)carboxamides.

This is also in line with the conclusions of Bharatam et al. who have analyzed the electron delocalization in isocyanates, formamides and ureas by theoretical calculations. Bharatam et al. conclude that in these systems the electronegativity is not the determining factor but the electron delocalization which is higher in compounds with sulfur than in compounds with oxygen. Because of the longer C=S bond and the diffuse orbitals of sulfur the interaction between C and S is weaker, compared to C and O, leading to an energetically lower π^* orbital which can then be easier filled with electrons from the lone pair of nitrogen.[90] The better $n_N \rightarrow \pi^*_{C=S}$ interaction strengthens the double bond character of the CN bond and leads to higher rotation barriers about this bond. A further contribution to the higher barrier is a hyperconjugation in TS1. This transition state is influenced by a $n_N \rightarrow \sigma^*_{C-X}$ orbital interaction which becomes stronger with increasing electronegativity of X. Because of the minor electronegativity of sulfur compared to oxygen, TS1 in thiourea is less stabilized and hence higher in energy leading also to a higher rotation barrier.[90]

2.2.2 Conformational preferences of *N*-mono- and *N,N'*-disubstituted alkyl- and aryl(thio)urea derivatives

In the following section the conformation of substituted ureas and thioureas is discussed. Hay et al. have analyzed substitutent effects by theoretical calculations for monosubstituted alkyl- and phenyl(thio)ureas. For monosubstituted molecules, *trans* and *cis* conformations are possible (Scheme 6), where *trans* and *cis* denote the position of the hydrogen atom at the substituted nitrogen relative to the oxygen atom. For alkyl-substituted urea and thiourea compounds, the *trans* conformation is generally lower in energy. However the preference for the *trans*-conformation is significantly stronger for substituted ureas than for thioureas. This agrees with crystal structure data, where predominantly *trans* conformations are realized for *N*-alkyl ureas. In comparison the *cis*-conformation is more frequently found for *N*-alkyl thiourea. Hay et al. explain this

different behavior with an increased steric demand of the sulfur atom compared to the oxygen atom.[91]

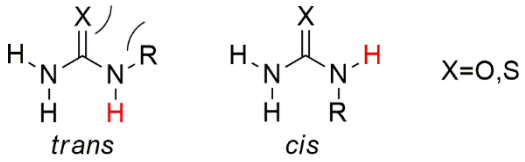

Scheme 6. Possible conformations of *N,N'*-monosubstituted (thio)ureas. The repulsion between O/S atom and the substituent in the *trans* form is indicated.

In agreement with the results shown in the previous section, the CN rotation barrier for alkyl-substituted thioureas is higher than for ureas. The calculations indicate that the CN double bond character is higher in thiourea, which is reflected by a shorter CN bond and a decreased pyramidalization of the nitrogen center in the calculated structure.

The influence of the ligand's steric demand becomes apparent especially in the case of the phenyl substituted derivatives. Theoretical calculations by Hay et al. reveal that for thiourea the *trans* conformation is 11 kJ mol^{-1} higher than the *cis* conformation, whereas in the case of urea this energy difference is only 4 kJ mol^{-1}. Presumably the repulsion between the *ortho*-hydrogen atoms and the sulfur atom is larger than that between those hydrogen atoms and the oxygen atom, as indicated by the larger angle between the (thio)urea and phenyl planes (55°) in phenylthiourea compared to phenylurea (21°).[91]

Going from *N*-monosubstituted to *N,N'*-disubstituted alkyl and aryl(thio)ureas leads to four possible conformers, namely *trans-trans*, *cis-trans*, *trans-cis* and *cis-cis* (Scheme 7). In case of symmetrically substituted (thio)ureas, the *cis-trans* and *trans-cis* forms are identical ($R_1 = R_2 = R$). Due to the steric hindrance of the two substituents the *cis-cis* conformer is rarely observed. Bouteiller et al. have studied, theoretically and experimentally, the structure of a series of symmetrically *N,N'*-disubstituted alkyl and arylureas (for example R = Me, Et, Pr, Bu, di-^{i}Pr-phenyl). These calculations and IR spectroscopic investigations in solution indicate that, with the exception of one sterically hindered *N,N'*-diaryl-substituted urea, the *trans-trans* conformer is the most stable structure. In the exceptional case, the phenyl substituent is *ortho*-disubstituted by two *iso*-propyl groups which leads to the formation of the *cis-trans* conformer with reduced repulsion between the oxygen atom and the substituent.[78]

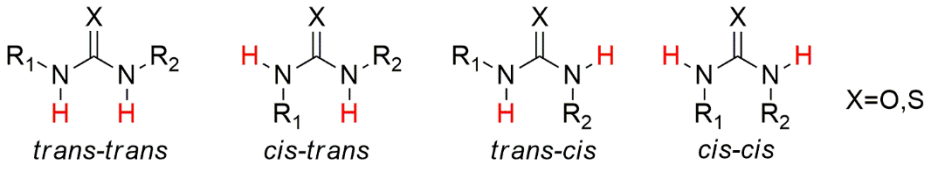

Scheme 7. Possible conformations of *N,N'*-disubstituted (thio)ureas.

IR spectroscopic studies on the *N,N'*-dialkylsubstituted thioureas Me-HNCSNH-Me and Et-HNCSNH-Et by Rao et al. in solution (chloroform) show mainly the presence of the *trans-trans* conformation. However, the sterically hindered thiourea ^{t}Bu-HNCSNH-^{t}Bu exists as a mixture of *trans-trans* and either *cis-trans* or *cis-cis* rotamers.[66] Indeed, the theoretical calculations of Custelcean et al. performed on *N,N'*-disubstituted alkylthioureas R-HNCSNH-R (R = Me, Et, ^{i}Pr, ^{t}Bu) support a preference for the *cis-trans* and *trans-trans* conformations, but predict a significantly higher energy for the *cis-cis* conformation.[92]

2.2.3 Hydrogen bonding motifs of *N,N'*-disubstituted (thio)urea compounds in the solid state

In contrast to urea compounds, which favor the *trans-trans* conformation in solution as well as in the solid state, thiourea compounds exist in the *trans-trans* and *cis-trans* conformations likewise. Generally, (thio)urea molecules in the *cis-trans* conformation form dimers in which the *cis* protons are involved in hydrogen bonds. Additionally, the *trans* proton can also participate in hydrogen bonds which connect neighboring dimers (Scheme 8). In the *trans-trans* conformation both NH protons are involved in intermolecular hydrogen bonds yielding a chain structure. In 2005 Custelcean et al. have compared 23 crystal structures of disubstituted thioureas in the CSD database of which 12 form dimers and 10 form chains.[92] In contrast, urea compounds have a clear preference to form chains in the solid state.[93] The hydrogen bonds in chains of urea compounds are linearly aligned, whereas in thiourea compounds the hydrogen bonds run in a zig-zag pattern (Scheme 8). To explain this behavior, Custelcean et al. have investigated theoretically the electrostatic potential on molecular surfaces of *N,N'*-dimethylurea and its thiourea analog. Based on their calculations, the most negative potential of the urea molecule is located in an axial position of the oxygen atom, whereas in the thiourea molecule the highest electron density is distributed on the equatorial torus around the S

atom. To achieve an effective interaction of the NH hydrogen with the torus of the S atom thiourea molecules are tilted towards each other (Scheme 8).[94]

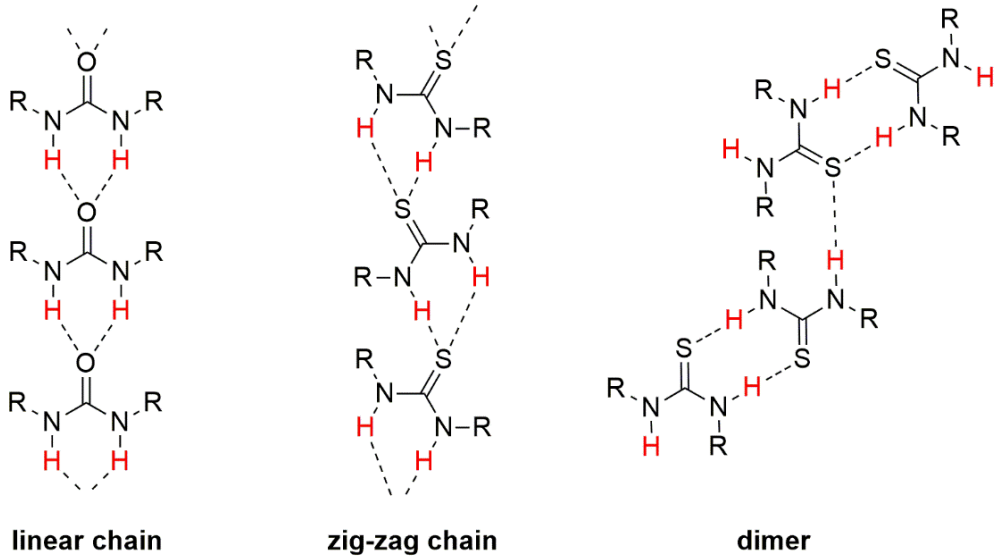

Scheme 8. Favored hydrogen bond motifs in the solid state of (thio)ureas.

Custelcean et al. observed that dimers in the solid state structures are connected by a hydrogen bond between sulfur and the *trans* proton. Further they find that introduction of sterically demanding substituents like *tert*-butyl leads to a strong shielding of the *trans* protons, hence the formation of hydrogen bonds between the dimer molecules is not feasible anymore and an aggregation to chains instead of dimers is preferred.

In general the formation of chains in the solid state is promoted by a cooperative effect as shown by Dannenberg et al. on the basis of theoretical calculations conducted for urea and thiourea. With rising number of urea molecules in the chain the dipole moment of the chain increases which in turn increases the strength of the hydrogen bonds.[95,96]

2.3 IR and NMR spectroscopic analysis of hydrogen bond formation

IR spectroscopy belongs to the most applied methods for the characterization of the conformation of (thio)urea compounds. The urea bridge [-NH-CX-NH-] (X = O, S) displays characteristic IR vibrations for the NH groups and the CO group as shown in Scheme 9. In view of the subject of this work only the vibrational modes of symmetrical and asymmetrical *N*,*N*'-disubstituted ferrocenyl(thio)ureas are discussed. In the case of

the *trans-trans* conformation a symmetrical ($\tilde{\nu}_s$) and a (much less intense) asymmetrical ($\tilde{\nu}_{as}$) NH valence vibration are predicted by DFT calculations, irrespective of the second substituent R. The *cis-trans* and *trans-cis* conformations both show separate bands for the NH vibrations of the protons orientated in *trans* and *cis* positions.

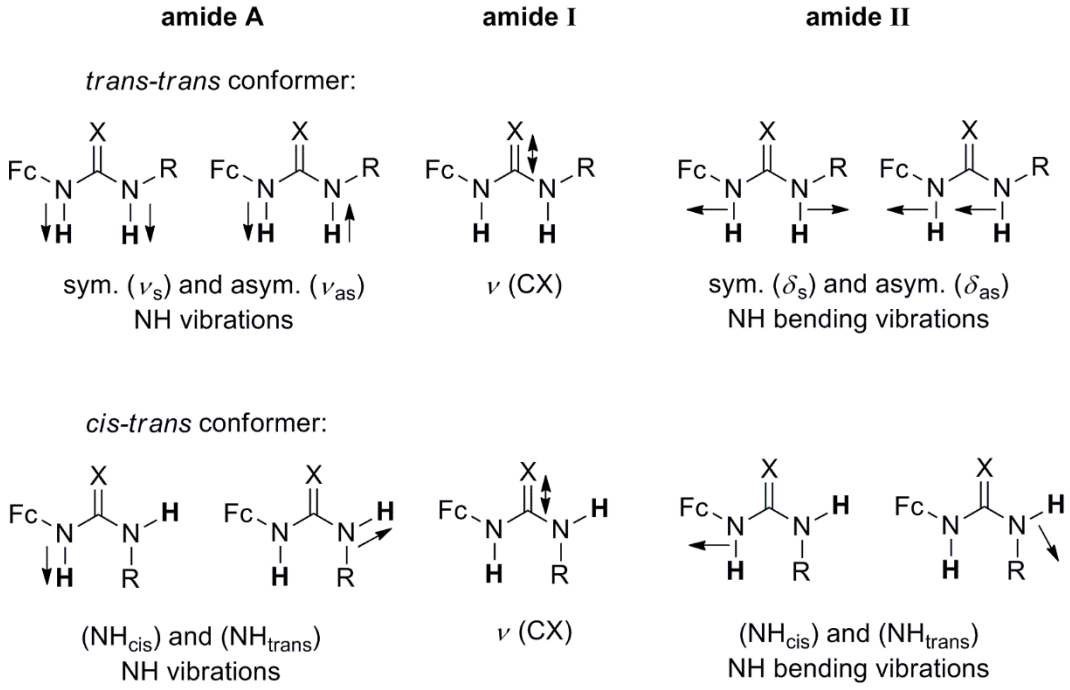

Scheme 9. IR vibrations of the *trans-trans* and *cis-trans* (*trans-cis*) conformations of ferrocenyl(thio)ureas, X = O, S.

If the NH groups are free, then the NH valence vibration band (amide A) is usually observed around 3400 cm^{-1}. If the NH groups involved in hydrogen bonds, then the NH bonds are elongated and their vibration shifts to lower energy (~3300 cm^{-1}). Further typical bands for the urea functionality are the amide I and amide II bands. The amide I band corresponds primarily to a stretching vibration of the CO group (~1680 cm^{-1}), which is elongated when involved in hydrogen bonds leading to a shift of the CO band to lower energy (~1630 cm^{-1}). The amide II band is composed of the NH bending vibration and the CN vibration and is observed at about 1580 cm^{-1}. Hydrogen bonds hamper the bending vibration of the NH groups and cause a shift to higher energy for the corresponding absorption bands.

The assignment of the CS vibrational band for thiourea compounds is not as clear as in case of the urea analog because of a strong coupling of the CS vibration with the CN and

NH vibrations. Rao et al. have compared thioamides and related compounds and have identified regions which can be generally assigned to N-C=S vibrational modes: 1395 – 1570 cm^{-1} (thioamide I), 1260 – 1420 cm^{-1} (thioamide II) and 940 – 1140 cm^{-1} (thioamide III).[65]

Concentration dependent IR spectroscopy is useful to study the aggregation behavior of (thio)urea molecules in solution. Jadzyn et al. have developed a corresponding theoretical model based on thermodynamic equations.[81]

The formation of hydrogen bonds between (thio)urea molecules can also be studied with concentration dependent (VC) and temperature dependent (VT) ^{1}H-NMR spectroscopy. The NH···O hydrogen bond formation leads to temperature and concentration dependent chemical shifts of the NH protons, which move towards lower field (when the equilibrium is shifted towards hydrogen bond formation) upon temperature decrease or concentration increase. The lowest level of aggregation of urea is dimerization. Within the framework of this work the dimerization constant for the formation of dimers from synthesized *N,N'*-disubstituted ureas is determined. A relation based on thermodynamic considerations between the chemical shift and the law of mass action can be derived as presented in the following.

In solution the monomers and dimers exist in a dynamic equilibrium:

$$2\,M \rightleftharpoons D$$

For the dimerization constant *K* applies:

$$K = \frac{[D]}{[M]^2}, \qquad \text{Equation 1}$$

with [M] = monomer concentration and [D] = dimer concentration. The total monomer concentration *c* consists of [M] and two [D] as one dimer contains two monomers:

$$c = [M] + 2[D] \qquad \text{Equation 2}$$

From equations 1 and 2, [D] can be expressed as:

$$[D] = K[M]^2 \qquad \text{Equation 3}$$

$$[D] = \frac{c}{2} - \frac{[M]}{2} \qquad \text{Equation 4}$$

Setting equations 3 and 4 equal yields:

$$0 = K[M]^2 - \frac{c}{2} + \frac{[M]}{2} \qquad \text{Equation 5}$$

Equation 5 is a classical quadratic equation and solved by:

$$[M] = \frac{1}{4K}(\sqrt{1 + 8cK} - 1) \qquad \text{Equation 6}$$

If the dimerization reaction is fast compared to the NMR time scale, the observed chemical shift for a proton is given by a weighted linear combination of the proton's chemical shifts in the pure dimer (δ_D) and monomer (δ_M):

$$\delta = \frac{1}{c}(2[D]\delta_D + [M]\delta_M) \qquad \text{Equation 7}$$

Replacing [D] by the expression in equation 4 and reformulation yields:

$$\delta = \delta_D + \frac{[M]}{c}(\delta_M - \delta_D) \qquad \text{Equation 8}$$

Finally, [M] is inserted using equation 6:

$$\delta = \delta_D + \frac{1}{4cK}(\sqrt{1 + 8cK} - 1)(\delta_M - \delta_D) \qquad \text{Equation 9}$$

The unknowns δ_D, δ_M and K are determined through a fit of this analytical expression to measured chemical shifts δ (ppm) as a function of concentration c (mol L^{-1}).
Based on the model of Jadzyn, Koll et al. have determined K for *N*,*N*'-disubstituted alkylureas from concentration dependent IR spectroscopic measurements and obtained values in the range K = 1.5 – 3.2 L mol^{-1} in $CHCl_3$. In the non-polar solvent CCl_4, the dimerization constant is significantly higher (K = 12.7 – 37.6 L mol^{-1}) due to the lower ability of the solvent to stabilize the monomer.[82]

2.4 Electronic communication between ferrocenyl centers

In organometallic chemistry, the properties of (thio)urea as mediator for intramolecular electron transfer (IET) have been investigated. In these systems the (thio)urea unit is connected to redox-active centers, for example bimetallic complexes, and enables electron transfer between those through bond or through space.[97–99] The (thio)urea unit

represents an example for a cross-conjugated bridge. In the classical description a cross-conjugated bridge contains three unsaturated groups, one of which is branched and in the center of the bridge. The two terminal groups are in conjugation to the central group but not to each other. In general, the rate of electron transfer in cross-conjugated bridges is lower than in linear conjugated bridges. Because of the existence of two nitrogen atoms instead of two double bonds, the (thio)urea unit is a nonclassical cross-conjugated bridge.

2.4.1 General considerations

With respect to inorganic compounds, mixed-valence (MV) systems contain metal redox centers in different oxidation states and are linked directly or through a bridging ligand. Homonuclear mixed valence complexes consist of two or more identical metal centers, whereas heteronuclear complexes contain different metal centers. The Creutz-Taube ion, a pyrazine bridged diruthenium(II/III) complex $Ru(NH_3)_5$-N∩N-$Ru(NH_3)_5$, is considered as the most famous homonuclear mixed-valence complex. In this complex the parazine spacer enables almost complete charge delocalization.[100,101] Robin and Day classify MV compounds according to the extent of electron delocalization into three classes. Compounds with no electronic communication belong to class I. In these systems the charges of the metal centers are fully localized and there is no electronic coupling. A weak communication between the metal redox centers exists in compounds of class II. In class III compounds the electronic communication is strong and the charge is fully delocalized. In terms of the Robin and Day classification the Creutz-Taube ion belongs to class II/III (borderline case).

The electron transfer (ET) within mixed-valence compounds in solution has been theoretically studied by Marcus.[102] The Marcus theory is generally accepted and provides the basis for further electron transfer theories (Marcus–Hush, Mulliken–Hush). In these theories, the reactant state (**R**) and product state (**P**) of a class I mixed valence compound without electronic communication is described by two parabolic functions as shown in Scheme 10a. In symmetrical complexes the **R** and **P** states are degenerate, whereas in asymmetrical complexes the two parabola are energetically offset. The following focuses on symmetrical compounds. The ET may occur in two ways (apart from tunneling): a) optically induced or b) thermally induced. Optically induced ET is a vertical excitation (according to the Franck-Condon principle) into a vibrationally excited state of the

electronic state **P**. For this transfer the reorganization energy λ is needed, which is a sum of solvation and inner (e.g. changes in bond lengths) reorganization energy. From the excited state the electron relaxes into the vibrational ground state of **P**. For thermally induced electron transfer the activation energy $\Delta G^{\ddagger}$ is needed.

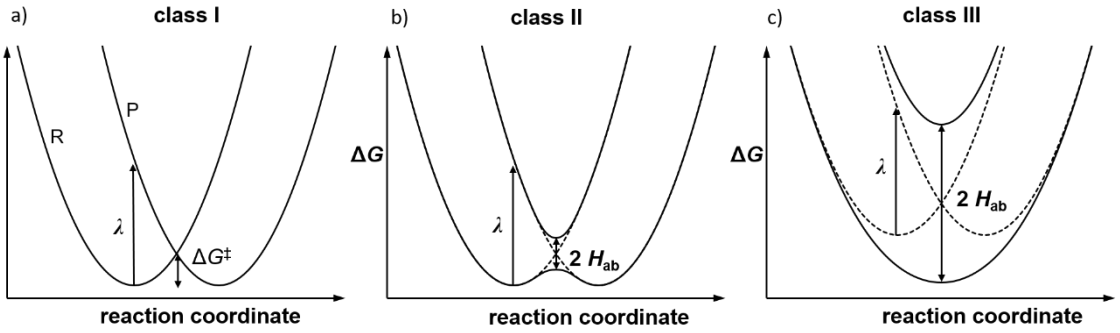

Scheme 10. Schematic description of the electronic states of a symmetric two-metal compound in terms of Robin and Day.

In systems where a weak interaction of the two metal centers is present, the two parabolic functions are coupled through the coupling constant H_{ab} and split into an electronic ground state and an excited state. The separation between the electronic ground state and the excited state at the transition state corresponds to 2 H_{ab}. In terms of Robin and Day, the electronic coupling of class II compounds is smaller than half the Marcus reorganization energy ($0 < H_{ab} < \lambda/2$, Scheme 10b).

Compounds with a coupling constant $H_{ab} > \lambda/2$ belong to class III. The strong interaction between the redox centers results in a ground state with a single energy minimum. In these systems optical and thermal charge transfer do not occur (Scheme 10c).

Experimentally, the H_{ab} value for class II compounds can be determined from UV-Vis spectroscopic measurements. According to Hush, a relationship between the intervalence charge transfer absorption (IVCT) for the electronic charge transfer between the redox centers and H_{ab} is provided by equation 10, with $\tilde{\nu}_{max}$ (cm^{-1}) = absorption maximum, ε_{max} (M^{-1} cm^{-1}) = extinction coefficient, $\Delta\tilde{\nu}_{max}$ (cm^{-1}) = full-width-at-half-maximum and r_{AB} (Å) = distance between the metal centers.[103]

$$H_{ab} = 2.06 \cdot 10^{-2}(\tilde{\nu}_{max} \times \varepsilon_{max} \times \Delta\tilde{\nu}_{max})^{0.5} \cdot r_{AB}^{-1} \qquad \text{Equation 10}$$

Besides UV-Vis spectroscopy, in some cases cyclic voltammetry (CV) can also be sensitive to electronic communication between redox centers.[104] In case of a homobimetallic system the gap between the oxidation waves (ΔE) can be used to estimate the efficiency of the electronic communication. If the metal centers do not interact with each other, then the value in the experiment theoretically should be (RT/F)ln 4 = 36 mV.[105] Compounds with a small ΔE value exhibit a weak interaction between redox centers, vice versa a larger ΔE value can be due to a strong electronic communication in a system. Large ΔE values are related to the comproportionation constant $K_c = e^{\Delta EF/(RT)}$. Thus high ΔE values generally mean high K_c values and reverse. Factors like solvation, electrostatic interactions, ion pairing with the electrolyte and structural distortions from oxidation or reduction processes can also influence the separation between the redox waves.[106]

2.4.2 Electronic communication between bridged ferrocene centers

The intramolecular electronic communication between redox centers depends on the nature of the metals, the orbital interaction of the bridge with the metals and the structure of the bridge. Generally conjugated rigid spacers transfer charge effectively through their π-orbitals.[106,107] Some examples for class II diferrocenyl compounds are shown in Scheme 11. Launey and Spangler have analyzed the influence of the length of the bridge on the electronic communication by studying diferrocenylpolyene compounds. They observe a decrease of the electronic communication (ΔE = 170 – 100mV) when increasing the length of the polyenic bridge (Scheme 11a).[108] Heinze et al. have investigated the electronic interaction of a series of amide-bridged ferrocene compounds. For these compounds an averaged value of ΔE = 123 mV for the separation is determined (Scheme 11 b).[109] Electrochemical investigations of the ureylene-bridged *N*,*N*'-diferrocenylurea CH_3OOCFc-NHCONH-$FcCOOCH_3$ (ΔE = 137 mV) have been conducted by Kraatz et al.[98] A similar value (ΔE = 130 mV)[110] has been observed by Zhong et al. for *N*,*N*'-diferrocenylurea first reported by Schlögl et al. in 1958.[111] The ureylene-bridged bis(biferrocene) $CH_3OOCFcFc$-NHCONH-$FcFcCOOCH_3$ synthesized by Heinze et al. exhibits a 1e/1e/2e process. The first two oxidations are ascribed to the inner ferrocene moieties (ΔE = 140 mV), which have a higher electron density than the outer ferrocene groups due to the electron donation from the nitrogen atom, while the second 2e

redoxwave is ascribed to the outer ferrocene moieties (ΔE = 540 mV, Scheme 11c).[97] In spite of the cross-conjugated character, the ureylene bridge allows a similar communication between the ferrocene centers as the amide linker and the butadiene bridge (n = 2).

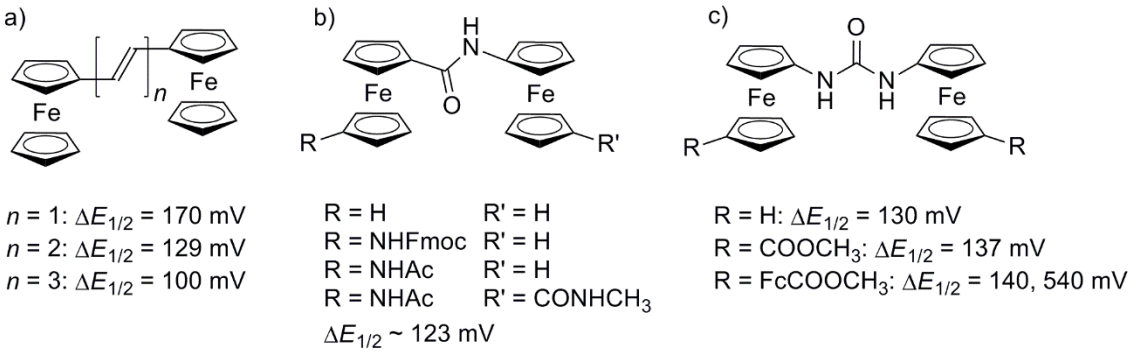

n = 1: $\Delta E_{1/2}$ = 170 mV
n = 2: $\Delta E_{1/2}$ = 129 mV
n = 3: $\Delta E_{1/2}$ = 100 mV

R = H R' = H
R = NHFmoc R' = H
R = NHAc R' = H
R = NHAc R' = $CONHCH_3$
$\Delta E_{1/2}$ ~ 123 mV

R = H: $\Delta E_{1/2}$ = 130 mV
R = $COOCH_3$: $\Delta E_{1/2}$ = 137 mV
R = $FcCOOCH_3$: $\Delta E_{1/2}$ = 140, 540 mV

Scheme 11. Selected class II compounds with different kinds of bridges: a) diferrocenylpolyenes,[108] b) diferrocenylamides (Fmoc = fluorenylmethyloxycarbonyl)[109] and c) diferrocenylureas.[97,98,110]

3 Sulfite oxidase mimicking molybdenum complexes

3.1 Molybdenum-containing enzymes

Molybdenum is taken up from organisms as molybdate ($[MoO_4]^{2-}$) and incorporated into metal cofactors.[112] Two types of molybdenum cofactors can be distinguished: the iron-molybdenum cofactor (FeMoco) and the molybdenum cofactor (Moco).[113] In the former, molybdenum is surrounded by three sulfur atoms of an iron-sulfur cluster and two oxygen atoms of a homocitrate molecule (Scheme 2a). FeMoco is part of the enzyme nitrogenase which is present in certain bacteria as for example *Rhizobia*, which is located at the roots of some plants,[114]and is responsible for nitrogen fixation. Moco consists of an electron-rich pterin-based ligand connected to a C6 pyrano ring, which is substituted by a phosphate and a molybdenum-binding dithiolene group (Scheme 2b). Depending on the enzyme, molybdenum is coordinated by either one or two pyranopterin dithiolene ligand. Further ligands are oxido/hydroxido groups, and/or sulfido groups and an amino acid (serine, cysteine, selenocysteine or aspartate residues).[115] In general, enzymes with a Moco unit catalyze the oxygen atom transfer (OAT) by using H_2O as oxygen source.

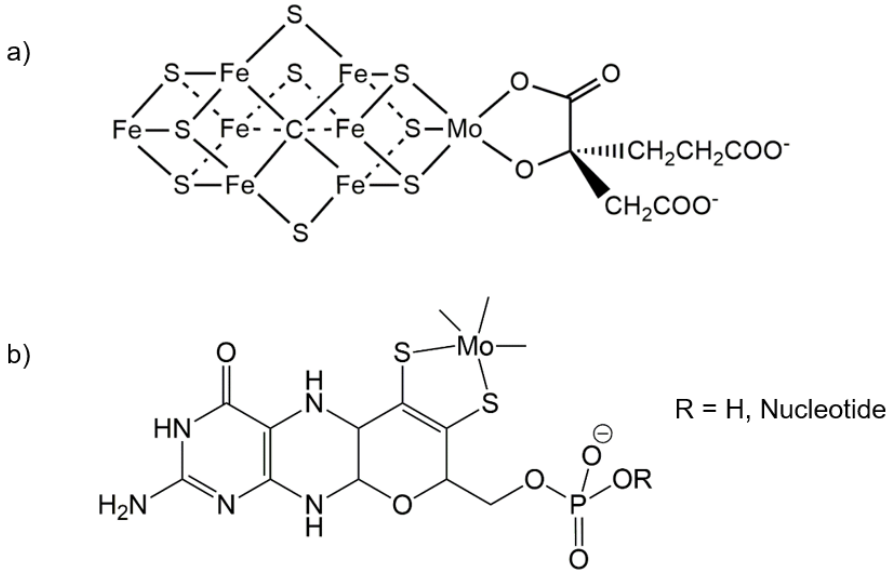

Scheme 12. Structures of a) FeMoco and b) Moco.

The OAT reaction is coupled to an electron transfer (ET) process. The electrons are transferred from Moco to further cofactors such as iron-sulfur clusters, hemes or flavins.[115] During the catalysis, molybdenum switches between the oxidation states VI, V and IV. Moco-containing enzymes can be categorized, depending on the kind of reaction, into two groups: hydroxylases and oxotransferases.[116] Hydroxylases catalyze the hydroxylation of aldehydes and aromatic heterocycles (Equation 1), while oxotransferases catalyze the OAT reactions to or from substrates (Equation 2).[117]

$$RH + H_2O \rightarrow ROH + 2H^+ + 2e^- \qquad \text{(Equation 1)}$$

$$R + H_2O \rightarrow RO + 2H^+ + 2e^- \qquad \text{(Equation 2)}$$

Generally accepted is Hille's classification of Moco-containing enzymes into three families based on the structure of the catalytic center: xanthine oxidases, sulfite oxidases and DMSO reductases (Scheme 13).[13,117]

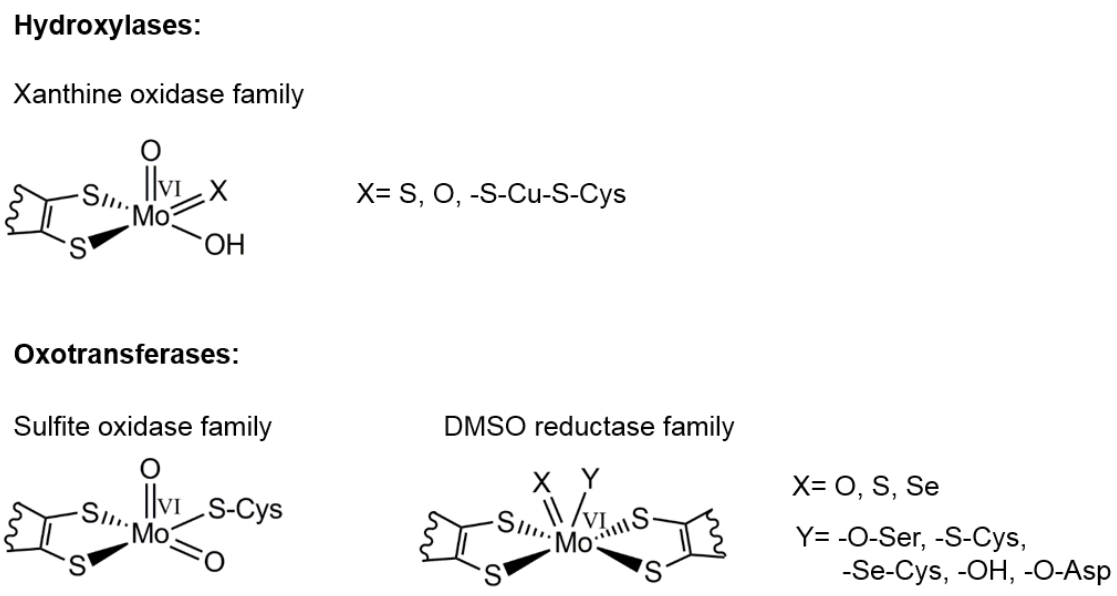

Scheme 13. Moco-containing enzyme families.

X-ray structures of the enzymes show that molybdenum is square pyramidally coordinated by the ligands in the catalytic centers of xanthine and sulfite oxidases, whereas the catalytic unit of the DMSO reductase family possesses a trigonal prismatic coordination geometry.[13] The family of xanthine oxidases belongs to the hydroxylases and is needed for the degradation of the purine bases xanthine and hypoxanthine

(degradation products of the nucleobases guanidine and adenosine) to uric acid. The catalytic centers contain a $Mo^{VI}OS(OH)$ group with the oxido ligand in the apical position and a catalytically active hydroxido ligand and frequently a sulfido ligand in the equatorial positions. The CO dehydrogenase represents an exception within the xanthine oxidase family because it contains a sulfido-bridged Cu^{I} unit. The sulfite oxidases possess a $Mo^{VI}O_2$(S-Cys) group with an apical Mo=O group and one oxido ligand and a cysteinato ligand in the equatorial positions. They convert toxic sulfite into harmless sulfate. The most diverse family is the DMSO reductase family. In the catalytic center, the molybdenum atom is coordinated by one or two pyranopterin dithiolene ligands. In the $Mo^{VI}X(Y)$ unit the ligands X and Y are represented predominantly by an oxido (X) and a serinato (Y) ligand. Other members of the family contain cysteinato, selenocysteinato, a hydroxido group or aspartate instead of a serinato ligand. Sulfur and Selenium atoms in place of the oxido ligand have also been found in some members. The DMSO reductase exists in anaerobic bacteria which need DMSO as electron and proton acceptor to generate dimethyl sulfide and water.[13]

In view of the present work's focus, the family of sulfite-oxidizing enzymes is presented in detail in the following section.

3.2 Sulfite-oxidizing enzymes

The family of sulfite-oxidizing enzymes includes the plant assimilatory nitrate reductases (NRs) and the sulfite oxidases (SOs) from animals, plants and bacteria, where the SOs are subdivided into plant and animal SOs and bacterial sulfite dehydrogenases (SDH).[118] In animals, sulfite is generated by degradation of the sulfur-containing amino acids cysteine and methionine. Because of its high nucleophilicity, sulfite reacts with disulfide bridges from proteins and forms sulfonated cysteine derivatives (Equation 3).[119]

$$R\text{-}S\text{-}S\text{-}R + SO_3^{2-} \rightarrow R\text{-}S\text{-}SO_3^{-} + RS^{-} \qquad \text{(Equation 3)}$$

Since disulfide bridges are important for the tertiary structure of proteins, the reaction with sulfite leads to the loss of protein function. It is known that a SO deficiency causes massive aberrations with lethal consequences.[113,120–122] Therefore sulfite is oxidized by SOs to the harmless SO_4^{2-} molecule (Equation 4). At the same time, molybdenum is reduced from Mo^{VI} to Mo^{IV}. To close the catalytic cycle, two electrons are released from

Mo^{IV} and transferred to the electron acceptor cytochrome (cyt *c*) leading to the restoration of the the Mo^{VI} center.

$$SO_3^{2-} + H_2O + 2\ \text{cyt}\ c_{ox} \rightarrow SO_4^{2-} + 2\ \text{cyt}\ c_{red} + 2\ H^+ \qquad \text{(Equation 4)}$$

Animal SOs have been found in the intermembrane space of mitochondria.[123] Like animals, bacteria use cytochromes as electron acceptor in the sulfite metabolism. The sulfite dehydrogenase in bacteria is localized in the periplasm of the cell. In contrast, the plant SO is localized in the peroxisomes of cells and does not interact with cyt *c*. Studies on the plant SO from *A. thaliana* have shown that during the sulfite metabolism the electrons are transferred to dioxygen which forms toxic H_2O_2 that is converted further into H_2O and O_2 by the enzyme catalase due to its toxicity. Strictly only the SO from plants is a true sulfite oxidase because of its ability to reduce oxygen, whereas the sulfite-oxidizing enzymes from bacteria and animals belong to the class of sulfite dehydrogenases. However, for historical reasons the sulfite-oxidizing enzymes in animals are also referred to as sulfite oxidases.[124]

3.2.1 Protein structure of sulfite-oxidizing enzymes

Well explored is the protein structure of the sulfite dehydrogenase from the bacterium *Starkeya novella*. The X-ray diffraction data reveals that the enzyme is a heterodimer (SorAB) that consists of two subunits, a Moco-binding subunit (SorA) and a cytochrome subunit (SorB), as shown in Figure 1. SorA includes two domains (domain 1 and domain 2) that resemble the domains of the chicken sulfite oxidase (CSO) and plant sulfite oxidase (PSO).[125] Domain 1 binds Moco, whereas domain 2 has a dimerization function, which is however not used in the SorAB complex. In contrast, eukaryotic SOs dimerize through this interface with a second monomer to form homodimeric protein structures. The second subunit SorB binds a *c*-type heme with histidine and methionine in the axial positions, which accepts electrons from Moco during the catalytic cycle. The interaction of SorA and SorB is very strong, due to the comparatively high number of bonds in the subunit interface, i.e. 30 hydrogen bonds and 2 salt bridges. One of the salt bridges links a propionate residue of the heme with an amino acid arginine (Arg-55) of SorA.

In the crystal structure, molybdenum exists in the reduced form with a hydroxido or water molecule instead of an oxido ligand in the coordination sphere. The Mo···Fe distance is

16.6 Å and the distance between Mo and the propionate residue of the heme cofactor amounts to 8.5 Å. The substrate-binding site contains three amino acids that are conserved in all members of sulfite-oxidizing enzymes: tyrosine (Tyr-236) and two arginines (Arg-55 and Arg-109). Tyr-236A and Arg-55A are engaged in hydrogen bonds to the hydroxido ligand of Moco. The hydroxido ligand is further involved in hydrogen bonds to two or three water molecules, which are present in the substrate-binding channel between SorA and SorB. Water molecules are involved in the catalytic cycle of the SO.[125]

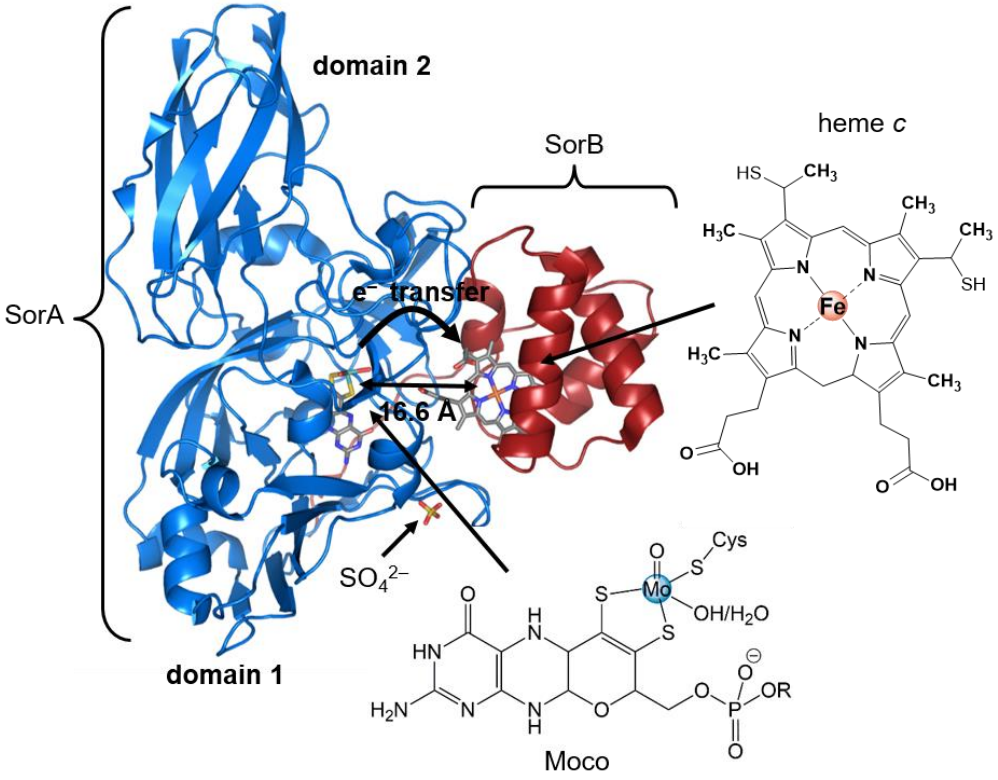

Figure 1. Molecular structure of the reduced form of the sulfite dehydrogenase from *S. novella* (PDB, 2BLF, presented with PyMOL[126]).

A special type of bacterial sulfite dehydrogenase is found in *Thermus Thermophilus*, which lives in hot springs.[127–129] A feature in the electronic pathway of this enzyme is that the electrons from Moco are transferred to a diheme cytochrome (c_{550}). The purpose of two heme units is supposed to be the storage of both of the two electrons generated during the oxidation of sulfite and their effective transfer via a further cytochrome (c_{552}) to the final electron acceptor O_2.

In contrast to the SDH from *S. novella*, the SO from chicken and the plant SO from *A. thaliana* exist as α_2 homodimers (Figure 2). The protein structure of the monomer of CSO contains three domains: a heme *b* domain, a Moco-binding domain and a dimerization domain. Unlike the SO from CSO, the plant sulfite oxidase (PSO) *A. thaliana* lacks the heme domain.[130]

The crystal structure of the chicken liver sulfite oxidase (CSO) contains Moco, presumably in its reduced form (Mo^{IV}), indicated by the hydroxido/water molecule that is found in the equatorial plane. Obviously, the Mo center of the enzyme is reduced during the X-ray measurements. The distances between Mo and the coordinated atoms amount to 1.7 Å (Mo=O), 2.3 Å (Mo-OH/H_2O), 2.4 Å (Mo-S1/Mo-S2, with the sulfur atoms from the dithiolene ligand) and 2.5 Å (Mo-S$(Cys)_{185}$).

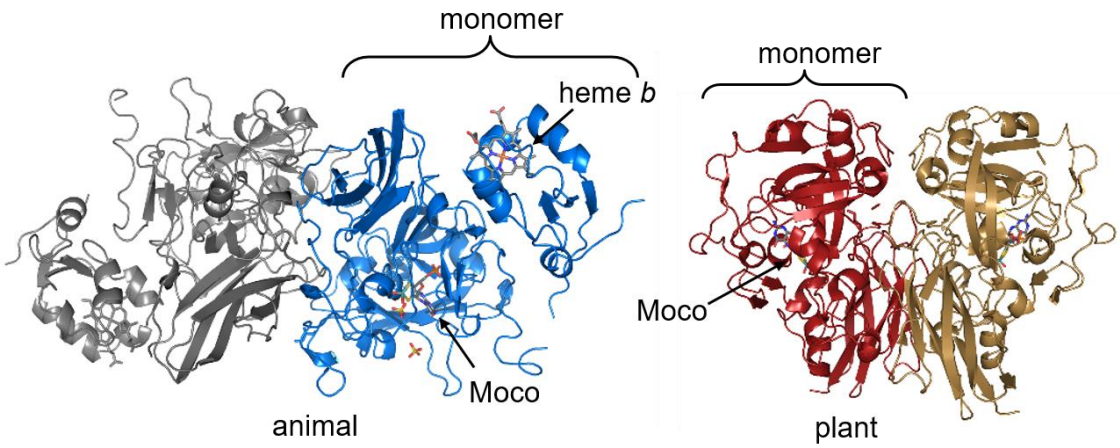

Figure 2. Molecular structure of the sulfite oxidase in animal (chicken) and plant (*A. thaliana*) (PDB, 1SOX and 1OGP, presented with PyMOL[126]).

The heme *b* domain and the Moco domain are connected via a flexible 10 amino acids long loop. Kisker et al. have found that the Mo-Fe distance in the crystal is 32 Å. Intramolecular electron transfer (IET) between two centers over such a large distance would only allow a low electron transfer rate (< 100 s^{-1}).[131,132] However, Enemark et al. have observed an electron transfer rate of around 2000 s^{-1} indicating a smaller distance than 32 Å between Mo and Fe during the electron transfer.[133] Enemark et al. suppose that the enzyme undergoes a conformational change that decreases the distance between Moco and heme domain to a degree that enables an IET fast enough for the catalytic reaction.[133] Computational modeling of the active state suggests that the Mo···Fe distance is smaller

than < 20 Å.[134] Based on docking studies, Kisker et al. have proposed a Mo···Fe distance of about 12 Å.[135] Pulse-EPR studies of human SO in frozen solution provide a Mo···Fe distance of 32 Å, the same as for the CSO in the crystal.[136] In the crystal structure, the sulfate molecule that results from the enzymatic reaction is embedded in a positively charged pocket of three arginine residues.

3.2.2 Mechanism of the OAT reaction

The generally accepted reaction mechanism for the OAT to sulfite has been postulated by Hille (Scheme 14).[117,137–140] This mechanism relies on experimental studies by Holm et al. [141,142] and DFT calculations by Hall et al. on dioxido molybdenum model complexes.[143,144] In the first step of the cycle, the lone pair of sulfite reacts with the equatorial Mo=O π^* orbital of the fully oxidized state Mo^{VI}/Fe^{III} (**1**) forming a $Mo^{IV}O(O\text{-}SO_3)$ species (**2**). After release of a sulfate molecule, the free coordination site is occupied by a water molecule (**3**). In the next step, a proton-coupled intramolecular electron transfer (IET) from Moco to heme (cyt *b*) follows and a Mo^{V}/Fe^{II} (**4**) state is generated that is detectable by EPR spectroscopy (Mo^{V}, d^1). Cyt *b* is reoxidized through electron transfer to an external electron acceptor, cytochrome *c* (**5**). From the Mo^{V}/Fe^{III} state a second proton-coupled IET occurs (**6**), followed by a second ET to cyt *c*, which yields the initial state (**1**).

Methylation of the three oxide anion groups of SO_3^{2-} leads to a similar function of the enzyme, confirming Hille's proposal that the lone pair of sulfite and not the oxo anion ligands attack the molybdenum ion.[139,140] DFT calculations of the OAT reaction also support this and are in good agreement with the experimental kinetic parameters.[145] The structures of the two EPR-active species **4** and **5** have been investigated by Pulse-EPR spectroscopy to get insight into the catalytic mechanism. In the framework of these measurements, the pH dependence, the influence of anions (SO_3^{2-}, SO_4^{2-}, Cl^-, PO_4^{3-}) and mutations have been investigated.[146–151]

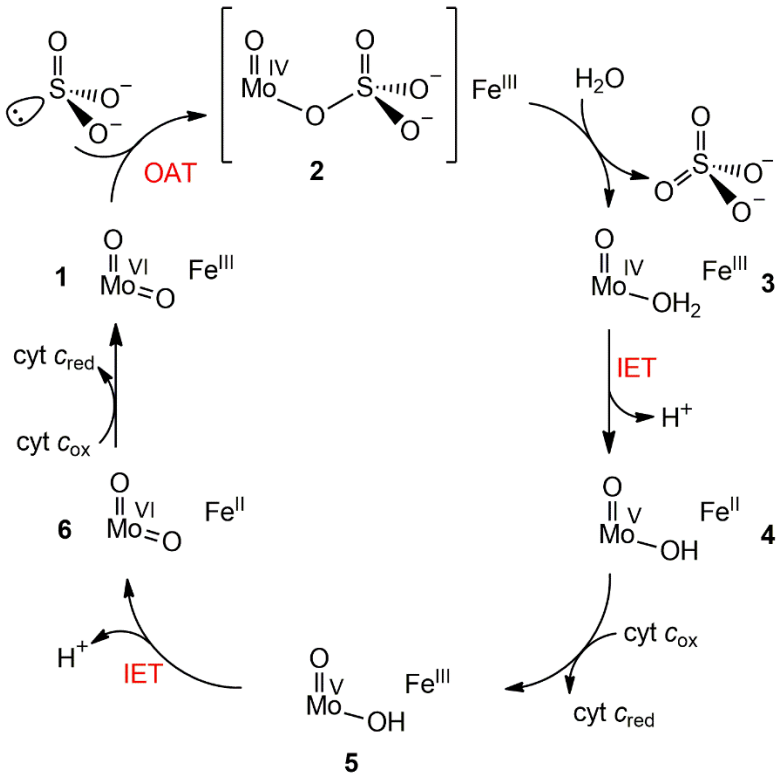

Scheme 14. Generally accepted mechanism of the catalysis in SO.

3.2.3 Insights into the IET between Moco and heme

With respect to IET in SOs, two main questions have been in the focus of recent research: a) How can the conformational change in the CSO be proven? b) In which way does the IET between Moco and heme occur? The answer to the first question is provided by several studies. Feng et al. have shown that the increase of solution viscosity through polyethylene or sucrose leads to a decrease in the IET rate constant for the CSO, pointing to a motion of residues within the protein. In contrast, the increase of solution viscosity does not affect the IET rate constant for the SDH, indicating that IET in the SDH occurs without conformational changes of the protein.[120] The conformational flexibility of CSO is confirmed by EPR spectroscopy which shows a distribution of intramolecular Mo···Fe distances.[152] Experimental determination of the IET rate constant k_{et} reveals that the ET process is independent of SO concentration, also pointing to an intramolecular process.[120] To give an answer to the second question, the role of the conserved amino acids (tyrosine, arginine and arginine) for the IET has been investigated. For this purpose mutated forms of SOs have been studied by various methods.[121,147,153–159] From the crystal structure it is known that one arginine (Arg-138 in the CSO) is involved in hydrogen bonds to the

sulfate molecule and to the hydroxido/water ligand of Moco (Scheme 15).[160] Enemark et al. have shown that the replacement of this arginine by the neutral amino acid glutamine (Gln) in the human SO (a mutation that was also found in patients with SO deficiency) leads to a decrease of the IET rate constant by three orders of magnitude.[159] Comparative studies with human SO mutants containing the basic amino acid lysine instead of arginine reveal a smaller (four-fold) decrease of the IET rate constant.[159] These results imply that the positive charge of arginine and not its location is necessary to allow the best orientations of Moco for effective IET between Mo and Fe and to orient the sulfate molecule optimally in the proximity of molybdenum.[160]

In contrast to the results with the CSO, the IET rate of mutants of the SDH with Arg to Gln substitution is three times higher than in the wild type SDH,[154] indicating that arginine in the SDH and CSO is not an absolutely required part of the electron transfer path between Moco and heme. Based on the results from experiments with the SDH, arginine is attributed the function to control the $Mo^{VI/V}$ potential through the influence of its positive charge and in that way to regulate the electron transfer rate.[154]

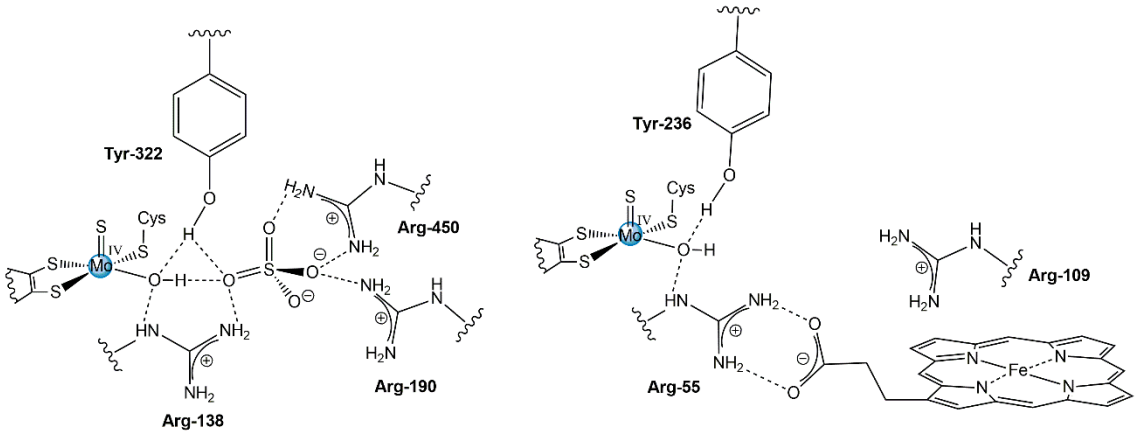

Scheme 15. Catalytic center of the reduced state of the CSO with bound sulfate molecule (left) and of the reduced state of the SDH (right) in the crystal structure. For clarity only one substituent (propiate group) at the heme molecule of the SDH is shown.

An alternative electron transfer path between Mo and Fe involves the aromatic amino acids in the proximity of the Moco and heme units.[125] These aromatic amino acids (Phe-168, Tyr-236, Trp-231, Phe-230, Tyr-61) are arranged with an edge-to-edge distance of 4 Å. The amino acids Phe-168 and Tyr-61 at the end of the row interact with the aromatic pterin moiety of Moco and a pyrrole ring of heme through π-π-stacking. According to this

hypothesis, the electrons are transported through electron hopping along this chain of amino acids between the two redox centers. Despite a variety of studies on mutants, the electron transfer mechanism is still not understood in detail.

3.3 Model complexes for the sulfite oxidase

Model complexes for enzymes are developed to obtain a better understanding of the reaction mechanisms in enzymes. The complexes are designed with respect to two aspects: *structural analogy* and *functional analogy*.[161] The primary purpose of structurally analogous complexes is to imitate the electronic structure and geometry of the catalytic center. The comparison of the analytic data of the model compound and the protein can help to gain a better understanding of the geometry of the catalytic center in the oxidation states VI, V and IV. The elucidation of the structure of the catalytic center in the Mo^{V} state mainly relies on EPR spectroscopic data. Crystal structures have been only obtained from SOs where molybdenum exists in the oxidation state VI or IV. For that reason the EPR data of molybdenum(V) model complexes contribute considerably to the understanding of the structure of enzymes in the Mo^{V} state.[162]

Functionally analogous model complexes for the SO attempt to imitate the OAT reaction and switch between the biologically relevant oxidation states VI, V and IV. One challenge in the development of such complexes is the suppression of the dimerization reaction of Mo^{VI} and Mo^{IV} centers to a μ-oxido Mo^{V} dimer. A further challenge is the use of sulfite as substrate. Because of its low oxophilicity and solubility in organic solvents, phosphanes are frequently used as substrates instead.

3.3.1 Structurally analogous complexes

A variety of model complexes for all families of sulfite-oxidizing enzymes have been synthetized based on mono- and bisdithiolene ligands. These ligands mimic the structural and electronic properties of the sulfur-containing ligands in the SO.[161,163] An example for a dioxido molybdenum(VI) complex based on a monodithiolene ligand as structurally analogous model for the SO is shown in Scheme 16a. The benzene-1,2-dithiolato ligand corresponds to the pyranopterin dithiolene ligand and the ^{i}Pr-substituted thiophenolate imitates the cysteinato ligand.[164,165] The complex exhibits a square pyramidal structure

and the bond lengths are similar to those found for the oxidized form of the CSO (determined from EXAFS analysis).[166]

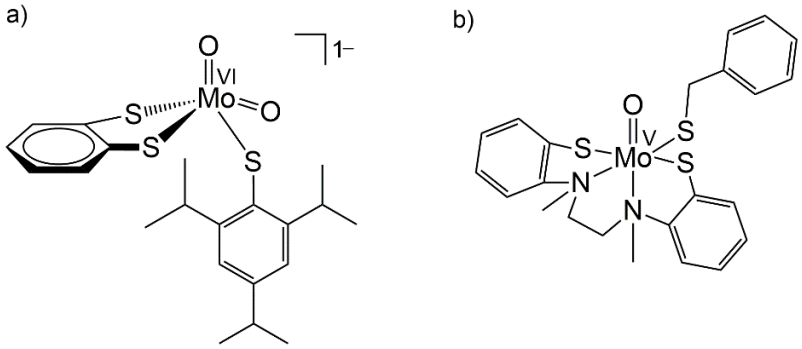

Scheme 16. Selected structurally analogous model complexes for the SO.[162,164]

Enemark et al. have synthetized a model complex based on a chelate ligand with (*N*,*S*)$_2$-coordination (Scheme 16b).[162] The EPR data (g_1 = 2.022, g_2 = 1.963, g_3 = 1.956) are closer to the EPR parameters (g_1 = 2.0037, g_2 = 1.972, g_3 = 1.9658)[148] for the low pH form of the SO than model compounds with two or four thiolate donors.[162]

3.3.2 Early functionally analogous complexes and fundamental studies of the OAT mechanism

The early studies by Holm et al. contribute substantially to the understanding of the mechanism of OAT in sulfite-oxidizing enzymes. Berg and Holm were among the first to develop functional model complexes for Moco-containing enzymes and have published a thorough analysis of the OAT reaction.[167,168] They have synthesized dioxido molybdenum(VI) complexes based on a tridentate ligand (LNS_2) with an *S*,*N*,*S*-coordination (Scheme 17).[169–171] The $Mo^{VI}O_2(LNS_2)$ complex is able to catalyze the reaction between PPh_3 and DMSO in DMF, forming $OPPh_3$ and DMS (Scheme 17). During the OAT reaction to PPh_3, the free coordination site in the molybdenum(IV) complex is supposed to be occupied by a DMF molecule. In spite of the high steric demand of the ligand, aggregation is possible and the reaction of $Mo^{VI}O_2(LNS_2)$ with PPh_3 yields the μ-oxido dimer with a $[Mo_2^{V}O_3]$ core.[172]

In later works Holm et al. have developed model complexes based on bidentate ligands with *N*,*O*- and *N*,*S*-coordination.[173] Especially the OAT reaction from $Mo^{VI}O_2(^t$Bu-$LNS)_2$

(LNS = (4-*tert*-butylphenyl)-2-pyridylmethanethiolate) to PEt_3 using the sterically most demanding ligand has been investigated in detail.

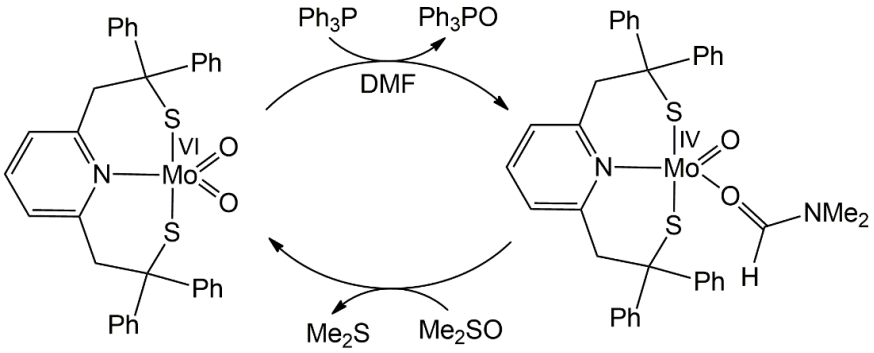

Scheme 17. Model complex based on a ligand with *S*,*N*,*S*-coordination.

This complex has several advantages compared to the system with the LNS_2 ligand: formation of a five-coordinated oxido molybdenum(IV) complex, good solubility in various solvents and reactivity of $Mo^{IV}O(^{t}Bu\text{-}LNS)_2$ with a variety of oxidized substrates.[173] Dimer formation is not observed in solvents like acetonitrile, THF and DMF, but in benzene. According to Holm et al. the coordination of solvent suppresses the μ-oxido dimer formation.

Enemark et al. have reported six-coordinated model complexes containing the tripodal ligand hydrotris(3,5-dimethyl-1-pyrazoyl)borate (Tp*).[174–176] Among those, especially complexes of the type $Mo^{VI}O_2(Tp^*)X$ (X = Cl, Br, NCS, OMe, OEt, OPh, S^{i}Pr, SPh and SCH_2Ph) are important.[176,177] The complex $Mo^{VI}O_2(Tp^*)(SPh)$ is the first that has been characterized in all biologically relevant oxidation states VI, V and IV (Scheme 18).[174,178] $Mo^{VI}O_2(Tp^*)(SPh)$ is successfully reduced with PPh_3 yielding $Mo^{IV}O(Tp^*)(SPh)$(solvent) in DMF or MeCN, where the free coordination site is occupied by a solvent molecule. A highlight of the studies on this model system is that in the presence of water the comproportionation reaction of the Mo^{VI} and Mo^{IV} form leads to the product $Mo^{V}O(OH)(Tp^*)(SPh)$, which represents a suitable model for the $[Mo^{V}O(OH)]^{2+}$ state in the sulfite oxidase. The incorporation of an oxygen atom from water is clearly proven by EPR experiments employing $H_2{}^{17}O$.[179] In presence of oxygen the Mo^{V} complex is reoxidized to the initial Mo^{VI} complex.

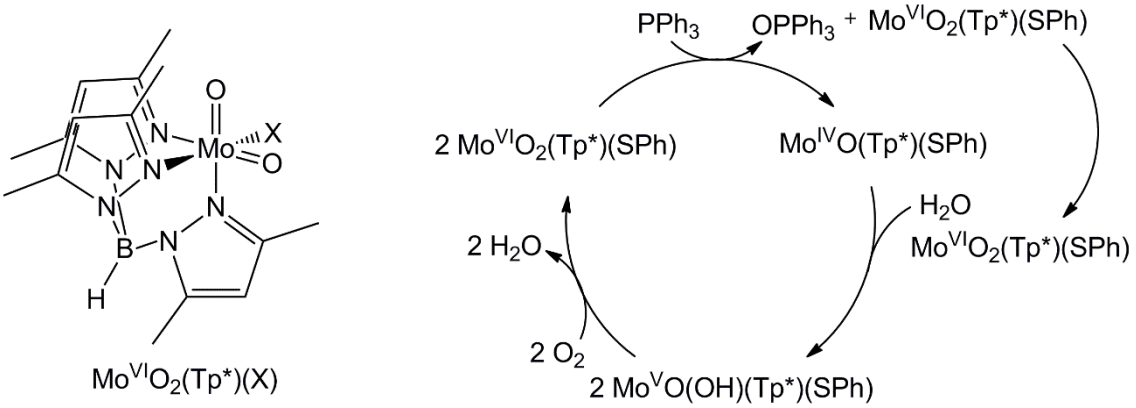

Scheme 18. Left: Model complex $MoO_2(Tp^*)(X)$, X = Cl, Br, NCS, OMe, OEt, OPh, S^{i}Pr, SPh or SCH_2Ph. Right: Catalytic oxygen atom transfer in wet solvents and upon admission of oxygen.

Hall et al. have performed theoretical calculations for the reaction of $Mo^{VI}O_2(Tp^*)(SPh)$ with PPh_3. In their model system $Mo^{VI}O_2(NH_3)_2(SH)_2$ they have replaced the tripodal ligand and the thiolate ligand by two ammonia and two SH^- ligands. As substrate trimethylphosphane has been used instead of PPh_3. The first step of their proposed mechanism for the OAT reaction is the attack of the lone pair of PMe_3 at the Mo=O π^* orbital generating the intermediate phosphoryl Mo^{IV} complex which is about 289 kJ mol^{-1} lower in energy than the starting materials. At the transition state, the Mo–O bond is longer (up to 1.83 Å) while the bond of the unreacted Mo=O group is only slightly shorter (decreased from 1.68 Å to 1.66 Å).[180] Further, their calculations show that after the formation of the intermediate, the addition of one water molecule takes place by an associative mechanism, i.e. concerted exchange of a $OPMe_3$ molecule against a H_2O molecule and not by a dissociative one ($OPMe_3$ leaving before H_2O coordinates).[143]

The theoretically predicted formation of a phosphoryl Mo^{IV} complex is confirmed experimentally through the isolation and characterization of phosphoryl Mo^{IV} complexes based on Tp* and Tp^{iPr} (Tp^{iPr} = hydrotris(3-isopropylpyrazoyl-1-yl)borate) ligands.[181–186] The kinetics of the OAT reaction of $Mo^{VI}O_2(Tp^{iPr})(OPh)$ with PR_3 and the solvolysis of a series of $Mo^{VI}O_2(Tp^{iPr})(OPh)(OR)$ complexes (R = PMe_3, PEt_3, PMe_2Ph, P^{n}Bu$_3$, $PEtPh_2$ and $PMePh_2$) have been studied by UV-Vis spectroscopy.[187] The values for the activation enthalpy for the formation of $Mo^{IV}O(Tp^{iPr})(OPh)(OPMe_3)$ ($\Delta G^{\ddagger}$ = 90.4 kJ mol^{-1}) and solvolysis with acetonitrile ($\Delta G^{\ddagger}$ = 93.8 kJ mol^{-1}) indicates that the nucleophilic attack by PMe_3 is faster than the solvolysis. In case of sterically more demanding phosphanes, however, the first step is rate limiting.[187] The solvolysis reaction

follows a dissociative mechanism for most of the phosphoryl complexes, as evident from the positive value for the entropy of activation. In contrast, in case of the trimethylphosphane complex a negative entropy of activation is observed which indicates an associative mechanism.[187] The electrochemical investigation shows that for the acetonitrile-coordinated complex $Mo^{IV}O(Tp^{iPr})(OPh)(NCMe)$, the redox potential for the $Mo^{IV/V}$ couple is by about 350 to 390 mV more positive than the redox potential for the phosphoryl complexes $Mo^{IV}O(Tp^{iPr})(OPh)(OPR_3)$. It is concluded that the coordination of a phosphoryl ligand has a more stabilizing effect on the Mo^{V} state.[187]

The Tp*-based model system has been extended by Basu and Enemark through the attachment of a porphyrinato iron(III) unit (Scheme 19). This additional complex unit mimics the heme component of the SO. The tri-*p*-tolylporphyrin (TPP) is coordinated to a Mo^{V} center through oxygen atoms of a catecholato substituent, in which the position of the hydroxyl groups is varied (2,3-OH-TTP and 3,4-OH-TTP) to modulate the Mo···Fe distance.

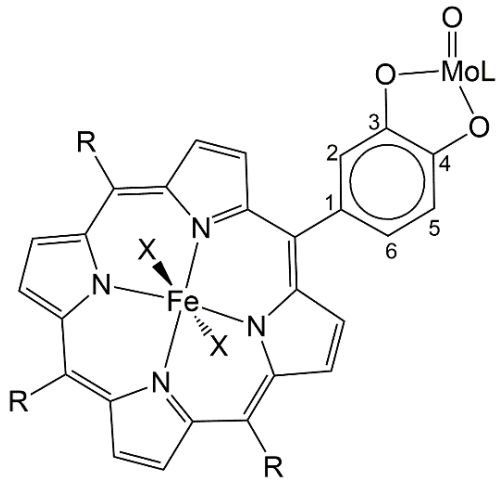

Scheme 19. Mo^{VI}-Fe^{III} model system imitating the Moco and heme component of the SO (R = 4-MePh, X = *N*-methyl imidazole, L = Tp*).

In this new model systems the magnetic interaction of the Mo^{V} and Fe^{III} centers has been investigated. In case of the 2,3-OH-TTP ligand, the Mo···Fe distance amounts to 7.9 Å resulting in weak exchange coupling. Coordination of 3,4-OH-TPP leads to a longer distance (9.4 Å) and hence a negligible exchange interaction.[188,189] However, no electron transfer studies have been conducted with this model complex.

3.3.3 Further functionally analogous complexes

The model complexes discussed in the previous section are able to transfer successfully oxygen to artificial substrates like phosphane molecules. However, an OAT to the physiological substrate sulfite has not been demonstrated with these compounds. Sarkar et al. have shown an OAT reaction to bisulfite on the structural-functional model complex $[Bu_4N]_2[Mo^{VI}O_2(mnt)_2]$ based on the dithiolene ligand mnt^{2-} (1,2-dicyanoethylene-1,2-dithiolate).[190,191] The OAT reaction is performed in an acetonitrile-water mixture and follows a Michaelis–Menten saturation kinetics, which is typical for enzymatically catalyzed reactions (Scheme 20). Due to the negative charge, the formation of a μ-oxido dimer is not observed.

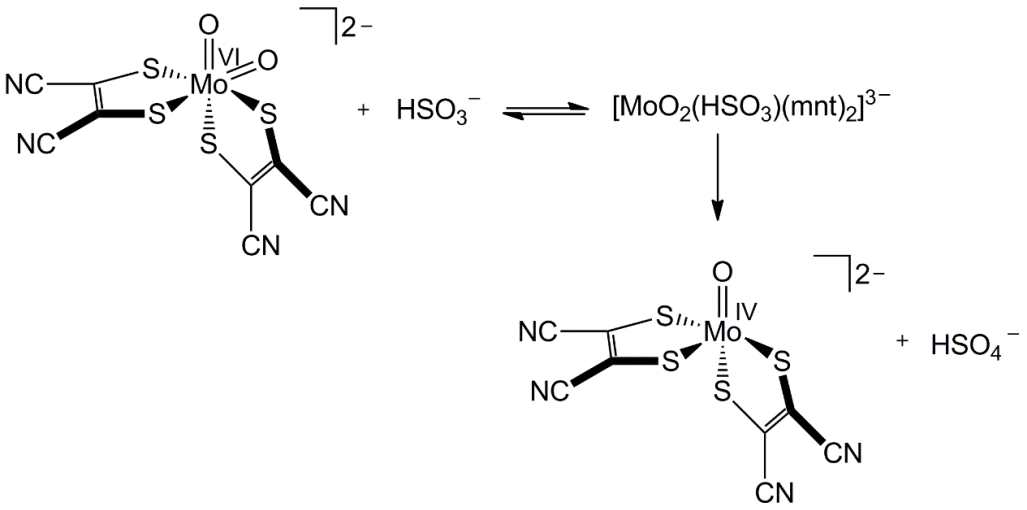

Scheme 20. OAT to bisulfite using the structural-functional model complex $[Bu_4N]_2[Mo^{VI}O_2(mnt)_2]$.

Based on DFT calculations, Sarkar suggests a mechanism in which the oxide anion of HSO_3^- attacks at the Mo^{VI} center and forms an intermediate seven-coordinated complex.[192] With that hypothesis, Sarkars' mechanism differs from the mechanism in the SO where the attack occurs by the lone pair of the HSO_3^- anion. Oxidation of the $[Mo^{IV}O(mnt)_2]^{2-}$ complex by iodine, in dichloromethane yields the EPR-active $[Mo^{V}O(mnt)_2]^-$ complex. In the presence of Cl^- anions during the oxidation with iodine the $[Mo^{V}OCl(mnt)_2]^{2-}$ complex (g_{iso} = 1.974) can be isolated, which is a suitable model for the low pH form of the molybdenum(V) state of the SO (g = 1.980).[151]

Recently, Sarkar et al. have reported a series of complexes of the type $[Mo^{IV}O(mnt)(SR)(N\text{-}N)]^-$ (R = Ph, Nap, *p*-Cl-Ph, *p*-CO_2H-Ph, *p*-NO_2-Ph; N-N = 2,2'-

bipyridine or 1,10-phenanthroline) as model systems for the reduced form of the SO. In contrast to the other complexes which show a Mo^{V} signal in the EPR spectrum upon oxidation, the $[Mo^{IV}O(mnt)(SPh)(phen)]^{-}$ complex provides a ligand-based EPR signal, induced by an unpaired electron on the dithiolene ligand. From this observation, Sarkar deduce the suggestion that in the SO enzyme the pyranopterin ligand is part of the electron transfer pathway.[193]

A series of dioxido and imido-oxido molybdenum(VI) model complexes based on *β*-ketiminato ligands ($L^{R,R'}$) has been synthetized by Mösch-Zanetti et al. (Scheme 21). In these complexes the MoO_2 moiety mimics the catalytic unit of the sulfite oxidase while the imido ligand imitates the sulfido group in the enzyme xanthine oxidase. The introduction of trifluoromethyl groups at the ligands removes electron density at the metal center and increases the electron donating effect of the imido group.[194–196] The reaction of $Mo^{VI}OX(L^{R,R'})_2$ complexes (X = O, N^{t}Bu) with trimethylphosphane yields $OPMe_3$ and the oxido phosphane molybdenum complexes $Mo^{IV}O(PMe_3)(L^{R,R'})_2$ with a coordinated phosphane molecule. In contrast, the complexes of Enemark, Basu and Holm coordinate a solvent molecule instead of a substrate in the reduced state. Through the introduction of an imido ligand, dimer formation is prevented during the reaction.[194] Kinetic studies of the OAT reactions reveal that the activation enthalpy $\Delta H^{\ddagger}$ (12 kJ mol^{-1}) is considerably lower for the fluorinated compound (R' = CF_3) than for the analogous non-fluorinated derivative ($\Delta H^{\ddagger}$ = 61 kJ mol^{-1}), implying an increase in the OAT reaction rate by fluorination. In the case of R = ^{i}Pr, no reaction with PMe_3 is observed when R' = Me, but a slow reaction when R' = CF_3. These results are rationalized by the electron-withdrawing effect of the CF_3 groups, which leads to a more facile nucleophilic attack by the lone pair of the PMe_3 molecule.[196] Independent of fluorination, the reaction rate of imido-oxido Mo^{VI} complexes is lower than that of dioxido Mo^{VI} complexes, however, fluorination does have a significant enhancing effect on the reaction rate difference (14:2). The rates for the fluorinated dioxido Mo^{VI} complex (R = Me) and imido-oxido Mo^{VI} complex (R = Me) are higher than those for the analogous CH_3-substituted complexes by a factor of 92 and 15, respectively. The reason for the lower reactivity of the imido-oxido Mo^{VI} complexes is the electron donation capability of the imido ligand, leading to a lower reactivity of the oxido ligand towards the nucleophilic attack.[196]

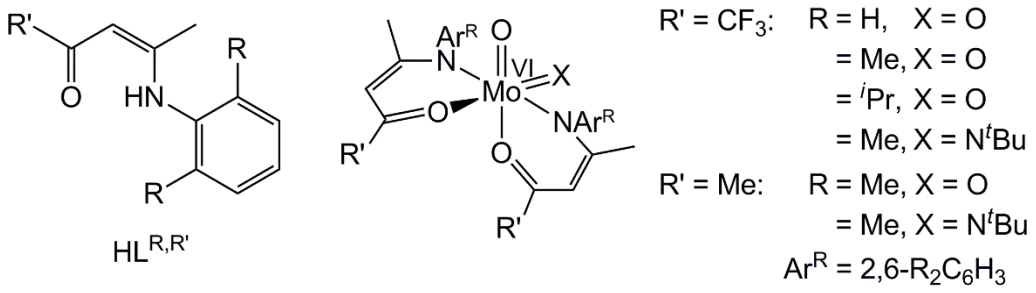

Scheme 21. Model complexes based on β-ketiminato ligands.

For the $Mo^{IV}O(PMe_3)(L^{Me,Me})_2$ complex a reaction with dry oxygen yields the oxido peroxido complex $Mo^{VI}O(O_2)(L^{Me,Me})_2$. This complex has been characterized with X-ray diffraction analysis. This reaction is an exceptional result, since oxido peroxido complexes are rare in synthetic coordination chemistry.[197]

Heinze et al. have employed a bidentate Schiff ligand with *N,N'*-coordination ($HL^{R,R'}$; R = OMe, OSiMe, ^{t}Bu; R' = H, ^{i}Pr) for the synthesis of octahedral dioxido and imido-oxido complexes of the type $Mo^{VI}OX(L^{R,R'})_2$ (X = O, N^{t}Bu) as model systems for sulfite-oxidizing enzymes, especially sulfite oxidase (Scheme 22).[198–202]

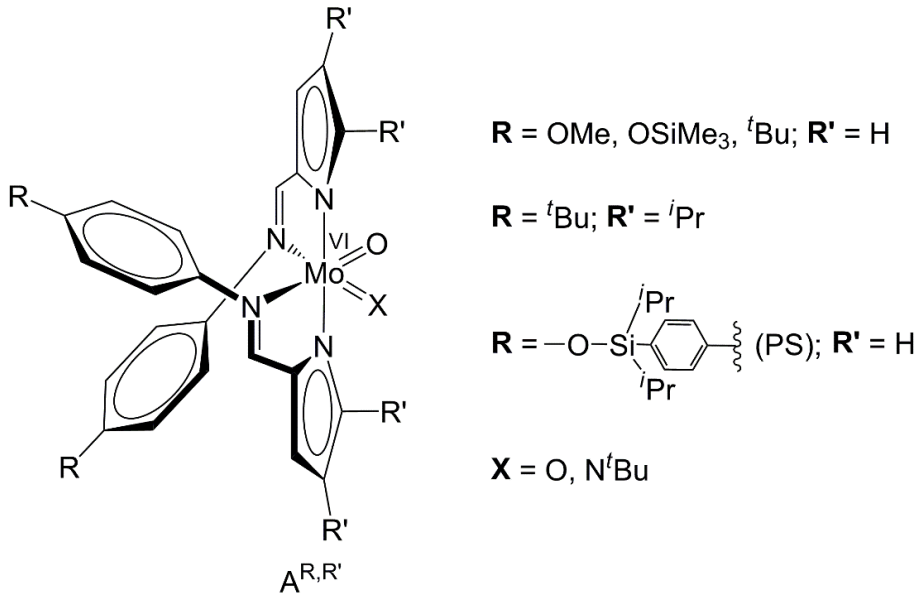

Scheme 22. Dioxido and imido-oxido Mo^{VI} complexes containing bidentate *N,N'*- chelate ligands.

These complexes have been used to investigate the OAT to several phosphanes such as PMe_3 and PPh_3. For the synthesis of the Mo^{VI} complexes the ligands are treated with a base (NEt_3, KHMDS) and then converted with the precursors MoO_2Cl_2(dme) and MoO(N^{t}Bu)(dme) (dme = 1,2-dimethoxyethane), respectively. The introduction of the

N^{t}Bu group suppresses a dimerization reaction, as already observed by Mösch-Zanetti et al. (vide supra).

In order to modify the properties of the Mo^{VI} complexes, the substituents at the ligands have been altered. The introduction of a *tert*-butyl group at the phenyl moiety of the ligands increases the solubility of the complexes and facilitates the formation of crystals suited for X-ray diffraction. A further way to suppress dimerization is achieved by attaching *iso*-propyl groups to the pyrrolato moiety. [202]

The reaction mechanism of the OAT reaction has been theoretically investigated with DFT calculations on the model complex $Mo^{VI}O_2(L^{H,H})_2$.[199] In the first step, a nucleophilic attack of phosphane at the MoO_2 π^* orbital occurs ($\Delta G^{\ddagger}$ = 65 kJ mol^{-1}) and intermediately the phosphoryl Mo^{IV} complex is formed, in agreement with the calculations of Basu and Hall. The cleavage of the Mo-$OPMe_3$ bond in the next step of the reaction yields the five-coordinated $Mo^{IV}O(L^{H,H})_2$ complex. The first step of the reaction is rate-limiting, since the second step requires less free enthalpy of activation ($\Delta G^{\ddagger}$ = 27 kJ mol^{-1}) than the nucleophilic attack. The five-coordinated Mo^{IV} complex reacts with a molecule of $Mo^{VI}O_2(L^{H,H'})_2$ to the $(L^{H,H'})_2OMo^{V}$-O-$Mo^{V}O(L^{H,H'})_2$ dimer. However, in presence of an excess of phosphane, the dimer is split and the free coordination site of the $Mo^{IV}O(L^{H,H})_2$ complex is occupied by a PMe_3 molecule, yielding the phosphane complex $Mo^{IV}O(PMe_3)(L^{H,H})_2$.

Kinetic studies of the reaction of $Mo^{VI}O_2(L^{OSiMe_3,H})_2$ with several phosphanes have been performed with UV-Vis spectroscopy, for the determination of the reaction rate using the evolution of the characteristic π-π^* absorption band of the μ-oxido dimer at ~550 nm. The reaction rate decreases with increasing steric demand of the phosphane ligand. The resulting activation barrier for the reaction with PMe_3 ($\Delta H^{\ddagger}$ = 50 kJ mol^{-1}) is lower than for the complexes based on the ß- ketiminato ligand from Mösch-Zanetti et al. ($\Delta H^{\ddagger}$ = 61 kJ mol^{-1}) or the Tp^{iPr} ligand from Basu et al. ($\Delta H^{\ddagger}$ = 75 kJ mol^{-1}).

Analogous OAT reactions have been performed in heterogeneous phase by immobilizing the ligands via a trimethylsilylether at a polystyrene backbone (L^{PS}) and the subsequent conversion to the dioxido Mo^{VI} complex. The fixation of the complexes suppresses the dimerization reaction of the molybdenum centers. Thus, the polymer backbone fulfills a similar task as the protein scaffold in the enzyme. A fully catalytic OAT reaction has been achieved at the solid phase (Scheme 23). Addition of PMe_3, $[Fe(AcC_5H_4)_2][BF_4]$ as

electron acceptor, water as oxygen donor and P_1-^{t}Bu as proton acceptor to the polymer-supported Mo^{VI} complex gives 25 eq. $OPMe_3$ within 48h.[198] Labeling experiments with $^{18}OH_2$ confirm the incorporation of oxygen from water into $OPMe_3$. A catalysis in homogeneous solution under these conditions is not feasible because the corresponding $Mo^V(H_2O)(L^{OSiMe_3,H})$ complex would react to a μ-oxido dimer. While the observed catalysis involves an ET step from Mo^{IV} to Fe^{III}, $[Fe(AcC_5H_4)_2]^+$ acts as an external electron acceptor, in contrast to the biological system that involves intramolecular electron transfer (IET).

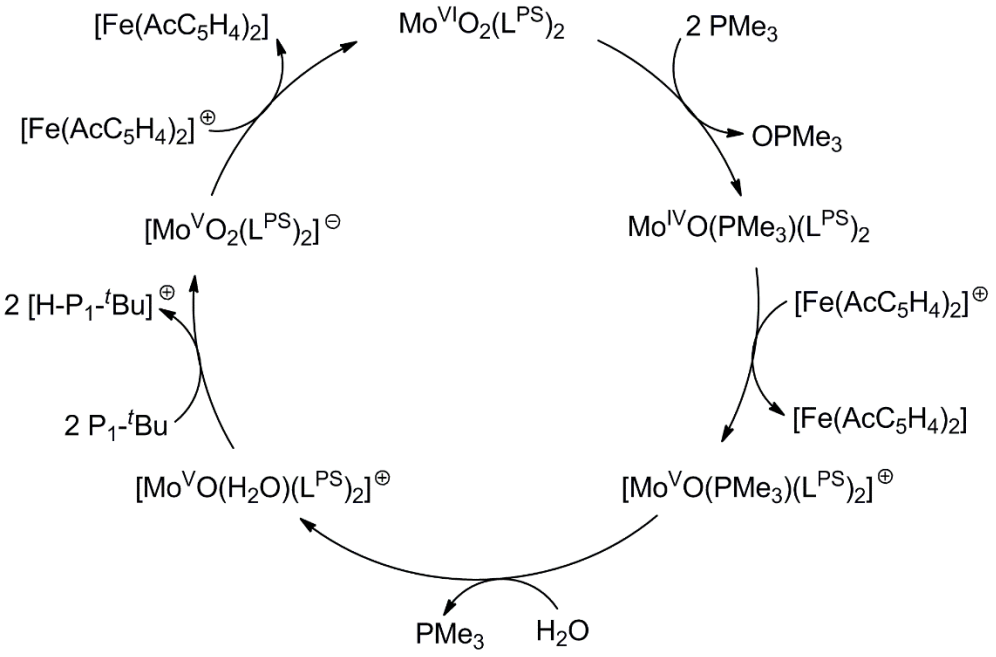

Scheme 23. Catalytic conversion of PMe_3 to $OPMe_3$ with $Mo^{VI}O_2(L^{PS})_2$.[198]

Duhme-Klair et al. report a Ru^{II}-Mo^{VI} dyad which is able to catalyze the OAT from DMSO to PPh_3 involving a light-induced IET. In the dyad $[Ru(bpy)_2(L)MoO_2(solv)]^{2+}$ (bpy = bipyridyl), the ruthenium complex unit and the molybdenum complex unit are linked via a phenanthroline-thiosemicarbazone ligand (L) (Scheme 24). In the first step of the catalysis, the photoexcited $[Ru^{II}*(bpy)_2(L)MoO_2(solv)]^{2+}$ complex is quenched by the mediator methylviologen (MV^{2+}), yielding $[Ru^{III}(bpy)_2(L)MoO_2(solv)]^{2+}$ and $MV^{\bullet+}$. An intramolecular electron transfer leads to $[Ru^{II}(bpy)_2(L^+)MoO_2(solv)]^{2+}$. From this state an IET-coupled OAT to $PPhe_3$ occurs, forming the Mo^V complex $[Ru^{II}(bpy)_2(L)Mo^VO(solv)]^{2+}$ and $OPPh_3$. The cycle is closed by regeneration of the initial

Mo^{VI} complex and MV^{2+} with DMSO. The OAT cycle runs faster through the involvement of the photo-active ruthenium complex unit than in the absence of light.[203]

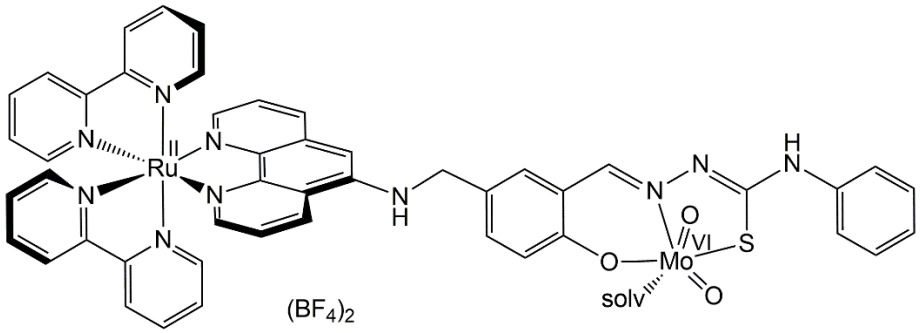

Scheme 24. Photo-active model complex $[Ru^{II}(bpy)_2(L)MoO_2(solv)][BF_4]_2$.

3.4 EPR spectroscopy

Paramagnetic species and radicals are common intermediates of enzymatic reactions in biological systems. In sulfite-oxidizing enzymes, for example, the formation of paramagnetic Mo^{V} species is part of the catalytic cycle, as already discussed in the previous sections. For detection of compounds with one unpaired electron, electron paramagnetic resonance (EPR) spectroscopy is used. Similar to NMR spectroscopy, EPR spectroscopy is based on the excitation of a spin, in this case the electron spin of unpaired electrons. The sensitivity of the method is considerably higher than that of NMR spectroscopy.

3.4.1 General considerations

Through application of an external magnetic field, the energy level of an electron splits into two states (*Zeeman* splitting), where the energetic splitting increases with the magnitude of the magnetic field: $\Delta E = h\ \nu = g\ \mu_B\ B_0$ (g = Landé factor, μ_B = Bohr magneton, B_0 = magnetic field). The proportionality factor g corresponds to the chemical shift δ in NMR spectroscopy. An orientation of the spin parallel to the external magnetic field is energetically favorable and corresponds to the ground state. The absorption of irradiated energy (microwaves) raises the electronic spin into the excited level.

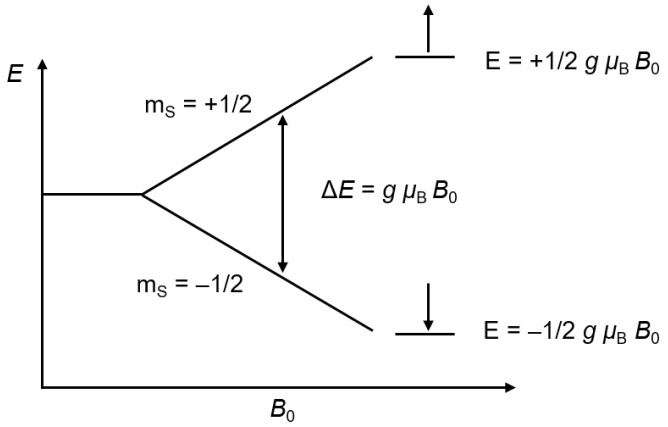

Scheme 25. *Zeeman* splitting with increasing magnetic field.

Usually paramagnetic samples are measured with a continuous wave (CW) spectrometer. During the measurement the sample is irradiated with microwaves of constant frequency, which is usually ~9.4 GHz (X-band). Through variation of the magnetic field, the magnetic field strength required for the transition is passed through. Because of the large line widths of the signals, the first derivative of the absorption spectrum is analyzed. The zero-crossing of the derivative spectrum corresponds to the *g*-factor. For free electrons, the *g*-value amounts to $g_e = 2.0023$.[204]

A further consideration is the magnetic interaction of an electronic spin with a nuclear spin causing an additional splitting of the energy levels. The electronic spin experiences in addition to the external magnetic field also the magnetic field of the nuclei. The interaction of magnetic moments of the unpaired electrons with the magnetic nuclear spins is called *hyperfine coupling*. The resulting multiplicity of the EPR line splitting corresponds to $m_I = 2nI + 1$ (I = nuclear spin, n = number of equal nuclei). The strength of this coupling is described by the hyperfine coupling constant A and corresponds to the distance between the hyperfine coupling lines in the spectrum. For the transitions, the following selection rules hold: $\Delta m_I = 0$, $\Delta m_S = \pm 1$. For example, the coupling of one electron with one nitrogen atom (^{14}N; $I = 1$) causes three lines in the spectrum, because of $2nI+1 = 3$. The coupling of an electron to adjacent atoms (e.g. ^{1}H; $I = ½$ or ^{31}P; $I = ½$) within the molecule can cause additional splitting of the hyperfine coupling lines (a doublet in case of ^{1}H of ^{31}P) and is called *superhyperfine coupling*.

In spherical molecules, the *g*-factor is equal for the three spacial directions x, y and z, i.e. an isotropic EPR spectrum is obtained. In the general case, a molecule is not symmetrical

and exhibits different *g*-values (g_x, g_y and g_z) and *A*-constants (A_x, A_y and A_z) for the three spacial directions. The resolution of the three parameters depends on the sample preparation. Dissolved compounds at room temperature are able to rotate such that the initial orientation of the molecules changes during the measurement. Thus an averaged EPR signal is obtained with $g_{iso} = (g_x + g_y + g_z)/3$ and $A_{iso} = (A_x + A_y + A_z)/3$. In frozen solution or in powder, the orientation of the molecules does not change and therefore the *g* and *A* parameters depend on the spacial direction. If $g_x = g_y \neq g_z$, an axial anisotropic spectrum is obtained. In case of $g_x \neq g_y \neq g_z$, the spectrum is called rhombic.

3.4.2 EPR spectroscopy of transition metals

Because of the heavy mass of transition metals, spin orbit coupling causes a greater deviation of the g-value from g_e than for organic compounds. Spin orbit coupling leads to a mixing of electronic states in which the unpaired electrons occupy different molecular orbitals. The additional shifts of g_x, g_y and g_z mainly result from a mixing of the states in which these orbitals are related to the orbitals of the unpaired electrons without spin orbit coupling through a rotation around the x, y or z axes, respectively. Because the magnitude of these shifts depends on orbital types and orbital energy differences, g_x, g_y and g_z are generally shifted by different amounts with respect to g_e.

The element iron contains four naturally occurring isotopes: ^{54}Fe (5.84%), ^{56}Fe (91.75%), ^{57}Fe (2.12%) and ^{58}Fe (0.03%). Only ^{57}Fe possesses a nonzero nuclear spin (I = ½). Due to the low abundance of ^{57}Fe in nature, no hyperfine coupling lines are observed for ferrocenium compounds (Fe^{III}, low-spin d^5).[205]

Usually substituted ferrocenium compounds show EPR signals at 77 K and not at room temperature because of the fast relaxation of the electron spin. Unsubstituted ferrocenium shows EPR signals at 20 K, with $g_{x,y} = 1.26$ and $g_z = 4.35$.[206] Due to the fast spin-lattice relaxation, the EPR resonances of ferrocenium compounds are in general very broad.[206] Frequently, ferrocenium compounds show an axial spectrum due to the ligand field splitting (Figure 3). An important contribution to the shift of g_z comes from d_{xy} which is related to the singly occupied orbital $d_{x^2-y^2}$ through a rotation around the z axis. The double occupation of d_{xy} causes an enhancement of the magnetic field. Thus the required external magnetic field is lowered, i.e. the g_z value is higher. In contrast, the contributions

from the d_{xz} and d_{yz} orbitals lead to a decrease of the magnetic field and hence to a decrease of the g_x and g_y values.

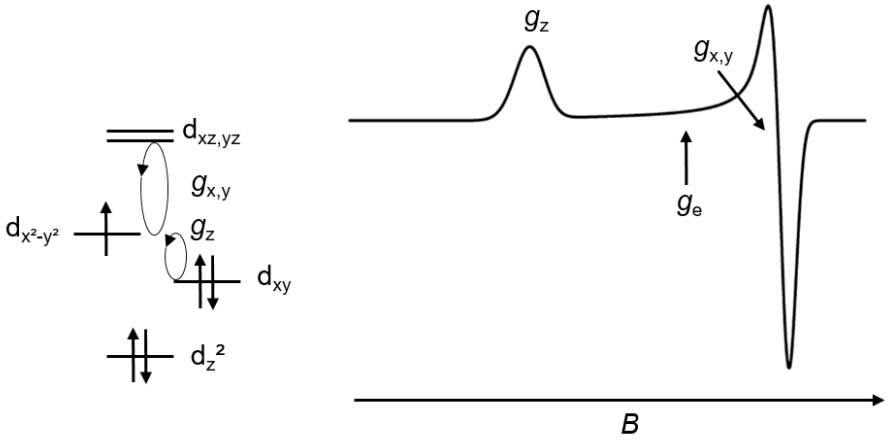

Figure 3. Left: Ligand field splitting of a ferrocenium (low-spin d^5) compound. Right: Simulated anisotropic axial spectrum of the corresponding ferrocenium compound.

In contrast to ferrocenium ions, paramagnetic molybdenum(V) complexes show hyperfine coupling in the EPR spectrum. Molybdenum contains two isotopes with a nuclear spin of I = 5/2: ^{95}Mo (15.87%) and ^{97}Mo (9.58%). The nuclear spin of the remaining isotopes ^{92}Mo (14.65%), ^{94}Mo (9.19%), ^{96}Mo (1.67%), ^{98}Mo (24.29%), and ^{100}Mo (9.74%) is I = 0. As an example, Figure 4 shows an isotropic spectrum of a Mo^V compound.[205]

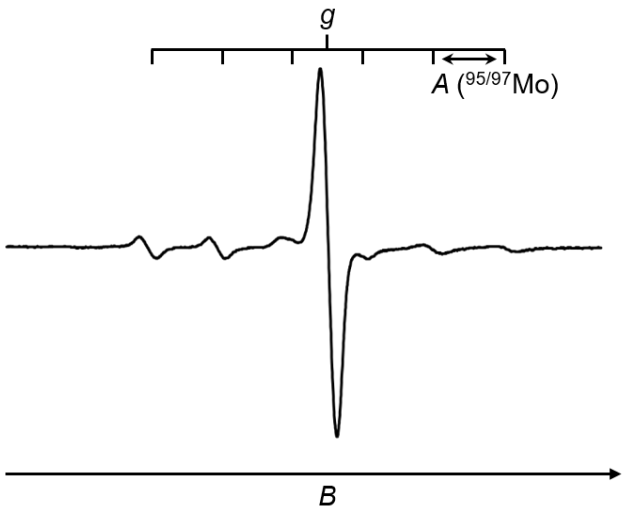

Figure 4. Measured isotropic EPR spectrum of a Mo^V (d^1) complex.

The g value of molybdenum(V) complexes is lower than g_e, because in d^1 compounds there are only unoccupied d orbitals which can involve in spin orbit coupling, always leading to an increase of the external magnetic field. The main signal in the center of the spectrum comes from the isotopes with $I = 0$, which contribute 75% of the overall intensity. The isotopes ^{95}Mo and ^{97}Mo cause the other six signals ($2nI+1 = 6$), which are weaker in intensity because of the smaller isotopic abundance in nature. The hyperfine coupling constant A ($^{95/97}$Mo) corresponds to the distance between the weaker signals (satellites). A is similar for both isotopes because of their similar magnetic moments ($\mu(^{95}\text{Mo}) = -0.9098\ \mu_N$, $\mu(^{97}\text{Mo}) = -0.9289\ \mu_N$).[207]

4 Results and discussion

The results of this thesis are reported and discussed in this chapter in the form of four original research articles, three of which are reprinted publications. Before presenting the full manuscripts, the following list gives an overview of the compiled articles and specifies the contributions made by the author of this thesis. Generally, X-ray crystallographic analyses were performed by Dr. C. Förster. Also, further analytical measurements (e.g. mass spectrometry and elemental analysis) were performed by the staff of the chemical institutes of the University of Mainz.

Solution conformation and self-assembly of ferrocenyl(thio)ureas

Reprinted with permission from

Kristina Hanauer, Minh Thu Pham, Christoph Förster and Katja Heinze, *Eur. J. Inorg. Chem.* **2017**, 433–445.

The first author performed and analyzed most of the experiments (except for a part of the syntheses and measurements that were performed by M. T. P. under the first author's guidance), carried out the DFT calculations, contributed a write-up of the material as first draft for the manuscript and compiled the supporting information.

Stereochemical consequences of oxygen atom transfer and electron transfer in imido/oxido molybdenum(IV, V, VI) complexes with two unsymmetric bidentate ligands

Reprinted with permission from

Kristina Hüttinger, Christoph Förster, Timo Bund, Dariush Hinderberger and Katja Heinze, *Inorg. Chem.* **2012**, *51*, 4180–4192.

The first author conducted all of the experimental work and analyses except for the 2D-EPR measurement (including analysis) and the analytical fit to the reaction kinetics data. Approximately half of the material has been generated and published within this author's

diploma thesis (Kristina Hüttinger, *Synthese, Struktur und Reaktivität von Dioxido- und Imido-Oxido-Molybdänkomplexen*, diploma thesis, Institute for Inorganic and Analytical Chemistry, University of Mainz, 2010).

Intramolecular electron transfer between molybdenum and iron mimicking bacterial sulphite dehydrogenase

Reproduced from

Kristina Hüttinger, Christoph Förster and Katja Heinze, *Chem. Commun.* **2014**, *50*, 4285–4288.

with permission from the Royal Society of Chemistry.

The first author conducted all of the experimental work and analyses except for the analytical fits to the UV-Vis spectra.

Coupled oxygen atom and electron transfer in dioxido molybdenum (VI) complexes bearing neutral and oxidized ferrocenyl substituents

Kristina Hanauer, Christoph Förster and Katja Heinze, *modified version to be submitted* **2017**.

The author of this thesis conducted all of the experimental work and analyses, carried out the DFT calculations and wrote the manuscript including the supporting information. A modified version of the manuscript will be submitted in due course.

4.1 Solution conformation and self-assembly of ferrocenyl(thio)ureas

Kristina Hanauer, Minh Thu Pham, Christoph Förster and Katja Heinze, *Eur. J. Inorg. Chem.* **2017**, 433–445.

DOI: 10.1002/ejic.201600918

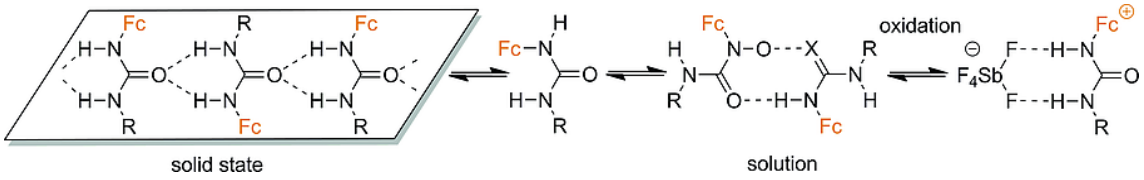

ChemPubSoc Europe

DOI: 10.1002/ejic.201600918

EurJIC European Journal of Inorganic Chemistry

Full Paper

CLUSTER ISSUE

Ferrocenyl(thio)ureas

Solution Conformation and Self-Assembly of Ferrocenyl(thio)ureas

Kristina Hanauer,[a] Minh Thu Pham,[a] Christoph Förster,*[a] and Katja Heinze*[a]

Abstract: Conformations and (dis)assembly processes of ureas and thioureas are of fundamental importance in supramolecular chemistry, anion binding, or crystal engineering, both in solution and in the solid state. For sensing and switching processes a redox-active unit, such as the ferrocene/ferrocenium couple, is especially suitable. Here, self-assembly processes of redox-active ferrocenyl(thio)ureas FcNHC(X)NHR [X = O, R = Fc (**1**), Ph (**2**), 1-naphthyl (**3**), Me (**4**), Et (**5**); X = S, R = Fc (**6**), 1-anthracenyl (**7**)] through hydrogen bonds – both in the solid state and in THF and CH_2Cl_2 solution – are reported. Special emphasis is placed on the impact of nonclassical intramolecular NH···Fe hydrogen bonds in these organometallic systems [these are absent in conventional organic (thio)ureas] on conformation and assembly. Furthermore, conformational switching and disassembly of **1**–**6** is induced by oxidation of **1**–**6** to the corresponding ferrocenium cations $\mathbf{1}^+$–$\mathbf{6}^+$ (redox switch).

Introduction

Directional hydrogen bonding of urea and thiourea and their derivatives in self-assembly processes or with other partners opens a broad range of applications in crystal engineering,[1] supramolecular chemistry,[2] and organocatalysis,[3–7] and also as anion receptors and sensors.[8–13] In solution, *trans-trans*, *cis-trans*, and *cis-cis* isomers of *N*,*N*′-disubstituted (thio)ureas equilibrate and direct the self-assembly process (Scheme 1).[14–19] In noncoordinating solvents, ureas prefer the *trans-trans* conformation, leading to supramolecular polymeric tape structures with bifurcated intermolecular hydrogen bonds (Scheme 1).[17,18] In contrast, thioureas show a significantly reduced aggregation tendency, forming dimers of *cis-trans* isomers (Scheme 1).[19] The hydrogen-bonding tendency of (thio)ureas is associated with the proton acceptor ability of the C=X group, which is lower for thioureas,[20] and with the acidity of the NH groups, which is higher for thioureas.[21] Because the acidity plays only a minor role in self-aggregation in solution, thioureas are less prone to such aggregation.[22] Similar trends are observed in the solid state, with ureas forming linear tape structures, whereas thioureas crystallize as hydrogen-bonded dimers or zigzag tapes (Scheme 1).[1,23]

Redox-active ferrocenyl (Fc) substituents are suitable building blocks for anion and cation receptors and sensors, both as electrochemical signaling units and as emission quenchers[24] of luminescent signaling units through energy or electron transfer.[25–28] The combination of ferrocene and urea (ferrocenylurea receptors) has been pioneered by Tucker,[29] Beer,[30,31] and Kaifer,[32,33] as well as by Tárraga and Molina.[34–37] Electronic

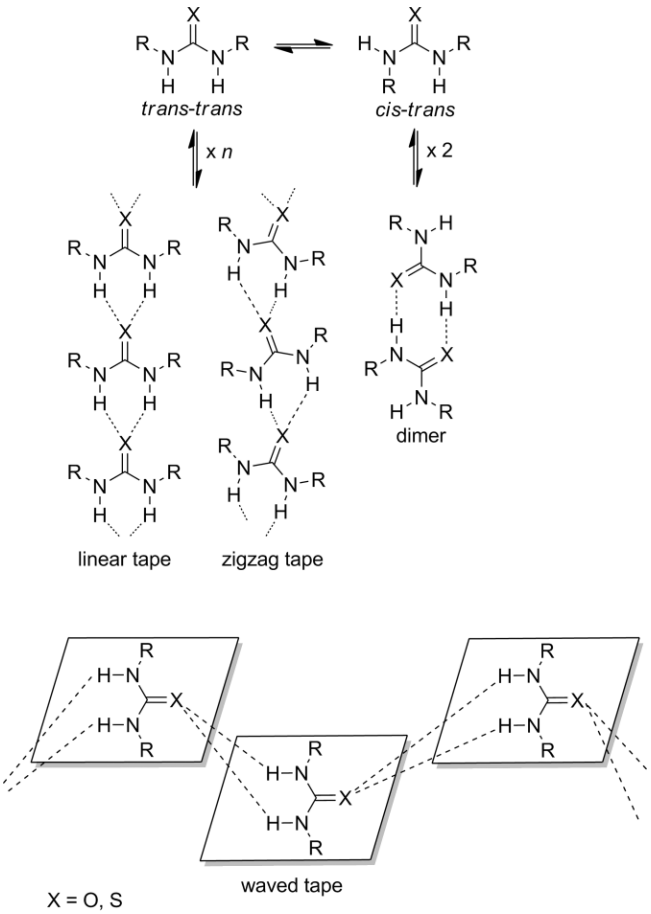

Scheme 1. Conformations and hydrogen bonding motifs of *N*,*N*′-disubstituted (thio)ureas.

[a] *Institute of Inorganic Chemistry and Analytical Chemistry, Johannes Gutenberg University Mainz*
Duesbergweg 10–14, 55128 Mainz, Germany
E-mail: cfoerster@uni-mainz.de
katja.keinze@uni-mainz.de
https://www.ak-heinze.chemie.uni-mainz.de/

Supporting information for this article is available on the WWW under http://dx.doi.org/10.1002/ejic.201600918.

communication between two ferrocenyl units through a ureylene bridge has been investigated by Kraatz, Heinze, and Zhong.[38–40] The hydrogen-bonded secondary structures of ferrocenylurea–peptide conjugates have been elucidated by Rapić and Heinze.[39,41,42]

The first examples of ferrocenylurea derivatives with the FcNHC(O)NHR binding motif [*N*,*N*′-diferrocenylurea (**1**)[43,44] and *N*-ferrocenyl-*N*′-phenylurea (**2**)[43]] were reported in the late 1950s by Schlögl and Silverstein. However, the solid-state structure of **1** has only recently been published.[40] Compounds of this type find applications as anion sensors and as host–guest receptors,[32,33,45–51] as labels for oligonucleotides,[52] and for potential pharmaceutical uses.[53,54] Electronic communication between two redox-equivalent ferrocenyl centers through hydrogen-bonded urea units in a hydrogen-bonded dimer has been investigated.[55] Similarly, photoinduced triplet–triplet energy transfer has been observed in a hydrogen-bonded 2-ureido-4(1*H*)-pyrimidinone-bridged ferrocene–fullerene conjugate.[56]

Despite the importance of the thiourea motif in organocatalysis,[57,58] examples of related ferrocenylthioureas FcNHC(S)NHR are rare. Although several ferrocenylureas have been reported, a detailed combined structural and conformational study on symmetric and unsymmetric *N*,*N*′-disubstituted ferrocenyl(thio)ureas in the solid state and, especially, in solution is lacking. Moreover, the ferrocenyl substituent provides the opportunity to investigate the impact of a positive charge on a (thio)urea on self-assembly processes in solution and in the solid state simply by oxidation of the Fc moiety to the ferrocenium cation. Such fundamental information is crucial for the rational design of ferrocenylurea-containing pharmaceuticals, sensors, catalysts, or stimuli-responsive materials. In this study, the conformation, assembly, and redox-induced switching of ferrocenylureas FcNHC(O)NHR [R = Fc (**1**), Ph (**2**), 1-naphthyl (Nap; **3**), Me (**4**), Et (**5**)] and ferrocenylthioureas FcNHC(S)NHR [R = Fc (**6**), 1-anthracenyl (Ant; **7**)] is reported.

Results and Discussion

Synthesis of Ferrocenylureas FcNHC(O)NHR [R = Fc (1), Ph (2), Nap (3), Me (4), Et (5)], Ferrocenylthioureas FcNHC(S)NHR [R = Fc (6), Ant (7)], and 1[SbF$_6$]$_2$

Ferrocenylureas **1**–**5** were synthesized according to Schlögl's general synthetic procedure,[43] starting from ferrocenecarboxylic acid, via ferrocenoyl azide and ferrocenyl isocyanate (Scheme 2a).[41] Nucleophilic addition of primary amines in toluene precipitates the ureas, and the products can be easily isolated from the reaction mixtures in moderate to good yields (36–90 %).

Thioureas **6** and **7** were synthesized in a one-pot fashion, from 1,1′-thiocarbonyldiimidazole and aminoferrocene (FcNH$_2$)[59,60] and from a mixture of FcNH$_2$ and 1-aminoanthracene, respectively, according to a procedure by Staab (Scheme 2b).[61] In the latter reaction, both **6** and **7** form concomitantly. Unfortunately, separation of these compounds by column chromatography or large-scale crystallization failed. However, a few single crystals of **7** could be obtained by recrystallization from a mixture of dichloromethane and ethyl acetate.

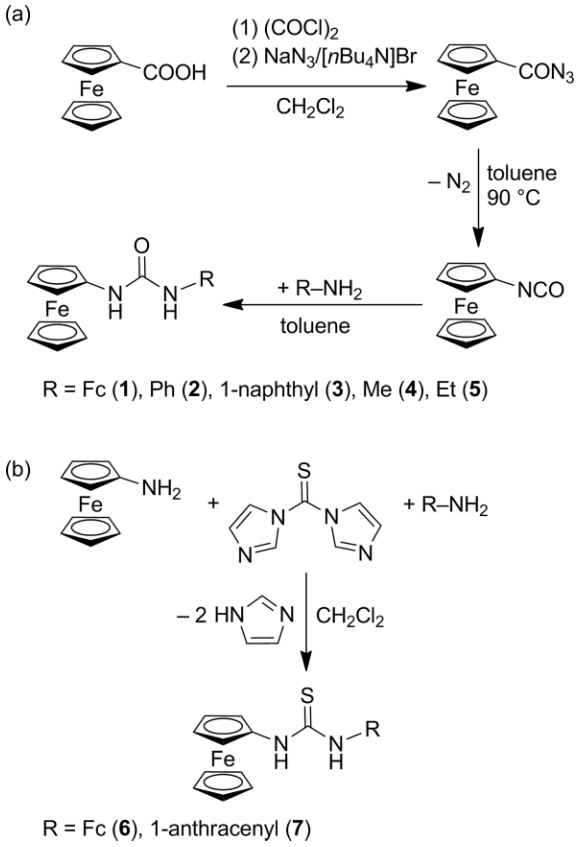

Scheme 2. Synthesis of (a) ureas **1**–**5**, and (b) thioureas **6** and **7**.

Crystals of the bis(ferrocenium) salt **1**[SbF$_6$]$_2$ formed during the attempt to oxidize **1** chemically to **1**$^+$ with 1 equiv. of silver hexafluoroantimonate (AgSbF$_6$). In the course of the crystallization of **1**[SbF$_6$], the mixed-valent cation **1**$^+$ disproportionates to **1** and **1**$^{2+}$, precipitating single crystals of **1**[SbF$_6$]$_2$.

Ferrocenyl(thio)ureas **1**–**6** were fully characterized by multinuclear and two-dimensional NMR, IR, and UV/Vis spectroscopy, mass spectrometry, cyclic voltammetry (CV), and elemental analysis. The aggregation motifs of **1**–**7** and of **1**[SbF$_6$]$_2$ in the solid state were determined by single-crystal X-ray diffraction (XRD) analyses.

Structures of 1–7 in the Solid State

Crystals of **1**–**7** suitable for XRD analyses were obtained by recrystallization from the solvents and solvent mixtures given in the Experimental Section. The structure of **1** has already been published,[40] but has been redetermined and is discussed in comparison with the structures of **2**–**7**. All ureas **1**–**5** form polymeric tapes with the monomers in the *trans-trans* conformation linked by bifurcated (NH)$_2$···O=C hydrogen bonds with *syn* or *anti* orientations of the Fc moieties and in some cases with a waving distortion (Scheme 1, Figure 1; Supporting Information).

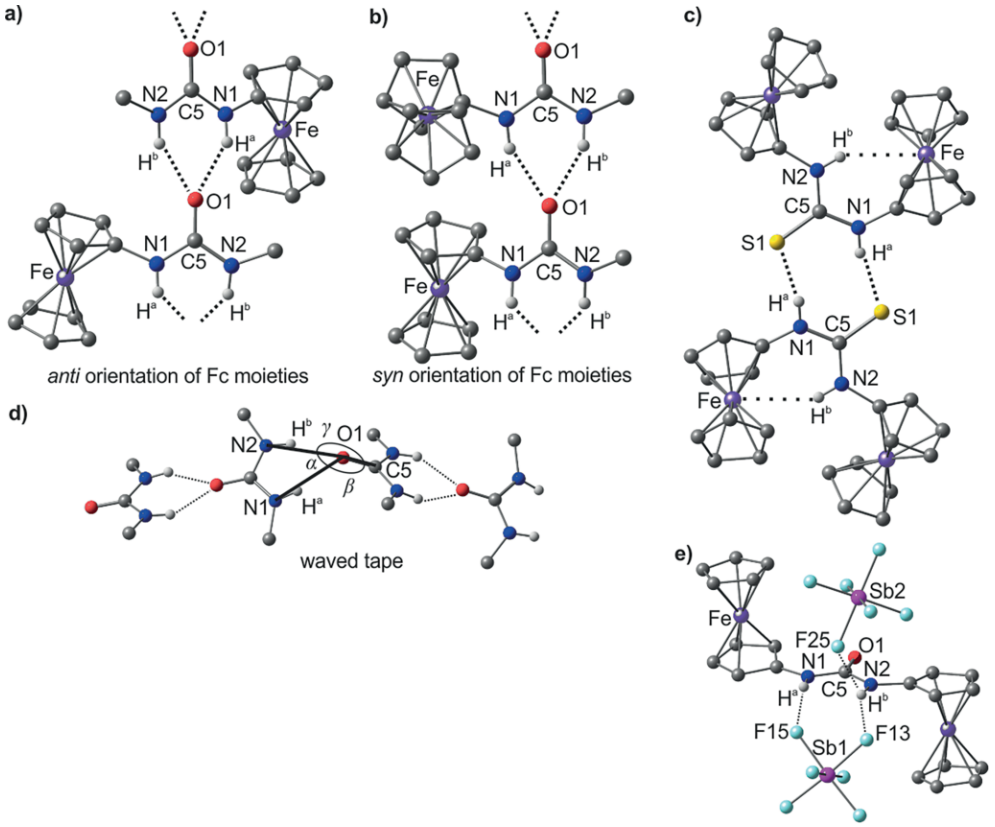

Figure 1. Hydrogen bonding motifs in crystals of **1**–**7** with relevant atom numbering: (a) *anti* orientation of the Fc moieties of **2**, **3**, and **4**, (b) *syn* orientation of the Fc moieties of **5**, (c) NH···S=C hydrogen bonding motif of ferrocenylthioureas **6** and **7**, shown for **6**, including NH···Fe hydrogen bonds, (d) waving distortion of hydrogen-bonded tapes described by angles α, β, and γ, and (e) hydrogen-bonded ion pair **1**$[SbF_6]_2$ in the solid state.

The metrics of the ferrocenyl substituents are as expected. All NH···O distances are similar to those of reported ferrocenylureas.[40,51,62]

In contrast, ferrocenylthioureas **6** and **7**·2CH_2Cl_2 crystallize as centrosymmetric dimers of *cis-trans* isomers in the triclinic space group $P\bar{1}$ (Figure 1c; Supporting Information). These are the first crystallographic reports of ferrocenylthioureas containing the motif FcNHC(S)NHR, according to a CSD search.[63] The NH···S distances within the hydrogen-bonded rings are similar to those in organic thioureas.[64–66] In addition to the intermolecular NH···S hydrogen bonds, the diferrocenyl derivative **6** forms an intramolecular nonclassical NH···Fe hydrogen bond (Figure 1c). The six-membered ring of the hydrogen-bonding motif is analogous to those in recently reported dimetallocenyl tosyl hydrazones (Mc)Mc′C=N–NHTs (Mc, Mc′ = Fc, ruthenocenyl; Ts = tosyl).[67,68] In the absence of other factors, this nonclassical NH···M hydrogen-bond-type appears to represent a favorable bonding situation in Mc–A–B–NH structural motifs with sufficiently acidic NH groups and electron-rich metal centers (Mc = Fc, ruthenocyl). In the aggregate $\mathbf{6}_2$ in the solid state, this NH···Fe hydrogen bond profits from cooperative NH···S hydrogen bonds (Figure 1c).

However, the nonclassical NH···Fe hydrogen bond is absent in the anthracenyl derivative **7**, although the anthracenyl substituent features π–π interactions to neighboring molecules of adjacent dimers, similar to those in the solid-state packing of the naphthyl derivative **3**, with a smallest distance of 3.6781(1) Å between centroids Cg(C6,C7,C8,C9,C10,C19) and Cg2(C10,C11,C12,C17,C18,C19) (Scheme 3). Possibly, this π-stacking of the organic substituent between dimers prevents the formation of the NH···Fe hydrogen bond within a *cis-trans* isomer of **7**. Again, the common solid-state dimer motif of thioureas is conserved, irrespective of the shape of the second substituent R (R = Fc, Ant).

A similar structural impact on formal O/S exchange has been observed for related ferrocenyl carboxamides and thioamides FcNHC(X)Me (X = O, S). The ferrocenyl carboxamide forms hydrogen-bonded tapes (N···O 2.73, 2.87 Å) with hydrogen bond lengths comparable to those in **1**–**5**, whereas the sulfur homologue crystallizes as centrosymmetric dimers of *cis*-thioamides (N···S 3.393 Å) analogously to **6** and **7** (Table 1).[60,69]

The diferrocenium salt **1**$[SbF_6]_2$ crystallizes in the monoclinic space group $P2_1/n$ with **1**$[SbF_6]_2$ as asymmetric unit. The presence of the SbF_6^- anions breaks the hydrogen-bonded tapes of **1** with bifurcated NH···O hydrogen bonds (Figure 1a), due to the formation of stronger charge-assisted NH···F hydrogen bonds of $\mathbf{1}^{2+}$ to the SbF_6^- anions (Figure 1e). One counter ion binds to both NH groups of the urea unit of $\mathbf{1}^{2+}$, whereas the second one is bound in a monodentate fashion (Figure 1e). Anion (e.g., PF_6^- or SO_4^{2-}) coordination to (thio)urea moieties is

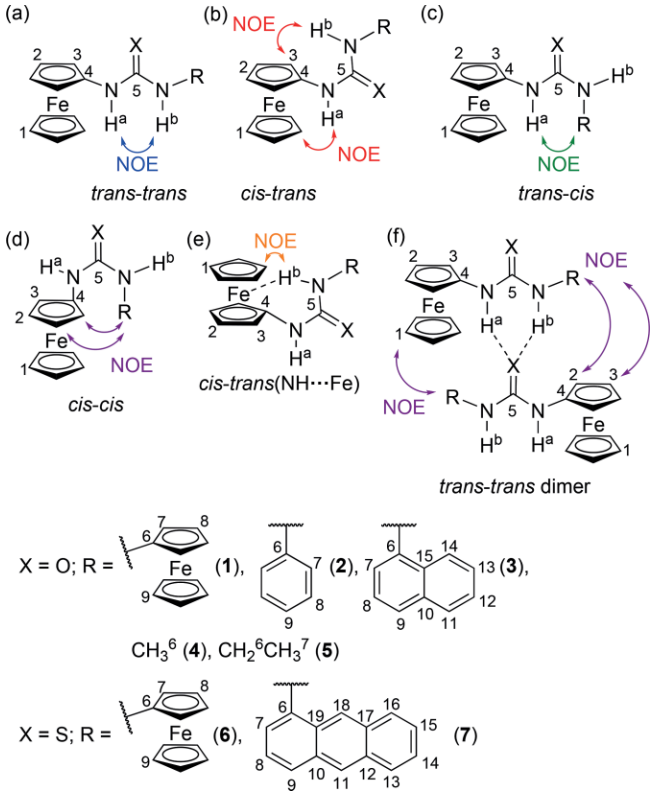

Scheme 3. Possible conformations of (thio)ureas **1**–**7** with characteristic NOE contacts (colour scheme) and relevant atom numbering for NMR and solid-state structure assignment.

Table 1. Selected ^{1}H and ^{13}C NMR spectroscopic data (δ [ppm]) for **1**–**7**.

	$NH^{a[a]/[b]}$	$NH^{b[a]/[b]}$	$C^{5[a]}$
1	6.83/6.11	6.83/6.11	153.2[c]
2	7.01/5.79	7.55/7.00	153.5
3	7.37/5.95	7.86/7.03	153.8
4	6.84/5.57	5.17/4.92	156.9
5	6.72/5.55	5.22/5.02	156.4
6	8.46/7.26 (*cis*)	8.46/7.99 (*trans*)	180.5[c]
7	8.26/–	9.18/–	–

[a] $[D_8]$THF. [b] CD_2Cl_2, c = 5.0 mM. [c] $[D_6]$DMSO.

well established in crystal engineering,[1] anion sensing,[8–13] and organocatalysis.[3–7] In solution, coordination of anions to positively charged [Fc^+–NH–R] units has also been observed before.[28,69] The conformation and assembly of neutral and charged ferrocenyl(thio)ureas in solution is addressed in the next sections.

NMR Spectroscopic Characterization and Studies on Hydrogen Bonding in Solution

For satisfactory signal/noise ratios in the ^{13}C NMR spectra, the low solubilities of **1**–**6** in $CDCl_3$ or CD_2Cl_2 required the preparation of NMR samples either in $[D_8]$THF (compounds **2**–**5**) or in $[D_6]$DMSO (compounds **1** and **6**). All ^{1}H and ^{13}C NMR resonances of **1**–**6** could be straightforwardly assigned (Experimental Section, Supporting Information). Because of problems in the separation of **7** from **6** and slow decomposition of **7** in solution, **7** was only characterized by ^{1}H NMR and $^{1}H,^{1}H$ NOE spectroscopy.

In the ureas **1**–**5**, the ^{1}H chemical shifts (δ) of the NH protons H^a and H^b show a dependency on the R substituent δ(R = Me, Et; **4**, **5**) < δ(R = Fc; **1**) < δ(R = Ph, Nap; **2**, **3**), due to inductive and ring-current effects. As would be expected, the NH^b resonance is more strongly affected than the NH^a resonance (Table 1, Scheme 3; Experimental Section). A larger paramagnetic shielding term[70] of the C=S group of thioureas **6** and **7** shifts the NH proton resonances to lower field than in the case of the urea congeners. Similar observations pertain to the ^{13}C NMR chemical shift of the thiocarbonyl carbon atom C^5 (δ = 180.5 ppm) of **6**, relative to the chemical shift of the carbonyl carbon atom C^5 of **1** (δ = 153.2 ppm; $\Delta\delta$ = 27.3 ppm).

The symmetric diferrocenylurea (**1**) displays only a single sharp NH proton resonance in $[D_8]$THF, suggesting symmetric *trans-trans*, *cis-cis* isomers or rapid equilibration between isomers (Scheme 3a; Supporting Information). For dissymmetric ureas **2**–**5**, strong NOE contacts of NH^a and NH^b appear in $^{1}H,^{1}H$ NOESY experiments (mixing time 1.0 s), confirming the preference of *trans-trans* conformers in $[D_8]$THF. According to weak NOE cross peaks between NH^b and H^3 of **2**, **4**, and **5** (Scheme 3b), *cis-trans* isomers are only present to a minor extent. Furthermore, weak NOE contacts between NH^a and the protons of the alkyl substituents R of **4** and **5** are observed, indicative of some *trans-cis* isomer (Scheme 3c).

Similarly to **1**, and in contrast with its own solid-state conformation, thiourea **6** exhibits only a single NH proton resonance in $[D_8]$THF, indicative of a *trans-trans* conformation, a *cis-cis* conformation, or fast rotation of the FcNH moiety around the HN–CS bond on the ^{1}H NMR timescale. No further cross peaks indicative of a *cis-cis* conformer could be identified (Scheme 3d), excluding this conformation. Anthracenyl-substituted thiourea **7** features a cross peak between the Cp proton H^3 and NH^b (Scheme 3b, e; Supporting Information). This perfectly fits with *cis-trans* conformations as found in the solid-state structure of **7**. In this conformer, nonclassical NH···Fe hydrogen bonds are conceivable, but their existence is not supported by the expected H^1/NH^b cross peak (Scheme 3e).

In essence, ureas **1**–**5** and thioureas **6** and **7** appear to be monomeric in THF solution, as might be expected from the good hydrogen-atom-accepting capabilities of THF, which solvates all NH groups. Hence, no intermolecular NH···O=C, NH···S=C, or intramolecular NH···Fe hydrogen bonds are required.

In contrast, the noncoordinating solvent CD_2Cl_2 should favor self-assembly processes of (thio)ureas. This was investigated as well, although the study is confined by the poor solubility of **1**, **2**, and **3** in CD_2Cl_2 and by the unsuccessful separation of **7** from **6**. In dilute CD_2Cl_2 solution, the proton resonances of the NH groups are found at higher field (Table 1; Supporting Information). Furthermore, the NH proton resonances are significantly broadened (Supporting Information).

$^{1}H,^{1}H$ NOESY experiments (mixing time 1.0 s) were performed in CD_2Cl_2 with **2**–**5** at concentrations at which self-as-

sembly is almost negligible, according to IR spectroscopy (see below). Because of their low solubility and the resulting poor signal/noise ratios, the data for *N*-aryl-*N*′-ferrocenylureas **2** and **3** are difficult to interpret (Supporting Information). However, contacts between NH^a and NH^b and between NH^b and H^3 reveal the presence of *trans-trans* and *cis-trans* isomers, respectively (Scheme 3a, b; Supporting Information). The *N*-ferrocenyl-*N*′-methylurea (**4**) exists exclusively in a *cis-trans* conformation with an intramolecular NH···Fe hydrogen bond, as can be concluded from a strong NOE cross peak between NH^b and H^3 and a weak NOE cross peak between NH^b and H^1 (Supporting Information; Scheme 3b, e). The same situation applies to **5**, with an additional contact between NH^a and NH^b indicating the presence of some *trans-trans* isomer (Scheme 3a). The $^1H,^1H$ NOESY spectrum of **5** at c = 50.0 mM features even more cross peaks, suggesting intermolecular contacts (Supporting Information). Significant self-assembly at this concentration is observable by IR spectroscopy as well (see below). Additional contacts are observed between NH^a and the methylene protons H^6 either for the *trans-cis* isomer or due to the formation of dimers/oligomers from *trans-trans* isomers (Scheme 3c, f). Similarly, contacts between the ferrocenyl protons H^1, H^2, and H^3 and the methyl protons H^7 and between H^3 and the methylene protons H^6 indicate either the presence of *cis-cis* isomers or (more likely) the aggregation of *trans-trans* monomers (Scheme 3d, f). According to DFT calculations (see below), the dimerization/oligomerization of *trans-trans* isomers leading to these NOE contacts is indeed probable.

Interestingly, two sets of NH resonances are observed for ferrocenylthiourea **6** in CD_2Cl_2, whereas only one was found in [D_8]THF (vide supra). This indicates a slow isomerization of dissymmetric thiourea conformers (either *cis-trans* or *trans-cis* isomers) on the ^1H NMR timescale. The resonance at lower field is assigned to NH^b in *trans* conformation, involved in an intramolecular NH···Fe hydrogen bond, as also seen in the solid-state assembly of **6**. This is further confirmed by low-temperature $^1H,^1H$ NOESY/EXSY NMR experiments (see below; Supporting Information).

Variable-temperature ^1H NMR (VT NMR) experiments over a temperature range of –25 to 25 °C in CD_2Cl_2 were performed to obtain a deeper insight into the isomerization dynamics of **1**–**6** in solution (Supporting Information). Coalescence of the $NH^{a/b}$ resonances of **1** is estimated at T_c = (258 ± 5) K (Supporting Information). The Eyring equation gives a Gibbs free energy of activation $\Delta G^{\ddagger}_{258}$ = (49 ± 1) kJ mol^{-1} for the rotation around the HN–CO bond (Supporting Information).

A distinct splitting of ferrocenyl and NH protons of diferrocenylthiourea **6** into two sets of sharp signals with $\delta(NH^a)$ = 7.26 ppm and $\delta(NH^b)$ = 7.99 ppm, consistent with the *cis-trans* isomer (Scheme 3). Coalescence of $H^{1/9}$ occurs at T_c = (283 ± 5) K (Figure 2; Supporting Information). The calculated Gibbs free energy of activation for the rotation around the HN–CS bond amounts to $\Delta G^{\ddagger}_{283}$ = (58 ± 1) kJ mol^{-1}. A $^1H,^1H$ NOESY/EXSY NMR experiment with **6** at 248 K clearly supports the dynamic exchange of orientations of the FcNH moieties (Supporting Information). The values for the Gibbs free energies of activation obtained from DFT calculations excellently fit with the experimentally determined ones ($\Delta G^{\ddagger}_{258}$ = 45 kJ mol^{-1} for **1** and $\Delta G^{\ddagger}_{283}$ = 59 kJ mol^{-1} for **6**; Supporting Information).

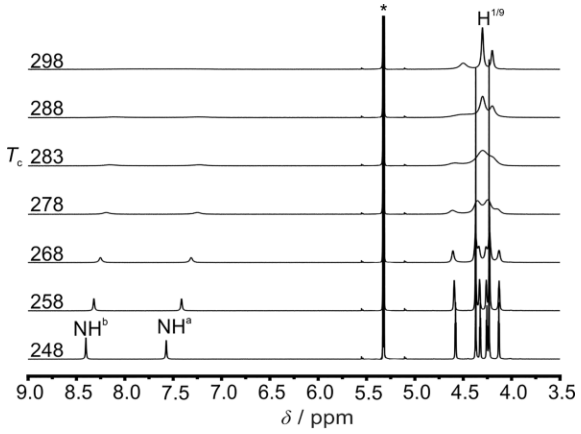

Figure 2. VT ^1H NMR spectra of **6** in CD_2Cl_2 (c = 5.0 mM, 400 MHz) with coalescence of $H^{1/9}$ at T_c = (283 ± 5) K; * denotes the signal of $CHDCl_2$.

The $NH^{a,b}$ proton resonances of **2**–**5** only broaden and shift to lower field with decreasing temperature (Supporting Information). No splitting of ^1H NMR resonances is observed over the temperature range from –25 to 25 °C. Interestingly, the proton signals of NH^a for **3**–**5** strongly depend on the variation of the temperature, indicating intermolecular NH^a···OC hydrogen bonds between *cis-trans* isomers. Upon cooling, all ferrocenylureas precipitate from solution, this being especially pronounced for **2**. This might explain the minor temperature dependence of the chemical shifts of NH^a and NH^b of **2**.

The higher solubility of ferrocenyl(thio)ureas **4**, **5**, and **6** enables variable-concentration NMR (VC NMR) spectroscopic investigations of the self-assembly in CD_2Cl_2 over the concentration ranges of 2.5–100.0 mM, 1.3–50.0 mM, and 2.5–18.0 mM, respectively. The appearance of doubled sets of signals for monomer–dimer/oligomer equilibria is not expected, due to fast equilibration on the ^1H NMR timescale. Hence, averaged NH proton resonances are observed in all cases.[41,71] With increasing concentration, the NH^a proton resonances of **4** and **5** are shifted significantly to lower field, indicating involvement in intermolecular NH^a···OC hydrogen bonding and increases in the dimer/oligomer/monomer ratios, whereas the chemical shifts of the NH^b signals are only slightly shifted to lower field in a linear fashion (Supporting Information).

These data support dimerization of **4** and **5** in predominantly *cis-trans* conformation through NH^a···O hydrogen bonds (Figure 1c), which has been also proposed for an *N*,*N*′-diarylurea in CCl_4.[17] Furthermore, the formation of dimers of **4** and **5** fits with the low reported relative molecular masses (average molecular mass of aggregates/molecular mass of monomer) of aggregates of *N*,*N*′-dialkylurea monomers in $CHCl_3$.[18] In this monomer/dimer model, the proton chemical shift (δ) of the NH^a signal is the fraction-weighted average of the chemical shifts for the dimer (δ_D) and for the monomer (δ_M). The relative proportions of the monomer and of the dimer are given by the association constant (K), describing the monomer/dimer equi-

librium. This can be transformed into the chemical shift (δ) of the NH[a] protons as a function of concentration (c) of **4** and **5** (Supporting Information) with K, δ_D, and δ_M as fit parameters. The dimerization constants for **4** [K = (4.9 ± 0.8) M^{-1}, δ_M = (5.46 ± 0.01) ppm, δ_D = (8.18 ± 0.27) ppm, R^2 = 0.9991] and **5** [K = (4.1 ± 0.3) M^{-1}, δ_M = (5.42 ± 0.01) ppm, δ_D = (8.45 ± 0.12) ppm, R^2 = 0.9996] are identical within uncertainty. Furthermore, the dimerization constants (K) are similar to those of *N*,*N*′-dialkylureas, as determined IR spectroscopically in chloroform from a two-equilibrium-constant approach (dimerization/oligomerization).[16,18] The dependence of the chemical shift (δ) of the NH[b] signal on the concentration is small and shows a linear behavior with an extrapolated axis intercept (δ_0) that corresponds to the chemical shift at infinite dilution (δ_0 = 4.90 ppm for **4**, 5.01 ppm for **5**).

The chemical shifts of the NH signals of **6** are essentially independent of the concentration (Figure 3). For concentrations up to 18.0 mM, negligible dimerization/oligomerization is observed. This finding clearly supports the conjecture of the lower self-assembly tendency of thioureas.[19,22]

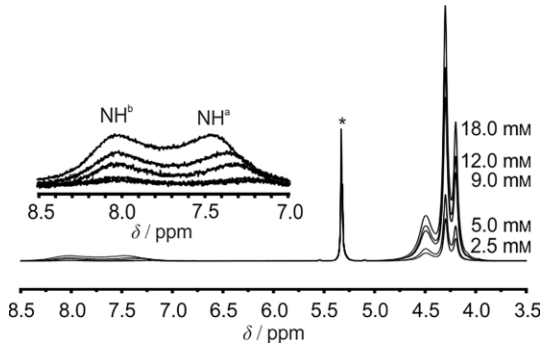

Figure 3. VC ^{1}H NMR spectra of **6** in CD_2Cl_2; * denotes the signal of $CHDCl_2$. The inset shows the region of the NH resonances.

IR Spectroscopic Monitoring of the Self-Assembly

The IR spectra of solid **1**–**5** (as KBr discs) clearly show the association of the NH and CO groups through hydrogen bonds with low-energy NH stretching vibrations at $\tilde{\nu}$(NH) = 3292–3339 cm^{-1} and CO vibrations at $\tilde{\nu}$(CO) = 1634–1651 cm^{-1}, respectively (Table 2; Supporting Information). The NH bands for the *N*-alkyl-*N*′-ferrocenylureas **4** and **5** appear at an energy similar to that for $FcNHC(O)NH(CH_2)_5CH_3$[51] [$\tilde{\nu}$(NH) = 3327 cm^{-1}], but at slightly higher wavenumbers than their ferrocenyl and aryl counterparts **1**, **2**, and **3** and at lower wavenumbers than those of *N*,*N*′-dialkylureas.[72] No simple correlation between NH···O=C distances in the solid state and the energy of the NH and CO stretching vibrations could be identified (Table 2; Supporting Information). Hence, the R substituents also exert an electronic influence. Diferrocenylthiourea (**6**) forms a dimer based on *cis-trans* conformers in the solid state. According to DFT calculations, the IR absorption bands at $\tilde{\nu}$ = 3269 and 3171 cm^{-1} are attributable to the NH stretches of the NH group in the intramolecular NH···Fe hydrogen bond and of the NH group in the intermolecular NH···S=C hydrogen bond, respectively (Figure 1c; see below). The weak C=S stretching band, typically appearing at $\tilde{\nu} \approx$ 700 cm^{-1}, could not be unambiguously assigned, due to severe overlap of skeletal vibrations.[73,74]

Table 2. Selected IR data ($\tilde{\nu}$ [cm^{-1}]) for (thio)ureas **1**–**6**.

	$\tilde{\nu}$(NH)[a]/[b]	$\tilde{\nu}$(CO)[a]/[b]
1	3292/3423, 3341	1636/1686
2	3306/3424 (sh), 3416, 3341	1645/1686
3	3292/3422, 3335	1634/1686
4	3339/3447, 3433, 3390 (sh)	1651/1682
5	3321/3433, 3381	1634/1676
6	3269, 3171/3404, 3385 (sh), 3372 (sh), 3275	–

[a] KBr. [b] CH_2Cl_2, c = 3.0–5.0 mM.

IR spectra of (thio)ureas **1**–**6** in dichloromethane as a noncoordinating solvent are depicted in the Supporting Information. Because of the low solubility of ureas **1**, **2**, and **3**, all IR spectra were recorded at a low concentration of c = 3.0–5.0 mM. Generally, bands for the stretching vibration of free NH groups of *N*,*N*′-dialkyl- or *N*,*N*′-diarylureas appear at $\tilde{\nu}(NH_{free}) \approx$ 3400–3470 cm^{-1} in CCl_4,[14,17,18,75] whereas the NH bands of diarylureas are observed at slightly lower energy. The IR spectra of **1**–**5** feature several overlapping bands corresponding to NH stretching vibrations for non-associated NH groups in the region of $\tilde{\nu}$ = 3422–3447 cm^{-1}, which is consistent with the ^{1}H NMR spectroscopic observation of equilibrating isomers. As expected, the NH stretching vibration absorption bands of arylureas **1**–**3** appear at lower energy. In particular, the IR spectra of **1**, **2**, and **5** each show a broad, weak, but distinct band at lower wavenumbers ($\tilde{\nu}$ = 3335–3390 cm^{-1}; Supporting Information). These bands are each assigned to the NH stretching vibration of an NH group involved in an NH···Fe hydrogen bond in a *cis-trans* isomer (Scheme 3e). This interpretation is further supported by VC IR experiments on ferrocenyl(thio)ureas **4**, **5**, and **6**, which exhibit sufficient solubility. The relative intensities of the NH bands in the region $\tilde{\nu}$ = 3320–3450 cm^{-1} are concentration-independent, clearly supporting the intramolecular nature of the NH hydrogen bonds (namely NH···Fe hydrogen bonds). The intensities of the NH···Fe absorption bands increase in the orders **3** < **2** < **1** and **4** < **5**, respectively, suggesting increasing fractions of conformers with intramolecular NH···Fe hydrogen bonds in these series (Supporting Information). In solution, the band of the carbonyl stretching vibration for each of the ferrocenylureas **1**–**5** is found at high wavenumbers, corresponding to non-associated carbonyl groups (Table 2). This confirms the absence of dimers and oligomers under these conditions. The bands for free NH groups of diferrocenylthiourea (**6**) are observed at $\tilde{\nu}$ = 3404–3372 cm^{-1}, again showing the equilibration of isomers. The quite intense band at $\tilde{\nu}$ = 3275 cm^{-1} is assigned to a strong NH···Fe hydrogen bond in a *cis-trans* conformer of **6**.

When the concentrations of **4** and **5** are increased above 10 mM, two new bands appear in the $\tilde{\nu}$ = 3150–3350 cm^{-1} region, partially overlapping with the NH···Fe band ($\tilde{\nu}$ = 3390 and 3381 cm^{-1}, respectively). These bands are attributable to NH groups involved in self-assembled intermolecular hydrogen bonds (Figure 4; Supporting Information). For diferrocenylthiourea (**6**) no new low-energy bands for NH stretching vibrations

appear upon increasing the concentration up to 16 mM (limited by the low solubility) (Supporting Information). This finding again confirms the lower self-aggregation tendency of diferrocenylthiourea (**6**).

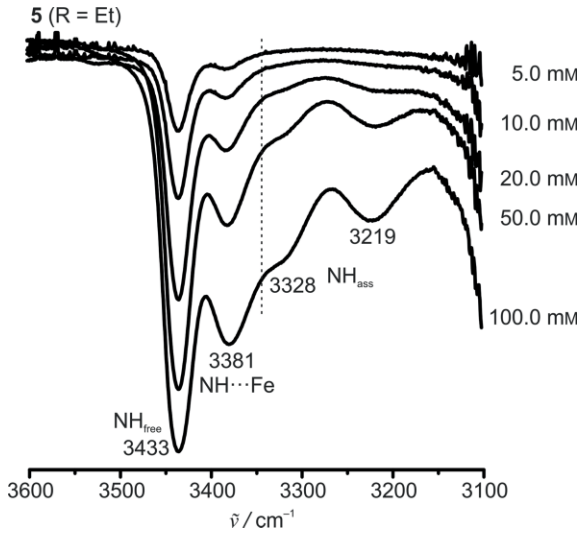

Figure 4. VC IR spectra of **5** in CH_2Cl_2 (NH region, c = 5.0–100.0 mM).

DFT Calculations on 1–7

In [D_8]THF, ureas **1**–**5** prefer the *trans-trans* conformation, whereas thiourea **7** favors the *cis-trans* conformation. However, DFT calculations at the B3LYP/LANLDZ (with polarization functions) level with empirical dispersion correction and use of a polarizable continuum model (PCM THF) to include the influence of the solvent (Experimental Section) did not accurately describe the preference for the *trans-trans* isomers of **1**–**5** in THF solutions. In fact, the explicit coordination of tetrahydrofuran to NH moieties has to be included (Figure 5). According to calculations on **1**, the *trans-trans* conformer with a single coordinated THF molecule in a bifurcated $(NH)_2$···O(THF) hydrogen bond together with one noncoordinated THF (*trans-trans*-**1**·THF+THF) is significantly preferred. Furthermore, coordination of a single THF molecule is entropically preferred over the coordination of two THF molecules, as exemplified by calculations on *cis-trans*-**1**·THF+THF and *cis-trans*-**1**·2THF (Figure 5). The intramolecular NH···Fe hydrogen bond seems to have only a marginal stabilizing effect on the *cis-trans* isomer [*cis-trans*-**1**(NH···Fe)·THF+THF] (Figure 5), reflecting the lower NH acidity of ureas.[21]

In CH_2Cl_2 (PCM), the DFT-calculated, dispersion-corrected Gibbs free energies of relevant isomers of **1**–**7** indicate a slight preference for the *cis-trans* conformation with NH···Fe hydrogen bond [*cis-trans*(NH···Fe)]. For **3**, the *trans-cis* isomer is essentially isoenergetic with the *cis-trans*(NH···Fe) isomer (Table 3; Supporting Information). Notably, with the exception of the high-energy *cis-cis* isomers, all calculated energy differences between the isomers of **1**–**5** fall within a narrow range of 11 kJ mol^{-1}.

Hence, the simultaneous presence of the *cis-trans*, *trans-trans*, and *trans-cis* isomers in CH_2Cl_2 is probable. These results

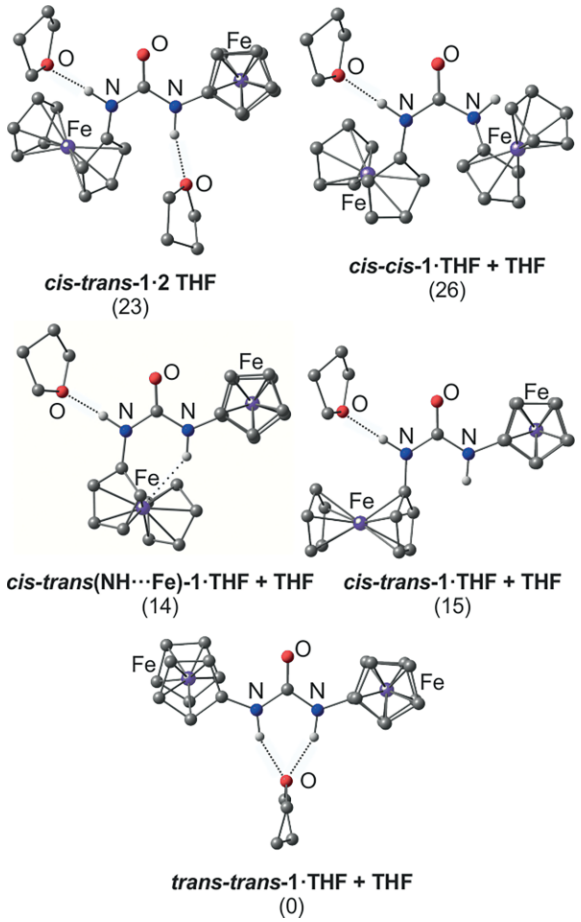

Figure 5. DFT-calculated (B3LYP/LANL2DZ with polarization functions, PCM THF, dispersion correction) geometries and relative Gibbs free energies (ΔG [kJ mol^{-1}]) of tetrahydrofuran adducts of different isomers of **1**.

Table 3. DFT[a]-calculated relative Gibbs free energies (ΔG [kJ mol^{-1}]) of relevant isomers of ferrocenyl(thio)ureas **1**–**7**.

	cis-trans(NH···Fe)	*cis-trans*	*trans-trans*	*trans-cis*	*cis-cis*
1					
monomer	0	4	2	–	17
dimer	10 (–12)[b]	0 (–22)	23 (+1)		
2					
monomer	0	5	8	7	17
3					
monomer	1	6	11	0	13
4					
monomer	0	4	6	10	19
5					
monomer	0	3	6	7	20
dimer	0 (–12)	0 (–12)	18 (+6)	19 (+7)	34 (+22)
6					
monomer	0	9	21	–	13
dimer	0 (–1)	9 (+8)	37 (+36)		
7					
monomer	0	4	21	6	6

[a] B3LYP/LANLDZ with polarization functions, PCM CH_2Cl_2, dispersion correction. [b] Gibbs free energy (ΔG [kJ mol^{-1}]) of dimerization, relative to the monomer of lowest energy.

fully support the NMR spectroscopic findings. The calculated Gibbs free energies for the ferrocenylthioureas **6** and **7** suggest a clear preference for the *cis-trans*(NH···Fe) isomer with NH···Fe hydrogen bond. The relative energies of the *trans-trans* isomers of **6** and **7** are quite high.

The calculated trends for the Gibbs free energies of dimerization, exemplified for **1**, **5**, and **6**, parallel the VC NMR spectroscopic results. Ureas **1** and **5** dimerize to rings $\mathbf{1}_2$ and $\mathbf{5}_2$ with negative driving force (Figure 1c, Table 3; Supporting Information). In both cases the formation of NH···Fe hydrogen bonds is unfavorable or thermoneutral, which is likely an effect of the weak acidity of ureas.[21] On the other hand, the higher acidity of thiourea **6** favors the *cis-trans*(NH···Fe) conformer both in the monomer **6** and in the dimer $\mathbf{6}_2$. However, the dimerization of **6** is essentially thermoneutral. This result nicely corroborates the lower tendency of **6** to self-assemble as concluded from the VC ^{1}H NMR and VC IR spectroscopic studies.

Electrochemistry

The ferrocenyl moieties in **1**–**6** are reversibly oxidized to give the ferrocenium cations $\mathbf{1}^+$–$\mathbf{6}^+$ (Experimental Section, Supporting Information). The half-wave potentials for the first oxidation of ferrocenylureas **1**–**5** show a dependency on the electron-withdrawing character of the R substituent $E_{1/2}$(R = Me, Et; **4**, **5**) < $E_{1/2}$(R = Fc; **1**) < $E_{1/2}$(R = Ph, Nap; **2**, **3**) (Table 4). The C=S group of thiourea **6** is more strongly electron-withdrawing than the C=O group in urea homologue **1**, leading to higher half-wave potentials for the first and the second oxidation of the ferrocenyl moieties. An analogous trend was observed for Fc-NHC(O)R and Fc-NHC(S)R pairs.[69] For the sulfur derivative **6**, a third irreversible oxidation wave was found at E_p = 800 mV (vs. FcH/FcH^+); this is assigned to a sulfur-centered oxidation.[69]

Table 4. Electrochemical data {$E_{1/2}$ and E_p (irrev.)[a] [mV]} for ferrocenyl(thio)ureas **1**–**6**.

1	2	3	4	5	6
–120 70	–90	–110	–140	–140	–30 180 (irrev.) 800

[a] Versus FcH/FcH^+, CH_2Cl_2, $[nBu_4N][B(C_6F_5)_4]$.

EPR Spectroscopy of Ferrocenium Cations

Chemical oxidation of **1**, **2**, **4**, and **5** with 1 equiv. of silver hexafluoroantimonate ($AgSbF_6$) in CH_2Cl_2 gives the corresponding ferrocenium cations $\mathbf{1}^+$, $\mathbf{2}^+$, $\mathbf{4}^+$, and $\mathbf{5}^+$. Their hexafluoroantimonate salts **1**[SbF_6], **2**[SbF_6], **4**[SbF_6], and **5**[SbF_6] are even less soluble in CH_2Cl_2 than their parent neutral ferrocene derivatives. EPR spectra of **1**[SbF_6], **2**[SbF_6], **4**[SbF_6], and **5**[SbF_6] at 77 K give broad axial resonances ($g_{x,y} \approx 1.880$, $g_z \approx 3.155$; Supporting Information), confirming the iron-centered oxidation The line broadening is likely based on the formation of microcrystallites upon freezing to 77 K, giving non-averaged orientations.[76]

UV/Vis Spectroscopy

The UV/Vis/NIR spectra of **1**–**6** in CH_2Cl_2 each show the characteristic ferrocene absorption at λ_{max} = 437–440 nm (Experimental Section, Supporting Information). The characteristic ferrocenium band is observed for the monocations $\mathbf{1}^+$–$\mathbf{6}^+$ at λ_{max} = 807–819 nm (Supporting Information). Additionally, weak intervalence charge-transfer bands at λ_{max} = 970 nm and λ_{max} = 1175 nm could be identified after Gaussian band-shape analysis of the UV/Vis/NIR spectra of redox-symmetric mixed-valent cations $\mathbf{1}^+$ and $\mathbf{6}^+$, respectively (Supporting Information). The optical electron transfer of the thio homologue $\mathbf{6}^+$ (E_{op} = 8511 cm^{-1}) requires less energy than that of $\mathbf{1}^+$ (E_{op} = 10300 cm^{-1}), Which is similar to the observations for ferrocenyl(thio)amides.[69] The electronic coupling of the iron redox centers in $\mathbf{1}^+$ and $\mathbf{6}^+$ amounts to H_{AB} = 120 and 110 cm^{-1} (±10 cm^{-1}), respectively, as calculated by the Hush formula with parameters from the Gaussian band-shape analysis and an estimated Fe···Fe distance of 7.5 Å from DFT calculations.[77] According to Robin and Day, these moderate values of H_{AB} assign $\mathbf{1}^+$ and $\mathbf{6}^+$ to class II mixed-valent species.[78]

The influence of the positive charge of $\mathbf{1}^+$–$\mathbf{6}^+$ and the counter anion SbF_6^- on self-assembly was investigated by IR spectroscopy, conductivity measurements, and DFT calculations. The introduction of a positive charge should acidify the NH^a group adjacent to Fc^+, increasing the hydrogen bond strengths with this moiety. However, Coulomb attractions between cations and anions should become important as well.

IR Spectroscopic Characterization and Studies on Hydrogen Bonding in 1[SbF_6]–6[SbF_6] in Solution

IR spectra of **1**[SbF_6]–**6**[SbF_6] in CH_2Cl_2 at $c \approx 5.0$ mM show several, partially overlapping bands for the NH stretching vibrations (Supporting Information). The intense bands at $\tilde{\nu}$ = 3399–3437 cm^{-1} are assigned to non-associated NH groups. These bands are slightly shifted to lower wavenumbers than in neutral ferrocenylureas **1**–**5**. A second, less intense band is found in the $\tilde{\nu}$ = 3362–3377 cm^{-1} region in each case; these correspond to associated NH groups. Intramolecular NH···Fe hydrogen bonds and formation of dimers of $\mathbf{1}^+$–$\mathbf{5}^+$ can be neglected for the oxidized monoferrocenylureas, due to the accumulation of a positive charge at the iron atom upon oxidation.[67] Rather, the coordination of hexafluoroantimonate counterions, resulting in strong charge-assisted NH···F hydrogen bonds, is probable. Similar coordination of counterions has been proposed for the (acetylamino)ferrocenium cation $[FcNHC(O)Me]^+$. Oxidation of FcNHC(O)Me to $[FcNHC(O)Me]^+$ shifts the NH stretching vibration from $\tilde{\nu}$ = 3435 cm^{-1} to $\tilde{\nu}$ = 3360 cm^{-1} in CH_2Cl_2 solution, suggesting the coordination of the counter ion X^- at NH.[60,79] For the unsymmetric ferrocenium ureas $\mathbf{2}^+$–$\mathbf{5}^+$, a third, less intense band for associated NH groups is observed at $\tilde{\nu}$ = 3250–3267 cm^{-1} in each case (Supporting Information), suggesting that both NH groups can engage in intermolecular hydrogen bonds (to counter ions).

The solubility of **5**[SbF_6] is fairly high; therefore, VC IR experiments were performed. With increasing concentration, the band at $\tilde{\nu}$ = 3372 cm^{-1} grows relative to the band at $\tilde{\nu}$ =

3426 cm^{-1} demonstrating progressive association (Figure 6). This finding supports aggregation in contact ion pairs or even as ion clusters. The association of **5**[SbF_6] as contact ion pairs or as clusters of ions at higher concentration is further supported by conductivity measurements.

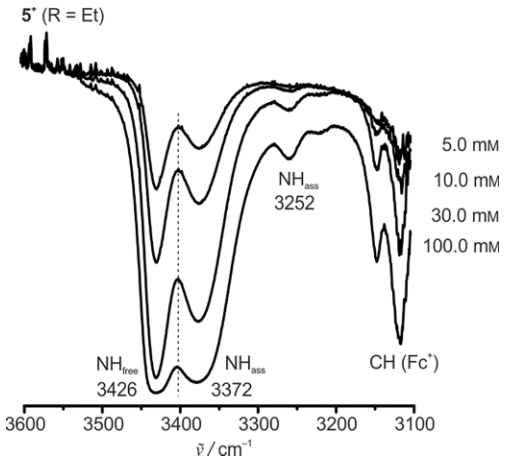

Figure 6. VC IR spectra of **5**[SbF_6] in CH_2Cl_2 (NH region, c = 5.0–100.0 mM).

Conductivity Measurements on 5[SbF_6]

At high concentrations (>1.25 mM), the ionic conductivity of **5**[SbF_6] in CH_2Cl_2 clearly deviates from Kohlrausch's law for strong electrolytes, confirming its aggregation into contact ion pairs. The molar conductivity of **5**[SbF_6] in the concentration range of 0.31–1.25 mM is proportional to the square root of the concentration, yet the conductivity of **5**[SbF_6] at infinite dilution (Λ_o = 6.9 S cm^2 mol^{-1}) is significantly lower than that of Fc[SbF_6] (Λ_o = 32.9 S cm^2 mol^{-1}), lacking the hydrogen-bonding unit, and other typical 1:1 electrolytes (Supporting Information).[80] This low ionic conductivity of **5**[SbF_6] is clearly evidence of the formation of contact ion pairs with strong charge-assisted NH···F hydrogen bonds in CH_2Cl_2, even at high dilution.

DFT Calculations on the Formation of Contact Ion Pairs of 5[SbF_6]

DFT (PCM, CH_2Cl_2) calculations on different isomers of $\mathbf{5}^+$ reveal the preference for the *trans-trans* and *trans-cis* isomers (Figure 7; Supporting Information). The *cis-trans* and *cis-cis* isomers are destabilized by more than 10 kJ mol^{-1}. Coordination of a hexafluoroantimonate anion to both NH groups through two NH···F hydrogen bonds in a chelating fashion stabilizes the *trans-trans* isomer by more than 10 kJ mol^{-1} over the *trans-cis* isomer. According to the calculation, this coordination mode involves a strong, charge-assisted NH^a···F and a weaker NH^b···F bond. Chelating and monodentate coordination modes of SbF_6^- ions to doubly charged *trans-trans* diferrocenylurea is also observed in the solid state for **1**$[SbF_6]_2$ (Figure 1e). As expected, NH···Fe hydrogen bonds play no role in ferrocenium cations (Supporting Information).[67,68]

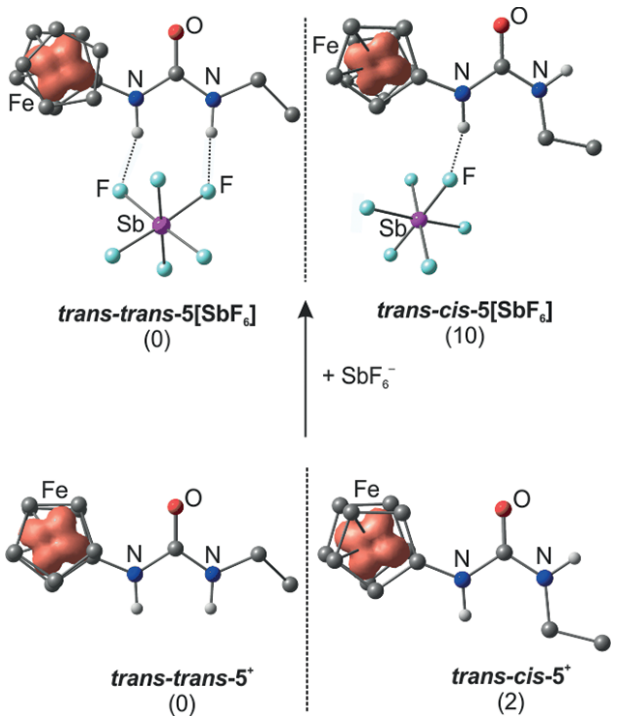

Figure 7. DFT-calculated geometries (UB3LYP/LANL2DZ with polarization functions, PCM, CH_2Cl_2, dispersion correction) and relative Gibbs free energies (ΔG [kJ mol^{-1}]) of relevant isomers of $\mathbf{5}^+$ and relevant hydrogen-bonded contact ion pairs **5**[SbF_6] with DFT-calculated spin-density distributions (isosurface value 0.01 a.u.).

Conclusions

In the solid state, ferrocenylureas **1**–**5** (R = Fc, Ph, Nap, Me, Et) self-assemble into tapes of monomers in *trans-trans* conformation linked by bifurcated $(NH)_2$···O=C hydrogen bonds, whereas ferrocenylthioureas **6** and **7** (R = Fc, Ant) dimerize as *cis-trans* isomers into rings with NH···S=C hydrogen bonds (Scheme 4). In diferrocenylthiourea (**6**) the remaining NH groups in the dimer are engaged in nonclassical intramolecular NH···Fe hydrogen bonds [*cis-trans*(NH···Fe) dimer; Scheme 4].

In THF solution, single THF molecules coordinate to ureas **1**–**5** through bifurcated $(NH)_2$···O(THF) hydrogen bonds. This suggests a simple assembly/disassembly process of ureas in the *trans-trans* conformation in THF (Scheme 4). Thioureas **6** and **7** appear to prefer the *cis-trans* isomer form in THF, which is also consistent with their conformations in the solid state.

In the noncoordinating solvent dichloromethane, however, several isomers of **1**–**5** equilibrate, especially the *cis-trans*, *trans-trans*, and *trans-cis* isomers. A slight preference for the *cis-trans*(NH···Fe) isomer featuring a nonclassical NH···Fe hydrogen bond is noted, although the effect is not particularly large, due to the low acidity of ureas. The acidity of thioureas **6** and **7** is higher, and hence the *cis-trans*(NH···Fe) isomer including the nonclassical NH···Fe hydrogen bond is more stabilized. All (thio)ureas appear to dimerize into rings of *cis-trans* isomers at higher concentrations in CH_2Cl_2 (Scheme 4). The intramolecular

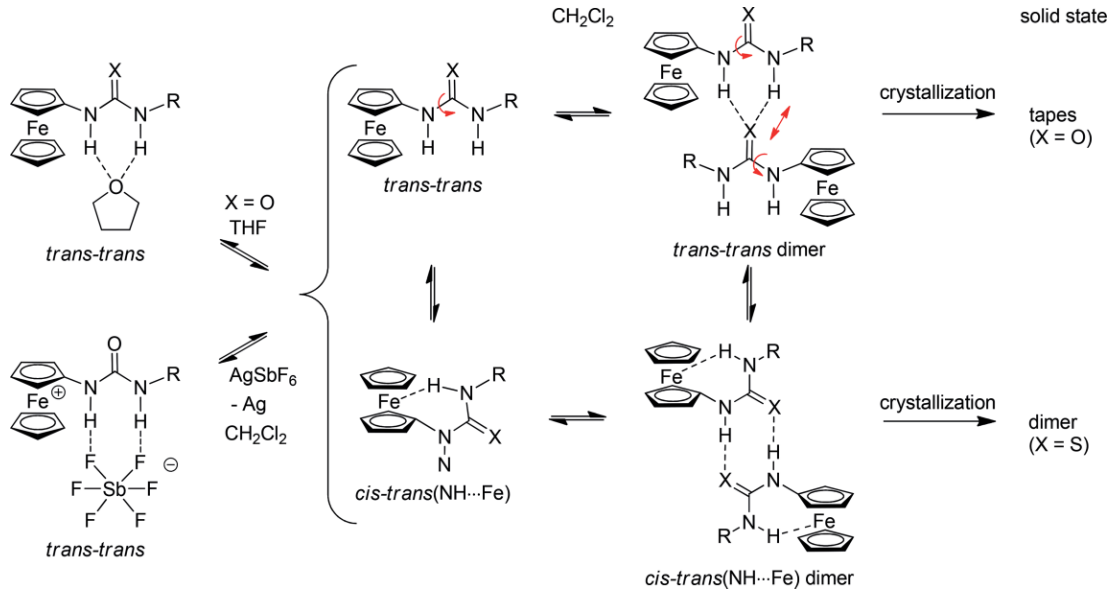

Scheme 4. Summary of conformational equilibria of ferrocenyl(thio)ureas in coordinating and noncoordinating solvents (THF, CH_2Cl_2); influence on crystallization and ion-pair formation upon oxidation.

NH···Fe hydrogen bond is especially pronounced for (*cis-trans*-**6**)$_2$. Equilibrium constants for *cis-trans*-**4**/(*cis-trans*-**4**)$_2$ and *cis-trans*-**5**/(*cis-trans*-**5**)$_2$ dimerizations amount to $K \approx 4.1\ M^{-1}$. In spite of the preorganization of thioureas as *cis-trans* isomers, their dimerization tendency is lower, due to their lower proton-acceptor capability.

The nucleation of ureas in CH_2Cl_2 starts with the formation of rings of *cis-trans* monomers, whereas the crystals contain tapes of *trans-trans* isomers, so a further rearrangement is clearly required. We suggest that the rings of *cis-trans* monomers rearrange into dimers of *trans-trans* isomers through dissociation of one NH···OC hydrogen bond and cooperative rotation of the R–NHC(O) moieties of both monomer units (Scheme 4). This double rotation results in a zigzag dimer of *trans-trans* isomers that can further relax into a linear dimer. These dimers further assemble into tapes of *trans-trans* isomers. The Gibbs free energy of activation for such a rotation has been determined as $\Delta G^{\ddagger}_{258} = (49 \pm 1)$ kJ mol^{-1} (in a monomer of **1**).

From this information, we conclude that self-assembly of ferrocenyl(thio)ureas in the solid state is dictated by balancing the maximum number of (strong) NH···X hydrogen bonds (X = O, S) and the preferred conformation of the NHC(X)NH unit (*trans-trans*, *cis-trans*). Ferrocenylthioureas prefer the *cis-trans* conformation, which translates into rings in the solid state, leaving one NH group nonbonded. This NH moiety can further engage in weak nonclassical NH···Fe hydrogen bonds. Ureas equilibrate with several isomers of similar energy, so tapes of *trans-trans* isomers with bifurcated (NH)$_2$···O=C hydrogen bonds involving all NH groups are thermodynamically favored in the solid state (Scheme 4).

Oxidation of ureas with $AgSbF_6$ to the corresponding ferrocenium cations disassembles all homomeric aggregates and instead favors the coordination of an SbF_6^- counter ion to both NH groups, giving strong charge-assisted NH···F hydrogen bonds in contact ion pairs and ion clusters (Scheme 4). Again, the *trans-trans* isomer form is favored in this anion binding, similar to the situation of the neutral ferrocenylureas in THF and their self-assembly in the solid state. In the dication **1**$^{2+}$ of diferrocenylurea even two SbF_6^- counter ions bind to the NH groups of **1**$^{2+}$ in a *trans-trans* conformation in the solid state, supporting the ion clustering hypotheses for positively charged ureas and thioureas.

Experimental Section

General Procedures: All reactions were performed under argon unless otherwise noted. A glovebox (UniLab/MBraun, Ar 4.8, O_2 < 1 ppm, H_2O < 1 ppm) was used for storage and weighing of sensitive compounds. All analytical samples that required the absence of oxygen were prepared in the same glovebox. Dichloromethane was dried with CaH_2 and distilled prior to use. THF and toluene were distilled from potassium. All reagents were used as received from commercial suppliers (ABCR, Acros Organics, Alfa Aesar, Fischer Scientific, Fluka, and Sigma–Aldrich). Deuterated solvents were purchased from euriso-top. Aminoferrocene (Fc–NH_2),[59,60] ferrocenecarboxylic acid (Fc–COOH),[41] ferrocenyl isocyanate (Fc–NCO), and ureas **1** and **2**[43] were prepared according to literature procedures. NMR spectra were recorded with a Bruker Avance DRX 400 spectrometer at 400.31 MHz (^{1}H) and 100.07 MHz [^{13}C{^{1}H}]. All resonances are reported in ppm with respect to the solvent signal as internal standard [CD_2Cl_2 (^{1}H: δ = 5.32 ppm; ^{13}C: δ = 53.8 ppm), [D_8]tetrahydrofuran (^{1}H: δ = 1.73, 3.58 ppm; ^{13}C: δ = 67.4, 25.3 ppm), [D_6]DMSO (^{1}H: δ = 2.50 ppm; ^{13}C: δ = 39.5 ppm)].[81] EPR spectra were recorded with a Miniscope MS 300 X-band CW spectrometer (Magnettech GmbH, Germany). Values of *g* are referenced to Mn^{2+} in ZnS as external standard (*g* = 2.118, 2.066, 2.027, 1.986, 1.946). Simulations were performed with the EasySpin program package.[82] ^{57}Fe Mössbauer measurements of powder samples were performed in transmission geometry with a constant-acceleration spectrometer and the source ^{57}Co(Rh). Recoil 1.03 Mössbauer Analysis Software was used to fit the experimental spectra with Lorentzian peaks.[83] Isomer shift values are

quoted relative to α-Fe at 293 K. IR spectra were recorded with a BioRad Excalibur FTS 3100 spectrometer as KBr disks or by use of KBr cells [in CH_2Cl_2 or in CD_2Cl_2 (**6**) with a larger transparent window for the NH vibration region]. Electrochemical experiments were carried out with a BioLogic SP-50 voltammetric analyzer and use of a platinum working electrode, a platinum wire as counter electrode, and a 0.01 M $Ag/AgNO_3$ electrode as reference electrode. The measurements were carried out at a scan rate of 100 mV s^{-1} for cyclic voltammetry experiments and at 50 mV s^{-1} for square-wave voltammetry experiments in $[n\mathrm{Bu_4N}][\mathrm{B(C_6F_5)_4}]$ (0.1 M) as supporting electrolyte in CH_2Cl_2. Potentials are referenced against the ferrocene/ferrocenium couple. UV/Vis/NIR spectra were recorded with a Varian Cary 5000 spectrometer and use of 1.0 cm cells (Hellma, Suprasil). FD mass spectra were recorded with a Thermo Fisher DFS mass spectrometer with a LIFDI upgrade (Linden CMS) or with an FD Finnigan Mat95 spectrometer. Melting points were determined with a Gallenkamp MFB 595 010 capillary melting point apparatus and were not corrected. Elemental analyses were performed by the microanalytical laboratory of the chemical institutes of the University of Mainz. Conductivities were measured with a Greisinger conductivity cell, model 6MH 3431 LFE-210 with platinum electrodes in the concentration range c = 0.31–1.25 mM in CH_2Cl_2. The equivalent conductivity (Λ_e) was plotted as a function of $\sqrt{c}$, with c being the equivalent concentration. To determine Λ_o, Λ_e was extrapolated to infinite dilution. $\Lambda_o - \Lambda_e$ was plotted vs. $\sqrt{c}$ to obtain an Onsager plot. From this plot, the slopes of various electrolyte types can be easily compared (Supporting Information).

Crystal Structure Determinations: Suitable crystals for single-crystal X-ray analyses were obtained after slow evaporation of the solvent variously from solutions of **3**, **4**, **5**, **6**, and **1**$[SbF_6]$ in dichloromethane, from a solution of **2** in ethanol, from a solution of **1** in ethyl acetate, and from a solution of **7** in dichloromethane/ethyl acetate. Intensity data were collected with a Bruker AXS Smart1000 CCD diffractometer with an APEX II detector and an Oxford cooling system or with a STOE IPDS-2T diffractometer and were corrected for absorption and other effects with the aid of Mo-K_α radiation (λ = 0.71073 Å). The diffraction frames were integrated by use of the Bruker SAINT or STOE X-RED package, and most were corrected for absorption with MULABS or SADABS.[84–86] The structures were solved by direct methods and refined by the full-matrix method based on F^2 with use of the SHELXTL software package.[87,88] All non-hydrogen atoms were refined anisotropically, whereas the positions of all hydrogen atoms were generated with appropriate geometric constraints and allowed to ride on their corresponding parent carbon/nitrogen atoms with fixed isotropic thermal parameters. CCDC 1494851 (for **1**), 1494852 (for **1**$[SbF_6]_2$), 1494853 (for **2**), 1494854 (for **3**), 1494855 (for **4**), 1494856 (for **5**), 1494857 (for **6**), and 1494858 (**7**•$2CH_2Cl_2$) contain the supplementary crystallographic data for this paper. These data can be obtained free of charge from The Cambridge Crystallographic Data Centre.

Density Functional Theory Calculations: These were carried out with the Gaussian 09/DFT series[89] of programs. The B3LYP[90] formulation of density functional theory was used with employment of the LANL2DZ[91–94] basis set, including Huzinaga polarization functions on hydrogen, carbon, nitrogen, and oxygen/sulfur of the NHCXNH moiety (X = O, S), on fluorine atoms of the SbF_6^- anion, and on oxygen atoms of THF molecules.[95] No symmetry constraints were imposed on the molecules. The presence of energy minima of the ground states was checked by analytical frequency calculations. The calculated transition states each exhibit a single imaginary frequency. Solvent modeling was carried out by employing the integral equation formalism polarizable continuum model (IEFPCM, tetrahydrofuran or dichloromethane). The approximate Gibbs free energies at 298 K were obtained through thermochemical analysis of the frequency calculation, with use of the thermal correction to the Gibbs free energy as reported by Gaussian 09. Additionally, Grimme's empirical dispersion correction to density functionals DFT-D3 was employed.[96]

General Procedure for the Synthesis of Ferrocenylureas 1–5: An equimolar amount of a primary amine R–NH_2 (R = Fc, Ph, Nap, Me, Et) was added to a solution of ferrocenyl isocyanate Fc–NCO in toluene. The reaction mixture was stirred overnight. The resulting yellow precipitate was separated from the solution by filtration. The precipitate was washed with several portions of toluene and further with petroleum ether (40/60) and dried under reduced pressure. All ureas **1**–**5** were obtained as yellow, crystalline solids.

***N,N′*-Diferrocenylurea (1):** Fc–NCO (500 mg, 2.20 mmol), Fc–NH_2 (443 mg, 2.20 mmol), toluene (20 mL). Yield: 850 mg (1.99 mmol, 90 %). M.p. > 208 °C (decomp.). ^{1}H NMR ([D$_8$]THF): δ = 6.83 (s, 2 H, NH), 4.51 (s, 4 H, H^3), 4.12 (s, 10, H^1), 3.89 (s, 4 H, H^2) ppm. ^{13}C{^{1}H} NMR ([D$_6$]DMSO): δ = 153.2 (s, C^5), 97.2 (s, C^4), 68.5 (s, C^1), 63.4 (s, C^2), 60.2 (s, C^3) ppm. IR (KBr): $\tilde{\nu}$ = 3292 (s, NH), 3088 (m, CH), 1636 (s, C=O), 1584 (s), 1477 (m), 1256 (m) cm^{-1}. IR (CH_2Cl_2, c = 5.0 mM): $\tilde{\nu}$ = 3423 (m, NH), 3341 (w, NH), 1686 (s, C=O), 1541 (s), 1497 (w), 1481 (w) cm^{-1}. UV/Vis (CH_2Cl_2): λ_{max} = 438 nm (360 M^{-1} cm^{-1}). CV {CH_2Cl_2, ($n\mathrm{Bu_4N}$)[$\mathrm{B(C_6F_5)_4}$]}: $E_{1/2}$ = –120, 70 mV vs. FcH/FcH$^+$. FD MS (THF): m/z (%) = 428.5 (100) [M]$^+$.$C_{21}H_{20}Fe_2N_2O$ (428.09): calcd. C 58.92, H 4.71, Fe 26.09, N 6.54; found C 58.74, H 4.39, Fe 26.19, N 6.57. Mössbauer (300 K): *I.S.*(Fe^{2+}) = 0.417 mm s^{-1} ΔE_Q = 2.450 mm s^{-1}.

***N*-Ferrocenyl-*N′*-phenylurea (2):** Fc–NCO (258 mg, 1.18 mmol), Ph–NH_2 (0.11 mL, 1.18 mmol), toluene (40 mL). Yield: 238 mg (0.74 mmol, 63 %). M.p. > 206 °C (decomp.). ^{1}H NMR ([D$_8$]THF): δ = 7.55 (s, 1 H, NH^b), 7.47 (d, $^2J_{H,H}$ = 7.7 Hz, 2 H, H^7), 7.19 (pt, 2 H, H^8), 7.01 (s, 1 H, NH^a), 6.89 (pt, 1 H, H^9), 4.51 (s, 2 H, H^3), 4.11 (s, 5 H, H^1), 3.89 (s, 2 H, H^2) ppm. ^{13}C{^{1}H} NMR ([D$_8$]THF): δ = 153.3 (s, C^5), 141.4 (s, C^6), 129.3 (s, C^8), 122.2 (s, C^9), 118.8 (s, C^7), 98.6 (s, C^4), 69.6 (s, C^1), 64.4 (s, C^2), 61.1 (s, C^3) ppm. IR (KBr): $\tilde{\nu}$ = 3306 (m, NH), 3196 (vw, CH), 3097 (w, CH), 1645 (s, C=O), 1598 (m), 1562 (s), 1498 (m), 1248 (m) cm^{-1}. IR (CH_2Cl_2, c = 5.0 mM): $\tilde{\nu}$ = 3424 (m, sh, NH), 3416 (m, NH), 3341 (w, NH), 1686 (s, C=O), 1597 (m), 1531 (s), 1499 (m) cm^{-1}. UV/Vis (CH_2Cl_2): λ_{max} = 253 (7514), 440 nm (145 M^{-1} cm^{-1}). CV {CH_2Cl_2, ($n\mathrm{Bu_4N}$)[$\mathrm{B(C_6F_5)_4}$]}: $E_{1/2}$ = –90 mV vs. FcH/FcH$^+$. FD MS (THF): m/z (%) = 319.9 (100) [M]$^+$. $C_{17}H_{16}FeN_2O$ (320.17): calcd. C 63.77, H 5.04, N 8.75; found C 63.97, H 5.07, N 8.66.

***N*-Ferrocenyl-*N′*-(1-naphthyl)urea (3):** Fc–NCO (1.10 g, 4.84 mmol), Nap–NH_2 (694 mg, 4.84 mmol), toluene (40 mL). Purification: column chromatography [Alox II, CH_2Cl_2/ethyl acetate, 1:1 (v/v), R_f = 0.7]. Yield: 1.33 g (3.59 mmol, 74 %). M.p. > 200 °C (decomp.). ^{1}H NMR ([D$_8$]THF): δ = 8.19 (d, $^3J_{H,H}$ = 6.9 Hz, 1 H, H^7), 7.94–7.96 (m, 1 H, H^{14}), 7.86 (br., 1 H, NH^b), 7.82–7.84 (m, 1 H, H^{11}), 7.54 (d, $^3J_{H,H}$ = 8.2 Hz, 1 H, H^9), 7.44–7.46 (m, 1 H, H^{13}), 7.43–7.45 (m, 1 H, H^{12}), 7.39 (d, $^2J_{H,H}$ = 8.0 Hz, 1 H, H^8), 7.37 (s, 1 H, NH^a), 4.57 (pt, 2 H, H^3), 4.13 (s, 5 H, H^1), 3.92 (pt, 2 H, H^2) ppm. ^{13}C{^{1}H} NMR ([D$_8$]THF): δ = 153.8 (s, C^5), 135.9 (s, C^{15}), 135.3 (s, C^{10}), 129.5 (s, C^{11}), 127.2 (s, C^6), 126.8 (s, C^8), 126.2 (s, C$^{12/13}$), 126.1 (s, C$^{12/13}$), 123.5 (s, C^9), 121.4 (s, C^{14}), 118.0 (s, C^7), 98.8 (s, C^4), 69.6 (s, C^1), 64.5 (s, C^2), 61.2 (s, C^3) ppm. IR (KBr): $\tilde{\nu}$ = 3292 (m, NH), 3093 (w, CH), 1634 (s, C=O), 1624 (s), 1574 (s), 1553 (s), 1491 (m), 1248 (m) cm^{-1}. IR (CH_2Cl_2, c = 3.0 mM): $\tilde{\nu}$ = 3422 (m, NH), 3335 (w, NH), 1686 (s, C=O), 1539 (s), 1500 (m) cm^{-1}. UV/Vis (CH_2Cl_2): λ_{max} = 247 (8900), 286 (8675), 437 nm (175 M^{-1} cm^{-1}). CV {CH_2Cl_2, ($n\mathrm{Bu_4N}$)[$\mathrm{B(C_6F_5)_4}$]}: $E_{1/2}$ = –110 mV vs. FcH/FcH$^+$. FD MS (THF): m/z (%) = 369.9 (100) [M]$^+$. $C_{21}H_{18}FeN_2O$ (370.23): calcd. C 68.13, H 4.90, N 7.57; found C 67.79, H 4.74, N 7.48.

***N*-Ferrocenyl-*N*′-methylurea (4):** Fc–NCO (345 mg, 1.52 mmol), Me–NH_2 (0.76 mL, 1.52 mmol), toluene (60 mL). Purification: Precipitation from a CH_2Cl_2 solution of **4** with petroleum ether (40/60). Yield: 140 mg (0.54 mmol, 36 %). M.p. > 166 °C (decomp.). ^{1}H NMR ([D_8]THF): δ = 6.84 (s, 1 H, NH^a), 5.17 (br., 1 H, NH^b), 4.41 (pt, 2 H, H^3), 4.07 (s, 5 H, H^1), 3.84 (pt, 2 H, H^2), 2.69 (d, $^3J_{H,H}$ = 4.7 Hz, 3 H, H^6) ppm. $^{13}C\{^1H\}$ NMR ([D_8]THF): δ = 156.9 (s, C^5), 99.5 (s, C^4), 69.5 (s, C^1), 64.2 (s, C^2), 61.2 (s, C^3), 26.9 (s, C^6) ppm. IR (KBr): $\tilde{\nu}$ = 3339 (m, NH), 3091 (w, CH), 2943–2808 (w, CH), 1651 (s, C=O), 1577 (s), 1491 (m), 1255 (m) cm^{-1}. IR (CH_2Cl_2, *c* = 5.0 mM): $\tilde{\nu}$ = 3447 (m, NH), 3433 (m, NH), 3390 (w, sh, NH), 1682 (s, C=O), 1539 (s), 1485 (w) cm^{-1}. UV/Vis (CH_2Cl_2): λ_{max} = 327 (sh), 440 nm (130 M^{-1} cm^{-1}). CV {CH_2Cl_2, (nBu$_4$N)[B(C_6F_5)$_4$]}: $E_{1/2}$ = –140 mV vs. FcH/FcH$^+$. FD MS (THF): *m*/*z* (%) = 258.1 (100) $[M]^+$. $C_{12}H_{14}FeN_2O$ (258.10): calcd. C 55.84, H 5.47, N 10.85; found C 55.83, H 5.48, N 10.75.

***N*-Ethyl-*N*′-ferrocenylurea (5):** Fc–NCO (36 mg, 0.16 mmol), Et–NH_2 (0.08 mL, 0.16 mmol), toluene (30 mL). Purification: Precipitation from a CH_2Cl_2 solution of **5** with petroleum ether (40/60). Yield: 33 mg (0.12 mmol, 76 %). M.p. > 173 °C (decomp.). ^{1}H NMR ([D_8]THF): δ = 6.72 (s, 1 H, NH^a), 5.22 (br., 1 H, NH^b), 4.41 (s, 2 H, H^3), 4.07 (s, 5 H, H^1), 3.83 (s, 2 H, H^2), 3.20–3.13 (dvq, $^3J_{H,H}$ = 5.7, $^3J_{H,H}$ = 7.2 Hz, 2 H, H^6), 1.08 (t, $^3J_{H,H}$ = 7.2 Hz, 3 H, H^7) ppm. $^{13}C\{^1H\}$ NMR ([D_8]THF): δ = 156.2 (s, C^5), 99.4 (s, C^4), 69.5 (s, C^1), 64.2 (s, C^2), 61.2 (s, C^3), 35.4 (s, C^6), 16.0 (s, C^7) ppm. IR (KBr): $\tilde{\nu}$ = 3321 (s, NH), 3099–2930 (w, CH), 1634 (s, C=O), 1584 (s), 1259 (m) cm^{-1}. IR (CH_2Cl_2, *c* = 5.0 mM): $\tilde{\nu}$ = 3433 (m, NH), 3381 (w, NH), 1676 (s, C=O), 1531 (s), 1495 (w), 1483 (w) cm^{-1}. UV/Vis (CH_2Cl_2): λ_{max} = 439 nm (140 M^{-1} cm^{-1}). CV {CH_2Cl_2, (nBu$_4$N)[B(C_6F_5)$_4$]}: $E_{1/2}$ = –140 mV vs. FcH/FcH$^+$. FD MS (THF): *m*/*z* (%) = 272.0 (100) $[M]^+$. $C_{13}H_{16}FeN_2O$ (272.12) •1/12CH_2Cl_2: calcd. C 56.28, H 5.84, N 10.03; found C 56.24, H 5.63, N 10.06.

***N*,*N*′-Diferrocenylthiourea (6):** Aminoferrocene Fc–NH_2 (150 mg, 0.75 mmol), and 1,1′-thiocarbonylbisimidazole (72 mg, 0.40 mmol) were dissolved in CH_2Cl_2 (7 mL). The reaction mixture was stirred overnight. The volume of the mixture was reduced to ca. 3–4 mL under reduced pressure. After crystallization at –30 °C, the precipitate was washed with cold CH_2Cl_2 (3 mL). Compound **6** was obtained as a yellow, crystalline solid after further purification by column chromatography [Alox II, CH_2Cl_2/ethyl acetate, 12:1 (v/v), R_f = 0.5] Yield: 75 mg (0.17 mmol, 23 %). M.p. > 190 °C (decomp.). ^{1}H NMR ([D_8]THF): δ = 8.46 (s, NH), 4.59 (s, 2 H, $H^{3/7}$), 4.29 (s, 5 H, $H^{1/9}$), 4.11 (s, 2 H, $H^{2/8}$) ppm. $^{13}C\{^1H\}$ NMR ([D_6]DMSO): δ = 180.5 (s, C^5), 95.03 (s, $C^{4/6}$), 68.9 (s, $C^{1/9}$), 64.7 (s, $C^{2/8}$), 64.6 (s, $C^{3/7}$) ppm. IR (KBr): $\tilde{\nu}$ = 3269 (m, NH), 3171 (s, NH), 3080 (w, CH), 3024 (m, CH), 1553 (s), 1528 (s), 1277 (s), 1105 (m), 831 (m) cm^{-1}. IR (CH_2Cl_2, *c* = 5.0 mM): $\tilde{\nu}$ = 3404 (m, NH), 3385 (sh, NH), 3372 (sh, NH), 3275 (w, NH), 1555 (m), 1521 (m), 1506 (m), 1483 (w) cm^{-1}. UV/Vis (CH_2Cl_2): λ_{max} = 439 nm (425 M^{-1} cm^{-1}). CV {CH_2Cl_2, (nBu$_4$N)[B(C_6F_5)$_4$]}: $E_{1/2}$ = –30, 180 mV; E_p = 800 (irrev.) mV vs. FcH/FcH$^+$. FD MS (THF): *m*/*z* (%) = 443.8 (100) $[M]^+$. $C_{21}H_{20}Fe_2N_2S$ (444.15): calcd. C 56.79, H 4.54, N 6.31; found C 56.99, H 4.40, N 6.26.

***N*-(1-Anthracenyl)-*N*′-ferrocenylthiourea (7):** Aminoferrocene (Fc–NH_2, 334 mg, 1.66 mmol), 1,1′-thiocarbonylbisimidazole (296 mg, 1.66 mmol), and 1-aminoanthracene (321 mg, 1.66 mmol) were dissolved in CH_2Cl_2 (40 mL). The reaction mixture was stirred overnight. The solvent was removed under reduced pressure. The crude product was a mixture of **6** and **7**. The compounds could not be separated by column chromatography [Alox II, CH_2Cl_2/ethyl acetate, 13:1 (v/v), R_f = 0.56]. After double crystallization from a solution of the crude product in ethyl acetate at –25 °C, a small batch of almost pure **7**, sufficient for ^{1}H NMR spectroscopic and mass spectrometric characterization, could be obtained as a yellow solid. ^{1}H NMR ([D_8]THF): δ = 9.18 (br., 1 H, NH^b), 8.63 (s, 1 H, H^{18}), 8.52 (s, 1 H, H^{11}), 8.26 (br., 1 H, NH^a), 8.10 (dvd, 1 H, H^{16}), 8.02 (dvd, 1 H, H^{13}), 7.97 (d, $^3J_{H,H}$ = 8.5 Hz, 1 H, H^9), 7.60 (d, $^3J_{H,H}$ = 6.9 Hz, 1 H, H^7), 7.48–7.46 (m, 3 H, $H^{8/14/15}$), 4.66 (s, 2 H, H^3), 4.14 (s, 5 H, H^1), 4.03 (s, 2 H, H^2) ppm. FD MS (THF): *m*/*z* (%) = 435.9 (100) $[M]^+$.

Preparation of Ferrocenium Cations: (Thio)ureas **1**–**6** (2 mg) were dissolved in CH_2Cl_2 (6 mL). A solution of $AgSbF_6$ in CH_2Cl_2 (5.8 mg in 4 mL, 1 equiv.) was added, precipitating silver. The resulting dark yellow solution was filtered with a syringe filter (pore size = 0.20 µm) to remove silver and subjected to EPR, IR, or UV/Vis spectroscopic analyses, as well as to conductivity studies.

Acknowledgments

We thank Regine Jung-Pothmann for the collection of the diffraction data, Dr. Johannes Liermann for the VT NMR spectroscopic measurements, Dr. Vadim Ksenofontov for the Mößbauer measurement, and the Johannes Gutenberg University (Germany) for financial support to C. F. (Internal University Research Funding). Financial support from the COST Action CM1302 SIPs is gratefully acknowledged.

Keywords: Ferrocene · (Thio)ureas · Hydrogen bonds · Self-assembly · Conformation analysis · Density functional calculations · Solid-state structures

[1] R. Custelcean, *Chem. Commun.* **2008**, 295–307.
[2] J. W. Steed, *Chem. Soc. Rev.* **2010**, *39*, 3686–3699.
[3] P. R. Schreiner, *Chem. Soc. Rev.* **2003**, *32*, 289.
[4] Y. Takemoto, *Org. Biomol. Chem.* **2005**, *3*, 4299–4306.
[5] M. S. Taylor, E. N. Jacobsen, *Angew. Chem. Int. Ed.* **2006**, *45*, 1520–1543; *Angew. Chem.* **2006**, *118*, 1550–1573.
[6] A. G. Doyle, E. N. Jacobsen, *Chem. Rev.* **2007**, *107*, 5713–5743.
[7] Z. Zhang, P. R. Schreiner, *Chem. Soc. Rev.* **2009**, *38*, 1187–1198.
[8] G. W. Bates, P. A. Gale, *Struct. Bonding (Berlin)* **2008**, *129*, 1–44.
[9] B. P. Hay, *Chem. Soc. Rev.* **2010**, *39*, 3700–3708.
[10] A.-F. Li, J.-H. Wang, F. Wang, Y.-B. Jiang, *Chem. Soc. Rev.* **2010**, *39*, 3729–3745.
[11] P. A. Gale, *Chem. Soc. Rev.* **2010**, *39*, 3746–3771.
[12] V. Amendola, L. Fabbrizzi, L. Mosca, *Chem. Soc. Rev.* **2010**, *39*, 3889–3915.
[13] V. Blažek Bregović, N. Basarić, K. Mlinarić-Majerski, *Coord. Chem. Rev.* **2015**, *295*, 80–124.
[14] Y. Mido, *Spectrochim. Acta, Part A* **1973**, *29*, 1–6.
[15] Y. Mido, T. Gohda, *Bull. Chem. Soc. Jpn.* **1975**, *48*, 2704–2707.
[16] J. Jadzyn, M. Stockhausen, B. Zywucki, *J. Phys. Chem.* **1987**, *91*, 754–757.
[17] F. Lortie, S. Boileau, L. Bouteiller, *Chem. Eur. J.* **2003**, *9*, 3008–3014.
[18] M. Obrzud, M. Rospenk, A. Koll, *J. Phys. Chem. B* **2010**, *114*, 15905–15912.
[19] M. Obrzud, M. Rospenk, A. Koll, *J. Mol. Struct.* **2012**, *1018*, 54–63.
[20] P. A. Wood, E. Pidcock, F. H. Allen, *Acta Crystallogr., Sect. B* **2008**, *64*, 491–496.
[21] F. G. Bordwell, D. J. Algrim, J. A. Harrelson, *J. Am. Chem. Soc.* **1988**, *110*, 5903–5904.
[22] M. Obrzud, M. Rospenk, A. Koll, *Phys. Chem. Chem. Phys.* **2014**, *16*, 3209–3219.
[23] R. Custelcean, N. L. Engle, P. V. Bonnesen, *CrystEngComm* **2007**, *9*, 452.
[24] S. Fery-Forgues, B. Delavaux-Nicot, *J. Photochem. Photobiol. A* **2000**, *132*, 137–159.
[25] P. Molina, A. Tárraga, A. Caballero, *Eur. J. Inorg. Chem.* **2008**, 3401–3417.
[26] S. R. Bayly, P. D. Beer, G. Z. Chen in *Ferrocenes – Ligands, Materials and Biomolecules* (Ed.: P. Štěpnička), J. Wiley, Chichester, England, Hoboken, NJ, **2008**.
[27] S. R. Bayly, P. D. Beer, *Struct. Bonding (Berlin)* **2008**, *129*, 45–94.
[28] D. Siebler, C. Förster, K. Heinze, *Eur. J. Inorg. Chem.* **2010**, 523–527.
[29] H. Miyaji, S. R. Collinson, I. Prokeš, J. H. R. Tucker, *Chem. Commun.* **2003**, 64–65.

[30] A. J. Evans, S. E. Matthews, A. R. Cowley, P. D. Beer, *Dalton Trans.* **2003**, 4644.
[31] M. D. Pratt, P. D. Beer, *Polyhedron* **2003**, *22*, 649–653.
[32] B. Alonso, C. M. Casado, I. Cuadrado, M. Morán, A. E. Kaifer, *Chem. Commun.* **2002**, 1778–1779.
[33] K. Moon, A. E. Kaifer, *J. Am. Chem. Soc.* **2004**, *126*, 15016–15017.
[34] F. Otón, A. Tarraga, A. Espinosa, M. D. Velasco, D. Bautista, P. Molina, *J. Org. Chem.* **2005**, *70*, 6603–6608.
[35] F. Otón, A. Tárraga, M. D. Velasco, P. Molina, *Dalton Trans.* **2005**, 1159–1161.
[36] F. Otón, A. Tárraga, A. Espinosa, M. D. Velasco, P. Molina, *Dalton Trans.* **2006**, 3685–3692.
[37] F. Otón, A. Tárraga, A. Espinosa, M. D. Velasco, P. Molina, *J. Org. Chem.* **2006**, *71*, 4590–4598.
[38] K. Mahmoud, Y.-T. Long, G. Schatte, H.-B. Kraatz, *J. Organomet. Chem.* **2004**, *689*, 2250–2255.
[39] D. Siebler, C. Förster, T. Gasi, K. Heinze, *Organometallics* **2011**, *30*, 313–327.
[40] Z.-L. Gong, Y.-W. Zhong, *Sci. China: Chem.* **2015**, *58*, 1444–1450.
[41] J. Lapić, G. Pavlović, D. Siebler, K. Heinze, V. Rapić, *Organometallics* **2008**, *27*, 726–735.
[42] J. Lapić, S. Djaković, M. Cetina, K. Heinze, V. Rapić, *Eur. J. Inorg. Chem.* **2010**, 106–114.
[43] K. Schlögl, H. Seiler, *Naturwissenschaften* **1958**, *45*, 337.
[44] E. M. Acton, R. M. Silverstein, *J. Org. Chem.* **1959**, *24*, 1487–1490.
[45] M. Arroyo, P. R. Birkin, P. A. Gale, S. E. García-Garrido, M. E. Light, *New J. Chem.* **2008**, *32*, 1221.
[46] D. P. Cormode, A. J. Evans, J. J. Davis, P. D. Beer, *Dalton Trans.* **2010**, *39*, 6532–6541.
[47] M. Li, B. Wu, F. Cui, Y. Hao, X. Huang, X.-J. Yang, *Z. Anorg. Allg. Chem.* **2011**, *637*, 2306–2311.
[48] M. Li, Y. Hao, B. Wu, C. Jia, X. Huang, X.-J. Yang, *Org. Biomol. Chem.* **2011**, *9*, 5637–5640.
[49] M. Li, B. Wu, C. Jia, X. Huang, Q. Zhao, S. Shao, X.-J. Yang, *Chem. Eur. J.* **2011**, *17*, 2272–2280.
[50] X. Huang, B. Wu, C. Jia, B. P. Hay, M. Li, X.-J. Yang, *Chem. Eur. J.* **2013**, *19*, 9034–9041.
[51] G. Cooke, H. A. de Cremiers, F. M. Duclairoir, J. Leonardi, G. Rosair, V. M. Rotello, *Tetrahedron* **2003**, *59*, 3341–3347.
[52] S. C. Hillier, C. G. Frost, A. A. Jenkins, H. T. Braven, R. W. Keay, S. E. Flower, J. M. Clarkson, *Bioelectrochemistry* **2004**, *63*, 307–310.
[53] A. J. Salmon, M. L. Williams, Q. K. Wu, J. Morizzi, D. Gregg, S. A. Charman, D. Vullo, C. T. Supuran, S.-A. Poulsen, *J. Med. Chem.* **2012**, *55*, 5506–5517.
[54] W. Liu, Y. Tang, Y. Guo, B. Sun, H. Zhu, Y. Xiao, D. Dong, C. Yang, *Appl. Organomet. Chem.* **2012**, *26*, 189–193.
[55] H. Sun, J. Steeb, A. E. Kaifer, *J. Am. Chem. Soc.* **2006**, *128*, 2820–2821.
[56] K. Feng, M.-L. Yu, S.-M. Wang, G.-X. Wang, C.-H. Tung, L.-Z. Wu, *ChemPhysChem* **2013**, *14*, 198–203.
[57] Q. Zhang, B. Zhao, Y. Song, C. Hua, X. Gou, B. Chen, J. Zhao, *Heteroat. Chem.* **2015**, *26*, 348–354.
[58] Y.-F. Yuan, L.-Y. Zhang, J.-P. Cheng, J.-T. Wang, *Trans. Met. Chem.* **1997**, *22*, 281–283.
[59] B. Bildstein, M. Malaun, H. Kopacka, K. Wurst, M. Mitterböck, K.-H. Ongania, G. Opromolla, P. Zanello, *Organometallics* **1999**, *18*, 4325–4336.
[60] K. Heinze, M. Schlenker, *Eur. J. Inorg. Chem.* **2004**, 2974–2988.
[61] H. A. Staab, *Angew. Chem. Int. Ed. Engl.* **1962**, *1*, 351–367; *Angew. Chem.* **1962**, *74*, 407–423.
[62] Cambridge Crystallographic Data Centre (CCDC reference number 1042201).
[63] CSD search (ConQuest) (www.ccdc.cam.ac.uk) on May 11, **2016**. Search parameters: FcNHC(X)NHR, X = S, R = non-donor-atom containing substituent.
[64] P. Pansuriya, H. B. Friedrich, G. E. Maguire, *Acta Crystallogr., Sect. E* **2011**, *67*, o2621.
[65] J. van Rooyen, R. Betz, B. J. van Brecht, *Acta Crystallogr., Sect. E* **2011**, *67*, o2889.
[66] X. Li, W. Liu, *Acta Crystallogr., Sect. E* **2011**, *67*, m1744.
[67] C. Förster, P. Veit, V. Ksenofontov, K. Heinze, *Chem. Commun.* **2015**, *51*, 1514–1516.
[68] P. Veit, E. Prantl, C. Förster, K. Heinze, *Organometallics* **2016**, *35*, 249–257.
[69] T. Kienz, C. Förster, K. Heinze, *Organometallics* **2014**, *33*, 4803–4812.
[70] J. Mason, *Multinuclear NMR*, Springer US, Boston, MA, **1987**.
[71] L. Barisic, M. Cakic, K. A. Mahmoud, Y.-n. Liu, H.-B. Kraatz, H. Pritzkow, S. I. Kirin, N. Metzler-Nolte, V. Rapić, *Chem. Eur. J.* **2006**, *12*, 4965–4980.
[72] Y. Mido, *Spectrochim. Acta, Part A* **1972**, *28*, 1503–1518.
[73] R. K. Ritchie, H. Spedding, D. Steele, *Spectrochim. Acta, Part A* **1971**, *27*, 1597–1608.
[74] Y. Mido, H. Mizuno, K. Machida, *Spectrochim. Acta, Part A* **1988**, *44*, 445–447.
[75] Y. Mido, *Bull. Chem. Soc. Jpn.* **1974**, *47*, 1833–1837.
[76] D. M. Duggan, D. N. Hendrickson, *Inorg. Chem.* **1975**, *14*, 955–970.
[77] B. S. Brunschwig, N. Sutin, *Coord. Chem. Rev.* **1999**, *187*, 233–254.
[78] M. B. Robin, *Adv. Inorg. Chem. Radiochem.* **1968**, *10*, 247–422.
[79] A. Neidlinger, V. Ksenofontov, K. Heinze, *Organometallics* **2013**, *32*, 5955–5965.
[80] R. D. Feltham, R. G. Hayter, *J. Chem. Soc.* **1964**, 4587.
[81] G. R. Fulmer, A. J. M. Miller, N. H. Sherden, H. E. Gottlieb, A. Nudelman, B. M. Stoltz, J. E. Bercaw, K. I. Goldberg, *Organometallics* **2010**, *29*, 2176–2179.
[82] S. Stoll, A. Schweiger, *J. Magn. Reson.* **2006**, *178*, 42–55.
[83] K. Lagarec, D. G. Rancourt, *Nucl. Instr. Meth. Phys. Res. B* **1997**, *129*, 266–280.
[84] *SMART Data Collection* and *SAINT-Plus Data Processing*, Software for the SMART System (various versions), Bruker Analytical X-ray Instruments, Inc., Madison, WI, **2000**.
[85] B. Blessing, *Acta Crystallogr., Sect. A* **1995**, *51*, 33–38.
[86] *SADABS Area-Detector Absorption Correction*, Siemens Industrial Automation Inc., Madison, WI, **1996**.
[87] G. M. Sheldrick, University of Göttingen, Göttingen, Germany **1997**.
[88] G. M. Sheldrick, *SHELXTL*, version 5.1, Bruker AXS, Madison, WI, **1998**.
[89] M. J. Frisch, G. W. Trucks, H. B. Schlegel, G. E. Scuseria, M. A. Robb, J. R. Cheeseman, G. Scalmani, V. Barone, B. Mennucci, G. A. Petersson, H. Nakatsuji, M. Caricato, X. Li, H. P. Hratchian, A. F. Izmaylov, J. Bloino, G. Zheng, J. L. Sonnenberg, M. Hada, M. Ehara, K. Toyota, R. Fukuda, J. Hasegawa, M. Ishida, T. Nakajima, Y. Honda, O. Kitao, H. Nakai, T. Vreven, J. A. Montgomery Jr., J. E. Peralta, F. Ogliaro, M. Bearpark, J. J. Heyd, E. Brothers, K. N. Kudin, V. N. Staroverov, R. Kobayashi, J. Normand, K. Raghavachari, A. Rendell, J. C. Burant, S. S. Iyengar, J. Tomasi, M. Cossi, N. Rega, J. M. Millam, M. Klene, J. E. Knox, J. B. Cross, V. Bakken, C. Adamo, J. Jaramillo, R. Gomperts, R. E. Stratmann, O. Yazyev, A. J. Austin, R. Cammi, C. Pomelli, J. W. Ochterski, R. L. Martin, K. Morokuma, V. G. Zakrzewski, G. A. Voth, P. Salvador, J. J. Dannenberg, S. Dapprich, A. D. Daniels, Ö. Farkas, J. B. Foresman, J. V. Ortiz, J. Cioslowski, D. J. Fox, *Gaussian 09*, revision A.02, Gaussian, Inc., Wallingford, CT, **2009**.
[90] A. D. Becke, *J. Chem. Phys.* **1993**, *98*, 5648–5652.
[91] C. E. Dykstra, *Chem. Phys. Lett.* **1977**, *45–52*, 466–469.
[92] P. J. Hay, W. R. Wadt, *J. Chem. Phys.* **1985**, *82*, 299–310.
[93] P. J. Hay, W. R. Wadt, *J. Chem. Phys.* **1985**, *82*, 270–283.
[94] W. R. Wadt, P. J. Hay, *J. Chem. Phys.* **1985**, *82*, 284–298.
[95] S. Huzinaga, J. Andzelm, M. Klobukowski, E. Radzio-Andzelm, Y. Sakai, H. Tatewaki, *Gaussian Basis Sets for Molecular Calculations*, Elsevier, Amsterdam, **1984**.
[96] S. Grimme, J. Antony, S. Ehrlich, H. Krieg, *J. Chem. Phys.* **2010**, *132*, 154104–154119.

Received: July 25, 2016
Published Online: October 28, 2016

4.2 Stereochemical consequences of oxygen atom transfer and electron transfer in imido/oxido molybdenum(IV, V, VI) complexes with two unsymmetric bidentate ligands

Kristina Hüttinger, Christoph Förster, Timo Bund, Dariush Hinderberger and Katja Heinze, *Inorg. Chem.* **2012**, *51*, 4180–4192.

DOI: 10.1021/ic202588u

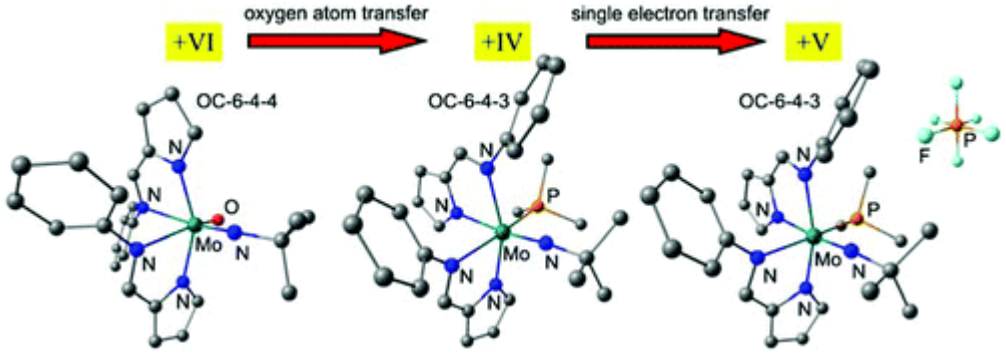

Inorganic Chemistry

Article

pubs.acs.org/IC

Stereochemical Consequences of Oxygen Atom Transfer and Electron Transfer in Imido/Oxido Molybdenum(IV, V, VI) Complexes with Two Unsymmetric Bidentate Ligands

Kristina Hüttinger,[†] Christoph Förster,[†] Timo Bund,[‡] Dariush Hinderberger,[‡] and Katja Heinze*[,†]

[†]Institute of Inorganic Chemistry and Analytical Chemistry, Johannes Gutenberg-University of Mainz, Duesbergweg 10-14, 55128 Mainz, Germany

[‡]Max Planck Institute for Polymer Research, Ackermannweg 10, 55128 Mainz, Germany

Supporting Information

ABSTRACT: Two equivalents of the unsymmetrical Schiff base ligand $(\mathbf{L}^{t\mathbf{Bu}})^-$ (4-*tert*-butyl phenyl(pyrrolato-2-ylmethylene)amine) and $MoCl_2(NtBu)O(dme)$ (dme = 1,2-dimethoxyethane) gave a single stereoisomer of a mixed imido/oxido Mo^{VI} complex $\mathbf{2}^{t\mathbf{Bu}}$. The stereochemistry of $\mathbf{2}^{t\mathbf{Bu}}$ was elucidated using X-ray diffraction, NMR spectroscopy, and DFT calculations. The complex is active in an oxygen atom transfer (OAT) reaction to trimethyl phosphane. The putative intermediate five-coordinate Mo^{IV} imido complex coordinates a PMe_3 ligand, giving the six-coordinate imido phosphane Mo^{IV} complex $\mathbf{5}^{t\mathbf{Bu}}$. The stereochemistry of $\mathbf{5}^{t\mathbf{Bu}}$ is different from that of $\mathbf{2}^{t\mathbf{Bu}}$ as shown by NMR spectroscopy, DFT calculations, and X-ray diffraction. Single-electron oxidation of $\mathbf{5}^{t\mathbf{Bu}}$ with ferrocenium hexafluorophosphate gave the stable cationic imido phosphane Mo^V complex $[\mathbf{5}^{t\mathbf{Bu}}]^+$ as the PF_6^- salt. EPR spectra of $[\mathbf{5}^{t\mathbf{Bu}}](\mathbf{PF_6})$ confirmed the presence of PMe_3 in the coordination sphere. Single-crystal X-ray diffraction analysis of $[\mathbf{5}^{t\mathbf{Bu}}](\mathbf{PF_6})$ revealed that electron transfer occurred under retention of the stereochemical configuration. The rate of OAT, the outcome of the electron transfer reaction, and the stabilities of the imido complexes presented here differ dramatically from those of analogous oxido complexes.

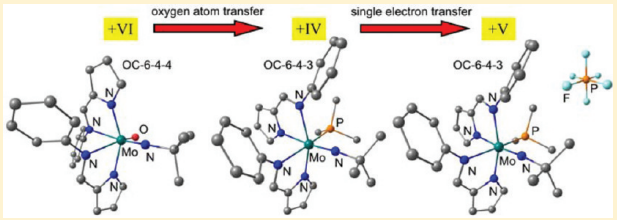

INTRODUCTION

Oxygen atom transfer OAT[1] as seen, e.g., in molybdenum-containing oxotransferases[2,3] is very well studied using model chemistry.[4,5] The oxygen atom is transferred from a $[Mo^{VI}{=}O]$ species to the substrate giving a $[Mo^{IV}]$ species, and the oxygenated substrate, e.g., SO_4^{2-}, is formed from SO_3^{2-}.[6] We[7−9] and others[4,5] observed that in some reactions employing dioxido $Mo^{VI}O_2(X{\cap}Y)_2$ model complexes, e.g., of type **A** (Chart 1), as oxygen atom donor the resulting five-coordinate $Mo^{IV}O(X{\cap}Y)_2$ species form a μ-oxido dimer $(X{\cap}Y)_2(O)Mo^V{-}O{-}Mo^V(O)(X{\cap}Y)_2$ as very stable intermediate by comproportionation with the starting material. This is a quite general phenomenon using uncharged and sterically less congested complexes.[4,5] With excess substrate, e.g., PR'_3, the vacant coordination site of the intermediate $Mo^{IV}O(X{\cap}Y)_2$ species can be filled by the phosphane substrate.[7−10] When two dissymmetric chelate ligands X∩Y are employed several stereoisomers $Mo(X{\cap}Y)_2(O)(PR'_3)$ are conceivable. We were able to deduce the stereochemistry of such molybdenum(IV) phosphane complexes by NMR spectroscopy and DFT calculations for complexes of dissymmetric imino pyrrolato chelate ligands $(L^R)^-$ (Chart 1; R = $OSiMe_3$).[7−9]

To close a catalytic cycle the two-electron-reduced molybdenum(IV) species has to be reoxidized to molybdenum(VI) via molybdenum(V) complexes in two single-electron transfer (SET) oxidation steps. One-electron oxidation of $Mo^{IV}(L^R)_2(O)(PR'_3)$ to the molybdenum(V) species $[Mo^V(L^R)_2(O)(PR'_3)]^+$ resulted in rapid loss of the coordinated phosphane PR'_3 (R′ = Me, Ph).[9] However, neither Mo^{IV} species nor mononuclear Mo^V species could be characterized in this system by X-ray diffraction methods so far due to solubility and stability reasons. We therefore decided (i) to improve the solubility of the complexes by introducing a *tert*-butyl group at the chelate ligand $HL^{t\mathbf{Bu}}$ and (ii) to modify solubility and electronics by replacing one oxido ligand by a *tert*-butyl imido ligand. In this report we describe our attempts to stabilize and characterize mononuclear Mo^{IV} and Mo^V complexes with imido ligands and two dissymmetric chelate ligands X∩Y. Parallel to our work on mixed imido/oxido complexes for oxygen atom transfer studies the group of Mösch-Zanetti recently reported the synthesis of $Mo^{VI}O(NtBu)(X{\cap}Y)_2$ complexes with bidentate β-diketiminato supporting ligands (Chart 1, **B**).[11] Six-coordinate mixed imido/oxido complexes **C1** and **C2** with tetradentate salpen and salen ligands have also been reported by Sullivan (Chart 1).[12] Tetrahedral and pseudotetrahedral Mo^{VI} complexes with a mixed imido/oxido donor set have also been reported.[18−21] As can be seen from Chart 1, the

Received: December 1, 2011
Published: March 20, 2012

Chart 1. Ligands $(L^R)^-$ and Dioxido Molybdenum(VI) Complexes A of Bidentate Imino Pyrrolato Chelate Ligands $(L^R)^-$,[7−9] Imido/Oxido Molybdenum(VI) Complexes B of Bidentate β-Diketiminato Ligands,[11] and Imido/Oxido Molybdenum(VI) Complexes C1/C2 of Tetradentate Schiff Base Ligands[12] [a]

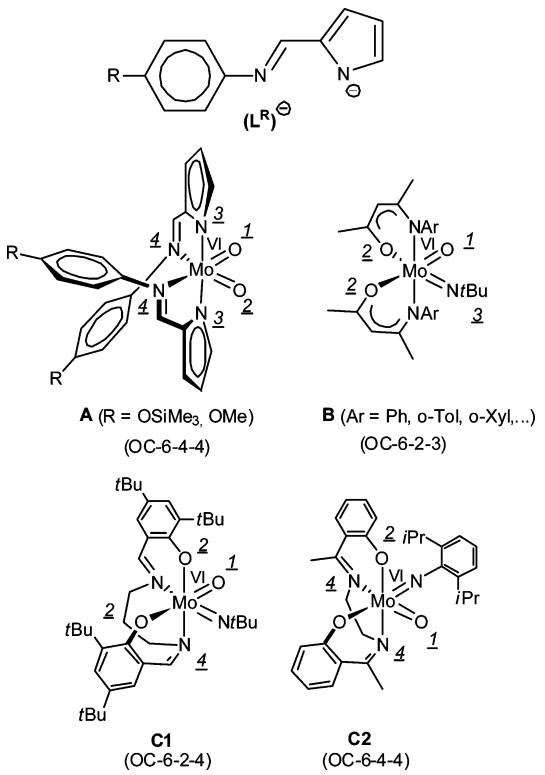

[a]The underlined numbers indicate the CIP priority for the stereodescriptor.[13−17]

stereochemistry (**C1**, **C2**)[13−17] is not easily predicted in six-coordinate imido/oxido Mo^{VI} complexes. Even less is known about the stereochemistry of six-coordinate Mo^{IV} and Mo^{V} complexes with dissymmetric X∩Y chelate ligands. To the best of our knowledge, a detailed stereochemical and electronic analysis of Mo^{IV} and Mo^{V} complexes derived from $Mo^{VI}O(NtBu)(X∩Y)_2$ complexes by OAT and SET has not been reported yet.

EXPERIMENTAL SECTION

General Procedures. All reactions were performed under an inert atmosphere (Schlenk techniques, glovebox). THF was distilled from potassium, diethyl ether, petroleum ether 40−60 °C, triethyl amine, and acetonitrile from calcium hydride. $MoCl_2O_2(dme)$[22] and $MoCl_2(NtBu)O(dme)$[20,23] were prepared according to literature procedures. All other reagents were used as received from commercial suppliers (Acros, Sigma-Aldrich). NMR spectra were recorded on a Bruker Avance DRX 400 spectrometer at 400.31 (^{1}H), 100.66 (^{13}C{^{1}H}), 162.05 (^{31}P{^{1}H}), and 40.56 MHz (^{15}N). All resonances are reported in ppm versus the solvent signal as internal standard [d_8-THF (^{1}H: δ = 1.24, 3.57; ^{13}C: δ = 25.5, 67.7 ppm)], versus external H_3PO_4 (85%) (^{31}P: δ = 0 ppm) or versus external CH_3NO_2 (90% in $CDCl_3$) (^{15}N: δ = 380.23 ppm). ^{15}N data are reported vs liquid NH_3 as reference (δ = 0 ppm). IR spectra were recorded with a BioRad Excalibur FTS 3100 spectrometer as KBr disks. Electrochemical experiments were carried out on a BioLogic SP-50 voltammetric analyzer using platinum wires as counter and working electrodes and a 0.01 *m* $Ag/AgNO_3$ electrode as reference electrode. Cyclic voltammetry measurements were carried out at a scan rate of 50−100 mV s^{-1} using 0.1 *m* (nBu_4N)($B(C_6F_5)_4$) as supporting electrolyte in THF. Potentials are referenced to the ferrocene/ferrocenium couple ($E_{1/2}$ = 270 ± 5 mV under the experimental conditions). UV−vis−NIR spectra were recorded on a Varian Cary 5000 spectrometer using 1.0 cm cells (Hellma, suprasil). FD mass spectra were recorded on a FD Finnigan MAT90 spectrometer. ESI mass spectra were recorded on a Micromass Q-TOF-Ultima spectrometer. X-band CW EPR spectra were recorded on a Magnettech MS 300 spectrometer with a frequency counter Hewlett-Packard 5340A at a microwave frequency of 9.39 GHz in THF or frozen THF solution (77 K). Mn^{2+} in ZnS was used as external standard. Simulations were performed with the program package EasySpin.[24] Details of the HYSCORE experiments can be found in the Supporting Information. Elemental analyses were performed by the microanalytical laboratory of the chemical institutes of the University of Mainz.

Crystal Structure Determination. Intensity data were collected with a Bruker AXS Smart1000 CCD diffractometer with an APEX II detector and an Oxford cooling system and corrected for absorption and other effects using Mo Kα radiation (λ = 0.71073 Å) at 173(2) K. Diffraction frames were integrated using the SAINT package, and most were corrected for absorption with MULABS.[25,26] Structures were solved by direct methods and refined by the full-matrix method based on F^2 using the SHELXTL software package.[27,28] All non-hydrogen atoms were refined anisotropically, while the positions of all hydrogen atoms were generated with appropriate geometric constraints and allowed to ride on their respective parent carbon atoms with fixed isotropic thermal parameters. Crystallographic data (excluding structure factors) for the structures reported in this paper have been deposited with the Cambridge Crystallographic Data Centre as supplementary publication nos. CCDC-831113 (HL^{tBu}), 831108 (1^{tBu}), 831109 (2^{tBu}), 831110 (4^{tBu}), 831112 (5^{tBu}), and 831111 ($[5^{tBu}](PF_6)$). Copies of the data can be obtained free of charge on application to CCDC, 12 Union Road, Cambridge CB2 1EZ, U.K. (fax (0.44) 1223-336-033; e-mail deposit@ccdc.cam.ac.uk).

Density functional calculations were carried out with the Gaussian03/DFT[29] series of programs. The B3LYP formulation of density functional theory was used employing the LANL2DZ basis set with d-type polarization functions on O (ζ = 1.154), N (ζ = 0.864), and P (ζ = 0.340) for geometry optimization.[30] No symmetry constraints were imposed on the molecules. For calculations of EPR parameters the EPR-II basis set[31] was used for C, H, and N, the WTBS basis set[32] for Mo, and 6-311++G(2d,2p) for P. For some calculations a solvent model was employed (integral equation formalism polarizable continuum model; IEFPCM; THF).

Synthesis of HL^{tBu}. 1*H*-Pyrrole-2-carbaldehyde (2 g, 21.03 mmol), 4-*tert*-butylaniline (3.35 mL, 21.03 mmol), $MgSO_4$ (2 g, 16.61 mmol), and ethyl acetate (100 mL) were heated under reflux for 4 h. The suspension was filtered while hot, and the solvent was removed under reduced pressure. The resulting orange-colored oil solidified upon cooling, and the solid was recrystallized from acetonitrile, giving pale yellow crystals in 75% yield (3.56 g, 15.72 mmol). Mp 116 °C. ^{1}H NMR (d_8-THF): δ = 11.09 (br s, 1H, NH), 8.27 (s, 1H, H^7), 7.37 (d, 2H, $H^{3,5}$, $^3J_{HH}$ = 8.8 Hz), 7.10 (d, 2H, $H^{2,6}$, $^3J_{HH}$ = 8.8 Hz), 6.93 (s, 1H, H^{11}), 6.60 (dvd, 1H, H^9), 6.20 (dvd, 1H, H^{10}), 1.33 (s, 9H, CH_3). ^{13}C{^{1}H} NMR (d_8-THF): δ = 151.2 (s, C^1), 150.1 (s, C^7), 148.6 (s, C^4), 132.5 (s, C^8), 126.7 (s, $C^{3,5}$), 123.8 (s, C^{11}), 121.3 (s, $C^{2,6}$), 116.8 (s, C^9), 110.5 (s, C^{10}), 35.2 (s, C^q), 32.1 (s, CH_3). ^{15}N NMR (d_8-THF): δ = 285.6 (N^p), 199.8 (N^i). IR (KBr): ν = 3131 (w, NH), 2953 (m, CH_3), 1618 (m, C=N), 1587 (s), 1500 (m), 1418 (m), 1034 (m) cm^{-1}. UV−vis (THF): λ = 329 (22 560 M^{-1} cm^{-1}) nm. MS (FD): *m*/*z* (%) = 226.2 (100, M^+). Anal. Calcd. for $C_{15}H_{18}N_2$ (226.31): C, 79.61; H, 8.02; N, 12.38. Found: C, 79.38; H, 8.16; N, 12.16.

Synthesis of 1^{tBu}. The ligand HL^{tBu} (346 mg, 1.19 mmol) was dissolved in THF (20 mL) and deprotonated with triethyl amine (1.0 mL, 7.14 mmol) for 30 min. In a separate flask $MoCl_2O_2(dme)$[22] (539 mg, 2.38 mmol) was dissolved in THF (50 mL), and the deprotonated ligand was added. After heating to reflux for 3 h the suspension was filtered, and the red filtrate was dried under reduced pressure. The

dx.doi.org/10.1021/ic202588u | Inorg. Chem. 2012, 51, 4180−4192

product was washed three times with methanol and dried under reduced pressure, giving a red crystalline solid in 81% yield (555 mg, 0.96 mmol). Mp 199 °C. ^{1}H NMR (d_8-THF): δ = 7.95 (s, 1H, H^7), 7.25 (s, 1H, H^{11}), 7.16 (d, $^3J_{HH}$ = 8.43 Hz, 2H, H^{3,5}), 6.99 (d, $^3J_{HH}$ = 8.43 Hz, 2H, H^{2,6}), 6.35 (d, 1H, H^9), 6.08 (dd, 1H, H^{10}), 1.26 (s, 9H, CH$_3$). ^{13}C{^{1}H} NMR (d_8-THF): δ = 158.6 (s, C^7), 149.4 (s, C^4), 147.2 (s, C^1), 144.0 (s, C^{11}), 140.1 (s, C^8), 126.0 (s, C^{3,5}), 122.4 (s, C^{2,6}), 120.0 (s, C^9), 115.2 (s, C^{10}), 35.2 (s, C^q), 31.8 (s, CH$_3$). ^{15}N NMR (d_8-THF): δ = 248.3 (N^i), 215.1 (N^p). IR (KBr): ν = 2959 (m, CH$_3$), 1606 (m, C=N), 1581 (s), 1500 (m), 1431 (m), 1399 (s), 1296 (m), 1038 (m), 928 (m, Mo=O), 902 (m, Mo=O) cm^{-1}. UV−vis (THF): λ = 235 (32 345), 303 (66 760), 436 (9440 M^{-1} cm^{-1}) nm. MS (FD): m/z (%) = 578.5 (76, M$^+$). CV (THF): E_p = −0.86 V (irr). Anal. Calcd for $C_{30}H_{34}N_4O_2Mo$ (578.55): C, 62.28; H, 5.92; N, 9.68. Found: C, 60.93; H, 6.18; N, 9.50.

Synthesis of 2^{tBu}. The ligand **HL^{tBu}** (1.32 g, 5.8 mmol) was dissolved in THF (15 mL) and deprotonated with triethyl amine (2.4 mL, 17 mmol) for 30 min. In a separate flask $MoCl_2$(N*t*Bu)O-(dme)[20,23] (1.0 g, 2.9 mmol) was dissolved in THF (50 mL), and the deprotonated ligand was added. After heating to reflux for 7 h the suspension was filtered, and the red filtrate was dried under reduced pressure (95% raw yield). The product was washed with petroleum ether 40−60 °C (1:1), giving an orange-colored crystalline solid in 50% yield (950 mg, 1.5 mmol). Mp 174 °C. ^{1}H NMR (d_8-THF): δ = 7.89 (s, 1H, H$^{7'}$), 7.76 (s, 1H, H^7), 7.28 (m, 1H, H$^{11'}$), 7.14 (m, 1H, H^{11}), 7.11 (d, $^3J_{HH}$ = 8.6 Hz, 2H, H$^{3',5'}$), 7.08 (d, $^3J_{HH}$ = 8.5 Hz, 2H, H^{3,5}), 6.99 (d, $^3J_{HH}$ = 8.5 Hz, 2H, H$^{2',6'}$), 6.78 (d, $^3J_{HH}$ = 8.5 Hz, 2H, H^{2,6}), 6.34 (dvd, 1H, H^9), 6.27 (dvd, 1H, H$^{9'}$), 6.11 (dvd, 1H, H^{10}), 6.06 (dvd, 1H, H$^{10'}$), 1.50 (s, 9H, NC(CH$_3$)), 1.25 (2 s, 18H, CH$_3$/CH$_3$′). ^{13}C{^{1}H} NMR (d_8-THF): δ = 157.4 (s, C^7), 156.6 (s, C$^{7'}$), 148.8 (s, C$^{4'}$), 148.4 (s, C^4), 148.1 (s, C^1), 147.1 (s, C$^{1'}$), 143.2 (s, C$^{11'}$), 142.2 (s, C^{11}), 140.9 (s, C$^{8'}$), 139.1 (s, C^8), 125.8 (pd, C$^{3,5,3',5'}$), 122.4 (s, C^{2,6}), 122.0 (s, C$^{2',6'}$), 118.9 (s, C$^{9'}$), 118.2 (s, C^9), 114.3 (s, C$^{10'}$), 114.2 (s, C^{10}), 35.1 (s, C$^{q,q'}$), 31.9 (s, CH$_3$, CH$_3$′), 30.2 (s, NC−CH$_3$), 73.0 (s, NC−CH$_3$). ^{15}N NMR (d_8-THF): δ = 477.4 (N^{imido}), 253.2 (N$^{i'}$), 242.6 (N^i), 213.3 (N$^{p'}$), 205.1 (N^p). IR (KBr): ν = 2961 (m, CH$_3$), 1580 (s), 1518 (m), 1433 (w), 1395 (m), 1298 (m), 1039 (m), 897 (s, Mo=O) cm^{-1}. UV−vis (THF): λ = 296 (16 780), 395 (8335 M^{-1} cm^{-1}) nm. MS (FD): m/z (%) = 633.4 (86, M$^+$). CV (THF): E_p = −0.87 V (irr). Anal. Calcd for $C_{34}H_{43}N_5OMo$ (633.67): C, 64.44; H, 6.84; N, 11.05. Found: C, 63.34; H, 5.96; N, 11.04.

Synthesis of 4^{tBu}. Dioxido complex **1^{tBu}** (360 mg, 0.55 mmol) was dissolved in THF (20 mL), and trimethylphosphane (1 M in THF, 3.11 mL, 3.02 mmol) was added. After stirring for 7 days at room temperature volatiles were removed under reduced pressure to give a green powder in 91% yield (320 mg, 0.50 mmol). Attempts to completely remove the phosphane oxide by recrystallization from THF failed. Mp 203 °C (dec.). ^{1}H NMR (d_8-THF): δ = 8.00 (d, $^4J_{PH}$ = 2.3 Hz, 1H, H^7), 7.63 (bs, 1H, H^{11}), 7.50 (bs, 1H, H$^{7'}$), 7.24 (d, $^3J_{HH}$ = 8.7 Hz, 2H, H$^{3',5'}$), 7.11 (d, $^3J_{HH}$ = 8.7 Hz, 2H, H$^{2',6'}$), 7.08 (d, $^3J_{HH}$ = 8.5 Hz, 2H, H^{3,5}), 7.01 (d, $^3J_{HH}$ = 2.7 Hz, 2H, H^9), 6.61 (d, $^3J_{HH}$ = 8.5 Hz, 2H, H^{2,6}), 6.5 (dd, 1H, H^{10}), 6.33 (dd, 1H, H$^{9'}$), 6.32 (pd, 1H, H$^{10'}$), 5.80 (bs, 1H, H$^{11'}$), 1.34 (s, 9H, CH$_3$′), 1.31 (s, 9H, CH$_3$), 1.31 (d, $^2J_{PH}$ = 8.5 Hz, 9H, P(CH$_3$)$_3$). ^{13}C{^{1}H} NMR (d_8-THF): δ = 158.0 (s, C^7), 151.9 (s, C$^{1'}$), 151.2 (s, C$^{7'}$), 150.9 (s, C^1), 148.8 (s, C^4), 148.7 (s, C$^{4'}$), 147.9 (s, C^{11}), 144.9 (s, C^8), 141.3 (s, C$^{8'}$), 138.5 (s, C$^{11'}$), 126.2 (s, C^{3,5}), 125.8 (s, C$^{3',5'}$), 124.0 (s, C$^{2',6'}$), 123.0 (s, C^{2,6}), 119.3 (s. C^9), 115.8 (s. C$^{9'}$), 114.9 (s. C^{10}), 113.6 (s. C$^{10'}$), 35.2 (pd, C$^{q,q'}$), 32.0 (s, CH$_3$, CH$_3$′), 16.4 (d, $^1J_{PC}$ = 23.4 Hz, P(CH$_3$)$_3$). ^{31}P{^{1}H} NMR (d_8-THF): δ = 1.3 (s, major), −5.3 (s, minor) ppm. ^{31}P NMR (d_8-THF): δ = 1.3 (m, major, $^2J_{PH}$ = 8.5 Hz, $^4J_{PH}$ = 2.3 Hz). ^{15}N NMR (d_8-THF): δ = 236.6 (N^i, N$^{i'}$), 230.3 (N$^{p'}$), 219.0 (N^p). IR (KBr): ν = 2960 (w, CH$_3$), 1506 (w), 1390 (w), 935 (m, Mo=O) cm^{-1}. UV−vis (THF): λ = 303 (8160), 345 (8180), 386 (sh), 479 (1420), 610 (250), 715 (200 M^{-1} cm^{-1}) nm. MS (FD): m/z (%) = 638.4 (100, M$^+$). CV (THF): E_p = −0.29 V (irr).

Synthesis of 5^{tBu}. Imido/oxido complex **2^{tBu}** (400 mg, 0.63 mmol) was dissolved in THF (10 mL), and trimethylphosphane (1 M in THF, 5.00 mL, 5.0 mmol) was added. After stirring for 4 days at room temperature volatiles were removed under reduced pressure to give a black powder in 74% yield (325 mg, 0.47 mmol). Repeated recrystallization with a high loss of material was necessary to obtain a product almost free of $OPMe_3$. Mp 133 °C (dec.). ^{1}H NMR (d_8-THF): δ = 7.85 (d, $^4J_{PH}$ = 2.8 Hz, 1H, H^7), 7.37 (bs, 1H, H^{11}), 7.28 (bs, 1H, H$^{7'}$), 7.17 (d, $^3J_{HH}$ = 8.3 Hz, 2H, H^{3,5}), 7.15 (d, $^3J_{HH}$ = 8.3 Hz, 2H, H$^{3',5'}$), 6.85 (d, $^3J_{HH}$ = 2.8 Hz, 1H, H^9), 6.79 (d, $^3J_{HH}$ = 8.6 Hz, 2H, H$^{2',6'}$), 6.64 (d, $^3J_{HH}$ = 8.5 Hz, 2H, H^{2,6}), 6.31 (dd, $^3J_{HH}$ = 1.9 Hz, 1H, H^{10}), 6.30 (d, $^3J_{HH}$ = 3.4 Hz, 1H, H$^{9'}$), 5.85 (dd, $^3J_{HH}$ = 1.7 Hz, 1H, H$^{10'}$), 5.73 (bs, 1H, H$^{11'}$), 1.30 (2 s, 18H, CH$_3$/CH$_3$′), 1.24 (d, $^2J_{PH}$ = 7.8 Hz, 9H, P(CH$_3$)$_3$), 1.01 (s, 9H, NC(CH$_3$)). ^{13}C{^{1}H} NMR (d_8-THF): δ = 157.9 (s, C^7), 153.8 (s, C$^{1'}$), 152.0 (s, C^1), 148.4 (s, C$^{4'}$), 148.2 (2 s, C$^{4,7'}$), 145.4 (s, C^{11}), 144.8 (s, C$^{8'}$), 142.2 (s, C^8), 136.2 (s, C$^{11'}$), 125.8 (s, C^{3,5}), 125.2 (s, C$^{3',5'}$), 123.8 (s, C$^{2',6'}$), 123.2 (s, C^{2,6}), 117.3 (s, C^9), 113.7 (s, C$^{9'}$), 112.9 (s, C^{10}), 112.7 (s, C$^{10'}$), 35.0 (2 s, C$^{q,q'}$), 31.8 (2 s, CH$_3$, CH$_3$′), 30.7 (s, NC−CH$_3$), 69.1 (s, NC−CH$_3$), 18.7 (d, $^1J_{PC}$ = 22.3 Hz, P(CH$_3$)$_3$). ^{31}P{^{1}H} NMR (d_8-THF): δ = 9.2 (s) ppm. ^{31}P NMR (d_8-THF): δ = 9.2 (m, $^2J_{PH}$ = 7.8 Hz, $^4J_{PH}$ = 2.8 Hz). ^{15}N NMR (d_8-THF): δ = 273.7 (N^{imido}), 252.2 (N$^{i'}$), 234.2 (N^i), 231.1 (N$^{p'}$), 212.0 (N^p). IR (KBr): ν = 2963 (w, CH$_3$), 1573 (s), 1506 (m), 1433 (w), 1389 (m), 1296 (m), 1035 (m) cm^{-1}. UV−vis (THF): λ = 299 (10 820), 340 (10 080), 377 (sh), 490 (1465), 594 (1000), 735 (265 M^{-1} cm^{-1}) nm. MS (FD): m/z (%) = 693.5 (82, M$^+$). CV (THF): $E_{1/2}$ = −0.71 V (rev oxidation). Anal. Calcd for $C_{37}H_{52}N_5MoP$ (693.77): C, 64.06; H, 7.55; N, 10.09. Found: C, 63.03; H, 7.67; N, 10.55.

Oxidation of 4^{tBu}. Oxido phosphane complex **4^{tBu}** (50 mg, 0.076 mmol) was dissolved in THF (5 mL), and a suspension of ferrocenium hexafluorophosphate (26 mg, 0.078 mmol) in THF (5 mL) was added. After stirring for 12 h at room temperature the solvent was removed under reduced pressure, giving a dark brown product (55 mg, possibly several paramagnetic species of unknown composition, see text). EPR (THF, 298 K): g_{iso} = 1.9459, A_{iso}($^{95/97}$ Mo) = 49.8 G. EPR (THF, 77 K): $g_{1,2,3}$ = 1.9618, 1.9555, 1.9362.

Synthesis of [5^{tBu}](PF$_6$). Imido phosphane complex **5^{tBu}** (100 mg, 0.144 mmol) was dissolved in THF (5 mL), and a suspension of ferrocenium hexafluorophosphate (47.7 mg, 0.144 mmol) in THF (5 mL) was added. After stirring for 12 h at room temperature the solvent was removed under reduced pressure, giving a black product, which was washed with petroleum ether 40−60 °C and repeatedly recrystallized from THF/petroleum ether 40−60 °C. The yield after the first recrystallization was 75 mg (0.09 mmol, 62%). Mp 151 °C (dec.). EPR (THF, 298 K): g_{iso} = 1.9810, A_{iso}($^{95/97}$ Mo) = 40.3 G, A_{iso}(^{31}P) = 28.7 G. EPR (THF, 77 K): $g_{1,2,3}$ = 1.9825, 1.9785, 1.9615, $A_{1,2,3}$(^{31}P) = 23, 33, 29 G. HYSCORE (THF, 20 K): $A_{1,2,3}$(^{14}N$_{large}$) = 1.5, 2.0, 3.8 G, $A_{1,2,3}$(^{14}N$_{small,A}$) = 1.3, 1.4, 1.7 G, $A_{1,2,3}$(^{14}N$_{small,B}$) = 0.8, 0.8, 0.9 G, $A_{1,2,3}$(^{1}H) = 3.4, 4.1, 5.0 G, A_{iso}(^{14}N$_{large}$) = 2.4 G, A_{iso}(^{14}N$_{small,A}$) = 1.5 G, A_{iso}(^{14}N$_{small,B}$) = 0.8 G, A_{iso}(^{1}H) = 4.2 G. IR (KBr): ν = 2962 (w, CH$_3$), 1572 (m), 1506 (w), 1433 (w), 1390 (m), 1269 (m), 840 (s, PF) cm^{-1}. UV−vis (THF): λ = 298 (29 865), 405 (12 815, sh), 532 (1165, sh), 787 (905 M^{-1} cm^{-1}) nm. MS (ESI+): m/z (%) = 693.3 (81, M$^+$). CV (THF): $E_{1/2}$ = −0.73 V (rev reduction). μ_{eff} (THF, 298 K) = 1.71 ± 0.05 μ_B. Anal. Calcd for $C_{37}H_{52}N_5MoP_2F_6$ (838.73): C, 52.99; H, 6.25; N, 8.35. Found: C, 51.98; H, 7.34; N, 7.97.

RESULTS AND DISCUSSION

All complex syntheses performed as well as compound abbreviations are summarized in Scheme 1.

Synthesis and Properties of the Chelate Ligand and Its Mo(VI) Complexes. The highly soluble chelate ligand **HL^{tBu}** is easily obtained by Schiff base condensation of pyrrole-2-carbaldehyde and 4-(*tert*-butyl)aniline in the presence of magnesium sulfate in high yield similar to comparable syntheses.[7,8] It crystallizes from CH_3CN in the space group *Cc* as colorless long bricks with two independent molecules in the unit cell (Figure 1). The two molecules differ only in the aryl torsion angles C7−C8−N1−C11 = −20.8(2)°/C24−C23−N3−C26 = −31.6(2)°, and they are linked by N−H···N

dx.doi.org/10.1021/ic202588u | *Inorg. Chem.* 2012, 51, 4180−4192

Scheme 1. Synthesis of Molybdenum Complexes of Ligand HL^{tBu} (R = *t*Bu) and Atom Numbering for NMR Assignments

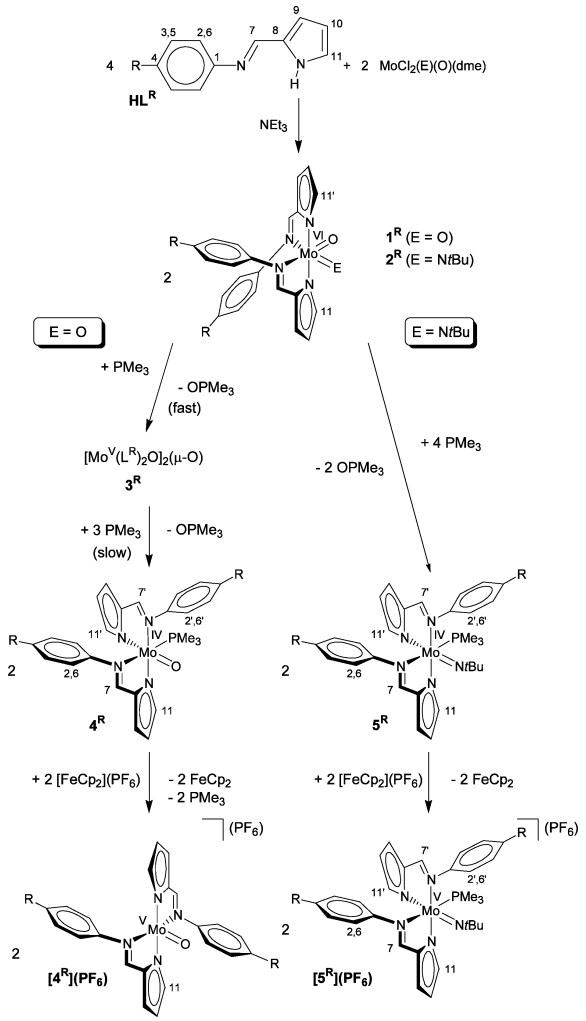

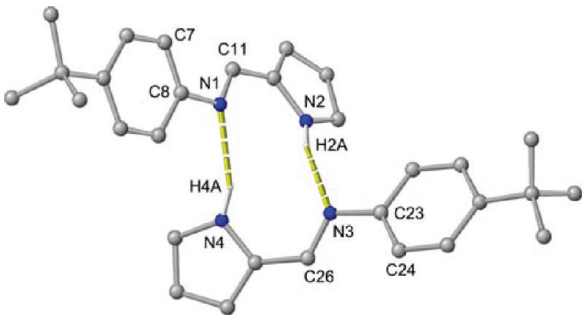

Figure 1. Molecular structure and intermolecular hydrogen bonding of HL^{tBu} in the crystal (CH hydrogen atoms omitted for clarity).

hydrogen bonds to give a dimer with an $R^2_2(10)$ motif[33,34] (N2···N3 = 2.987(2) Å; N4···N1 = 3.008(2) Å).

The bis(chelate) dioxido complex $\mathbf{1}^{tBu}$ was prepared similar to literature procedures[7,8] for $\mathbf{1}^{R}$ (R = OMe, $OSiMe_3$) from $MoCl_2O_2(dme)$[12] and the chelate ligand HL^{tBu} in the presence of triethyl amine as red crystalline solid. The mixed imido/oxido complex $\mathbf{2}^{tBu}$ was prepared from the convenient precursor complex $MoCl_2(NtBu)(O)(dme)$[20,23] and HL^{tBu} in the presence of triethyl amine as yellow solid. Both *tert*-butyl-substituted complexes $\mathbf{1}^{tBu}$ and $\mathbf{2}^{tBu}$ are excellently soluble in typical organic solvents like THF or diethyl ether, which greatly facilitates purification, spectroscopic characterization, and crystallization.

The most stable stereoisomer of $\mathbf{1}^{R}$ is the OC-6-4-4 isomer[13−17] with the two oxido ligands in cis positions as expected for d^0 complexes and each oxido ligand trans to the imine nitrogen atoms of the chelate ligands.[8] In the infrared spectrum of the *tert*-butyl derivative $\mathbf{1}^{tBu}$ the absorptions of the two Mo═O vibrations are found at 928 and 902 cm^{-1}, consistent with the expected cis dioxido moiety.[7,8] The proton NMR spectrum of $\mathbf{1}^{tBu}$ displays a single signal set for two chelate ligands, suggesting the presence of one diastereomer with C_2 symmetry. Upon coordination of the chelate to molybdenum the resonance of proton H^{11} experiences a large coordination shift to lower field from δ = 6.93 ppm to δ = 7.25 ppm, while the resonance of imine proton H^7 shifts from δ = 8.27 ppm to δ = 7.95 ppm. The nitrogen nuclei of ligand HL^{tBu} resonate at δ = 199.8 (N^i = N^{imine}) and 285.6 ppm (N^p = $N^{pyrrolato}$). These resonances are considerably shifted to δ = 248.3 (N^i) and 215.1 ppm (N^p) in the Mo^{VI} complex $\mathbf{1}^{tBu}$ (cf. $\mathbf{1}^{OSiMe3}$ [9]). Single-crystal X-ray structure analysis of $\mathbf{1}^{tBu}$ corroborates the proposed OC-6-4-4 stereochemistry (Figure 2). $\mathbf{1}^{tBu}$ crystallized from diethyl ether in the monoclinic space

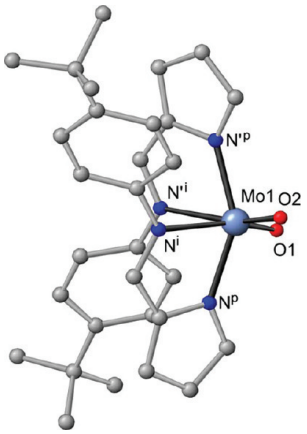

Figure 2. Molecular structure of $\mathbf{1}^{tBu}$ in the crystal (CH hydrogen atoms omitted for clarity).

group $P2_1/c$ with two independent molecules in the asymmetric unit (Table 1). DFT calculations (B3LYP, LANL2DZ with d-type polarization functions on O[30]) for the model system $\mathbf{1}^{H}$ are also in good agreement with the experimental metrical data (Table 2).[8]

In a previously reported mixed imido/oxido $Mo^{VI}(O)(NtBu)$(salpen) complex **C1** (Chart 1) the tetradentate salpen ligand with a $(CH_2)_3$ linker between the imino donor atoms induces an OC-6-2-4 configuration (imido/oxido cis to each other, oxido trans to phenolato, and imido trans to imine), while a salen ligand with a $(CH_2)_2$ linker between the imino donor atoms and a bulky aryl−imido ligand N(2,6-*i*Pr-C_6H_3) favors the OC-6-4-4 isomer **C2** (imido/oxido cis to each other, oxido trans to imine, and imido trans to phenolato).[12] Two bidentate β-diketiminato ligands induce OC-6-2-3 stereochemistry (complexes of type **B**, Chart 1).[11]

dx.doi.org/10.1021/ic202588u | *Inorg. Chem.* 2012, 51, 4180−4192

Table 1. Crystallographic Data and Structure Refinement of HL^{tBu}, 1^{tBu}, 2^{tBu}, 4^{tBu}, 5^{tBu}, and $[5^{tBu}](PF_6)$

	HL^{tBu}	1^{tBu}	2^{tBu}	4^{tBu}	5^{tBu}	$[5^{tBu}](PF_6)$
empirical formula	$C_{15}H_{18}N_2$	$C_{30}H_{34}MoN_4O_2$	$C_{34}H_{43}MoN_5O$	$C_{33}H_{43}MoN_4OP$	$C_{37}H_{52}MoN_5P$	$C_{45}H_{68}MoN_5O_2P_2F_6$
fw	226.31	578.55	633.67	638.62	693.75	982.92
cryst syst	monoclinic	monoclinic	tetragonal	monoclinic	monoclinic	orthorhombic
space group	*Cc*	$P2_1/c$	$I4_1/a$	$C2/c$	$P2_1/n$	*Pbca*
a/Å	11.3992(5)	16.2627(5)	25.2905(8)	35.703(7)	11.8934(6)	18.8771(9)
b/Å	16.8185(7)	25.0561(7)	25.2905(8)	7.4514(14)	24.7875(12)	19.6195(10)
c/Å	13.8657(6)	14.8107(5)	21.4037(14)	28.794(5)	12.7566(7)	26.9700(14)
β/deg	97.3820(10)	110.3530(10)	90	122.153(5)	94.515(2)	90
volume/Å^3	2636.3(2)	5658.3(3)	13690.0(11)	6485(2)	3749.1(3)	9988.6(9)
Z	8	8	16	8	4	8
density (calcd), Mg m^3	1.140	1.358	1.230	1.308	1.229	1.307
abs coeff, mm^{-1}	0.068	0.496	0.415	0.484	0.423	0.389
F(000)	976	2400	5312	2672	1464	4120
cryst size, mm^3	0.65 × 0.44 × 040	0.26 × 0.22 × 0.08	0.06 × 0.02 × 0.02	0.15 × 0.03 × 0.02	0.33 × 0.30 × 0.12	0.15 × 0.05 × 0.02
θ range for data collection	2.42−25.23	2.28−27.96	2.22−27.89	2.29−28.07	2.29−28.07	2.39−27.92
index ranges	$-13 \le h \le 13$	$-21 \le h \le 21$	$-33 \le h \le 33$	$-46 \le h \le 46$	$-15 \le h \le 15$	$-24 \le h \le 24$
	$-20 \le k \le 20$	$-32 \le k \le 32$	$-33 \le k \le 33$	$-9 \le k \le 9$	$-32 \le k \le 32$	$-25 \le k \le 25$
	$-16 \le h \le 16$	$-19 \le h \le 19$	$-28 \le h \le 28$	$-36 \le h \le 37$	$-16 \le h \le 16$	$-35 \le h \le 35$
no. of reflns collected	12 407	65 502	110 537	37 366	43 312	215 807
no. of indep reflns	4555	13 533	8179	7840	9016	11 896
R_{int}	0.0617	0.0932	0.2109	0.1764	0.0712	0.1033
completeness to θ_{max}	100.0	99.4	99.8	99.5	98.9	99.4
max/min transmn		0.9614/0.8818	0.990/0.992	0.9904/0.9309	0.9510/0.8730	0.9923/0.9440
goodness-of-fit on F^2	1.050	0.908	0.761	0.886	0.900	1.117
final *R* indices $[I > 2\sigma(I)]$	R_1 = 0.0323	R_1 = 0.0412	R_1 = 0.0381	R_1 = 0.0622	R_1 = 0.0334	R_1 = 0.0562
	wR_2 = 0.0817	wR_2 = 0.0721	wR_2 = 0.0567	wR_2 = 0.1029	wR_2 = 0.0666	wR_2 = 0.1474
R indices (all data)	R_1 = 0.0347	R_1 = 0.0752	R_1 = 0.1054	R_1 = 0.1640	R_1 = 0.0638	R_1 = 0.0916
	wR_2 = 0.0830	wR_2 = 0.0824	wR_2 = 0.0673	wR_2 = 0.1185	wR_2 = 0.0747	wR_2 = 0.1602
largest diff peak and hole, e/Å^3	0.137/−0.135	0.547/−0.805	0.347/−0.332	1.011/−0.613	0.425/−0.720	0.536/−0.562

Table 2. Selected Bond Lengths (Angstroms) and Angles (degrees) of 1^{tBu}, 2^{tBu}, 4^{tBu}, 5^{tBu}, and $[5^{tBu}](PF_6)$

	1^{tBu} (2 molecules)	2^{tBu}	4^{tBu}	5^{tBu}	$[5^{tBu}](PF_6)$
Mo1−O1	1.698(2)/1.702(2)	1.705(2)	1.686(4)		
Mo1−O2	1.702(2)/1.704(2)				
Mo1−N^{imido}		1.731(2)		1.743(2)	1.739(3)
Mo1−N^{i}	2.320(2)/2.349(2)	2.375(2)	2.182(4)	2.220(2)	2.198(3)
Mo1−N^{p}	2.081(2)/2.073(2)	2.129(2)	2.126(4)	2.155(2)	2.110(3)
Mo1−N^{i}	2.351(2)/2.353(2)	2.401(2)	2.213(4)	2.201(2)	2.143(3)
Mo1−N^{p}	2.066(2)/2.079(2)	2.087(2)	2.272(5)	2.218(2)	2.212(3)
Mo1−P1			2.482(2)	2.4532(6)	2.549(1)
Mo1−N^{imido}-C^{imido}		159.1(2)		178.7(2)	172.8(3)
O1−Mo1−O2	105.54(9)/106.0(1)				
O1−Mo1−N^{imido}		103.5(1)			
P1−Mo1−O1			92.3(1)		
P1−Mo1−N^{imido}				92.53(6)	99.2(1)

For our mixed imido/oxido complex 2^{tBu} DFT calculations on 2^{H} (B3LYP, LANL2DZ with d-type polarization functions on O and N[30]) suggest the OC-6-4-4 stereoisomer as the most stable one similar to the dioxido complex 1^{tBu} (Figure 3). The other plausible stereoisomers OC-6-3-4, OC-6-4-3, and OC-6-3-3 are calculated higher in energy by 6.7, 22.4, and 36.1 kJ mol^{-1}, respectively (Figure 3).

In any case, introduction of the imido ligand reduces the complex symmetry from C_2 (1^{tBu}) to C_1 (2^{tBu}). Thus, in the NMR spectra of 2^{tBu} two signal sets are expected for the two chelate ligands L and L′. For example, the resonances of H^{11}/$H^{11'}$ are found at δ = 7.14/7.28 ppm, and the resonances of H^{7}/$H^{7'}$ are observed at δ = 7.76/7.89 ppm. The ^{15}N resonances of 2^{tBu} are recorded at δ = 242.6/253.2 (N^{i}/N^{i}), 205.1/213.3 (N^{p}/N^{p}), and 477.4 ppm (N^{imido}). Proton−proton, nitrogen−proton, and carbon−proton correlation spectroscopy allowed us to unambiguously assign all proton signals to the two different coordinated chelate ligands (L^{tBu}: $H^{2,6}$/$H^{3,5}$/H^{7}/H^{9}/H^{10}/H^{11}; L'^{tBu}: $H^{2',6'}$/$H^{3',5'}$/$H^{7'}$/$H^{9'}$/$H^{10'}$/$H^{11'}$). Several *inter-ligand* nuclear Overhauser contacts which are relevant for the relative ligand orientations are observed for 2^{tBu}, namely, $H^{11'} \leftrightarrow H^{2,6}$, $H^{11'} \leftrightarrow H^{tBu,imido}$, $H^{7'} \leftrightarrow H^{2,6}$, and $H^{7} \leftrightarrow H^{2',6'}$. Some of these NOE contacts are indicated in Figure 3 for the calculated stereoisomers. The $H^{11'} \leftrightarrow H^{tBu,imido}$ correlation places the pyrrolato ring of L'^{tBu} (N'^{p}) in the cis position to the *tert*-butyl imido ligand with the $C^{11'}$−$H^{11'}$ vector oriented in the Mo=N-*t*Bu direction, i.e., the N'^{i} atom is located trans to N*t*Bu. This is fulfilled for the OC-6-4-4 and OC-6-3-4 isomers. A short $H^{11'}$

dx.doi.org/10.1021/ic202588u | *Inorg. Chem.* 2012, 51, 4180−4192

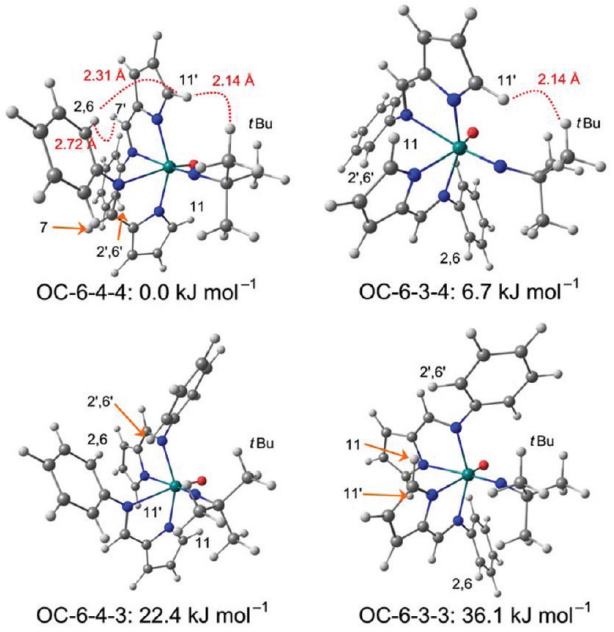

Figure 3. DFT-calculated stereoisomers of $\mathbf{2}^{H}$ together with relevant interligand H···H distances (shortest distance obtained by phenyl and *tert*-butyl rotations) and relative energies in kJ mol^{-1}.

↔ $H^{2,6}$ distance is found in the OC-6-4-4 isomer but not in the OC-6-3-4 isomer. The $H^{7'}$ ↔ $H^{2,6}$ and H^{7} ↔ $H^{2',6'}$ NOEs place N^{i} and $N^{i'}$ in close proximity, which is fulfilled in the OC-6-4-4 isomer (Figure 3). Thus, from the DFT-calculated H···H distances only the expected OC-6-4-4 isomer fits to the experimental data as all other isomers violate some of the NOE distance constraints.

Single crystals of $\mathbf{2}^{tBu}$ were grown from diethyl ether/petroleum ether 40−60° (1:1) at room temperature. $\mathbf{2}^{tBu}$ crystallized in the tetragonal space group $I4_1/a$ (Figure 4, Tables 1 and 2). Six-coordinate heteroleptic imido/oxido complexes are relatively unexplored with respect to structural data.[11,12] Recently, Mösch-Zanetti et al. reported the synthesis and structures of well-defined mixed imido/oxido complexes with β-ketiminato N, O chelate ligands.[11] They reported a slight elongation of the Mo═O bond length by replacing one oxido by an imido ligand for these complexes.[11] An analogous slight elongation is within experimental error when comparing the Mo═O bond lengths of $\mathbf{1}^{tBu}$ (1.698−1.704(2) Å) with that of $\mathbf{2}^{tBu}$ (1.705(2) Å) (Table 2). However, this slight elongation of the Mo═O bond is also reproduced by DFT calculations on $\mathbf{1}^{H}$ and $\mathbf{2}^{H}$ ($\mathbf{1}^{H}$, 1.713/1.715 Å; $\mathbf{2}^{H}$, 1.719 Å).

The quite short Mo1═N^{imido} bond length of 1.731(2) Å points to a significant triple-bond character (DFT $\mathbf{2}^{H}$, 1.746 Å). Mo═N distances in a similar range have been reported for six-coordinate imido/oxido complexes (type **B** complexes 1.742(2) and 1.734(6) Å[11] and complex **C1** 1.740(4) and 1.731(4) Å[12]). Almost linear imido ligands have been found for **B**-type complexes (175.6(2)°, 172.5(5)°)[11] and **C1** (174.2(4)°, 167.6(4)°)[12]. The Mo1═N^{imido}−C^{imido} angle of the imido ligand of $\mathbf{2}^{tBu}$ amounts to 159° in the X-ray structure analysis of $\mathbf{2}^{tBu}$. DFT calculations on $\mathbf{2}^{H}$ suggest a very shallow potential for the Mo═N−C deformation.[35] A 140−180° bending deformation lies within 11 kJ mol^{-1} (see Supporting Information, Figure S1). A minimum is calculated at 160°, in good agreement with the experimental value. This facile bending of the Mo═N−C angle should allow a nucleophilic associative attack at the oxido ligand in spite of the presence of the sterically demanding *tert*-butyl group at the imido nitrogen (vide infra). Additionally, the Mo1−$N^{i'}$ bond length trans to the imido ligand is significantly larger (2.394(3) Å) than the corresponding Mo1−N^{i} bond lengths trans to oxido ligands (2.32−2.37 Å), which reflects the stronger trans influence of the N*t*Bu ligand as compared to the oxido ligand.[36] This trend is also observed in the DFT-calculated structures (2.493 Å trans to imido; 2.413−2.481 Å trans to oxido).

The energies of the Mo═O stretching vibrations have been calculated for $\mathbf{1}^{H}$ and for $\mathbf{2}^{H}$ by DFT methods (and scaled by 0.9614[37]) as 940/914 ($\mathbf{1}^{H}$ [8]) and 910 cm^{-1} ($\mathbf{2}^{H}$), in good agreement with the experimental data 928/902 ($\mathbf{1}^{tBu}$) and 897 cm^{-1} ($\mathbf{2}^{tBu}$), Figure 5. From a structural and vibrational point of view the calculations reproduce and confirm the experimental data sufficiently well. Then, the electronic structures of the d^0 complexes $\mathbf{1}^{tBu}$ and $\mathbf{2}^{tBu}$ have been probed by UV−vis absorption spectroscopy and TD-DFT calculations. TD-DFT

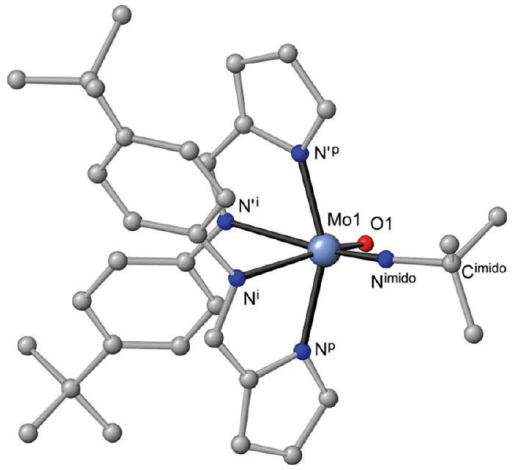

Figure 4. Molecular structure of $\mathbf{2}^{tBu}$ in the crystal (CH hydrogen atoms omitted for clarity).

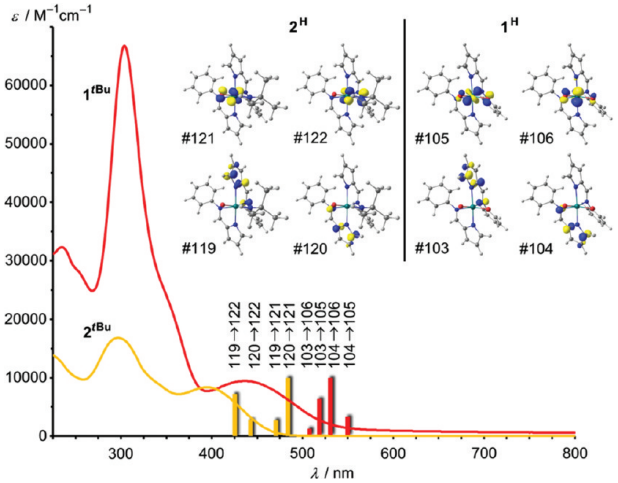

Figure 5. UV−vis spectra of $\mathbf{1}^{tBu}$ and $\mathbf{2}^{tBu}$ in THF; calculated low-energy transitions of $\mathbf{1}^{H}$ and $\mathbf{2}^{H}$ as stick representation; frontier Kohn−Sham molecular orbitals of $\mathbf{1}^{H}$ and $\mathbf{2}^{H}$ (contour value 0.1 au).

dx.doi.org/10.1021/ic202588u | *Inorg. Chem.* 2012, 51, 4180−4192

calculations have also been performed with inclusion of a solvent model (integral equation formalism polarizable continuum model; IEFPCM; THF). However, no significant improvement was noticed in the calculated spectra.

The red color of the dioxido complex $\mathbf{1}^{t\mathrm{Bu}}$ arises from an absorption band at λ = 436 nm (ε = 9440 M^{-1} cm^{-1}), which is absent in the ligand $\mathbf{HL}^{t\mathrm{Bu}}$. It is assigned LMCT/LLCT in character. TD-DFT calculations on $\mathbf{1}^{\mathrm{H}}$ find an absorption band at 528 nm, which is composed of four transitions with similar energy (λ = 508, 518, 531, 550 nm). All transitions involve the four frontier orbitals of the complex, namely, two occupied orbitals of the pyrrolato ligands (MO nos. 103, 104) and two π^* orbitals of the MoO_2 unit (MO nos. 105, 106). The yellow imido/oxido complex $\mathbf{2}^{t\mathrm{Bu}}$ lacks characteristic absorption maxima in the visible region (λ = 395 nm, ε = 8335 M^{-1} cm^{-1}; only tailing into the visible region). TD-DFT calculations on $\mathbf{2}^{\mathrm{H}}$ predict analogous transitions to $\mathbf{1}^{\mathrm{H}}$ involving the pyrrolato ligands (MO nos. 119, 120) and the Mo═O (MO no. 121) and Mo═N*t*Bu units (MO no. 122). However, these excitations occur at higher energy and with much more spread (λ = 426, 443, 470, 483 nm) due to the larger energy difference ΔE of the acceptor orbital energies ($\mathbf{1}^{\mathrm{H}}$, ΔE(105,106) = 0.10 eV; $\mathbf{2}^{\mathrm{H}}$, ΔE(121,122) = 0.24 eV). These effects explain the less intense color of the imido/oxido complex.

Oxygen Atom Transfer and Stereochemistry of Mo(IV) Products. The OAT from dioxido complexes $\mathbf{1}^{\mathrm{R}}$ (R = $OSiMe_3$, O−Si(*i*Pr)$_2$−polymer) to phosphanes PMe_nPh_{3-n} has been recently investigated experimentally[7,9] and on a theoretical basis (R = H).[8] After associative attack of the phosphane at a molybdenum-bound oxido ligand, formation, and dissociation of the phosphane oxide a five-coordinate molybdenum(IV) intermediate is formed. Its vacant coordination site is either filled with a remaining starting Mo^{VI} dioxido complex forming a binuclear oxido bridged complex $L^R_2(O)Mo^V{-}O{-}Mo^V(O)L^R_2$ ($\mathbf{3}^{\mathrm{R}}$) or by excess substrate PMe_nPh_{3-n} (n = 1 − 3) after longer reaction times.[10] For the resulting phosphane complexes $\mathbf{4}^{\mathrm{H}}$ (with R = H and n = 3; PMe_3) several stereoisomers have been considered by DFT calculations. The OC-6-3-3 and OC-6-4-3 isomers of $\mathbf{4}^{\mathrm{H}}$ are the lowest energy isomers with very similar energy, while the OC-6-4-4 isomer is calculated significantly higher in energy.[8] On the basis of NOE contacts and DFT calculations the OC-6-4-3 isomer of $\mathbf{4}^{\mathrm{OSiMe3}}$ is preferred in THF solution.[7−9]

For the reaction of $\mathbf{1}^{t\mathrm{Bu}}$ with PMe_3 similar results were obtained (Scheme 1). Due to the excellent solubility of the complexes two resonances for two stereoisomers $\mathbf{4}^{t\mathrm{Bu}}$ were discernible in the $^{31}P\{^1H\}$ NMR spectrum (δ = 1.3 and −5.3 ppm in a ratio ≈ 5 : 2). These two isomers can be distinguished in the ^1H NMR spectrum as well (four different signal sets for the chelate ligands are observed). All resonances of the major isomer could be assigned by correlation spectroscopy. The resonance of proton H^7 is split to a doublet with $^4J_{PH}$ = 2.3 Hz. The P−H correlation spectrum confirms that this doublet arises from coupling to phosphorus (δ = 1.3 ppm; see Supporting Information, Figure S8). Weaker cross peaks of the phosphorus nucleus are found to $H^{7'}$ and $H^{11'}$ (J_{PH} < 1.0 Hz). The ^{15}N resonances of the major isomer are observed at δ = 219.0 (N^p), 230.3 ($N^{p'}$), and 236.6 ppm (N^i + $N^{i'}$). By nuclear Overhauser spectroscopy it was possible to elucidate the orientation of one chelate ligand relative to the phosphane. A strong Me ↔ H^{11} contact (between phosphane and ligand L) places the nitrogen atom N^p cis to the phosphane with the $C^{11}{-}H^{11}$ vector pointing in the Mo−P direction, i.e., N^i is located trans to the phosphane. Two further NOE contacts Me ↔ $H^{11'}$ (medium) and Me ↔ $H^{2',6'}$ (medium) are compatible with the OC-6-4-3 and the OC-6-4-4 isomers. From the DFT calculations and NOE contacts we propose again the OC-6-4-3 isomer as the major isomer (compatible with all NOE contacts but not unambiguous). The other (minor) stereoisomer observed is most likely the OC-6-3-3 isomer from an energetic point of view.[8] In the infrared spectrum of complex $\mathbf{4}^{t\mathrm{Bu}}$ absorption of the Mo═O stretching vibration is observed at 935 cm^{-1}. For the model $\mathbf{4}^{\mathrm{H}}$ complexes the energies are calculated (and scaled by 0.9614[37]) as 935, 937, 956, and 957 cm^{-1} for isomers OC-6-4-3, OC-6-3-3, OC-6-3-4, and OC-6-4-4, respectively. These data also fit to OC-6-4-3 and OC-6-3-3 stereoisomers. One stereoisomer of $\mathbf{4}^{t\mathrm{Bu}}$ crystallized from THF in the monoclinic space group *C*2/*c* (Tables 1 and 2). As already suggested from combined NMR/DFT analysis the OC-6-4-3 major stereoisomer is indeed present in the crystal (Figure 6, top).

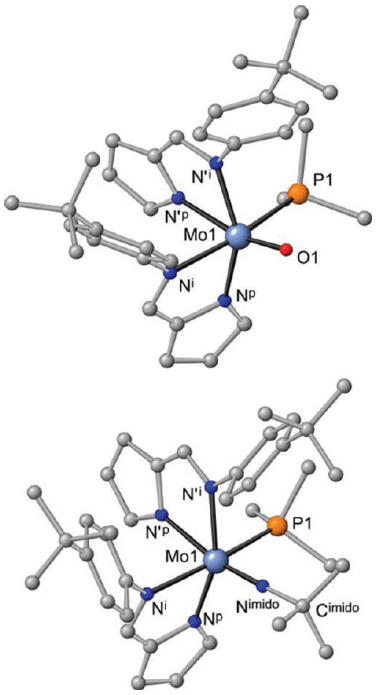

Figure 6. Molecular structures of $\mathbf{4}^{t\mathrm{Bu}}$ and $\mathbf{5}^{t\mathrm{Bu}}$ in the crystal (CH hydrogen atoms omitted for clarity).

Reaction of imido complex $\mathbf{2}^{t\mathrm{Bu}}$ with PMe_3 (Scheme 1) yields a single molybdenum(IV) phosphane complex $\mathbf{5}^{t\mathrm{Bu}}$ with $\delta(^{31}P)$ = 9.2 ppm and $\delta(^{15}N)$ = 212.0 (N^p), 231.1 ($N^{p'}$), 234.2 (N^i), and 252.2 ppm ($N^{i'}$) NMR spectral characteristics. The imido nitrogen nucleus experiences the largest shift from δ = 477.4 ppm ($\mathbf{2}^{t\mathrm{Bu}}$) to δ = 273.7 ppm ($\mathbf{5}^{t\mathrm{Bu}}$). The H^7 resonance of $\mathbf{5}^{t\mathrm{Bu}}$ is split into a doublet by coupling to ^{31}P ($^4J_{PH}$ = 2.8 Hz). In the P−H correlation spectrum a weak correlation peak (J_{PH} < 1.0 Hz) is also found to $H^{11'}$ similar to the oxido phosphane complex $\mathbf{4}^{t\mathrm{Bu}}$ (see Supporting Information, Figure S9).

The larger imido ligand in $\mathbf{2}^{t\mathrm{Bu}}$ should disfavor nucleophilic attack of the phosphane at the oxido ligand as compared to reaction of PMe_3 with $\mathbf{1}^{t\mathrm{Bu}}$. DFT calculations on $\mathbf{1}^{\mathrm{H}}$ and PMe_3 give a barrier of 64.6 kJ mol^{-1},[8] while with $\mathbf{2}^{\mathrm{H}}$ the calculated barrier indeed increases to 108.3 kJ mol^{-1}. In addition, the barrier calculated for dissociation of the coordinated phosphane

dx.doi.org/10.1021/ic202588u | *Inorg. Chem.* 2012, 51, 4180−4192

oxide amounts to only 26.3 kJ mol^{-1} in the case $\mathbf{1}^{H}$/PMe$_3$[8] and is almost doubled in the case $\mathbf{2}^{H}$/PMe$_3$ (50.1 kJ mol^{-1}). In spite of these decelerating effects the overall phosphane complex formation $\mathbf{2}^{tBu}$ + 2 PMe$_3$ → $\mathbf{5}^{tBu}$ + OPMe$_3$ proceeds roughly 10 times *faster* than the reaction $\mathbf{1}^{tBu}$ + 2 PMe$_3$ → $\mathbf{4}^{tBu}$ + OPMe$_3$ at room temperature as judged by ^{31}P{^{1}H} NMR spectroscopic reaction monitoring (see Supporting Information, Figure S2). This apparent discrepancy can be ascribed to the absence of dimer accumulation in the imido case as the steric bulk of the imido ligand prevents intermediate formation of imido- or oxido-bridged dimers with six-coordinate molybdenum centers.[38] In the oxido case dimerization retards formation of the phosphane complex $\mathbf{4}^{tBu}$. Thus, in the *overall* reaction the less sterically hindered complex $\mathbf{1}^{tBu}$ reacts slower due to the comproportionation equilibrium to $\mathbf{3}^{tBu}$.

Mösch-Zanetti et al. also observed formation of an imido phosphane complex by reaction of their bis(β-ketiminato)(imido)(oxido) complexes **B** (Chart 1) with PMe$_3$ (δ(^{31}P) = 6.5 ppm). They suggested formation of a stereoisomer in which the oxido ligand is replaced by the phosphane without isomerization in the five-coordinate intermediate. However, no experimental evidence for this stereochemical assignment has been given.[11] In our system DFT calculations on possible stereoisomers of $\mathbf{5}^{H}$ find the OC-6-4-3 isomer as the global minimum and the OC-6-4-4 and OC-6-3-3 isomers 9.8 and 13.6 kJ mol^{-1} higher in energy, respectively (Figure 7). Nuclear

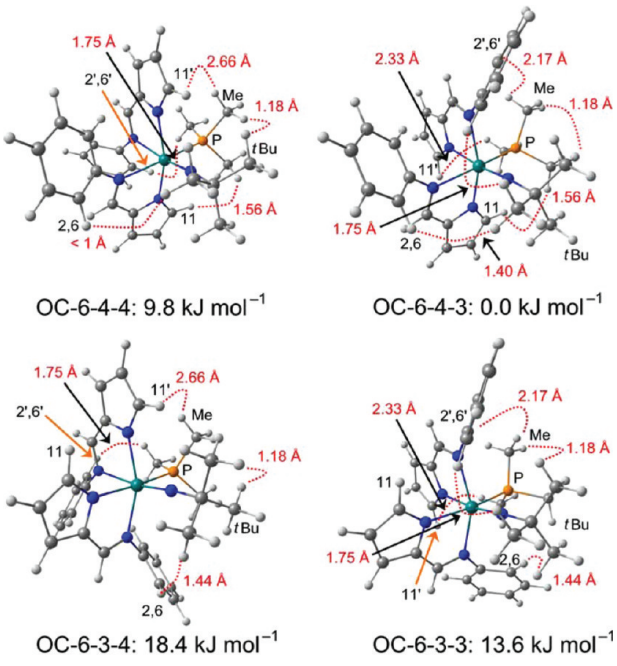

Figure 7. DFT-calculated stereoisomers of $\mathbf{5}^{H}$ together with relevant interligand H···H distances (shortest distance obtained by PMe$_3$, phenyl, and *tert*-butyl rotation) and relative energies in kJ mol^{-1}.

Overhauser spectroscopy experimentally clarifies the stereochemistry of $\mathbf{5}^{tBu}$ as six relevant interligand NOE contacts are observed, namely, three between PMe$_3$ and the chelate ligands (Me ↔ H^{11}, Me ↔ H$^{11'}$, Me ↔ H$^{2',6'}$; similar to $\mathbf{4}^{tBu}$), two between N*t*Bu and the chelate ligands (*t*Bu ↔ H^{2,6}; *t*Bu ↔ H$^{2',6'}$), and one between PMe$_3$ and N*t*Bu. The Me ↔ N*t*Bu contact places the phosphane cis to the imido ligand. The Me ↔ H^{11} contact locates the nitrogen atoms N^{p} cis and N^{i} trans to the phosphane as found for $\mathbf{4}^{tBu}$. Finally, the imido ligand displays contacts to ortho protons H^{2,6} and H$^{2',6'}$ of both chelate ligands, which places both imino nitrogen atoms N^{i} and N$^{i'}$ in cis positions to the N*t*Bu ligand. These neighborhood relations are only realized in the (energetically most stable) OC-6-4-3 isomer (Figure 7).

Six-coordinate $\mathbf{5}^{tBu}$ crystallized from diethyl ether/acetonitrile in the monoclinic space group $P2_1/n$ (Table 1). As suggested from the unequivocal NMR/DFT analysis the OC-6-4-3 stereoisomer is present in the crystal (Figure 6, bottom). The Mo═N bond length of $\mathbf{5}^{tBu}$ is slightly larger (1.743(2) Å, Table 2) than that of $\mathbf{2}^{tBu}$ (1.731(2) Å, Table 2), which is also reproduced by the DFT calculation ($\mathbf{5}^{H}$, 1.751 Å; $\mathbf{2}^{H}$, 1.746 Å).The imido ligand in $\mathbf{5}^{tBu}$ is almost perfectly linear with Mo═N−C 178.7(2)° (DFT $\mathbf{5}^{H}$ 174.9°). The DFT-calculated Mo═N−C bending deformation potential is much steeper for the Mo^{IV} complex than for the Mo^{VI} complex (see Supporting Information, Figure S1). The P−Mo═N angle in six-coordinate $\mathbf{5}^{tBu}$ is smaller (92.53(6)°) than those found by Gibson et al. in pseudotetrahedral Mo^{IV}(N*t*Bu)$_2$(PMe$_3$)(L) complexes (~100°, L = olefin or acetylene).[39] In the DFT model $\mathbf{5}^{H}$ the angle is calculated as 94.6°, in good agreement with the experimental value. The Mo−P bond length is shorter for the imido derivative $\mathbf{5}^{tBu}$ (2.4532(6) Å) as compared to that of the oxido derivative $\mathbf{4}^{tBu}$ (2.482(2) Å), suggesting a stronger Mo−P dative bond in $\mathbf{5}^{tBu}$. This trend is also reproduced in the DFT calculation ($\mathbf{5}^{H}$, 2.533 Å; $\mathbf{4}^{H}$, 2.642 Å).

Given the fact that two isomers ($\mathbf{4}^{tBu}$) and one isomer ($\mathbf{5}^{tBu}$) are observed instead of a mixture of several isomers points to a thermodynamically driven product distribution. Thus, coordination of PMe$_3$ in $\mathbf{4}^{tBu}$ and $\mathbf{5}^{tBu}$ should be reversible. To probe this $\mathbf{4}^{tBu}$ and $\mathbf{5}^{tBu}$ were treated with 5 equiv of triethylphosphane PEt$_3$ at 293 ($\mathbf{4}^{tBu}$) and 333 K ($\mathbf{5}^{tBu}$), respectively (Scheme 2). Indeed, in the ^{31}P{^{1}H} NMR spectra (see

Scheme 2. Phosphane Exchange via Five-Coordinate Intermediates

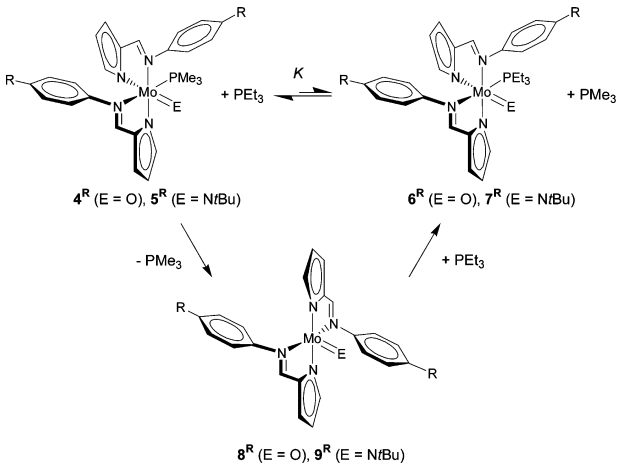

Supporting Information, Figure S10, S11) new resonances at δ = 23.1 ($\mathbf{4}^{tBu}$/ PEt$_3$) and 33.5 ppm ($\mathbf{5}^{tBu}$/ PEt$_3$) were observed, respectively, together with the resonance of free PMe$_3$ (δ = −63.1 ppm) and free PEt$_3$ (δ = −20.1 ppm). The low-field resonances are assigned to the corresponding PEt$_3$ complexes $\mathbf{6}^{tBu}$ and $\mathbf{7}^{tBu}$. The former was also prepared independently by synthesis from $\mathbf{1}^{tBu}$ with PEt$_3$, confirming the assignment. Integration of the resonances assigned to $\mathbf{4}^{tBu}$/$\mathbf{6}^{tBu}$ and $\mathbf{5}^{tBu}$/

dx.doi.org/10.1021/ic202588u | *Inorg. Chem.* 2012, 51, 4180−4192

7^{tBu} and the free phosphanes allows one to estimate the equilibrium constants as $K_{293} = 12 \times 10^{-3}$ ($4^{tBu}/6^{tBu}$) and $K_{333} = 2 \times 10^{-3}$ ($5^{tBu}/7^{tBu}$). Expectedly, the sterically less encumbered PMe_3 complexes are favored due to the smaller Tolman cone angle[40] of PMe_3 (118°) as compared to that of PEt_3 (132°), which is even more pronounced for the imido complexes 5^{tBu} and 7^{tBu}.

The five-coordinate oxido intermediate 8^H has been previously characterized by DFT,[8] and the corresponding calculation of the imido intermediate 9^H is presented here (Scheme 2, Supporting Information). The largest calculated N−Mo−N angles of the oxido complex 8^H amount to 153.3° and 123.5° describing a geometry between trigonal bipyramidal and tetragonal pyramidal ($\tau = 0.50$[41]), while the corresponding angles in the imido derivative 9^H amount to 149.9° and 132.9° describing a more tetragonal pyramidal geometry ($\tau = 0.28$).

Complexes 1^{tBu} and 2^{tBu} react at different rates in the OAT to PMe_3 with the sterically encumbered imido complex 2^{tBu} (via 9^{tBu}) reacting faster than the oxido complex 1^{tBu} (via 8^{tBu} and then the μ-oxido dimer 3^{tBu}) as shown by NMR spectroscopy. In a catalytic *double* OAT reaction[42] from dmso to PMe_3 giving dimethyl sulfide dms and $OPMe_3$ the imido complex should be the faster catalyst. Initial rates were determined under pseudo-first-order conditions ($[1^{tBu}]$, $[2^{tBu}] = 0.025$ mM; $[PMe_3]_0 = 0.25$ mM in dmso) at 298 K (see Supporting Information, Figures S12, S13). Indeed, rate constants of $k_{298} = 1.5(1) \times 10^{-5}$ s^{-1} (1^{tBu}) and $k_{298} = 3.0(1) \times 10^{-5}$ s^{-1} (2^{tBu}) were determined, confirming the initial faster overall double OAT reactions with the imido system. However, product formation is quantitative only with the oxido but not with the imido catalyst. These findings point to catalyst inhibition during catalysis in the case of 2^{tBu}. Proton and ^{31}P NMR spectroscopy reveal that during turnover of 2^{tBu} the phosphane complex 5^{tBu} is formed in appreciable amounts, which significantly slows down catalysis (substrate inhibition). No evidence was obtained for formation of a dms complex (product inhibition), which has been recently proposed for the natural enzyme DMSO reductase in the course of turnover.[43] Attempts to displace PMe_3 in 5^{tBu} by a large excess dimethyl sulfide failed. Furthermore, the phosphane complex 5^{tBu} is shown to be stable in the presence of dmso (^1H NMR, $^{31}P\{^1H\}$ NMR) and thus is not a competent catalyst for oxygenation of PMe_3 by dmso. Thus, the major reactivity difference between intermediates 8^{tBu} and 9^{tBu} is their affinity to the molybdenum(VI) catalyst itself ($1^{tBu}/2^{tBu}$) and to the substrate PMe_3. The five-coordinate oxido complex 8^{tBu} strongly binds to 1^{tBu}, giving the μ-oxido dimer 3^{tBu}, while the five-coordinate imido species 9^{tBu} preferentially coordinates the substrate PMe_3.

The electronic structures of the green d^2 complexes 4^{tBu} and 5^{tBu} were investigated by optical spectroscopy. Both complexes feature several ligand field bands in the visible spectral region, namely, at λ = 715 (sh), 610 (sh), and 479 (1420) nm (4^{tBu}) and at λ = 735 (265), 594 (1000), and 490 (1490) nm (5^{tBu}) in THF (Figure 8). TD-DFT calculations find low-energy absorption bands at 728, 659, 453, and 435 nm (4^H) and 695, 598, 482, and 458 nm (5^H), in reasonable agreement with experiment (Figure 8). The bands are largely composed of $d_{xy} \rightarrow d_{xz}/d_{yz}$ ligand field transitions with some admixture of the chelate and the imido/oxido ligands (Figure 8).

One-Electron Oxidation of Molybdenum(IV) Complexes to Molybdenum(V) Complexes. Outer-sphere one-electron oxidation of oxido phosphane complexes 4^R (R = $OSiMe_3$) with ferrocenium salts has been previously reported

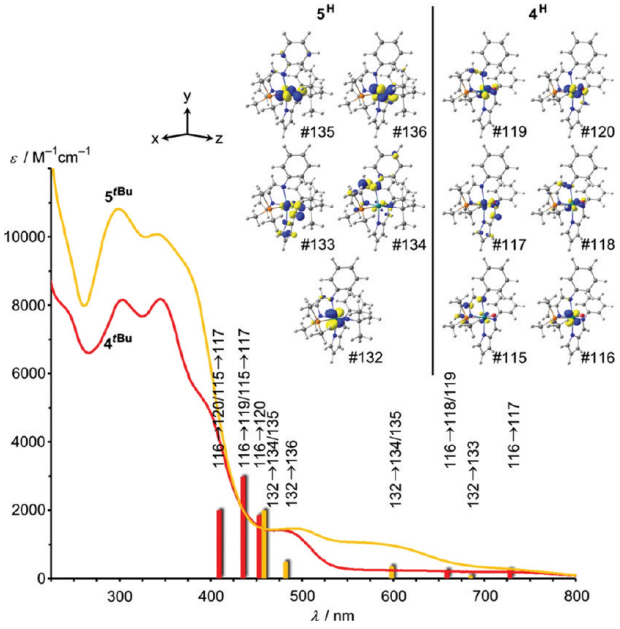

Figure 8. UV−vis spectra of 4^{tBu} and 5^{tBu} in THF; calculated low-energy transitions of 4^H and 5^H as a stick representation; frontier molecular orbitals of 4^H (contour value 0.1 au) and 5^H (contour value 0.07 au).

by us.[7,9] It was observed that the larger the coordinated phosphane ligand PMe_nPh_{3-n} (n = 1−3) the more facile the phosphane dissociates from the Mo^V complex.[9] Similarly, the oxido phosphane complex 4^{tBu} features only an irreversible oxidation wave in the cyclic voltammogram with $E_p = -0.29$ V vs FcH/FcH^+ with a rereduction peak ($E_p = -0.85$ V) clearly associated with a different chemical species (Figure 9, top, left). Higher scan rates or the presence of PMe_3 (100 equiv) do not alter the appearance of this cyclic voltammogram significantly. Chemical oxidation of 4^{tBu} with ferrocenium hexafluorophosphate gives EPR-active d^1 Mo^V species with an average g_{iso} = 1.9459 and $A_{iso}(^{95/97}\text{Mo}) = 49.8$ G ($I(^{95/97}\text{Mo}) = 5/2$). No superhyperfine coupling of the unpaired electron to phosphorus ($I(^{31}P) = 1/2$) is observed, which points to facile dissociation of PMe_3 after electron transfer to Mo^{IV} also in this case (Figure 9, top, right). The EPR spectrum in frozen solution at 77 K shows a signal with $g_{1,2,3}$ = 1.9618, 1.9555, and 1.9362 lacking obvious hyperfine splitting (for simulation see Supporting Information, Figure S14) comparable to that of the previously reported Mo(V) complex with L^{OSiMe3} chelate ligands ($g_{1,2,3}$ = 1.9703, 1.9503, 1.9413).[9] Unrestricted DFT geometry optimization on five-coordinate $[4^H]^+$ suggests a geometry between trigonal-bipyramidal and tetragonal pyramidal (largest angles 155.1°, 127.7°; $\tau = 0.46$[41]). Calculated principal g values $g_{1,2,3}$ = 1.9740, 1.9638, and 1.9593 are in reasonably good agreement with the experiment (UB3LYP, WTBS basis set for Mo/EPR-II basis set for C, H, N). However, the presence of other species, e.g., like a THF adduct, or different stereoisomers cannot be excluded on the basis of the EPR spectrum. Such species could also be responsible for the additional peaks in the spectrum, which hampers a reliable simulation of the spectrum (Figure 9, top).

On the other hand, the imido phosphane complex 5^{tBu} is *reversibly* oxidized in the cyclic voltammogram at $E_{1/2} = -0.71$ V vs FcH/FcH^+ (Figure 9, bottom, left). Simple outer-sphere

dx.doi.org/10.1021/ic202588u | Inorg. Chem. 2012, 51, 4180−4192

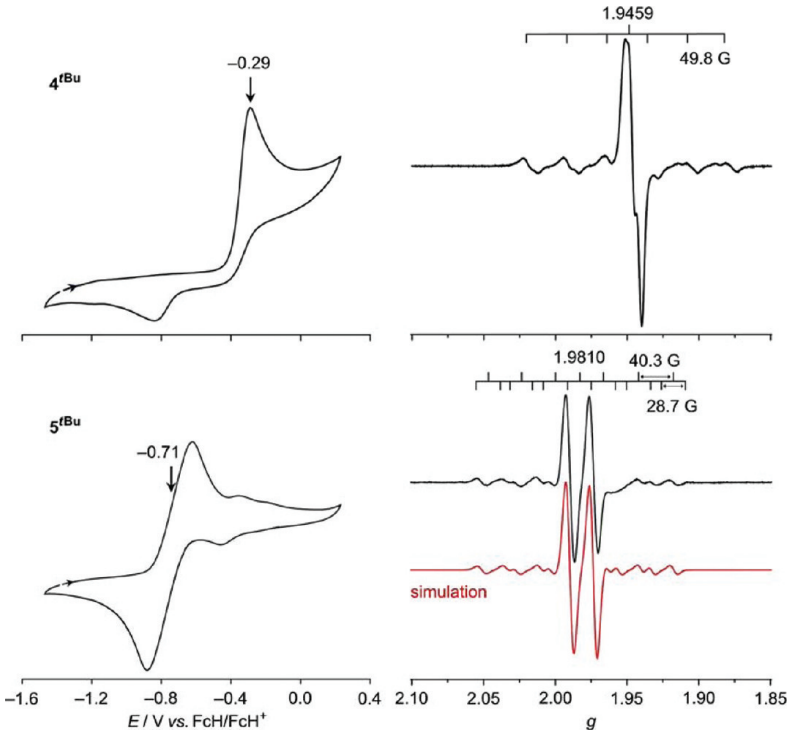

Figure 9. Cyclic voltammograms of $\mathbf{4}^{t\mathrm{Bu}}$ and $\mathbf{5}^{t\mathrm{Bu}}$ (left) and X-band CW-EPR spectra of $\mathbf{4}^{t\mathrm{Bu}}$ and $\mathbf{5}^{t\mathrm{Bu}}$ oxidized with $[\mathrm{FcH}](\mathrm{PF_6})$ at 298 K.

one-electron oxidation of $\mathbf{5}^{t\mathrm{Bu}}$ should retain the stoichiometry and also the OC-6-4-3 stereochemistry. Thus, under these conditions the kinetic six-coordinate $\mathrm{Mo^V}$ product $[\mathbf{5}^{t\mathrm{Bu}}]^+$ with OC-6-4-3 configuration should be formed. This metastable complex should be unable to isomerize to another stereoisomer as trigonal twists are usually quite energy demanding in six-coordinate complexes as long as dissociation is prevented.[44] According to unrestricted DFT calculations the *thermodynamically* most stable stereoisomer $[\mathbf{5}^{\mathrm{H}}]^+$ is the OC-6-4-4 isomer, followed by the OC-6-4-3 isomer (6.3 kJ $\mathrm{mol^{-1}}$), the OC-6-3-4 isomer (11.1 kJ $\mathrm{mol^{-1}}$), and the OC-6-3-3 isomer (16.2 kJ $\mathrm{mol^{-1}}$). To confirm the assumption of formation of the kinetic OC-6-4-3 product $\mathbf{5}^{t\mathrm{Bu}}$ is chemically oxidized with ferrocenium hexafluorophosphate to the $\mathrm{Mo^V}$ complex $[\mathbf{5}^{t\mathrm{Bu}}](\mathbf{PF_6})$. The isotropic CW EPR spectrum of the product reveals a doublet signal at $g_{\mathrm{iso}} = 1.9810$ with $A_{\mathrm{iso}}(^{31}\mathrm{P}) = 28.7$ G and $A_{\mathrm{iso}}(^{95/97}\mathrm{Mo}) = 40.3$ G (Figure 9, bottom, right). This doublet signal remains stable for days in solution at room temperature. In frozen THF solution the coupling of the unpaired electron to the ^{31}P nucleus is also discernible. Simulation[24] of the rhombic spectrum yields $g_{1,2,3} = 1.9825$, 1.9785, and 1.9615 and $A_{1,2,3}(^{31}\mathrm{P}) = 23$, 33, and 29 G (see Supporting Information, Figure S15). To probe the direct nuclear environment around the central d^1 molybdenum ion it is necessary to measure the weak hyperfine couplings (HFC) that are not resolved in the CW EPR spectra. To this end, X-band HYSCORE spectra[45,46] of $[\mathbf{5}^{t\mathrm{Bu}}](\mathbf{PF_6})$ (Figure 10) in frozen THF solution were recorded at 20 K and analyzed. Experimental details can be found in the Supporting Information. Several off-diagonal cross peaks are detected both in the (−,+) and in the (+,+) quadrant. The HYSCORE data could be satisfactorily simulated[46b] assuming anisotropic couplings to several ^{14}N nuclei. Two weak ^{14}N hyperfine and quadrupolar couplings (see Supporting Information) and one distinctly larger HFC can be inferred

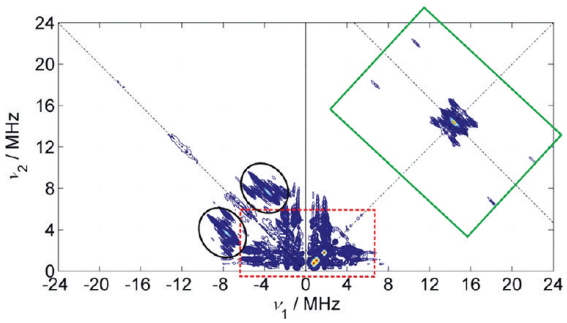

Figure 10. X-band HYSCORE spectrum of $[\mathbf{5}^{t\mathrm{Bu}}](\mathbf{PF_6})$ at 20 K as measured on the maximum of the low-temperature, echo-detected EPR spectrum. ^{1}H coupling region is marked by a tilted green rectangle, the weak ^{14}N coupling region is marked by a dashed red rectangle, and the main features of the strongly coupled ^{14}N nucleus are marked by black ovals. Detailed spectra and their simulations are shown in Figure S16 in the Supporting Information.

$[A_{1,2,3}(^{14}\mathrm{N_{small,A}}) = 1.3$, 1.4, 1.7 G, $A_{\mathrm{iso}}(^{14}\mathrm{N_{small,A}}) = 1.5$ G; $A_{1,2,3}(^{14}\mathrm{N_{small,B}}) = 0.8$, 0.8, 0.9 G, $A_{\mathrm{iso}}(^{14}\mathrm{N_{small,B}}) = 0.8$ G; $A_{1,2,3}(^{14}\mathrm{N_{large}}) = 1.5$, 2.0, 3.8 G, $A_{\mathrm{iso}}(^{14}\mathrm{N_{large}}) = 2.4$ G]. Furthermore, indirect indications for one strongly coupled proton that may be coupled via a nitrogen atom could be found with $A_{1,2,3}(^1\mathrm{H}) = 3.4$, 4.1, and 5.0 G and $A_{\mathrm{iso}}(^1\mathrm{H}) = 4.2$ G (see Supporting Information[46c]). Note that the ^{1}H couplings are not directly observed in Figure 10 but by the double-quantum transitions of ^{1}H and a ^{14}N nucleus. This can be explained by cross-suppression of the ^{1}H coupling through nuclei with large modulation amplitudes such as ^{14}N and is explained in detail in ref 46c. All hyperfine and quadrupole couplings derived from the simulations are summarized in Table S1 in the Supporting Information.

dx.doi.org/10.1021/ic202588u | *Inorg. Chem.* 2012, 51, 4180−4192

Table 3. Characteristic EPR Data Calculated for the Stereoisomers of $[5^{H}]^{+}$ and Experimental Data for $[5^{tBu}](PF_6)$

	g_{iso}	$g_{1,2,3}$	$A_{iso}(^{31}P)$/G	$A_{iso}(^{14}N^{imido})$/G	$A_{iso}(^{1}H)$/G (largest)
OC-6-4-4	1.9755	1.9813, 1.9766, 1.9686	22.9	3.3	1.2/1.7 ($H^{9\prime}$, $H^{10\prime}$)
OC-6-4-3	1.9728	1.9822, 1.9759, 1.9603	25.2	4.0	2.1 ($H^{11\prime}$)
OC-6-3-4	1.9748	1.9813, 1.9733, 1.9700	27.7	3.4	1.2/1.5 ($H^{9\prime}$, $H^{10\prime}$)
OC-6-3-3	1.9822	1.9845, 1.9824, 1.9798	28.4	3.1	2.2 ($H^{11\prime}$)
exp	1.9810	1.9825, 1.9785, 1.9615	28.7[a]	2.4[b]	4.2[c]

[a] A_{iso} is extracted from the X-band CW EPR spectrum. [b] A_{iso} is calculated as the average value of the full hyperfine coupling matrix extracted from the HYSCORE spectrum, not taking into account quadrupolar couplings. [c] This value is inferred from the double-quantum transitions of one ^{14}N and one ^{1}H from the HYSCORE spectrum.[46c]

EPR parameters g_{iso}, $g_{1,2,3}$, $A_{iso}(^{31}P, ^{14}N, ^{1}H)$ have been calculated by DFT (UB3LYP, WTBS basis set for Mo, 6-311++G(2d,2p) basis set for P and EPR-II basis set for C, H, N) for the four different isomers of $[5^{H}]^{+}$ (Table 3). Calculated g_{iso} values of the stereoisomers are very similar, impeding any reliable assignment, while the anisotropic data fit best to the OC-6-4-3 isomer. In all stereoisomers the imido nitrogen nucleus N^{imido} is strongly coupled to the unpaired electron with $A_{iso}(^{14}N^{imido})$ = 3.1−4.0 G, while the other nitrogen atoms of the chelate ligands give rise to smaller couplings with $A_{iso}(^{14}N^{i,p})$ = 0.2−2.1 G. This compares nicely with the experimental HFC data but does not allow distinguishing between the isomers with certainty. Significant couplings to protons with $A_{iso}(^{1}H)$ > 1.0 G are calculated for protons of one pyrrolato ring ($H^{9\prime}$, $H^{10\prime}$, $H^{11\prime}$) with the largest ones found for the OC-6-4-3 and OC-6-3-3 isomers ($A_{iso}(^{1}H, H^{11\prime})$ > 2.0 G). This assignment is in accord with the suggested stereoisomer OC-6-4-3.

Fortunately, crystals of $[5^{tBu}](PF_6)$ grown from THF/petroleum ether 40−60° solution were suitable for X-ray crystallographic analyses (Table 1). The salt $[5^{tBu}](PF_6)$ crystallized in the orthorhombic space group *Pbca* with additional THF solvent molecules in the unit cell. As expected, the OC-6-4-3 stereoisomer is observed in the crystal (Figure 11).

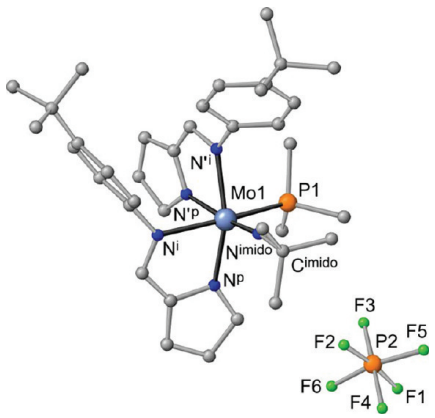

Figure 11. Molecular structure of $[5^{tBu}](PF_6)$ in the crystal (CH hydrogen atoms omitted for clarity).

Upon oxidation of 5^{tBu} to $[5^{tBu}](PF_6)$ the Mo1−P1 bond length is elongated from 2.4532(6) to 2.549(1) Å (Table 2), while the Mo1=N^{imido} distance remains almost constant (5^{tBu}, 1.743(2) Å; $[5^{tBu}](PF_6)$, 1.739(3) Å). In the cation the Mo1=N^{imido}−C^{imido} angle is slightly more bent (172.8(3)°) than in the neutral complex (178.8(2)°). The calculated Mo=N−C bending deformation potential for the d^1 Mo^{V} complex is very similar to that of the d^2 Mo^{IV} complex, suggesting steric rather than electronic reasons for the ligand coordination mode in this system (see Supporting Information, Figure S1).

The magnetic susceptibility χ of $[5^{tBu}](PF_6)$ was measured in d_8-THF at room temperature by the Evans method.[47,48] The experimental magnetic moment μ_{eff} = 2.828 $(\chi T)^{1/2}$ = 1.71 ± 0.05 μB corresponds to one unpaired electron (S = 1/2; $\mu_{eff,expected} = g \times (S(S+1))^{1/2}$ = 1.716 μB[49]).

In the UV−vis spectrum of $[5^{tBu}](PF_6)$ in THF several low-energy absorptions can be distinguished, namely, at 787 (ε = 905 M^{-1} cm^{-1}) and 532 (sh, 1165 M^{-1} cm^{-1}) nm, which account for the dark color (Figure 12). TD-DFT calculation on

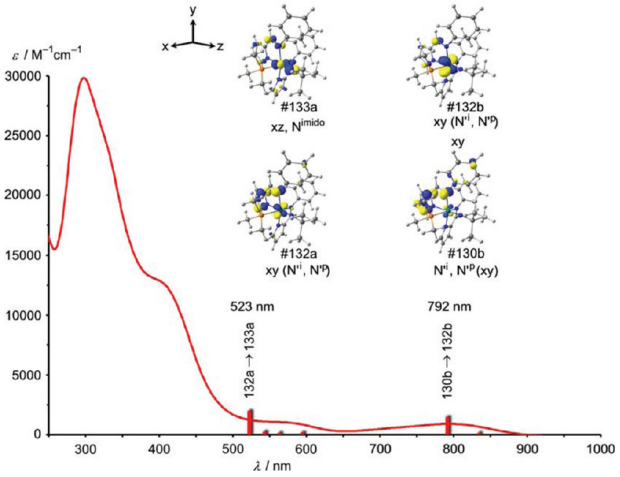

Figure 12. UV−vis spectrum of $[5^{tBu}](PF_6)$ in THF; calculated low-energy transitions of 5^{H} as a stick representation; relevant frontier molecular orbitals of 5^{H} (contour value 0.07 au).

$[5^{H}]^{+}$ assigns the stronger low-energy absorption (λ_{calcd} = 792 nm) mainly to a ligand-to-metal charge transfer from the L′ chelate ligand (MO no. 130b) to the singly occupied d_{xy} orbital (MO no. 132b). The second low-energy absorption band is assigned to a ligand field transition from the singly occupied d_{xy} orbital (MO no. 132a) to the d_{xz} orbital (π^* orbital, MO no. 133a) with some contribution of N^{imido} (λ_{calcd} = 523 nm).

CONCLUSIONS

Molybdenum(VI) dioxido (1^{tBu}) and mixed imido/oxido complexes (2^{tBu}) were prepared and fully characterized with respect to stereochemistry (OC-6-4-4), optical properties, and reactivity toward phosphanes as oxygen atom acceptors. Counterintuitively, the sterically more demanding imido ligand promotes a faster overall reaction. The final molybdenum(IV) products 4^{tBu} and 5^{tBu} of the OAT reactions were isolated, and

dx.doi.org/10.1021/ic202588u | Inorg. Chem. 2012, 51, 4180−4192

their OC-6-4-3 stereochemistry was confirmed by NMR analysis, X-ray diffraction, and DFT calculations. In a catalytic *double* OAT reaction[42] from dmso to PMe_3 giving dms and $OPMe_3$ the imido complex $\mathbf{2}^{t\mathrm{Bu}}$ is initially approximately twice as fast as the oxido complex $\mathbf{1}^{t\mathrm{Bu}}$. However, inhibition by the substrate prevents full conversion with the imido catalyst $\mathbf{2}^{t\mathrm{Bu}}$. The optical properties of the d^2 complexes $\mathbf{4}^{t\mathrm{Bu}}$ and $\mathbf{5}^{t\mathrm{Bu}}$ were analyzed by TD-DFT calculations, and the low-energy absorptions were assigned $d_{xy} \rightarrow d_{xz}/d_{yz}$ transitions with some admixture of the chelate and the imido/oxido ligands. One-electron oxidation gives the corresponding d^1 molybdenum(V) complexes. The oxido phosphane complex is unstable with respect to dissociation of coordinated phosphane ($[\mathbf{4}^{t\mathrm{Bu}}]^+$), while the imido phosphane complex $[\mathbf{5}^{t\mathrm{Bu}}]^+$ has been isolated and fully characterized. The higher stability of the Mo−P bond in $\mathbf{5}^{t\mathrm{Bu}}$ and $[\mathbf{5}^{t\mathrm{Bu}}]^+$ as compared to $\mathbf{4}^{t\mathrm{Bu}}$ and $[\mathbf{4}^{t\mathrm{Bu}}]^+$ is most likely due to electronic rather than steric reasons. The OC-6-4-3 stereochemistry is retained in the molybdenum(V) complex. The unpaired electron in $[\mathbf{5}^{t\mathrm{Bu}}]^+$ couples to the metal center ($^{95/97}$Mo), to the coordinated ^{31}P nucleus (CW EPR), as well as to ^{14}N and ^{1}H of the ligands (HYSCORE). The optical absorption bands of $[\mathbf{5}^{t\mathrm{Bu}}]^+$ are assigned to ligand field and charge transfer transitions. In conclusion, the imido/oxido π-donor ligands dramatically control the reactivity and stability of the reported Schiff base molybdenum complexes. The reactivity of the novel six-coordinate imido phosphane Mo^{IV} and Mo^{V} complexes is currently investigated in greater detail, especially with respect to exploiting the latent free coordination site by removing the phosphane.

■ ASSOCIATED CONTENT

Supporting Information

Energy profile of the Mo═N−C bending deformation in $\mathbf{2}^{\mathrm{H}}$, $\mathbf{5}^{\mathrm{H}}$, and $[\mathbf{5}^{\mathrm{H}}]^+$ obtained by DFT calculation fixed Mo═N−C angle and optimized geometry; $^{31}P\{^1H\}$ NMR reaction monitoring of the reactions $\mathbf{1}^{t\mathrm{Bu}}$ + PMe_3 and $\mathbf{2}^{t\mathrm{Bu}}$ + PMe_3 in THF at room temperature; NH-HMBC of $\mathbf{1}^{t\mathrm{Bu}}$, $\mathbf{2}^{t\mathrm{Bu}}$, $\mathbf{4}^{t\mathrm{Bu}}$, and $\mathbf{5}^{t\mathrm{Bu}}$ in d_8-THF; PH-COSY of $\mathbf{4}^{t\mathrm{Bu}}$ and $\mathbf{5}^{t\mathrm{Bu}}$ in d_8-THF; $^{31}P\{^1H\}$ NMR of the equilibrium reaction $\mathbf{4}^{t\mathrm{Bu}}$ + $SPEt_3$ in d_8-THF at 298 K; $^{31}P\{^1H\}$ NMR of the equilibrium reaction $\mathbf{5}^{t\mathrm{Bu}}$ + $SPEt_3$ in d_8-THF at 333 K; plots of $[PMe_3]$ vs time and $[PMe_3]/[PMe_3]_0$ vs time for the reaction between d_6-dmso and PMe_3 catalyzed by $\mathbf{1}^{t\mathrm{Bu}}$ at 298 K; plots of $[PMe_3]$ vs time and $[PMe_3]/[PMe_3]_0$ vs time for the reaction between d_6-dmso and PMe_3 catalyzed by $\mathbf{2}^{t\mathrm{Bu}}$ at 298 K; X-band EPR spectra of $[\mathbf{4}^{t\mathrm{Bu}}](\mathbf{PF_6})$ and $[\mathbf{5}^{t\mathrm{Bu}}](\mathbf{PF_6})$ in frozen THF at 77 K and simulation; Cartesian coordinates of DFT-optimized complexes. This material is available free of charge via the Internet at http://pubs.acs.org.

■ AUTHOR INFORMATION

Corresponding Author

*Fax: +49-6131-39-27277. E-mail: katja.heinze@uni-mainz.de.

Notes

The authors declare no competing financial interest.

■ ACKNOWLEDGMENTS

We thank the Deutsche Forschungsgemeinschaft for continuously supporting our work. We are grateful to Dr. Mihail Mondeshki for excellent NMR support, Regine Jung-Pothmann for X-ray data collection, and Dr. Andreas Fischer for exploratory experimental work.

■ REFERENCES

(1) Holm, R. *Chem. Rev.* **1987**, *87*, 1401−1449.
(2) Hille, R. *Chem. Rev.* **1996**, *96*, 2757−2816.
(3) Hille, R. *Trends Biochem. Sci.* **2002**, *27*, 360−367.
(4) John H. Enemark, J. H.; Cooney, J. J. A.; Wang, J.-J.; Holm, R. H. *Chem. Rev.* **2004**, *104*, 1175−1200.
(5) Schulzke, C. *Eur. J. Inorg. Chem.* **2011**, 1189−1199.
(6) Feng, C.; Tollin, G.; Enemark, J. H. *Biochim. Biophys. Acta* **2007**, *1774*, 527−539.
(7) Heinze, K.; Fischer, A. *Eur. J. Inorg. Chem.* **2007**, 1020−1026.
(8) Heinze, K.; Marano, G.; Fischer, A. *J. Inorg. Biochem.* **2008**, *102*, 1199−1211.
(9) Heinze, K.; Fischer, A. *Eur. J. Inorg. Chem.* **2010**, 1939−1947.
(10) Lyashenko, G.; Saischek, G.; Judmaier, M. E.; Volpe, M.; Baumgartner, J.; Belaj, F.; Jancik, V.; Herbst-Irmer, R.; Mösch-Zanetti, N. C. *Dalton Trans.* **2009**, 5655−5665.
(11) Mösch-Zanetti, N. C.; Wurm, D.; Volpe, M.; Lyashenko, G.; Harum, B.; Belaj, F.; Baumgartner, J. *Inorg. Chem.* **2010**, *49*, 8914−8921.
(12) Ramnauth, R.; Al-Juaid, S.; Motevalli, M.; Parkin, B. C.; Sullivan, A. C. *Inorg. Chem.* **2004**, *43*, 4072−4079.
(13) The stereochemistry of the complexes under study will be described by the configuration index according to the Cahn−Ingold−Prelog system in an octahedral complex OC-6-*x*-*y* with the priority sequence used as follows: PMe_3 > O > N^{imido} > $N^{pyrrolato}$ > N^{imine}. The first index *x* refers to the ligand priority of the ligand trans to the ligand of the highest priority (axial ligands), and the second index *y* refers to the ligand priority trans to the ligand of the equatorial plane which has the highest priority of these four equatorial ligands. Thus, molybdenum(VI) complexes $\mathbf{1}^{\mathrm{R}}$ and $\mathbf{2}^{\mathrm{R}}$ possess OC-6-4-4 stereochemistry, while molybdenum(IV) complexes $\mathbf{4}^{\mathrm{R}}$ and $\mathbf{5}^{\mathrm{R}}$ are OC-6-4-3 stereoisomers as depicted in Scheme 1. For the sake of better comparison with $\mathbf{2}^{\mathrm{R}}$ we enumerated both oxido ligands in $\mathbf{1}^{\mathrm{R}}$. Correctly, the preferred isomer of $\mathbf{1}^{\mathrm{R}}$ should be described by OC-6-3-3 as there is no distinguished fourth donor atom present.
(14) Cahn, R. S.; Ingold, C. K.; Prelog, V. *Angew. Chem., Int. Ed. Engl.* **1966**, *5*, 385−415.
(15) Prelog, V.; Helmchen, G. *Angew. Chem., Int. Ed. Engl.* **1982**, *21*, 567−583.
(16) Block, B. P.; Powell, W. H.; Fernelius, W. C. *Inorganic chemical nomenclature:principles and practice*; ACS Professional Reference Book; American Chemical Society: Washington, DC, 1990.
(17) von Zelewsky, A. *Stereochemistry of Coordination Compounds*: John Wiley & Sons Ltd.: New York, 1996.
(18) Cross, W. B.; Anderson, J. C.; Wilson, C. S. *Dalton Trans.* **2009**, 1201−1205.
(19) Cross, W. B.; Anderson, J. C.; Wilson, C.; Blake, A. J. *Inorg. Chem.* **2006**, *45*, 4556−4561.
(20) Gibson, V. C.; Graham, A. J.; Jolly, M.; Mitchell, J. P. *Dalton Trans.* **2003**, 4457−4465.
(21) Radius, U.; Wahl, G.; Sundermeyer, J. *Z. Anorg. Allg. Chem.* **2004**, *630*, 848−857.
(22) Rufanov, K. A.; Zarubin, D. N.; Ustynyuk, N. A.; Gourevitch, D. N.; Sundermeyer, J.; Churakov, A. V.; Howard, J. A. K. *Polyhedron* **2001**, *20*, 379−385.
(23) Merkoulov, A.; Harms, K.; Sundermeyer, J. *Eur. J. Inorg. Chem.* **2005**, 4902−4906.
(24) Stoll, S.; Schweiger, A. *J. Magn. Reson.* **2006**, *178*, 42−55.
(25) *SMART Data Collection and SAINT-Plus Data Processing Software for the SMART System (various versions)*; Bruker Analytical X-Ray Instruments, Inc.: Madison, WI, 2000.
(26) Blessing, B. *Acta Crystallogr.* **1995**, *A51*, 33−38.
(27) Sheldrick, G. M. *SHELXTL*, Version 5.1; Bruker AXS: Madison, WI, 1998.
(28) Sheldrick, G. M. *SHELXL-97*; University of Göttingen, Göttingen, Germany, 1997.
(29) Frisch, M. J.; Trucks, G. W.; Schlegel, H. B.; Scuseria, G. E.; Robb, M. A.; Cheeseman, J. R.; Montgomery, J. A.; Vreven, Jr., T.; Kudin, K. N.; Burant, J. C.; Millam, J. M.; Iyengar, S. S.; Tomasi, J.;

Barone, V.; Mennucci, B.; Cossi, M.; Scalmani, G.; Rega, N.; Petersson, G. A.; Nakatsuji, H.; Hada, M.; Ehara, M.; Toyota, K.; Fukuda, R.; Hasegawa, J.; Ishida, M.; Nakajima, T.; Honda, Y.; Kitao, O.; Nakai, H.; Klene, M.; Li, X.; Knox, J. E.; Hratchian, H. P.; Cross, J. B.; Adamo, C.; Jaramillo, J.; Gomperts, R.; Stratmann, R. E.; Yazyev, O.; Austin, A. J.; Cammi, R.; Pomelli, C.; Ochterski, J. W.; Ayala, P. Y.; Morokuma, K.; Voth, G. A.; Salvador, P.; Dannenberg, J. J.; Zakrzewski, V. G.; Dapprich, S.; Daniels, A. D.; Strain, M. C.; Farkas, O.; Malick, D. K.; Rabuck, A. D.; Raghavachari, K.; Foresman, J. B.; Ortiz, J. V.; Cui, Q.; Baboul, A. G.; Clifford, S.; Cioslowski, J.; Stefanov, B. B.; Liu, G.; Liashenko, A.; Piskorz, P.; Komaromi, I.; Martin, R. L.; Fox, D. J.; Keith, T.; Al-Laham, M. A.; Peng, C. Y.; Nanayakkara, A.; Challacombe, M.; Gill, P. M. W.; Johnson, B.; Chen, W.; Wong, M. W.; Gonzalez, C. Pople, J. A. *Gaussian 03*, Revision B.03; Gaussian, Inc.: Pittsburgh, PA, 2003.

(30) Huzinaga, S.; Andzelm, J.; Klobukowski, M.; Radzio-Andzelm, E.; Sakai, Y.; Tatewaki, H. *Gaussian Basis Sets for Molecular Orbital Calculations*; Elsevier: Amsterdam, 1984.

(31) Barone, V. In *Recent Advances in Density Functional Methods*; Chong, D. P., Ed.; World Scientific: Singapore, 1995; Part 1.

(32) The WTBS basis set was obtained from the Extensible Computational Chemistry Environment Basis Set Database, Version 02/02/06, as developed and distributed by the Molecular Science Computing Facility, Environmental and Molecular Sciences Laboratory, which is part of the Pacific Northwest Laboratory, P.O. Box 999, Richland, WA 99352, and funded by the U.S. Department of Energy. The Pacific Northwest Laboratory is a multiprogram laboratory operated by the Battelle Memorial Institute of the U.S. Department of Energy under Contract DE-AC06-76RLO.

(33) $R^{x}_{y}(n)$: The superscript x denotes the number of hydrogen acceptors, the subscript y the number of hydrogen donors, and n the ring size.

(34) Bernstein, J.; Davis, R. E.; Shimoni, L.; Chang, N.-L. *Angew. Chem., Int. Ed. Engl.* **1995**, *34*, 1555−1573.

(35) Ciszewski, J. T.; Harrison, J. F.; Odom, A. L. *Inorg. Chem.* **2004**, *43*, 3605−3617.

(36) Korn, K.; Schorm, A.; Sundermeyer, J. *Z. Anorg. Allg. Chem.* **1999**, *625*, 2125−2132.

(37) Koch, W.; Holthausen, M. C. *A Chemist's Guide to Density Functional Theory*; Wiley-VCH: Weinheim, 2001; p 134.

(38) An imido-bridged Mo^{V} dimer has been reported, although with five-coordinate molybdenum centers, i.e., with less steric congestion: Ortiz, C. G.; Abboud, K. A.; Boncella, J. M. *Organometallics* **1999**, *18*, 4253−4260.

(39) Dyer, P. W.; Gibson, V. C.; Howard, J. A. K.; Whittle, B.; Wilson, C. *Polyhedron* **1995**, *14*, 103−111.

(40) Tolman, C. A. *Chem. Rev.* **1977**, *77*, 313−348.

(41) Addison, A. W.; Rao, T. N.; Reedijk, J.; van Rijn, J.; Verschoor, G. C. *J. Chem. Soc., Dalton Trans.* **1984**, 1349−1356.

(42) Mayilmurugan, R.; Harum, B. N.; Volpe, M.; Sax, A. F.; Palaniandavar, M.; Mösch-Zanetti, N. C. *Chem. − Eur. J.* **2011**, *17*, 704−713.

(43) Mtei, R. P.; Lyashenko, G.; Stein, B.; Rubie, N.; Hille, R.; Kirk, M. L. *J. Am. Chem. Soc.* **2011**, *133*, 9762−9774.

(44) Bickely, D. G.; Serpone, N. *Inorg. Chem.* **1976**, *15*, 2577−2582.

(45) (a) Höfer, P.; Grupp, A.; Nebenführ, H.; Mehring, M. *Chem. Phys. Lett.* **1986**, *132*, 279−282. (b) Calle, C.; Sreekanth, A.; Fedin, M. V.; Forrer, J.; Garcia-Rubio, I.; Gromov, I. A.; Hinderberger, D.; Kasumaj, B.; Léger, P.; Mancosu, B.; Mitrikas, G.; Santangelo, M. G.; Stoll, S.; Schweiger, A.; Tschaggelar, R.; Harmer, J. *Helv. Chim. Acta* **2006**, *89*, 2495−2521. (c) Schweiger, A.; Jeschke, G. *Principles of Pulsed Electron Paramagnetic Resonance*; Oxford University Press, 2001.

(46) (a) Hinderberger, D.; Piskorski, R.; Goenrich, M.; Thauer, R. K.; Schweiger, A.; Harmer, J.; Jaun, B. *Angew. Chem., Int. Ed.* **2006**, *45*, 3602−3607. (b) Madi, Z.; van Dorslaaer, S.; Schweiger, A. *J. Magn. Reson.* **2002**, *154*, 181−191. (c) Kasumaj, B.; Stoll, S. *J. Magn. Reson.* **2008**, *190*, 233−247.

(47) Evans, D. F. *J. Chem. Soc.* **1959**, 2003−2005.

(48) Sur, S. K. *J. Magn. Reson.* **1989**, *82*, 169−173.

(49) Hare, C. R.; Bernal, I.; Gray, H. B. *Inorg. Chem.* **1962**, *1*, 831−835.

4.3 Intramolecular electron transfer between molybdenum and iron mimicking bacterial sulphite dehydrogenase

Kristina Hüttinger, Christoph Förster and Katja Heinze, *Chem. Commun.* **2014**, *50*, 4285–4288.

DOI: 10.1039/c3cc46919k

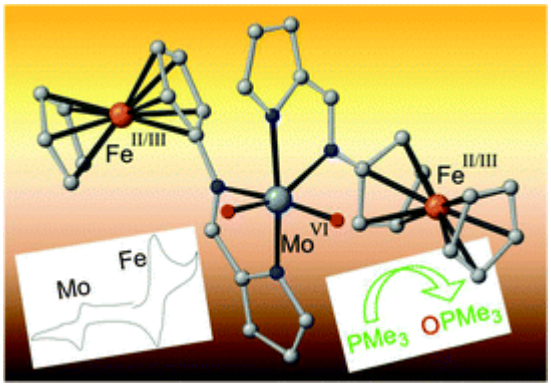

Volume 50 | Number 33 | 28 April 2014 | Pages 4261–4384

ChemComm

Chemical Communications
www.rsc.org/chemcomm

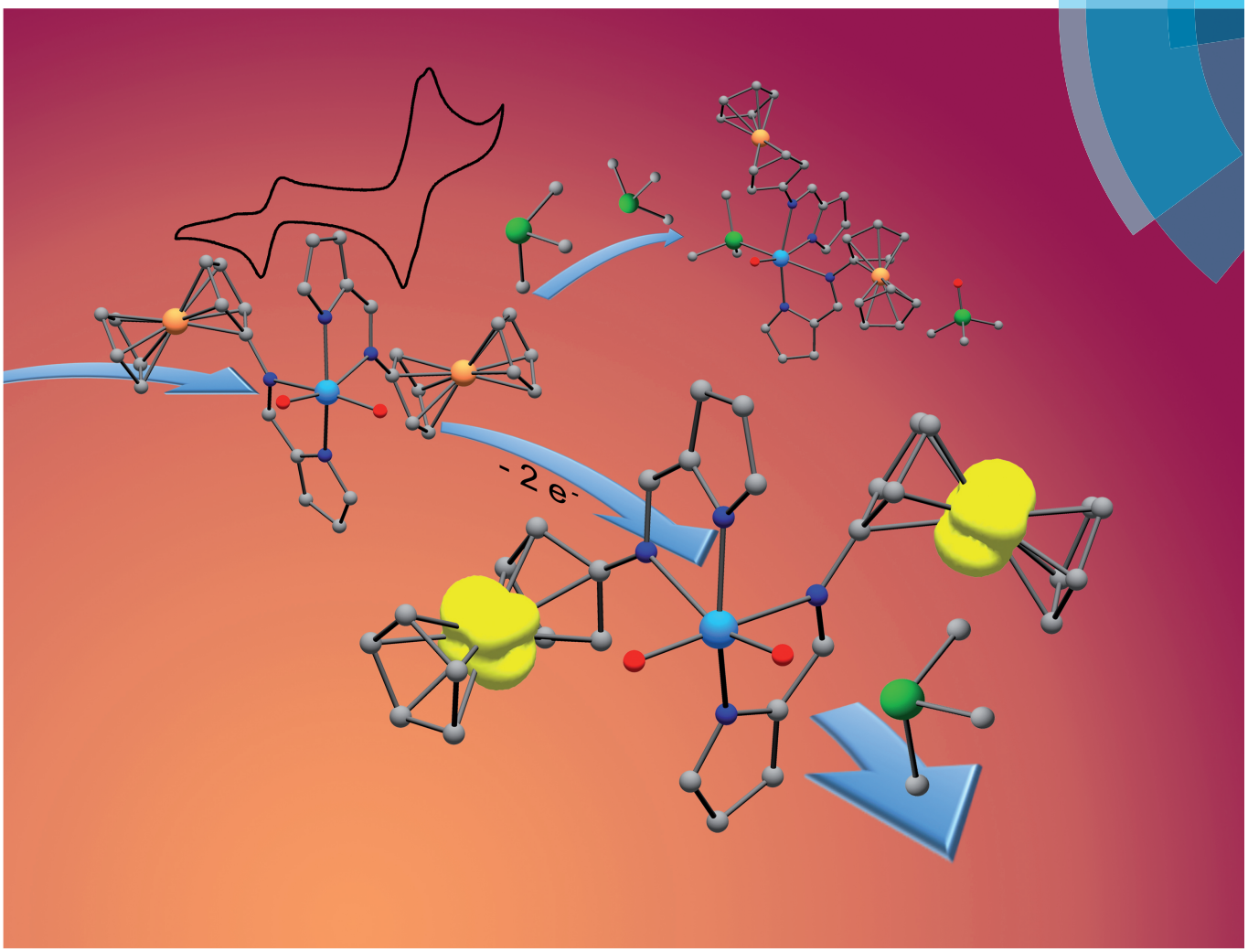

ISSN 1359-7345

ROYAL SOCIETY OF CHEMISTRY

COMMUNICATION
Katja Heinze *et al.*
Intramolecular electron transfer between molybdenum and iron mimicking bacterial sulphite dehydrogenase

ChemComm

COMMUNICATION

View Article Online
View Journal

Intramolecular electron transfer between molybdenum and iron mimicking bacterial sulphite dehydrogenase†

Cite this: DOI: 10.1039/c3cc46919k

Received 10th September 2013,
Accepted 7th January 2014

DOI: 10.1039/c3cc46919k

www.rsc.org/chemcomm

Kristina Hüttinger, Christoph Förster and Katja Heinze*

Diferrocenyl/diferrocenium substituted dioxido molybdenum(VI) complexes $[Fe_2MoO_2]$ $2^{Fc}/[2^{Fc}]^{2+}$ mimic the catalytic active site including the redox subunits as well as the catalytic function of bacterial sulphite oxidases.

Sulphite-oxidising molybdenum enzymes transform toxic sulphite into sulphate using H_2O as the oxygen source.[1–4] The active site of sulphite oxidases (SOs) comprises a $[Mo^{VI}O_2]$ centre (Scheme 1a) capable of binding SO_3^{2-} and transferring an oxygen atom to give SO_4^{2-} (oxygen atom transfer, OAT).

The reduced $[Mo^{IV}O]$ site undergoes two subsequent proton-coupled one-electron transfer steps to (oxidised) cytochrome units, *e.g.* cyt b_5 in animal SO or cyt *c* in bacterial SO (sulphite dehydrogenase, SHD).[3] In animal and human SOs the electron accepting cyt b_5 subunit is connected to the Mo domain by a flexible peptide tether with a Mo···Fe distance of 32 Å.[5,6]

Current mechanistic proposals suggest that the enzyme undergoes a conformational change before the electron transfer step with the heme unit approaching the molybdenum active site more closely.[3] On the other hand, in bacterial SDH of *Starkeya novella* the electron accepting cyt *c* is rigidly located close to the Mo domain with a Mo···Fe distance of 16.6 Å[7] providing a rapid and efficient intramolecular electron transfer (IET) pathway between $Mo^{IV/V}$ and Fe^{III} (Scheme 1a).[3] The IET from Mo^{IV} to Fe^{III} is coupled to a proton release from coordinated water (Scheme 1b). After electron transfer from Fe^{II} to oxidized external cyt *c* a further proton-coupled IET between Fe^{III} and Mo^{V} is proposed (Scheme 1b).[3] Although several molecular structural models and functional OAT model systems are known,[8–10] only very few biomimetic complexes model the proton-coupled electron transfer steps.[11–16] To the best of our knowledge ET in reported model systems occurs only for *external* electron acceptors (intermolecular ET).

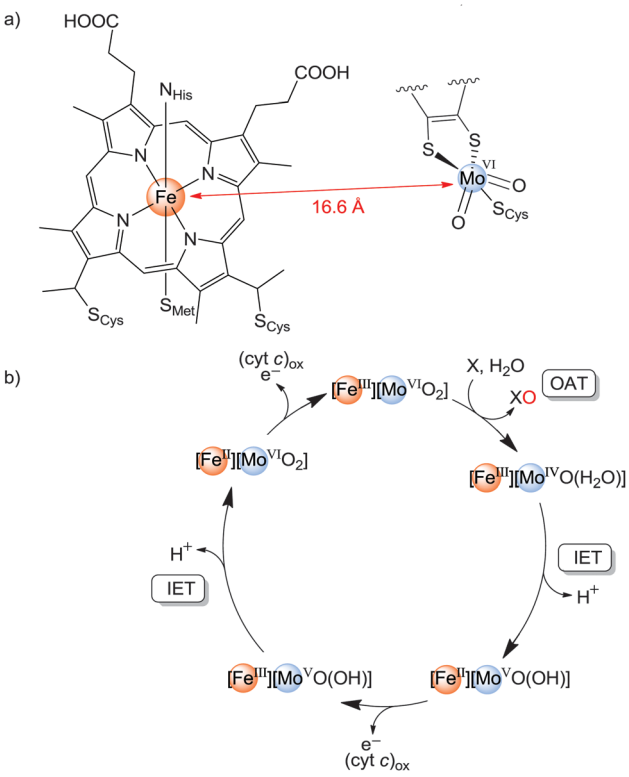

Scheme 1 (a) Sketch of the molybdenum and iron active sites of SDH from *Starkeya novella* and (b) proposed catalytic cycle of SOs.

We have previously designed functional Mo^{VI} model complexes to study the OAT between $[Mo^{VI}O_2]$ units and an artificial substrate as well as the subsequent ETs to an artificial *external* one-electron oxidant (ferrocenium).[13–16] We and others could demonstrate the occurrence of well-defined $[Mo^{IV}E]$ and $[Mo^{V}E]$ species (E = O, N^tBu) during the catalytic cycle with a further substrate coordinated to reduced $[Mo^{IV/V}E]$ centres at high substrate concentrations.[13,16,17] Later, Enemark *et al.* provided strong EPR evidence that

Institute of Inorganic Chemistry and Analytical Chemistry, Johannes Gutenberg-University of Mainz, Duesbergweg 10-14, 55128 Mainz, Germany. E-mail: katja.heinze@uni-mainz.de; Fax: +49-6131-39-27277; Tel: +49-6131-39-25886

† Electronic supplementary information (ESI) available: Experimental procedures, spectral and X-ray diffraction details, nomenclature of stereochemistry, DFT calculations. CCDC 956709 and 956710. For ESI and crystallographic data in CIF or other electronic format see DOI: 10.1039/c3cc46919k

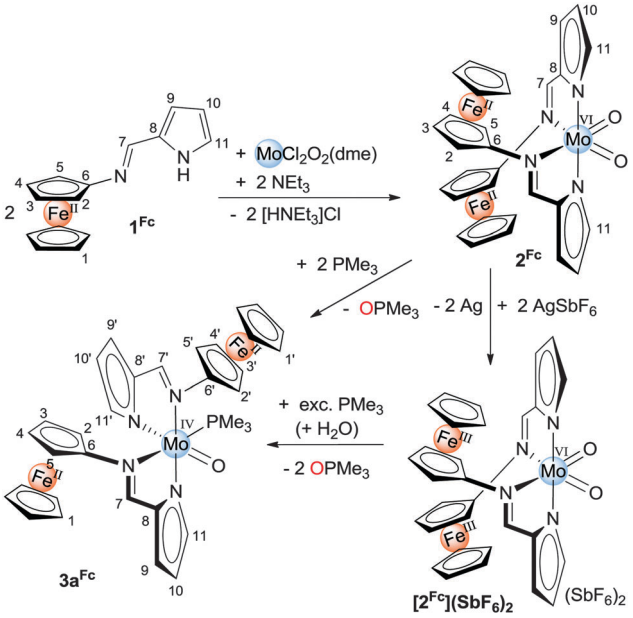

Scheme 2 Synthesis of the biomimetic model complexes $\mathbf{2^{Fc}}$/$\mathbf{[2^{Fc}](SbF_6)_2}$ and $\mathbf{3a^{Fc}}$ including atom numbering for NMR assignments.

SO_3^{2-} also binds to reduced Mo^V in a mutant of human SO ("blocked form").[18]

In this contribution we present the elaborate SDH model $\mathbf{2^{Fc}}$ (Scheme 2) comprising a functional $[Mo^{VI}O_2]$ catalytic unit[13–16] and two low spin $Fe^{II/III}$ complexes as functional cytochrome mimics (Fc/Fc^+ couple) in the second coordination sphere in order to model the IET step(s) of SDHs. The presence of *two* Fc units is especially interesting as the molybdenum enzyme of *Thermus thermophilus* is reported to contain a di-heme[19] cytochrome *c*550.[20] The close proximity of two heme units to the molybdenum active site is proposed to accelerate the two consecutive IET steps as two electrons can be stored at two Fe centres.[20] Ferrocenyl phosphane ligands have been amply used in catalysis but mostly as inert scaffolds. Redox active ligands with functional Fc/Fc^+ subunits have been successfully incorporated into an olefin-metathesis catalyst of the Grubbs–Hoveyda type for recycling purposes.[21] Rauchfuss *et al.* employed a functional Fc/Fc^+ unit in the second coordination sphere of a carbonyl diiron platform giving an active [FeFe] hydrogenase model system with Fc/Fc^+ mimicking the 4Fe–4S cluster of the enzyme.[22] Enemark has studied a bimetallic structural and spectroscopic SO model composed of a $[Mo^VO]$ complex linked to an Fe^{III} porphyrin.[23]

The Fc containing chelate $\mathbf{1^{Fc}}$ (Scheme 2) is readily prepared from aminoferrocene and pyrrol-2-carbaldehyde. $\mathbf{1^{Fc}}$ crystallises as a hydrogen-bonded dimer, similar to its *p*-^{t}Bu-C_6H_4 substituted ferrocene-free analogue $\mathbf{1^{tBu}}$ (Fig. 1a).[16] Stirring two equivalents of the bright red chelate $\mathbf{1^{Fc}}$ in the presence of a base with $MoCl_2O_2$(dme) yields the dark red $[Fe_2MoO_2]$ complex $\mathbf{2^{Fc}}$ (Scheme 2). The MoO stretching vibrations of $\mathbf{2^{Fc}}$ (929/905 cm^{-1}) are similar to those of $\mathbf{2^{tBu}}$ (928/902 cm^{-1}).[16] Single crystal XRD of $\mathbf{2^{Fc}}$ reveals the double coordination of deprotonated $\mathbf{1^{Fc}}$ at molybdenum giving the expected OC-6-4-4 stereoisomer (Fig. 1b, ESI†). The Mo–O (1.6983(19)–1.7014(17) Å) and Mo–N distances ($Mo–N^{pyrrol}$ = 2.0674(19)–2.0925(21) Å; $Mo–N^{imine}$ = 2.3329(19)–2.4256(19) Å) in

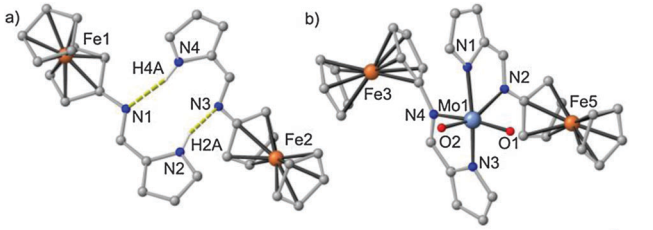

Fig. 1 Molecular structures derived from single crystal XRD of (a) $\mathbf{1^{Fc}}$ and (b) $\mathbf{2^{Fc}}$ (one of the two independent molecules shown). CH hydrogen atoms omitted.

$\mathbf{2^{Fc}}$ are fully compatible with those of $\mathbf{2^{tBu}}$.[16] The Fe–Cp(centroid) distances (1.65 Å) in $\mathbf{2^{Fc}}$ are very similar to those found in $\mathbf{1^{Fc}}$ (Fig. 1). These structural data confirm that $\mathbf{2^{Fc}}$ is best described as a $[Fe^{II}{}_2Mo^{VI}O_2]$ complex. In the solid state the intramolecular Mo···Fe distances are between 4.8 and 5.3 Å. The Cp rings of the chelate ligands are twisted with respect to the chelate plane with torsion angles ranging between ±13° and ±48° suggesting a certain conformational flexibility of the appended redox centres. In solution full rotation of the Fc substituents relative to their chelate planes is hindered as suggested by the appearance of separate resonances for H^2/H^5 and H^3/H^4, respectively (Scheme 2), similar to the situation found in Pt(NC–CH=CH–CN)(Fc–N=CH–py).[24] Proton H^5 experiences a high-field shift due to the ring current of the nearby pyrrolate of the other chelate ligand as well as an NOE contact to H^{11} of that chelate. DFT calculations (B3LYP; LANL2DZ + polarisation functions for N, O; PCM THF) fully support the $[Fe^{II}{}_2Mo^{VI}O_2]$ valence description and furthermore corroborate one rather coplanar Fc unit (±14°) and a more twisted one (±46°) in $\mathbf{2^{Fc}}$ with short $H^5···H^{11}$ (2.9–3.3 Å) and $H^5···$pyrrol(centroid) contacts (2.5–3.2 Å) in the optimised geometry (ESI†). The pyrrolate → $MoO_2(\pi^*)$ CT absorption of $\mathbf{2^{Fc}}$ is shifted to a higher energy (385 nm, 8420 M^{-1} cm^{-1}) as compared to $\mathbf{2^{tBu}}$ (436 nm, 9440 M^{-1} cm^{-1}) (ESI†). A Fc → $MoO_2(\pi^*)$ CT absorption is found at 549 nm. TD-DFT calculations indeed assign the lowest energy absorption to a CT essentially composed of the filled $d_{x^2-y^2}$ orbital of the more coplanar Fc unit to the two Mo=O π^* orbitals (ESI†) suggesting the presence of an IET pathway with the substituted Cp ring of Fc being coplanar to the chelate.

Similar to $\mathbf{2^{tBu}}$ complex $\mathbf{2^{Fc}}$ is capable of transferring an oxygen atom to PMe_3 to give $OPMe_3$ ($\delta(^{31}P)$ = 29.8 ppm) and substrate-bound complexes $\mathbf{3^{Fc}}$ within hours (Scheme 2).[16] $\mathbf{3^{Fc}}$ forms two stereoisomers in solution ($\delta(^{31}P)$ = 2.1 and −5.6 ppm for $\mathbf{3a^{Fc}}$ and $\mathbf{3b^{Fc}}$ in THF, respectively; ratio 5 : 2; ESI†) fully congruent with the reactivity of $\mathbf{3^{tBu}}$.[16] The $[Fe^{II}{}_2Mo^{IV}O]$ complexes $\mathbf{3^{Fc}}$ correspond to the fully reduced form of SO suggested by Hille to be formed in a slow side reaction.[25] The major stereoisomer $\mathbf{3a^{Fc}}$ possesses the OC-6-4-3 configuration according to NOE data and by comparison with $\mathbf{3a^{tBu}}$ (ESI†).[16] The Fe^{II} centres in $\mathbf{1^{Fc}}$ and $\mathbf{2^{Fc}}$ are reversibly oxidised at −45 mV and −30/+80 mV *vs.* FcH/FcH^+, respectively (Fig. 2). For $\mathbf{2^{Fc}}$ the small separation of the oxidation waves (≈100 mV) indicates a weak electronic interaction of the appended $Fe^{II/III}$ moieties either *via* the Mo^{VI} centre or electrostatically through space in $[\mathbf{2^{Fc}}]^+$ ($\mathbf{2^{Fc}}$: Fe···Fe = 8 Å). A quasireversible reduction of the Mo^{VI} core in $\mathbf{2^{Fc}}$ is observed at −1540 mV (Fig. 2b). The Fe^{III} centres in $[\mathbf{2^{Fc}}]^{2+}$ should be able to oxidise Mo^{IV} to Mo^V and further to Mo^{VI}.[13,16]

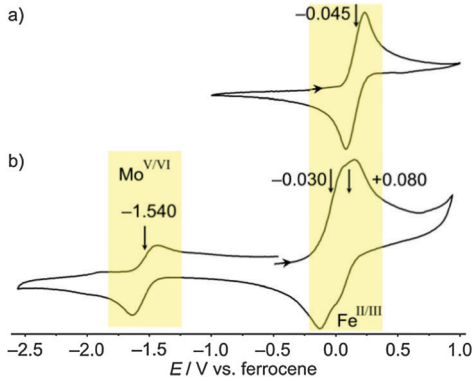

Fig. 2 Cyclic voltammograms of (a) $\mathbf{1}^{\mathbf{Fc}}$ and (b) $\mathbf{2}^{\mathbf{Fc}}$ (bottom) in $[^{n}Bu_4N][B(C_6F_5)_4]$/THF.

Addition of two equivalents of $AgSbF_6$ to a solution of $\mathbf{2}^{\mathbf{Fc}}$ in THF oxidises both Fe^{II} centres to the $[Fe^{III}{}_2Mo^{VI}O_2]$ dication $[\mathbf{2}^{\mathbf{Fc}}]^{2+}$ (Scheme 2, Fig. 3a). The ESI+ mass spectrum displays cluster peaks corresponding to $[\mathbf{2}^{\mathbf{Fc}}]^{+}$ (m/z 684.0) and $\{[\mathbf{2}^{\mathbf{Fc}}](\mathbf{SbF_6})\}^{+}$ (m/z 918.9) confirming the successful charging of $\mathbf{2}^{\mathbf{Fc}}$. The UV/Vis spectrum of $[\mathbf{2}^{\mathbf{Fc}}]^{2+}$ in CH_3CN features an absorption band at 934 nm (445 M^{-1} cm^{-1}) which is assigned to a pyrrol(at)e → Fc^{+} CT by comparison with the corresponding band of $[\mathbf{1}^{\mathbf{Fc}}]^{+}$ (917 nm; 610 M^{-1} cm^{-1}; ESI†). The pyrrolate → $MoO_2(\pi^*)$ bands of $[\mathbf{2}^{\mathbf{Fc}}]^{2+}$ are slightly shifted to a lower energy (442 nm, 5295 M^{-1} cm^{-1}) as compared to $\mathbf{2}^{\mathbf{tBu}}$.[16] Spectroelectrochemical oxidation of $\mathbf{2}^{\mathbf{Fc}}$ in THF/$[^{n}Bu_4N][B(C_6F_5)_4]$ yields similar data including isosbestic points at 559 and 679 nm (ESI†). The ^{1}H NMR spectrum of $[\mathbf{2}^{\mathbf{Fc}}]^{2+}$ shows paramagnetically broadened and shifted resonances at δ = 27.9, 24.2, 21.6 ($H^{1,2,3,4,5}$), 7.1, 5.2, 0.3 ($H^{9,10,11}$) and −8.4 (H^{7}) ppm (ESI†). The strong shift to a lower field (δ > 20 ppm) is characteristic for ferrocenium ions[26] while the rather sharp resonances at δ = 7.1, 5.2 and 0.3 ppm are correlated in the HH COSY suggesting that these belong to the pyrrolate unit bearing less spin density than the ferrocenium moieties. A frozen solution of the monoferrocenium cation $[\mathbf{1}^{\mathbf{Fc}}]^{+}$ (S = 1/2) is EPR active at 77 K (ESI†)[27] while $[\mathbf{2}^{\mathbf{Fc}}]^{2+}$ is EPR silent possibly due to the increased relaxation rate in $[\mathbf{2}^{\mathbf{Fc}}]^{2+}$ with two rather close paramagnetic ferrocenium ions.

Addition of 1 eq. PMe_3 to $[\mathbf{2}^{\mathbf{Fc}}]^{2+}$ to CD_3CN results in a rapid reaction (in contrast to the slow reaction of neutral $\mathbf{2}^{\mathbf{Fc}}$ with PMe_3) with consumption of PMe_3 within minutes (disappearance of $\delta(^{31}P)$ = −54.7 ppm resonance). The ^{1}H NMR spectrum of the reaction mixture shows shifted and broadened resonances different from those of pure $[\mathbf{2}^{\mathbf{Fc}}]^{2+}$. Excess PMe_3 finally yields a mixture of the phosphane Mo^{IV} complexes $\mathbf{3a}^{\mathbf{Fc}}/\mathbf{3b}^{\mathbf{Fc}}$ ($\delta(^{31}P)$ = 3.0 and −4.8 ppm in CD_3CN) as well as $OPMe_3$ ($\delta(^{31}P)$ = 36.2 ppm in CD_3CN) in a 5 : 4 : 18 ratio (ESI†). This ratio implies that one eq. $[\mathbf{2}^{\mathbf{Fc}}]^{2+}$ produces two eq. of $OPMe_3$, *i.e.* 1 eq. more than neutral $\mathbf{2}^{\mathbf{Fc}}$ (Scheme 2). Hence, we propose that after the initial attack of PMe_3 on $[\mathbf{2}^{\mathbf{Fc}}]^{2+}$ to give transient $[\mathbf{4}^{\mathbf{Fc}}]^{2+}$ (Fig. 3b) $OPMe_3$ is substituted by (inadvertently present) H_2O (Scheme 1b). The coordinated water at the doubly charged complex is then simply deprotonated to give neutral $\mathbf{2}^{\mathbf{Fc}}$ after or synchronous to double IET. Spin densities, natural atomic charges and Fe···Cp(centroid) distances of the proposed initially formed transient $OPMe_3$ adduct $[\mathbf{4}^{\mathbf{Fc}}]^{2+}$ clearly show that a single IET has already occurred to give the mixed-valent $[Fe^{II}Fe^{III}Mo^{V}O(OPMe_3)]^{2+}$ complex $^3[\mathbf{4}^{\mathbf{Fc}}]^{2+}$ in the triplet state (Fig. 3b).‡ These findings suggest that OAT is intimately coupled to ET in such compact systems with close contacts between redox units. It is conceivable that the OAT step is accelerated with the aid of concomitant IET or that ET might even precede the OAT with Mo=O acting as a redox relay between Fe^{III} and the substrate. Current studies are aimed at identifying more intermediates during and after OAT/IET in the $[\mathbf{2}^{\mathbf{Fc}}]^{2+}$/substrate system as well as probing the distance dependence of IET between Fe and the Mo active sites.

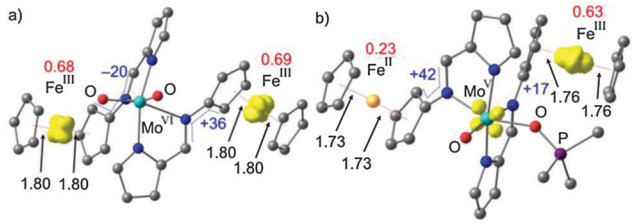

Fig. 3 DFT optimised geometry of (a) $[\mathbf{2}^{\mathbf{Fc}}]^{2+}$ and (b) $[\mathbf{4}^{\mathbf{Fc}}]^{2+}$ in the triplet states (spin densities at 0.05 a.u.; distances in Å; angles in deg; natural atomic charges at iron in red; hydrogen atoms omitted).

Notes and references

‡ According to DFT in the thermodynamically less favoured singlet state even both Fc^{+} sites are reduced giving formally the $[Fe^{II}{}_2Mo^{VI}O(OPMe_3)]^{2+}$ valence isomer $^1[\mathbf{4}^{\mathbf{Fc}}]^{2+}$ by double IET (see ESI†).

1 C. Kisker, H. Schindelin and D. C. Rees, *Annu. Rev. Biochem.*, 1997, **66**, 233.
2 (*a*) R. Hille, *Chem. Rev.*, 1996, **96**, 2757; (*b*) R. Hille, T. Nishino and F. Bittner, *Coord. Chem. Rev.*, 2011, **255**, 1179.
3 C. Feng, G. Tollin and J. H. Enemark, *Biochim. Biophys. Acta*, 2007, **1774**, 527.
4 K. Johnson-Winters, G. Tollin and J. H. Enemark, *Biochemistry*, 2010, **49**, 7242.
5 C. Kisker, H. Schindelin, A. Pacheco, W. A. Wehbi, R. M. Garrett, K. V. Rajagopalan, J. H. Enemark and D. C. Rees, *Cell*, 1997, **91**, 973.
6 A. V. Astashkin, A. Rajapakshe, M. J. Cornelison, K. Johnson-Winters and J. H. Enemark, *J. Phys. Chem. B*, 2012, **116**, 1942.
7 U. Kappler and S. Bailey, *J. Biol. Chem.*, 2005, **280**, 24999.
8 J. H. Enemark, J. J. A. Cooney, J.-J. Wang and R. H. Holm, *Chem. Rev.*, 2004, **104**, 1175.
9 J. H. Enemark and J. J. A. Cooney, in *Concepts and Models in Bioinorganic Chemistry*, ed. H. B. Kraatz and N. Metzler-Nolte, Wiley-VCH, Weinheim, Germany, 2006, p. 237.
10 C. Schulzke, *Eur. J. Inorg. Chem.*, 2011, 1189.
11 Z. Xiao, M. A. Bruck, J. H. Enemark, C. G. Young and A. G. Wedd, *Inorg. Chem.*, 1996, **35**, 7508.
12 A. Rajapakshe, R. A. Snyder, A. V. Astashkin, P. Bernardson, D. J. Evans, C. G. Young, D. H. Evans and J. H. Enemark, *Inorg. Chim. Acta*, 2009, **362**, 4603.
13 K. Heinze and A. Fischer, *Eur. J. Inorg. Chem.*, 2007, 1020.
14 K. Heinze, G. Marano and A. Fischer, *J. Inorg. Biochem.*, 2008, **102**, 1199.
15 K. Heinze and A. Fischer, *Eur. J. Inorg. Chem.*, 2010, 1939.
16 K. Hüttinger, C. Förster, T. Bund, D. Hinderberger and K. Heinze, *Inorg. Chem.*, 2012, **51**, 4180.
17 M. Volpe and N. C. Mösch-Zanetti, *Inorg. Chem.*, 2012, **51**, 1440.
18 (*a*) E. L. Klein, A. M. Raitsimring, A. V. Astashkin, A. Rajapakshe, K. Johnson-Winters, A. R. Arnold, A. Potapov, D. Goldfarb and J. H. Enemark, *Inorg. Chem.*, 2012, **51**, 1408; (*b*) R. C. Bray, M. T. Lamy, S. Gutteridge and T. Wilkinson, *Biochem. J.*, 1982, **201**, 241.
19 Z. Chen, M. Koh, G. Van Driessche, J. J. Van Beeumen, R. G. Bartsch, T. E. Meyer, M. A. Cusanovich and F. Scott Mathews, *Science*, 1994, **266**, 430.
20 (*a*) S. Robin, M. Arese, E. Forte, P. Sarti, A. Giuffrè and T. Soulimane, *J. Bacteriol.*, 2011, **193**, 3988; (*b*) S. Robin, M. Arese, E. Forte, P. Sarti, O. Kolaj-Robin, A. Giuffrè and T. Soulimane, *PLoS One*, 2013, **8**, e55129, DOI: 10.1371/journal.pone.0055129.

21 M. Süßner and H. Plenio, *Angew. Chem., Int. Ed.*, 2005, **44**, 6885.
22 J. M. Camara and T. B. Rauchfuss, *Nat. Chem.*, 2012, **4**, 26.
23 P. Basu, A. M. Raitsimring, M. J. LaBarre, I. K. Dhawan, J. L. Weibrecht and J. H. Enemark, *J. Am. Chem. Soc.*, 1994, **116**, 7166.
24 K. Heinze and S. Reinhardt, *Organometallics*, 2007, **26**, 5406.
25 M. S. Brody and R. Hille, *Biochemistry*, 1999, **38**, 6668.
26 (*a*) T.-Y. Dong, M.-Y. Hwang, T.-L. Hsu, C.-C. Schei and S.-K. Yeh, *Inorg. Chem.*, 1990, **29**, 80; (*b*) D. Siebler, M. Linseis, T. Gasi, L. M. Carrella, R. F. Winter, C. Förster and K. Heinze, *Chem.–Eur. J.*, 2011, **17**, 4540.
27 D. Siebler, C. Förster, T. Gasi and K. Heinze, *Organometallics*, 2011, **30**, 313.

4.4 Coupled oxygen atom transfer and electron transfer in dioxido molybdenum(VI) complexes bearing neutral and oxidized ferrocenyl substituents

Kristina Hanauer, Christoph Förster and Katja Heinze

Modified version to be submitted **2017**.

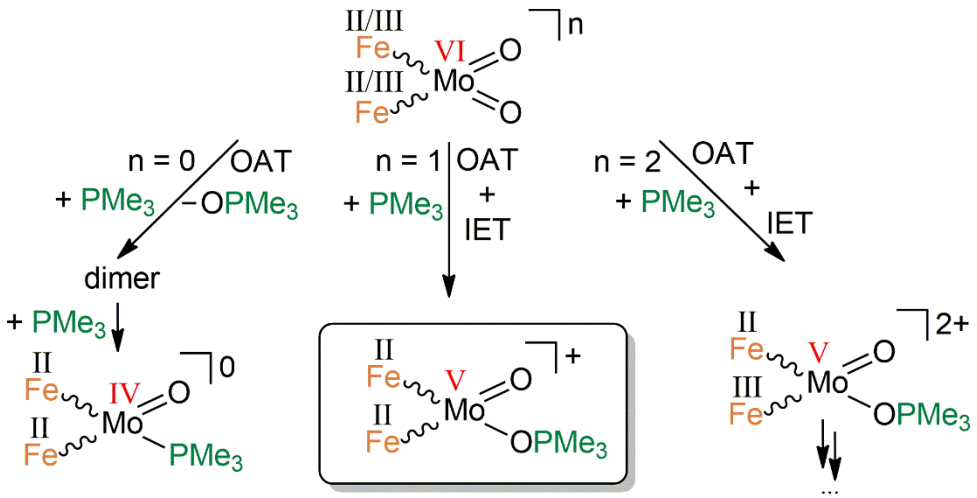

Coupled oxygen atom transfer and electron transfer in dioxido molybdenum(VI) complexes bearing neutral and oxidized ferrocenyl substituents

Kristina Hanauer, Christoph Förster, Katja Heinze

ABSTRACT

The dioxido molybdenum(VI) complex $Mo^{VI}(L^{Fc})_2O_2$ (**2^{Fc}**) with **L**^{Fc} = *N*-((pyrrolato-2-yl)methylene)ferrocenylamine (**1^{Fc}**) is the first reported model system for the enzyme sulfite dehydrogenase which allows to study intramolecular electron transfer (IET) coupled oxygen atom transfer (OAT).[208] An extension of this study with focus on the role of the ligands' oxidation states in these reactions is presented. Single and double oxidation of the redox-active ferrocenyl-substituted ligands of **2^{Fc}** give the stable paramagnetic complexes $[Mo^{VI}(L^{Fc})_2O_2]^+$ (**[2^{Fc}]$^+$**) and $[Mo^{VI}(L^{Fc})_2O_2]^{2+}$ (**[2^{Fc}]$^{2+}$**), with one or two ferrocenium units, respectively. Addition of an excess of PMe_3 to **2^{Fc}** leads to $OPMe_3$ and the $Mo^{IV}(L^{Fc})_2O(PMe_3)$ complex **3^{Fc}**. The $Mo^{IV/V}$ oxidation of **3^{Fc}** is irreversible. OAT of **2^{Fc}** to PPh_3 finally yields the dimer $[Mo^{V}(L^{Fc})_2O]_2(\mu$-O) (**4^{Fc}**) which can be reversibly oxidized four times. Reaction of PMe_3 with **[2^{Fc}]$^{2+}$** shows formation of **3^{Fc}** and concomitant attack of PMe_3 at the Cp ring and iron center. Reaction of PMe_3 with **[2^{Fc}]$^+$** yields an EPR-active Mo^V species. Based on DFT calculations and spectroscopic data, we propose the formation of the phosphoryl molybdenum(V) complex $[Mo^{V}(L^{Fc})_2O(OPMe_3)]^+$. This valence isomer is generated by OAT ($[Mo^{VI}(Fe^{II/III})_2O_2]^+ + PMe_3 \rightarrow [Mo^{IV}(Fe^{II/III})_2O(OPMe_3)]^+$) followed by IET ($[Mo^{IV}(Fe^{II/III})_2O(OPMe_3)]^+ \rightarrow [Mo^{V}(Fe^{II/II})_2O(OPMe_3)]^+$).

INTRODUCTION

Oxygen atom transfer (OAT) is an essential reaction in various biological systems.[13,117,209,210] The design of model complexes aims at a better understanding of the enzymatic reaction mechanisms.[142,163,211,212] We and others have developed model complexes for the molybdenum-containing enzyme sulfite oxidase (SO).[174,193,195,196,213–215] In SOs one oxygen atom is transferred from a $[Mo^{VI}O_2]^{2+}$ unit to SO_3^{2-}, whereby molybdenum is reduced from the oxidation state +VI to +IV in the biological cycle. The initial Mo^{VI} state is restored by two single proton-coupled intramolecular electron transfer (IET) steps to an adjacent heme unit which is integrated in the SO. The transferred oxygen atom is replaced by an oxygen atom from a water molecule. Model complexes featuring two chelate ligands and a $[MoO_2]^{2+}$ unit are active towards artificial substrates such as phosphane molecules, e.g. trimethylphosphane (Scheme 26, $\mathbf{HL^{R,R'}}$, $\mathbf{A^{R,R'}}$).[213] Recently we have presented a dioxido molybdenum (VI) complex $Mo(L^{Fc})_2O_2$ with a redox-active ferrocenyl moiety integrated into the chelate ligand $\mathbf{L}^{Fc}$ = $\mathbf{1^{Fc}}$ as model system for the sulfite dehydrogenase (SDH) *Thermus Thermophilus*[127,128] (Scheme 26, $\mathbf{1^{Fc}}$, $\mathbf{2^{Fc}}$).[208] A special feature of this enzyme is the electron transfer (ET) to a diheme cytochrome.[127] This diheme unit is represented by the two ferrocenyl-substituted ligands in the model system. Double oxidation of the ferrocenyl moieties of the $Mo(L^{Fc})_2O_2$ complex $\mathbf{2^{Fc}}$ to $[\mathbf{2^{Fc}}]^{2+}$ followed by reduction at the molybdenum center via OAT with PMe_3 imitates an IET-coupled OAT reaction.[208] $\mathbf{2^{Fc}}$ is the first reported model complex for SOs with internal electron acceptors. Very recently, Duhme-Klair et al. have reported a Ru^{II}-Mo^{VI} dyad imitating also an IET-coupled OAT reaction, in which the IET step occurs light-induced. After photoexcitation of Ru^{II}, an oxidative quenching with a mediator yields Ru^{III} and an electron transfer from ligand L to Ru^{III} occurs and forms the dyad $[Ru^{II}(bpy)_2(L^+)Mo^{VI}O_2(solv)]^{2+}$ (bpy = bipyridyl, L = phenanthroline-thiosemicarbazone ligand). In this state the dyad catalyzes OAT from DMSO to triphenylphosphane including an IET step to L^+. The OAT cycle runs faster with the involvement of the redox-active unit, which is necessary for the IET, than without the light-induced process.[203]

Starting from neutral $\mathbf{2^{Fc}}$ and using an excess of PMe_3, the $Mo(L^{Fc})_2O(PMe_3)$ complex $\mathbf{3^{Fc}}$ forms. OAT to the fully oxidized $[Mo(L^{Fc})_2O_2]^{2+}$ complex $[\mathbf{2^{Fc}}]^{2+}$ yields complex $\mathbf{3^{Fc}}$ as well. For the reaction with $[\mathbf{2^{Fc}}]^{2+}$ and PMe_3 we propose that in the first step a phosphoryl molybdenum(V) complex $[Mo^V(L^{Fc})_2O(OPMe_3)]^{2+}$ forms by transferring one

electron from Mo^{IV} to Fe^{III}. In the next step, $OPMe_3$ is substituted by an H_2O molecule (which is supposed to be present in tiny amounts) followed by deprotonation and a second electron transfer from Mo^{V} to the second Fe^{III}. Unfortunately, the reaction is accompanied by side reactions shown with ^{31}P-NMR spectroscopy and mass spectrometry.[208]

Here, we present an analysis of the OAT/IET reaction of $\mathbf{2^{Fc}}$ and $[\mathbf{2^{Fc}}]^{2+}$ with PMe_3 and the side reactions of $[\mathbf{2^{Fc}}]^{2+}$ with PMe_3. Additionally we study the OAT reaction with PPh_3 which leads to the $Mo_2(L^{Fc})_4O_3$ dimer bearing four Fc centers. In order to avoid the side reactions observed for $[\mathbf{2^{Fc}}]^{2+}$, we also investigate the IET-coupled OAT reaction starting from the singly oxidized $[Mo(L^{Fc})_2O_2]^{+}$ complex $[\mathbf{2^{Fc}}]^{+}$ and PMe_3 by EPR spectroscopy and DFT calculations.

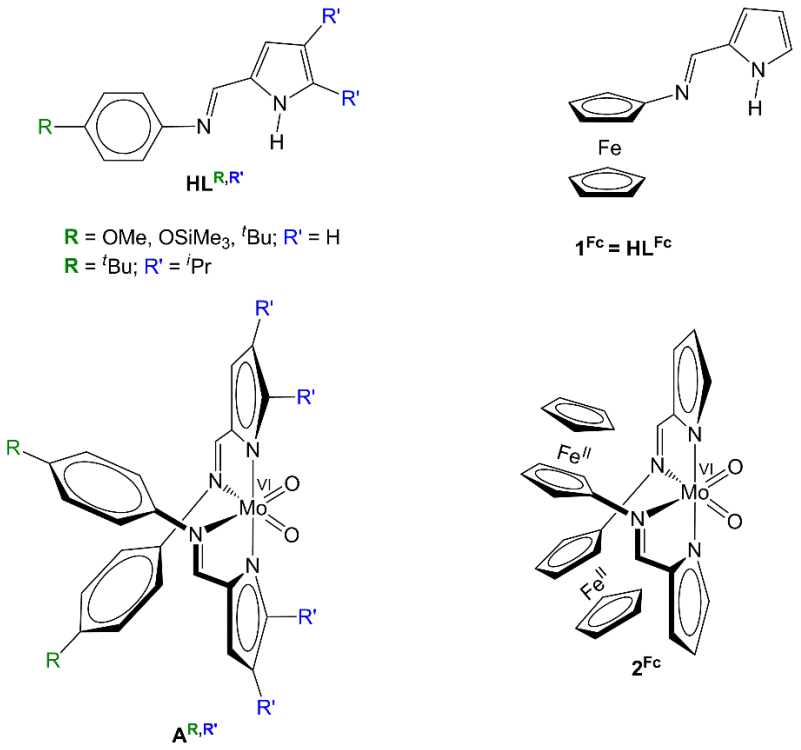

Scheme 26. Bidentate *N,N'*-iminopyrrolato chelate ligand (top) based model complexes for SO (bottom).

RESULTS AND DISCUSSION

OAT to PPh_3. As already known from the OAT reactions of dioxido molybdenum complexes, treatment of $\mathbf{2^{Fc}}$ with PPh_3 does not yield the phosphane complex, as in the case of PMe_3 addition, because of the steric demand of the phenyl groups (PPh_3: Tolman cone angle = 145°, PMe_3: Tolman cone angle = 118°).[216] Instead, it yields the dimer $\mathbf{4^{Fc}}$ (Scheme 27). The reaction occurs according to a mechanism known for similar dioxido

complexes.[199,201] Treating **2^{Fc}** with an excess of PPh_3 (5-10 eq.) gives red crystals of **4^{Fc}** in tetrahydrofuran after several days at room temperature.

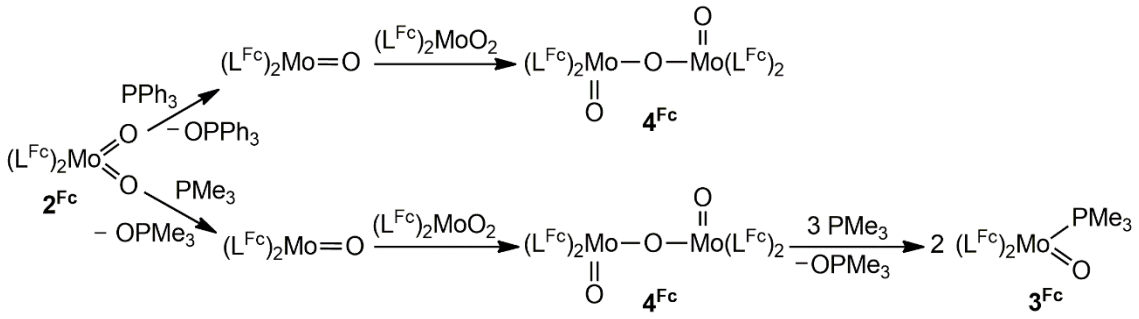

Scheme 27. Synthesis of **3^{Fc}** and **4^{Fc}**.

The isolated dimer **4^{Fc}** was fully characterized by usual spectroscopic methods. **4^{Fc}** crystallizes as *Λ,Λ*-isomer (*meso*-isomer) with the local OC-6-4-4 configuration[217] in the monoclinic space group $P2_1/c$ (Figure 5). The Mo^V centers of **4^{Fc}** are antiferromagnetically coupled (Mo1···Mo1A: 3.745 Å) and hence **4^{Fc}** is EPR silent. Because of the crystallographic inversion symmetry, the Mo1-O1-Mo1A angle is linear. The bond lengths of Mo-*μ*-O (1.8725(5) Å) and Mo=O (1.691(2) Å) are similarly long as those of the analogous dimer $[Mo^V(L^{tBu,H})_2O_2]_2(\mu\text{-}O)$.[202] Selected bond lengths and angles are presented in Table 1. Further crystallographic data is reported in the Supporting Information (SI), Table S1.

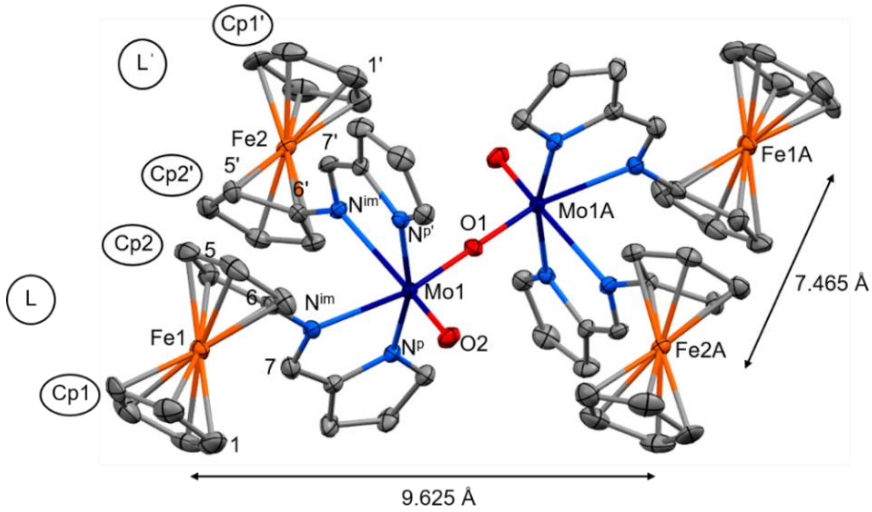

Figure 5. Molecular structure of **4^{Fc}** in the crystal (hydrogen atoms are omitted for clarity). Thermal ellipsoids at 50% probability.

Table 1. Selected bond lengths (Å) and angles (°) for $\mathbf{3^{Fc}}$ and $\mathbf{4^{Fc}}$ (Z = centroid of the Cp ring).

	$\mathbf{3^{Fc}}$	$\mathbf{3^{Fc}}$**(DFT)**	$\mathbf{4^{Fc}}$	$\mathbf{4^{Fc}}$**(DFT)**
Mo-O1	1.685(2)	1.709	1.8725(5)	1.699
Mo-O2/P	2.5076(10)	2.549	1.691(2)	1.886
Mo-N^{im}	2.172(3)	2.244	2.212(3)	2.266
Mo-$N^{im'}$	2.206(3)	2.278	2.370(3)	2.430
Mo-N^{p}	2.134(3)	2.137	2.103(3)	2.109
Mo-$N^{p'}$	2.237(3)	2.288	2.128(3)	2.154
O1-Mo-O2/P	90.49(8)	92.89	106.10(9)	103.376
Mo1-O1-Mo1A	-	-	180	180
N^{im}-Mo-N^{p}	76.27(10)	76.14	75.01(11)	75.189
$N^{im'}$-Mo-$N^{p'}$	72.85(10)	72.56	72.06(11)	71.579
C5-C6-N^{im}-C7	70.5(5)	–36.76	–49.9(5)	–41.10
C5'-C6'-$N^{im'}$-C7'	–29.9(5)	37.18	–28.7(5)	–39.20
Z1-Fe-Z2	175.98	179.26	178.78	179.17
Z1'-Fe-Z2'	177.59	178.43	177.79	178.91
C1-Z1-Z2-C6	6.96	3.19	–10.30	6.34
C1'-Z1'-Z2'-C6'	20.17	–0.33	8.26	–1.16

The iron centers Fe1 and Fe2 bound to the same Mo center are 7.465 Å apart from each other. Compared to the molecular structure of $\mathbf{2^{Fc}}$ (8.041 Å), the distance between the iron centers is shorter due to the sterical restriction by the other complex unit. The distance Fe1···Fe2A between iron centers of the two complex units amounts to 9.265 Å.

The IR spectrum in CsI of $\mathbf{4^{Fc}}$ features a band at ν = 955 cm^{-1} which is ascribed to the Mo=O vibration (Figure S1). A similar value (ν = 960 cm^{-1}) for this kind of vibration has been found for the μ-oxido dimer based on the $HL^{OSiMe3,H}$ ligand.[198] A second similarly intense band at 935 cm^{-1} is assigned to Cp ring vibrations coupled with Mo-N^{im} vibrations based on DFT calculations (ν = 913 cm^{-1}, scaled by 0.9614[218]).

The ^{1}H-NMR spectrum of $\mathbf{4^{Fc}}$ shows two sets of signals for the chelate ligands **L** and **L'** due to the inequivalence of the two oxygen atoms in *trans* position to the pyrrolato groups (Figure 6). The signals are assigned with help of the 2D ^{1}H-NMR experiments ^{1}H^{1}H-COSY and ^{1}H^{1}H-NOESY. The two chelate ligands are distinguished by NOE contacts of the pyrrol protons H^{11} and $H^{11'}$ in the ^{1}H^{1}H-NOESY spectrum (Figure 7 and SI, Figure

S2). While H^{11} exhibits one contact to a ferrocenyl proton ($H^{5'}$), $H^{11'}$ shows NOE contacts to two ferrocenyl protons, H^{5} and $H^{5'}$.

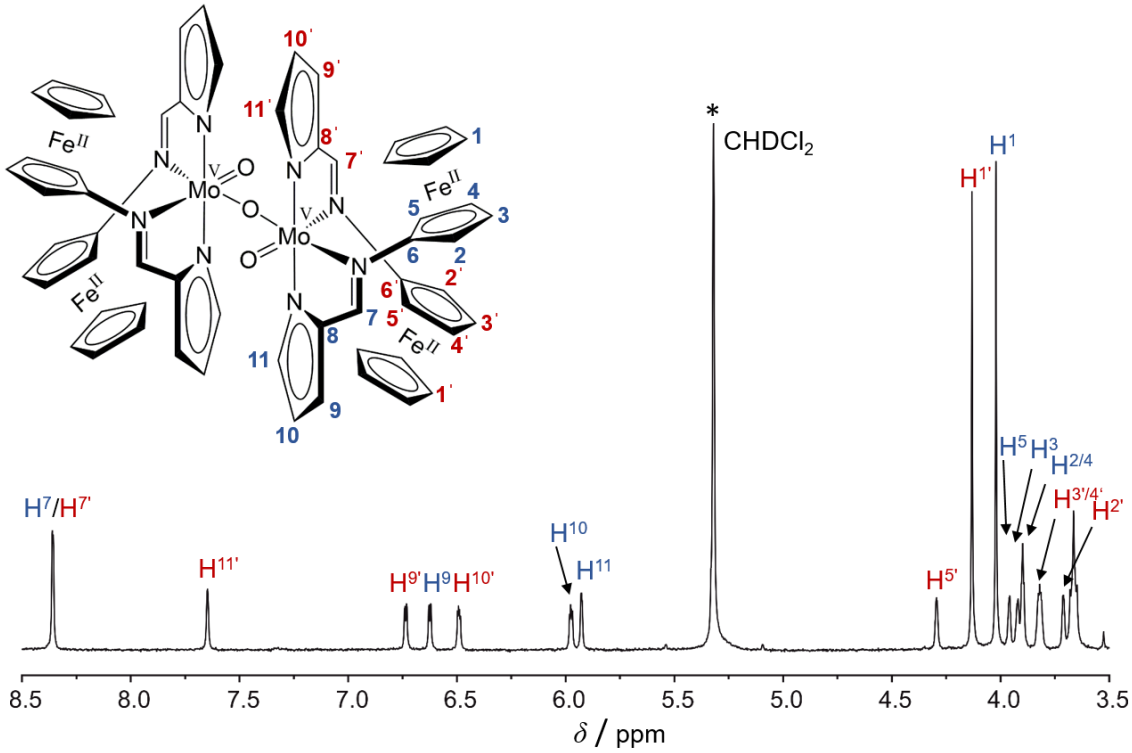

Figure 6. ^{1}H-NMR spectrum of $\mathbf{4^{Fc}}$ in CD_2Cl_2. The solvent signal is indicated by *.

The different chemical environments influence the chemical shifts of the protons H^7 and $H^{7'}$ only marginally (8.360 / 8.357 ppm). For the chemical shift of H^{11} and $H^{11'}$, a large deviation is observed, similar to the observations made for the μ-oxido dimer $[Mo^V(L^{OSiMe3,H})_2O_2]_2(\mu\text{-}O)$[198] and oxido phosphane molybdenum(IV) complexes in our group.[198–200] Proton H^{11} is shifted to higher field compared to $H^{11'}$ because of shielding through the ring current caused by the pyrrol ring (py) from L' of the other complex unit ($H^{11}\cdots$py(centroid): 2.465 Å).

The reaction of $\mathbf{2^{Fc}}$ with 5 eq. PPh_3 was monitored by ^{1}H-NMR spectroscopy for several hours (Figure 8). Within 45 min the resonances of $\mathbf{2^{Fc}}$ decrease and resonances of $OPPh_3$ and of several new species arise. The two main products of the reaction mixture are assigned to the *Δ,Λ*-isomer (*meso*-isomer, $\mathbf{4a^{Fc}}$**)** and the *Λ,Λ*-isomer (*rac*-isomer, $\mathbf{4b^{Fc}}$**)** of $\mathbf{4^{Fc}}$, indicated by purple ($\mathbf{4a^{Fc}}$) and green symbols ($\mathbf{4b^{Fc}}$). Within the first 45 min an increased formation of both products is observed, however, the increase of $\mathbf{4b^{Fc}}$ is more

intense. This situation changes after 45 min and **4a**^{Fc} becomes the main product, while the concentration of **4b**^{Fc} decreases.

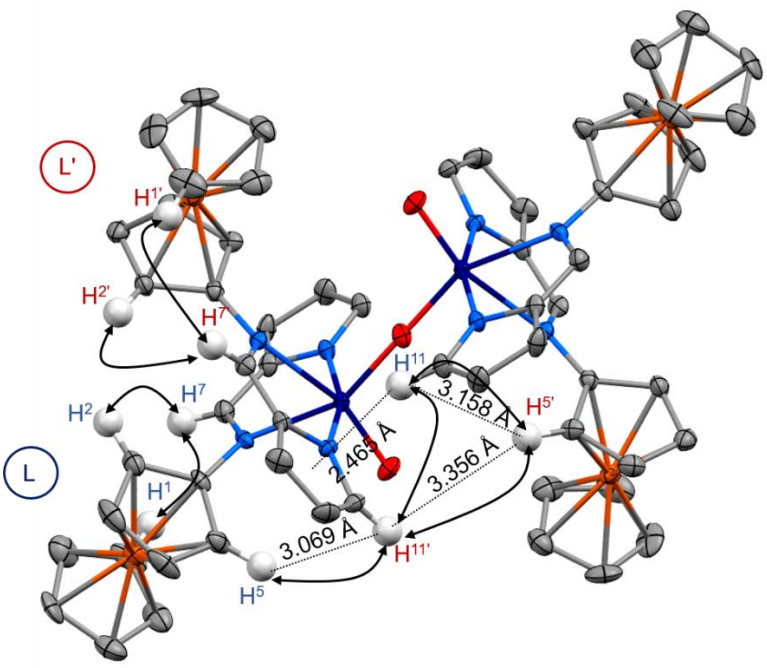

Figure 7. Selected NOE contacts (indicated by the arrows in the molecular structure) and distances of **4**^{Fc}. Thermal ellipsoids at 50% probability.

DOSY measurements during the reaction reveal similar diffusion coefficients ($\log(D/m^2s^{-1}) = -9.22$) for **4a**^{Fc} and **4b**^{Fc} which confirms the presence of two isomers of the dimer **4**^{Fc} (SI Figure S3). The obtained value is similar to that determined for the dimer $[Mo^{V}(L^{tBu,H})_2O_2]_2(\mu\text{-}O)$ ($\log(D/m^2s^{-1}) = -9.23$).[202] For comparison, the diffusion coefficient for **2**^{Fc} is higher with $\log(D/m^2s^{-1}) = -9.02$, consistent with the value for **A**^{tBu,H} ($\log(D/m^2s^{-1}) = -9.04$).[202]

DFT calculations provide an energy difference of 11 kJ mol^{-1} between the *Δ,Λ*- and the *Λ,Λ*-isomer and thereby support the assignment of the major isomer to **4a**^{Fc}. Obviously **4b**^{Fc} represents the kinetic product of the reaction and is converted over several hours to the thermodynamically stable product **4a**^{Fc}. Most likely the conversion of **4b**^{Fc} occurs through dissociation into *Λ*-**2**^{Fc} and the formation of a five-coordinated Mo^{IV} complex, since dimerization is an equilibrium reaction. Rebinding of the *Δ*-isomer of **2**^{Fc} to the five-coordinated Mo^{IV} complex leads to the energetically favorable **4a**^{Fc} (Scheme 28).

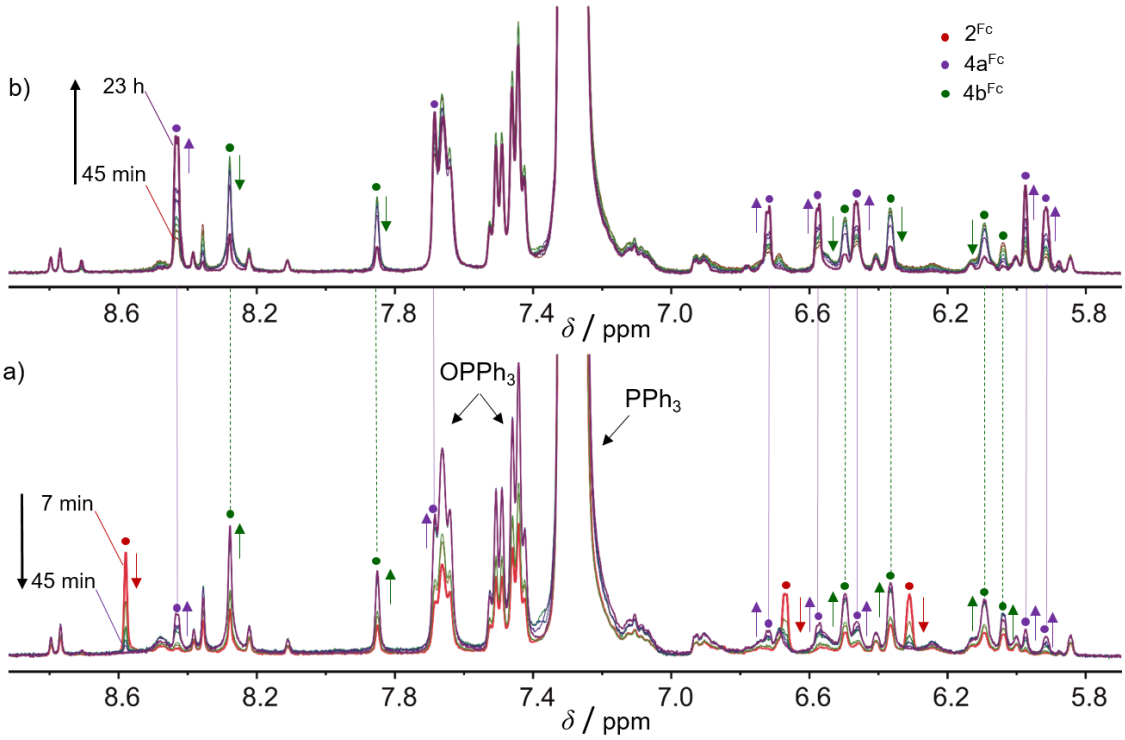

Figure 8. Evolution of the ^{1}H-NMR spectra during the reaction of **2^{Fc}** with 5 eq. PPh_3 in d_8-THF (c = 0.01 mol L^{-1}), a) 7 – 45 min and b) 45 min – 23 h.

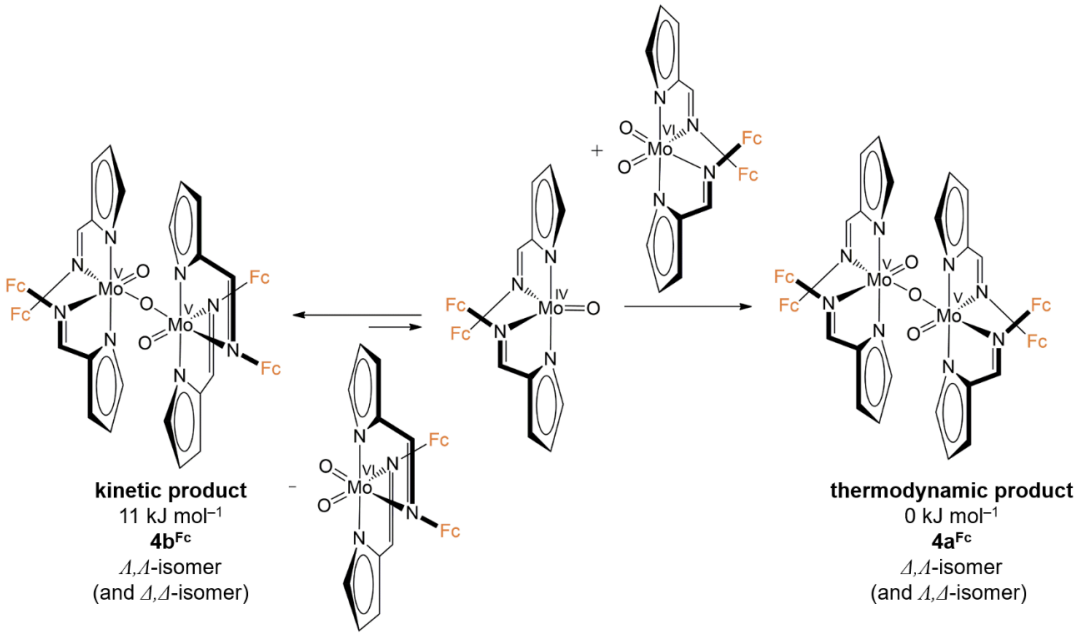

Scheme 28. Conversion of **4b^{Fc}** to **4a^{Fc}**. The ΔG values of the DFT-optimized geometries (B3LYP/LANL2DZ with polarization functions, PCM, THF, dispersion correction) of **4a^{Fc}** and **4b^{Fc}** are given in kJ mol^{-1}.

The cyclic voltammogram of **4^{Fc}** features four reversible oxidation waves at –130, 0, 160 and 270 mV (referenced against FcH / FcH$^+$) for the ferrocenyl substituents and one quasi-reversible reduction process at –1870 mV for the Mo$^{IV/V}$ redox couple (Figure 9, SI Figure S4).

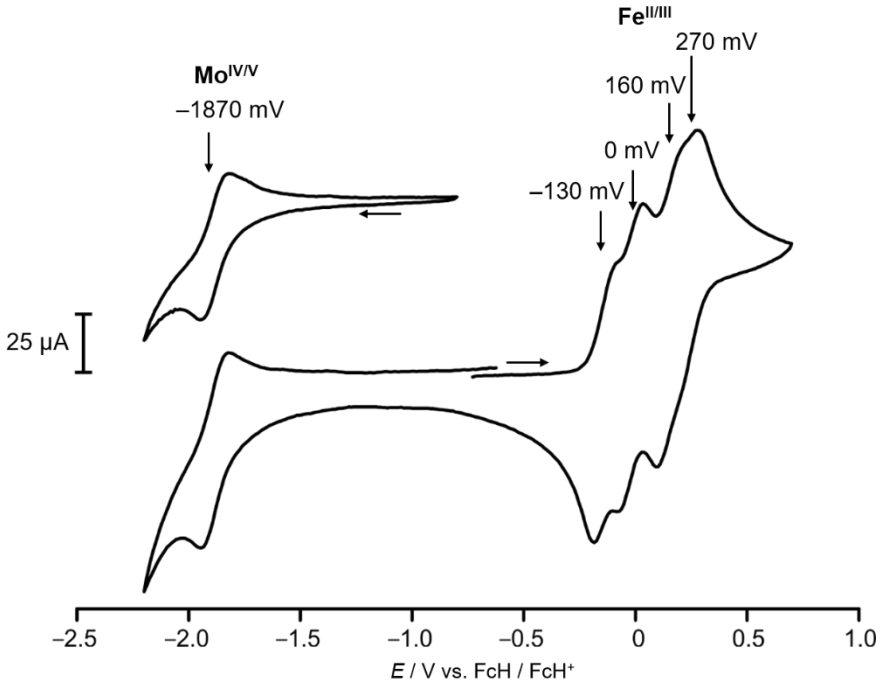

Figure 9. Cyclic voltammogram of **4^{Fc}** in CH_2Cl_2 / [^{n}Bu$_4$N][B(C$_6$F$_5$)$_4$].

The oxidation of the ferrocenyl substituents occurs in four one-electron steps to the tetracation with splitting values of 130, 160 and 110 mV. The larger splitting value between the oxidation wave forming [**4^{Fc}**]$^{2+}$ and [**4^{Fc}**]$^{3+}$ reflects the chemical nonequivalence of the first two ligands compared with the last two ligands.

In line with this, DFT calculations of the singly oxidized [**4^{Fc}**]$^+$ show that the first oxidation occurs on the ferrocenyl substituent with the imino nitrogen atom oriented *trans* to a terminal oxido ligand due to its higher electron donor effect compared to the μ-oxido ligand (Figure 10). The oxidation of the iron center leads to a longer N$^{im'}$-Mo1 bond (2.531 Å) compared to the analogous bond in the neutral state (2.430 Å). This may be explained by a withdrawal of electron density from the imino nitrogen atom to the electron-poor ferrocenium substituent and hence to a lower electron donor ability of the same imino nitrogen atom towards the Mo1 center. As expected, the Fe^{III}-Z(Cp centroid) distance in [**4^{Fc}**]$^+$ (1.803/1.796 Å) is longer than the Fe^{II}-Cp distance in **4^{Fc}**

(1.728/1.730 Å) and is similar to the values calculated for $[\mathbf{2}^{\mathbf{Fc}}]^{2+}$ (1.799/1.798 Å and 1.802/1.802 Å).[208] As expected, the second oxidation occurs at the ligand which is symmetric to the first oxidized ligand. The additional oxidation affects the bond lengths involving Mo1 only marginally (Figure 10).

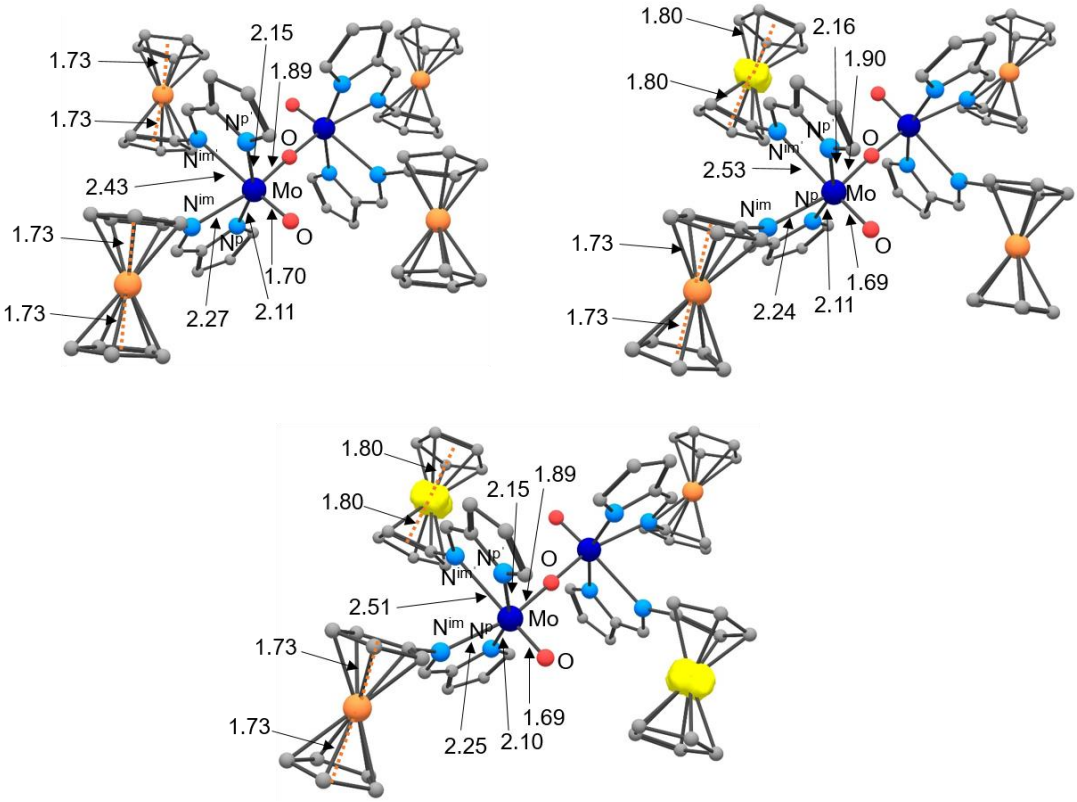

Figure 10. DFT-optimized structures (B3LYP/LANL2DZ with polarization functions, PCM, CH_2Cl_2) of $\mathbf{4a}^{\mathbf{Fc}}$ (top left), $[\mathbf{4a}^{\mathbf{Fc}}]^{+}$ (top right) and $[\mathbf{4a}^{\mathbf{Fc}}]^{2+}$ (bottom). Numbers before arrows specify bond lengths in Å. Spin density in yellow at 0.05 a.u.

The UV-Vis spectrum of $\mathbf{4}^{\mathbf{Fc}}$ shows a characteristic absorption band at 545 nm which is mainly assigned to the $\pi \rightarrow \pi^*$ transition within the $[\text{Mo-O-Mo}]^{4+}$ unit, based on a comparison with the similar dimer $[Mo^{V}(L^{tBu,H})_2O_2]_2(\mu\text{-O})$ (λ = 545 nm, SI Figure S5) and TD-DFT calculations (SI Figure S6). A further absorption band at λ = 498 nm is assigned to LMCT (Fc → MoO(π^*), with Fc *trans* to the oxido ligand) by comparison with the second most intense transition predicted by TD-DFT (λ = 606 nm).

In course of stepwise chemical oxidation of $\mathbf{4}^{\mathbf{Fc}}$ with $AgSbF_6$ in CH_2Cl_2, the UV-Vis/NIR spectra show the formation of an absorption band which shifts hypochromically with increasing amount of Ag^+ from λ = 1050 nm upon addition of one equivalent of Ag^+ to

λ = 950 nm upon addition of four equivalents of Ag^+ (Figure 11, SI Figure S7). Through comparison with $\mathbf{[1^{Fc}]^+}$ (917 nm),[208] these absorptions are ascribed to pyrrolato → Fc^+ transitions (λ = 768 nm in $\mathbf{[1^{Fc}]^+}$ by TD-DFT).

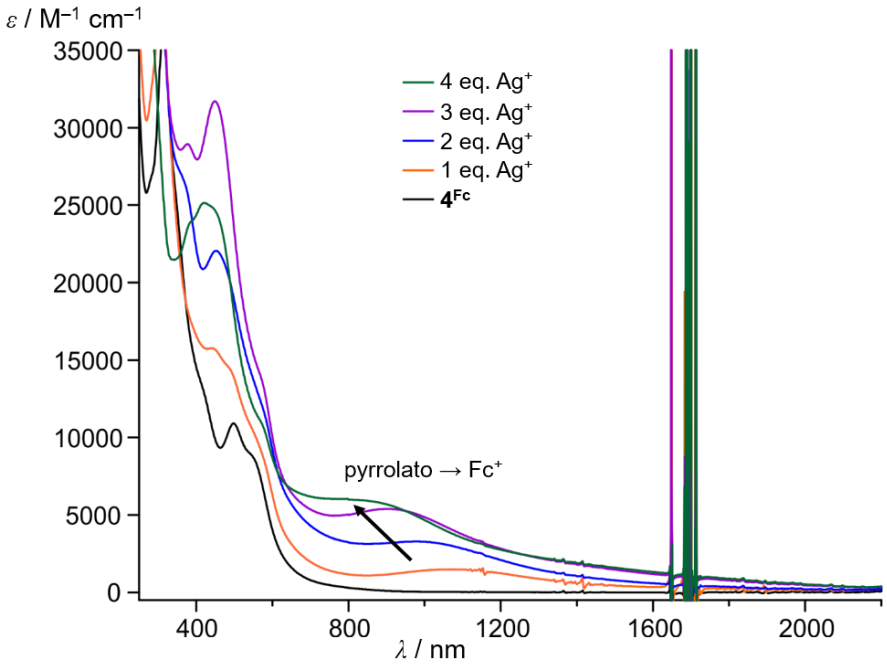

Figure 11. UV-Vis/NIR spectra of $\mathbf{4^{Fc}}$ in CH_2Cl_2 upon oxidation with 1-4 eq. $AgSbF_6$.

Presumably the absorption band shifts hypochromically due to the increasing positive charge of the molecule leading to a lowering of the HOMO orbital of the pyrrolato moiety. The Gaussian band shape analysis provides for the oxidation products $\mathbf{[4a^{Fc}]^{3+}}$ and $\mathbf{[4a^{Fc}]^{4+}}$ a further absorption band at λ = 1390 nm, which is likely another pyrrolato → Fc^+ transition that occurs mainly in the chelate ligand trans to the μ-oxido bridge (Scheme 29). This transition is expected to be energetically lower because of the lower energy of the ferrocenium orbitals in these ligands compared to the ones that are oxidized first, as indicated by the higher redox potential for the last two oxidations in the cyclic voltammogram.

For the oxidation products $\mathbf{[4a^{Fc}]^+}$ to $\mathbf{[4a^{Fc}]^{4+}}$, a characteristic absorption band at λ = 570 – 580 nm is determined. As for the neutral dimer, this band is assigned to the $\pi \rightarrow \pi^*$ transition within the $[Mo\text{-}O\text{-}Mo]^{4+}$ unit. The fitted absorption bands at λ = 690 – 750 nm for $\mathbf{[4a^{Fc}]^+}$ to $\mathbf{[4a^{Fc}]^{4+}}$ can be assigned to ferrocenium transitions, as they appear in a typical range[97,219,220] and gain intensity with increasing degree of oxidation.

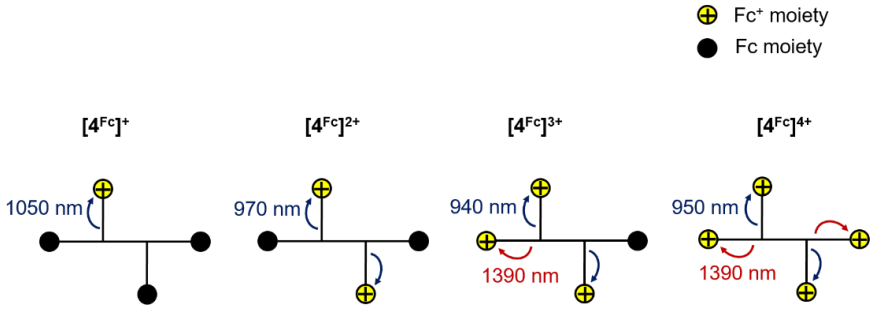

Scheme 29. Assigned pyrrolato → Fc^+ transitions in $\mathbf{[4a^{Fc}]^+}$ to $\mathbf{[4a^{Fc}]^{4+}}$, indicated by blue and red arrows.

OAT to PMe_3. As already previously reported, OAT in presence of an excess of PMe_3 leads to the oxido phosphane complex $\mathbf{3^{Fc}}$, which exists in solution in the form of two isomers ($\mathbf{3a^{Fc}}$ and $\mathbf{3b^{Fc}}$) with the OC-6-4-3 conformation as major product.[208] In the present work we could crystallize $\mathbf{3^{Fc}}$ from a tetrahydrofuran / diethyl ether solution at room temperature. The XRD results confirm that $\mathbf{3^{Fc}}$ exists in the crystal in the OC-6-4-3 configuration ($\mathbf{3a^{Fc}}$), in agreement with the configuration of the oxido phosphane Mo^{IV} complex $\mathbf{3^{tBu}}$ (Figure 12).[201]

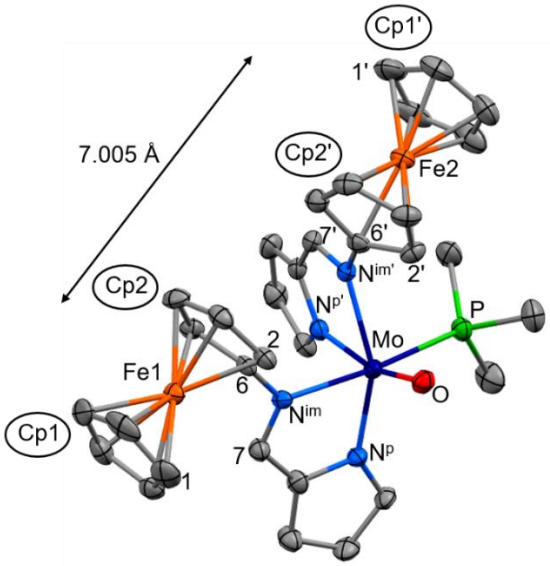

Figure 12. Molecular structure of $\mathbf{3^{Fc}}$ in the crystal (hydrogen atoms are omitted for clarity). Thermal ellipsoids at 50% probability.

Generally, the bond lengths and angles between Mo and the coordinated atoms are similar to those found for $\mathbf{3^{tBu}}$ (Table 1). The Fe···Fe distance (7.005 Å) is shorter than in the molecular structures of $\mathbf{2^{Fc}}$ and $\mathbf{4^{Fc}}$.

^{1}H-NMR spectra of just-dissolved crystals in d_8-THF exhibit only signals of the isomer **3a^{Fc}**. After several days, new signals develop which are assigned to the second isomer **3b^{Fc}** with OC-6-4-4 configuration (SI Figure S8). We suggest that the isomerization follows a trigonal twist mechanism (Scheme 30a), converting *Δ*-**3a^{Fc}** into *Λ*-**3b^{Fc}**.[221] The configuration of **3b^{Fc}** has been elucidated with a ^{1}H^{1}H-NOESY experiment (SI Figure S9). The spectrum contains EXSY signals for each pair of corresponding protons on the two ligands of the isomer **3b^{Fc}**. These are caused by switching the positions of the PMe_3 ligand with the oxido ligand through dissociation and rebinding of the PMe_3 ligand at a different position reforming the OC-6-4-4 isomer, since this automerization implies a formal exchange of the two chelate ligands (Scheme 30b). On the other hand, an exchange of PMe_3 and oxido ligands in **3a^{Fc}** (OC-6-4-3) leads to the isomer OC-6-3-4 without implying formal exchange of the chelate ligands, such that no EXSY signals are expected for this isomer. Therefore, based on the spectroscopic data, presence of small amounts of the isomer OC-6-3-4 in fast equilibrium with the major isomer **3a^{Fc}** cannot be ruled out.

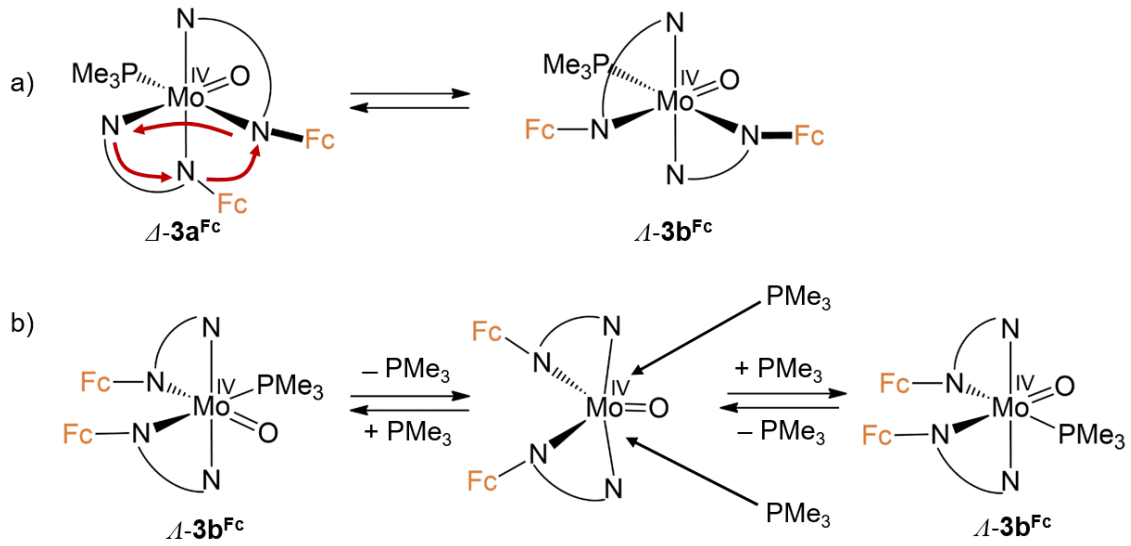

Scheme 30. a) Isomerization of *Δ*-**3a^{Fc}** to *Λ*-**3b^{Fc}** by the trigonal twist mechanism. b) Exchange of chelate ligands in **3b^{Fc}** through dissociation and rebinding of PMe_3.

DFT calculations of the possible isomers of **3^{Fc}** are in agreement with the results from XRD and NMR spectroscopic measurements (Figure 13). The OC-6-4-3 isomer has the lowest energy, whereas the OC-6-4-4 isomer is energetically higher by only 6 kJ mol^{-1}. Interestingly, the isomer OC-6-3-4 is stabilized stronger by accounting for intramolecular dispersion and predicted to be higher than OC-6-4-3 by just 4 kJ mol^{-1}. In contrast, DFT

calculations of $\mathbf{3}^{t\mathbf{Bu}}$ reveal the OC-6-3-3 isomer[201] as the second lowest in energy, which is in the case of $\mathbf{3}^{\mathbf{Fc}}$ the energetically highest.

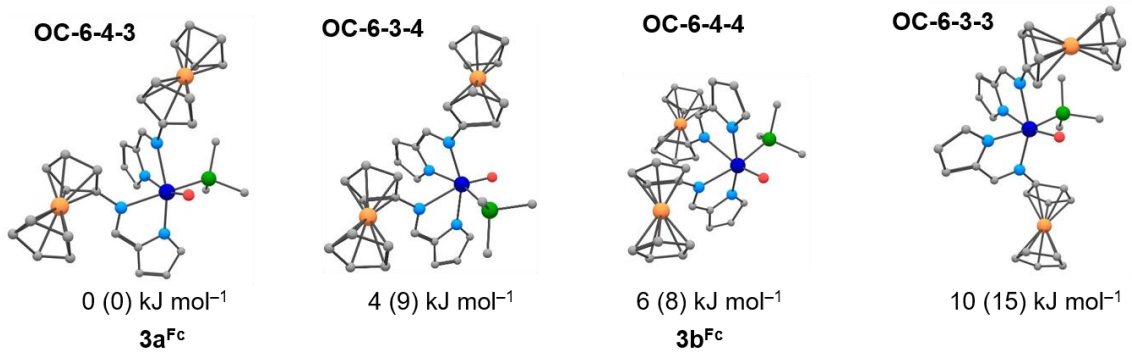

Figure 13. DFT-optimized geometries and Δ*G* values (B3LYP/LANL2DZ with polarization functions, PCM, THF, dispersion correction) of the possible isomers of $\mathbf{3}^{\mathbf{Fc}}$ (hydrogen atoms are omitted for clarity). Values in parentheses are without dispersion correction.

The calculated vibrational frequency of the Mo=O vibration for the major isomer OC-6-4-3 (926 cm^{-1}, scaled by 0.9614[218]) is lower than the experimental value in CsI (941 cm^{-1}, SI Figure S10). A similar value is obtained for isomer OC-6-3-3 where the oxygen atom is also in *trans* position to the pyrrolato nitrogen atom. The Mo=O vibrations for the isomers OC-6-4-4 and OC-6-3-4 differ with 936 cm^{-1} and 942 cm^{-1} more from $\mathbf{3a}^{\mathbf{Fc}}$, because in these cases the imino nitrogen atom is *trans* to the oxido ligand instead of the pyrrolato nitrogen atom. This strong dependence of the Mo=O vibration on the type of ligand *trans* to the oxido ligand is in line with computational data for the analogous complex $Mo(L^{tBu,H})_2O(PMe_3)$ $\mathbf{C}^{t\mathbf{Bu,H}}$.[201] Compared to $\mathbf{C}^{t\mathbf{Bu,H}}$ (935 cm^{-1}), $\mathbf{3a}^{\mathbf{Fc}}$ exhibits a higher value for the Mo=O vibration because the electron withdrawing effect of the ferrocenyl moieties is larger than that of the aryl substituents in $\mathbf{C}^{t\mathbf{Bu,H}}$.

For comparison with the kinetic study of the dimer formation using PPh_3, the OAT reaction of $\mathbf{2}^{\mathbf{Fc}}$ with 5 eq. PMe_3 at room temperature in d_8-THF was followed with ^{1}H-NMR spectroscopy. Consistent with the observations made using PPh_3, the isomer $\mathbf{4b}^{\mathbf{Fc}}$ of the dimer represents the major component in the beginning of the reaction. Within three hours, the main product becomes $\mathbf{4a}^{\mathbf{Fc}}$, accompanied by an increasing formation of $\mathbf{3a}^{\mathbf{Fc}}$. A complete conversion of $\mathbf{4}^{\mathbf{Fc}}$ to $\mathbf{3}^{\mathbf{Fc}}$ requires several days, since the dissociation of the dimer into Mo^{IV} and Mo^{VI} complexes and the following attack of PMe_3 at the dioxido Mo^{VI} complex is a slow process (SI Figure S11). These observations are in agreement

with the theoretical calculations by Heinze et al. which reveal that the PMe_3 attack at the oxido ligand of the dioxido molybdenum(VI) complex $\mathbf{A^{H,H}}$ is the rate-limiting step in the OAT reaction ($\Delta G^{\ddagger}$ = 65 kJ mol^{-1}).[199] Remarkably, $\mathbf{3b^{Fc}}$ is the dominant isomer of $\mathbf{3^{Fc}}$ in the beginning of the reaction. The reason for this kinetic preference for $\mathbf{3b^{Fc}}$ is likely that the configuration OC-6-4-4 of $\mathbf{2^{Fc}}$ is retained in the reaction, whereas formation of $\mathbf{3a^{Fc}}$ requires an additional trigonal twist isomerization (Scheme 30a).

Electrochemical oxidation of $\mathbf{3^{Fc}}$ at the Mo^{IV} center (E_p = –210 mV) leads to the formation of secondary products, indicated by the presence of irreversible redox waves in the cyclic voltammogram (SI Figure S12). The labile binding of the PMe_3 ligand at the Mo^{IV} core is also observed for previously reported oxido phosphane complexes.[200–202] A comparison among those shows that the PMe_3 ligand in $Mo(L^{t\mathrm{Bu},i\mathrm{Pr}})_2O(PMe_3)$ ($\mathbf{C^{tBu,iPr}}$) is stronger bound than in the other complexes. This complex exists mainly in the OC-6-3-3 configuration and is quasi-reversibly oxidized ($E_{1/2}$ = –400 mV) due to shielding by the sterically demanding ligands.[202]

The UV-Vis spectrum of $\mathbf{3^{Fc}}$ shows a similar, but more intense absorption band at λ = 484 nm (ε = 9890 M^{-1} cm^{-1}) as observed for the phosphane complex $\mathbf{C^{tBu,H}}$ (λ = 479 nm, ε = 1420 M^{-1} cm^{-1}). Based on DFT calculations, the band can be assigned to $Mo(d_{xz}/d_{yz}) \rightarrow \pi^*(MoO)$ and $Fc(d_{xy}/d_{x^2-y^2}) \rightarrow \pi^*(MoO)$/pyrrolato transitions. A weak absorption band around $\lambda \approx$ 700 nm is ascribed to Fc(d-d) transitions. (SI Figure S13).

Oxidation of $\mathbf{2^{Fc}}$ to $\mathbf{[2^{Fc}]^+}$ and $\mathbf{[2^{Fc}]^{2+}}$. Starting from the procedure published in our previous work,[208] we optimized the conditions of the oxidation reaction of $\mathbf{2^{Fc}}$ to the dication $\mathbf{[2^{Fc}]^{2+}}$ in order to reduce impurities. Complete oxidation is achieved in THF with 2 eq. $AgSbF_6$. Through proper choice of concentrations, a separation of silver is possible while keeping the $\mathbf{[2^{Fc}][SbF_6]_2}$ salt in solution. Upon resting of the $\mathbf{[2^{Fc}]^{2+}}$ solution at room temperature, partial precipitation of the $\mathbf{[2^{Fc}][SbF_6]_2}$ salt occurs which can then be isolated as powder. $\mathbf{2^{Fc}}$ was also stepwise oxidized and the degree of oxidation controlled by ^{1}H-NMR spectroscopy (Figure 14). The ^{1}H-NMR spectrum upon oxidation with 2 eq. of Ag^+ shows broad signals at δ = 40.50, 36.00, 29.55, 27.47 ($H^{2,3,4,5}$), 32.20 (H^1) and –25.68 ppm (H^7). Because of the predominant location of the charge on the iron centers, the paramagnetic influence on the signal shift of the pyrrolato protons $H^{9,10,11}$ (δ = 10.14, 8.67 and 2.86 ppm) is less than on the signals of the ferrocenyl protons.[208]

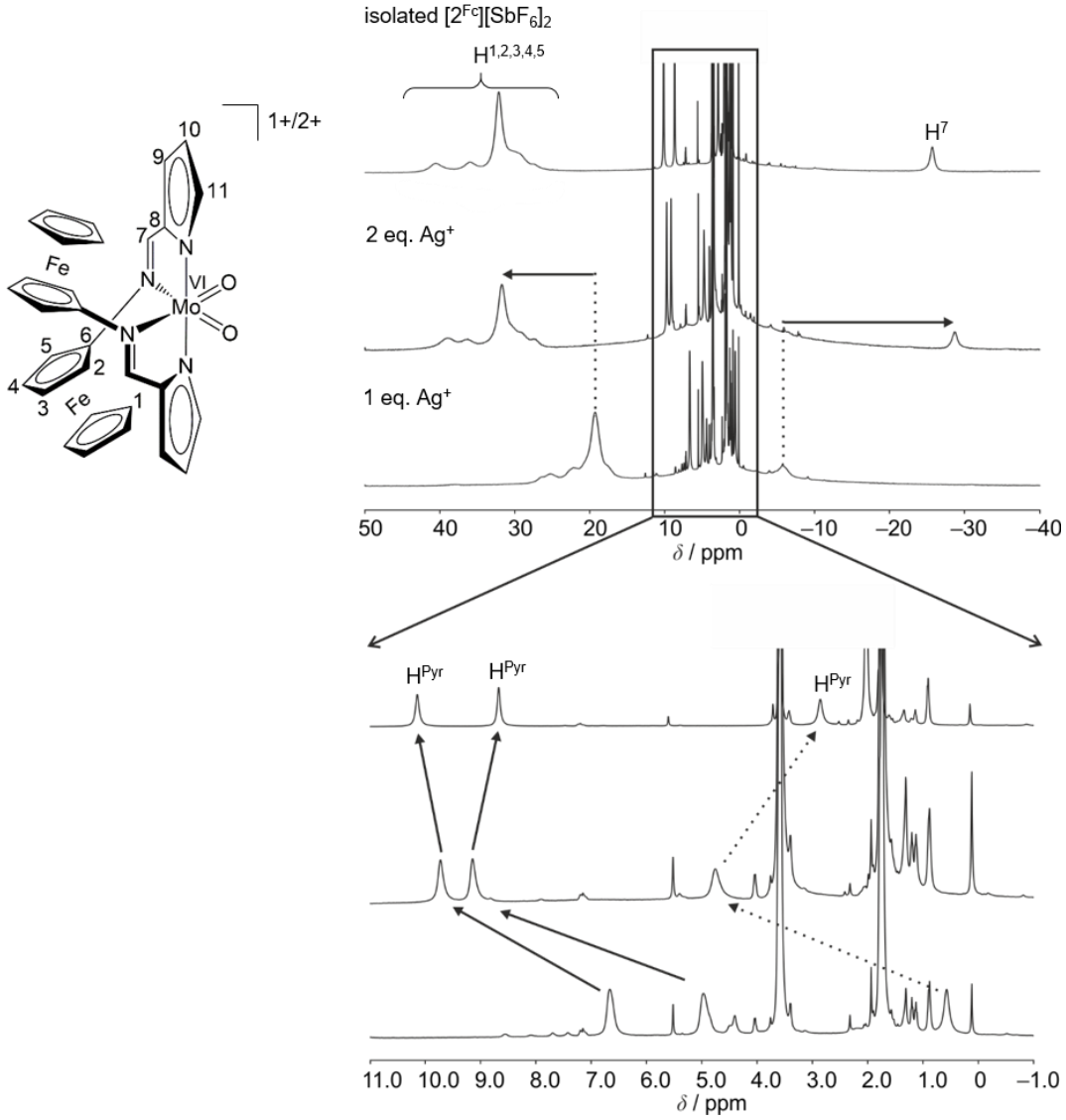

Figure 14. ^{1}H-NMR spectra of **[2^{Fc}]$^+$**, **[2^{Fc}]$^{2+}$** (d_8-THF) and isolated **[2^{Fc}][SbF$_6$]$_2$** (d_8-THF / d_6-acetone).

Oxidation with an excess of 5 eq. of Ag^+ does not further affect the shifts of the proton resonances, indicating that with 2 eq. Ag^+ a complete oxidation is already achieved. The ^{1}H-NMR spectrum of the isolated salt **[2^{Fc}][SbF$_6$]$_2$** shows less signals of impurities than the salt prepared in situ (Figure 14). Single oxidation with 1 eq. of Ag^+ to **[2^{Fc}]$^+$** leads to a smaller shift of the signals (δ = 19.3 ppm for H^1) and does not lead to a splitting into separate signals for **2^{Fc}**, **[2^{Fc}]$^+$** and **[2^{Fc}]$^{2+}$** due to the rapid self-exchange of Fc/Fc$^+$ sites (k_{ex} = 9.1·10^6 – 1.25·10^7 M^{-1} s^{-1})[222] on the NMR time scale (Figure 14).[97,220,223] DFT calculations give almost the same energies for the (open-shell) singlet and triplet state of **[2^{Fc}]$^{2+}$**, indicating that an almost statistical mixture of singlet and triplet states (1:3) exists in solution (Figure 15).

The presence of two ferrocene/ferrocenium redox waves in the cyclic voltammogram of $\mathbf{2^{Fc}}$ indicates that the equilibrium of the comproportionation reaction $\mathbf{[2^{Fc}]^{2+}} + \mathbf{2^{Fc}} \rightarrow 2\ \mathbf{[2^{Fc}]^{+}}$ is on the side of the monocation $\mathbf{[2^{Fc}]^{+}}$.[208] From the splitting ΔE between the first and second redox waves ($E_{1/2}$ = –0.03, 0.08 V), we can calculate the comproportionation constant K_c employing the Nernst equation: $\Delta E = \frac{RT}{zF} \ln K_c$, with R = 8.314 J mol^{-1} K^{-1}; T = 298.15 K; ΔE = 0.11 V; F = 96485 J V^{-1} mol^{-1}; z = 1. This yields K_c = 72 and confirms that the dioxido complex is stable in the singly oxidized state.

A comparison of ^{1}H-NMR spectra of the ferrocenium derivatives Fc^+, $[FcNHAc]^+$ and the ligand $[\mathbf{1^{Fc}}]^+$ reveals paramagnetic shifts of the ferrocenyl protons' signals in a similar ppm range (SI Figure S14). The single resonance for the ferrocenium protons exhibits a similar value for the chemical shift (δ = 28.65 ppm) as the signals from the unsubstituted Cp ring in $\mathbf{[2^{Fc}]^{2+}}$ (δ = 32.20 ppm). The signals of the pyrrolato rings in $\mathbf{[2^{Fc}]^{2+}}$ are stronger shifted towards lower field than those in the free oxidized ligand because of deshielding by a withdrawal of electron density from the nitrogen atoms to the molybdenum center upon coordination.

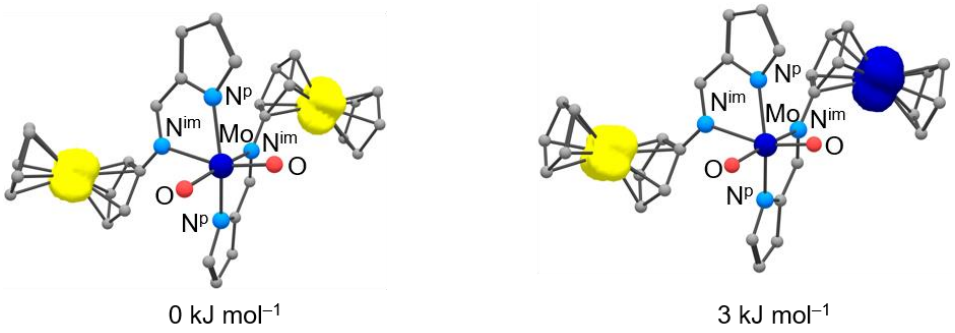

Figure 15. DFT-optimized geometries and ΔG values (B3LYP/LANL2DZ with polarization functions, PCM, THF, dispersion correction) of the triplet and (open-shell) singlet state of $\mathbf{[2^{Fc}]^{2+}}$ (spin density in yellow and blue at 0.01 a.u.).

OAT from $\mathbf{[2^{Fc}]^{+}}$ and $\mathbf{[2^{Fc}]^{2+}}$ to PMe_3. Based on DFT calculations, we have proposed that the phosphoryl Mo^V complex $\mathbf{[5^{Fc}]^{2+}}$ is an intermediate in the OAT reaction of $\mathbf{[2^{Fc}]^{2+}}$ with PMe_3.[208] Unfortunately, attempts to trap this EPR-active species by rapid-freeze techniques for characterization with EPR spectroscopy did not succeed. Detailed analysis by NMR and mass spectroscopy of the reaction of $\mathbf{[2^{Fc}]^{2+}}$ with an excess of PMe_3 reveals the formation of several products (Scheme 31).

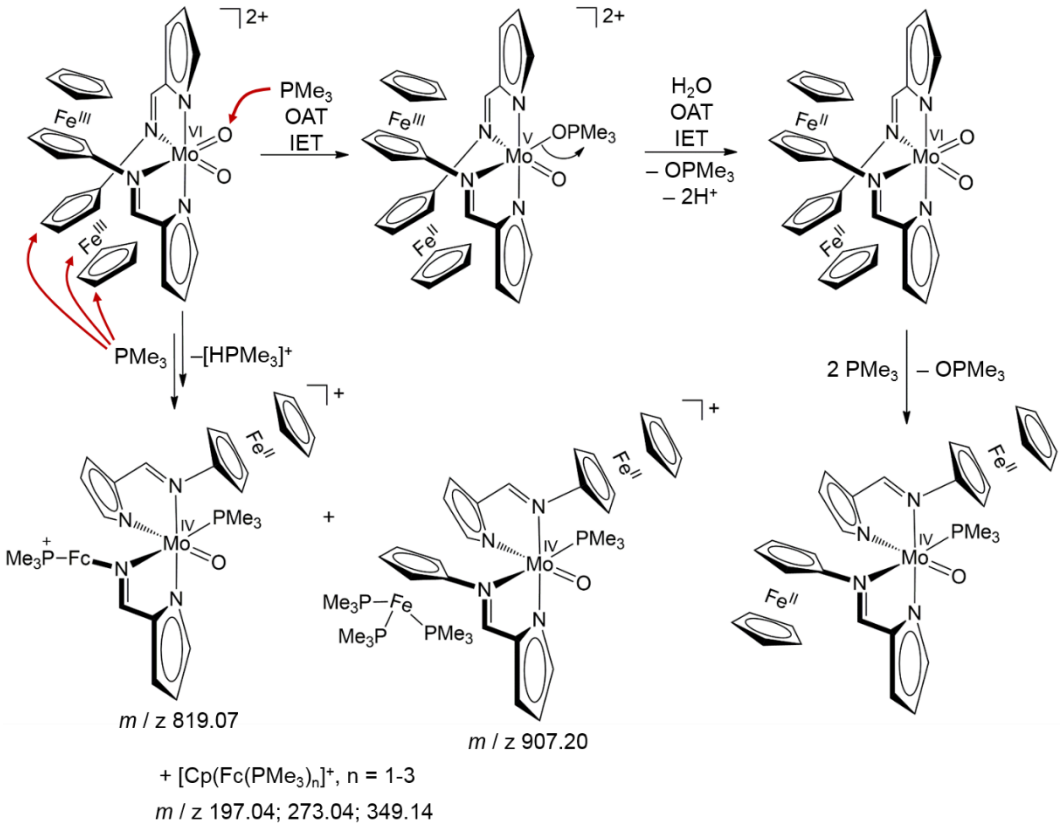

Scheme 31. Products of the reaction of $\mathbf{[2^{Fc}]^{2+}}$ with an excess of PMe_3. For simplicity, only the attack of PMe_3 at one of the chelate ligands is shown.

The ESI^+ mass spectrum of the reaction mixture (SI Figure S15) shows a peak at *m*/z 819.07 which can be ascribed to a derivative of $\mathbf{3^{Fc}}$ resulting from PMe_3 substitution at a Cp ring. The peak at *m*/z 743.03 corresponds to the same species without PMe_3 coordination at molybdenum. A further peak at *m*/z 907.20 corresponds to a derivative of $\mathbf{3^{Fc}}$ in which one unsubstituted Cp ring of one chelate ligand is substituted by three PMe_3 ligands. The replacement of the substituted Cp ring by PMe_3 ligands yielding $[CpFe^{II}(PMe_3)_3]^+$ (*m*/z 349.14) also takes place. The observed peaks at *m*/z 273.04 and *m*/z 197.04 can be assigned to $[CpFe^{II}(PMe_3)_2]^+$ and $[CpFe^{II}(PMe_3)]^+$, respectively, and are likely decomposition products of $[CpFe^{II}(PMe_3)_3]^+$ that form in the spectrometer. All in all, attack of PMe_3 occurs at the oxido ligand, the Cp ring and at the iron center.

ESI^+ mass spectrometric analysis of the reactions of PMe_3 with oxidized $\mathbf{[1^{Fc}]^+}$, *N*-Acetylaminoferrocenium ($[FcNHAc]^+$) and ferrocenium (Fc^+) also show substitution of PMe_3 at the (presumably unsubstituted) Cp ring (*m*/z 353.08, 318.10 and 261.07, SI Figure S16–S18). The ^{1}H-NMR spectra of the reaction mixtures show sharp signals in the

diamagnetic region, including proton signals of the neutral starting compounds (SI Figure S19). Proton signals in the ^{1}H-NMR spectrum and a signal in the ^{31}P-NMR spectrum of the reaction of Fc^+ and PMe_3 can be assigned to a ferrocenyl phosphonium ion (^{31}P-NMR: δ = 24.82 ppm). In the ^{31}P-NMR spectra of all reactions with PMe_3, several phosphorus compounds are discernible (SI Figure S20). The formation of half-sandwich complexes of the type $[Cp^RFe^{II}(PMe_3)_n]^+$ (n = 1 – 3, R = NCHPyr, NHAc or H) is also detected with ESI^+ mass spectra for the corresponding reactions of $[\mathbf{1}^{Fc}]^+$, $[FcNHAc]^+$ and Fc^+ with PMe_3 (*m*/z 441.14, 406.17 and 349.14 for $[Cp^RFe^{II}(PMe_3)_3]^+$, R = NCHPyr, NHAc and H). However, no proton signals in the ^{1}H-NMR and ^{31}P NMR spectra could be unambiguously assigned to these phosphane Fe^{II} species. The $[CpFe^{II}(PMe_3)_3]^+$ complex is a literature-known compound, synthesized by Buchner et al. through radiation of $[(\eta^5\text{-}(C_5H_5)(CO)_3Fe][BF_4]$ and PMe_3 (^{1}H-NMR: δ = 1.59 ppm, ^{31}P-NMR: δ = 24.1 ppm).[224] Taking into account the observed products, we suggest that besides the OAT reaction a competing reaction takes place in which the oxidized compounds react with PMe_3 to a ferrocenyl phosphonium complex, the neutral starting compound and $HPMe_3^+$. DFT calculations for the reaction of Fc^+ with PMe_3 predict that this reaction is thermodynamically feasible (Scheme 32).

$$2\ Fc^+ + 2\ PMe_3 \rightarrow FcPMe_3^+ + HPMe_3^+ + Fc \qquad \Delta G = -98\ kJ\ mol^{-1}$$

Scheme 32. Proposed reaction of ferrocenium with PMe_3 and corresponding ΔG value calculated with DFT (B3LYP/LANL2DZ with polarization functions, PCM, THF, dispersion correction).

For the reaction of ferrocenium with PMe_3, three considerable reaction paths are analyzed with DFT. One possibility is that a deprotonation of ferrocenium at the Cp ring occurs in the first step of the reaction (**II**, Scheme 33a), generating a radical center at the Cp ring. However, DFT calculations predict that deprotonation of ferrocenium with PMe_3 is unfeasible (ΔG = 201 kJ mol^{-1}) and requires much stronger bases, such as the base P_1-^{t}Bu as shown by Neidlinger.[225] Even the hypothetical reaction of this deprotonated ferrocenium with PMe_3 first leads to an Fe^I species with comparatively high energy (**III**, ΔG = 100 kJ mol^{-1}), and requires a subsequent oxidation of the Fe^I center to Fe^{II} with ferrocenium in order to reach the thermodynamically favorable product (**IV**, ΔG = –98 kJ mol^{-1}).

In an alternative reaction path, PMe_3 performs a nucleophilic attack at the Cp ring (Scheme 33b) and the Fe^{III} center is reduced to Fe^{I}, followed by rearrangement of a proton (**V**).[226] This nucleophilic reaction is energetically strongly favored over the deprotonation reaction in path a) (ΔG = 21 kJ mol^{-1}). Deprotonation followed by oxidation would lead to the final product through the intermediate **III**, as discussed also for path a). The reverse order, first oxidation (**VI**, ΔG = 71 kJ mol^{-1}) and then deprotonation (**IV**) is shown in Scheme 33c. This reaction path is compared to a) and b) energetically most favorable.

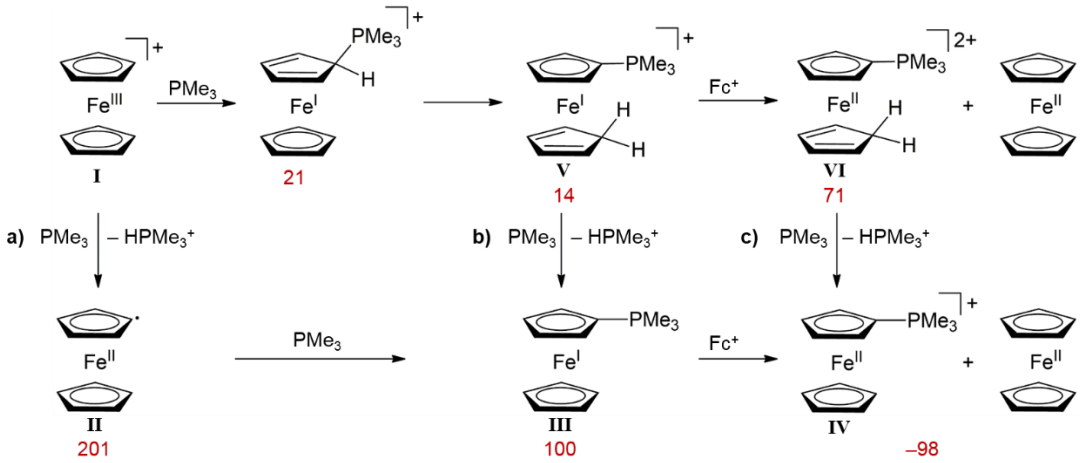

Scheme 33. Three potential paths a), b) and c) for the reaction of Fc^+ with PMe_3 calculated with DFT (B3LYP/LANL2DZ with polarization functions, PCM, THF, dispersion correction). The ΔG values for the reactions are given in kJ mol^{-1} (in red).

Presumably the attack of the PMe_3 molecule at $\mathbf{[2^{Fc}]^{2+}}$ occurs in a similar way. However, the fate of the side product $HPMe_3^+$ (^{31}P-NMR: –3 ppm)[227] is currently unclear. It might not have been observed due to precipitation or a secondary reaction as for example the protonation of a dissociated $[Cp^R]^-$ ($[Cp^R]^- + HPMe_3^+ \rightarrow HCp^R + PMe_3$).

An IET-coupled OAT to PMe_3 is also possible starting from the monocationic $Mo^{VI}Fe^{III}Fe^{II}$ complex $\mathbf{[2^{Fc}]^+}$. DFT calculations of the positively charged phosphoryl Mo^V complex $\mathbf{[5^{Fc}]^+}$ show spin density on the Mo center indicating that an IET from Mo^{IV} to Fe^{III} has occured. In $\mathbf{[5^{Fc}]^{2+}}$ the Mo-N^{im} bond is longer than in $\mathbf{[5^{Fc}]^+}$ due to the charged iron center, consistent with the $\mathbf{4^{Fc}}$ and $\mathbf{[4^{Fc}]^+}$ redox couple (Figure 16). As an aside, it should be mentioned that single occupation of the d_{x2-y2} orbital in the ferrocenium moiety of $\mathbf{[5^{Fc}]^{2+}}$ is energetically lower than the previously reported single occupation of d_{z2}.[208]

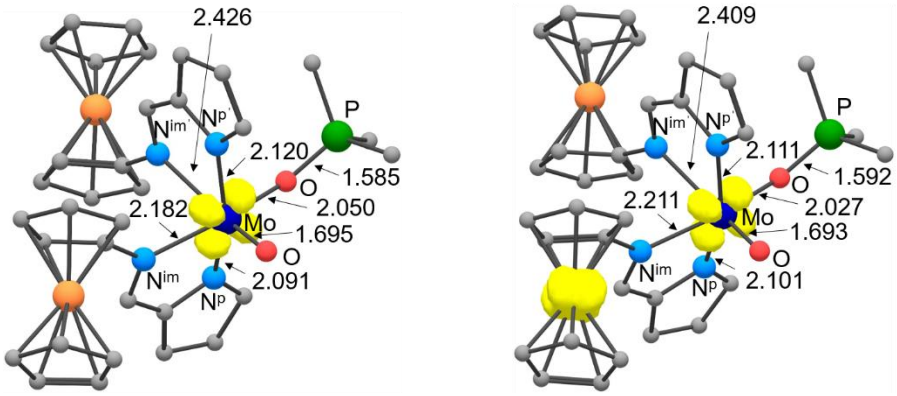

Figure 16. DFT-optimized geometries (B3LYP/LANL2DZ with polarization functions, PCM, THF) of the phosphoryl complexes $\mathbf{[5^{Fc}]^{+}}$ (doublet state) and $\mathbf{[5^{Fc}]^{2+}}$ (triplet state). The bond lengths are given in Å and the spin densities are at 0.03 a.u. in yellow.

Experimentally, the treatment of $\mathbf{[2^{Fc}]^{+}}$ with 1 eq. PMe_3 yields an EPR-active Mo^{V} complex $\mathbf{[5^{Fc}]^{+}}$ which is stable even at room temperature for several minutes. Simulation of the X-band CW EPR spectrum of the red reaction solution gives the best fit with g_{iso} = 1.9458 and a hyperfine coupling of $A_{iso}(^{95/97}Mo)$ = 47 G for the $^{95/97}Mo$ isotopomers (Figure 17). Further, a shoulder in the main signal is best described through a weak ^{31}P hyperfine coupling ($A(^{31}P)$ = 7.2 G). Based on this EPR analysis, we conclude that the Mo^{V} signal arises from the phosphoryl Mo(V) complex $\mathbf{[5^{Fc}]^{+}}$.

DFT calculations provide similar results for the isotopic ^{31}P coupling and the isotopic *g*-value ($A(^{31}P)$ = 8.4 G, g = 1.9507). The value for the hyperfine coupling of $^{95/97}Mo$ is underestimated by this method ($A(^{95/97}Mo)$ = 22.7 G). To increase the significance of this result, the EPR parameters for the well-characterized $[Mo(L^{tBu,H})_2(N^{t}Bu)(PMe_3)]^{+}$ complex were calculated by the same method (g = 1.9772, $A(^{95/97}Mo)$ = 19.6 G, $A(^{31}P)$ = 25.7 G), approximating the ^{t}Bu substituents at the phenyl rings by hydrogen atoms. The ^{31}P hyperfine coupling and g value are in good agreement with the reported experimental data (g = 1.9810, $A(^{95/97}Mo)$ = 40.3 G, $A(^{31}P)$ = 28.7 G), while the $^{95/97}Mo$ coupling is again underestimated.[201] This result additionally supports the formation of the $\mathbf{[5^{Fc}]^{+}}$ complex.

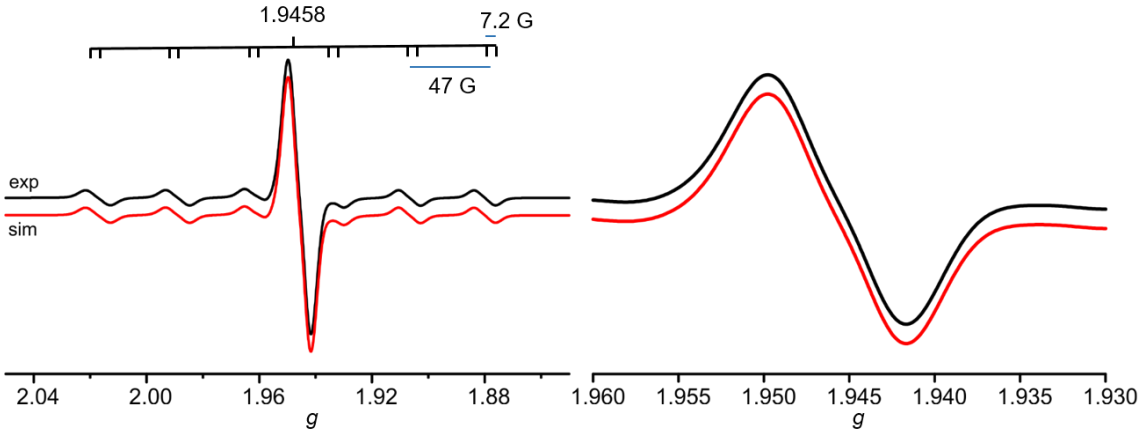

Figure 17. Simulated and experimental EPR spectrum of the reaction solution $[\mathbf{2}^{\mathbf{Fc}}]^+$ with 1 eq. PMe_3 in THF at 295 K (ν = 9.42 GHz, field = 3465.4 G, sweep = 94.74 G, sweep time = 60 s, modulation = 700 mG and MW attenuation = 10 dB, c = 23 mmol L^{-1}). Right: Detailed view of the main signal of the EPR spectrum.

Within 80 minutes the EPR signal of the solution decreases with a half-time $\tau_{1/2}$ = 38 ± 2 min (Figure 18 and Figure 19). A further signal at g = 1.953 can be assigned to a minor component and becomes increasingly visible through the decay of the signal intensity of $[\mathbf{5}^{\mathbf{Fc}}]^+$ (Figure 18 and SI Figure S21). Because the absolute intensity of the minor component's signal does not significantly change during the decay of the major signal, this species is likely no decomposition product of $[\mathbf{5}^{\mathbf{Fc}}]^+$. The spectrum of a second minor component is overlaid by a satellite signal of the major component at g = 1.963 (Figure 18).

Simulation of the rhombic spectrum at 77 K of the frozen solution of $[\mathbf{5}^{\mathbf{Fc}}]^+$ after 25 min yields $g_{1,2,3}$ = 1.9698, 1.9538 and 1.9375 and $A_{1,2,3}(^{31}P)$ = 5, 15 and 7 G (SI Figure S22). Basu et al. have reported in 2010 a phosphoryl Mo^{IV} complex based on the hydrotris(3-isopropylpyrazoyl-1-yl)borate ligand. Through electrochemical analysis they could show that in the Mo^{V} state the phosphoryl complex is more stabilized than in the Mo^{IV} state.[187] Studies on the enzyme sulfite oxidase show that the phosphate anion inhibits the enzyme in the Mo^{V} state, indicating the stabilizing effect of this oxidation state.[147,151,228] Pulse-EPR measurements by Enemark et al. of the blocked form of SO have revealed different conformations and provide ^{31}P coupling values in a similar order of magnitude ($A(^{31}P)$ = 7.5-15.3 G) as for $[\mathbf{5}^{\mathbf{Fc}}]^+$.[147] Taken together, these findings support the formation of $[\mathbf{5}^{\mathbf{Fc}}]^+$.

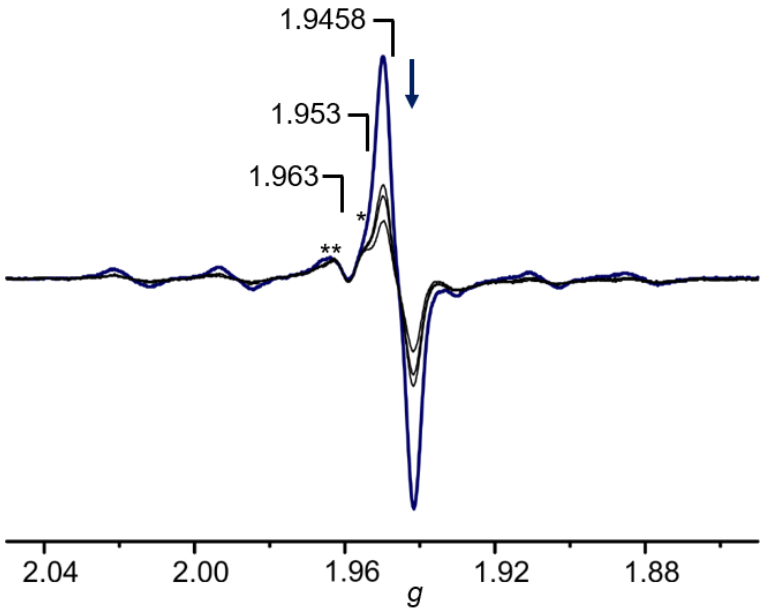

Figure 18. X-band CW EPR spectra of $[\mathbf{5}^{\mathbf{Fc}}]^{+}$ in THF at 295 K within 80 min (main signal). The temporal decay of the main EPR signal is indicated by the blue arrow. The two minor components are indicated by * and **, respectively.

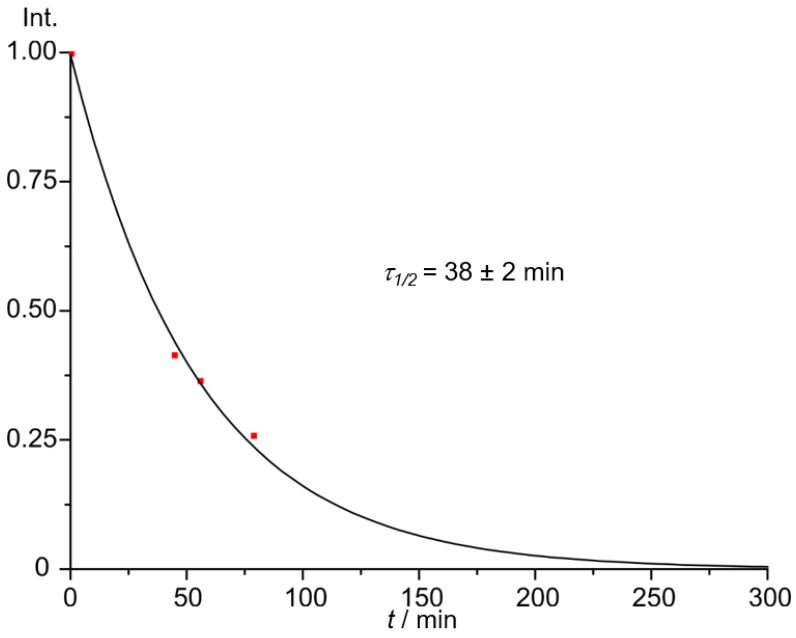

Figure 19. Exponential fit to the observed decay of the EPR signals of $[\mathbf{5}^{\mathbf{Fc}}]^{+}$.

Presumably, $[\mathbf{5}^{\mathbf{Fc}}]^{2+}$ could not be trapped under the chosen conditions because of its higher reactivity compared to $[\mathbf{5}^{\mathbf{Fc}}]^{+}$ due to the second charge being localized on an iron center. The ferrocenium moiety is reactive towards PMe_3 molecules resulting in substitution at

the Cp ring as discussed above. The high reactivity of ferrocenium moieties towards substitution reactions in presence of bases has already been shown for substituted oxidized ferrocenyl compounds.[225,229] In **[5^{Fc}]$^{+}$** both chelate ligands are uncharged, leading to a higher stability towards bases and nucleophiles.

DFT calculations of OAT reactions. The differences in reactivity of **[2^{Fc}]**, **[2^{Fc}]$^{+}$** and **[2^{Fc}]$^{2+}$** with respect to PMe_3 are analyzed with DFT calculations (Scheme 34).

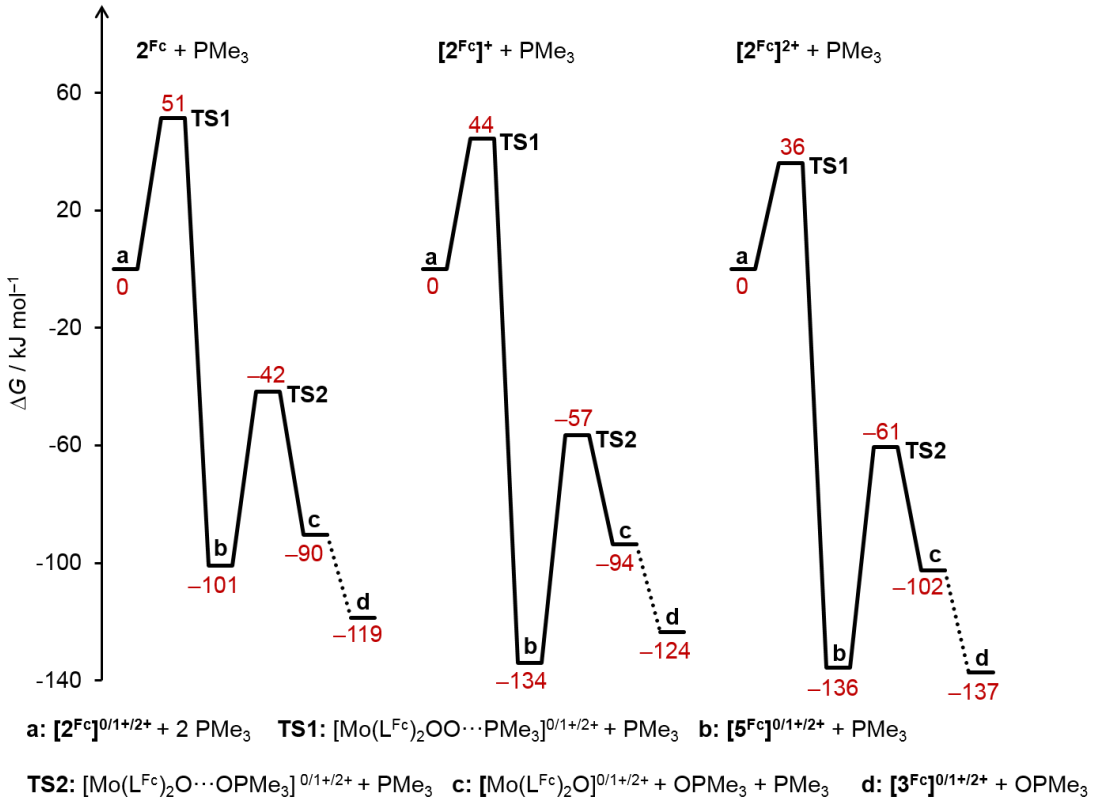

Scheme 34. DFT-calculated mechanisms of the reactions of **[2^{Fc}]**, **[2^{Fc}]$^{+}$** and **[2^{Fc}]$^{2+}$** with PMe_3. ΔG values (kJ mol^{-1}) are displayed in red.

The attack of PMe_3 at **2^{Fc}** requires a free enthalpy of activation $\Delta G^{\ddagger}$ = 51 kJ mol^{-1} which is somewhat lower than calculated for $Mo(L^{H,H})_2O_2$ ($\Delta G^{\ddagger}$ = 65 kJ mol^{-1}).[201] The formation of the phosphoryl complex $Mo^{IV}(L^{Fc})_2O(OPMe_3)$ (**5^{Fc}**) leads to an energetic lowering to ΔG = –101 kJ mol^{-1}. The low barrier for the dissociation of $OPMe_3$ ($\Delta G^{\ddagger}$ = 59 kJ mol^{-1}) allows fast follow-up reactions of **5^{Fc}** through the low-lying intermediate $Mo^{IV}(L^{Fc})_2O$ complex (ΔG = –90 kJ mol^{-1}). Indeed, the coordination of PMe_3 leads to the energetically favorable oxido phosphane complex **3^{Fc}** (ΔG = –119 kJ mol^{-1}), in agreement with the experimental observation.

In comparison, the reaction of $\mathbf{[2^{Fc}]^{+}}$ with PMe_3 is faster ($\Delta G^{\ddagger}$ = 44 kJ mol^{-1}) and gives the phosphoryl complex $[Mo^{V}(L^{Fc})_2O(OPMe_3)]^{+}$ ($\mathbf{[5^{Fc}]^{+}}$) which is by about ΔG = –33 kJ mol^{-1} more stable than its neutral analog. As mentioned above, the electron transfer from Mo^{IV} to Fe^{III} allows this stabilization through formation of the preferred Mo^{V} state (Figure 16). The higher barrier for the dissociation of $OPMe_3$ ($\Delta G^{\ddagger}$ = 77 kJ mol^{-1}) and the higher Gibbs energies of both $[Mo^{V}(L^{Fc})_2O]^{+}$ and the conceivable oxido phosphane complex $[\mathbf{3^{Fc}}]^{+}$ make $\mathbf{[5^{Fc}]^{+}}$ the thermodynamically most stable species in the reaction such that its detection by EPR spectroscopy is possible. However, given that the cyclic voltammogram of $[\mathbf{3^{Fc}}]$ features an irreversible oxidation process (SI Figure S12), the observed degradation of $\mathbf{[5^{Fc}]^{+}}$ possibly occurs through $[\mathbf{3^{Fc}}]^{+}$ as low-lying intermediate.

In case of $\mathbf{[2^{Fc}]^{2+}}$, the initial OAT reaction with PMe_3 is even further enhanced, as evident from the low barrier of TS1 ($\Delta G^{\ddagger}$ = 36 kJ mol^{-1}). The relative stabilization of the phosphoryl complex $\mathbf{[5^{Fc}]^{2+}}$ and the energetics of the dissociation of $OPMe_3$ are similar as in the singly oxidized case. However, the lower energy of the oxido phosphane complex $[\mathbf{3^{Fc}}]^{2+}$ indicates that the driving force for consecutive reactions (e.g. with PMe_3 or residual water) might be higher than for $\mathbf{[5^{Fc}]^{+}}$, in addition to the higher tendency towards side reactions (vide supra). In summary, these results coincide nicely with the experimental findings which show the formation of phosphoryl complex starting from $\mathbf{[2^{Fc}]^{+}}$, whereas the analogous complexes $\mathbf{5^{Fc}}$ and $\mathbf{[5^{Fc}]^{2+}}$ are not observed due to fast consecutive reactions.

Conclusion

The oxidation of the $Mo(L^{Fc})_2O_2$ complex $\mathbf{2^{Fc}}$ with $AgSbF_6$ to $\mathbf{[2^{Fc}]^{+}}$ and $\mathbf{[2^{Fc}]^{2+}}$ was investigated in detail by NMR spectroscopy. In the ^{1}H-NMR spectrum the ferrocenyl proton signals of $\mathbf{[2^{Fc}]^{2+}}$ are paramagnetically shifted to about 30 ppm. Through optimization of the reaction conditions, the salt $\mathbf{[2^{Fc}][SbF_6]_2}$ could be isolated as crystalline powder. The paramagnetic shift of the Cp signals of $\mathbf{[2^{Fc}]^{+}}$ corresponds to half of the shift for $\mathbf{[2^{Fc}]^{2+}}$, due to the rapid self-exchange between Fc and Fc^{+}.

The reaction with PMe_3 was investigated starting from $\mathbf{2^{Fc}}$, $\mathbf{[2^{Fc}]^{+}}$ and $\mathbf{[2^{Fc}]^{2+}}$. The OAT reaction of $\mathbf{2^{Fc}}$ with an excess of PMe_3 yields the oxido phosphane complex $\mathbf{3^{Fc}}$ which exists in the form of two isomers ($\mathbf{3a^{Fc}}$ and $\mathbf{3b^{Fc}}$). Based on XRD and NOESY/EXSY peaks, the configuration of $\mathbf{3a^{Fc}}$ (OC-6-4-3, possibly in fast equilibrium with the minor isomer OC-6-3-4) and $\mathbf{3b^{Fc}}$ (OC-6-4-4) could be identified. Electrochemical investigation

shows decomposition of **3^{Fc}** upon oxidation of Mo^{IV} to Mo^{V}. The OAT reaction with **2^{Fc}** employing the bulky phosphane PPh_3 gives the dimer $[Mo^{V}(L^{Fc})_2O]_2(\mu\text{-}O)$ (**4^{Fc}**). The analysis of ^{1}H-NMR spectra over time reveals the formation of two isomers of **4^{Fc}**, the *Δ,Λ*-isomer **4a^{Fc}** (*meso*-isomer) and the *Λ,Λ*-isomer **4b^{Fc}** (*rac*-isomer), where the *rac*-isomer **4b^{Fc}** represents the kinetic product whereas the *meso*-isomer **4a^{Fc}** is the thermodynamic product, which is also found in the crystals of **4a^{Fc}**.

Addition of PMe_3 to **[2^{Fc}]$^{2+}$** results in the formation of **3^{Fc}** and several byproducts. Next to the desired attack of PMe_3 at Mo=O, mass spectrometric analysis provides indications for the attack of PMe_3 at the Cp ring and at the iron center. Indeed, occurrence of the former reaction is further supported by formation of a ferrocenyl phosphonium ion in the analogous reaction of Fc^+ and PMe_3.

Due to its reactivity, the expected intermediate $Mo^{V}Fe^{II}Fe^{III}$ phosphoryl complex $[Mo(L^{Fc})_2O(OPMe_3)]^{2+}$ (**[5^{Fc}]$^{2+}$**) could not be trapped in the case of **[2^{Fc}]$^{2+}$**. However, treatment of **[2^{Fc}]$^{+}$** with 1 eq. PMe_3 yields an EPR-active Mo^{V} species. The best fit to the EPR spectrum of the reaction solution is achieved when accounting for a weak ^{31}P hyperfine coupling ($A(^{31}P)$ = 7.2 G), which strongly supports the formation of the $Mo^{V}Fe^{II}Fe^{II}$ phosphoryl complex $[Mo^{V}(L^{Fc})_2O(OPMe_3)]^{+}$ (**[5^{Fc}]$^{+}$**) as intermediate obtained by IET-coupled OAT.

EXPERIMENTAL SECTION

General Procedures

All reactions were performed under argon atmosphere. THF was distilled over potassium, petrol ether over sodium and dichloromethane over calcium hydride. A glovebox (UniLab/MBraun, Ar 4.8, O_2 < 100 ppm, H_2O < 1 ppm) was used for storage and weighing of sensitive compounds. Aminoferrocene ($FcNH_2$),[230] *N*-acetylaminoferrocene (FcNHAc),[230] $MoCl_2O_2(dme)$,[231] **1^{Fc}**, **2^{Fc}** and **3^{Fc}** [208] were prepared according to literature procedures. Other reagents were received from usual suppliers (ABCR, Acros Organics, Alfa Aesar, Fischer Scientific, Fluka and Sigma–Aldrich). Filtrations from precipitated silver after oxidation were performed with syringe filters (Rotilabo, Ø = 25 mm, pore size = 0.20 µm; Carl Roth GmbH + Co. KG, Germany). NMR spectra were recorded on a Bruker Avance DRX 400 spectrometer at 400.31 MHz (^{1}H) and 162.05 MHz ($^{31}P\{^1H\}$). All resonances are reported in ppm versus the solvent signal as internal standard [d_8-THF (^{1}H: δ = 1.73, 3.58), CD_2Cl_2 (^{1}H: δ = 5.32)] and versus external H_3PO_4 (85%) (^{31}P: δ = 0

ppm). IR spectra were recorded with a BioRad Excalibur FTS 3100 spectrometer as CsI or KBr disks. Electrochemical experiments were carried out on a BioLogic SP-50 voltammetric analyzer using platinum wires as counter and working electrodes and a 0.01 M $Ag/AgNO_3$ electrode as reference electrode. The cyclic voltammetry and square wave measurements were carried out at scan rates of 50–200 mV s^{-1} using 0.1 M $[^nBu_4N][B(C_6F_5)_4]$ in CH_2Cl_2 or THF as supporting electrolyte. Potentials are referenced against the ferrocene/ferrocenium couple. UV-Vis/NIR spectra were recorded on a Varian Cary 5000 spectrometer using 1.0 cm cells (Hellma, suprasil). FD mass spectra were recorded on an FD Finnigan MAT90 spectrometer. ESI^+ mass spectra were recorded on a Micromass Q-TOF-Ultima spectrometer. Elemental analyses were conducted by the microanalytical laboratory of the chemical institutes of the University of Mainz. X-band CW EPR spectra were recorded on a Magnettech MS 300 spectrometer with a Hewlett Packard 5340A frequency counter at a microwave frequency of 9.4 GHz in frozen THF solution (77 K). Mn^{2+} in ZnS was used as external standard. EPR simulations were performed with the program package EasySpin.[232]

X-ray structure determinations

Intensity data was collected with a Bruker AXS Smart 1000 CCD diffractometer with an APEX II detector and an Oxford cooling system and corrected for absorption and other effects using Mo K_α radiation (λ = 0.71073 Å) at 173(2) K. The diffraction frames were integrated using the SAINT package, and most were corrected for absorption with MULABS.[233,234] The structures were solved by direct methods and refined by the full-matrix method based on F^2 using the SHELXTL software package.[235,236] All non-hydrogen atoms were refined anisotropically, while the positions of all hydrogen atoms were generated with appropriate geometric constraints and allowed to ride on their respective parent atoms with fixed isotropic thermal parameters. The molecule $\mathbf{4^{Fc}}$ co-crystallizes with four tetrahydrofuran molecules.

Density functional theory calculations (DFT)

DFT calculations for geometry optimization were carried out with the Gaussian 09 package.[237] The B3LYP[238] functional was employed in conjunction with the LANL2DZ[239–242] basis set, including additional Huzinaga polarization functions on oxygen, nitrogen and phosphorus atoms.[243] The presence of energy minima of the ground states and first-order saddle points in case of transition states was checked by analytical

frequency calculations. No symmetry constraints were imposed on the molecules. A polarizable continuum model (IEFPCM, tetrahydrofuran or dichloromethane) was used for solvent modeling. Grimme's D3 dispersion correction[244] was applied to the resulting Gibbs free energies, unless otherwise noted. In the geometry optimizations of **[2^{Fc}]$^{+}$** and [Mo(L^{Fc})$_2$O]$^{+}$, convergence was only achieved with relaxed convergence criteria (using the Gaussian keyword opt=loose). In case of the EPR calculations performed with the program package ORCA 3.0.2.,[245] the functional B3LYP, the basis set SV(P) for carbon and hydrogen atoms and TVZPP for oxygen, nitrogen, phosphorus, molybdenum and iron atoms,[246,247] the RIJCOSX approximation,[248,249] the zeroth-order regular approximation (ZORA)[250,251] and the KDIIS algorithm[252] and a solvent model (COSMO, THF)[253] were used.

Synthesis of 4^{Fc}. Dioxido complex **2^{Fc}** (10.43 mg, 0.015 mmol) was dissolved in THF (0.5 mL). Separately, triphenylphosphane (3.25 mg, 0.012 mmol) was dissolved in THF (0.5 mL). The solutions were mixed and the reaction solution rested for 5 days at room temperature. The overlaying solution was removed by a syringe from the precipitated dark red crystals. The crystals were washed with THF (3 x 0.1 mL), yielding 5.94 mg (0.004 mmol, 60%) of **4^{Fc}**. ^{1}H-NMR (CD_2Cl_2): δ = 8.36 (s, 2H, H$^{7/7'}$), 7.65 (s, 1H, H$^{11'}$), 6.74 (d, 1H, H$^{9'}$), 6.63 (s, 1H, H^{9}), 6.49 (s, 1H, H$^{10'}$), 5.98 (s, 1H, H^{10}), 5.93 (s, 1H, H^{11}), 4.29 (s, 1H, H$^{5'}$), 4.13 (s, 1H, H$^{1'}$), 4.02 (s, 1H, H^{1}), 3.96 (s, 1H, H^{5}), 3.92 (m, 1H, H^{3}), 3.90 (m, 2H, H^{2,4}), 3.82 (m, 2H, H$^{3'/4'}$), 3.71 (m, 1H, H$^{2'}$) ppm. IR (CsI): $\tilde{\nu}$ = 3095 (w, CH), 1578 (s, CN), 1292 (m), 1284 (m), 1186 (m), 1039 (s), 955 (m, M=O), 821 (m), 746 (m), 491 (s) cm^{-1}. DOSY (d_8-THF): log(D/m^2 s^{-1}) = –9.22. UV-Vis (CH_2Cl_2): λ = 314 (36070), 498 (10900), 545 (sh, 8715) nm (M^{-1} cm^{-1}). MS (FD): *m*/*z* (%) = 1348.6 (100, M^{+}). CV (CH_2Cl_2): E_p = –1870 (qrev), –130 (rev.), 0 (rev.), +160, +270 mV. Elemental analysis calcd. (%) for $C_{60}H_{52}Fe_4Mo_2N_8O_3$: C 53.44, H 3.89, N 8.31; found C 54.29, H 3.16 N, 9.54.

Oxidation of 2^{Fc} to [2^{Fc}](SbF$_6$)$_2$. Dioxido complex **2^{Fc}** (16.76 mg, 0.025 mmol) was dissolved in THF (1.8 mL). $AgSbF_6$ (17.11 mg, 0.05 mmol) was dissolved in THF (1.3 mL). The silver salt solution was added to the complex solution and the reaction mixture was shaken several times. After 5 minutes the mixture was filtered from the silver by a syringe filter. A brown solid precipitated from the solution for one hour at room temperature. The overlaying solution was removed by a syringe and the solid was washed

with petrol ether (4 x 0.2 mL). After drying under reduced vacuum, 8.33 mg (0.007 mmol, 28%) of the salt was obtained. ^{1}H-NMR (d_8-THF / d_6-acetone): δ = 40.50 – 27.47 (br. s, 4H, $H^{2,3,4,5}$), 32.20 (br. s, 5H, H^1), 10.14, 8.67, 2.86 (3 x s, 3H, $H^{9,10,11}$), –25.68 (br. s, 1H, H^7) ppm.

General procedure of the oxidation of $\mathbf{1^{Fc}}$, Fc, FcNH2+and FcNHAc to $\mathbf{[1^{Fc}]^+}$, $\mathbf{Fc^+}$, $\mathbf{FcNH_2^+}$ and $\mathbf{[FcNHAc]^+}$ for ^{1}H-NMR measurements. For ^{1}H-NMR measurements in d_8-THF 0.020 mmol of the compounds were dissolved in d_8-THF (0.5 mL). 1 eq. of $AgSbF_6$ was dissolved in d_8-THF (0.5 mL) and added to the first solution. The solutions were mixed, shaken several times and then separated from silver through filtration. The ^{1}H-NMR spectra were recorded immediately.

General procedure of the reaction of $\mathbf{[1^{Fc}]^+}$, $\mathbf{Fc^+}$ and $\mathbf{[FcNHAc]^+}$ with an excess of $\mathbf{PMe_3}$ for ^{1}H-NMR measurements. To the dissolved ferrocenium compounds (prepared by the procedure described above), 5 eq. of trimethylphosphane (1 M in THF) was added with an Eppendorf pipette in case of $\mathbf{[1^{Fc}]^+}$. In case of $\mathbf{Fc^+}$ and $\mathbf{[FcNHAc]^+}$, 3 eq. and 1 eq. of PMe_3 were added, respectively. The ^{1}H-NMR spectra were recorded immediately.

Oxidation of $\mathbf{2^{Fc}}$ to $\mathbf{[2^{Fc}]^+}$ and addition of 1 eq. $\mathbf{PMe_3}$ for EPR measurement:
Dioxido complex $\mathbf{2^{Fc}}$ (15.24 mg, 0.022 mmol) was dissolved in 0.5 mL d_8-THF. $AgSbF_6$ (8.90 mg, 0.026 mmol) was dissolved in d_8-THF (0.2 mL). The silver salt solution was added to the complex solution. After shaking several times, the reaction mixture was filled into a washed (0.5 mL d_8-THF) syringe and filtered from silver (the degree of oxidation was checked by ^{1}H-NMR spectroscopy). To the 0.95 mL filtrate, 1 eq. trimethylphosphane (1 M in THF, 22.33 µL, 0.022 mmol) was added. The solution was frozen by immersion of the EPR tube in liquid nitrogen to obtain the anisotropic EPR spectrum. After warming up to room temperature, the isotropic EPR spectra were measured.

ACKNOWLEDGMENTS

We thank Mihail Mondeshki for excellent NMR support, Regine Jung-Pothmann for X-ray data collection, and Minh Thu Pham, Ali Abdulkarim and Lidia Pelin for preparative assistance.

5 Summary and Outlook

The focus of this thesis is the synthesis and characterization of functional ferrocenyl-based compounds: redox-switchable *N*,*N*'-disubstituted ferrocenyl(thio)ureas, and dioxido molybdenum(VI) complexes with ferrocenyl-substituted ligands as model systems for the enzyme sulfite oxidase (SO).

Concerning the first subject, this work presents a detailed investigation of the structure of novel *N*,*N*'-disubstituted ferrocenyl(thio)ureas Fc-NHCXNH-R (X = O: R = Me, Et, Ph, Nap, Fc; X = S: R = Ant, Fc) both in the solid state and in solution. In general, *N*,*N*'-disubstituted ferrocenyl(thio)ureas exist in the *trans-trans*, *cis-trans* (with *cis/trans* describing the position of an NH-proton relative to the carbonyl group), *trans-cis* and *cis-cis* conformation. In the solid state all investigated ferrocenylureas exist in the *trans-trans* conformation and are connected to chains through bifurcated $(NH)_2\cdots O=C$ hydrogen bonds. On the other hand, both of the studied ferrocenylthioureas dimerize as *cis-trans* isomers into rings via NH···S=C hydrogen bonds, with the feature that in Fc-NHCSNH-Fc the remaining NH proton forms a nonclassical NH···Fe hydrogen bond. These results are in line with X-ray diffraction data from the literature which also show ureas mainly in the *trans-trans*-conformation, while thioureas exist in the *trans-trans* and *cis-trans* conformation likewise.

The conformation of ferrocenyl(thio)ureas in solution has been investigated in the coordinating solvent tetrahydrofuran and in the non-coordinating solvent dichloromethane. For this purpose, IR and NMR spectroscopy have been used. In particular, $^1H^1H$-NOESY experiments turn out to be of high value in the conformational analysis and thus have been performed for all ferrocenyl(thio)ureas. The $^1H^1H$-NOESY spectra show that in tetrahydrofuran ferrocenylureas exist in the *trans-trans* conformation because of the energy gain from the coordination of the solvent molecule via $(NH)_2\cdots O$ hydrogen bonding, which is also in agreement with DFT calculations. For ferrocenylthioureas the energy gain from hydrogen bond formation is not sufficient, hence the *cis-trans* conformation is still preferred. In dichloromethane, however, the

ferrocenylureas exist as a mixture of *cis-trans*, *trans-cis* and *trans-trans* isomers in absence of a coordinating solvent, while ferrocenylthioureas retain their *cis-trans* conformation. The *cis-trans* conformation is additionally stabilized by the formation of a nonclassical NH···Fe hydrogen bond. This stabilizing effect is somewhat larger for thioureas because of their higher acidity. The experimental results are supported by DFT calculations which show a larger energy gap between *cis-trans* und *trans-trans* for ferrocenylthioureas than for ferrocenylureas. Presumably, the bigger atomic radius of sulfur compared to the oxygen atom leads to a higher repulsion with the Fc substituent and hence to a preference of the *cis-trans* conformation.

With increasing concentration or decreasing temperature, the ferrocenyl(thio)ureas aggregate to dimers. In course of this aggregation, the ^{1}H-NMR resonance of the NH proton *cis* to the carbonyl group shifts much stronger than the signal of the *trans* NH proton, which evidences the involvement of primarily the *cis* NH proton in hydrogen bonds and implies a formation of dimers from *cis-trans* isomers. At high concentration, the aggregation of molecules to higher oligomers is possible, as indicated by NOE signals characteristic for chains of *trans-trans* isomers. This change in the preferred conformation of the ferrocenylurea molecules from *cis-trans* to *trans-trans* can be rationalized by the larger number of hydrogen bonds in a chain compared to the number in tapes of dimers containing the same amount of monomers, and ultimately results in crystals featuring chains of ferrocenylurea molecules.

The oxidation of the ferrocenyl moiety with silver hexafluoroantimonate leads to a coordination of the $[SbF_6]^-$ anion to both NH protons, changing the *cis-trans* into a *trans-trans* conformation similar to the situation in THF. The crystal structure of [Fc-NHCONH-Fc][SbF_6]$_2$ provides a direct proof for this bifurcated coordination in the solid state. In solution, evidence comes from conductivity measurements on [Fc-NHCONH-Et][SbF_6] showing the formation of contact ion pairs through a substantial deviation of the ionic conductivity from Kohlrausch's law. Additionally, DFT calculations confirm the preference for the coordination of the anion over a single bifurcated hydrogen bond. Electrochemical measurements show a reversibility of the oxidation, meaning that the *trans-trans* conformation can be switched back to the *cis-trans* conformation upon reduction. With this property, ferrocenyl(thio)ureas can act as redox switches. Taken together, the conformation of ferrocenyl(thio)ureas is very sensitive with respect to

solvent, concentration and oxidation state, making these compounds useful in fields of application where molecules with tunable conformation are necessary.

Regarding the second subject of this thesis, a first step towards sulfite oxidase mimicking model complexes are the dioxido molybdenum(VI) complex $Mo^{VI}(L^{tBu})_2O_2$ (**1**, L^{tBu} = 4-*tert*-butyl phenyl(pyrrolato-2-ylmethylene)amine) and the imido oxido molybdebum(VI) complex $Mo^{VI}(L^{tBu})_2(N^tBu)O$ (**2**), which prove oxygen atom transfer (OAT) capability to PMe_3.

The OAT from **1** to PMe_3 leads to the formation of the $(L^{tBu})_2OMo^V–O–Mo^VO(L^{tBu})_2$ dimer and $OPMe_3$. With an excess of PMe_3 the dimer dissociates and the vacant coordination site is occupied by a PMe_3 molecule, yielding the phosphane complex $Mo^{IV}(L^{tBu})_2O(PMe_3)$ (**3**) in form of two isomers OC-6-4-3 and OC-6-3-3 (5:2). The larger imido ligand in **2** should make the nucleophilic attack of PMe_3 at the oxido ligand more difficult as also predicted by DFT calculations ($\Delta G^‡$ = 65 kJ mol^{-1} for **1** compared to $\Delta G^‡$ = 109 kJ mol^{-1} for **2**). However, ^{31}P-NMR spectroscopy over time shows that **2** reacts 10 times faster than **1** because the bulky imido ligand prevents the formation of a μ-oxido dimer. Similar to **3**, the $Mo^{IV}(L^{tBu})_2(N^tBu)(PMe_3)$ complex (**4**) is most stable as OC-6-4-3 isomer. However, in contrast to **3**, the presence of a further isomer is not observed. Catalytic double OAT reaction from DMSO to PMe_3, yielding DMS and $OPMe_3$, occurs in the case of **2** (k_{298} = 3.0x10^{-5} s^{-1}) faster than for **1** (k_{298} = 1.5x10^{-5} s^{-1}) because no dimer formation takes place such as for **1**. However, for **2**, product inhibition by the PMe_3 substrate is observed, leading to the formation of small amounts of phosphane complex **4** and hence to an incomplete conversion of the PMe_3 substrate. Oxidation of **3** to the molybdenum(V) complex **[3]**$^+$ leads to dissociation of the PMe_3 ligand, whereas the oxidation of **4** yields the stable $[Mo^V(L^{tBu})_2(N^tBu)(PMe_3)][PF_6]$ complex (**[4][PF$_6$]**) which has been characterized with X-ray diffraction. Obviously the imido ligand stabilizes the positive charge in **[4]**$^+$ through donation of electron density to the molybdenum center, whereas the oxido ligand in **[3]**$^+$ is destabilized by withdrawal of electron density from the central atom. In summary, **2** is stable in the biologically relevant oxidation states VI, V and IV and does not aggregate to the abiological μ-oxido dimer during the OAT reaction.

The use of the dioxido molybdenum(VI) complex $Mo^{VI}(L^{Fc})_2O_2$ (**1^{Fc}**), based on the redox-active ligand HL^{Fc} (*N*-((pyrrolato-2-yl)methylene)ferrocenylamine), offers the possibility to mimic the enzymatic intramolecular electron transfer (IET) coupled OAT. After oxidation, the generated ferrocenium units of the ligand act as electron acceptor, which can receive electrons from the molybdenum center. For this purpose, the oxidation products **[1^{Fc}]$^{+}$** and **[1^{Fc}]$^{2+}$** have been characterized, after synthesis via oxidation of **1^{Fc}** with 1 eq. and 2 eq. silver hexafluoroantimonate, respectively. In the ^{1}H-NMR spectrum, the paramagnetically shifted and broadened proton signals are clearly assigned to **[1^{Fc}]$^{+}$** and **[1^{Fc}]$^{2+}$**. While all of the states **1^{Fc}**, **[1^{Fc}]$^{+}$** and **[1^{Fc}]$^{2+}$** are capable of OAT to phosphanes, their reactivities and reaction products are quite different:

The OAT from **1^{Fc}** to PMe_3 follows the same mechanism that is observed for $Mo^{VI}(L^{tBu})_2O_2$ and is also known from similar dioxido molybdenum(VI) complexes. By employing an excess of PMe_3, the oxido phosphane molybdenum(IV) complex $Mo^{IV}(L^{Fc})_2O(PMe_3)$ (**3^{Fc}**) has been isolated. Similar to **3**, **3^{Fc}** exists in two isomers (OC-6-4-3 and OC-6-4-4, 5:2). Oxidation of **3^{Fc}** leads to decomposition due to the labile bonding of the PMe_3 ligand, similar to the behavior of **3**. In comparison, use of the large phosphane PPh_3 does not yield the corresponding oxido phosphane complex and hence the OAT reaction stops at the step of the $(L^{Fc})_2OMo^{V}–O–Mo^{V}O(L^{Fc})_2$ dimer (**4^{Fc}**). ^{1}H-NMR spectroscopy over time reveals the formation of two isomers of $(L^{Fc})_2OMo^{V}–O–Mo^{V}O(L^{Fc})_2$ during the OAT reaction. In the course of the reaction, the kinetically formed *rac*-isomer converts to the thermodynamically preferred *meso*-isomer.

With **[1^{Fc}]$^{+}$** as oxygen donor the characterization of the EPR-active intermediate $[Mo^{V}(L^{Fc})_2O(OPMe_3)]^{+}$ **[5^{Fc}]$^{+}$** is possible. The formation of this phosphoryl molybdenum(V) complex can be rationalized by an IET-coupled OAT. Through the attack of PMe_3 at the oxido ligand, molybdenum is reduced from Mo^{VI} to Mo^{IV}, followed by an IET from Mo^{IV} to Fe^{III}. DFT calculations confirm the experimental findings, as they predict a larger energetic stabilization of **[5^{Fc}]$^{+}$** compared to the analogous neutral phosphoryl complex, and an increased barrier for the subsequent dissociation of $OPMe_3$. The addition of an excess of PMe_3 to **[1^{Fc}]$^{2+}$** yields **3^{Fc}** and $OPMe_3$ in a ratio 1:2. The formation of **3^{Fc}** can be explained by OAT to PMe_3, followed by two electron transfer steps to the Fe^{III} center, replacement of the oxido ligand by an oxygen atom from residual water and a second OAT to PMe_3. In contrast to **[5^{Fc}]$^{+}$**, the $[Mo^{V}(L^{Fc})_2O(OPMe_3)]^{2+}$

complex $\mathbf{[5^{Fc}]^{2+}}$ from the reaction of $\mathbf{[1^{Fc}]^{2+}}$ with PMe_3 cannot be trapped using similar conditions, indicating faster consecutive reactions. Additionally, the trapping of $\mathbf{[5^{Fc}]^{2+}}$ is complicated by a higher reactivity of the complex due to the presence of a ferrocenium moiety which can be attacked by PMe_3 at the Cp ring or at the iron(III) center directly. Corresponding side products assigned in the mass spectra provide evidence for these reactions. Further, attack at the Cp ring also occurs in $[Fc][SbF_6]$ solutions in presence of PMe_3, in agreement with DFT calculations and as proven by NMR spectroscopic observation of the resulting product. Similar side reactions are not observed for $\mathbf{[5^{Fc}]^{+}}$ because the iron centers are not oxidized.

Potential ways to minimize the extent of the side reactions by reducing their reaction rates are to decrease the temperature or the concentration of $\mathbf{[1^{Fc}]^{2+}}$, or to slowly add phosphane (and potentially other reagents like water and base in order to close the catalytic cycle) to control its concentration during the reaction. Use of other substrates such as PPh_3 might prevent attacks of the substrate at the ligand or the molybdenum center and thus may be worth trying. In view of the stability of the $[Mo^{V}(L^{tBu})_2(N^{t}Bu)(PMe_3)]^{+}$ complex, the synthesis of the analogous $[Mo^{V}(L^{Fc})_2(N^{t}Bu)(PMe_3)]^{+}$ with similar stability is also conceivable. The characterization of this complex could additionally confirm the present experimental results for $\mathbf{[5^{Fc}]^{+}}$ and deepen our understanding of IET-coupled OAT reactions.

Overall, the $Mo^{VI}(L^{Fc})_2O_2$ model complex $\mathbf{1^{Fc}}$ successfully mimics the enzymatic IET-coupled OAT reaction. This coupling of intramolecular single-electron transfer to a formal two-electron transfer step (i.e. oxygen atom transfer) in $\mathbf{1^{Fc}}$ may also be regarded as a step towards the utilization of this principle in other catalytic reactions.

6 References

(1) Rosenfeld, L. *Clin. Chem.* **2003**, *49*, 699–705.

(2) Withers, P. C. *Clin. Exp. Pharmacol. Physiol.* **1998**, *25*, 722–727.

(3) Follmer, C. *Phytochemistry* **2008**, *69*, 18–28.

(4) Wöhler, F. *Ann. Phys.* **1828**, *88*, 253–256.

(5) Tsipis, C. A.; Karipidis, P. A. *J. Phys. Chem. A* **2005**, *109*, 8560–8567.

(6) Meessen, J. *Chemie-Ingenieur-Technik* **2014**, *86*, 2180–2189.

(7) Volz, N.; Clayden, J. *Angew. Chemie Int. Ed.* **2011**, *50*, 12148–12155.

(8) Wittkopp, A.; Schreiner, P. R. *Chem. Soc. Rev.* **2003**, *9*, 407–414.

(9) Piepenbrock, M.-O. M.; Lloyd, G. O.; Clarke, N.; Steed, J. W. *Chem. Rev.* **2010**, *110*, 1960–2004.

(10) Khan, S. A.; Singh, N.; Saleem, K. *Eur. J. Med. Chem.* **2008**, *43*, 2272–2277.

(11) Molina, P.; Tárraga, A.; Caballero, A. *Eur. J. Inorg. Chem.* **2008**, 3401–3417.

(12) Astruc, D. *Eur. J. Inorg. Chem.* **2017**, 6–29.

(13) Hille, R.; Hall, J.; Basu, P. *Chem. Rev.* **2014**, *114*, 3963–4038.

(14) Hine, F. J.; Taylor, A. J.; Garner, C. D. *Coord. Chem. Rev.* **2010**, *254*, 1570–1579.

(15) Kaim, W.; Schwederski, B. *Bioanorganische Chemie*, 4rd ed.; Teubner: Wiesbaden, 2005.

(16) Etter, M. C.; Panunto, T. W. *J. Am. Chem. Soc.* **1988**, *110*, 5896–5897.

(17) Etter, M. C.; Urbañczyk-Lipkowska, Z.; Zia-Ebrahimi, M.; Panunto, T. W. *J. Am. Chem. Soc.* **1990**, *112*, 8415–8426.

(18) Curran, D. P.; Kuo, L. H. *J. Org. Chem.* **1994**, *59*, 3259–3261.

(19) Schreiner, P. R. *Chem. Soc. Rev.* **2003**, *32*, 289–296.

(20) Wittkopp, A.; Schreiner, P. R. *Chem. Eur. J.* **2003**, *9*, 407–414.

(21) Sigman, M. S.; Jacobsen, E. N. *J. Am. Chem. Soc.* **1998**, *120*, 4901–4902.

(22) Sigman, M. S.; Vachal, P.; Jacobsen, E. N. *Angew. Chemie Int. Ed.* **2000**, *39*, 1279–1281.

(23) Yoon, T. P.; Jacobsen, E. N. *Angew. Chemie Int. Ed.* **2005**, *44*, 466–468.

(24) Boileau, S.; Bouteiller, L.; Lauprêtre, F.; Lortie, F. *New J. Chem.* **2000**, *24*, 845–848.

(25) Bouteiller, L.; Colombani, O.; Lortie, F.; Terech, P. *J. Am. Chem. Soc.* **2005**, *127*, 8893–8898.

(26) Lortie, F.; Boileau, S.; Bouteiller, L.; Chassenieux, C.; Demé, B.; Ducouret, G.; Jalabert, M.; Lauprêtre, F.; Terech, P. *Langmuir* **2002**, *18*, 7218–7222.

(27) Obert, E.; Bellot, M.; Bouteiller, L.; Andrioletti, F.; Lehen-Ferrenbach, C.; Boué, F. *J. Am. Chem. Soc.* **2007**, *129*, 15601–15605.

(28) Shikata, T.; Nishida, T.; Isare, B.; Linares, M.; Lazzaroni, R.; Bouteiller, L. *J. Phys. Chem. B* **2008**, *112*, 8459–8465.

(29) Sijbesma, R. P.; Beijer, F. H.; Brunsveld, L.; Folmer, B. J. B.; Ky Hirschberg, J. H. K.; Lange, R. F. M.; Lowe, J. K. L.; Meijer, E. W. *Science* **1997**, *278*, 1601–1604.

(30) Ávalos, M.; Babiano, R.; Cintas, P.; Gómez-Carretero, A.; Jiménez, J. L.; Lozano, M.; Ortiz, A. L.; Palacios, J. C.; Pinazo, A. *Chem. Eur. J.* **2008**, *14*, 5656–5669.

(31) de Loos, M.; Feringa, B. L.; van Esch, J. H. *Eur. J. Org. Chem.* **2005**, 3615–3631.

(32) Estroff, L. A.; Hamilton, A. D. *Angew. Chemie Int. Ed.* **2000**, *39*, 3447–3450.

(33) de Loos, M.; van Esch, J.; Kellogg, R. M.; Feringa, B. L. *Angew. Chemie Int. Ed.* **2001**, *113*, 633–636.

(34) Piepenbrock, M.-O. M.; Lloyd, G. O.; Clarke, N.; Steed, J. W. *Chem. Commun.* **2008**, 2644–2646.

(35) Rodriguez, J. M.; Hamilton, A. D. *Angew. Chemie Int. Ed.* **2007**, *46*, 8614–8617.

(36) Fischer, L.; Claudon, P.; Pendem, N.; Miclet, E.; Didierjean, C.; Ennifar, E.;

Guichard, G. *Angew. Chemie Int. Ed.* **2010**, *49*, 1067–1070.

(37) van Gorp, J. J.; Vekemans, J. A. J. M.; Meijer, E. W. *Chem. Commun.* **2004**, *2*, 60–61.

(38) Shimizu, L. S.; Smith, M. D.; Hughes, A. D.; Shimizu, K. D. *Chem. Commun.* **2001**, 1592–1593.

(39) Dawn, S.; Dewal, M. B.; Sobransingh, D.; Paderes, M. C.; Wibowo, A. C.; Smith, M. D.; Krause, J. A.; Pellechia, P. J.; Shimizu, L. S. *J. Am. Chem. Soc.* **2011**, *133*, 7025–7032.

(40) Liu, Y.; Li, Y.; Jiang, L.; Gan, H.; Liu, H.; Li, Y.; Zhuang, J.; Lu, F.; Zhu, D. *J. Org. Chem.* **2004**, *69*, 9049–9054.

(41) Lapić, J.; Djaković, S.; Cetina, M.; Heinze, K.; Rapić, V. *Eur. J. Inorg. Chem.* **2010**, 106–114.

(42) Smith, P. J.; Reddington, M. V.; Wilcox, C. S. *Tetrahedron Lett.* **1992**, *33*, 6085–6088.

(43) Fan, E.; Van Arman, S. A.; Kincaid, S.; Hamilton, A. D. *J. Am. Chem. Soc.* **1993**, *115*, 369–370.

(44) Amendola, V.; Fabbrizzi, L.; Mosca, L. *Chem. Soc. Rev.* **2010**, *39*, 3889–3915.

(45) Heinze, K.; Schlenker, M. *Eur. J. Inorg. Chem.* **2005**, 66–71.

(46) Siebler, D.; Förster, C.; Heinze, K. *Eur. J. Inorg. Chem.* **2010**, 523–527.

(47) Hussain, S.; Brotherhood, P. R.; Judd, L. W.; Davis, A. P. *J. Am. Chem. Soc.* **2011**, *133*, 1614–1617.

(48) McConnell, A. J.; Beer, P. D. *Angew. Chemie Int. Ed.* **2012**, *51*, 5052–5061.

(49) Molina, P.; Tárraga, A.; Alfonso, M. *Dalton Trans.* **2014**, *43*, 18–29.

(50) Otón, F.; Tárraga, A.; Espinosa, A.; Velasco, M. D.; Molina, P. *J. Org. Chem.* **2006**, *71*, 4590–4598.

(51) Beer, P. D.; Davis, J. J.; Drillsma-Milgrom, D. A.; Szemes, F. *Chem. Commun.* **2002**, *44*, 1716–1717.

(52) Evans, A. J.; Matthews, S. E.; Cowley, R.; Beer, P. D. *Dalton Trans.* **2003**, *2*,

4644–4650.

(53) Miyaji, H.; Collinson, S. R.; Prokeŝ, I.; Tucker, J. H. R. *Chem. Commun.* **2003**, *2*, 64–65.

(54) Pratt, M. D.; Beer, P. D. *Polyhedron* **2003**, *22*, 649–653.

(55) Otón, F.; Espinosa, A.; Tárraga, A.; Ratera, I.; Wurst, K.; Veciana, J.; Molina, P. *Inorg. Chem.* **2009**, *48*, 1566–1576.

(56) Mulas, A.; Willener, Y.; Carr-Smith, J.; Joly, K. M.; Male, L.; Moody, C. J.; Horswell, S. L.; Nguyen, H. V.; Tucker, J. H. R. *Dalton Trans.* **2015**, *44*, 7268–7275.

(57) Biot, C.; Franc, N.; Maciejewski, L.; Poulain, D. *Bioorg. Med. Chem. Lett.* **2000**, *10*, 839–841.

(58) Allardyce, C. S.; Dorcier, A.; Scolaro, C.; Dyson, P. J. *Appl. Organomet. Chem.* **2005**, *19*, 1–10.

(59) Hillard, E.; Vessières, A.; Thouin, L.; Jaouen, G.; Amatore, C. *Angew. Chemie Int. Ed.* **2005**, *45*, 285–290.

(60) Payen, O.; Top, S.; Vessières, A.; Brulé, E.; Plamont, M.-A.; McGlinchey, M. J.; Müller-Bunz, H.; Jaouen, G. *J. Med. Chem.* **2008**, *51*, 1791–1799.

(61) Jaouen, G.; Vessières, A.; Top, S. *Chem. Soc. Rev.* **2015**, *44*, 8802–8817.

(62) Venkatachalam, T. K.; Sudbeck, E. A.; Mao, C.; Uckun, F. M. *Bioorg. Med. Chem. Lett.* **2001**, *11*, 523–528.

(63) Kakadiya, R.; Dong, H.; Kumar, A.; Narsinh, D.; Zhang, X.; Chou, T.-C.; Lee, T.-C.; Shah, A.; Su, T.-L. *Bioorg. Med. Chem.* **2010**, *18*, 2285–2299.

(64) Liu, W.; Tang, Y.; Guo, Y.; Sun, B.; Zhu, H.; Xiao, Y.; Dong, D.; Yang, C. *Appl. Organomet. Chem.* **2012**, *26*, 189–193.

(65) Rao, C. N. R.; Venkataraghavan, R. *Spectrochim. Acta* **1962**, *18*, 541–547.

(66) Gosavi, R. K.; Agarwala, U.; Rao, C. N. R. *J. Am. Chem. Soc.* **1967**, *35*, 235–239.

(67) Ritchie, R. K.; Spedding, H.; Steele, D. *Spectrochim. Acta* **1971**, *27A*, 1597–1608.

(68) Mido, Y. *Spectrochim. Acta* **1972**, *28A*, 1503–1518.

(69) Mido, Y. *Spectrochim. Acta* **1973**, *29A*, 431–438.

(70) Aruna, S.; Shanmugam, G.; Manogaran, S.; Sathyanarayana, D. N. *Bull. Chem. Soc. Jpn.* **1982**, *55*, 3612–3616.

(71) Mido, Y.; Mizuno, H.; Suzuki, T.; Okuno, T. *Spectrochim. Acta* **1986**, *42A*, 807–809.

(72) Bala, S. S.; Panja, P. K.; Ghosh, P. N. *J. Mol. Struct.* **1987**, *157*, 339–351.

(73) Mido, Y.; Mizuno, H.; Machida, K. *Spectrochim. Acta* **1988**, *44A*, 445–447.

(74) Panja, P. K.; Bala, S. S.; Ghosh, P. N. *Spectrochim. Acta* **1988**, *176*, 203–211.

(75) Gray, J. L.; Barnes, C. M.; Carr, A. J.; McCain, K. S. *Appl. Spectrosc.* **2009**, *63*, 1409–1413.

(76) Stewart, J. E. *J. Chem. Phys.* **1957**, *26*, 248–254.

(77) Boileau, S.; Bouteiller, L.; Lauprêtre, F.; Lortie, F. *New J. Chem.* **2000**, *24*, 845–848.

(78) Lortie, F.; Boileau, S.; Bouteiller, L. *Chem. Eur. J.* **2003**, *9*, 3008–3014.

(79) Obrzud, M.; Rospenk, M.; Koll, A. *J. Mol. Struct.* **2012**, *1018*, 54–63.

(80) Obrzud, M.; Rospenk, M.; Koll, A. *Phys. Chem. Chem. Phys.* **2014**, *16*, 3209–3219.

(81) Jadżyn, J.; Stockhausen, M.; Żywucki, B. *J. Phys. Chem.* **1987**, *91*, 754–757.

(82) Obrzud, M.; Rospenk, M.; Koll, A. *J. Phys. Chem. B* **2010**, *114*, 15905–15912.

(83) Świergiel, J.; Jadżyn, J. *React. Funct. Polym.* **2016**, *105*, 129–133.

(84) Godfrey, P. D.; Brown, R. D.; Hunter, A. N. *J. Mol. Struct.* **1997**, *413-414*, 405–414.

(85) Bryantsev, V. S.; Firman, T. K.; Hay, B. P. *J. Phys. Chem. A* **2005**, *109*, 832–842.

(86) Kim, W.; Lee, H.-J.; Choi, Y. S.; Choi, J.-H.; Yoon, C.-J. *J. Chem. Soc., Faraday Trans.* **1998**, *94*, 2663–2668.

(87) Haushalter, K. A.; Lau, J.; Roberts, J. D. *J. Am. Chem. Soc.* **1996**, *118*, 8891–8896.

(88) Bordwell, F. G.; Algrim, D. J.; Harrelson, Jr., J. A. *J. Am. Chem. Soc.* **1988**, *110*,

5903–5904.

(89) Wiberg, K. B.; Rush, D. J. *J. Am. Chem. Soc.* **2001**, *123*, 2038–2046.

(90) Bharatam, P. V.; Moudgil, R.; Kaur, D. *J. Phys. Chem. A* **2003**, *107*, 1627–1634.

(91) Bryantsev, V. S.; Hay, B. P. *J. Phys. Chem. A* **2006**, *110*, 4678–4688.

(92) Custelcean, R.; Gorbunova, M. G.; Bonnesen, P. V. *Chem. Eur. J.* **2005**, *11*, 1459–1466.

(93) Chang, Y.-L.; West, M.-A.; Fowler, F. W.; Lauher, J. W. *J. Am. Chem. Soc.* **1993**, *115*, 5991–6000.

(94) Custelcean, R. *Chem. Commun.* **2008**, 295–307.

(95) Masunov, A.; Dannenberg, J. J. *J. Phys. Chem. B* **2000**, *104*, 806–810.

(96) Masunov, A.; Dannenberg, J. J. *J. Phys. Chem. A* **1999**, *103*, 178–184.

(97) Siebler, D.; Förster, C.; Gasi, T.; Heinze, K. *Organometallics* **2011**, *30*, 313–327.

(98) Mahmoud, K.; Long, Y.-T.; Schatte, G.; Kraatz, H.-B. *J. Organomet. Chem.* **2004**, *689*, 2250–2255.

(99) Gong, Z.-L.; Zhong, Y.-W.; Yao, J. *Chem. Eur. J.* **2015**, *21*, 1554–1566.

(100) Creutz, C.; Taube, H. *J. Am. Chem. Soc.* **1969**, *91*, 3988–3989.

(101) Creutz, C.; Taube, H. *J. Am. Chem. Soc.* **1973**, *95*, 1086–1094.

(102) Marcus, R. A. *Rev. Mod. Phys.* **1993**, *65*, 599–610.

(103) Hush, N. S. *Prog. Inorg. Chem.* **1967**, *8*, 391–444.

(104) Winter, R. F. *Organometallics* **2014**, *33*, 4517–4536.

(105) Flanagan, J. B.; Margel, S.; Bard, A. J.; Anson, F. C. *J. Am. Chem. Soc.* **1978**, *100*, 4248–4253.

(106) Aguirre-Etcheverry, P.; O'Hare, D. *Chem. Rev.* **2010**, *110*, 4839–4864.

(107) Ceccon, A.; Santi, S.; Orian, L.; Bisello, A. *Coord. Chem. Rev.* **2004**, *248*, 683–724.

(108) Ribou, A.-C.; Launay, J.-P.; Sachtleben, M. L.; Li, H.; Spangler, C. W. *Inorg.*

Chem. **1996**, *35*, 3735–3740.

(109) Heinze, K.; Siebler, D. *Z. Anorg. Allg. Chem.* **2007**, *633*, 2223–2233.

(110) Gong, Z.-L.; Zhong, Y.-W. *Sci. China Chem.* **2015**, *58*, 1444–1450.

(111) Schlögl, K.; Seiler, H. *Naturwissenschaften* **1958**, *45*, 337–337.

(112) Mendel, R. R. *Dalton Trans.* **2005**, 3404–3409.

(113) Schwarz, G.; Mendel, R. R.; Ribbe, M. W. *Nature* **2009**, *460*, 839–847.

(114) Erfkamp, J.; Müller, A. *Chemie unserer Zeit* **1990**, *6*, 267–279.

(115) Romão, M. J. *Dalton Trans.* **2009**, 4053–4068.

(116) Thapper, A.; Lorber, C.; Fryxelius, J.; Behrens, A.; Nordlander, E. *J. Inorg. Biochem.* **2000**, *79*, 67–74.

(117) Hille, R. *Chem. Rev.* **1996**, *96*, 2757–2816.

(118) Johnson-Winters, K.; Tollin, G.; Enemark, J. H. *Biochemistry* **2010**, *49*, 7242–7254.

(119) Bailey, J. L.; Cole, R. D. *J. Biol. Chem.* **1959**, *234*, 1733–1739.

(120) Feng, C.; Tollin, G.; Enemark, J. H. *Biochim. Biophys. Acta* **2007**, *1774*, 527–539.

(121) Karakas, E.; Wilson, H. L.; Graf, T. N.; Xiang, S.; Jaramillo-Busquets, S.; Rajagopalan, K. V.; Kisker, C. *J. Biol. Chem.* **2005**, *280*, 33506–33515.

(122) Workun, G. J.; Moquin, K.; Rothery, R. A.; Weiner, J. H. *Microbiol. Mol. Biol. Rev.* **2008**, *72*, 228–248.

(123) Hänsch, R.; Lang, C.; Riebeseel, E.; Lindigkeit, R.; Gessler, A.; Rennenberg, H.; Mendel, R. R. *J. Biol. Chem.* **2006**, *281*, 6884–6888.

(124) Kappler, U. *Biochim. Biophys. Acta* **2011**, *1807*, 1–10.

(125) Kappler, U.; Bailey, S. *J. Biol. Chem.* **2005**, *280*, 24999–25007.

(126) The PyMOL Molecular Graphics System, Version 1.3 Schrödinger, LLC http://www.pymol.org.

(127) Robin, S.; Arese, M.; Forte, E.; Sarti, P.; Kolaj-Robin, O.; Giuffrè, A.; Soulimane, T. *PLoS ONE* **2013**, *8*, e55129.

(128) Robin, S.; Arese, M.; Forte, E.; Sarti, P.; Giuffrè, A.; Soulimane, T. *J. Bacteriol.* **2011**, *193*, 3988–3997.

(129) Di Salle, A.; D'Errico, G.; La Cara, F.; Cannio, R.; Rossi, M. *Extremophiles* **2006**, *10*, 587–598.

(130) Schrader, N.; Fischer, K.; Theis, K.; Mendel, R. R.; Schwarz, G.; Kisker, C. *Structure* **2003**, *11*, 1251–1263.

(131) Gray, H. B.; Winkler, J. R. *Annu. Rev. Biochem.* **1996**, *65*, 537–561.

(132) Winkler, J. R. *Curr. Opin. Chem. Biol.* **2000**, *4*, 192–198.

(133) Pacheco, A.; Hazzard, J. T.; Tollin, G.; Enemark, J. H. *J. Biol. Inorg. Chem.* **1999**, *4*, 390–401.

(134) Utesch, T.; Mroginski, M. A. *J. Phys. Chem. Lett.* **2010**, *1*, 2159–2164.

(135) Rudolph, M. J.; Johnson, J. L.; Rajagopalan, K. V.; Kisker, C. *Acta Crystallogr.* **2003**, *D59*, 1183–1191.

(136) Astashkin, A. V; Rajapakshe, A.; Cornelison, M. J.; Johnson-Winters, K.; Enemark, J. H. *J. Phys. Chem. B* **2012**, *116*, 1942–1950.

(137) Hille, R. *Essays Biochem.* **1999**, *34*, 221–230.

(138) Hille, R. *Biochim. Biophys. Acta* **1994**, *1184*, 143–169.

(139) Brody, M. S.; Hille, R. *Biochemistry* **1999**, *38*, 6668–6677.

(140) Brody, M. S.; Hille, R. *Biochim. Biophys. Acta* **1995**, *1253*, 133–135.

(141) Holm, R. H. *Coord. Chem. Rev.* **1990**, *100*, 183–221.

(142) Holm, R. H. *Chem. Rev.* **1987**, *87*, 1401–1449.

(143) Pietsch, M. A.; Hall, M. B. *Inorg. Chem.* **1996**, *35*, 1273–1278.

(144) Thomson, L. M.; Hall, M. B. *J. Am. Chem. Soc.* **2001**, *123*, 3995–4002.

(145) Hernandez-Marin, E.; Ziegler, T. *Inorg. Chem.* **2009**, *48*, 1323–1333.

(146) Klein, E. L.; Astashkin, A. V.; Raitsimring, A. M.; Enemark, J. H. *Coord. Chem. Rev.* **2013**, *257*, 110–118.

(147) Klein, E. L.; Raitsimring, A. M.; Astashkin, A. V.; Rajapakshe, A.; Johnson-

Winters, K.; Arnold, A. R.; Potapov, A.; Goldfarb, D.; Enemark, J. H. *Inorg. Chem.* **2012**, *51*, 1408–1418.

(148) Enemark, J. H.; Astashkin, A. V; Raitsimring, A. M. *Dalton Trans.* **2006**, 3501–3514.

(149) Astashkin, A. V; Hood, B. L.; Feng, C.; Hille, R.; Mendel, R. R.; Raitsimring, A. M.; Enemark, J. H. *Biochemistry* **2005**, *44*, 13274–13281.

(150) Pacheco, A.; Basu, P.; Borbat, P.; Raitsimring, A. M.; Enemark, J. H. *Inorg. Chem.* **1996**, *35*, 7001–7008.

(151) Lamy, M. T.; Gutteridge, S.; Bary, R. C. *Biochem. J.* **1980**, *185*, 397–403.

(152) Codd, R.; Astashkin, A. V.; Pacheco, A.; Raitsimring, A. M.; Enemark, J. H. *J. Biol. Inorg. Chem.* **2002**, *7*, 338–350.

(153) Reschke, S.; Niks, D.; Wilson, H.; Sigfridsson, K. G. V.; Haumann, M.; Rajagopalan, K. V.; Hille, R.; Leimkühler, S. *Biochemistry* **2013**, *52*, 8295–8303.

(154) Emesh, S.; Rapson, T. D.; Rajapakshe, A.; Kappler, U.; Bernhardt, P. V.; Tollin, G.; Enemark, J. H. *Biochemistry* **2009**, *48*, 2156–2163.

(155) Astashkin, A. V.; Johnson-Winters, K.; Klein, E. L.; Feng, C.; Wilson, H. L.; Rajagopalan, K. V.; Raitsimring, A. M.; Enemark, J. H. *J. Am. Chem. Soc.* **2008**, *130*, 8471–8480.

(156) Kappler, U.; Bailey, S.; Feng, C.; Honeychurch, M. J.; Hanson, G. R.; Bernhardt, P. V.; Tollin, G.; Enemark, J. H. *Biochemistry* **2006**, *45*, 9696–9705.

(157) Wilson, H. L.; Wilkinson, S. R.; Rajagopalan, K. V. *Biochemistry* **2006**, *45*, 2149–2160.

(158) Feng, C.; Wilson, H. L.; Tollin, G.; Astashkin, A. V.; Hazzard, J. T.; Rajagopalan, K. V.; Enemark, J. H. *Biochemistry* **2005**, *44*, 13734–13743.

(159) Feng, C.; Wilson, H. L.; Hurley, J. K.; Hazzard, J. T.; Tollin, G.; Rajagopalan, K. V; Enemark, J. H. **2003**, *42*, 12235–12242.

(160) Kisker, C.; Schindelin, H.; Pacheco, A.; Wehbi, W. A.; Garrett, R. M.; Rajagopalan, K. V.; Enemark, J. H.; Rees, D. C. *Cell* **1997**, *91*, 973–983.

(161) Groysman, S.; Holm, R. H. *Biochemistry* **2009**, *48*, 2310–2320.

(162) Mader, M. L.; Carducci, M. D.; Enemark, J. H. *Inorg. Chem.* **2000**, *39*, 525–531.

(163) Holm, R. H.; Solomon, E. I.; Majumdar, A.; Tenderholt, A. *Coord. Chem. Rev.* **2011**, *255*, 993–1015.

(164) Jalilehvand, F.; Lim, B. S.; Holm, R. H.; Hedman, B.; Hodgson, K. O. *Inorg. Chem.* **2003**, *42*, 5531–5536.

(165) Lim, B. S.; Willer, M. W.; Miao, M.; Holm, R. H. *J. Am. Chem. Soc.* **2001**, *123*, 8343–8349.

(166) George, G. N.; Pickering, I. J.; Kisker, C. *Inorg. Chem.* **1999**, *38*, 2539.

(167) Speier, G. *Inorganica Chim. Acta* **1979**, *32*, 139–141.

(168) Spence, J. T.; Minelli, M.; Kroneck, P. *J. Am. Chem. Soc.* **1980**, *102*, 4538–4541.

(169) Berg, J. M.; Holm, R. H. *J. Am. Chem. Soc.* **1985**, *107*, 925–932.

(170) Berg, J. M.; Holm, R. H. *J. Am. Chem. Soc.* **1984**, *106*, 3035–3036.

(171) Holm, R. H.; Berg, J. M. *Acc. Chem. Res.* **1986**, *19*, 363–370.

(172) Doonan, C. J.; Slizys, D. A.; Young, C. G. **1999**, *2*, 6430–6436.

(173) Schultz, B. E.; Gheller, S. F.; Muetterties, M. C.; Scott, M. J.; Holm, R. H. *J. Am. Chem. Soc.* **1993**, *115*, 2714–2722.

(174) Xiao, Z.; Young, C. G.; Enemark, J. H.; Wedd, A. G. *J. Am. Chem. Soc.* **1992**, *114*, 9194–9195.

(175) Cleland, Jr., W. E.; Barnhart, K. M.; Yamanouchi, K.; Collison, D.; Mabbs, F. E.; Ortega, R. B.; Enemark, J. H. *Inorg. Chem.* **1987**, *26*, 1017–1025.

(176) Roberts, S. A.; Young, C. G.; Kipke, C. A.; Cleland, Jr., W. E.; Yamanouchi, K.; Carducci, M. D.; Enemark, J. H. *Inorg. Chem.* **1990**, *29*, 3650–3656.

(177) Xiao, Z.; Bruck, M. A.; Doyle, C.; Enemark, J. H.; Grittini, C.; Gable, R. W.; Wedd, A. G.; Young, C. G. *Inorg. Chem.* **1995**, *34*, 5950–5962.

(178) Xiao, Z.; Bruck, M. A.; Enemark, J. H.; Young, C. G.; Wedd, A. G. *Inorg. Chem.* **1996**, *35*, 7508–7515.

(179) Wilson, G. L.; Kony, M.; Tiekink, E. R. T.; Pilbrow, J. R.; Spence, J. T.; Wedd, A. G. *J. Am. Chem. Soc.* **1988**, *110*, 6923–6925.

(180) Rappé, A. K.; Goddard III, W. A. *J. Am. Chem. Soc.* **1980**, *102*, 5114–5115.

(181) Smith, P. D.; Millar, A. J.; Young, C. G.; Ghosh, A.; Basu, P. *J. Am. Chem. Soc.* **2000**, *122*, 9298–9299.

(182) Nemykin, V. N.; Laskin, J.; Basu, P. *J. Am. Chem. Soc.* **2004**, *126*, 8604–8605.

(183) Nemykin, V. N.; Basu, P. *Dalton Trans.* **2004**, 1928–1933.

(184) Nemykin, V. N.; Basu, P. *Inorg. Chem.* **2005**, *44*, 7494–7502.

(185) Millar, A. J.; Doonan, C. J.; Smith, P. D.; Nemykin, V. N.; Basu, P.; Young, C. G. *Chem. Eur. J.* **2005**, *11*, 3255–3267.

(186) Kail, B. W.; Pérez, L. M.; Zarić, S. D.; Millar, A. J.; Young, C. G.; Hall, M. B.; Basu, P. *Chem. Eur. J.* **2006**, *12*, 7501–7509.

(187) Basu, P.; Kail, B. W.; Young, C. G. *Inorg. Chem.* **2010**, *49*, 4895–4900.

(188) Basu, P.; Raitsimring, A. M.; LaBarre, M. J.; Dhawan, I. K.; Weibrecht, J. L.; Enemark, J. H. *J. Am. Chem. Soc.* **1994**, *116*, 7166–7176.

(189) Basu, P.; Raitsimring, A. M.; Enemark, J. H.; Walker, F. A. *Inorg. Chem.* **1997**, *36*, 1088–1094.

(190) Das, S. K.; Chaudhury, P. K.; Biswas, D.; Sarkar, S. *J. Am. Chem. Soc.* **1994**, *116*, 9061–9070.

(191) Majumdar, A.; Sarkar, S. *Coord. Chem. Rev.* **2011**, *255*, 1039–1054.

(192) Pal, K.; Chaudhury, P. K.; Sarkar, S. *Chem. Asian J.* **2007**, *2*, 956–964.

(193) Mitra, J.; Sarkar, S. *Inorg. Chem.* **2013**, *52*, 3032–3042.

(194) Lyashenko, G.; Saischek, G.; Judmaier, M. E.; Volpe, M.; Baumgartner, J.; Belaj, F.; Jancik, V.; Herbst-Irmer, R.; Mösch-Zanetti, N. C. *Dalton Trans.* **2009**, 5655–5665.

(195) Mösch-Zanetti, N. C.; Wurm, D.; Volpe, M.; Lyashenko, G.; Harum, B.; Belaj, F.; Baumgartner, J. *Inorg. Chem.* **2010**, *49*, 8914–8921.

(196) Volpe, M.; Mösch-Zanetti, N. C. *Inorg. Chem.* **2012**, *51*, 1440–1449.

(197) Lyashenko, G.; Saischek, G.; Pal, A.; Herbst-Irmer, R.; Mösch-Zanetti, N. C. *Chem. Commun.* **2007**, 701–703.

(198) Heinze, K.; Fischer, A. *Eur. J. Inorg. Chem.* **2007**, 1020–1026.

(199) Heinze, K.; Marano, G.; Fischer, A. *J. Inorg. Biochem.* **2008**, *102*, 1199–1211.

(200) Heinze, K.; Fischer, A. *Eur. J. Inorg. Chem.* **2010**, 1939–1947.

(201) Hüttinger, K.; Förster, C.; Bund, T.; Hinderberger, D.; Heinze, K. *Inorg. Chem.* **2012**, *51*, 4180–4192.

(202) Leppin, J.; Förster, C.; Heinze, K. *Inorg. Chem.* **2014**, *53*, 12416–12427.

(203) Ducrot, A. B.; Coulson, B. A.; Perutz, R. N.; Duhme-Klair, A.-K. *Inorg. Chem.* **2016**, *55*, 12583–12594.

(204) Atkins, P. W. *Physikalische Chemie*, 3rd ed.; Wiley-VCH: Weinheim, 2001.

(205) Meija, J.; Coplen, T. B.; Berglund, M.; Brand, W. A.; De Bièvre, P.; Gröning, M.; Holden, N. E.; Irrgeher, J.; Loss, R. D.; Walczyk, T.; Prohaska, T. *Pure Appl. Chem.* **2016**, *88*, 293–306.

(206) Prins, R. *Mol. Phys.* **1970**, *19*, 603–620.

(207) Proctor, W. G.; Yu, F. C. *Phys. Rev.* **1951**, *81*, 20–30.

(208) Hüttinger, K.; Förster, C.; Heinze, K. *Chem. Commun.* **2014**, *50*, 4285–4288.

(209) Hille, R. *Dalton Trans.* **2013**, *42*, 3029–3042.

(210) Hille, R.; Nishino, T.; Bittner, F. *Coord. Chem. Rev.* **2011**, *255*, 1179–1205.

(211) Schulzke, C. *Eur. J. Inorg. Chem.* **2011**, 1189–1199.

(212) Enemark, J. H.; Cooney, J. J. A.; Wang, J.-J.; Holm, R. H. *Chem. Rev.* **2004**, *104*, 1175–1200.

(213) Heinze, K. *Coord. Chem. Rev.* **2015**, *300*, 121–141.

(214) Wallace, D.; Gibson, L. T.; Reglinski, J.; Spicer, M. D. *Inorg. Chem.* **2007**, *46*, 3804–3806.

(215) Das, S. K.; Chaudhury, P. K.; Biswas, D.; Sarkar, S. *J. Am. Chem. Soc.* **1994**, *116*,

9061–9070.

(216) Tolman, C. A. *Chem. Rev.* **1977**, *77*, 313–348.

(217) Cahn, R. S.; Ingold, C.; Prelog, V. *Angew. Chemie Int. Ed.* **1966**, *5*, 385–415.

(218) Koch, W.; Holthausen, M. C. *A Chemist's Guide to Density Functional Theory*; Wiley-VCH, 2001.

(219) Siebler, D.; Förster, C.; Gasi, T.; Heinze, K. *Chem. Commun.* **2010**, *46*, 4490–4492.

(220) Siebler, D.; Linseis, M.; Gasi, T.; Carrella, L. M.; Winter, R. F.; Förster, C.; Heinze, K. *Chem. Eur. J.* **2011**, *17*, 4540–4551.

(221) Leppin, J.; Förster, C.; Heinze, K. *Inorg. Chem.* **2014**, *53*, 1039–1047.

(222) Nielson, R. M.; McManis, G. E.; Safford, L. K.; Weaver, M. J. *J. Phys. Chem.* **1989**, *93*, 2152–2157.

(223) Kienz, T.; Heinze, K. *Organometallics* **2014**, *33*, 4803–4812.

(224) Buchner, W.; Ries, W.; Malisch, W. *Magn. Reson. Chem.* **1990**, *28*, 515–518.

(225) Neidlinger, A.; Kienz, T.; Heinze, K. *Organometallics* **2015**, *34*, 5310–5320.

(226) Mayor-López, M. J.; Lüthi, H. P.; Koch, H.; Morgantini, P. Y.; Weber, J. *J. Chem. Phys.* **2000**, *113*, 8009–8014.

(227) Hesse, M.; Meier, H.; Zeeh, B. *Spektroskopische Methoden in der organischen Chemie*, 7th ed.; Thieme, 2005.

(228) Gutteridge, S.; Lamy, M. T.; Bray, R. C. *Biochem. J.* **1980**, 285–288.

(229) Neidlinger, A.; Förster, C.; Heinze, K. *Eur. J. Inorg. Chem.* **2016**, 1274–1286.

(230) Heinze, K.; Schlenker, M. *Eur. J. Inorg. Chem.* **2004**, 2974–2988.

(231) Rufanov, K. A.; Zarubin, D. N.; Ustynyuk, N. A.; Gourevitch, D. N.; Sundermeyer, J.; Churakov, A. V.; Howard, J. A. K. *Polyhedron* **2001**, *20*, 379–385.

(232) Stoll, S.; Schweiger, A. *J. Magn. Reson.* **2006**, *178*, 42–55.

(233) *SMART Data Collection and SAINT-Plus Data Processing Software for the SMART System (various versions)*; Bruker Analytical X-Ray Instruments, Inc.:

Madison, WI, 2000.

(234) Blessing, R. H. *Acta Crystallogr.* **1995**, *A51*, 33–38.

(235) Sheldrick, G. M. *SHELXTL, version 5*; Bruker AXS: Madison, WI, 1998.

(236) Sheldrick, G. M. *SHELXTL-97*; University of Göttingen: Germany, 1997.

(237) Frisch, M. J.; Trucks, G. W.; Schlegel, H. B.; Scuseria, G. E.; Robb, M. A.; Cheeseman, J. R.; Scalmani, G.; Barone, V.; Mennucci, B.; Petersson, G. A.; Nakatsuji, H.; Caricato, M.; Li, X.; Hratchian, H. P.; Izmaylov, A. F.; Bloino, J.; Zheng, G.; Sonnenberg, J. L.; Hada, M.; Ehara, M.; Toyota, K.; Fukuda, R.; Hasegawa, J.; Ishida, M.; Nakajima, T.; Honda, Y.; Kitao, O.; Nakai, H.; Vreven, T.; Montgomery, Jr., J. A.; Peralta, J. E.; Ogliaro, F.; Bearpark, M.; Heyd, J. J.; Brothers, E.; Kudin, K. N.; Staroverov, V. N.; Kobayashi, R.; Normand, J.; Raghavachari, K.; Rendell, A.; Burant, J. C.; Iyengar, S. S.; Tomasi, J.; Cossi, M.; Rega, N.; Millam, J. M.; Klene, M.; Knox, J. E.; Cross, J. B.; Bakken, V.; Adamo, C.; Jaramillo, J.; Gomperts, R.; Stratmann, R. E.; Yazyev, O.; Austin, A. J.; Cammi, R.; Pomelli, C.; Ochterski, J. W.; Martin, R. L.; Morokuma, K.; Zakrzewski, V. G.; Voth, G. A.; Salvador, P.; Dannenberg, J. J.; Dapprich, S.; Daniels, A. D.; Farkas, O.; Foresman, J. B.; Ortiz, J. V.; Cioslowski, J.; Fox, D. J. *Gaussian 09, Revision A.02*; Gaussian, Inc.: Wallingford, CT, 2009.

(238) Becke, A. D. *J. Chem. Phys.* **1993**, *98*, 5648–5652.

(239) Dykstra, C. E. *Chem. Phys. Lett.* **1977**, 466–469.

(240) Hay, P. J.; Wadt, W. R. *J. Chem. Phys.* **1985**, *82*, 299–310.

(241) Hay, P. J.; Wadt, W. R. **1985**, *82*, 270–283.

(242) Wadt, W. R.; Hay, P. J. *J. Chem. Phys.* **1985**, *82*, 284–298.

(243) Huzinaga, S.; Andzelm, J.; Klobukowski, M.; Radzio-Andzelm, E.; Sakai, Y.; Tatewaki, H. *Gaussian Basis Sets for Molecular Calculations*; Elsevier: Amsterdam, 1984.

(244) Grimme, S.; Antony, J.; Ehrlich, S.; Krieg, H. *J. Chem. Phys.* **2010**, *132*, 154104–154119.

(245) Neese, F. *WIREs Comput. Mol. Sci.* **2012**, *2*, 73–78.

(246) Schäfer, A.; Horn, H.; Ahlrichs, R. *J. Chem. Phys.* **1992**, *97*, 2571.

(247) Schäfer, A.; Huber, C.; Ahlrichs, R. *J. Chem. Phys.* **1994**, *100*, 5829.

(248) Neese, F.; Wennmohs, F.; Hansen, A.; Becker, U. *Chem. Phys.* **2009**, *356*, 98–109.

(249) Izsák, R.; Neese, F. *J. Chem. Phys.* **2011**, *135*, 144105.

(250) van Lethe, E.; Baerends, E. J.; Snijders, J. G. *J. Chem. Phys.* **1993**, *99*, 4597.

(251) van Wüllen, C. *J. Chem. Phys.* **1998**, *109*, 392.

(252) Kollmar, C. *J. Chem. Phys.* **1996**, *105*, 8204.

(253) Sinnecker, S.; Rajendran, A.; Klamt, A.; Diedenhofen, M.; Neese, F. *J. Phys. Chem. A* **2006**, *110*, 2235–2245.

7 Supporting information

In the following, the supporting information (SI) of all publications and the not yet published manuscript is presented. The Cartesian coordinates from the DFT calculations are omitted in the published material. These can be found in the online version of the respective journals.

7.1 Solution conformation and self-assembly of ferrocenyl(thio)ureas

Kristina Hanauer, Minh Thu Pham, Christoph Förster and Katja Heinze

Supporting Information

Structures of 1–7 in the solid state. 1 crystallized in the centrosymmetric space group *C*2/*c* with two molecules **A** and **B** in the asymmetric unit. **A** and **B** form waved tapes along the *b* direction (Scheme 1, Figure 1, Supporting Information). The sum of angles N1···O1···N2 (α), N1···O1=C5 (β) and N2···O1=C5 (γ) at the donor and acceptor sites of molecules **A** and **B** is a measure of the waving distortion of the tapes (Figure 1d, Table 1). An angular sum of 360.0° arises for N1**B**···O1**A**···N2**B**, N1**B**···O1**A**=C5**A** and N4**B**···O1**A**=C5**A** while a sum of 332.4° is found for N1**A**···O2**B**···N2**A**, N1**A**···O2**B**=C5**B** and N2**A**···O2**B**=C5**B**, respectively, indicating a stronger bending of the latter hydrogen bonded pair. The orientation of hydrogen bonds within a tape is defined by the NH···O=C vector. These tapes form layers with parallel orientation of the NH···O=C vectors, while the layers pack in a three-dimensional fashion with alternating NH···O=C vectors. The aryl ferrocenyl ureas **2** and **3** crystallize in the same monoclinic space group $P2_1/c$ forming tapes along the *c* direction with *anti* orientation of the Fc moieties (Figure 1a). These tapes form layers with parallel orientation of the NH···O=C vectors, while the packing of layers is of alternating direction of NH···O=C vectors. The tapes of **3** are slightly waved with a sum of angles of 351.4° (N1···O1···N2, N1···O1=C5 and N2···O1=C5), while **2** assembles in almost planar tapes (angular sum 359.4°). Interestingly, the α-naphthyl substituents of a tape of **3** show weak π-π interactions with α-naphthyl substituents of an adjacent tape with a distance of 5.0135(3) Å of the centroids (C10–C15, Scheme 3, Supporting Information) and a ring-slippage of 1.554 Å. On the other hand, the phenyl substituents in **2** do not realize any π-stacking.

N-Methyl derivative **4** crystallizes as racemic twin in the space group $P2_1$. The asymmetric unit contains two molecules **A** and **B** linked by hydrogen bonds to give waved tapes (Scheme 1, Figure 1). These tapes pack into layers with the same direction of the NH···O=C hydrogen bonds (Figure 1, Supporting Information). The 2_1 screw axis orients adjacent layers of tapes in an orthogonal manner. The angular sums $\alpha + \beta + \gamma$ around O1**B** and O1**A** amount to 358.8° and 354.5°, respectively. The large ferrocenyl moieties within a tape orient in an *anti* fashion (Figure 1a). In addition to the waving of the tapes, a significant zigzag chain orientation with unsymmetrical bifurcated $(NH)_2$···O=C hydrogen bonds is observed for **1**, **3** and **4** as manifested in the pair wise difference Δd_{NO} of N1/N2···O distances (Scheme 1, Table 1).

N-Ethyl-*N*'-ferrocenyl urea **5** crystallizes in the orthorhombic space group *Pbca* with one molecule in the asymmetric unit. The *trans-trans* conformers of **5** form planar tapes along the *b* direction. These tapes align in an antiparallel manner to give layers. The layers pack in a parallel fashion in the *bc* plane. In contrast to the methyl derivative **4**, the Fc substituents of **5** arrange in a *syn* orientation within a tape (Figure 1b). This is probably a result of van der Waals interactions of the ethyl groups between neighboring tapes, analogous to the packing of the hexyl derivative $FcNHC(O)NH(CH_2)_5CH_3$.[1]

Hence, the substituent R influences the *syn*/*anti* orientation within a tape and the packing of the tapes, yet the formation of tapes by linking *trans-trans* isomers via bifurcated $(NH)_2$···OC hydrogen bonds is conserved in all cases R (R = Fc, Ph, Nap, Me, Et).

[1] G. Cooke, H. A. de Cremiers, F. M. Duclairoir, J. Leonardi, G. Rosair, V. M. Rotello, *Tetrahedron* **2003**, *59*, 3341–3347.

Table S1. Selected distances (Å) and angles (°) of **1**–**7**.

	N···X[a]	N–H···X	$\alpha + \beta + \gamma$[b]
1			
N1**A**H···O1**B**	2.823(4)	152.2	
N2**A**H···O1**B**	2.896(4)	143.6	332.4
Δd_{NO}	0.073(4)		
N1**B**H···O1**A**	2.809(4)	148.4	
N2**B**H···O1**A**	2.834(3)	149.3	360.0
Δd_{NO}	0.025(4)		
2			
N1H···O1	2.862(2)	146.1	
N2H···O1	2.807(2)	153.9	359.4
Δd_{NO}	0.055(2)		
3			
N1H···O2	2.811(2)	144.8	
N2H···O2	2.971(2)	149.4	351.4
Δd_{NO}	0.160(2)		
4			
N1**A**H···O1**B**	3.199(12)	138.6	
N2**A**H···O1**B**	2.920(11)	147.5	358.8
Δd_{NO}	0.279(12)		
N1**B**H···O1**A**	3.034(11)	154.0	
N2**B**H···O1**A**	2.943(13)	148.7	354.5
Δd_{NO}	0.091(12)		
5			
N1H···O2	2.926(2)	150.3	
N2H···O2	2.881(2)	154.0	360.0
Δd_{NO}	0.045(2)		
6			
N1H···S1	3.364(3)	157.0	–
N2H···Fe1	3.601(3)	142.1	
7(·2 CH_2Cl_2)			
N1H···S1	3.413(1)	166.6	–

[a] X = O, S. [b] Sum of angles α, β and γ as defined in Figure 1d.

Empirical formula	$C_{21}H_{20}Fe_2N_2O$	
Formula weight	428.09	
Temperature	193(2) K	
Wavelength	0.71073 Å	
Crystal system	Monoclinic	
Space group	*C*2/*c*	
Unit cell dimensions	*a* = 18.625(4) Å	α = 90°
	b = 17.567(4) Å	β = 109.22(3)°
	c = 23.746(5) Å	γ = 90°
Volume	7337(3) Å^3	
Z	16	
Density (calculated)	1.550 Mg/m^3	
Absorption coefficient	1.593 mm^{-1}	
F(000)	3520	
Crystal size	0.200 x 0.110 x 0.050 mm^3	
Theta range for data collection	2.428 to 28.302°	
Index ranges	$-20 \le h \le 24$, $-20 \le k \le 23$, $-31 \le l \le 31$	
Reflections collected	24698	
Independent reflections	9032 [*R*(int) = 0.0590]	
Completeness to theta = 25.242°	99.3 %	
Absorption correction	Semi-empirical from equivalents	
Max. and min. transmission	1.03079 and 0.96501	
Refinement method	Full-matrix least-squares on F^2	
Data / restraints / parameters	9032 / 0 / 469	
Goodness-of-fit on F^2	1.005	
Final *R* indices [$I > 2\sigma(I)$]	R1 = 0.0451, wR2 = 0.1003	
R indices (all data)	R1 = 0.0875, wR2 = 0.1186	
Extinction coefficient	n/a	
Largest diff. peak and hole	0.456 and -0.493 e Å^{-3}	

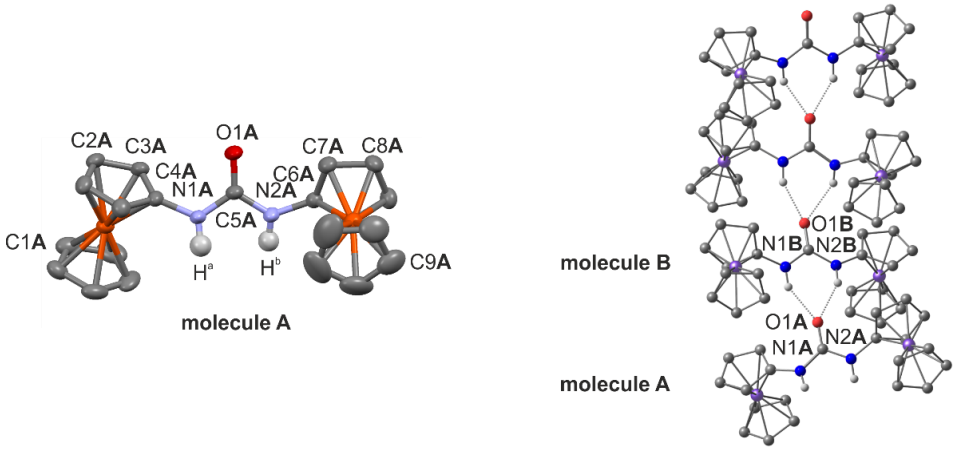

Figure S1. Selected XRD data of **1** with relevant atom numbering (CH hydrogen atoms omitted, thermal ellipsoids probability at 50 %).

Empirical formula	$C_{17}H_{16}FeN_2O$	
Formula weight	320.17	
Temperature	173(2) K	
Wavelength	0.71073 Å	
Crystal system	Monoclinic	
Space group	$P2_1/c$	
Unit cell dimensions	a = 7.3936(7) Å	α = 90°
	b = 23.584(2) Å	β = 107.956(3)°
	c = 9.1167(9) Å	γ = 90°
Volume	1512.3(3) Å^3	
Z	4	
Density (calculated)	1.406 Mg/m^3	
Absorption coefficient	0.996 mm^{-1}	
F(000)	664	
Crystal size	0.74 x 0.27 x 0.11 mm^3	
Theta range for data collection	2.50 to 28.02°	
Index ranges	$-9 \le h \le 9$, $-31 \le k \le 22$, $-12 \le l \le 11$	
Reflections collected	15807	
Independent reflections	3629 [R(int) = 0.0848]	
Completeness to theta = 28.02°	99.5 %	
Absorption correction	Semi-empirical from equivalents	
Max. and min. transmission	0.8983 and 0.5259	
Refinement method	Full-matrix least-squares on F^2	
Data / restraints / parameters	3629 / 0 / 190	
Goodness-of-fit on F^2	0.906	
Final R indices [I > 2sigma(I)]	R1 = 0.0340, wR2 = 0.0670	
R indices (all data)	R1 = 0.0572, wR2 = 0.0722	
Largest diff. peak and hole	0.392 and -0.252 e Å^{-3}	

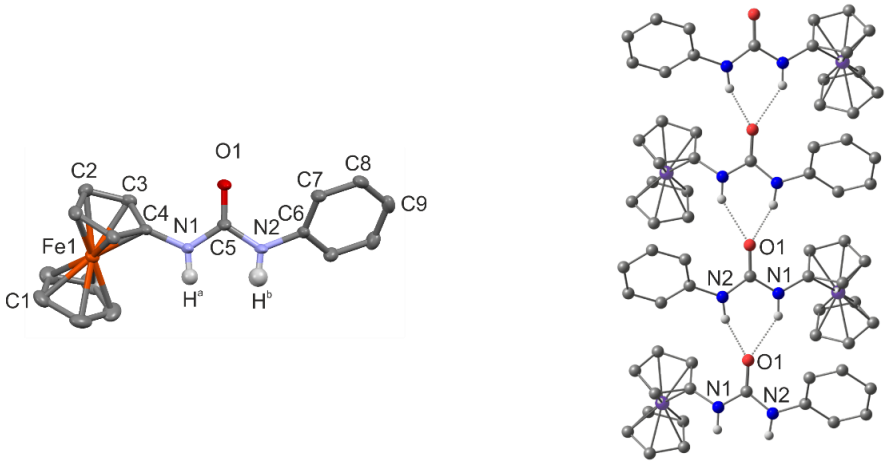

Figure S2. Selected XRD data of **2** with relevant atom numbering (CH hydrogen atoms omitted, thermal ellipsoids probability at 50 %).

Empirical formula	$C_{21}H_{18}FeN_2O$	
Formula weight	370.22	
Temperature	173(2) K	
Wavelength	0.71073 Å	
Crystal system	Monoclinic	
Space group	$P2_1/c$	
Unit cell dimensions	a = 7.5607(4) Å	α = 90°
	b = 24.0673(11) Å	β = 96.4578(12)°
	c = 9.1554(4) Å	γ = 90°
Volume	1655.40(14) Å^3	
Z	4	
Density (calculated)	1.485 Mg/m^3	
Absorption coefficient	0.922 mm^{-1}	
F(000)	768	
Crystal size	0.570 x 0.080 x 0.020 mm^3	
Theta range for data collection	1.692 to 27.884°	
Index ranges	$-9 \le h \le 9$, $-31 \le k \le 31$, $-12 \le l \le 12$	
Reflections collected	23675	
Independent reflections	3934 [R(int) = 0.0667]	
Completeness to theta = 25.242°	100.0 %	
Absorption correction	Semi-empirical from equivalents	
Max. and min. transmission	1.06709 and 0.94106	
Refinement method	Full-matrix least-squares on F^2	
Data / restraints / parameters	3934 / 0 / 226	
Goodness-of-fit on F^2	0.896	
Final R indices [I > 2sigma(I)]	R1 = 0.0324, wR2 = 0.0633	
R indices (all data)	R1 = 0.0571, wR2 = 0.0677	
Extinction coefficient	n/a	
Largest diff. peak and hole	0.310 and -0.300 e Å^{-3}	

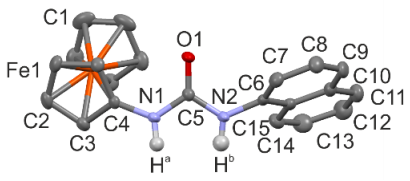

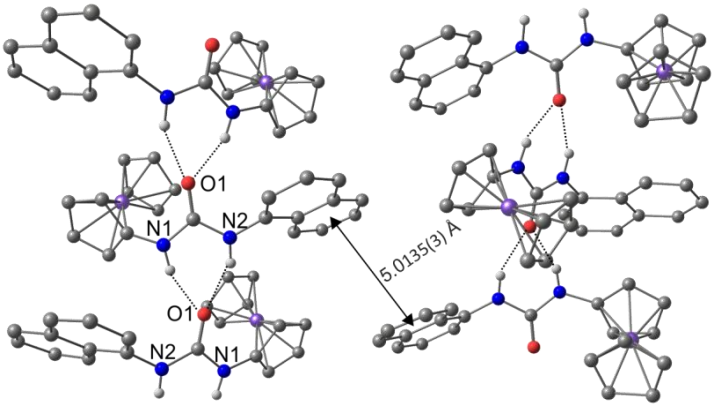

Figure S3. Selected XRD data of **3** with relevant atom numbering (CH hydrogen atoms omitted, thermal ellipsoids probability at 50 %). The π-π interaction between naphthyl residues of adjacent molecules is indicated.

Empirical formula	$C_{12}H_{14}FeN_2O$	
Formula weight	258.10	
Temperature	193(2) K	
Wavelength	0.71073 Å	
Crystal system	Monoclinic	
Space group	$P2_1$	
Unit cell dimensions	a = 5.8907(12) Å	α = 90°
	b = 7.4266(15) Å	β = 90.49(3)°
	c = 24.379(5) Å	γ = 90°
Volume	1066.5(4) Å^3	
Z	4	
Density (calculated)	1.607 Mg/m^3	
Absorption coefficient	1.391 mm^{-1}	
F(000)	536	
Crystal size	0.51 x 0.34 x 0.06 mm^3	
Theta range for data collection	2.87 to 28.17°.	
Index ranges	$-7 \le h \le 7$, $-9 \le k \le 8$, $-32 \le l \le 26$	
Reflections collected	6930	
Independent reflections	4332 [R(int) = 0.0312]	
Completeness to theta = 28.17°	98.8 %	
Absorption correction	Semi-empirical from equivalents	
Max. and min. transmission	0.9212 and 0.5373	
Refinement method	Full-matrix least-squares on F^2	
Data / restraints / parameters	4332 / 1267 / 578	
Goodness-of-fit on F^2	1.027	
Final R indices [I > 2sigma(I)]	R1 = 0.0284, wR2 = 0.0715	
R indices (all data)	R1 = 0.0394, wR2 = 0.0781	
Absolute structure parameter	0.47(4)	
Largest diff. peak and hole	0.289 and -0.273 e Å^{-3}	

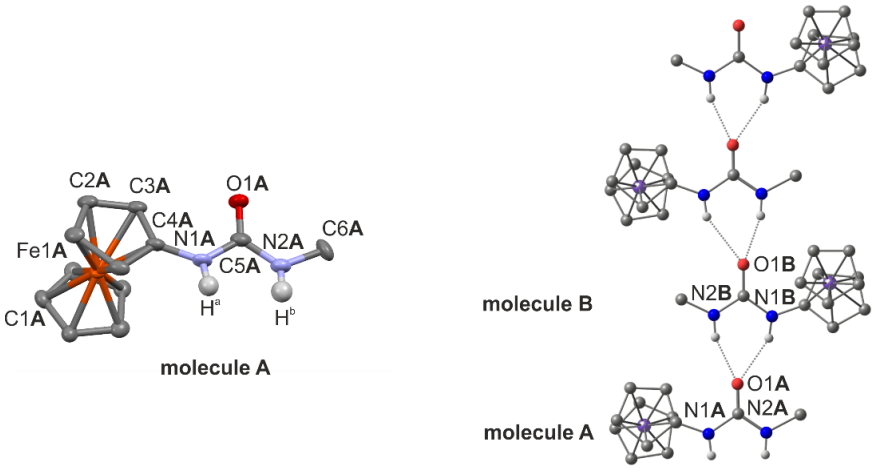

Figure S4. Selected XRD data of **4** with relevant atom numbering (CH hydrogen atoms omitted, thermal ellipsoids probability at 50 %).

Empirical formula	$C_{13}H_{16}FeN_2O$	
Formula weight	272.13	
Temperature	173(2) K	
Wavelength	0.71073 Å	
Crystal system	Orthorhombic	
Space group	*Pbca*	
Unit cell dimensions	a = 8.6271(5) Å	α = 90°
	b = 9.2703(5) Å	β = 90°
	c = 30.7949(17) Å	γ = 90°
Volume	2462.8(2) Å^3	
Z	8	
Density (calculated)	1.468 Mg/m^3	
Absorption coefficient	1.209 mm^{-1}	
F(000)	1136	
Crystal size	0.340 x 0.330 x 0.050 mm^3	
Theta range for data collection	2.646 to 27.995°.	
Index ranges	$-7 \le h \le 11$, $-12 \le k \le 12$, $-40 \le l \le 40$	
Reflections collected	15773	
Independent reflections	2974 [R(int) = 0.0531]	
Completeness to theta = 25.242°	99.9 %	
Absorption correction	Semi-empirical from equivalents	
Max. and min. transmission	1.10744 and 0.93889	
Refinement method	Full-matrix least-squares on F^2	
Data / restraints / parameters	2974 / 0 / 154	
Goodness-of-fit on F^2	0.913	
Final R indices [I > 2sigma(I)]	R1 = 0.0341, wR2 = 0.0759	
R indices (all data)	R1 = 0.0646, wR2 = 0.0861	
Extinction coefficient	n/a	
Largest diff. peak and hole	0.537 and -0.320 e Å^{-3}	

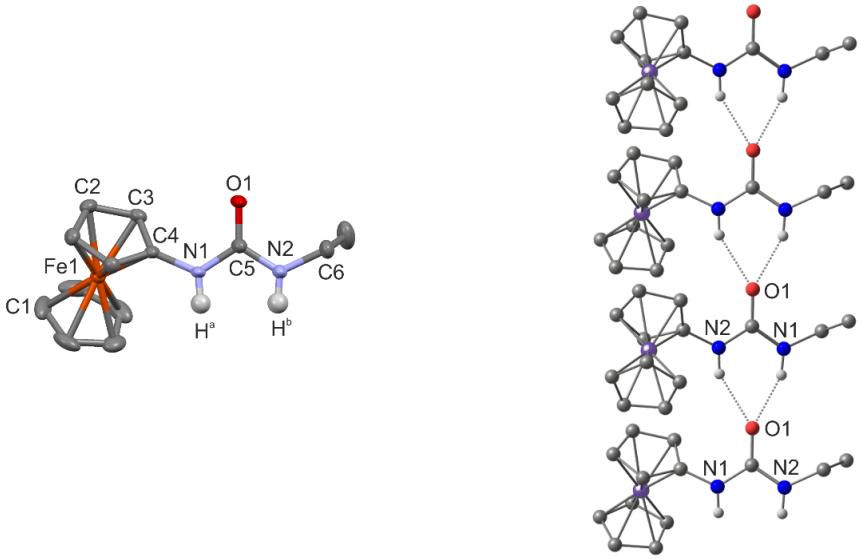

Figure S5. Selected XRD data of **5** with relevant atom numbering (CH hydrogen atoms omitted, thermal ellipsoids probability at 50 %).

Empirical formula	$C_{21}H_{20}Fe_2N_2S$	
Formula weight	444.15	
Temperature	298(2) K	
Wavelength	0.71073 Å	
Crystal system	Triclinic	
Space group	$P\bar{1}$	
Unit cell dimensions	a = 7.8369(7) Å	α = 97.676(2)°
	b = 9.4551(8) Å	β = 103.589(2)°
	c = 13.3018(12) Å	γ = 100.4268(19)°
Volume	926.11(14) Å^3	
Z	2	
Density (calculated)	1.593 Mg/m^3	
Absorption coefficient	1.686 mm^{-1}	
F(000)	456	
Crystal size	0.380 x 0.090 x 0.075 mm^3	
Theta range for data collection	2.228 to 27.982°	
Index ranges	$-10 \le h \le 10$, $-12 \le k \le 12$, $-16 \le l \le 17$	
Reflections collected	11142	
Independent reflections	4455 [R(int) = 0.0426]	
Completeness to theta = 25.242°	99.9 %	
Absorption correction	Semi-empirical from equivalents	
Max. and min. transmission	0.7456 and 0.6195	
Refinement method	Full-matrix least-squares on F^2	
Data / restraints / parameters	4455 / 0 / 237	
Goodness-of-fit on F^2	0.986	
Final R indices [I > 2sigma(I)]	R1 = 0.0447, wR2 = 0.1017	
R indices (all data)	R1 = 0.0710, wR2 = 0.1152	
Extinction coefficient	n/a	
Largest diff. peak and hole	0.616 and -0.284 e Å^{-3}	

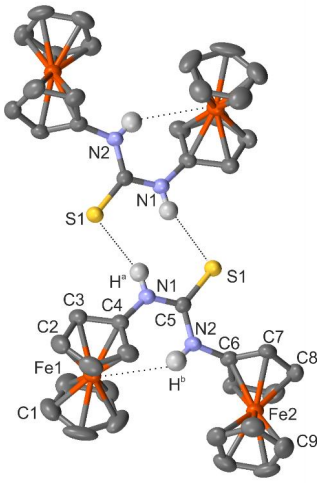

Figure S6. Selected XRD data of **6**·2 CH_2Cl_2 with relevant atom numbering (CH hydrogen atoms and cocrystallized CH_2Cl_2 omitted, thermal ellipsoids probability at 50 %).

Empirical formula	$C_{27}H_{24}Cl_4FeN_2S$	
Formula weight	606.19	
Temperature	173(2) K	
Wavelength	0.71073 Å	
Crystal system	Triclinic	
Space group	$P\bar{1}$	
Unit cell dimensions	a = 9.6008(3) Å	α = 77.5130(10)°
	b = 11.4322(3) Å	β = 82.2810(10)°
	c = 13.4550(4) Å	γ = 69.6280(10)°
Volume	1348.86(7) Å^3	
Z	2	
Density (calculated)	1.493 Mg/m^3	
Absorption coefficient	1.053 mm^{-1}	
F(000)	620	
Crystal size	0.35 x 0.33 x 0.12 mm^3	
Theta range for data collection	2.27 to 28.00°.	
Index ranges	$-12 \le h \le 12$, $-14 \le k \le 15$, $-17 \le l \le 17$	
Reflections collected	40479	
Independent reflections	6439 [R(int) = 0.0459]	
Completeness to theta = 28.00°	98.9 %	
Absorption correction	Semi-empirical from equivalents	
Max. and min. transmission	0.8841 and 0.7096	
Refinement method	Full-matrix least-squares on F^2	
Data / restraints / parameters	6439 / 12 / 372	
Goodness-of-fit on F^2	1.010	
Final R indices [I > 2sigma(I)]	R1 = 0.0302, wR2 = 0.0767	
R indices (all data)	R1 = 0.0425, wR2 = 0.0802	
Largest diff. peak and hole	0.349 and -0.288 e Å^{-3}	

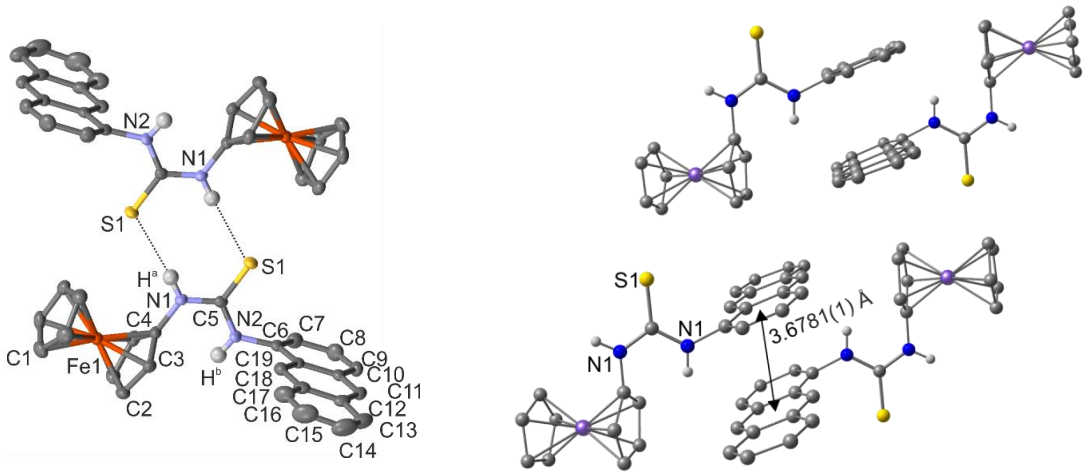

Figure S7. Selected XRD data of **7** with relevant atom numbering (CH hydrogen atoms omitted, thermal ellipsoids probability at 50 %). The π-π interaction between anthracenyl residues of adjacent molecules is indicated.

Empirical formula	$C_{21}H_{20}F_{12}Fe_2N_2OSb_2$	
Formula weight	899.59	
Temperature	173(2) K	
Wavelength	0.71073 Å	
Crystal system	Monoclinic	
Space group	$P2_1/n$	
Unit cell dimensions	a = 14.4936(14) Å	α = 90°
	b = 10.7645(10) Å	β = 98.714(2)°
	c = 17.6222(17) Å	γ = 90°
Volume	2717.6(4) Å^3	
Z	4	
Density (calculated)	2.199 Mg/m^3	
Absorption coefficient	3.115 mm^{-1}	
F(000)	1720	
Crystal size	0.530 x 0.150 x 0.040 mm^3	
Theta range for data collection	2.338 to 27.968°	
Index ranges	$-19 \le h \le 15$, $-14 \le k \le 14$, $-23 \le l \le 23$	
Reflections collected	28006	
Independent reflections	6530 [R(int) = 0.0487]	
Completeness to theta = 25.242°	99.9 %	
Absorption correction	Semi-empirical from equivalents	
Max. and min. transmission	1.24957 and 0.77106	
Refinement method	Full-matrix least-squares on F^2	
Data / restraints / parameters	6530 / 182 / 407	
Goodness-of-fit on F^2	0.964	
Final R indices [I > 2sigma(I)]	R1 = 0.0310, wR2 = 0.0684	
R indices (all data)	R1 = 0.0498, wR2 = 0.0740	
Extinction coefficient	n/a	
Largest diff. peak and hole	1.256 and -0.781 e Å^{-3}	

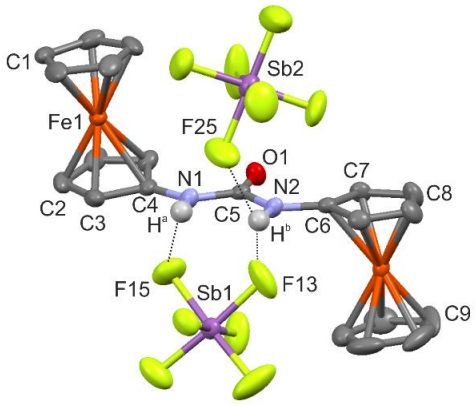

Figure S8. Selected XRD data of **1[SbF$_6$]$_2$** with relevant atom numbering (CH hydrogen atoms omitted, thermal ellipsoids probability at 50 %).

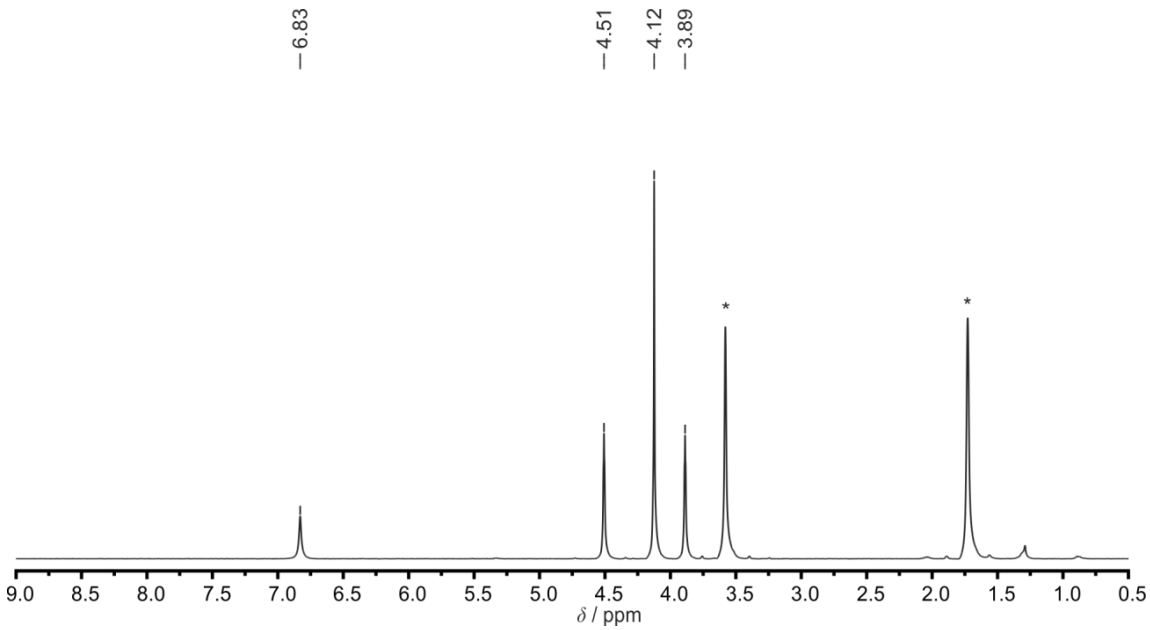

Figure S9. ^{1}H NMR spectrum of **1** in d_8-THF. Solvent signals are indicated by *.

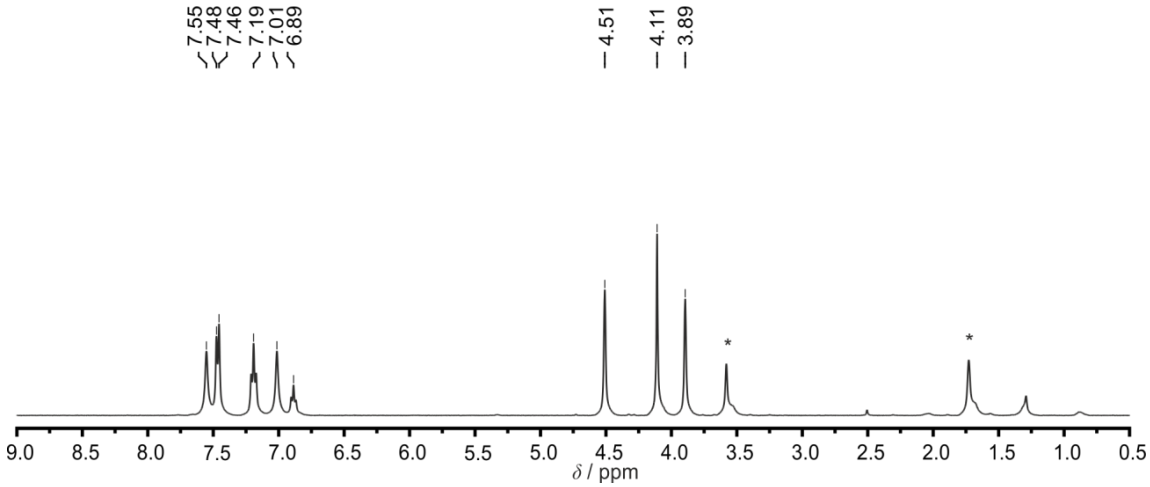

Figure S10. ^{1}H NMR spectrum of **2** in d_8-THF. Solvent signals are indicated by *.

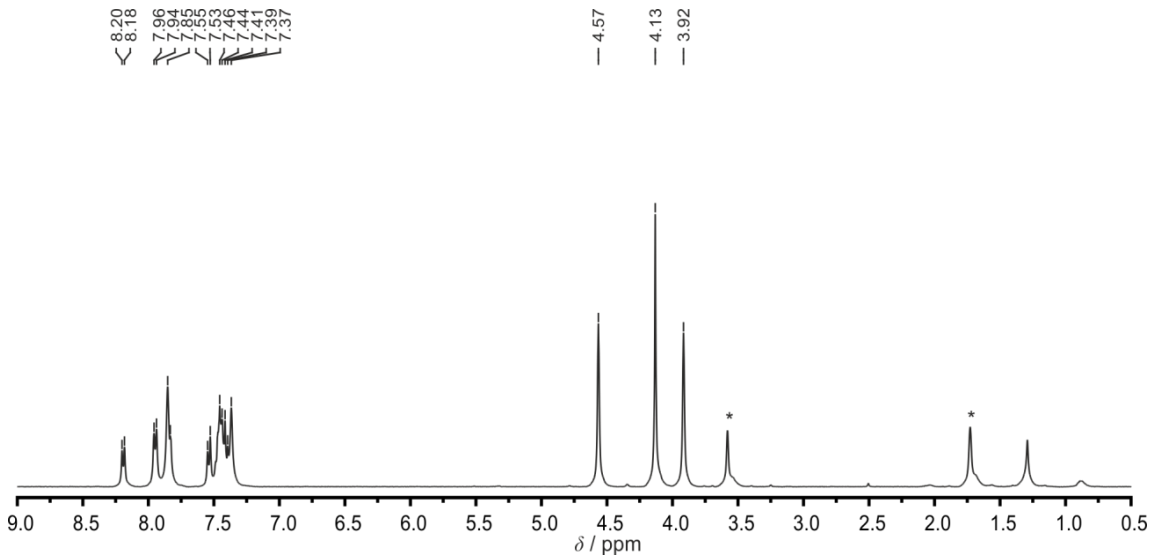

Figure S11. ^{1}H NMR spectrum of **3** in d_8-THF. Solvent signals are indicated by *.

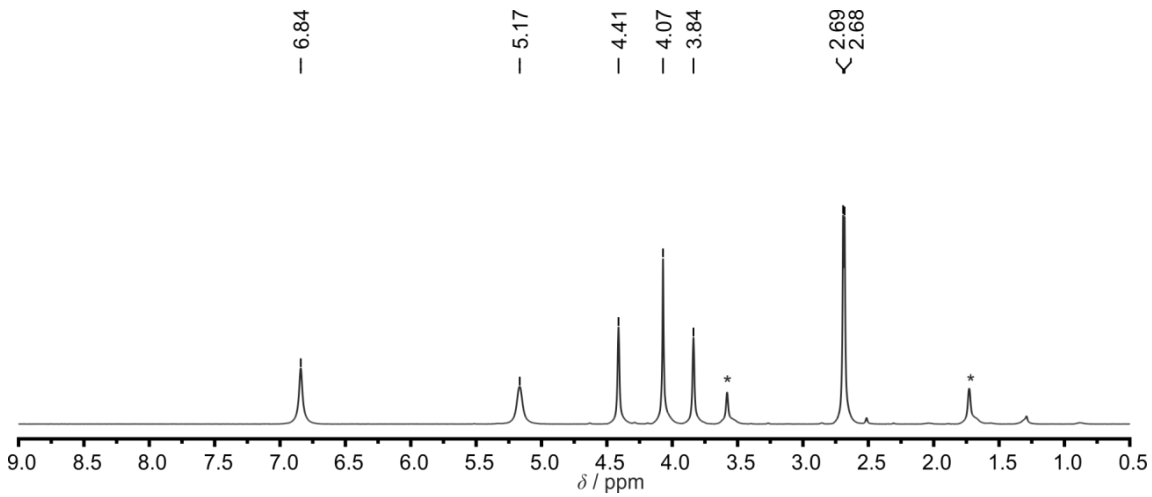

Figure S12. ^{1}H NMR spectrum of **4** in d_8-THF. Solvent signals are indicated by *.

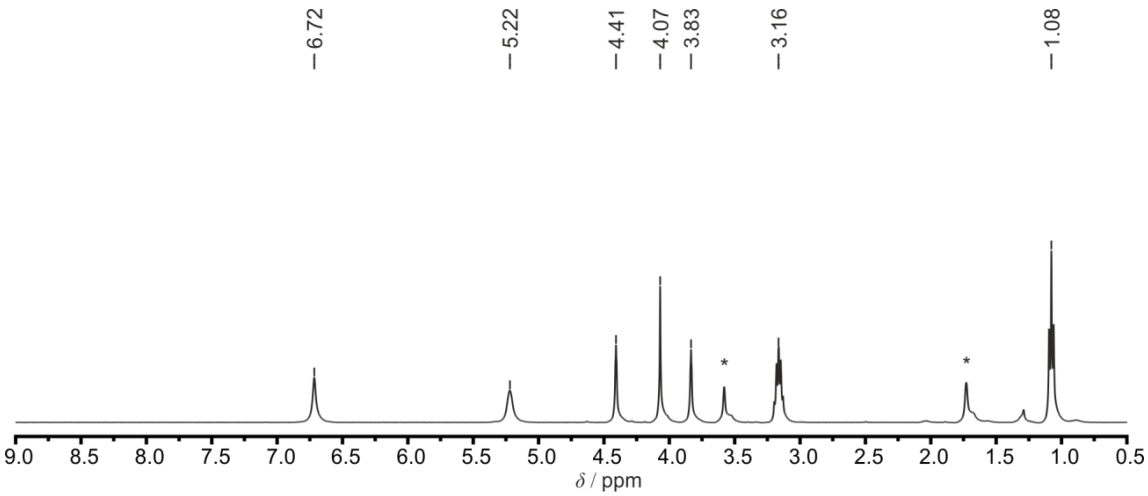

Figure S13. ^{1}H NMR spectrum of **5** in d_8-THF. Solvent signals are indicated by *.

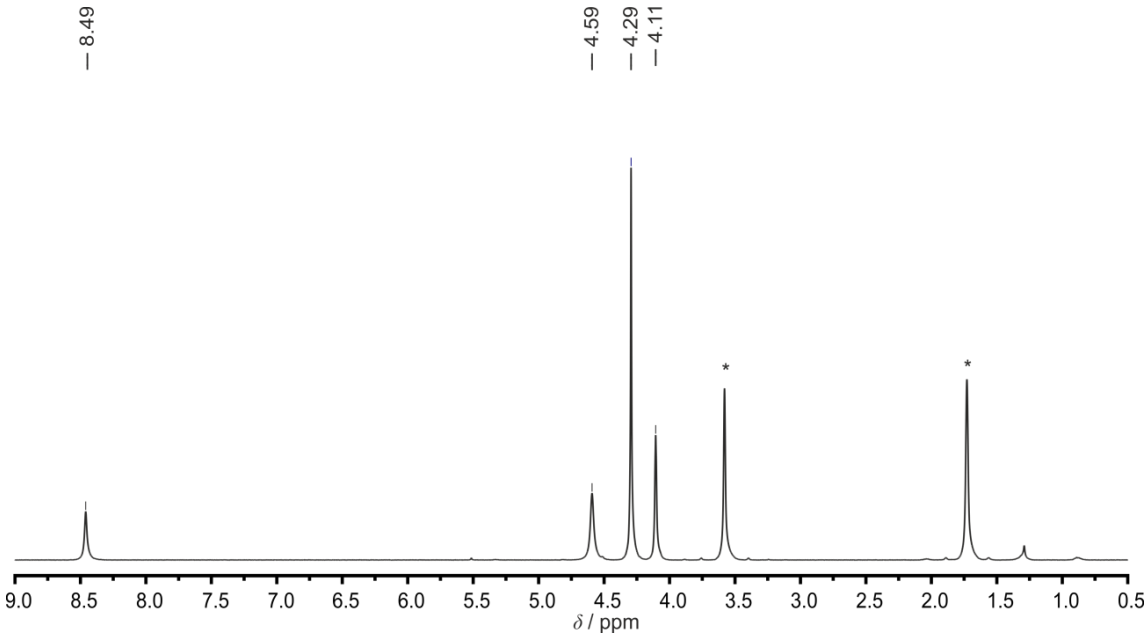

Figure S14. ^{1}H NMR spectrum of **6** in d_8-THF. Solvent signals are indicated by *.

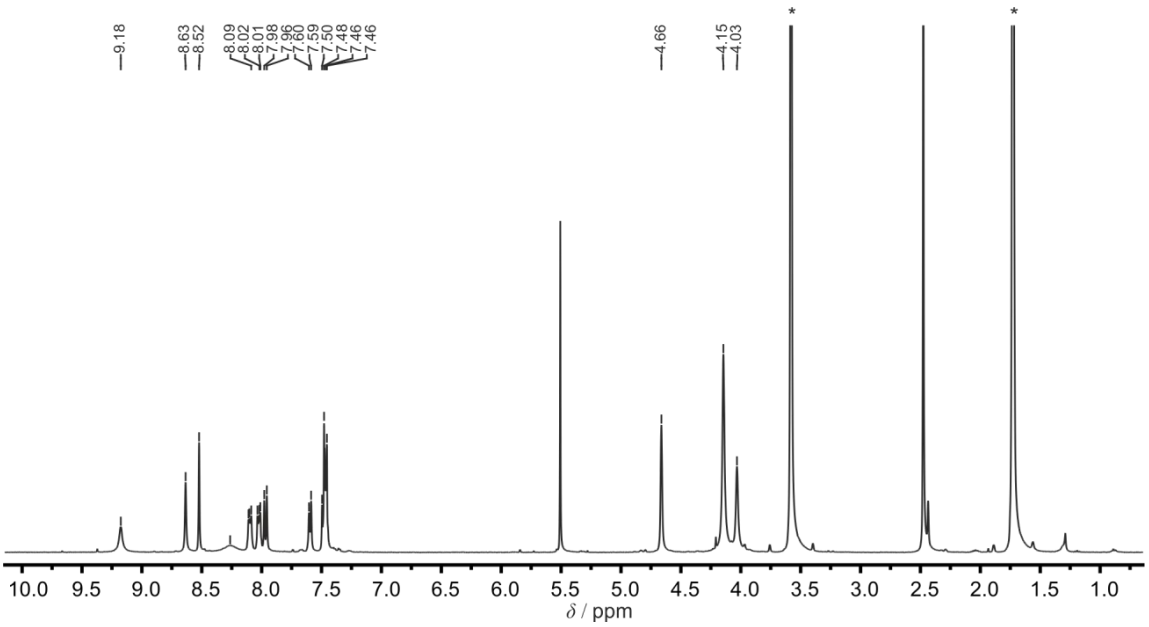

Figure S15. ^{1}H NMR spectrum of **7** in d_8-THF. Solvent signals are indicated by *.

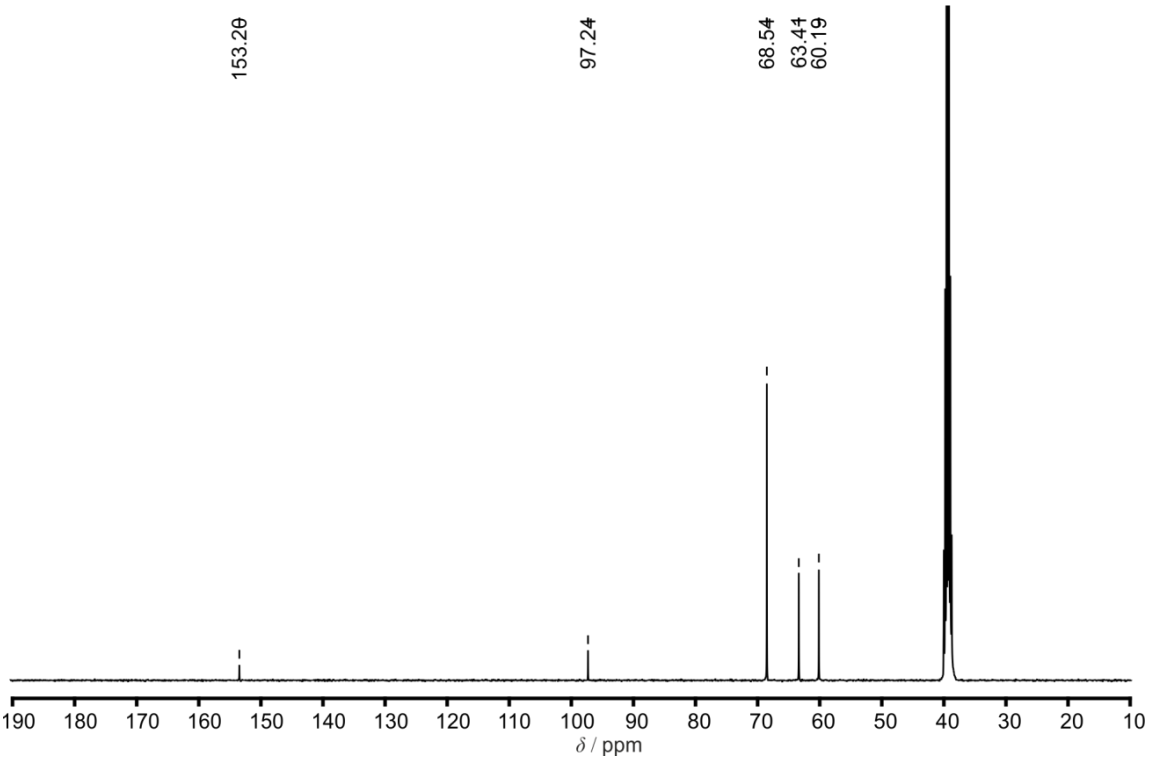

Figure S16. ^{13}C NMR spectrum of **1** in d_6-DMSO.

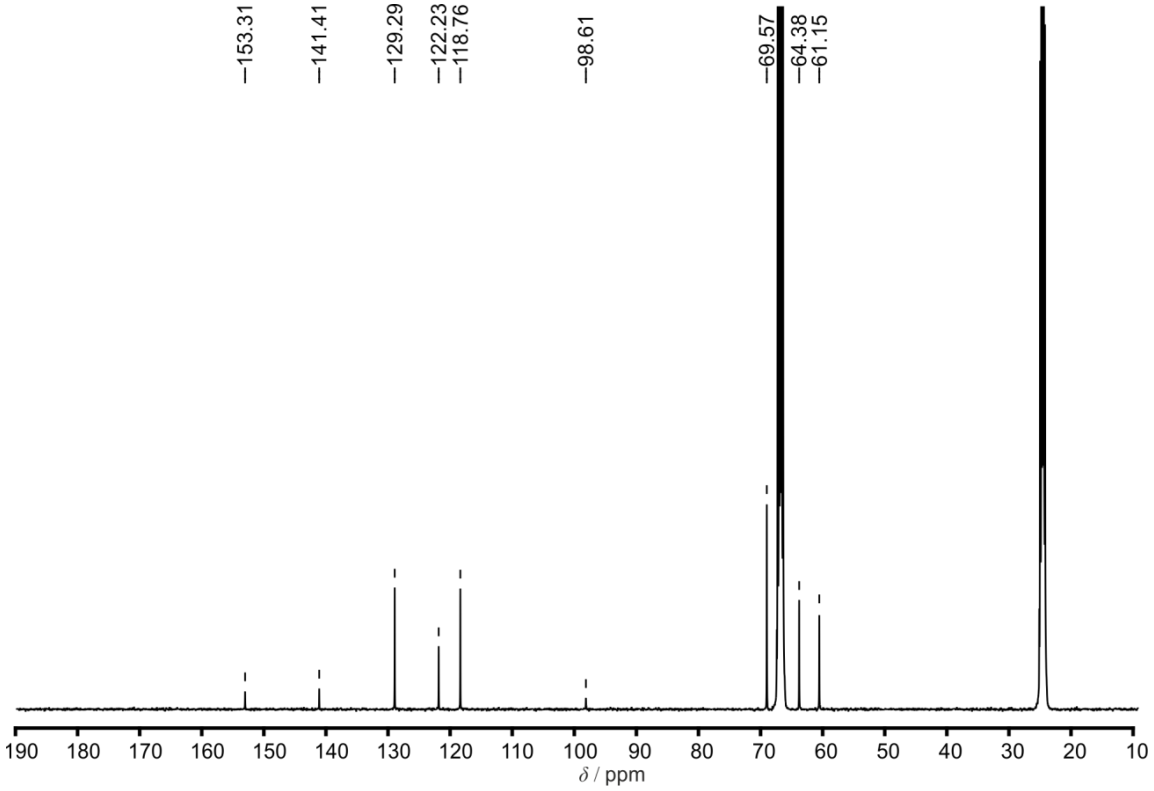

Figure S17. ^{13}C NMR spectrum of **2** in d_8-THF.

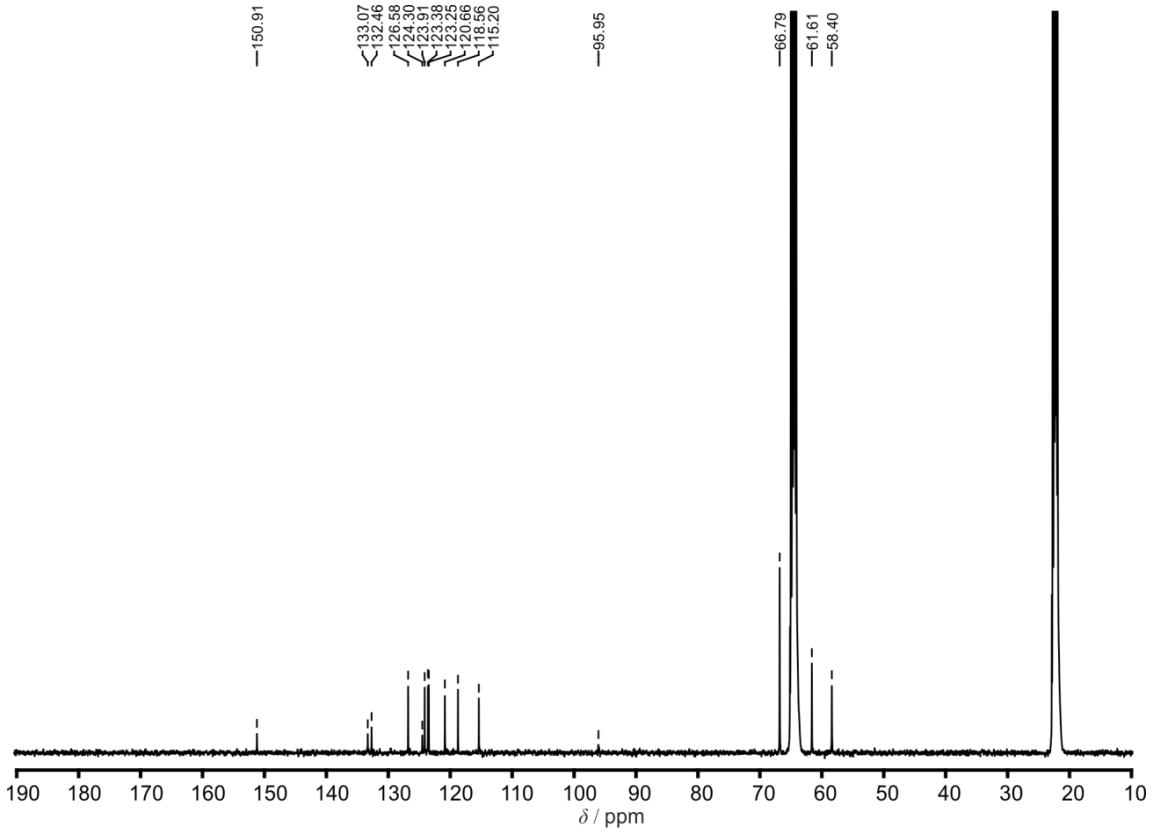

Figure S18. ^{13}C NMR spectrum of **3** in d_8-THF.

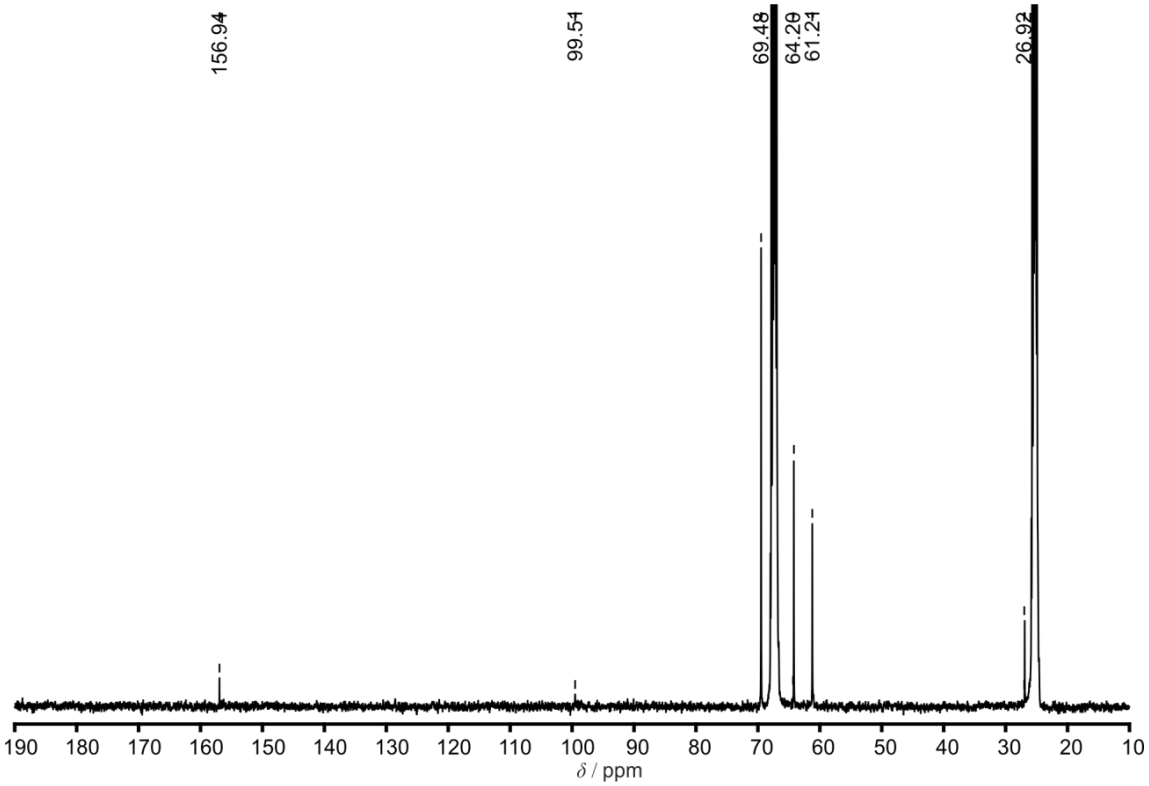

Figure S19. ^{13}C NMR spectrum of **4** in d_8-THF.

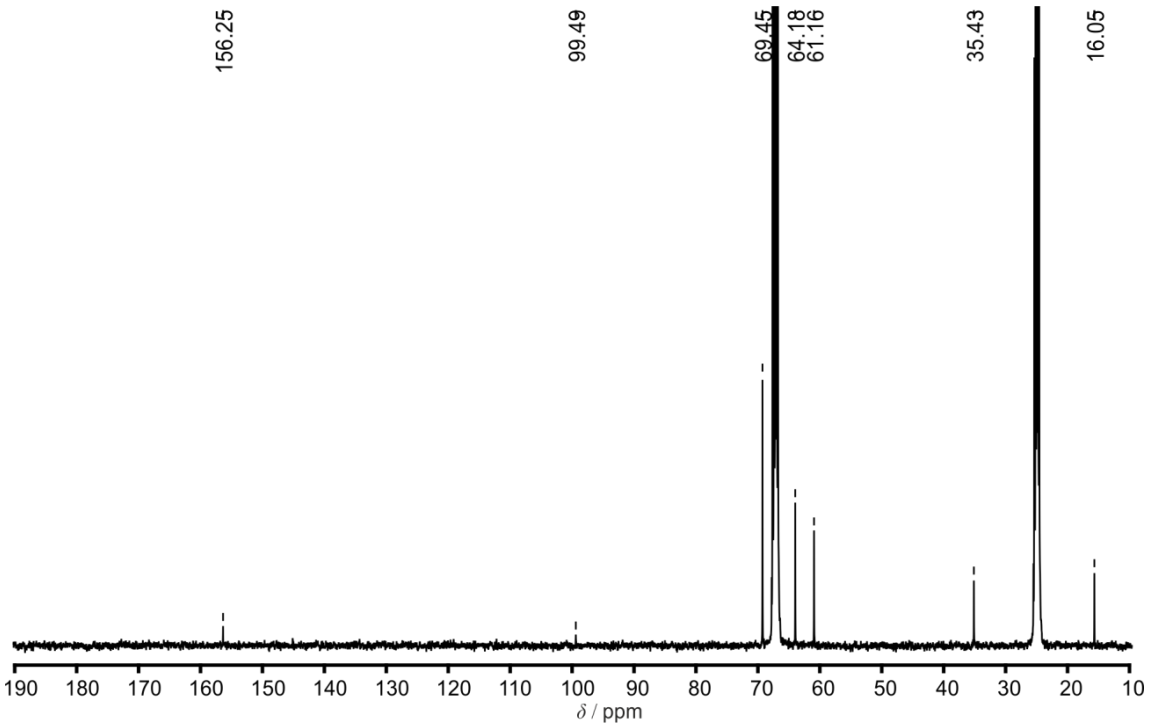

Figure S20. ^{13}C NMR spectrum of **5** in d_8-THF.

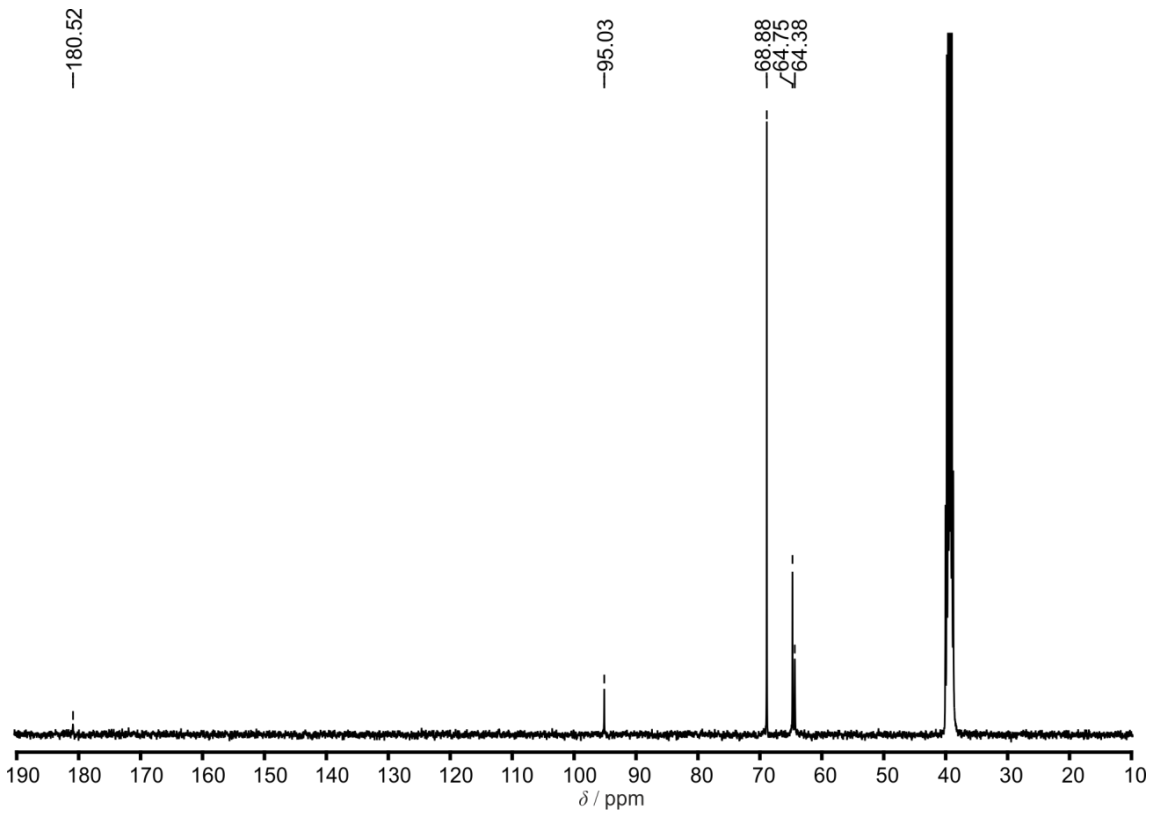

Figure S21. ^{13}C NMR spectrum of **6** in d_6-DMSO.

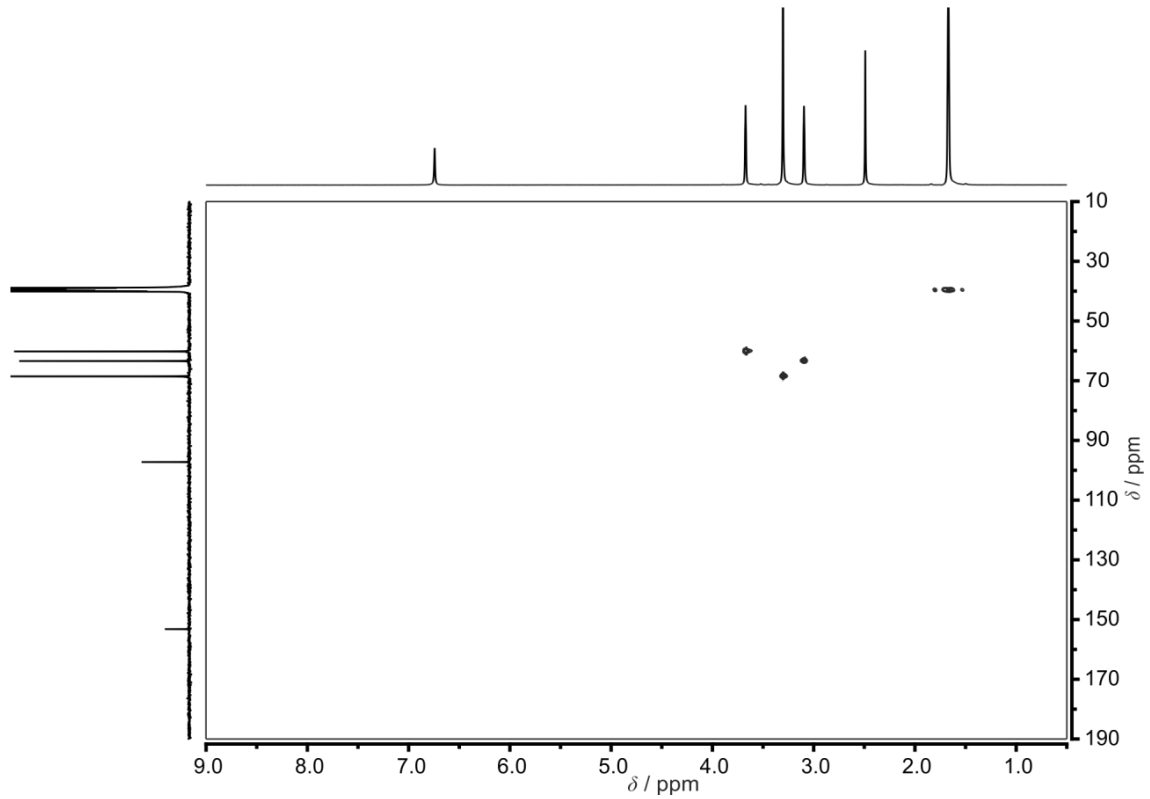

Figure S22. ^{13}C-^{1}H HSQC spectrum of **1** in d_6-DMSO.

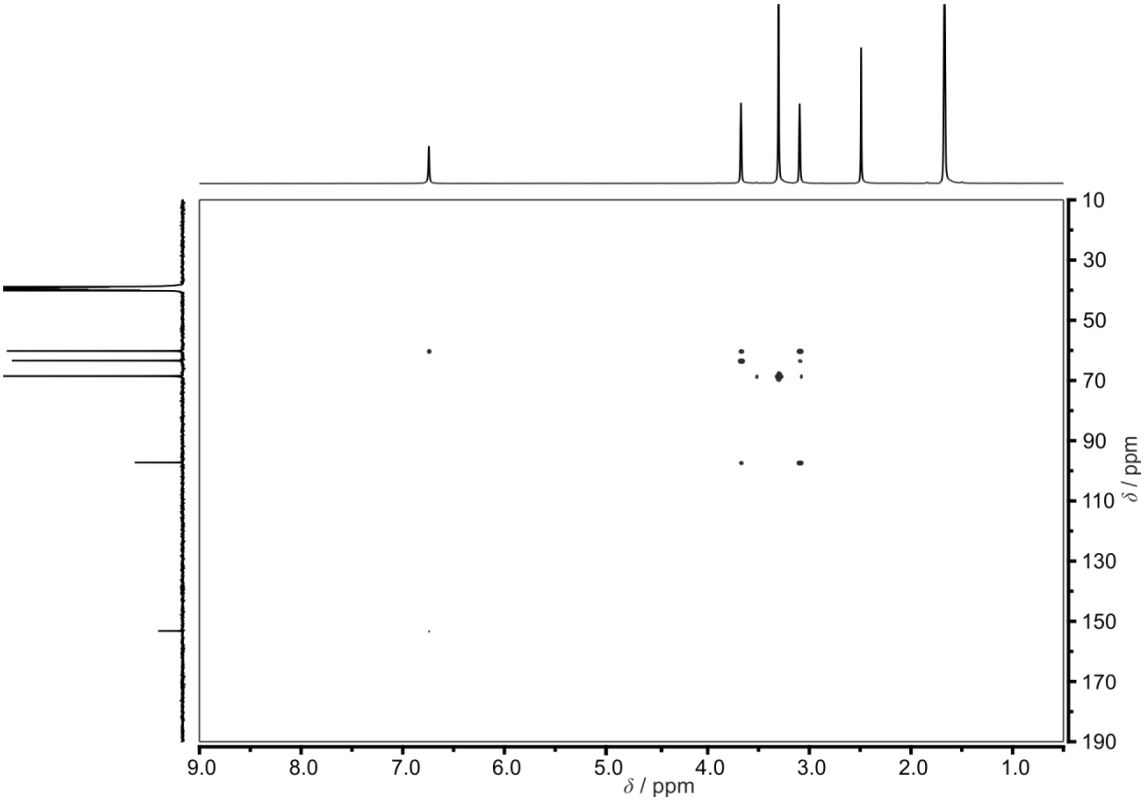

Figure S23. ^{13}C-^{1}H HMBC spectrum of **1** in d_6-DMSO.

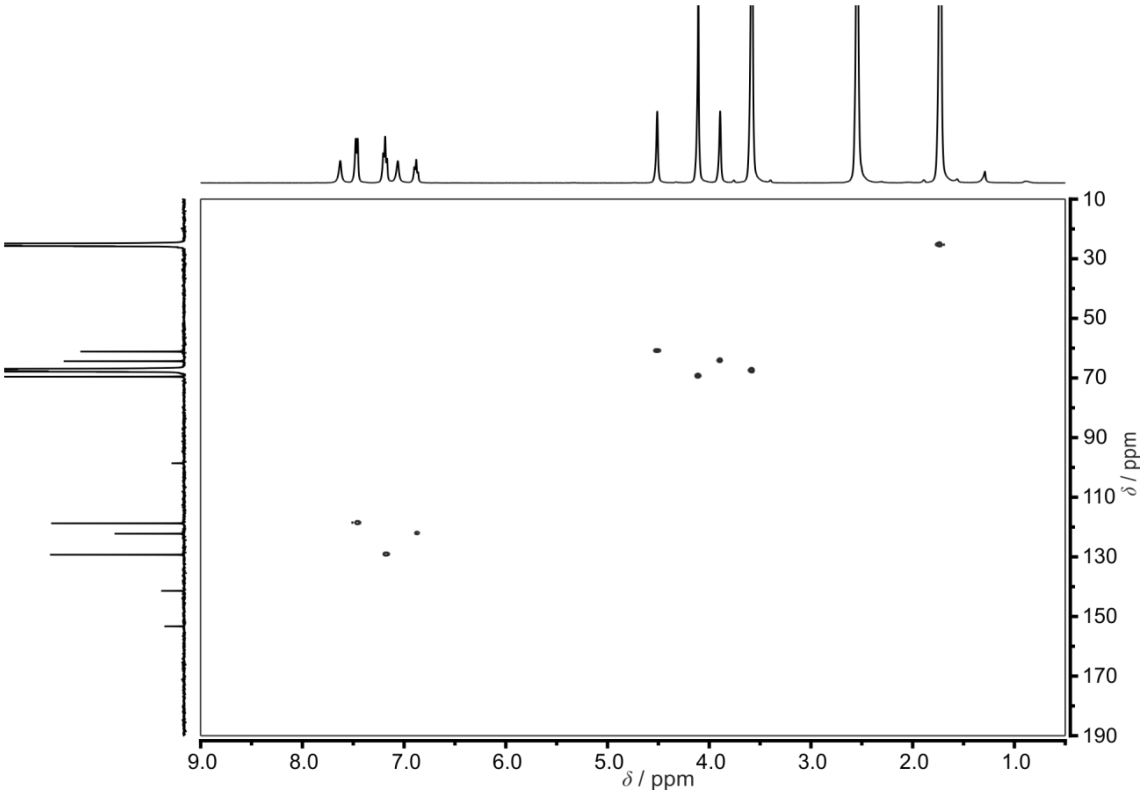

Figure S24. ^{13}C-^{1}H HSQC spectrum of **2** in d_8-THF.

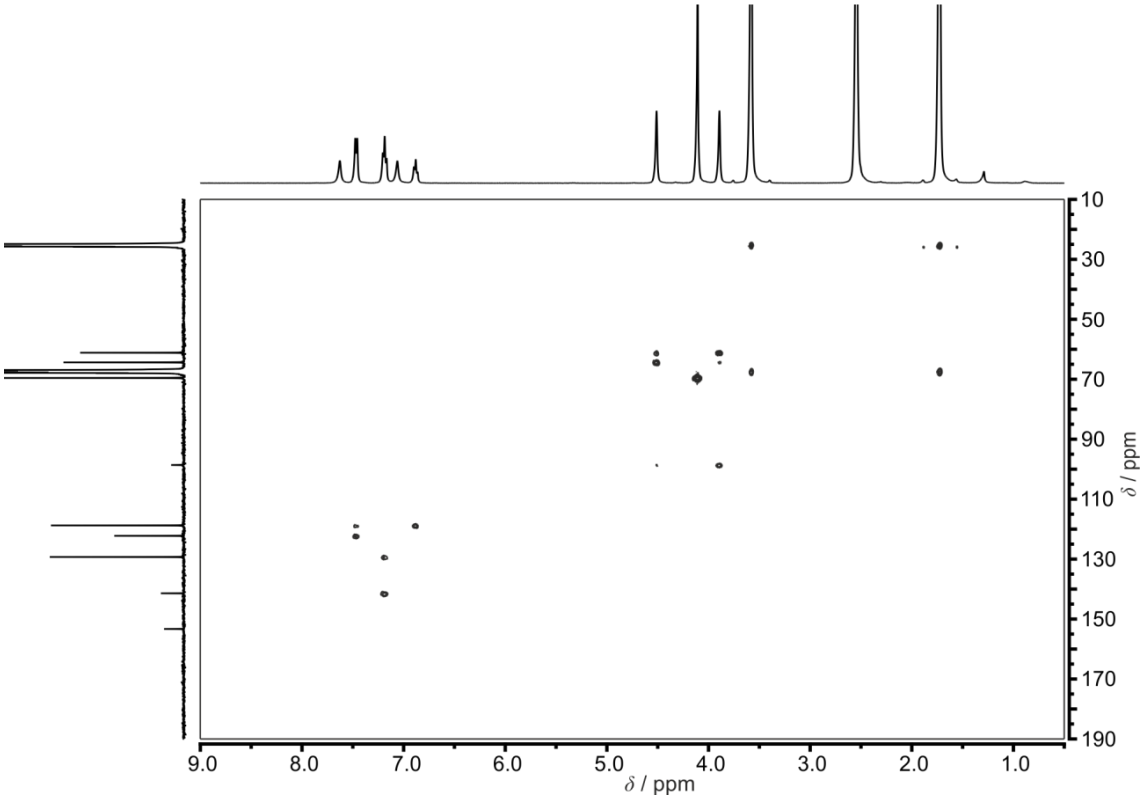

Figure S25. ^{13}C-^{1}H HMBC spectrum of **2** in d_8-THF.

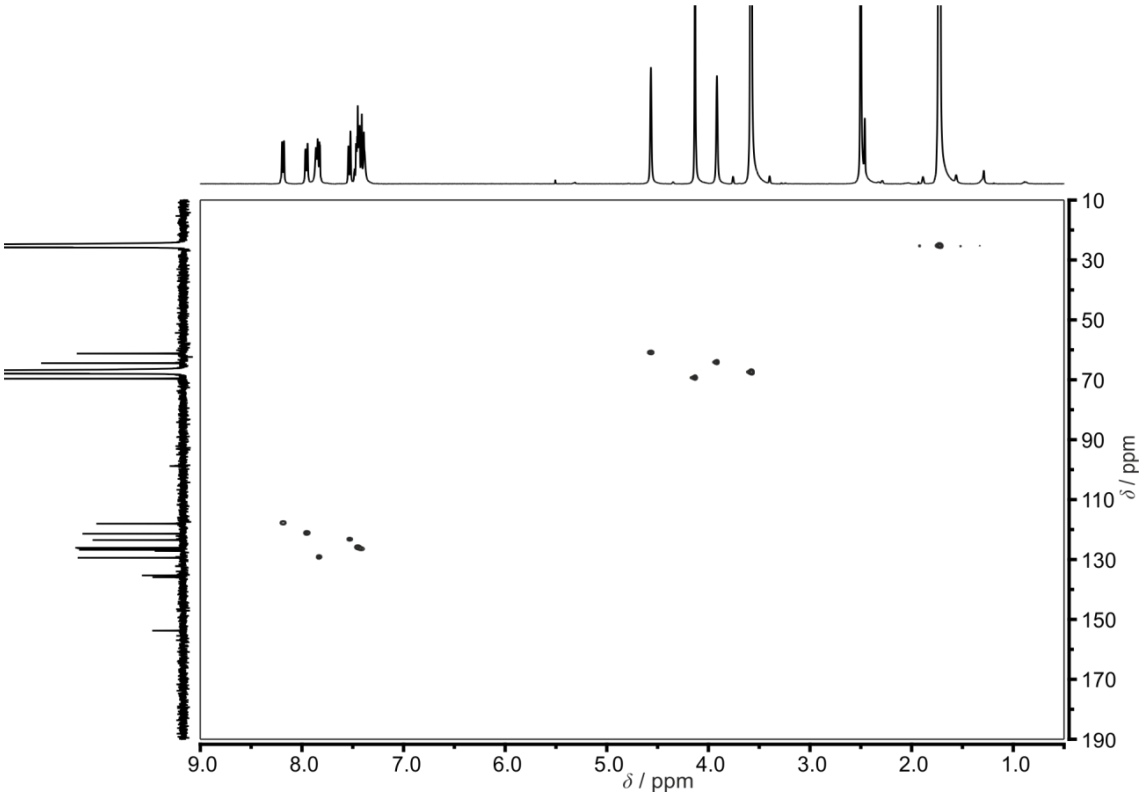

Figure S26: ^{13}C-^{1}H HSQC spectrum of **3** in d_8-THF.

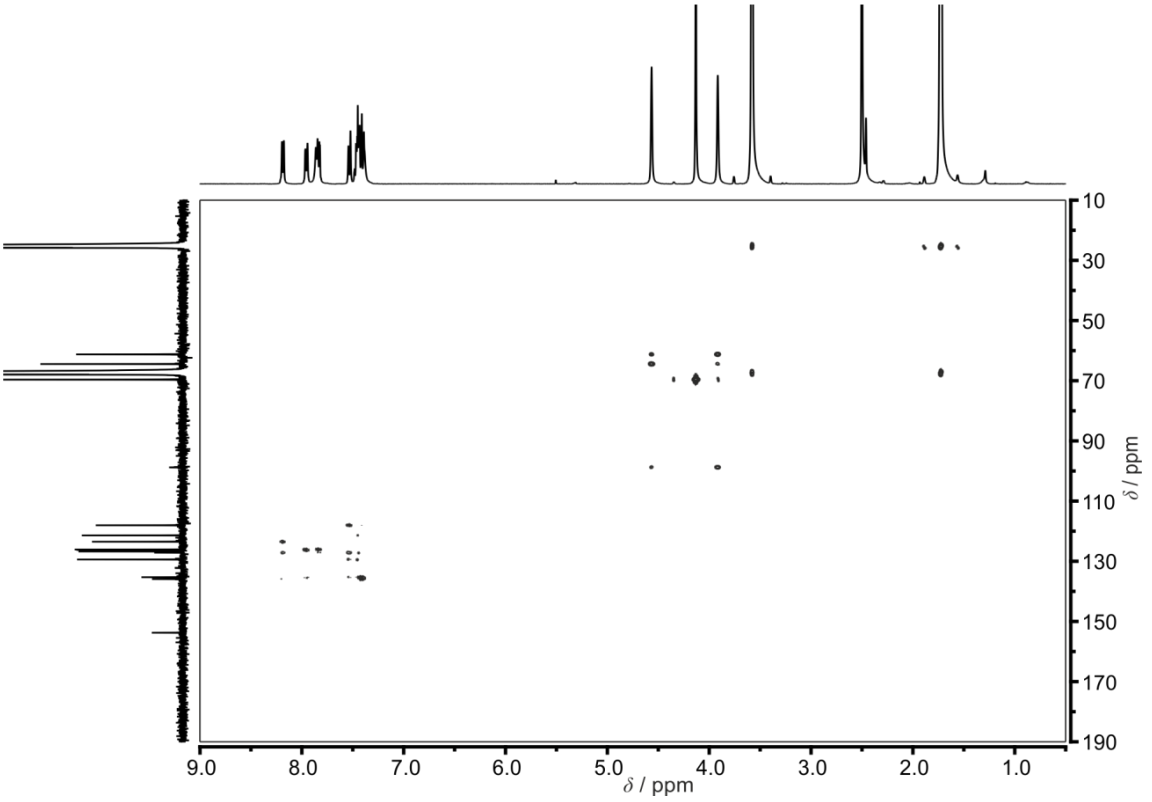

Figure S27. ^{13}C-^{1}H HMBC spectrum of **3** in d_8-THF.

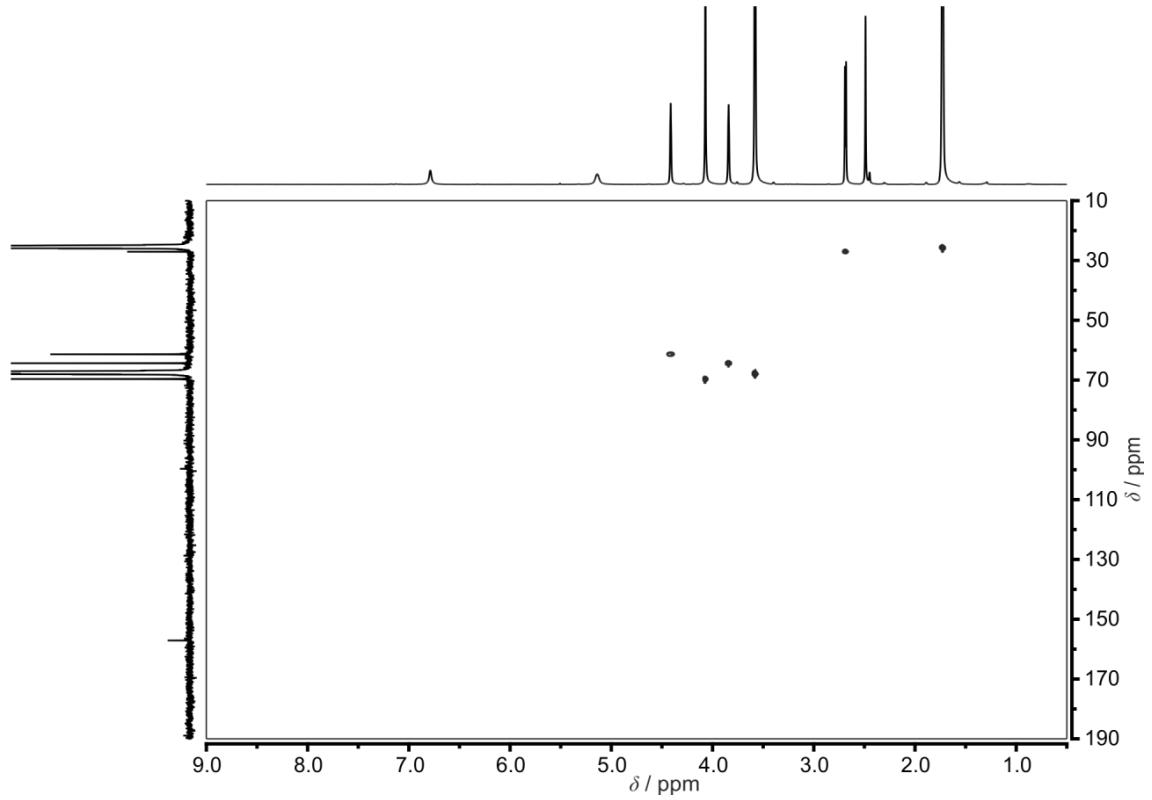

Figure S28. ^{13}C-^{1}H HSQC spectrum of **4** in d_8-THF.

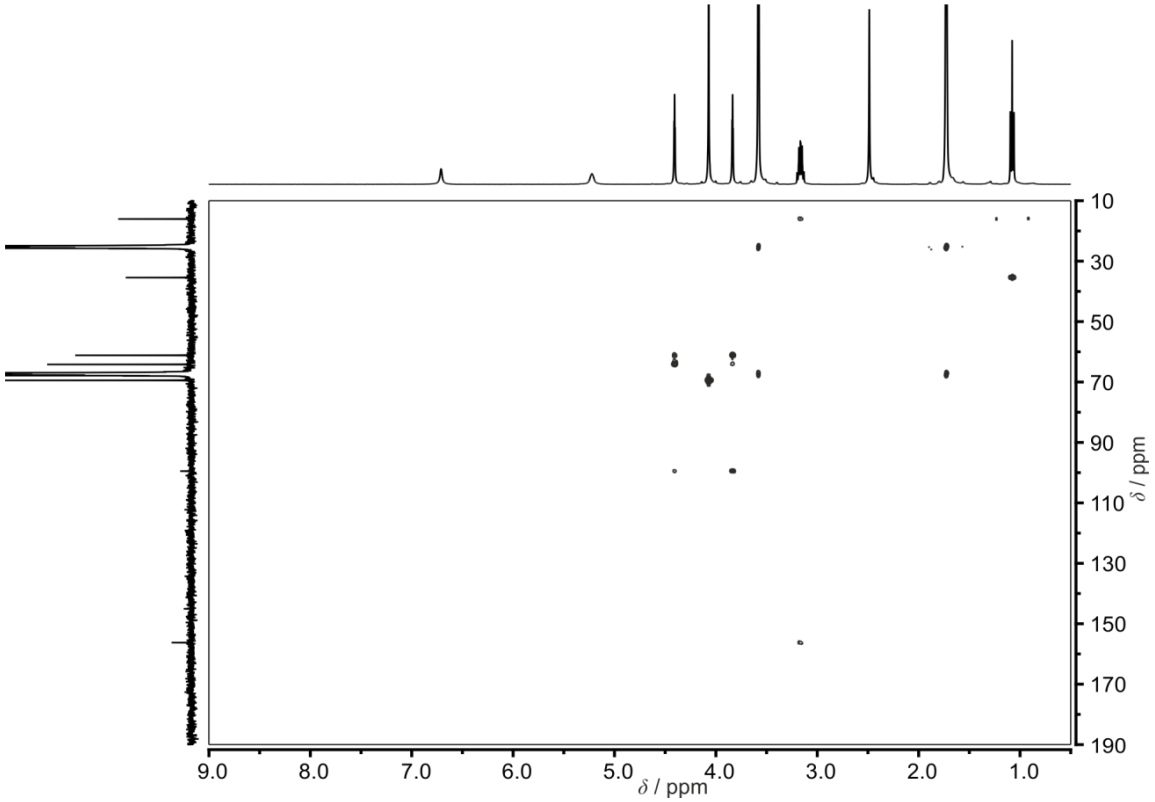

Figure S29. ^{13}C-^{1}H HMBC spectrum of **4** in d_8-THF.

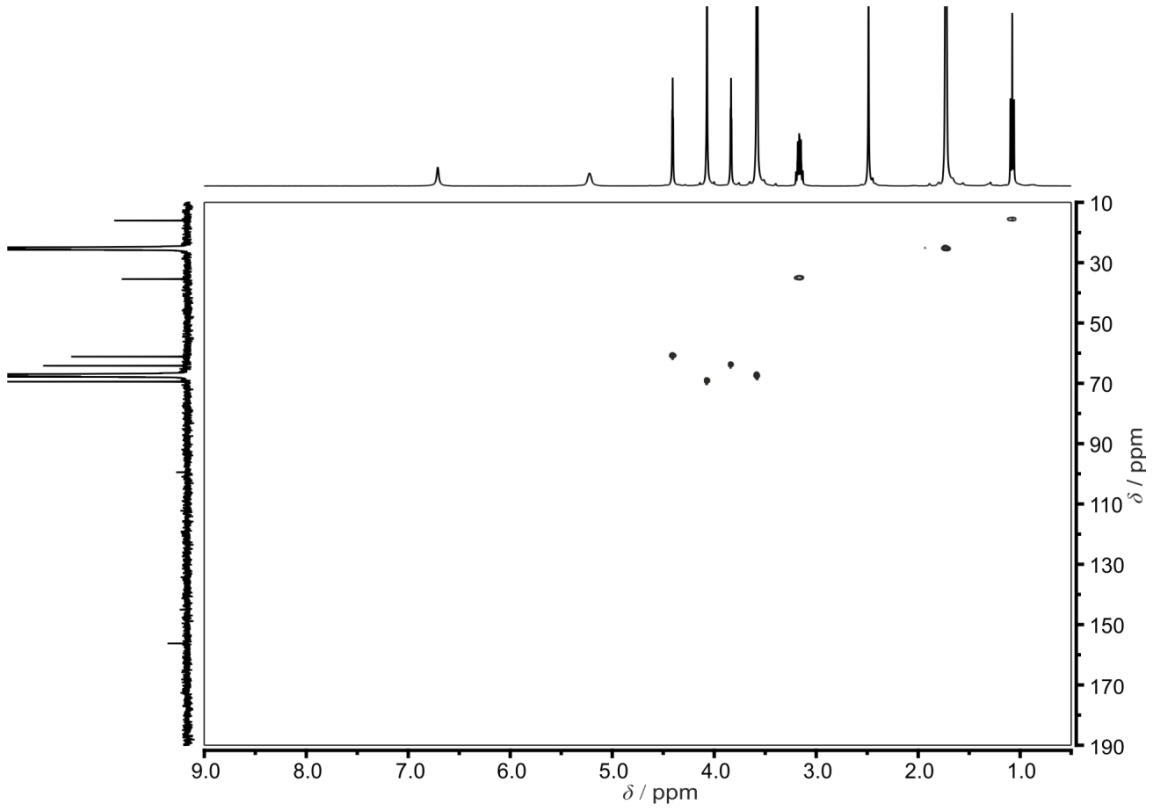

Figure S30. ^{13}C-^{1}H HSQC spectrum of **5** in d_8-THF.

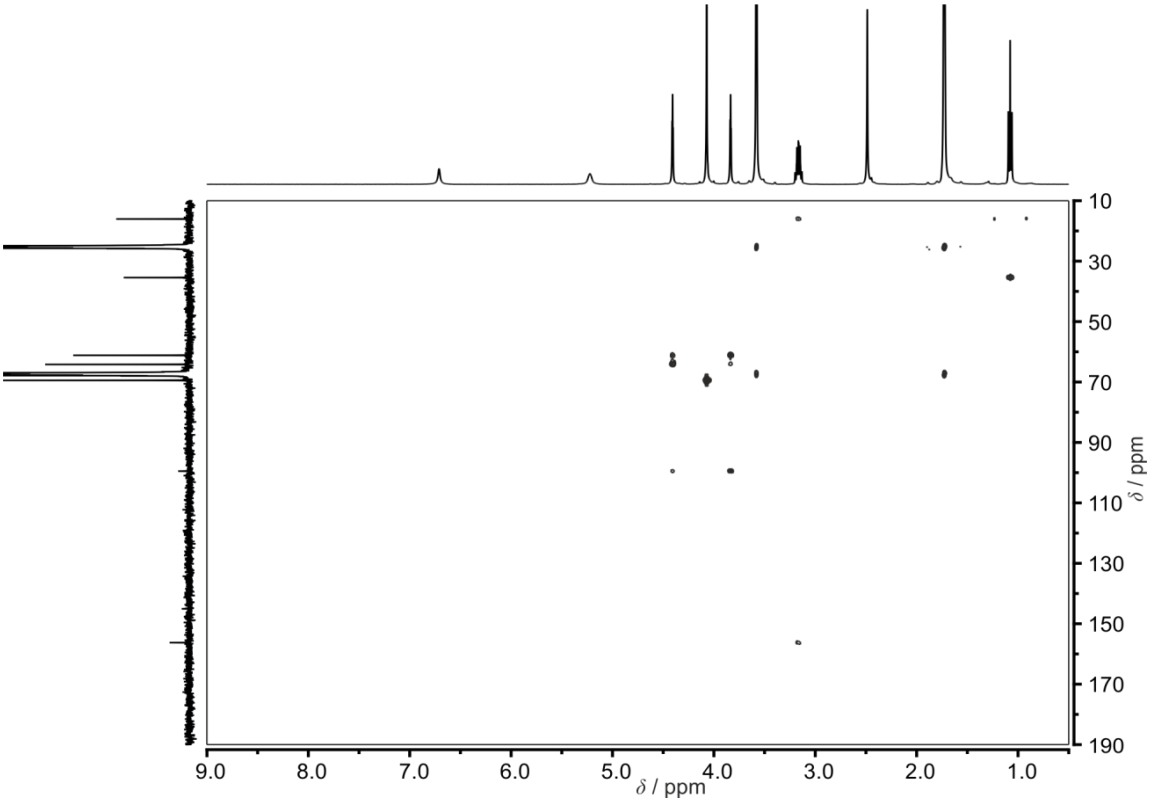

Figure S31. ^{13}C-^{1}H HMBC spectrum of **5** in d_8-THF.

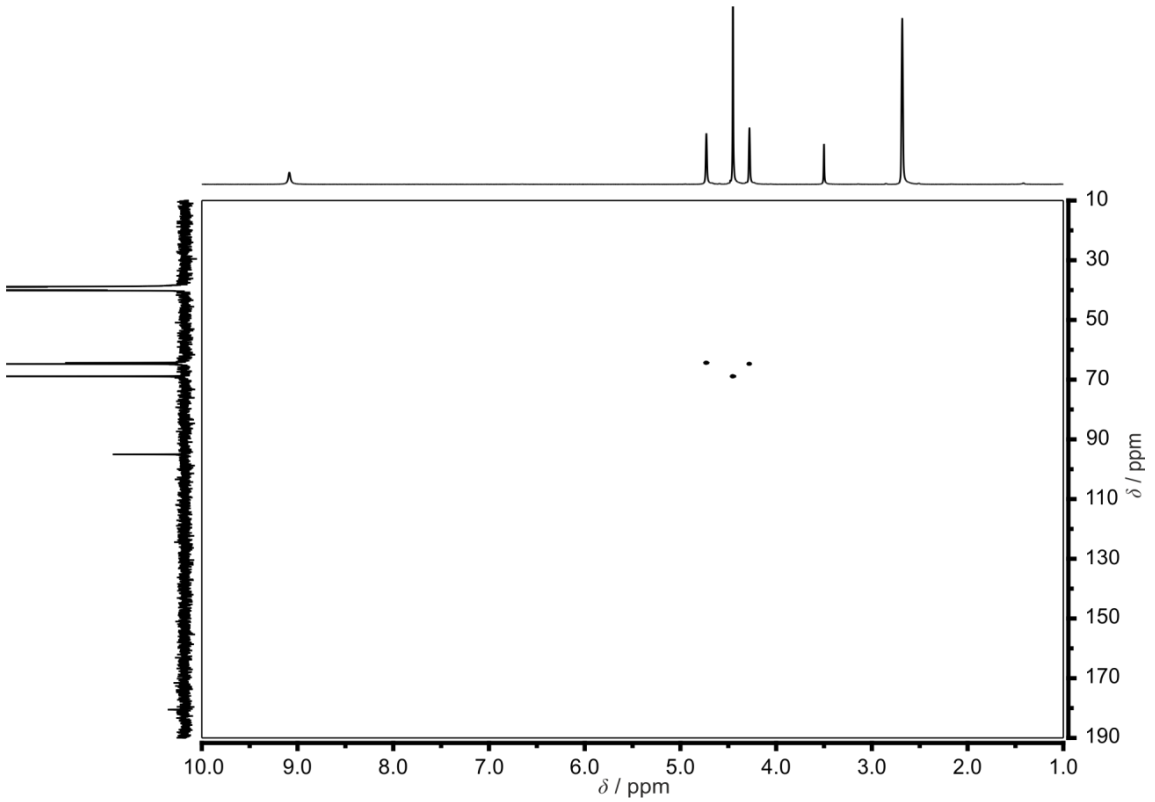

Figure S32. ^{13}C-^{1}H HSQC spectrum of **6** in d_6-DMSO.

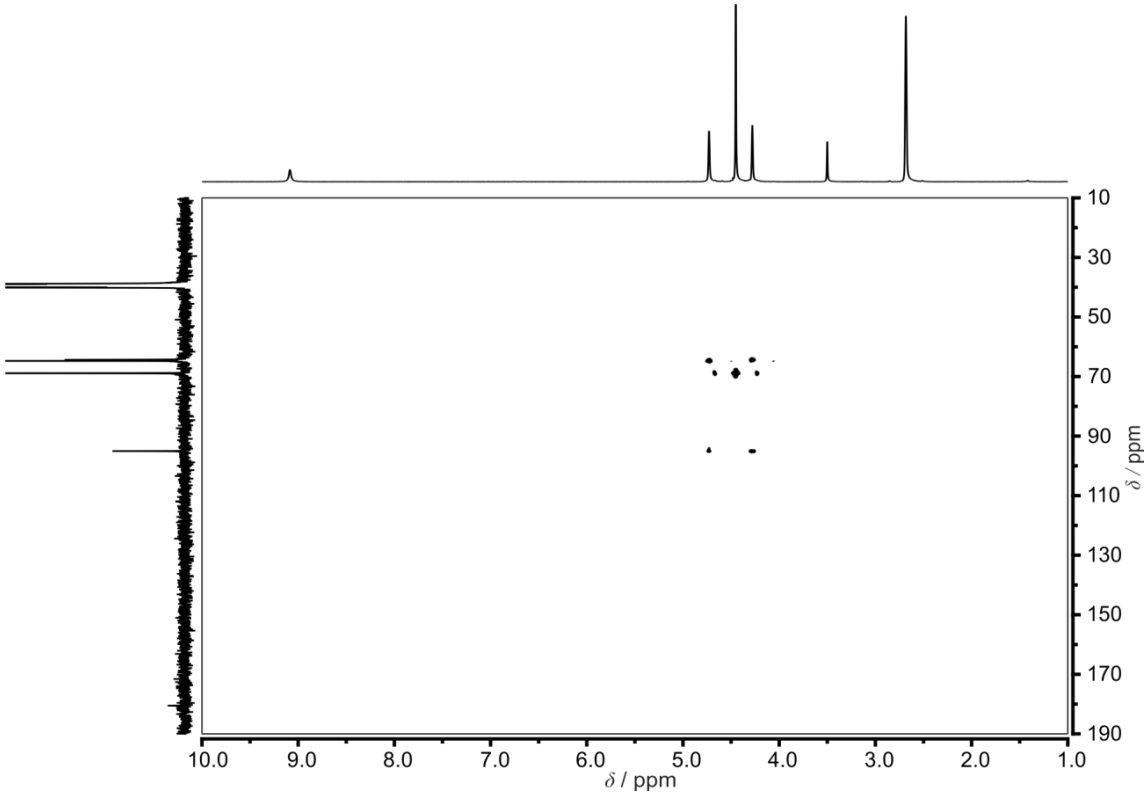

Figure S33. ^{13}C-^{1}H HMBC spectrum of **6** in d_6-DMSO.

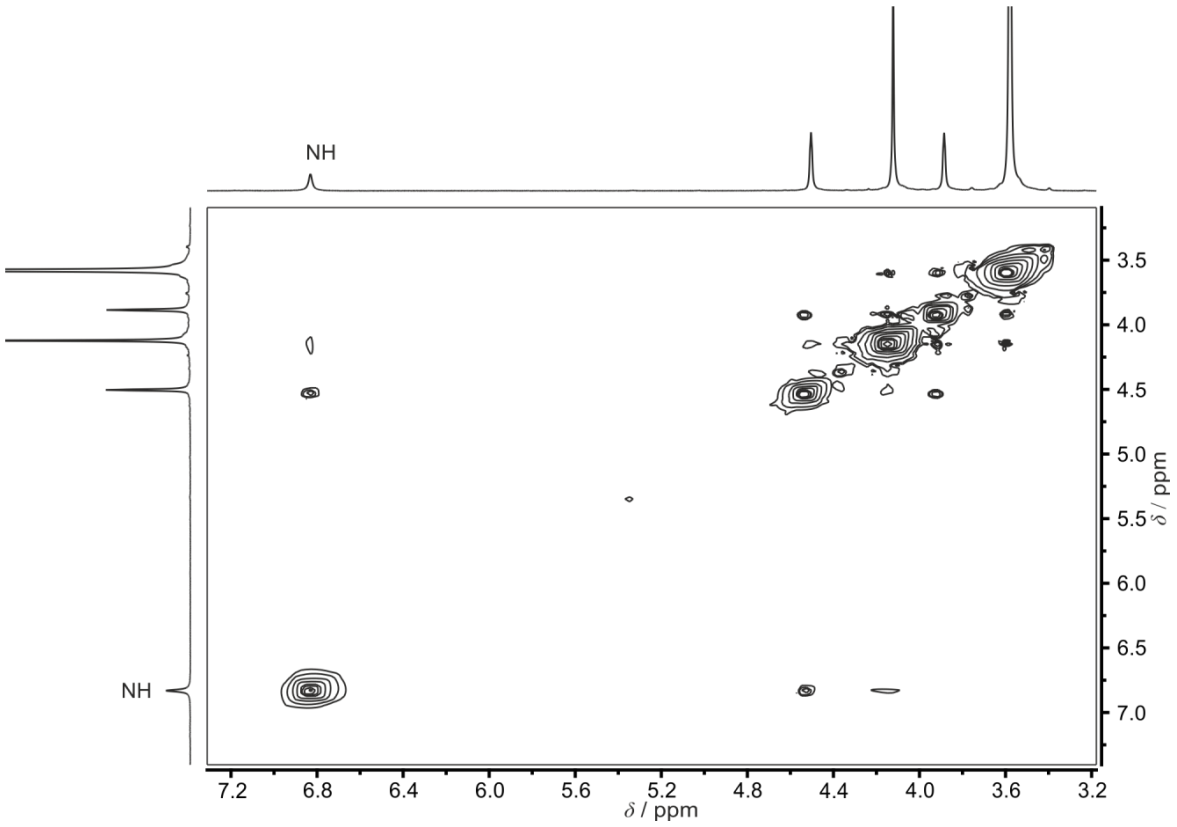

Figure S34. ^{1}H-^{1}H NOESY spectrum of **1** in d_8-THF.

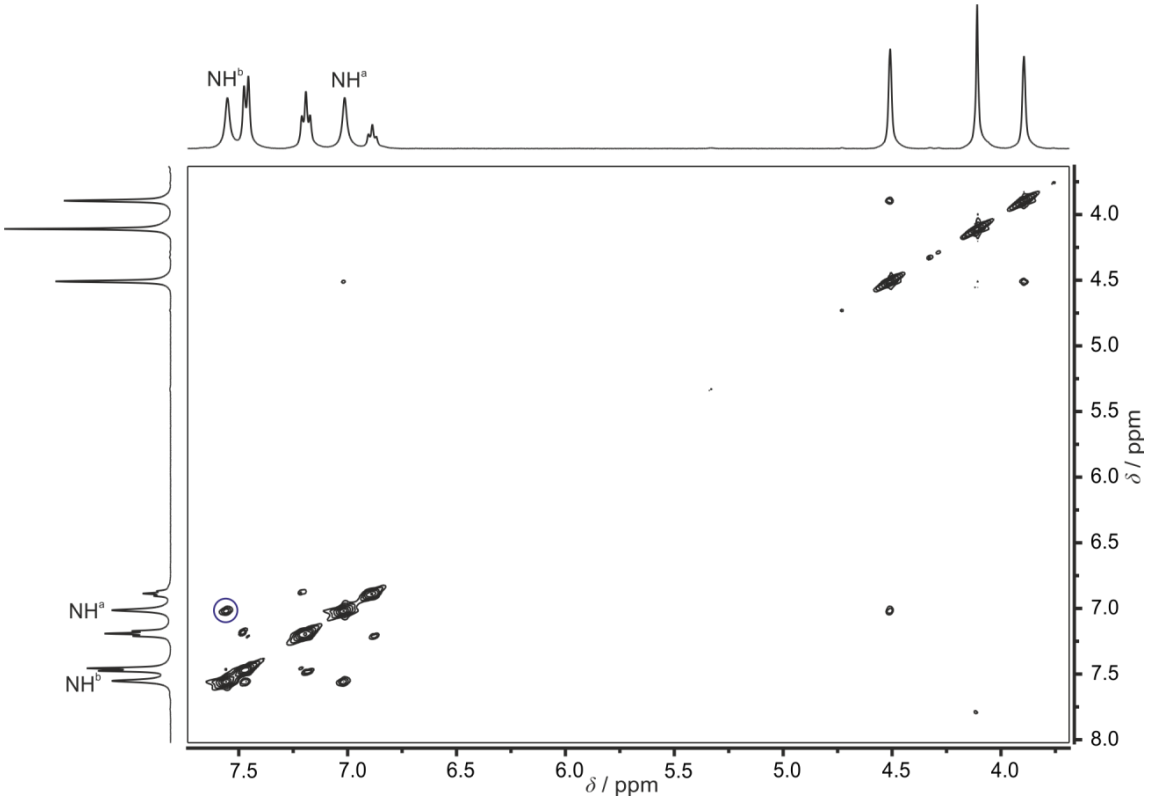

Figure S35. ^{1}H-^{1}H NOESY spectrum of **2** in d_8-THF.

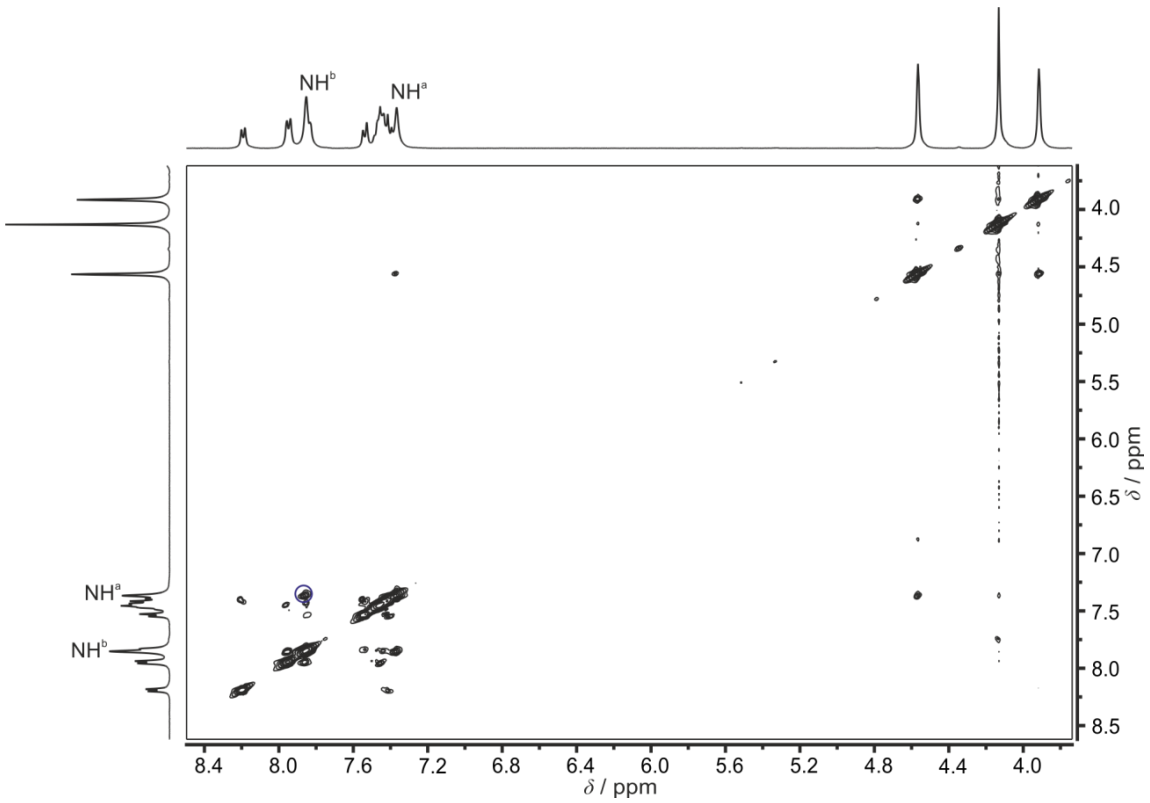

Figure S36. ^{1}H-^{1}H NOESY spectrum of **3** in d_8-THF.

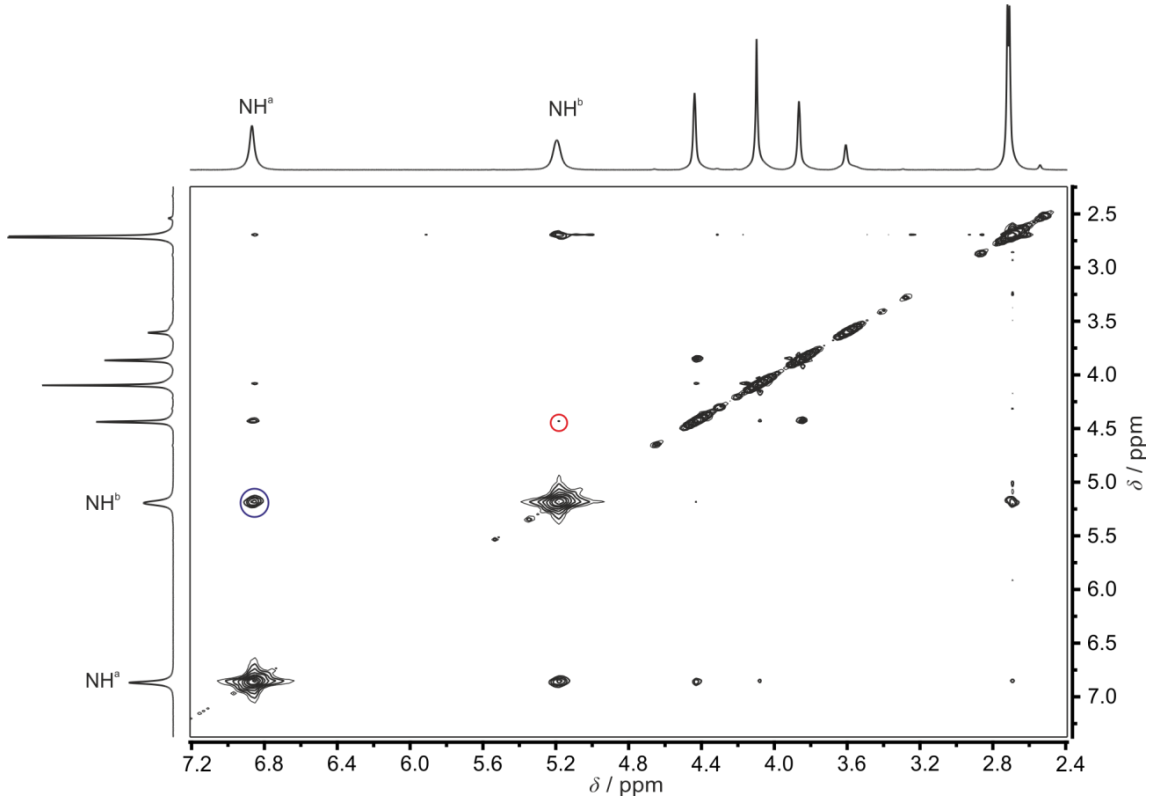

Figure S37. ^{1}H-^{1}H NOESY spectrum of **4** in d_8-THF.

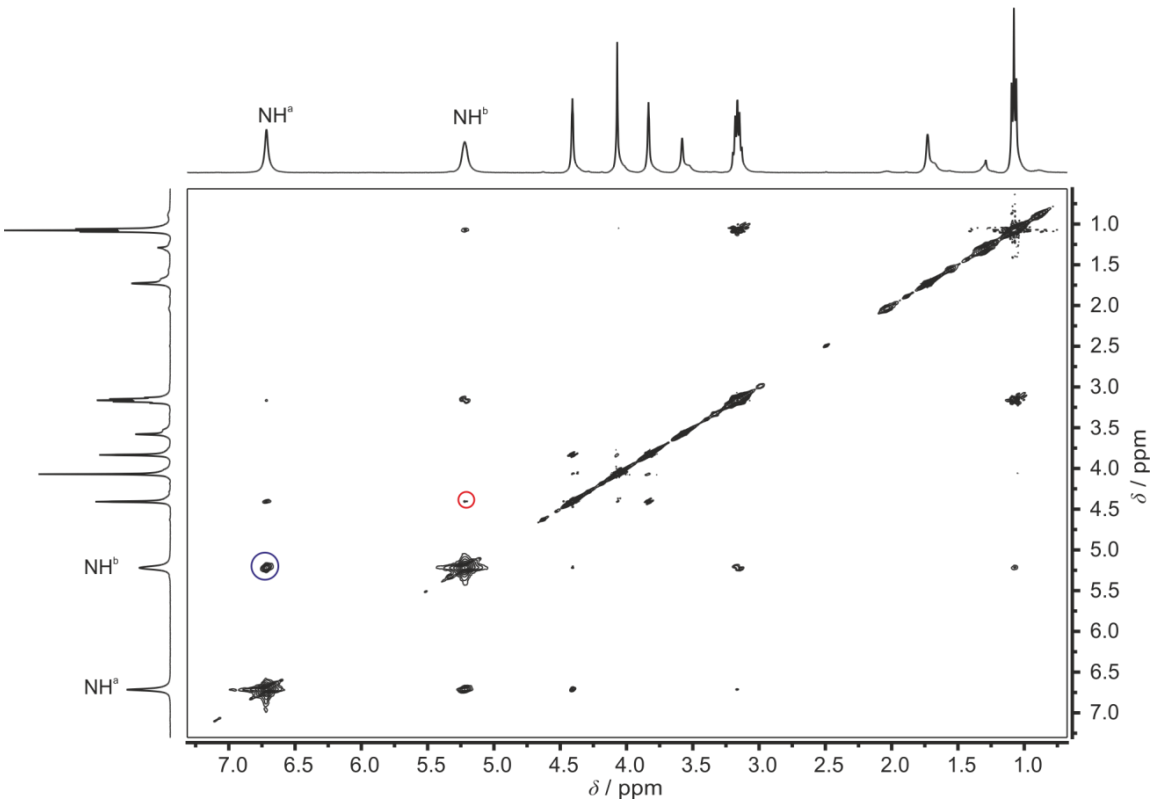

Figure S38. ^{1}H-^{1}H NOESY spectrum of **5** in d_8-THF.

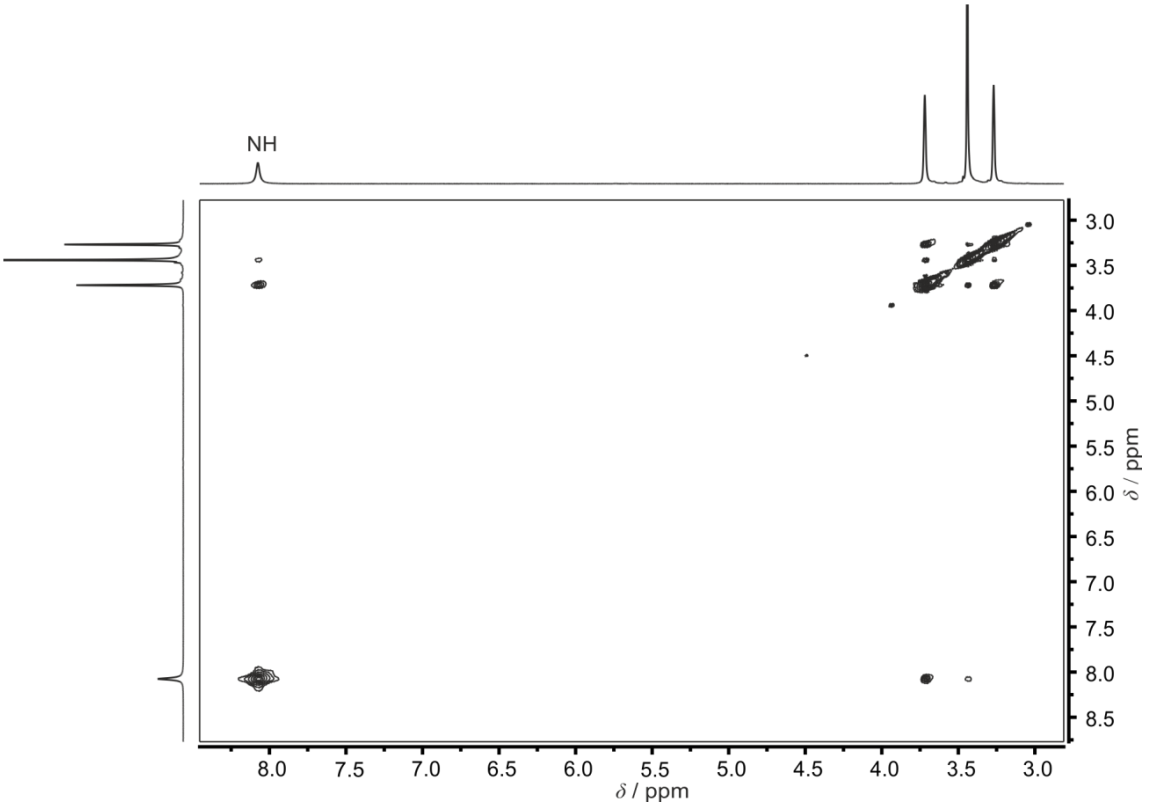

Figure S39. ^{1}H-^{1}H NOESY spectrum of **6** in d_8-THF.

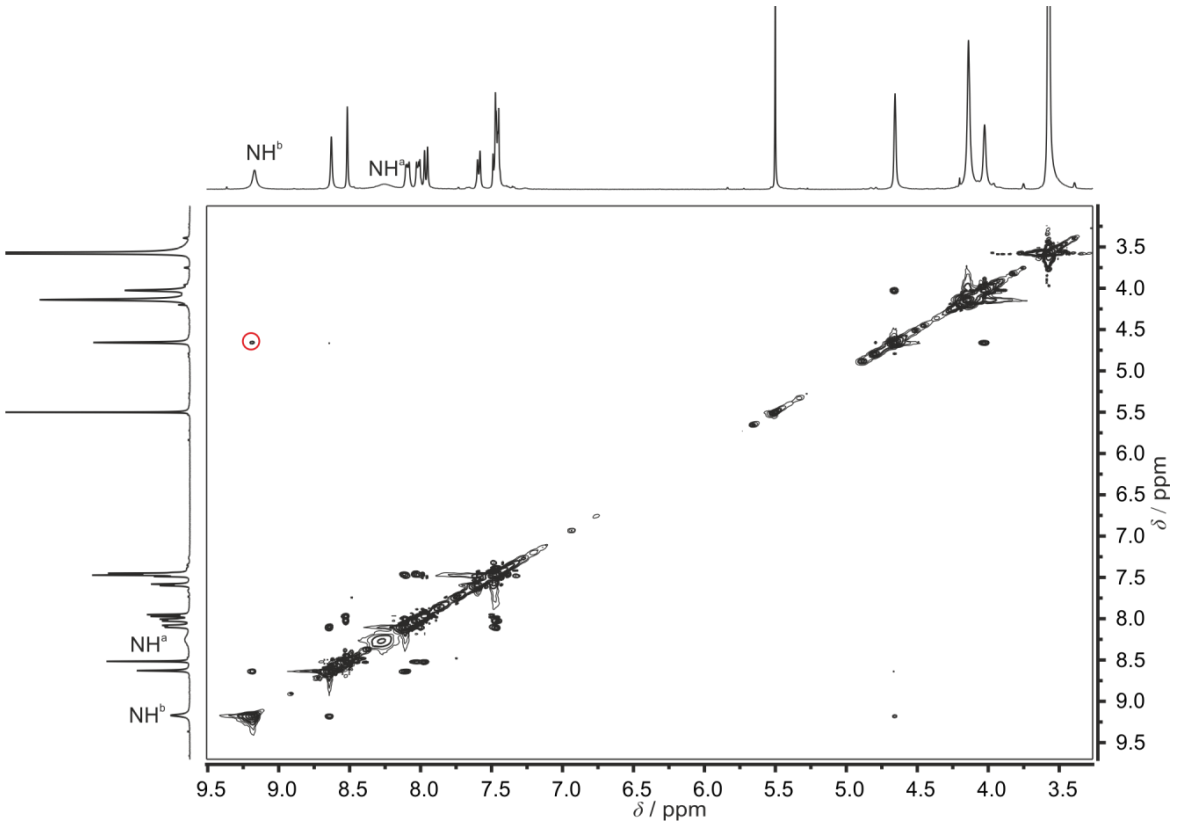

Figure S40. ^{1}H-^{1}H NOESY spectrum of **7** in d_8-THF.

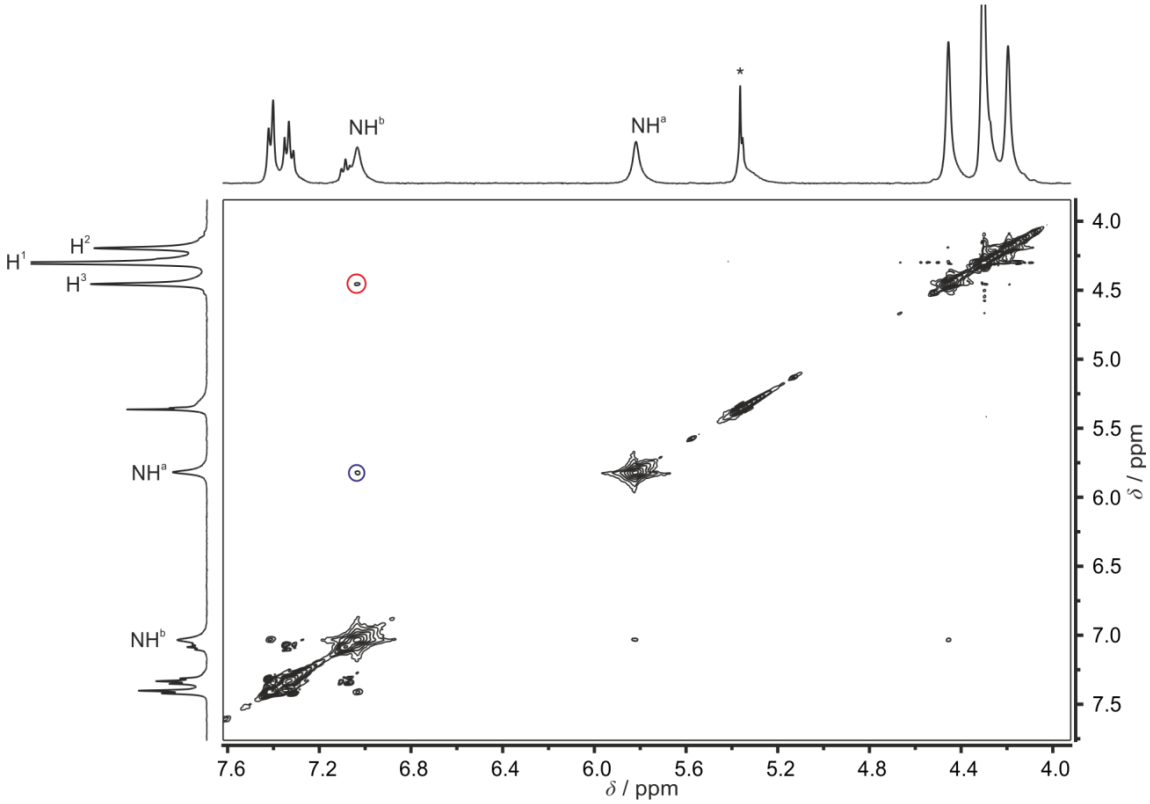

Figure S41. ^{1}H-^{1}H NOESY spectrum of **2** in CD_2Cl_2 (*c* = 0.005 mol / L).

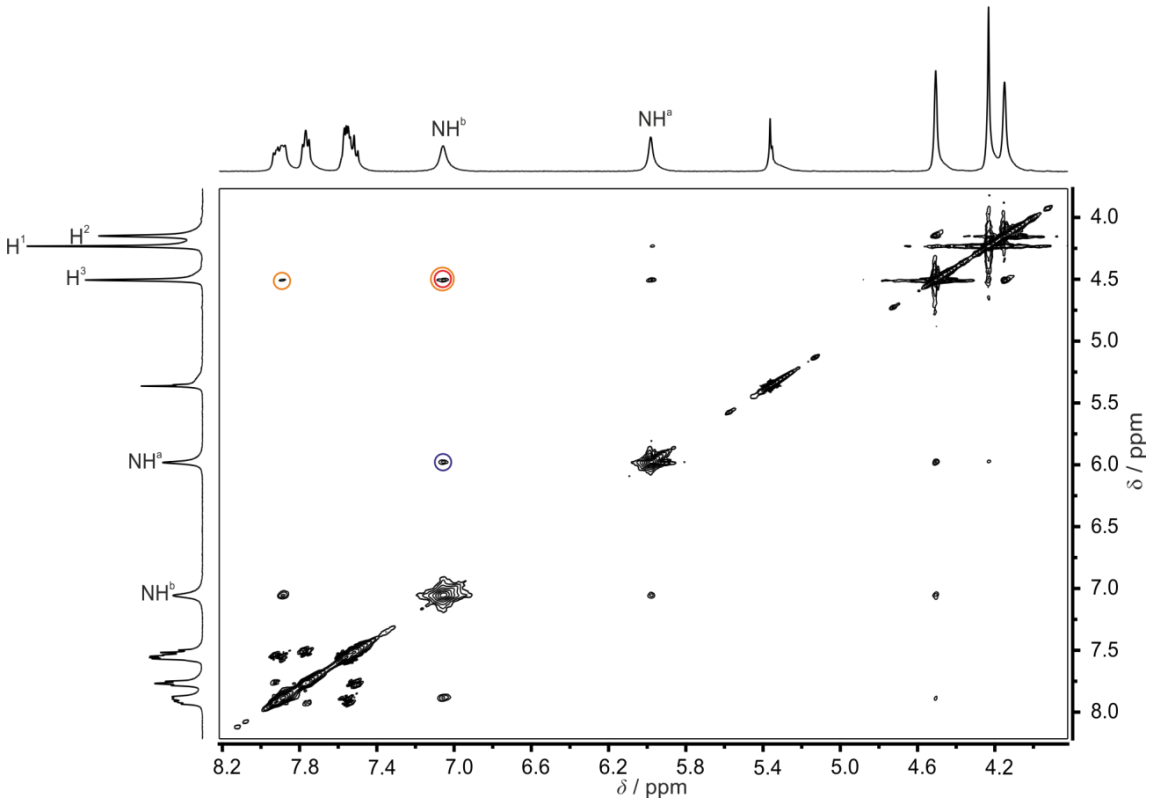

Figure S42. ^{1}H-^{1}H NOESY spectrum of **3** in CD_2Cl_2 (*c* = 0.005 mol / L).

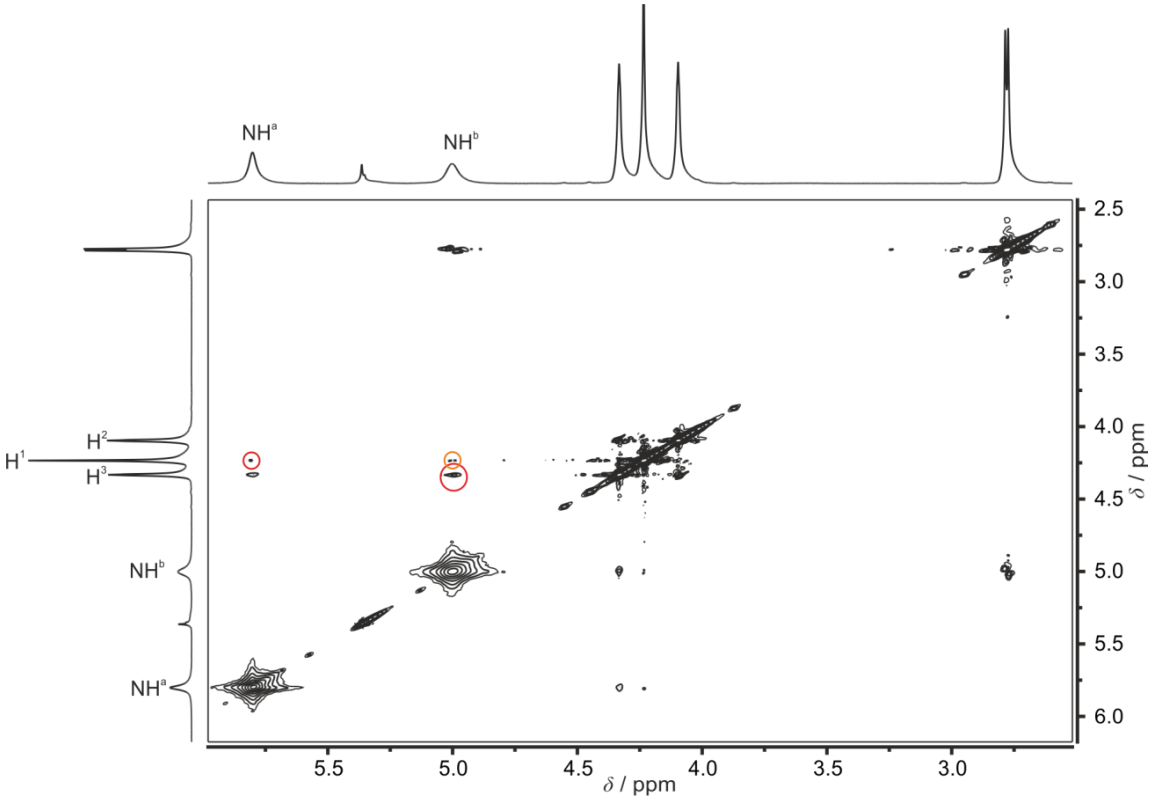

Figure S43. ^{1}H-^{1}H NOESY spectrum of **4** in CD_2Cl_2 (c = 0.01 mol / L).

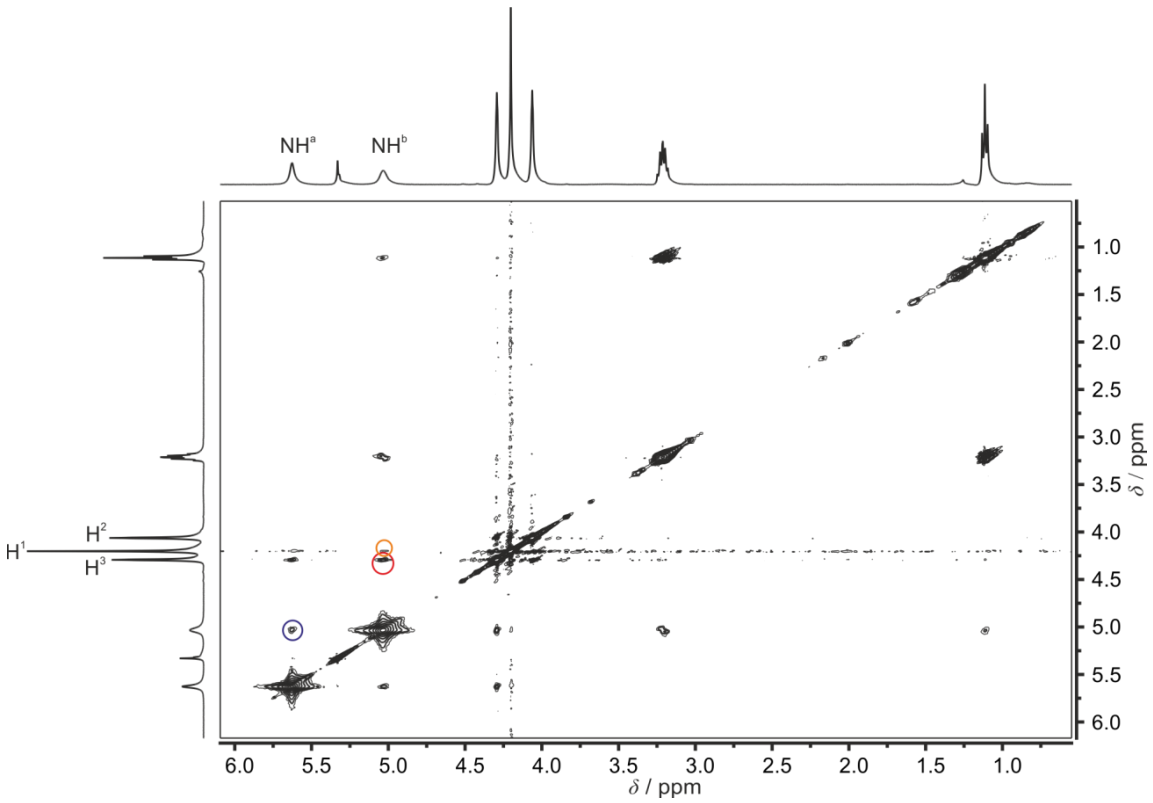

Figure S44. ^{1}H-^{1}H NOESY spectrum of **5** in CD_2Cl_2 (c = 0.01 mol / L).

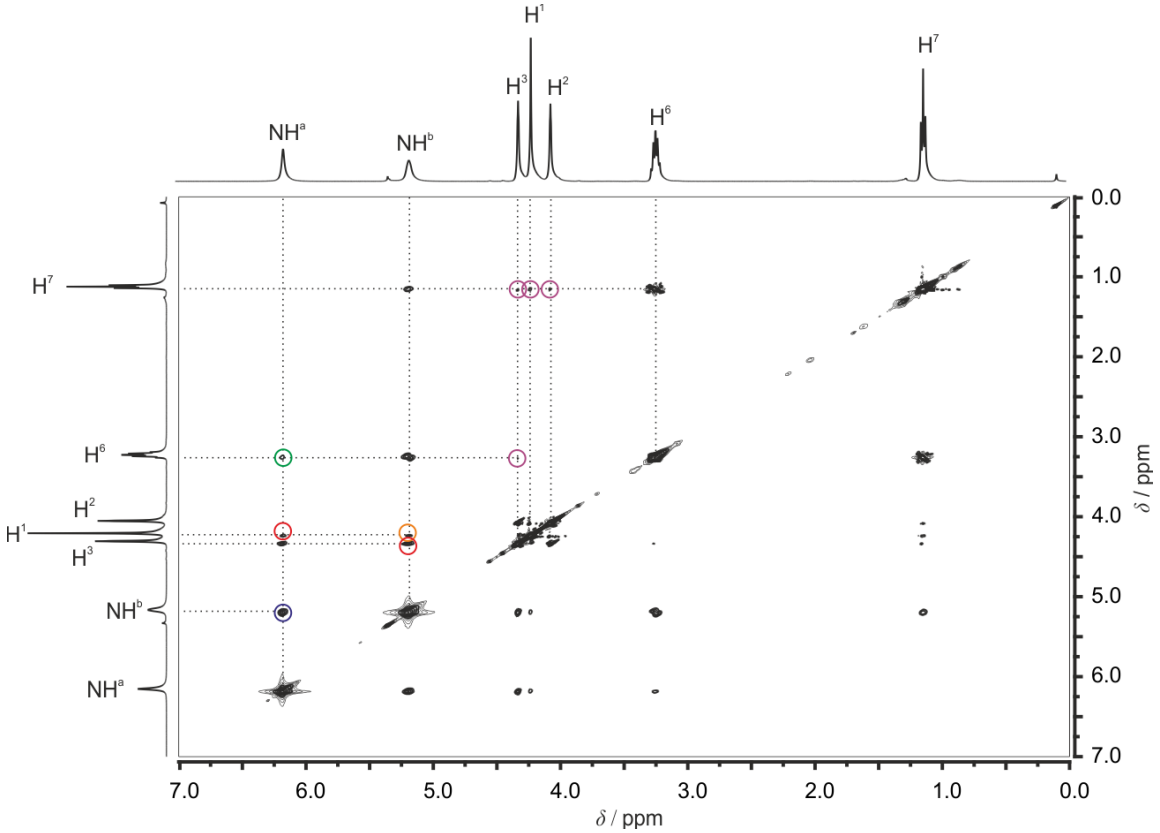

Figure S45. ^{1}H-^{1}H NOESY spectrum of **5** in CD_2Cl_2 (*c* = 0.5 mol / L).

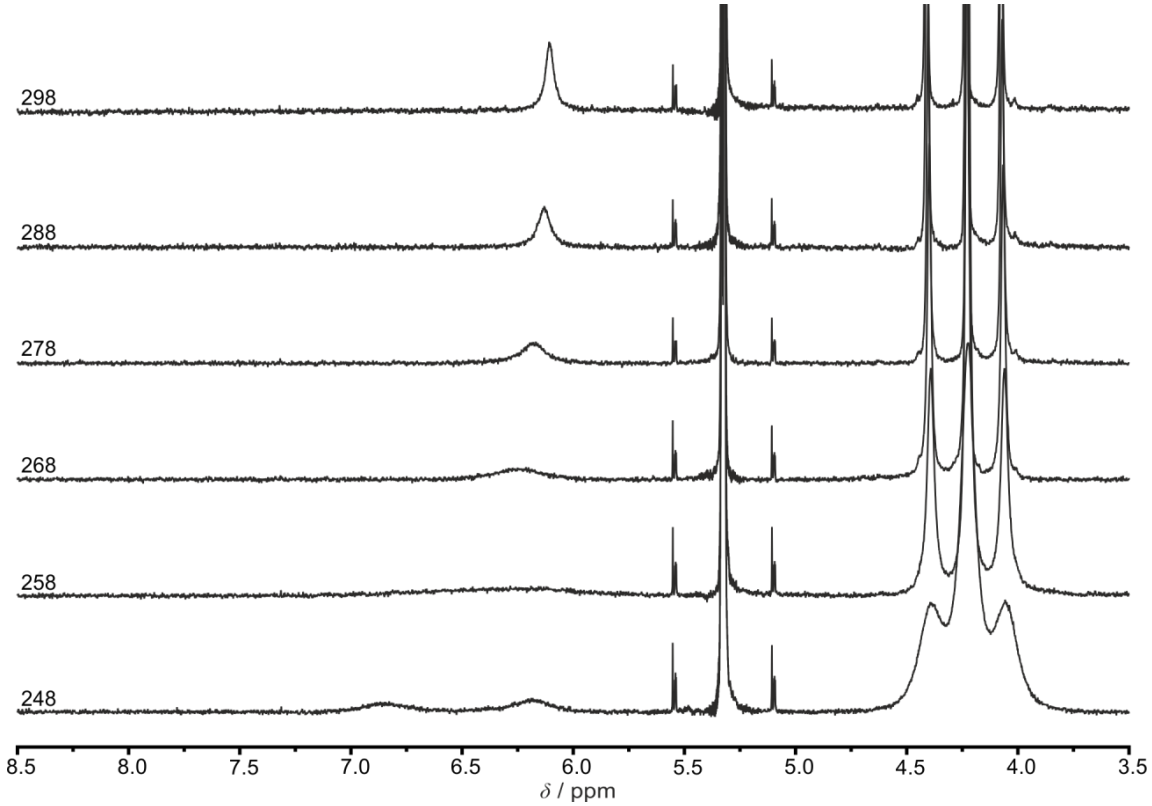

Figure S46. VT ^{1}H NMR spectra of **1** in CD_2Cl_2 (c ≤ 0.005 mol / L, 400 MHz).

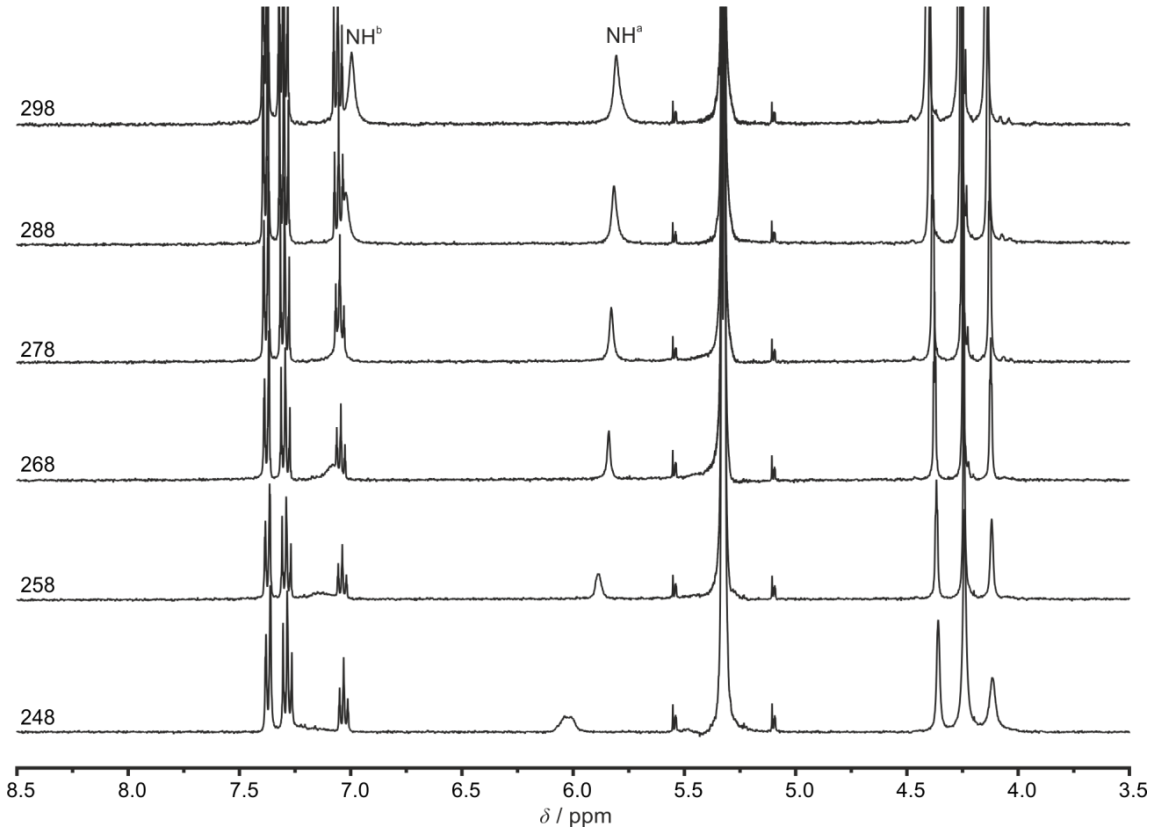

Figure S47. VT ^{1}H NMR spectra of **2** in CD_2Cl_2 (c ≤ 0.005 mol / L, 400 MHz).

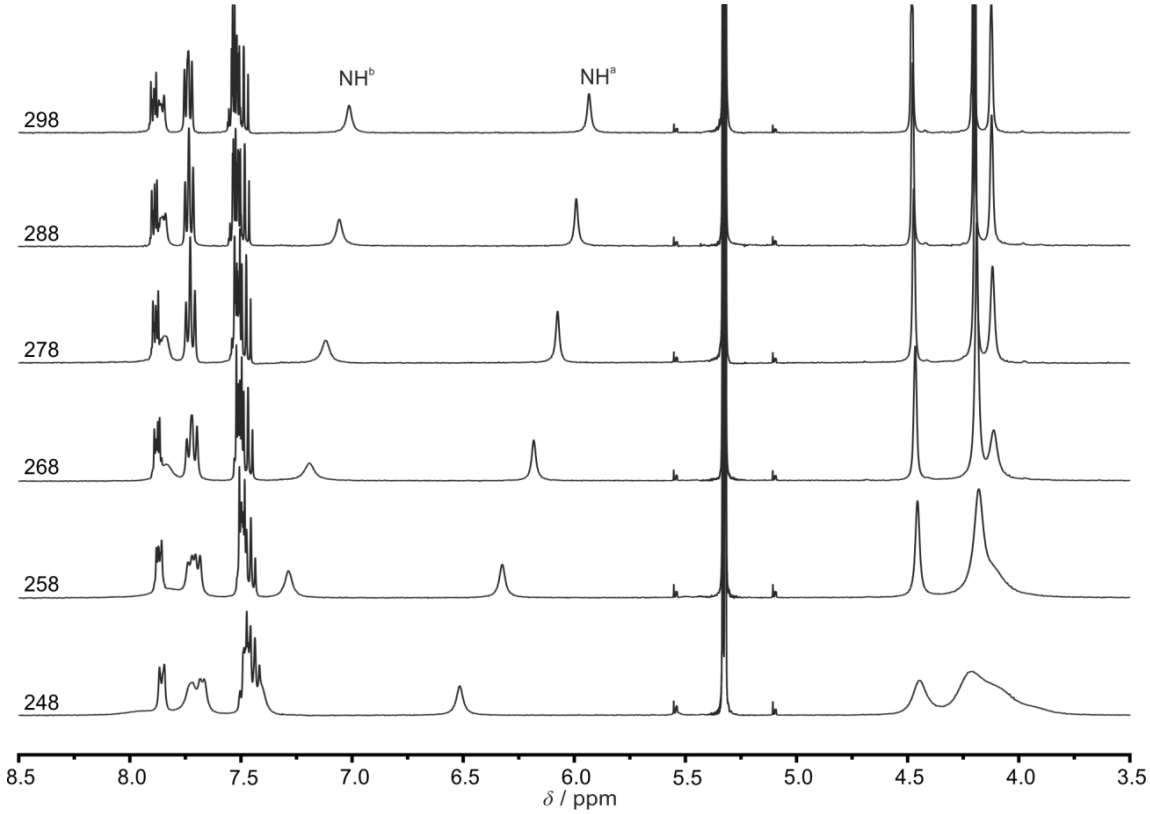

Figure S48. VT ^{1}H NMR spectra of **3** in CD_2Cl_2 ($c \leq 0.005$ mol / L, 400 MHz).

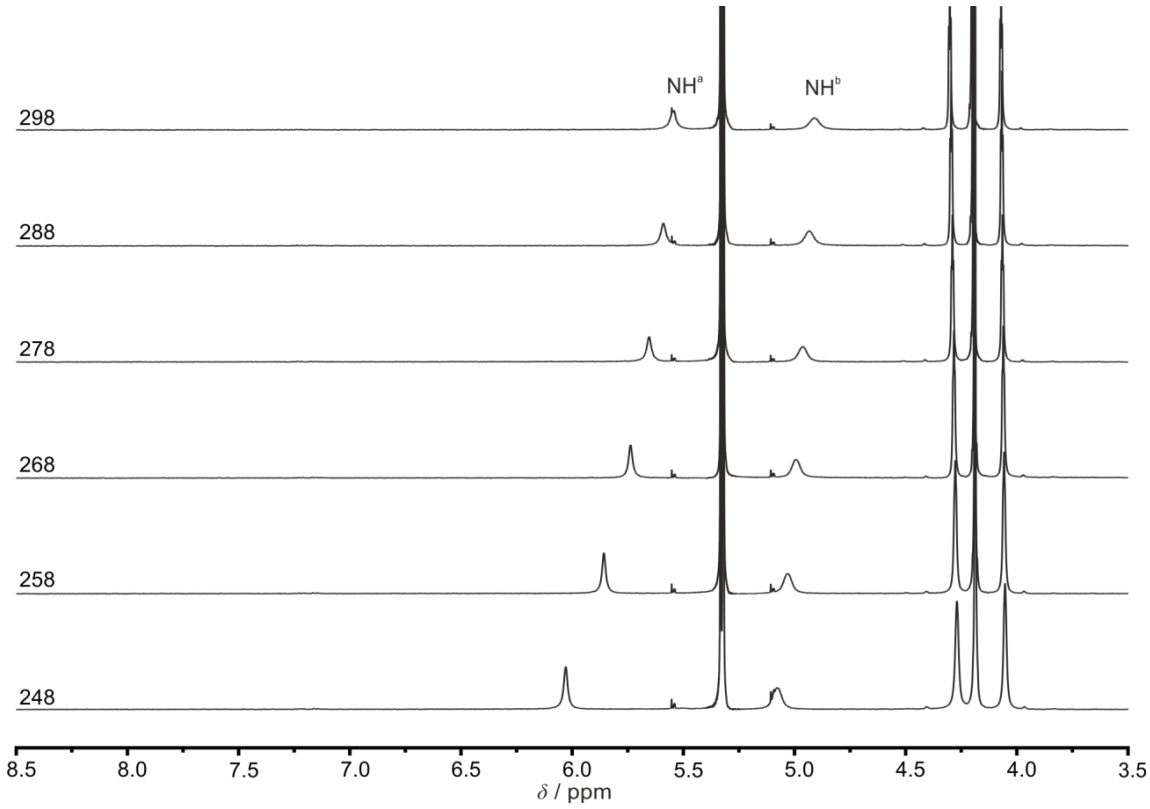

Figure S49. VT ^{1}H NMR spectra of **4** in CD_2Cl_2 ($c \leq 0.005$ mol / L, 400 MHz).

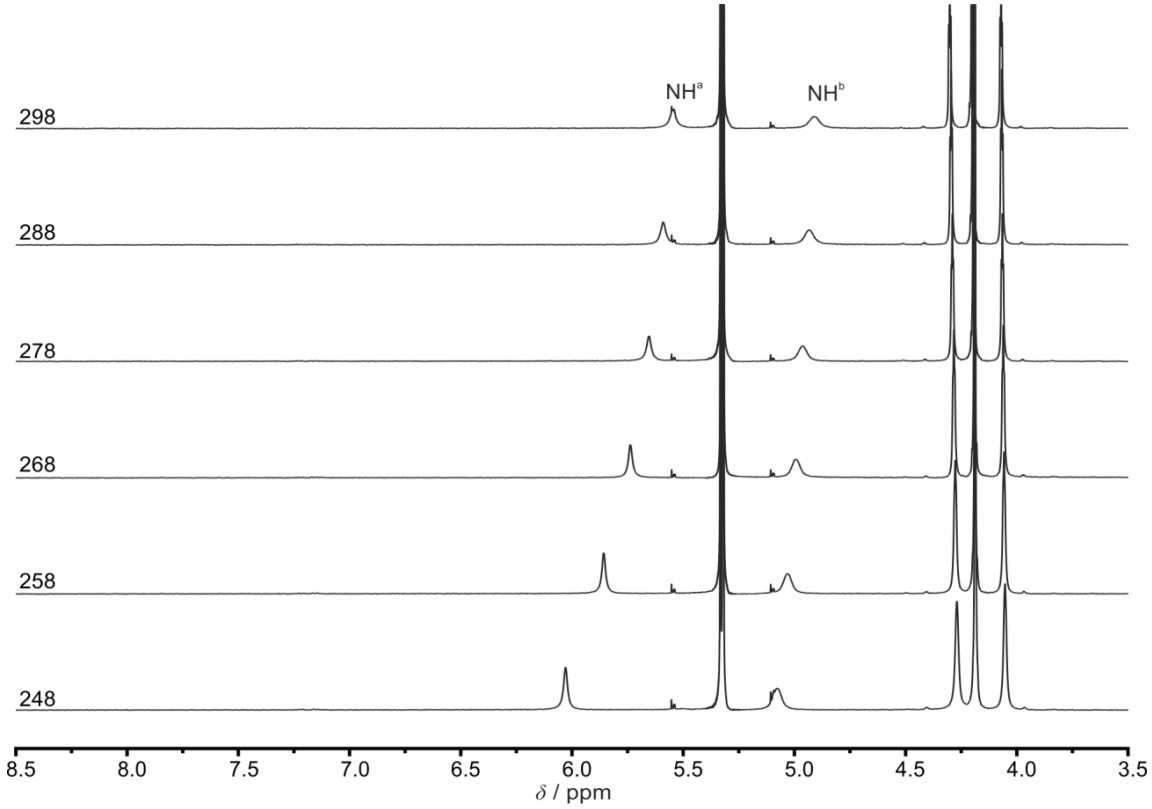

Figure S50. VT ^{1}H NMR spectra of **5** in CD_2Cl_2 (c ≤ 0.005 mol / L, 400 MHz).

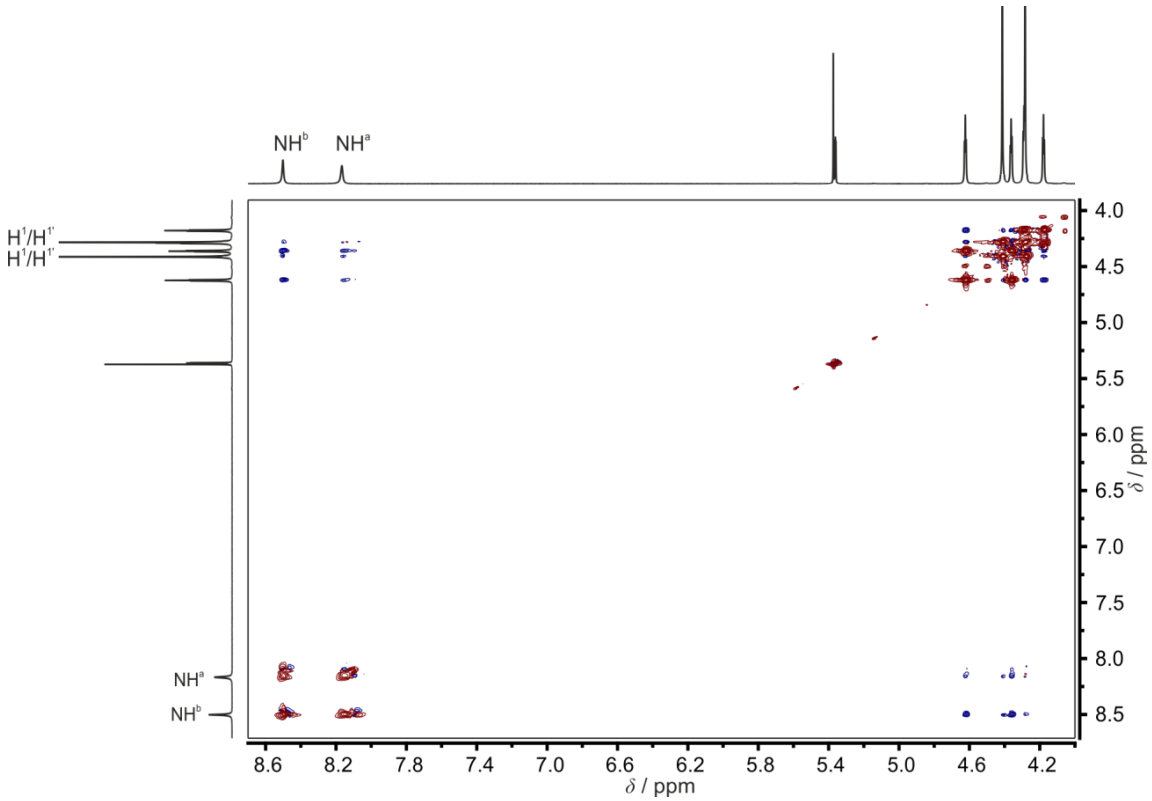

Figure S51. ^{1}H-^{1}H NOESY / EXSY spectrum of **6** in CD_2Cl_2 (c = 0.01 mol / L) at 248 K. NOE contacts are blue, exchange contacts are red.

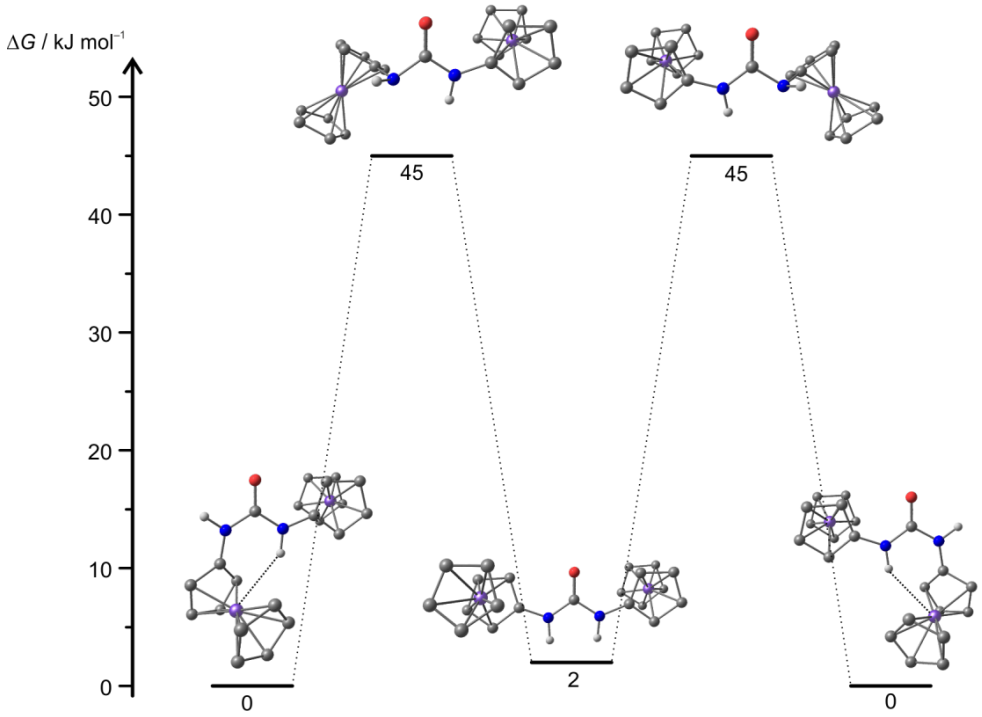

Figure S52. Calculated rotation barrier of **1**.

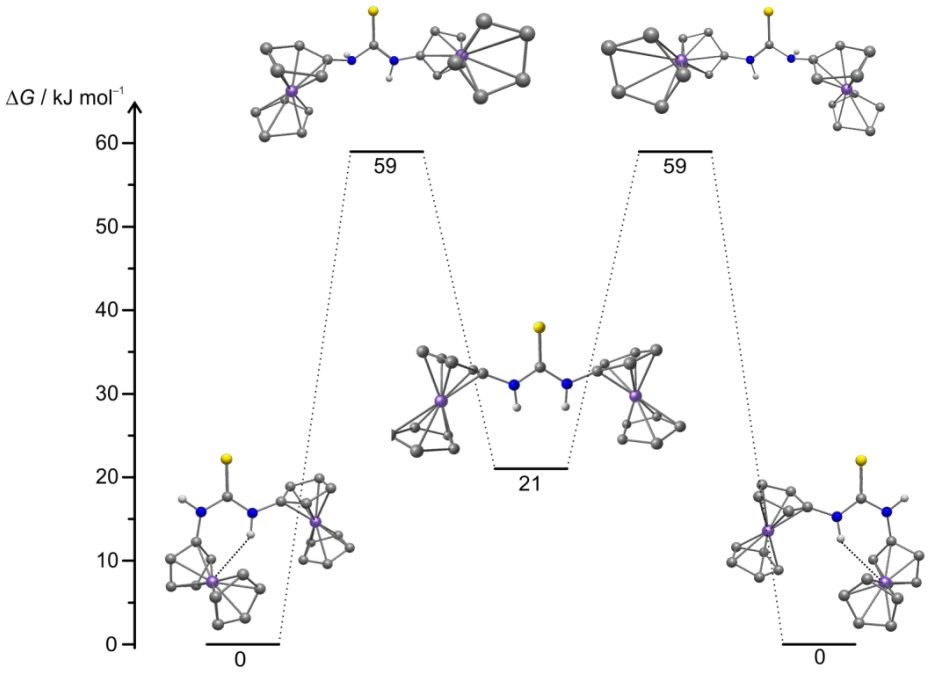

Figure S53. Calculated rotation barrier of **6**.

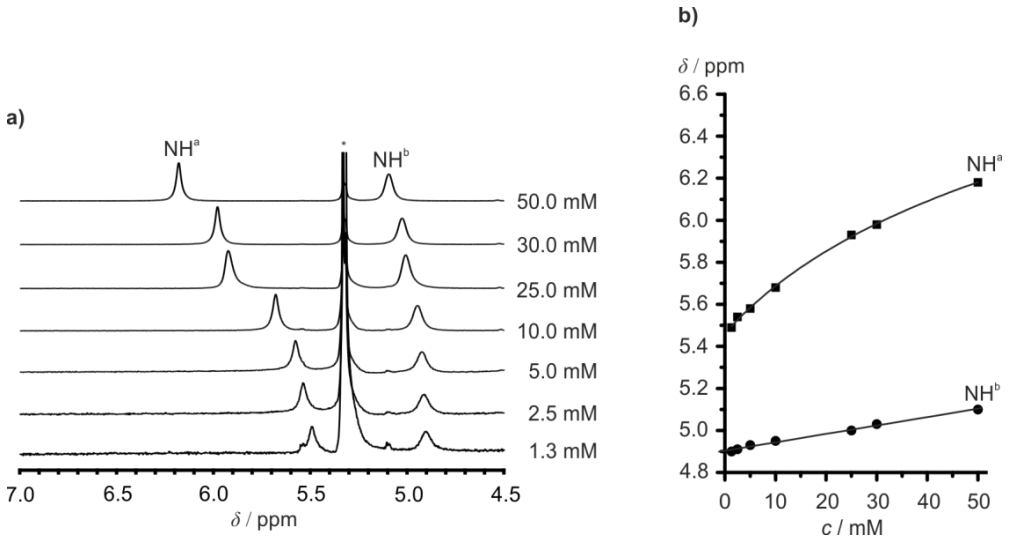

Figure S54. a) Partial VC ^{1}H NMR spectra of **4** in CD_2Cl_2 (* denotes the signal of $CHDCl_2$). b) Plot of the chemical shift δ of the NH proton resonances versus concentration c with linear fit for NH^b with y-axis intercept of δ_0 = 4.90 ppm and fitted curve for NH^a [K = (4.9±0.8) м$^{-1}$, δ_M = (5.46±0.01) ppm, δ_D = (8.18±0.27) ppm, R^2 = 0.9991].

$$\delta = \delta_D + (\delta_M - \delta_D)\left(-\frac{1}{4Kc} + \sqrt{\frac{1+8Kc}{16K^2c^2}}\right)$$

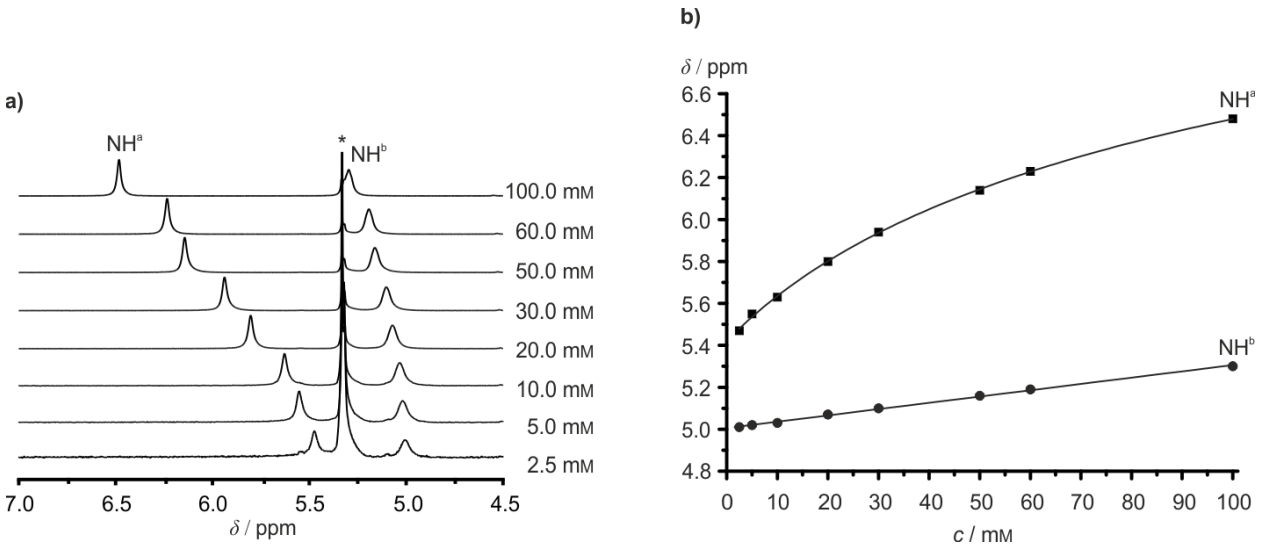

Figure S55. a) Partial VC ^{1}H NMR spectra of **5** in CD_2Cl_2 (* denotes the signal of $CHDCl_2$). b) Plot of the chemical shift δ of the NH proton resonances versus concentration c with linear fit for NH^b with y-axis intercept of δ_0 = 5.01 ppm and fitted curve for NH^a [K = (4.1±0.3) м$^{-1}$, δ_M = (5.42±0.01) ppm, δ_D = (8.45±0.12) ppm, R^2 = 0.9996].

$$\delta = \delta_D + (\delta_M - \delta_D)\left(-\frac{1}{4Kc} + \sqrt{\frac{1+8Kc}{16K^2c^2}}\right)$$

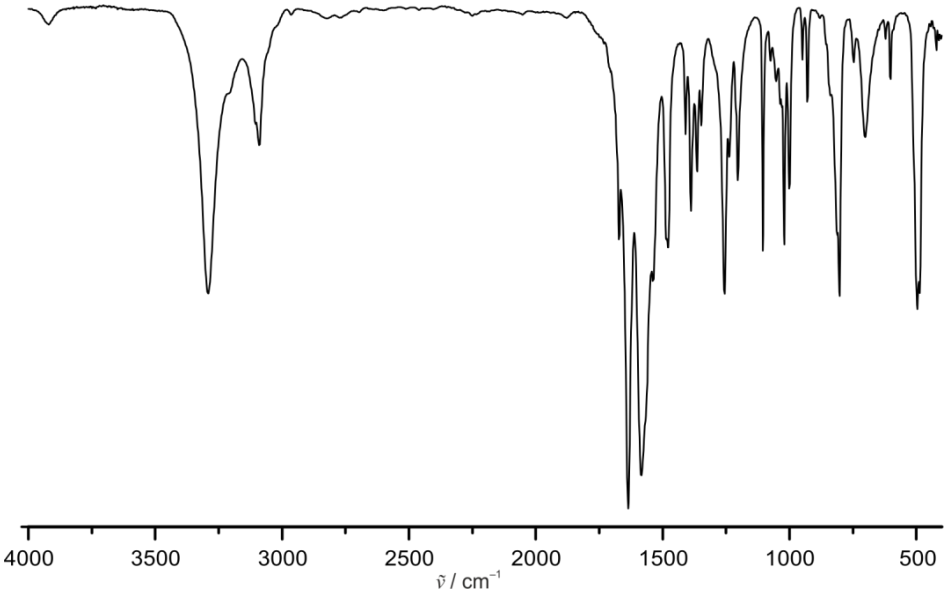

Figure S56. IR spectrum of **1** in KBr.

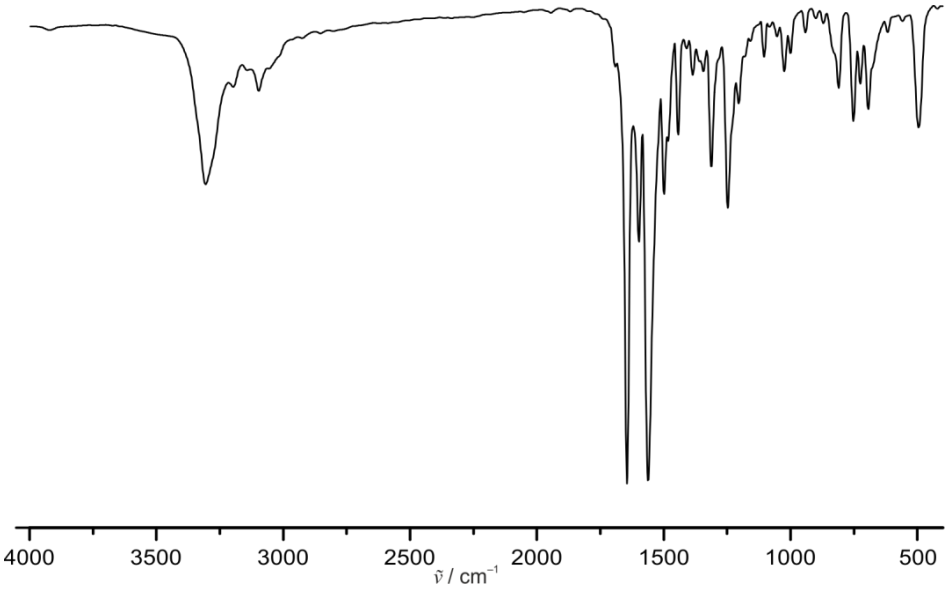

Figure S57. IR spectrum of **2** in KBr.

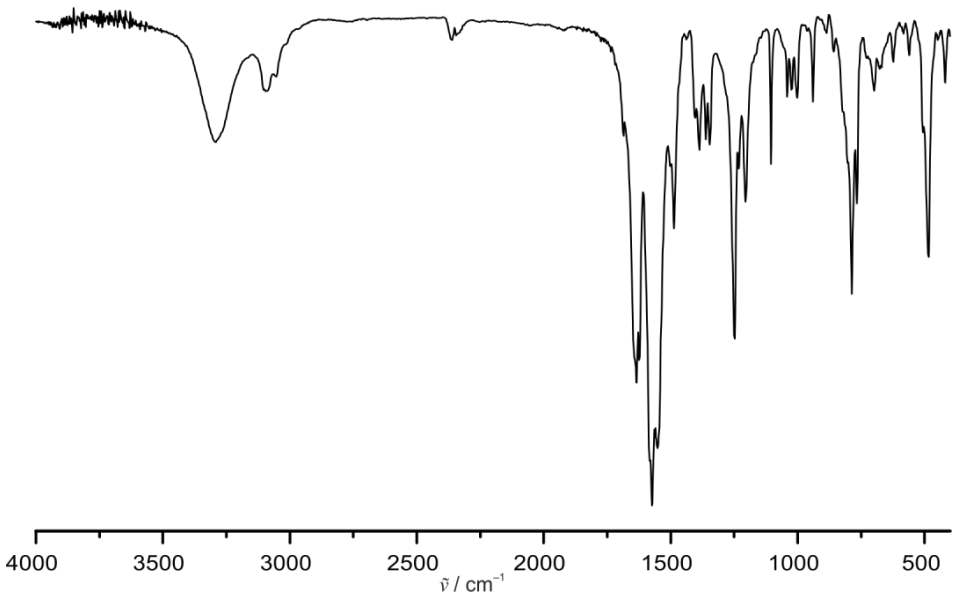

Figure S58. IR spectrum of **3** in KBr.

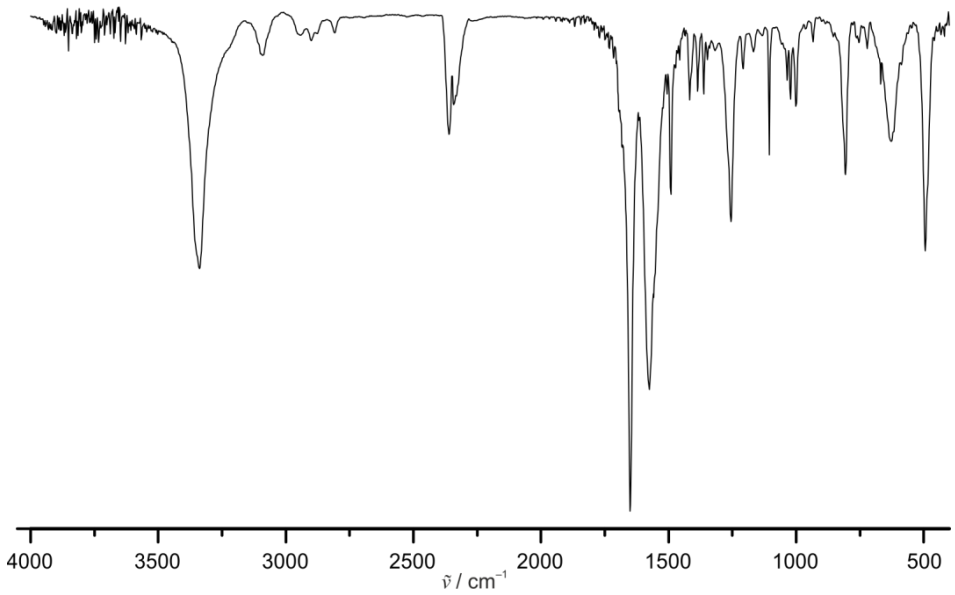

Figure S59. IR spectrum of **4** in KBr.

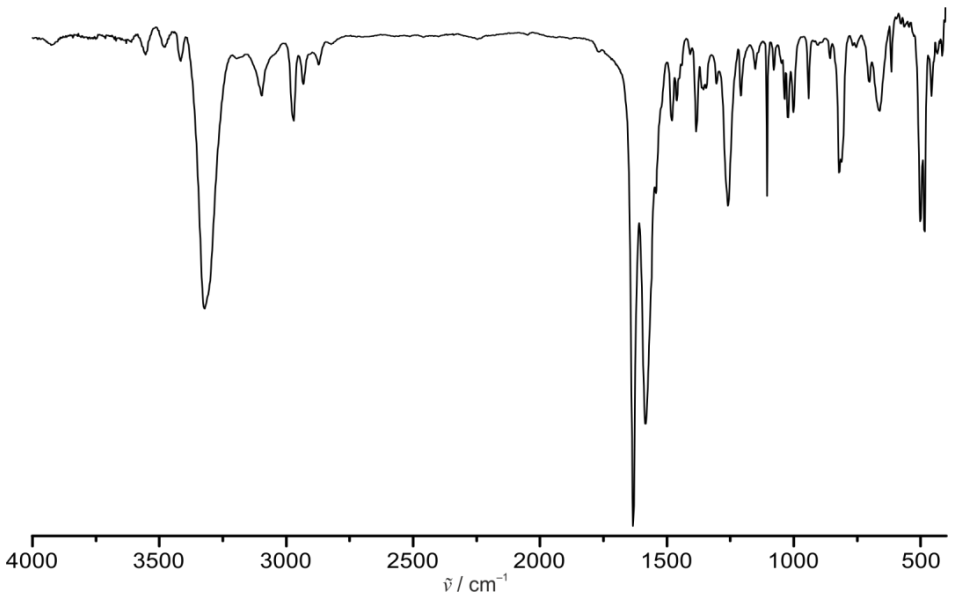

Figure S60. IR spectrum of **5** in KBr.

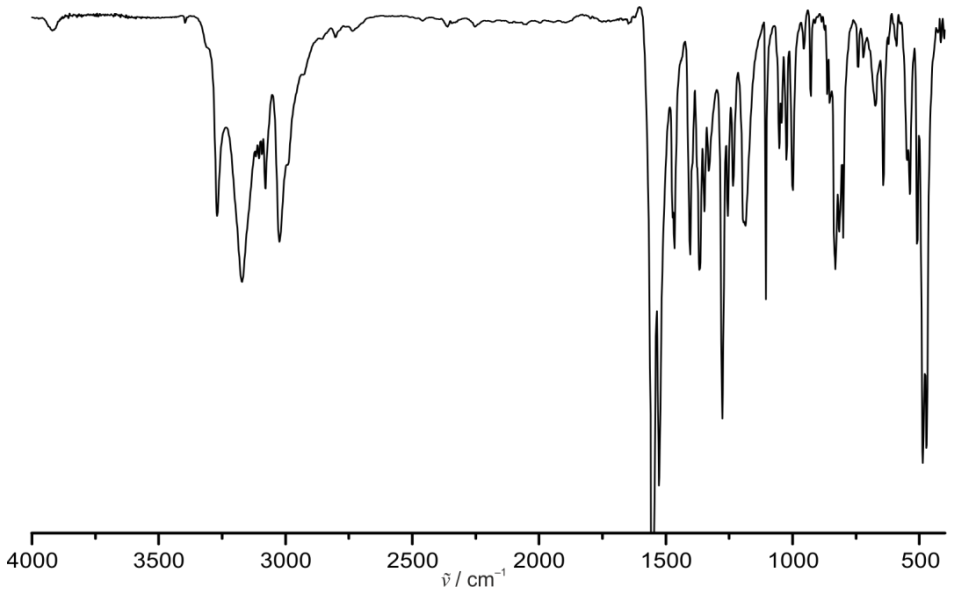

Figure S61. IR spectrum of **6** in KBr.

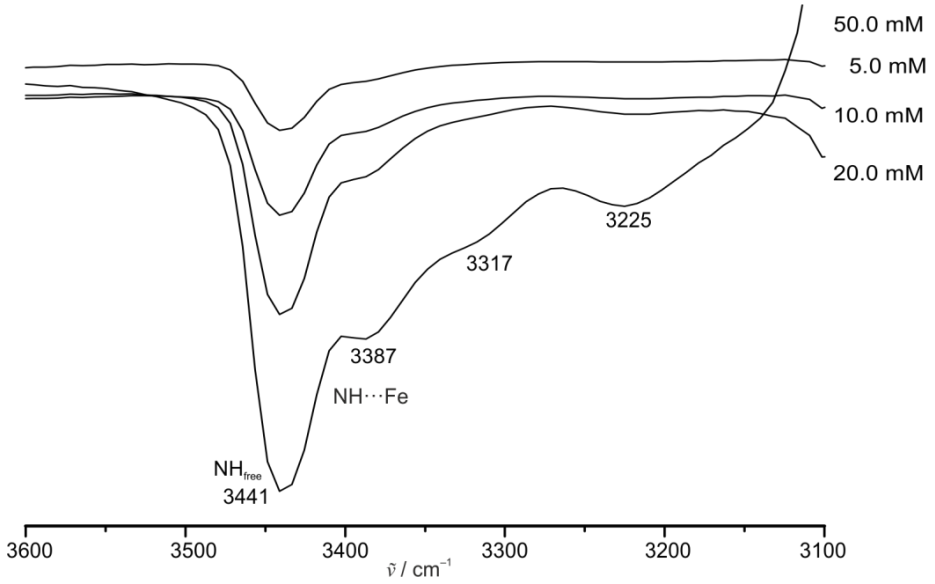

Figure S62. VC IR spectra of **4** in CH_2Cl_2.

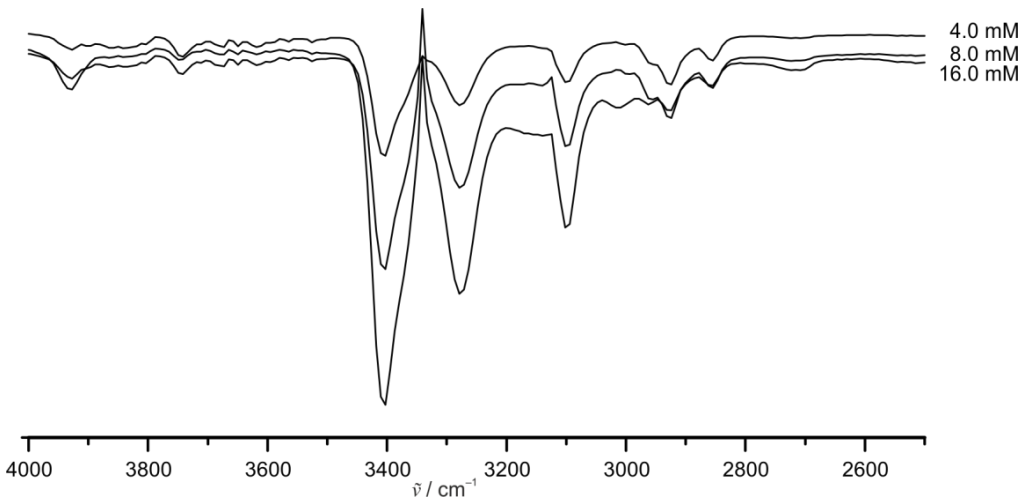

Figure S63. VC IR spectra of **6** in CD_2Cl_2.

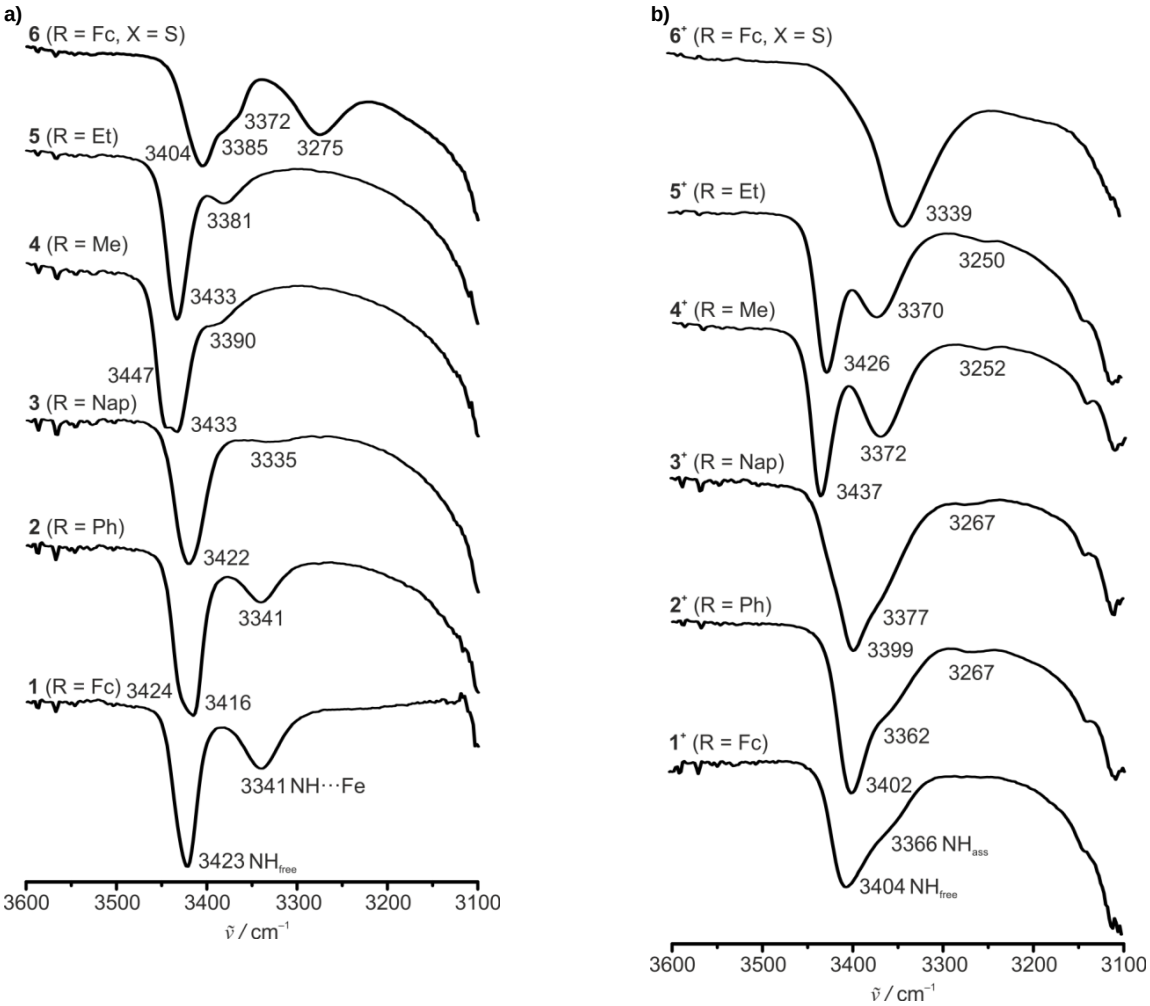

Figure S64. a) IR spectra of **1–6** in CH_2Cl_2 (NH region, *c* = 5.0 mM **1**, **2**, **4–6**; *c* = 3.0 mM **3**); b) IR spectra of **1[SbF6]–6[SbF6]** in CH_2Cl_2 (NH region, c ≈ 5.0 mM).

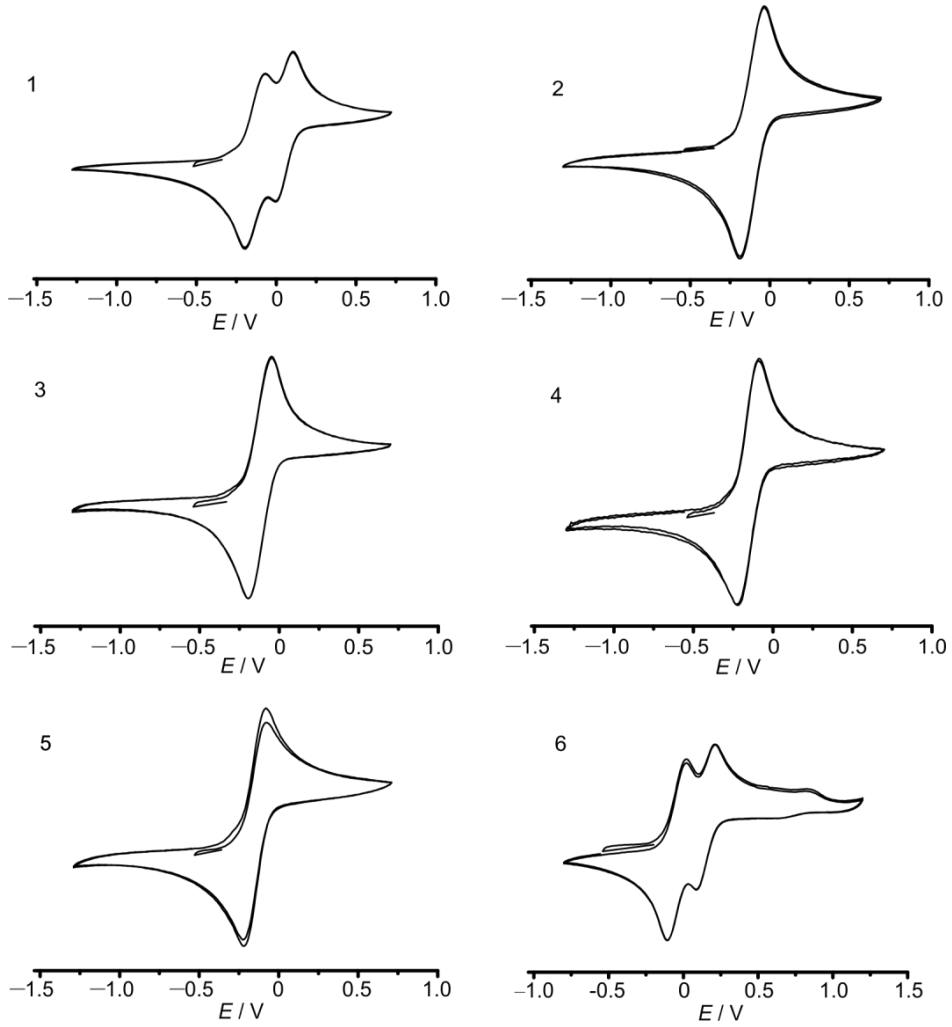

Figure S65. Cyclic voltammograms of **1**–**6** in CH_2Cl_2 ([*n*Bu_4N][$B(C_6H_5)_4$]).

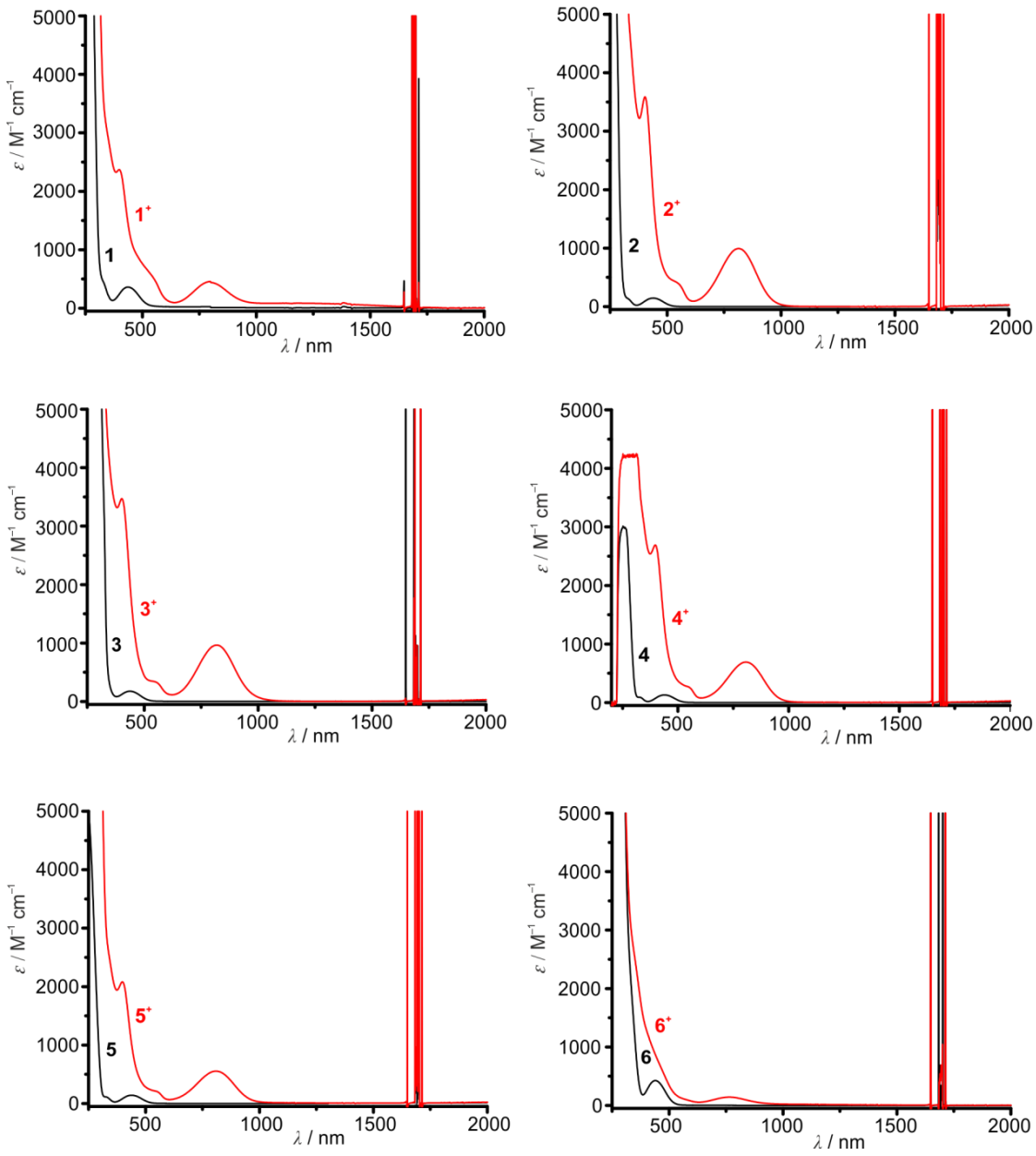

Figure S66. UV/Vis spectra of **1**–**6** (black) and **1⁺**–**6⁺** (red) in CH_2Cl_2.

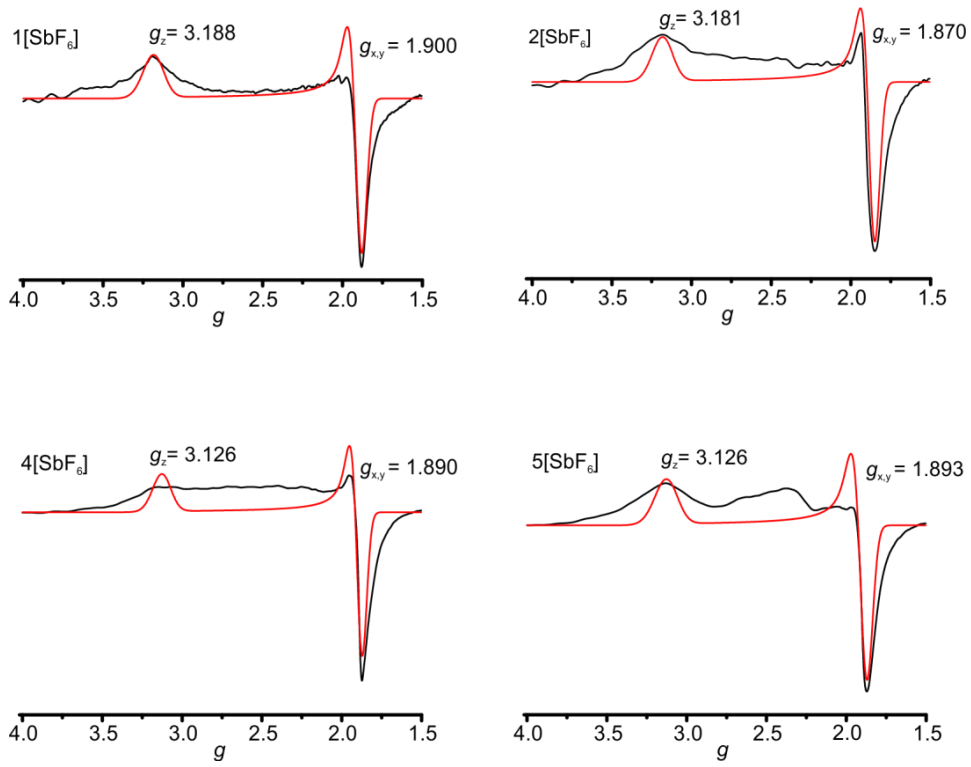

Figure S67. X-band EPR spectra of **1[SbF6]**, **2[SbF6]**, **4[SbF6]** and **5[SbF6]** in CH_2Cl_2 at 77K (black) and simulated spectra (red).

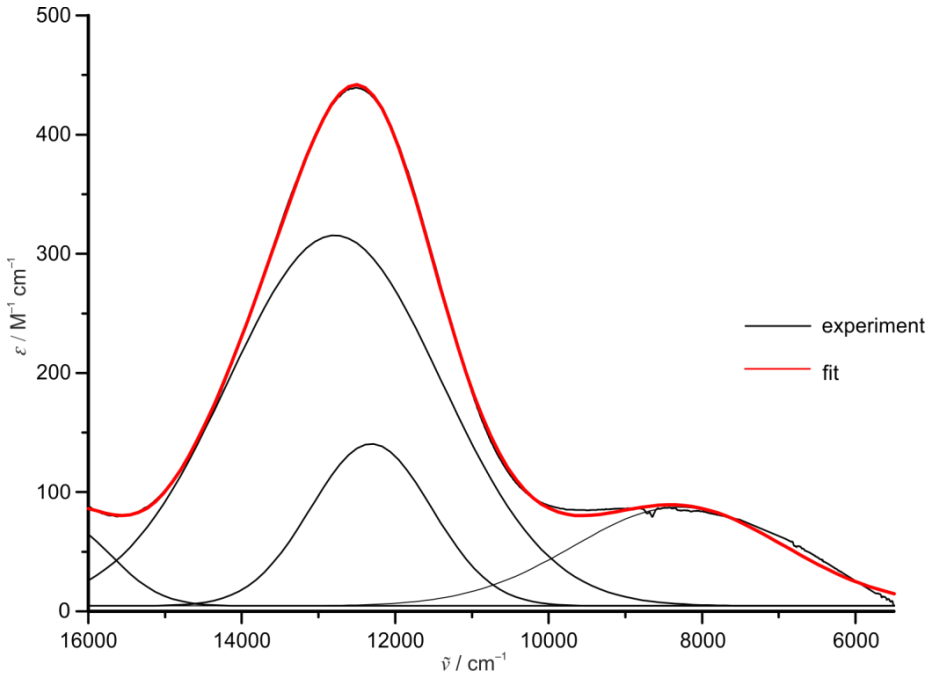

Figure S68. Gaussian deconvolution of the UV/Vis spectrum of **1** in CH_2Cl_2. The H_{AB} value was determined by the Hush formula:

$$H_{AB} = 2.06 \cdot 10^{-2} (\tilde{\nu}_{max} \cdot \varepsilon_{max} \cdot \Delta\tilde{\nu}_{0.5})^{\frac{1}{2}} \cdot r_{AB}^{-1}$$

$$\tilde{\nu}_{max} = 8301\,cm^{-1},\ \Delta\tilde{\nu}_{0.5} = 2750\,cm^{-1},\ \varepsilon_{max} = 87\ M^{-1}cm^{-1},\ r_{AB} = 7.5\ Å$$

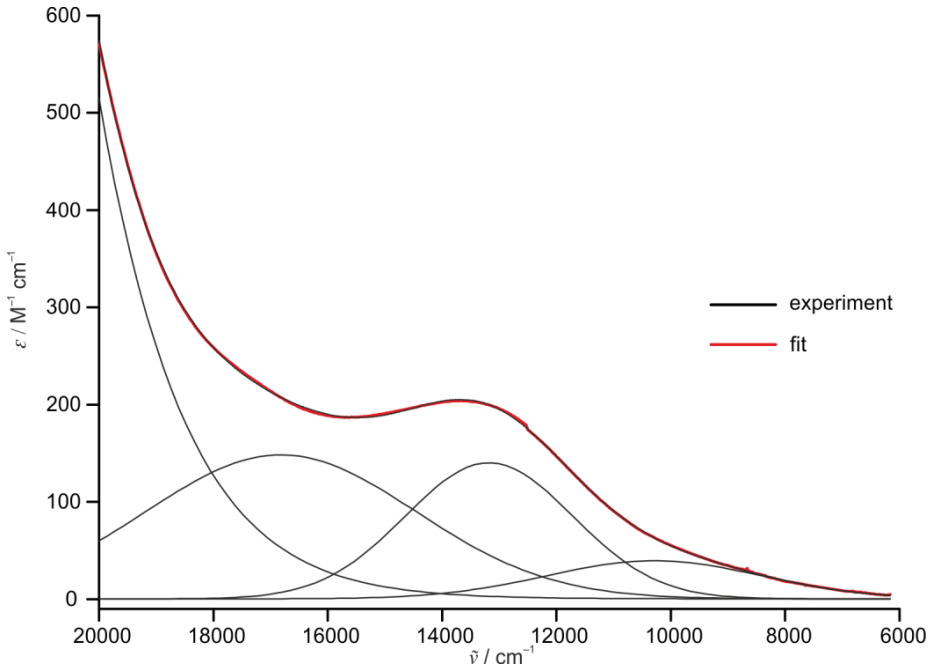

Figure S69. Gaussian deconvolution of the UV/Vis spectrum of **6** in CH_2Cl_2. The H_{AB} value was determined using:

$$\tilde{\nu}_{max} = 10293\,cm^{-1},\ \Delta\tilde{\nu}_{0.5} = 3751\,cm^{-1},\ \varepsilon_{max} = 40\ M^{-1}cm^{-1},\ r_{AB} = 7.5\ Å$$

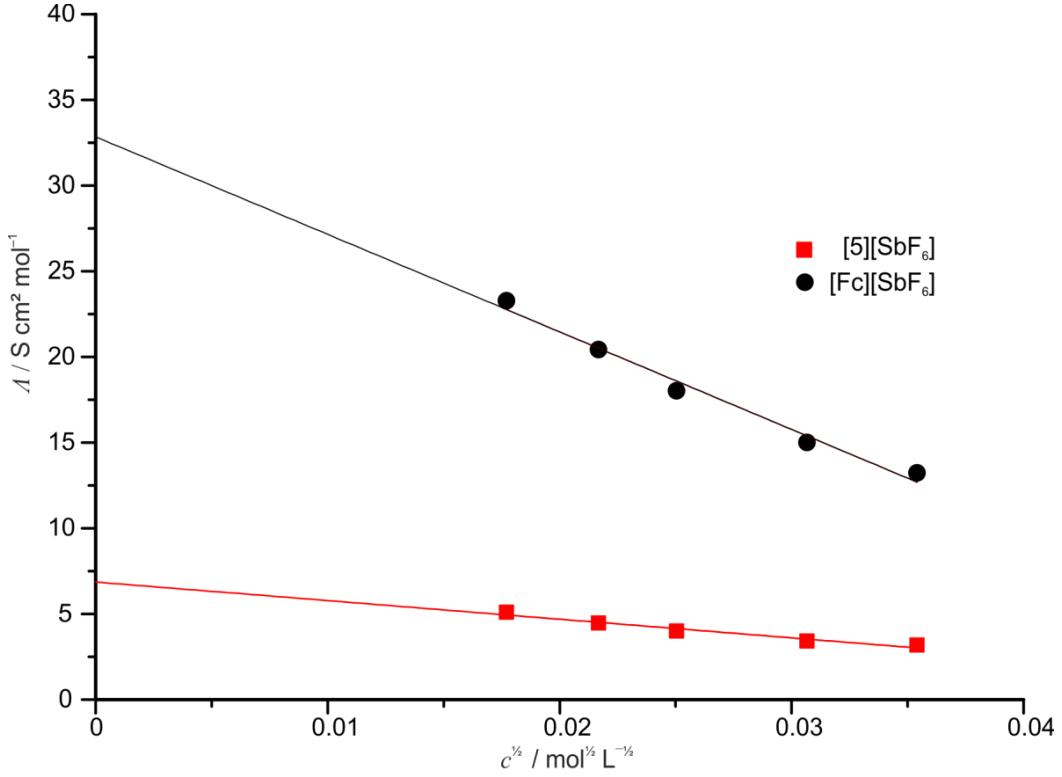

Figure S70. Molar conductivity of **[5][SbF₆]** and **[Fc][SbF₆]** in CH_2Cl_2.

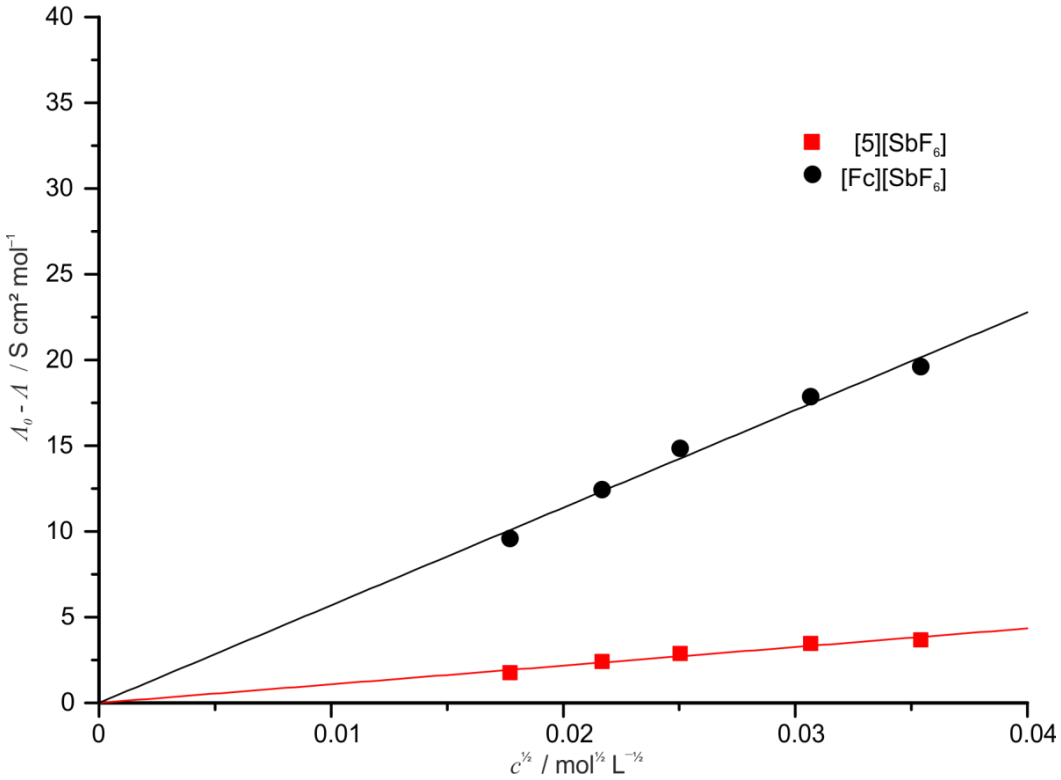

Figure S71. Onsager plots of **[5][SbF$_6$]** and **[Fc][SbF$_6$]** in CH_2Cl_2.

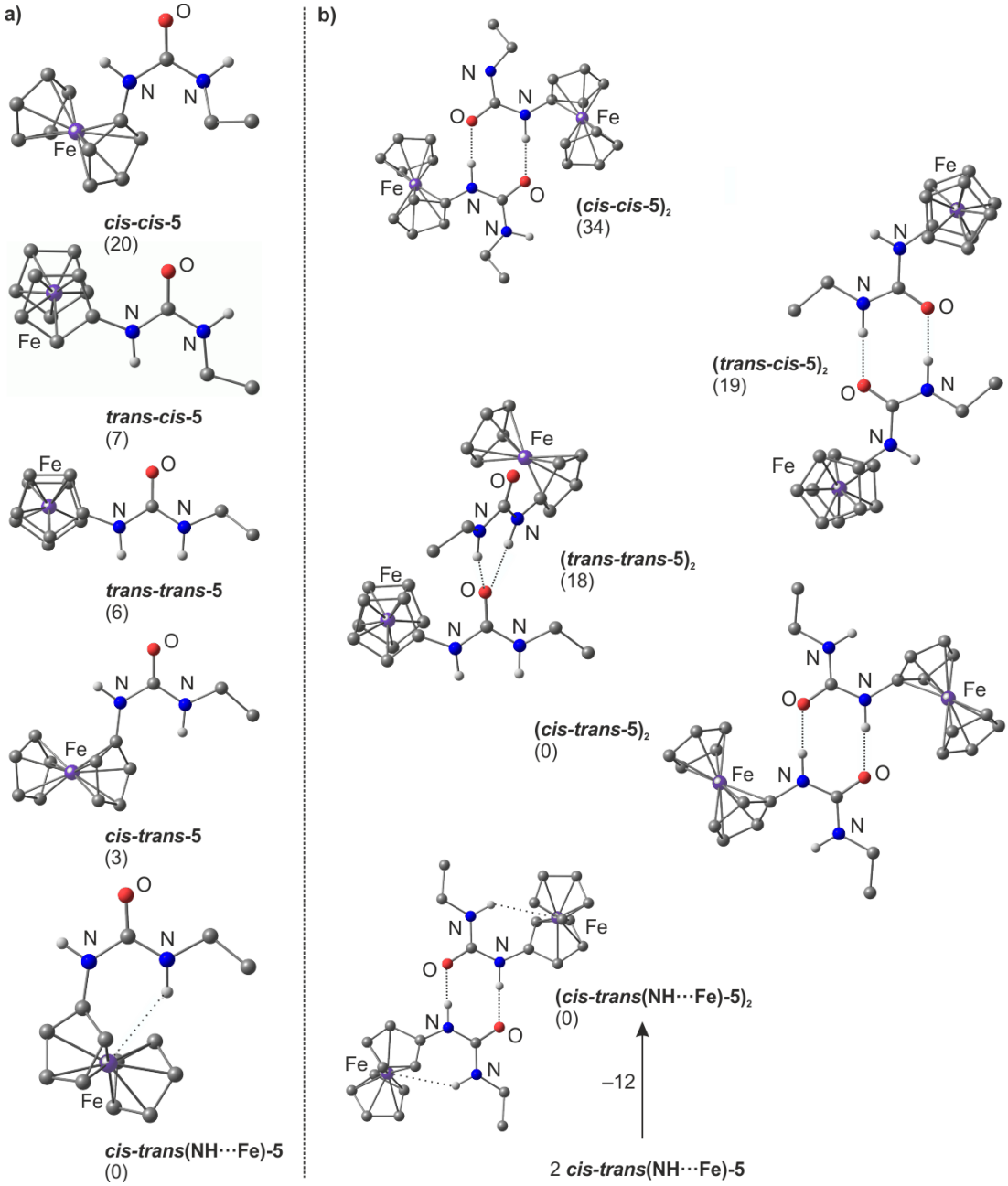

Figure S72. DFT calculated geometries and relative Gibbs free energies ΔG in kJ mol^{-1} of **a)** relevant isomers and **b)** dimers of **5**.

Table S2. DFT[a] calculated relative Gibbs free energies Δ*G* in kJ mol^{-1} of relevant isomers of singly oxidized ferrocenyl (thio)ureas **1**,**5** and **6**, both as cation and as ion pair with a coordinated SbF_6^- anion.

	***cis-trans*(NH···Fe^{III})**	***cis-trans***	***trans-trans***	***trans-cis*(NH···Fe^{II})**	***trans-cis***	***cis-cis***
1						
cation	–[b]	–[b]	7	4	0	24
ion pair	33	–[b]	0	39[c]	10	
5						
cation	18	15	0	–	2	23
ion pair	24	23	0	–	10	37
6						
cation	–[b]	–[b]	19	1	0	8
ion pair	19	–[b]	6	24[c]	0	7

[a] B3LYP/LANL2DZ with polarization functions, PCM CH_2Cl_2, dispersion correction. [b] The charge is preferentially localized on the Fc moiety next to the *trans*-NH, which is assigned as *trans-cis* conformation. [c] Intervalence charge transfer excited state of the *cis-trans*(NH···Fe^{III}) conformer.

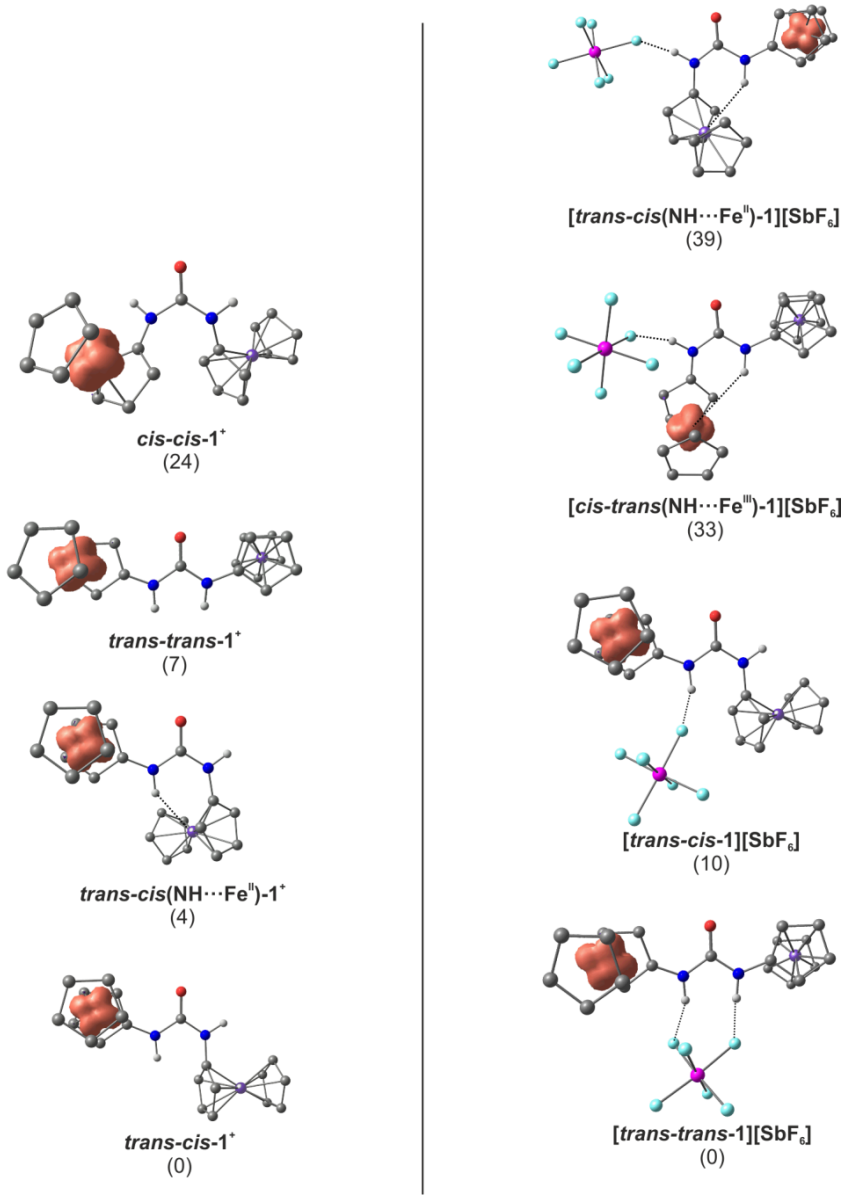

Figure S73. DFT calculated geometries and relative Gibbs free energies ΔG in kJ mol^{-1} of relevant isomers of singly oxidized diferrocenyl urea **1**$^{+}$.

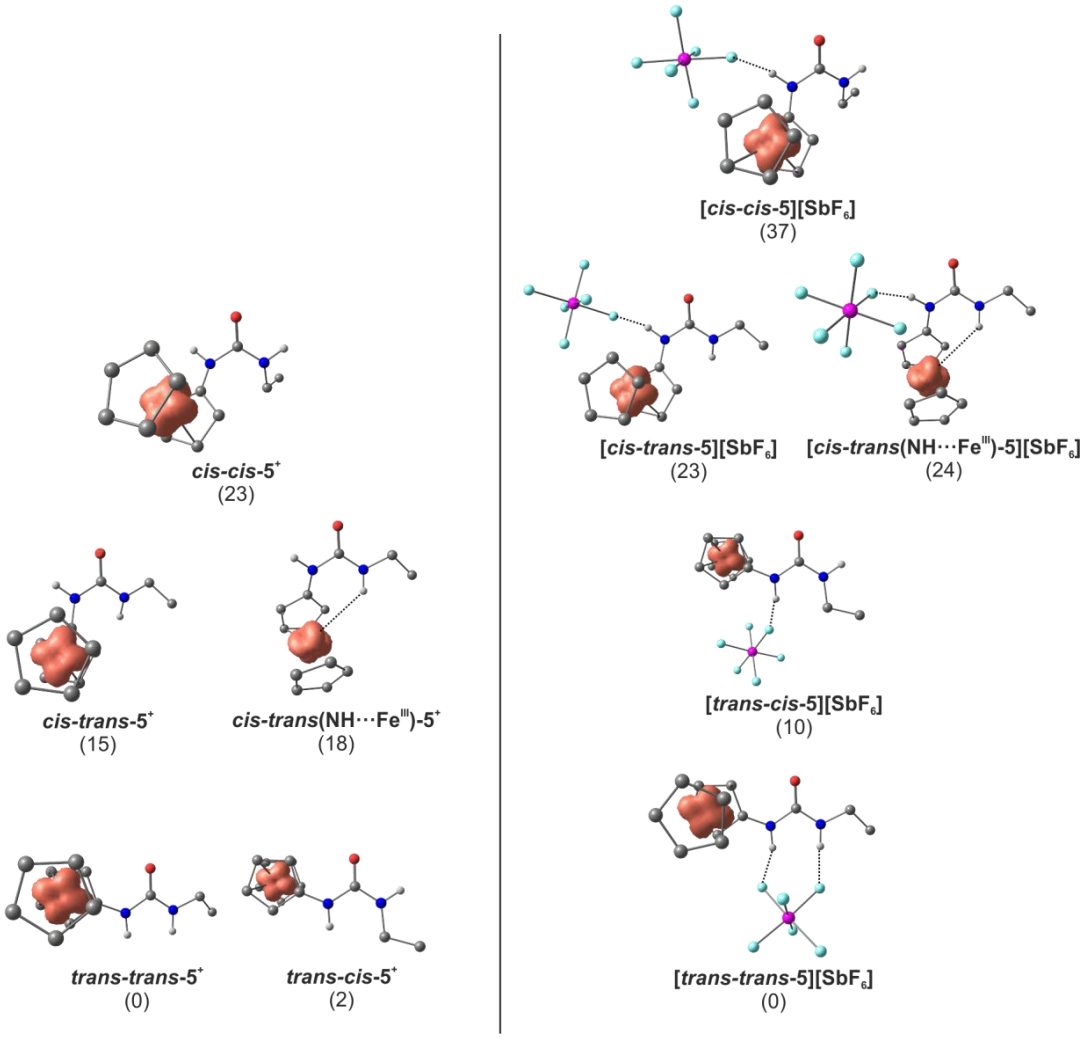

Figure S74. DFT calculated relative Gibbs free energies ΔG in kJ mol^{-1} of relevant isomers of oxidized ethyl ferrocenyl urea **5**$^{+}$.

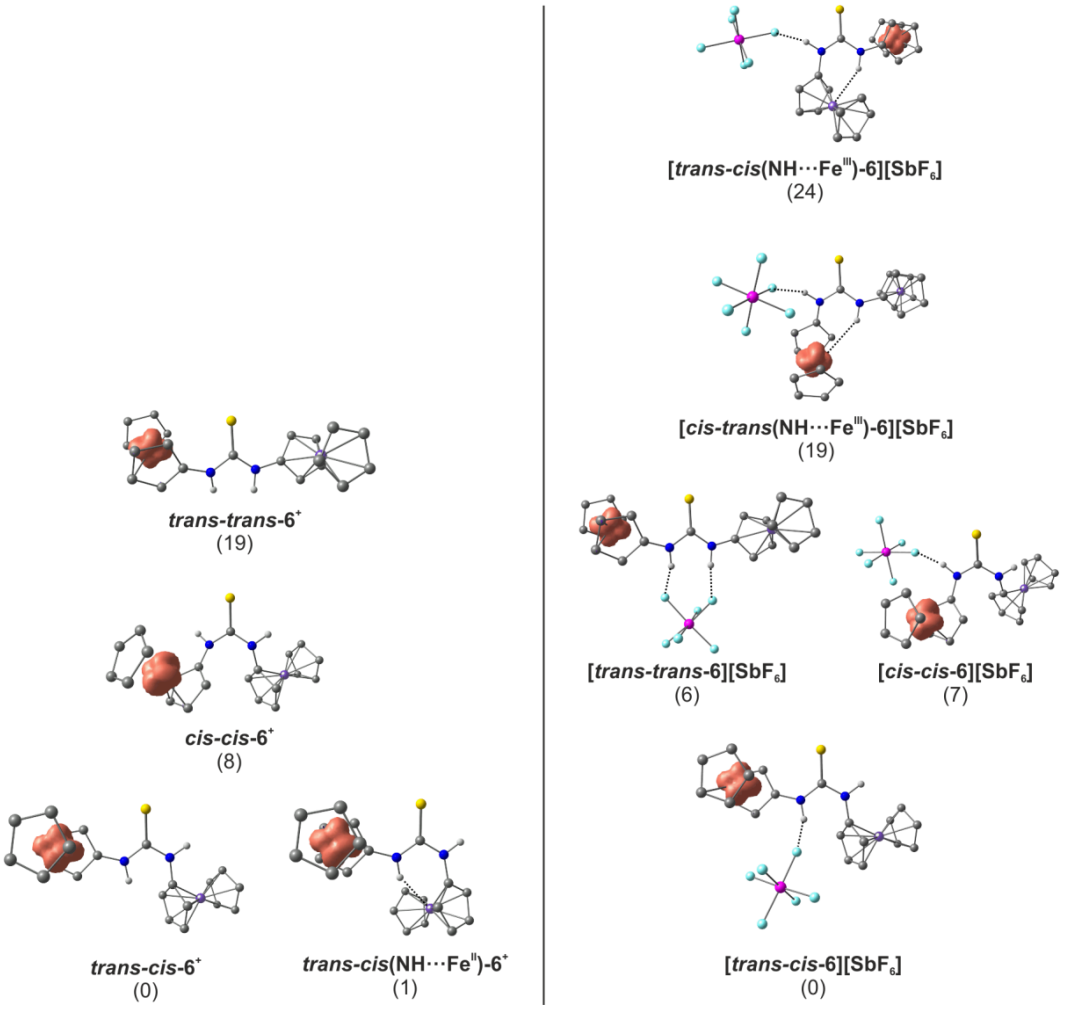

Figure S75. DFT calculated relative Gibbs free energies ΔG in kJ mol^{-1} of relevant isomers of singly oxidized diferrocenyl thiourea **6**$^+$.

7.2 Stereochemical consequences of oxygen atom transfer and electron transfer in imido/oxido molybdenum(IV, V, VI) complexes with two unsymmetric bidentate ligands

Kristina Hüttinger[a], Christoph Förster[a], Timo Bund[b], Dariush Hinderberger[b], and Katja Heinze[a]*

[a] Institute of Inorganic Chemistry and Analytical Chemistry, Johannes Gutenberg-University of Mainz, Duesbergweg 10-14, 55128 Mainz, Germany; Fax: +49-6131-39-27277

katja.heinze@uni-mainz.de

[b] Max Planck Institute for Polymer Research, Ackermannweg 10, 55128 Mainz, Germany

Supporting Information

Figure S1. Energy profiles of the Mo=N-C bending deformation in $\mathbf{2^H}$, $\mathbf{5^H}$ and $\mathbf{[5^H]^+}$ obtained by DFT calculations with fixed Mo=N-C angles and optimized geometry.

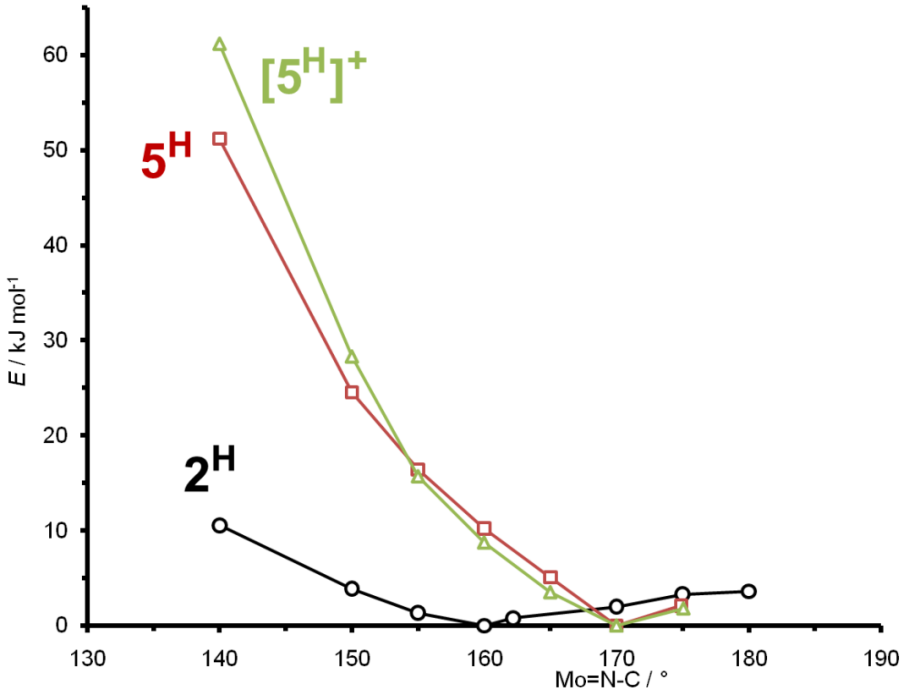

Figure S2. $^{31}P\{^{1}H\}$ NMR reaction monitoring of the reactions $\mathbf{1}^{t\mathbf{Bu}}$ + PMe_3 and $\mathbf{2}^{t\mathbf{Bu}}$ + PMe_3 in THF at room temperature.

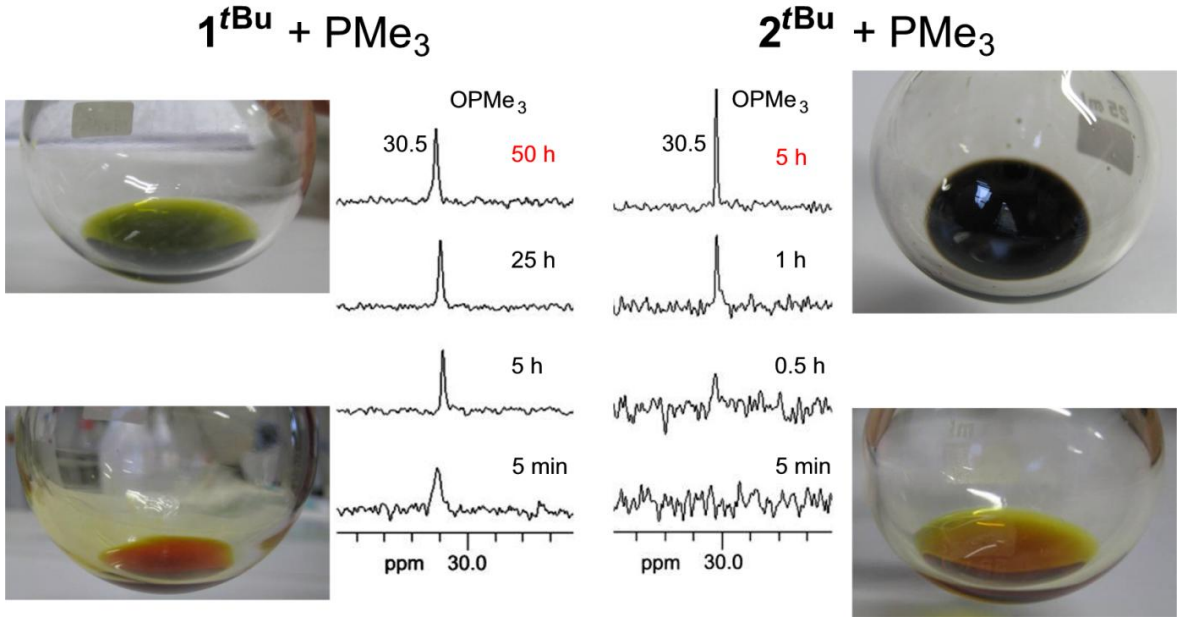

Figure S3. NH-HMBC of **HL**^{tBu} in d_8-THF.

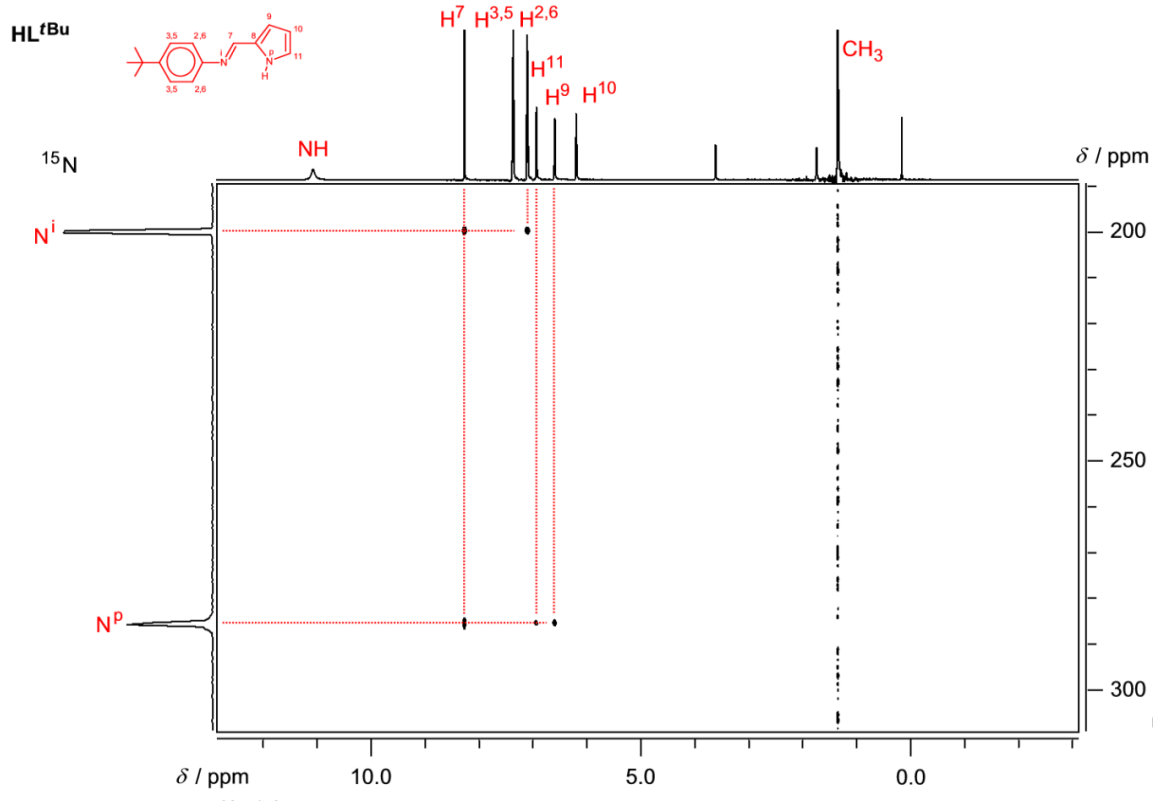

Figure S4. NH-HMBC of **1**^{tBu} in d_8-THF.

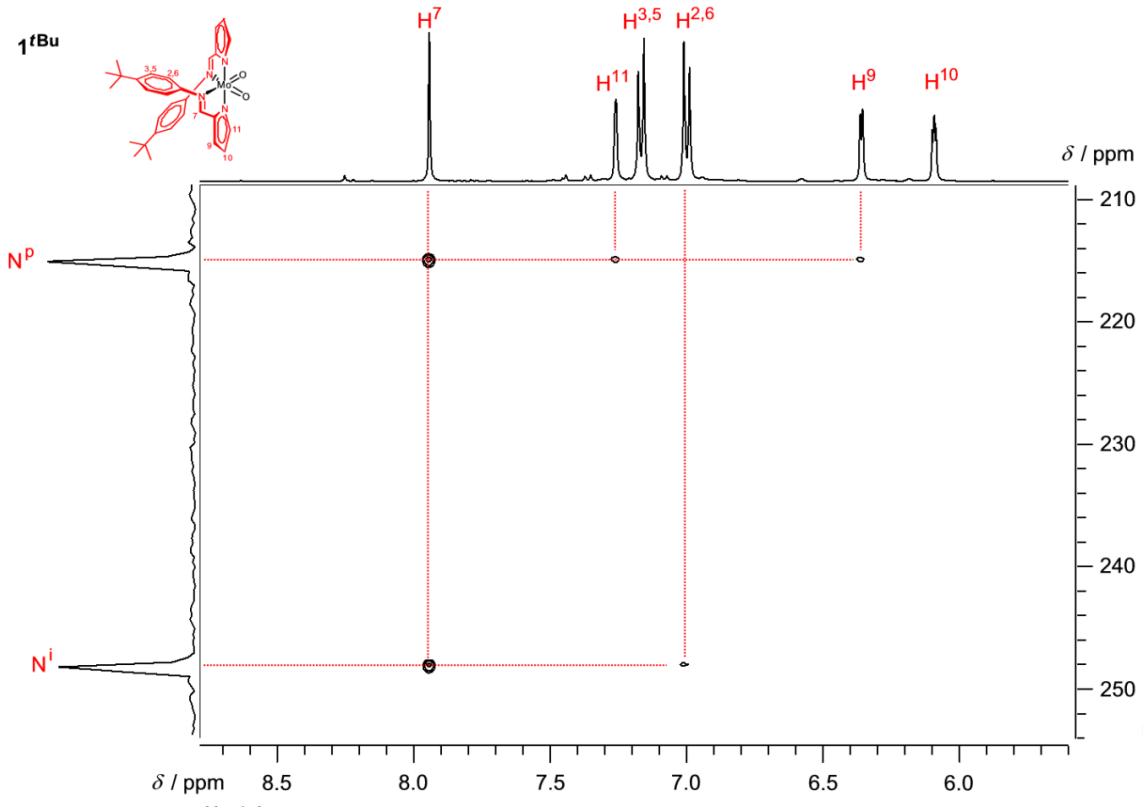

Figure S5. NH-HMBC of **2**^{tBu} in d_8-THF.

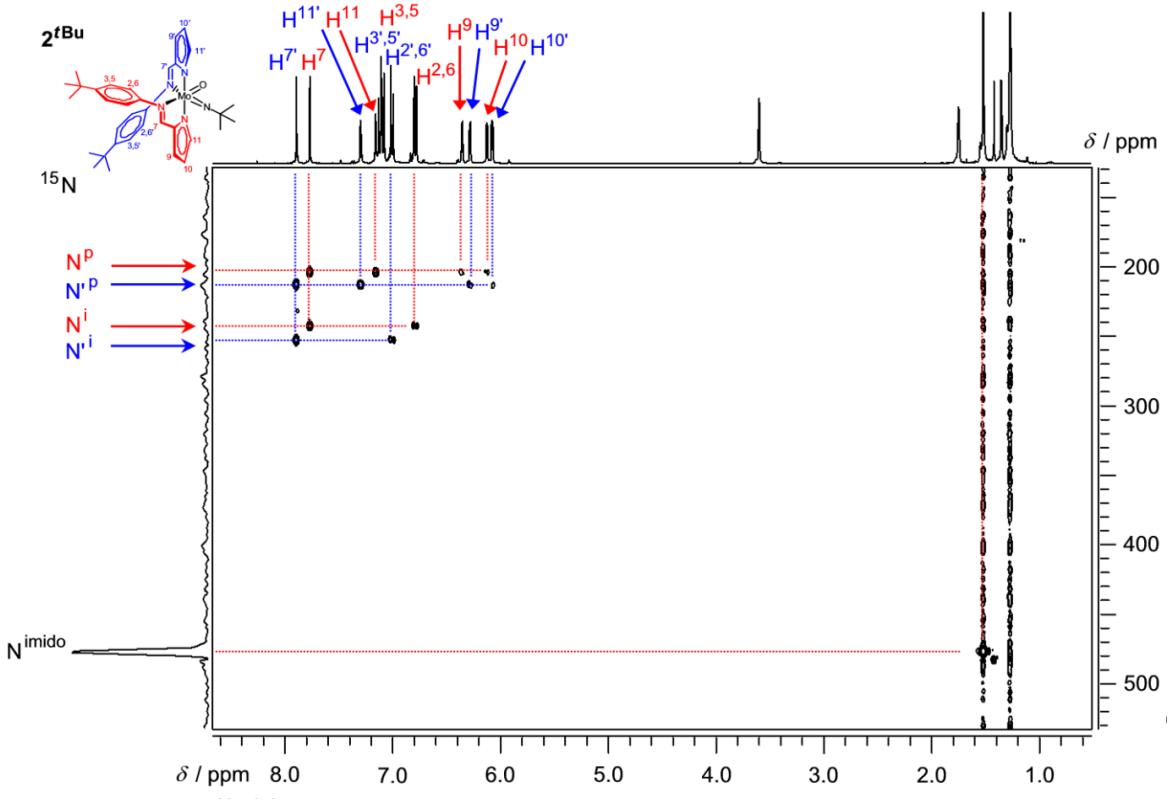

Figure S6. NH-HMBC of **4**^{tBu} in d_8-THF.

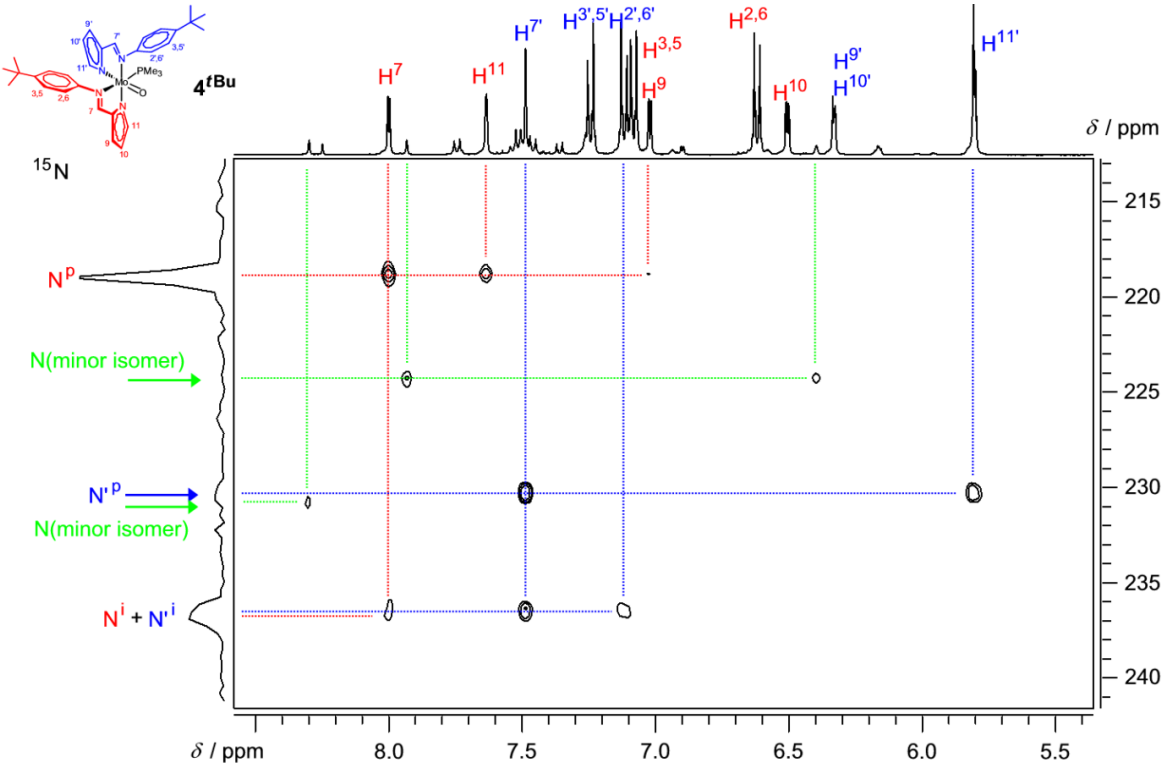

Figure S7. NH-HMBC of **5**^{tBu} in d_8-THF.

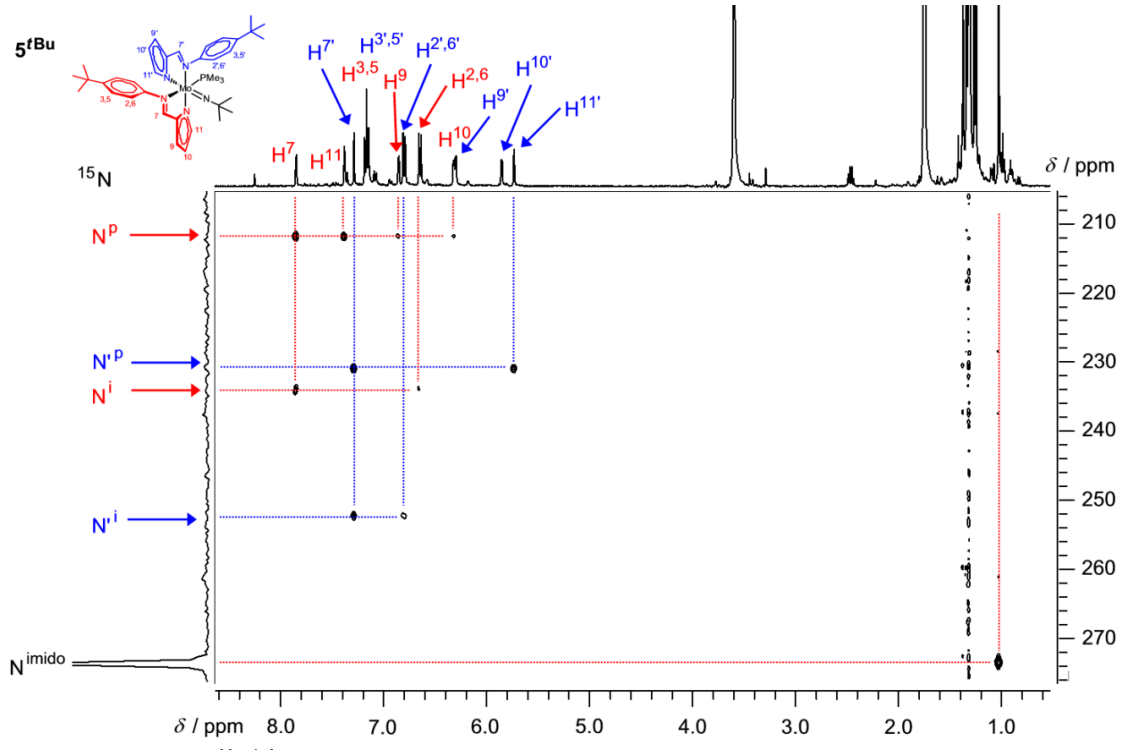

Figure S8. PH-COSY of **4**^{tBu} in d_8-THF.

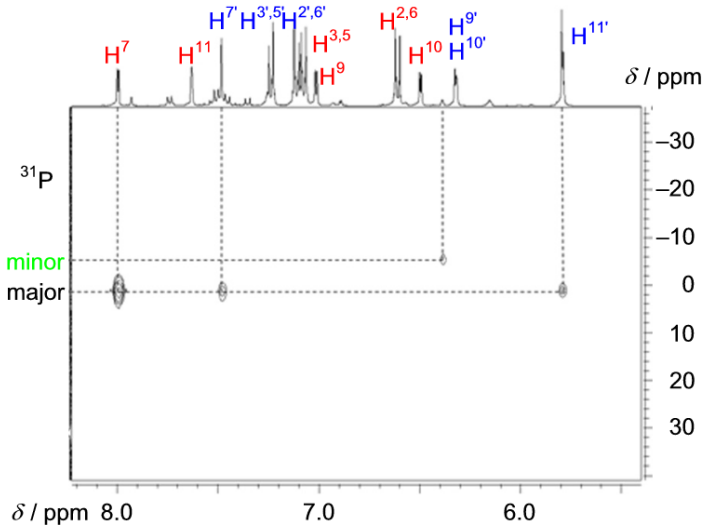

Figure S9. PH-COSY of **5**^{tBu} in d_8-THF.

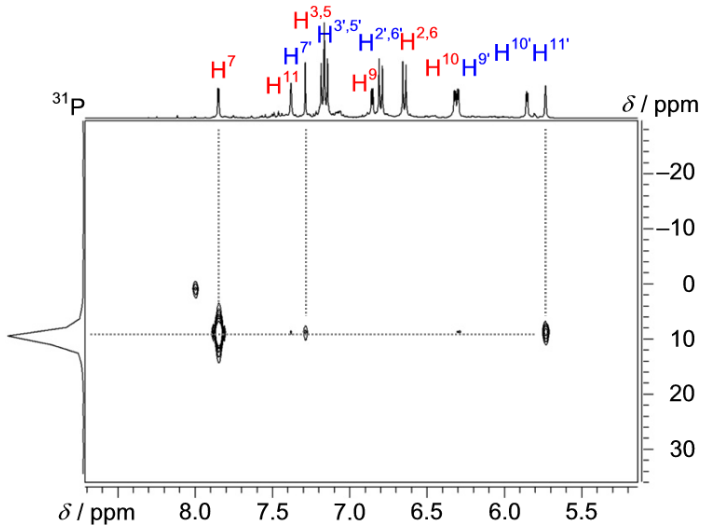

Figure S10. $^{31}P\{^1H\}$ NMR of the equilibrium reaction **4**^{tBu} + 5 PEt_3 in d_8-THF at 298 K.

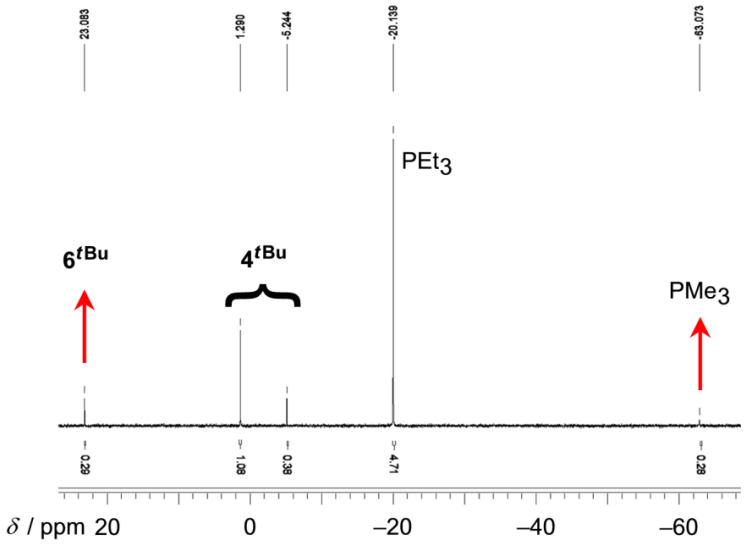

Figure S11. $^{31}P\{^1H\}$ NMR of the equilibrium reaction **5**^{tBu} + 5 PEt_3 in d_8-THF at 333 K.

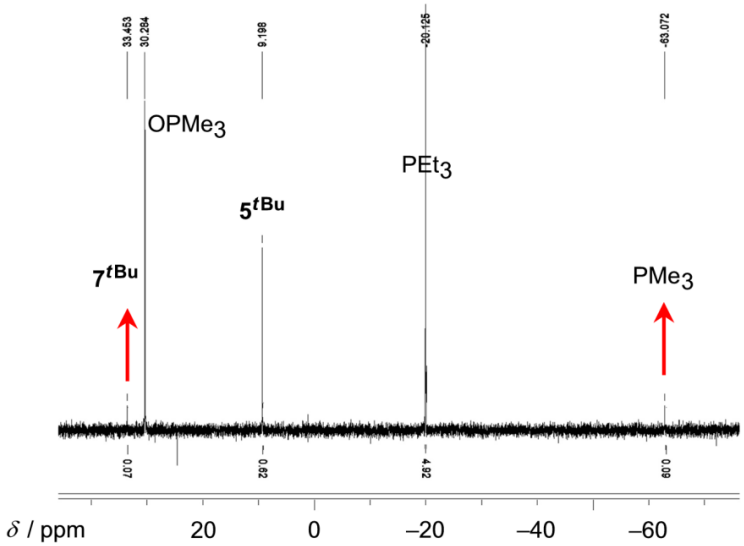

Figure S12. Plots of [PMe_3] vs. time and [PMe_3]/[PMe_3]$_0$ vs. time for the reaction between d_6-dmso and PMe_3 catalyzed by **1**^{tBu} at 298 K, [**1**^{tBu}] = 0.016 M; [PMe_3]$_0$ = 0.16 M in d_6-dmso.

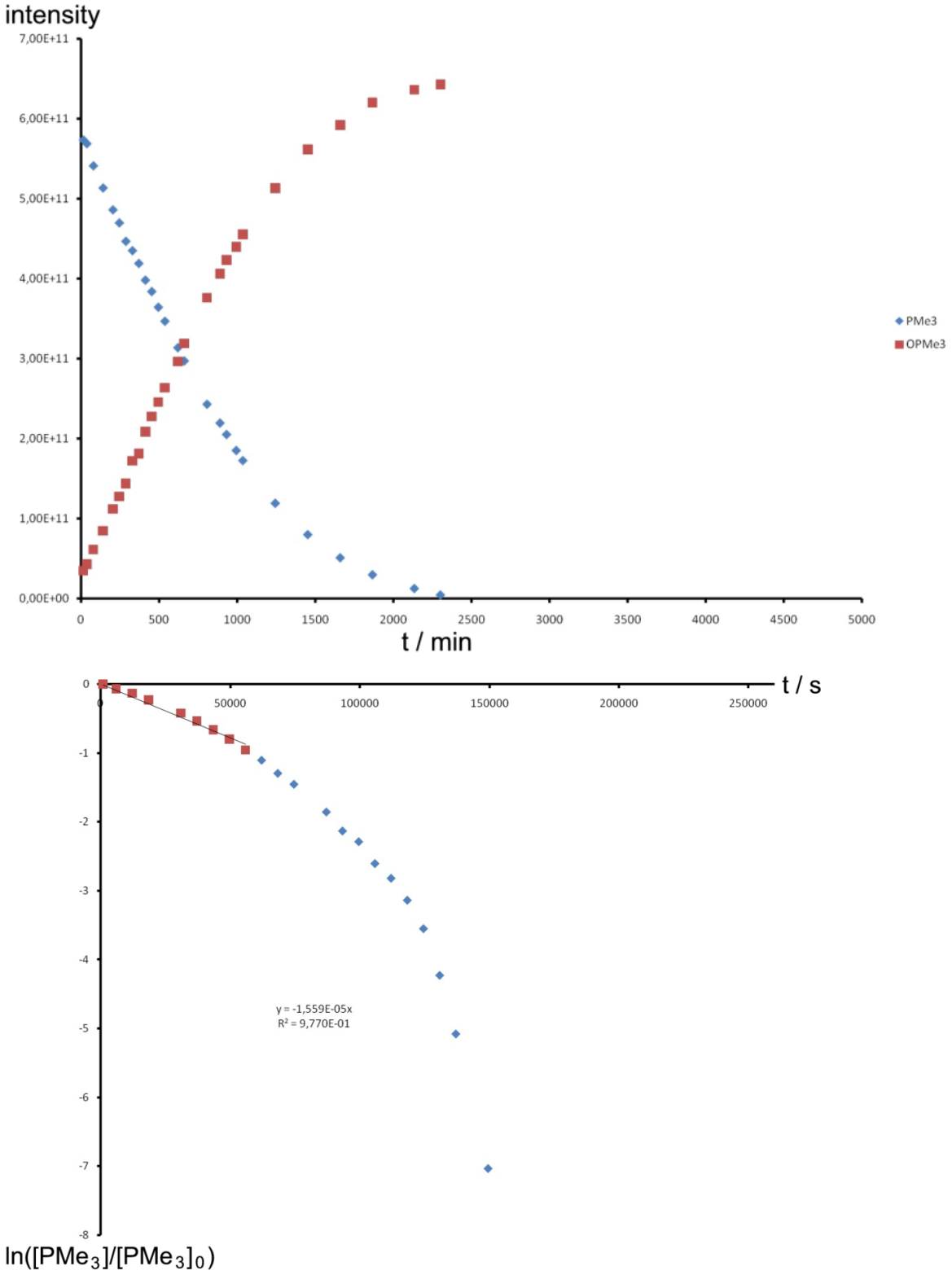

Figure S13. Plots of [PMe_3] vs. time and [PMe_3]/[PMe_3]$_0$ vs. time for the reaction between d_6-dmso and PMe_3 catalyzed by **2**^{tBu} at 298 K, [**2**^{tBu}] = 0.016 M; [PMe_3]$_0$ = 0.16 M in d_6-dmso.

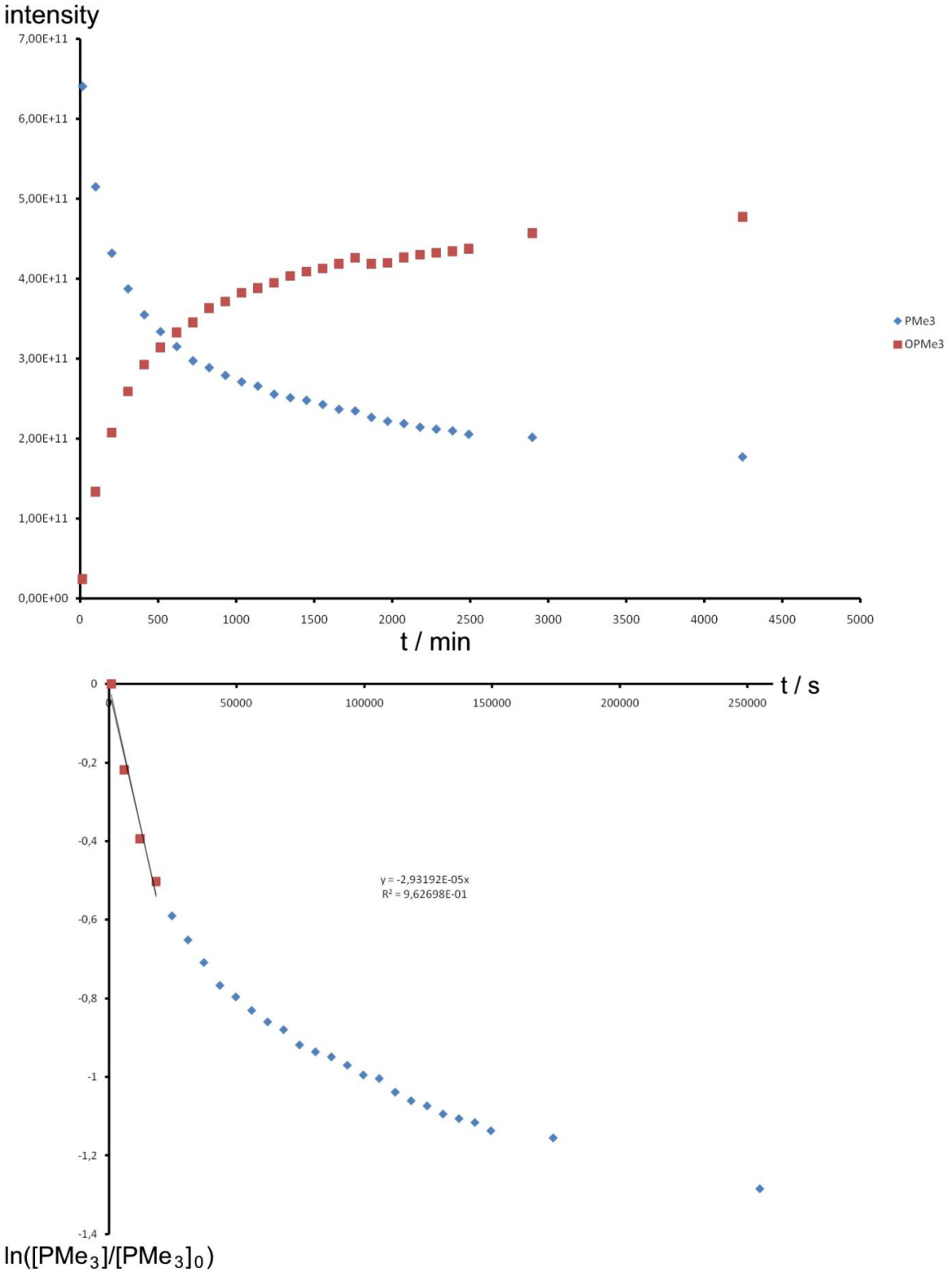

Figure S14. X-band EPR spectrum of **[4^{tBu}](PF$_6$)** in frozen THF at 77 K and simulation in red (without $^{95/97}$Mo satellites).

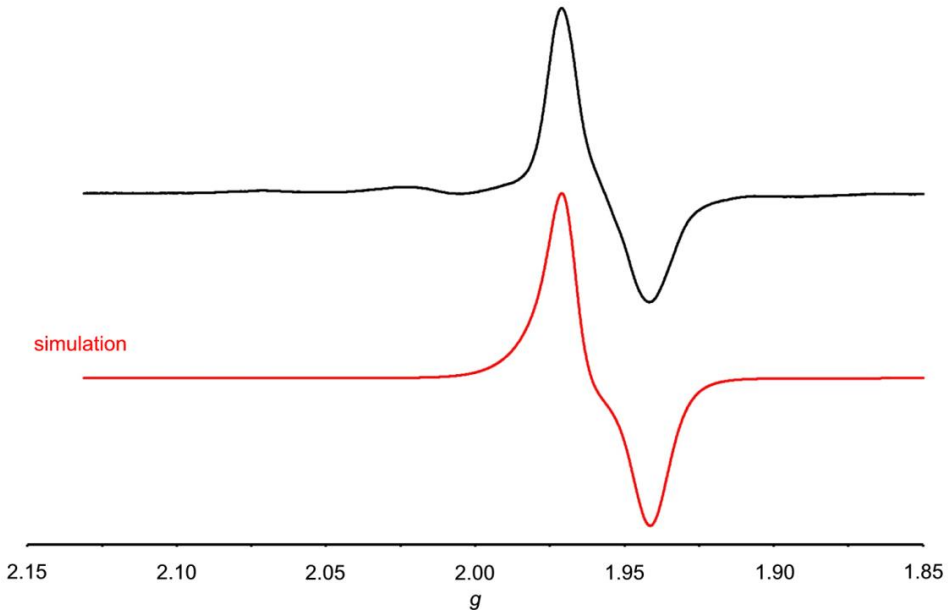

Figure S15. X-band EPR spectrum of **[5^{tBu}](PF$_6$)** in frozen THF at 77 K and simulation in red (without $^{95/97}$Mo satellites).

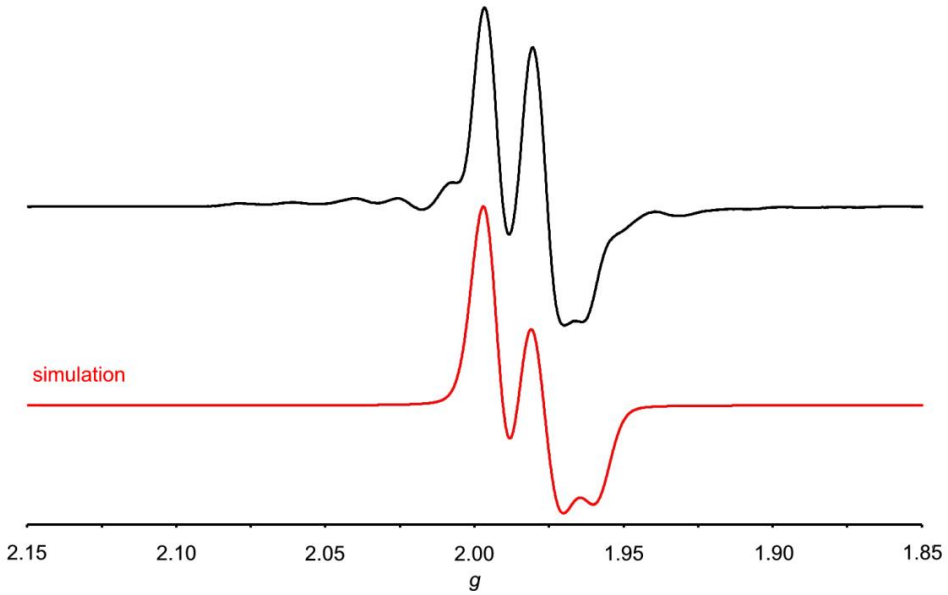

Figure S16. Detailed experimental (lower) and simulated (upper) HYSCORE spectra.

a) Experimental (lower) and simulated (upper) HYSCORE spectrum of one ^{14}N nucleus with large hyperfine and quadrupole coupling

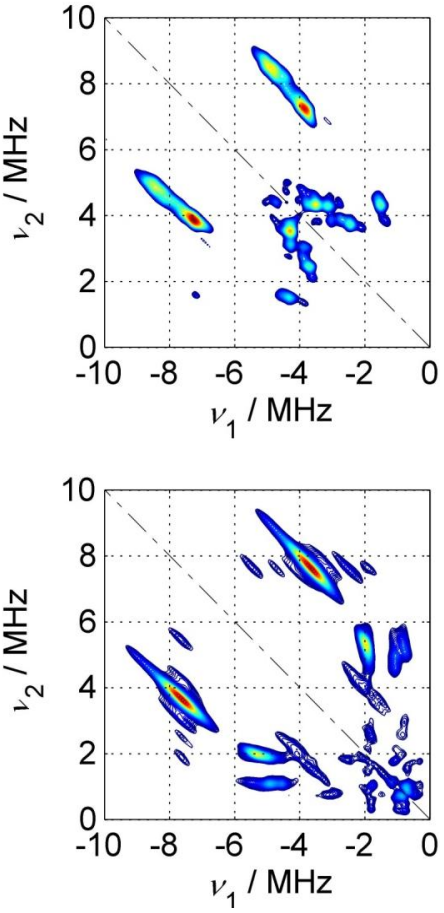

b) Experimental (lower) and simulated (upper) HYSCORE spectrum of one ^{1}H nucleus and one weakly coupled ^{14}N nucleus. Note that we tentatively assign experimentally only the double-quantum transitions, in line with cross-suppression of the ^{1}H main peaks (see Ref. 45c in the main text)

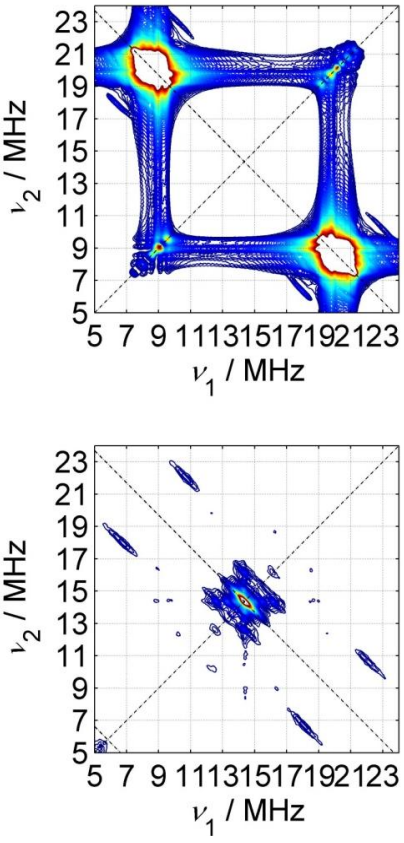

c) Experimental (lower) and simulated (upper) HYSCORE spectrum of two ^{14}N nuclei with small hyperfine and quadrupole couplings.

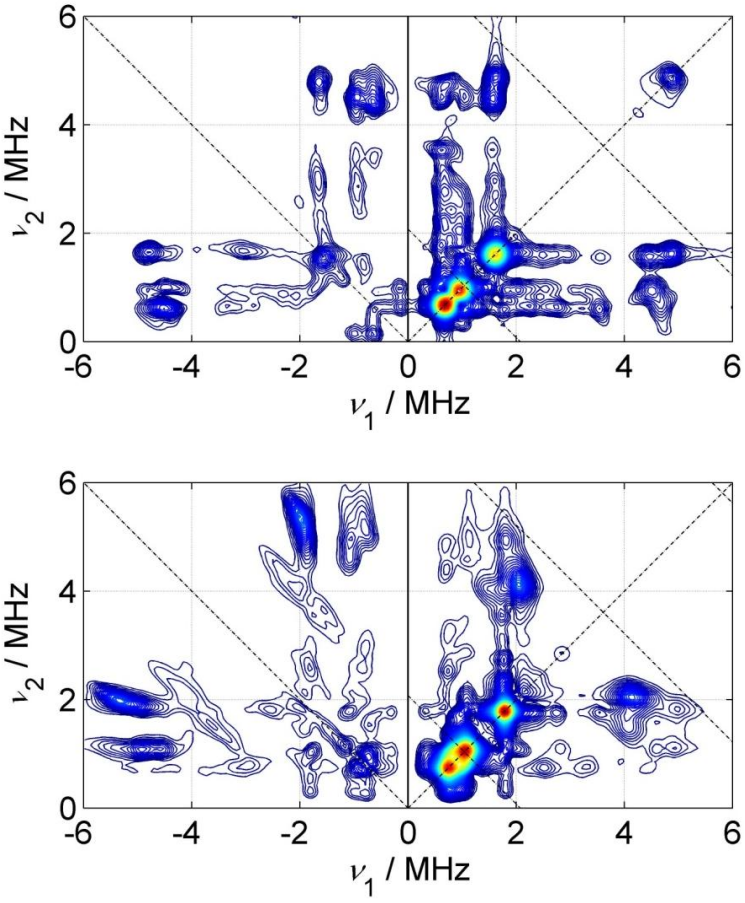

Table S1. ^{14}N hyperfine and nuclear quadrupole couplings and ^{1}H hyperfine couplings as determined from simulations of the experimental spectra.

The Euler angles α, β, γ define the passive rotation of the hyperfine (A) or nuclear quadrupole (Q) principal axes systems into the g-matrix principal axes system, e.g. $\mathbf{A}=\mathbf{R}(\alpha, \beta, \gamma)\mathbf{A}_{\text{diagonal}}\mathbf{R}^{\dagger}(\alpha, \beta, \gamma)$. The nuclear quadrupole interactions are: $\kappa = (e^2qQ/h)/(4I(2I\text{-}1))$ and the asymmetry parameters $\eta = (Q_x - Q_y)/Q_z$ with $Q_x = -\kappa(1-\eta)$, $Q_y = -\kappa(1+\eta)$, and $Q_z = 2\kappa$.

	A_x (G)	A_y (G)	A_z (G)	A_{iso} (G)	α, β, γ (°)	$\lvert e^2qQ/h \rvert$ (MHz)	η	α, β, γ (°)
$^{14}N_{large}$	1.5	2.0	3.8	2.4	0, 7, 0	1.8	2.2	-90, -80, 0
$^{14}N_{small,A}$	1.3	1.4	1.7	1.5	0, 90, 0	1.2	0.5	0, 0, 0
$^{14}N_{small,B}$	0.8	0.8	0.9	0.8	90,- 90, 0	1.5	1.2	90, -180, 0
^{1}H	3.4	4.1	5.0	4.2	0, 0, 0	n.a.	n.a.	n.a.

Experimental Section: Echo-detected, field-swept X-band EPR spectra were recorded with a primary echo sequence ($\pi/2$)-τ-(π)-τ-echo while sweeping the magnetic field using a Bruker ELEXSYS 580 spectrometer with a Flexline split-ring resonator (ER 4118X-MS3, overcoupled to Q-values of typically 100). All experiments were performed in glassy, shock-frozen solution at X-band frequencies (~9.4 GHz) at 20K.

HYSCORE experiments employed the pulse sequence $\pi/2-\tau-\pi/2-t_1-\pi-t_2-\pi/2-\tau-echo$. The following parameters were used: mw pulses of lengths $t_{\pi/2} = t_\pi = 16$ ns, starting times 96 ns for t_1 and t_2, and time increments $\Delta t = 16$ ns (data matrix 384 × 384). Spectra with different τ values were recorded. An eight-step phase cycle was used to remove unwanted echoes. The HYSCORE data were processed with MATLAB 6.5 (The MathWorks, Inc.). The time traces were baseline corrected with an exponential, apodized with a Gaussian window and zero filled. After a two-dimensional Fourier transformation absolute-value spectra were calculated. Spectra recorded with different τ values were recorded to check that τ-dependent blind spots do not distort the data. HYSCORE spectra were simulated applying the ZOMA package interfaced with MATLAB.[2]

In all cases the temperature was set to 20 K by cooling with an ARS cryostat and closed-cycle cooling system. The samples were prepared as concentrated solutions (concentrations typically >10 mM) and the sample volume was always large enough to fill the complete resonator volume in the probehead (>300 μL).

[1] Hinderberger, D.; Piskorski, R.; Goenrich, M.; Thauer, R. K.; Schweiger, A.; Harmer, J.; Jaun, B. *Angew. Chem. Int. Ed.* **2006**, *45*, 3602-3607.

[2] Madi, T.; van. Dorslaaer, S.; Schweiger, A.; *J. Magn. Reson.* **2002**, *154*, 181-191.

7.3 Intramolecular electron transfer between molybdenum and iron mimicking bacterial sulphite dehydrogenase

Kristina Hüttinger,[a] Christoph Förster[a] and Katja Heinze*[a]

Electronic Supporting Information

Fig. S1. DFT (B3LYP; LANL2DZ+polarisation functions for N, O; PCM THF) optimised geometry of **2**^{Fc} including natural atomic charges on Fe in red; distances in Å.

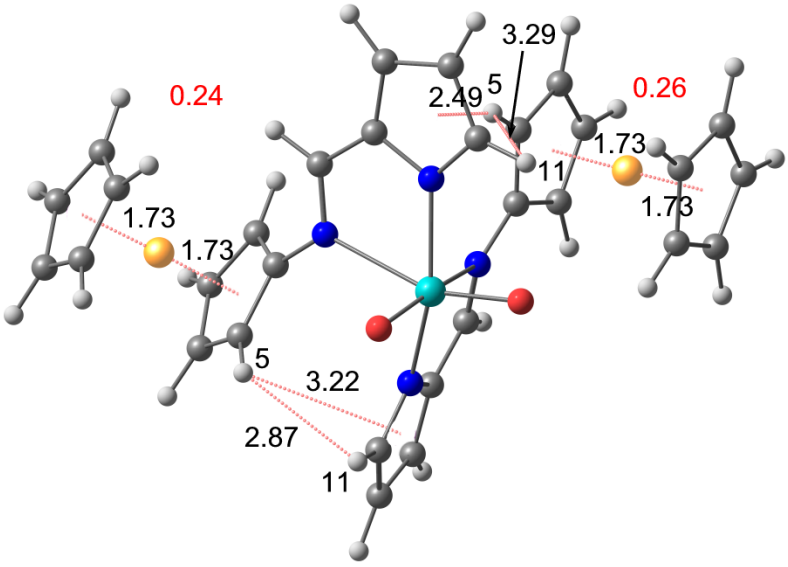

Fig. S2. UV/Vis spectra of **2**^{Fc} (and Gaussian deconvolution) and **2**^{tBu} in THF.

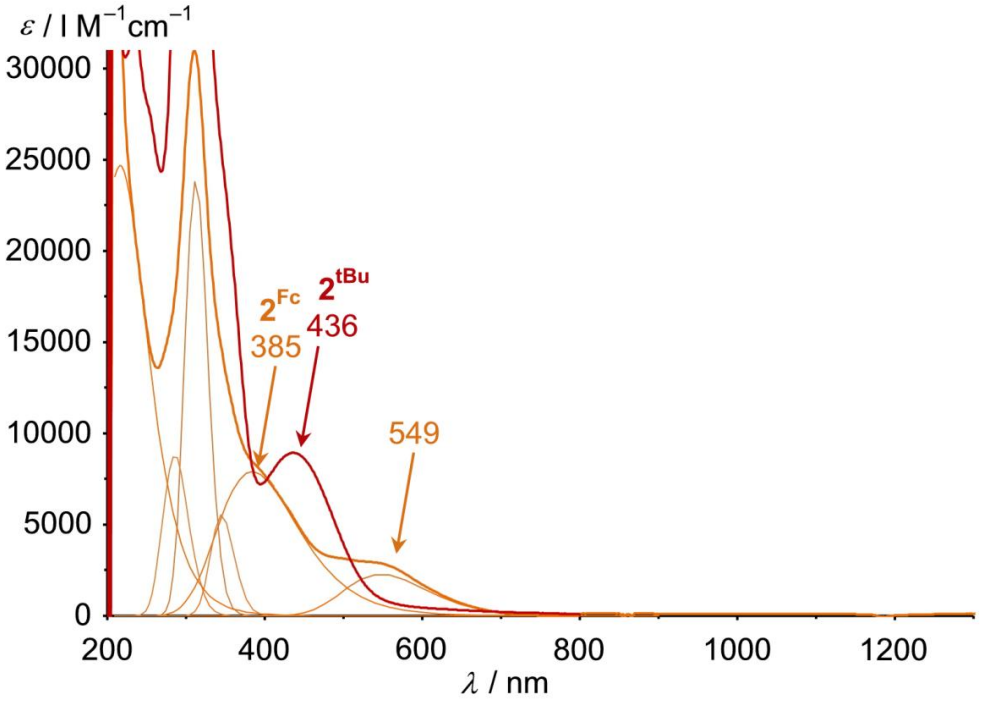

Fig. S3. Pictorial description of MO 148 (HOMO) and MOs 149 – 150 (LUMOs) of $\mathbf{2}^{Fc}$

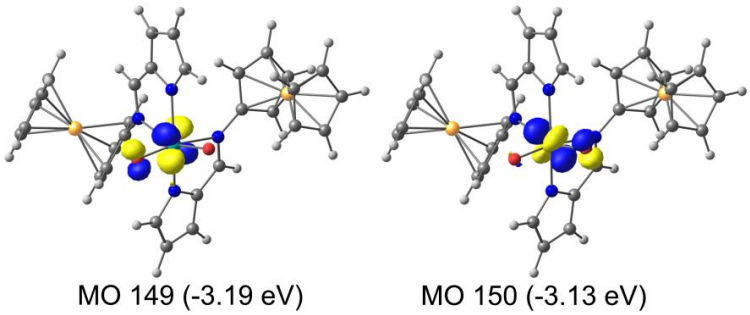

MO 149 (-3.19 eV) MO 150 (-3.13 eV)

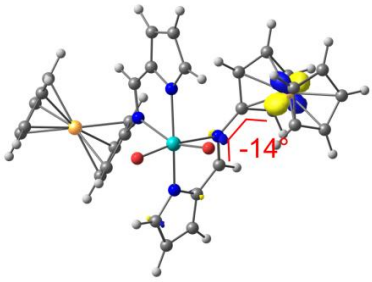

MO 148 (-5.57 eV)

Results of the TD-DFT calculation for **2**

```
Excited State   1:      Singlet-A      1.6788 eV  738.52 nm  f=0.0081
<S**2>=0.000
     144 ->157         0.12452
     146 ->155        -0.24498
     148 ->149         0.42505
     148 ->150        -0.34776
     148 ->153         0.11149
     148 ->156        -0.10660
     148 ->157         0.21958
```

Energy and intensity of the transition are governed by the relative orientation of the iron d orbital and Mo=O units. Hence, a perfect match between TD-DFT calculation and experiment is not expected.

Fig. S4. $^{31}P\{^{1}H\}$ NMR spectrum of **3a**^{Fc} and **3b**^{Fc} in d_8-THF.

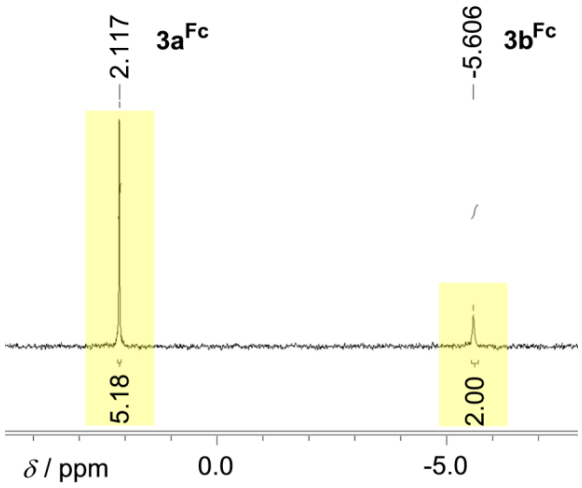

Fig. S5. NOE contacts in **3a**^{Fc} (red arrows, s = strong, m = medium, w = weak)

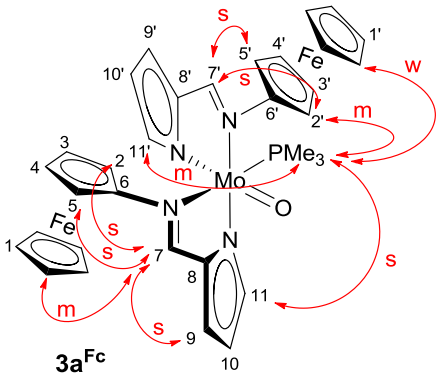

Fig. S6. DFT (B3LYP; LANL2DZ+polarisation functions for N, O; PCM THF) optimised geometry of **3a**^{Fc} including natural atomic charges on Fe in red; distances in Å; hydrogen atoms omitted.

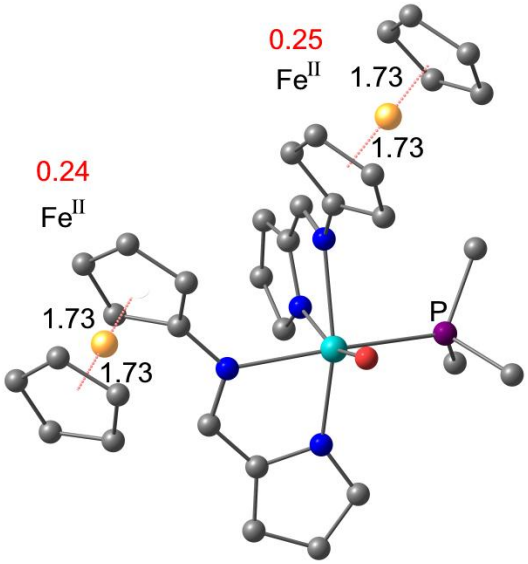
0.25
Fe^II
1.73
1.73
0.24
Fe^II
1.73
1.73
P

Fig. S7. UV/Vis spectra of $\mathbf{1}^{Fc}$ (orange) and $[\mathbf{1}^{Fc}]^{+}$ (blue) in THF including Gaussian band shape analyses.

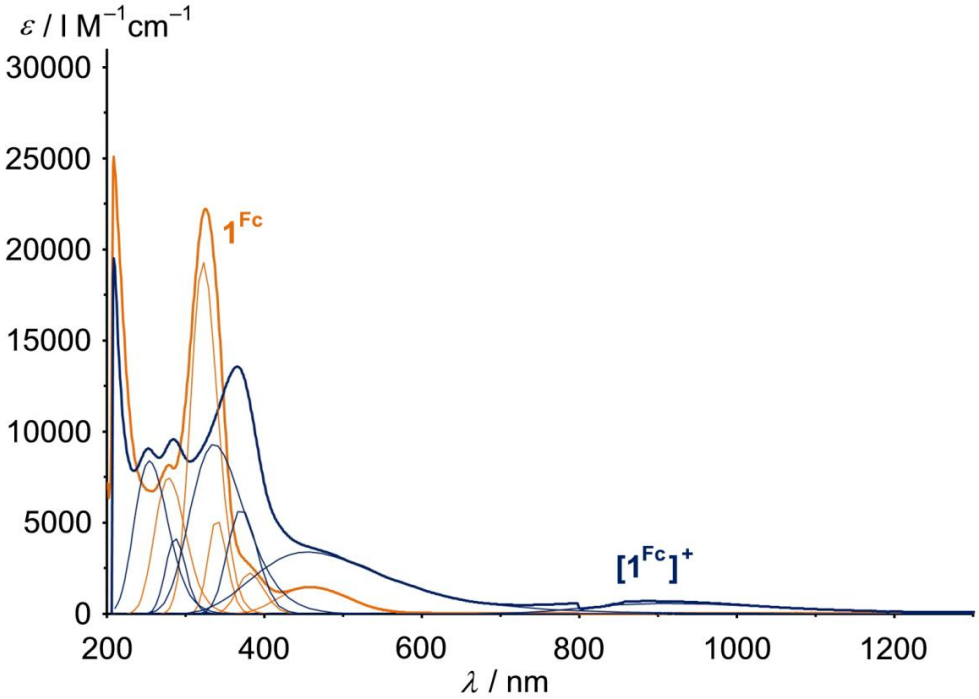

Fig. S8. UV/Vis spectra of $\mathbf{2}^{Fc}$ (orange) in THF and $[\mathbf{2}^{Fc}]^{2+}$ (blue) in CH_3CN including Gaussian band shape analyses.

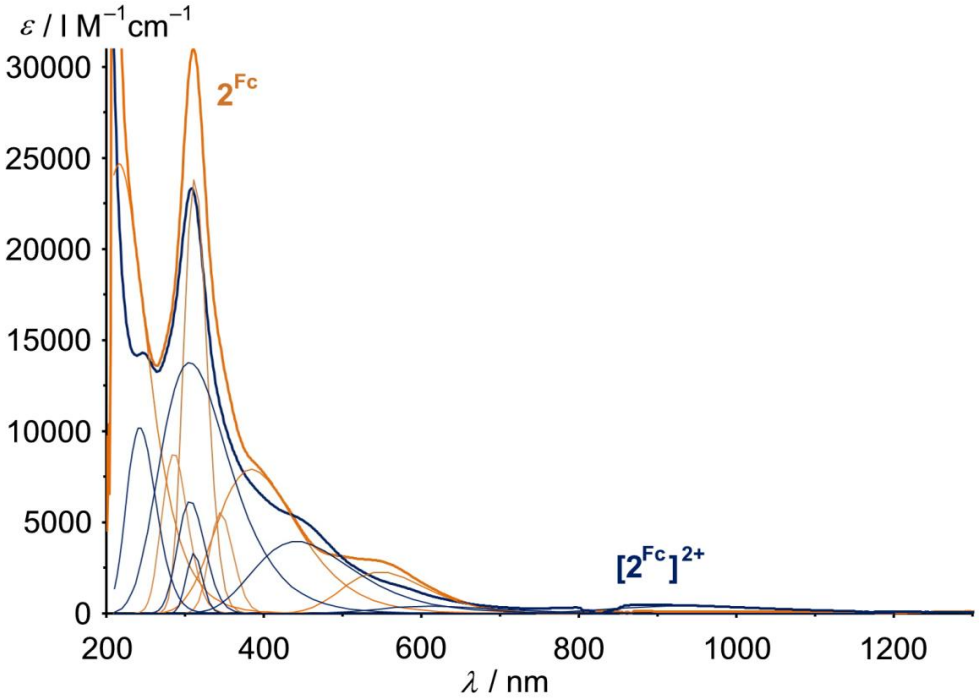

Fig. S9. Spectroelectrochemical oxidation of **2**$^{\mathbf{Fc}}$ in THF/[^{n}Bu$_4$N][B(C$_6$F$_5$)$_4$]; Pt electrodes; detector switch at 800 nm

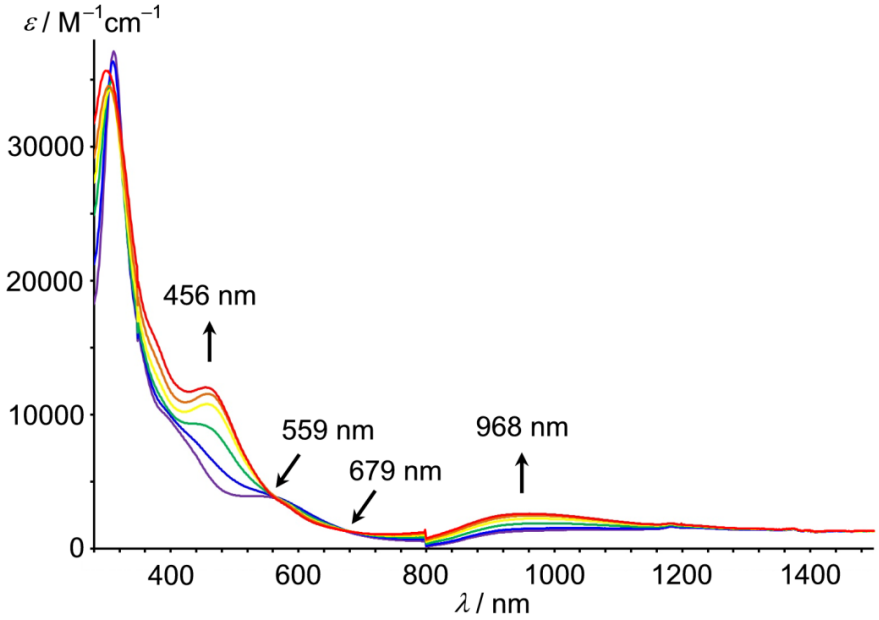

Fig. S10. Paramagnetic ^{1}H NMR spectra of $\mathbf{[2^{Fc}]^{2+}}$ in CD_3CN, including zoom in pyrrolate region; sharp resonances in the diamagnetic region are due to residual solvent.

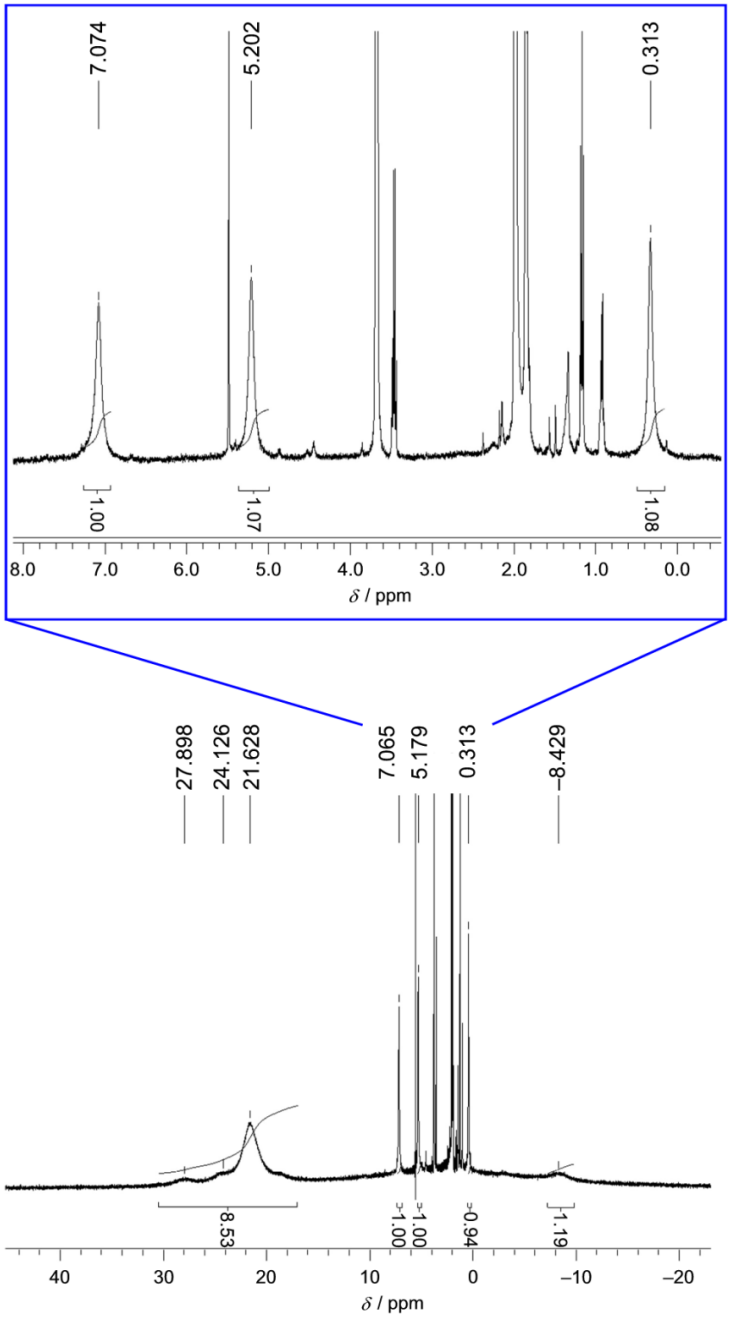

Fig. S11. DFT optimized geometry (B3LYP; LANL2DZ+polarisation functions for N, O, P; PCM THF) of a) $[\mathbf{2}^{Fc}]^{2+}$ and b) $[\mathbf{4}^{Fc}]^{2+}$ in the singlet states (distances in Å; angles in deg; natural atomic charges at iron in red; hydrogen atoms omitted).

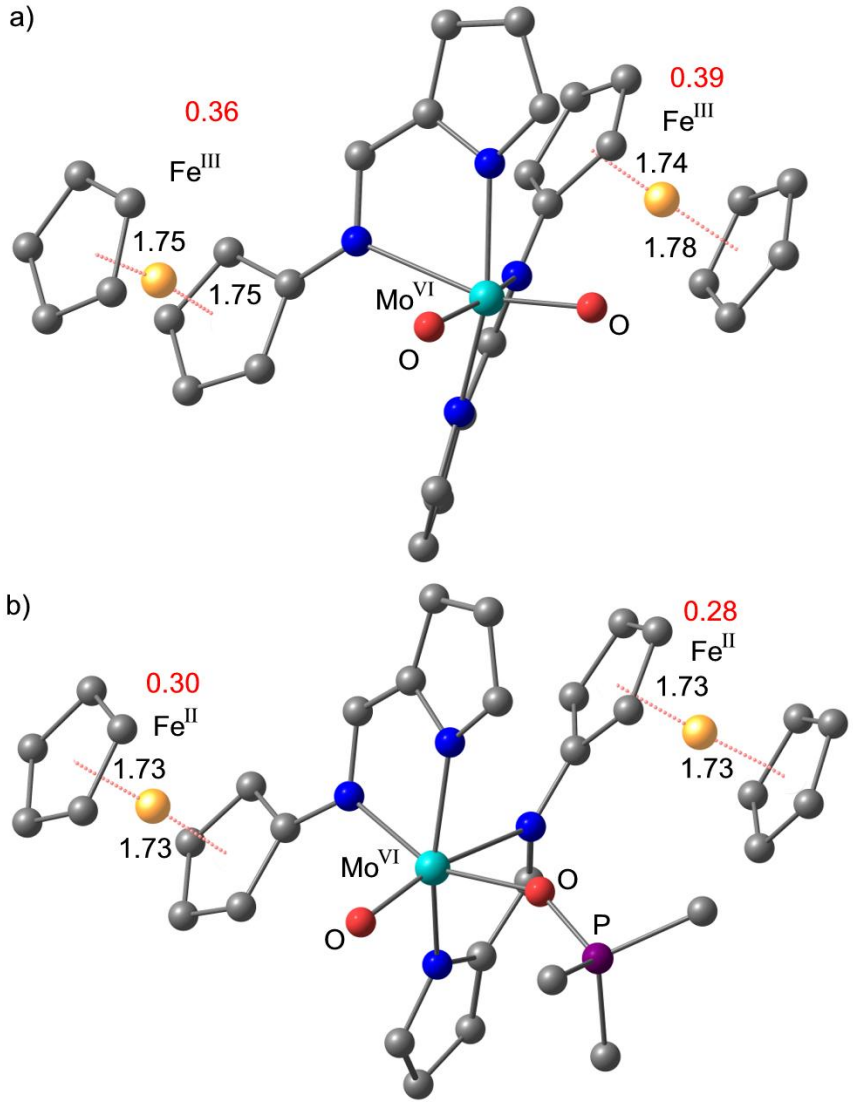

Fig. S12. $^{31}P\{^{1}H\}$ NMR spectrum of **2^{Fc}** and PMe_3 (exc.) in d_8-THF after removing volatiles (PMe_3).

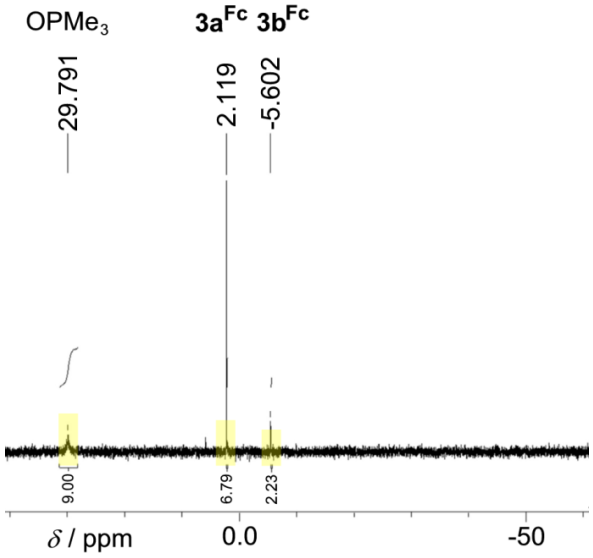

Fig. S13. $^{31}P\{^{1}H\}$ NMR spectrum of **[2^{Fc}]$^{2+}$** and PMe_3 (exc.) in CD_3CN.

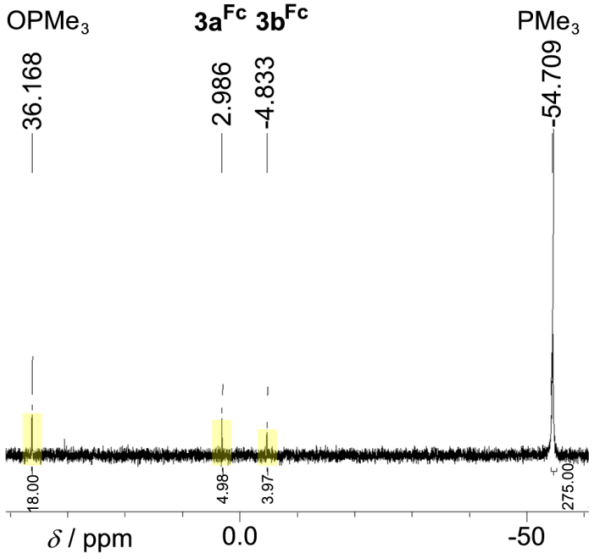

General Procedures

All reactions were performed under argon atmosphere unless otherwise noted. THF was distilled from potassium. Aminoferrocene[1,2] and $MoCl_2O_2(dme)$[3] were prepared according to literature procedures. Filtrations from precipitated silver after oxidation were performed with syringe filters (Rotilabo-Spritzenfilter, Ø = 25 mm, pore size = 0.20 µm; Carl Roth GmbH + Co. KG, Germany). NMR spectra were recorded on a Bruker Avance DRX 400 spectrometer at 400.31 MHz (^{1}H), 100.66 MHz (^{13}C{^{1}H}), 162.05 MHz (^{31}P{^{1}H}) and 40.56 MHz (^{15}N). All resonances are reported in ppm versus the solvent signal as internal standard [d_8-THF (^{1}H: δ = 1.73, 3.57; ^{13}C: δ = 25.5, 67.7 ppm); CD_3CN (^{1}H: δ = 1.94)], versus external H_3PO_4 (85%) (^{31}P: δ = 0 ppm) or versus external CH_3NO_2 (90% in $CDCl_3$) (^{15}N: δ = 380.23 ppm). ^{15}N data are reported vs. liquid NH_3 as reference (δ = 0 ppm). IR spectra were recorded with a BioRad Excalibur FTS 3100 spectrometer as KBr disks. Electrochemical experiments were carried out on a BioLogic SP-50 voltammetric analyzer using platinum wires as counter and working electrodes and a 0.01 M $Ag/AgNO_3$ electrode as reference electrode. The cyclic voltammetry measurements were carried out at scan rate of 50–100 mV s^{-1} using 0.1 M (nBu$_4$N)(B(C_6F_5)$_4$) as supporting electrolytes in THF. Potentials are referenced to the ferrocene/ferrocenium couple ($E_{½}$ = 270 ± 5 mV under the experimental conditions). Spectroelectrochemical experiments were performed using a thin layer quartz glass (path length 1 mm) cell kit (GAMEC Analysentechnik, Illingen, Germany) equipped with a Pt gauze working electrode, a Pt counter electrode and a $Ag/AgNO_3$ reference electrode in THF/0.1 M (nBu$_4$N)(B(C_6F_5)$_4$). UV/Vis/NIR spectra were recorded on a Varian Cary 5000 spectrometer using 1.0 cm cells (Hellma, suprasil). FD mass spectra were recorded on a FD Finnigan MAT90 spectrometer. ESI mass spectra were recorded on a Micromass Q-TOF-Ultima spectrometer. X-band CW EPR spectra were recorded on a magnettech MS 300 spectrometer with a frequency counter Hewlett Packard 5340A at a microwave frequency of 9.39 GHz in frozen THF solution (77 K). Mn^{2+} in ZnS was used as external standard. Simulations were performed with the program package EasySpin.[4]

Synthesis of 1^{Fc}

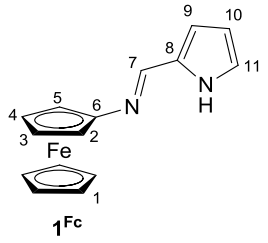

1^{Fc}

1H-Pyrrole-2-carbaldehyde (310 mg, 3.26 mmol), aminoferrocene[1,2] (650 mg, 3.23 mmol), molecular sieves (6 g) and toluene (80 ml) were heated to 90°C for 4 h. The suspension was filtered while hot and the solvent was removed under reduced pressure. The resulting red powder was purified by chromatography (Alox 15×3.5 cm, CH_2Cl_2) giving red crystals in 90% yield (926 mg, 2.88 mmol). M.p. 133°C. $R_f(CH_2Cl_2)$ = 0.7. ^{1}H NMR (d_8-THF): δ = 10.93 (br.s, 1H, NH), 8.38 (s, 1H, H^7), 6.90 (s, 1H, H^{11}), 6.46 (dd, 1H, H^9), 6.13 (dd, 1H, H^{10}), 4.45 (s, 2H, $H^{2,5}$), 4.12 (s, 2H, $H^{3,4}$), 4.09 (s, 5H, H^1) ppm. $^{13}C\{^1H\}$ NMR (d_8-THF): δ = 149.2 (s, C^7), 132.9 (s, C^8), 123.1 (s, C^{11}), 115.1 (s, C^9), 110.3 (s, C^{10}), 107.9 (s, C^6), 70.1 (s, C^1), 67.5 (s, $C^{3,4}$), 63.0 (s, $C^{2,5}$) ppm. NH-HMBC (d_8-THF): δ = 345.6 (s, N^p), 392.9 (s, N^i) ppm. IR (KBr): $\tilde{\nu}$ = 3447, 3158 (w, NH), 3095, 2956, 2850 (m, CH), 1602 (m, C=N), 1413 (m), 1129 (m), 1035 (m) cm^{-1}. UV/Vis (THF): λ = 457 (1470), 382 (sh, 2670), 323 (22060), 279 (8170 M^{-1} cm^{-1}) nm. MS (FD): *m*/*z* (%) = 278.3 (100, M^+). CV (THF): $E_{½}$ = –40 mV (rev.). Elemental analysis calcd. (%) for $C_{15}H_{14}N_2Fe$ (278.14): C 64.78, H 5.07, N 10.07; found C 64.39, H 5.31, N 9.87.

Synthesis of 2^{Fc}

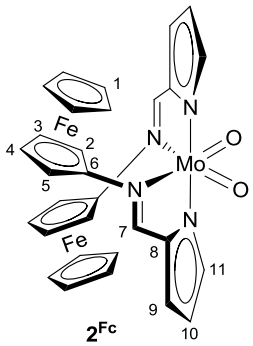

2^{Fc}

Ligand $\mathbf{1}^{Fc}$ (200 mg, 0.72 mmol) was dissolved in THF (10 ml) and deprotonated with triethyl amine (0.4 ml, 290 mg, 2.9 mmol). In a separate flask $MoCl_2O_2(dme)$[3] (104 mg, 0.36 mmol) was dissolved in THF (5 ml) and the deprotonated ligand was added. After stirring for 2 h the suspension was filtered and the red filtrate was dried under reduced pressure giving the raw product in nearly quantitative yield. The raw product was recrystallised from toluene/petroleum ether 40-60°C (1:1) at 8°C giving a dark red crystalline solid in 26% yield (65 mg, 0.095 mmol). Single crystals were obtained by recrystallisation from toluene/ petroleum ether 40-60°C (1:1). M.p. >250°C (decomp.). ^{1}H NMR (d_8-THF): δ = 8.58 (s, 1H, H^7), 7.33 (s, 1H, H^{11}), 6.67 (d, 1H, H^9), 6.31 (dd, 1H, H^{10}), 4.12 (s, 5H, H^1), 3.97 (m, 1H, H^2), 3.88 (m, 1H, H^3), 3.87 (m, H, H^4), 3.74 (m, 1H, H^5) ppm. $^{13}C\{^1H\}$ NMR (d_8-THF): δ = 159.0 (s, C^7), 143.9 (s, C^{11}), 140.2 (s, C^8), 119.4 (s, C^9), 115.4 (s, C^{10}), 106.7 (s, C^6), 70.5 (s, C^1), 66.2, 65.2 (2×s, $C^{3,4}$), 63.5 (s, C^5), 63.0 (s, C^2) ppm. IR (KBr): $\tilde{\nu}$ = 3094 (w, CH), 1579 (vs, C=N), 1421 (m), 1406 (m), 1292 (m), 1039 (s), 929 (m, Mo=O), 905 (m, Mo=O) cm^{-1}. UV/Vis (THF): λ = 549 (2865), 385 (8420), 312 (30875 M^{-1} cm^{-1}) nm. MS (FD): *m*/*z* (%) = 684.1 (62, M^+, correct isotopic distribution). CV (THF): E_p = –1540 (qrev), –30 (rev.), +80 (rev.) mV. Elemental analysis calcd. (%) for $C_{30}H_{26}N_4O_2Fe_2Mo$ (682.20)×0.2toluene: C 53.83, H 3.97, N 8.00; found C 54.48, H 4.23, N 8.85.

Synthesis of 3a^{Fc}

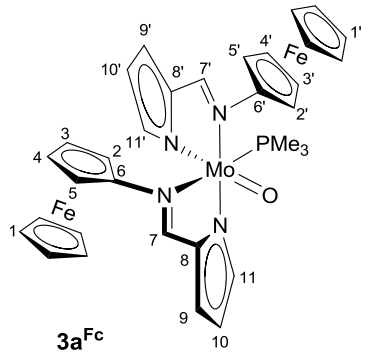

3a^{Fc}

Dioxido complex **2^{Fc}** (19 mg, 0.028 mmol) was dissolved in THF (3 ml) and trimethylphosphane (1M in THF, 0.11 ml, 0.11 mmol) was added. After stirring for 2 d at room temperature volatiles were removed under reduced pressure and the residue was washed with petroleum ether 40-60°C to give a green powder in 68% yield (14 mg, 0.019 mmol). ^{1}H NMR (d_8-THF): δ = 8.60 (d, $^{4}J_{PH}$ = 2.7 Hz, 1H, H^{7}), 8.22 (s, 1H, H$^{7'}$), 7.51 (bs, 1H, H^{11}), 6.99 (d, $^{3}J_{HH}$ = 3.4 Hz, 2H, H^{9}), 6.45 (m, 1H, H^{10}), 6.31 (m, 1H, H$^{10'}$), 5.78 (bs, 1H, H$^{11'}$), 5.75 (dd, 1H, H$^{9'}$), 4.87 (pt, 1H, H$^{2'}$), 4.70 (pt, 1H, H$^{5'}$), 4.41 4.37 (2×pt, 2×1H, pt, 1H, H^{2,5}), 4.23 (1, 5H, H$^{1'}$), 4.15 (m, 2H, H$^{3',4'}$), 4.02 (m, 2H, H^{3,4}), 3.97 (s, 5H, H^{1}), 1.27 (d, $^{2}J_{PH}$ = 8.64 Hz, 9H, P(CH$_3$)$_3$) ppm (major isomer **3a^{Fc}**). ^{31}P{^{1}H} NMR (d_8-THF): δ = 2.1 (s, major), –5.6 (s, minor) ppm (ratio 5:2).

Oxidation of $\mathbf{1^{Fc}}$ to $\mathbf{[1^{Fc}](SbF_6)}$

Ligand $\mathbf{1^{Fc}}$ (14 mg, 0.05 mmol) was dissolved in THF (3 ml) and $AgSbF_6$ (17.3 mg, 0.05 mmol) dissolved in THF (2 ml) was added ($E_{½}(Ag/Ag^+)$ = 410 mV vs. Fc/Fc^+ [16]). After stirring for 30 min the solution was filtered via syringe filters to remove precipitated silver. An aliquot of this solution was transferred into an EPR tube, frozen to 77 K and an EPR spectrum was recorded. A further aliquot of the solution was subjected to UV/Vis spectroscopic analysis. EPR (THF, 77 K): g = 3.37, 1.989, 1.815. UV/Vis (THF): λ_{max} = 917 (610), 456 (3690), 366 (13580), 284 (9580 M^{-1} cm^{-1}) nm. ESI-MS: *m*/*z* (%) = 278.0 (24, $\mathbf{[1^{Fc}]^+}$).

Oxidation of $\mathbf{2^{Fc}}$ to $\mathbf{[2^{Fc}](SbF_6)_2}$

Complex $\mathbf{2^{Fc}}$ (14.16 mg, 0.021 mmol) was dissolved in THF (3 ml) and $AgSbF_6$ (14.34 mg, 0.042 mmol) dissolved in THF (1 ml) was added. After stirring for 10 min the solution was allowed to stand for 12 h at room temperature. A precipitate including elemental silver had formed and was collected by filtration, washed three times with THF and dried to give a brown powder (12 mg). The solid material was dissolved in CH_3CN (3 ml) and filtered via syringe filters to remove undissolved silver. A part of the resulting solution was transferred into an EPR tube, frozen to 77 K and an EPR spectrum was recorded. A further part of the solution was subjected to UV/Vis spectroscopic analysis, mass spectrometry and NMR spectroscopy (after drying and redissolving in CD_3CN). EPR (CH_3CN, 77 K): silent. ^1H NMR (CD_3CN): δ = 27.9, 24.2, 21.6 (br. m, 9H, CpH), 7.1 (br., 1H, pyrrol-H), 5.2 (br., 1H, pyrrol-H), 0.3 (br., 1H, pyrrol-H), –8.4 (br., 1H, imine-H) ppm. UV/Vis (CH_3CN): λ_{max} = 934 (445), 442 (sh, 5295), 308 (23340), 247 (14305) nm. ESI-MS: *m*/*z* (%) = 684.0 (62%, $\mathbf{[2^{Fc}]^+}$), 918.9 (11%, $\mathbf{[2^{Fc}](SbF_6)}$).

Reaction of $\mathbf{[2^{Fc}](SbF_6)_2}$ with exc. $\mathbf{PMe_3}$

To a solution of $\mathbf{[2^{Fc}](SbF_6)_2}$ (7.7 mg, 0.0066 mmol) dissolved in CD_3CN (ca. 0.3 ml) and filtered via a syringe filter in an NMR tube was added an excess PMe_3 (1 M in THF, 20 µl, 0.02 mmol). ^1H and ^{31}P NMR spectra were recorded after a few minutes. All resonances appear in the diamagnetic region. In some instances traces of a pale, fluffy precipitate formed during this time. The (filtered and redissolved) precipitate is identified as $OPMe_3$ by ^1H NMR (δ = 1.34 ppm, d, $^2J_{PH}$ = 13.2 Hz) and ^{31}P NMR (δ = 36.2 ppm) in [D_6]-DMSO. ^1H NMR (CD_3CN): δ = 1.41 (d, $^2J_{PH}$ = 13.1 Hz, $OPMe_3$), 1.29 (d, $^2J_{PH}$ = 8.8 Hz, $\mathbf{3a^{Fc}}$), 0.85 (d, $^2J_{PH}$ = 8.5 Hz, $\mathbf{3b^{Fc}}$) ppm. $^{31}P\{^1H\}$ NMR (CD_3CN): δ = 36.2 (s, $OPMe_3$), 3.0 (s, $\mathbf{3a^{Fc}}$), –4.8 ($\mathbf{3b^{Fc}}$), –54.7 (PMe_3) ppm.

X-ray structure determinations

Intensity data were collected with a Bruker AXS Smart 1000 CCD diffractometer with an APEX II detector and an Oxford cooling system and corrected for absorption and other effects using Mo K_α radiation (λ = 0.71073 Å) at 173(2) K. The diffraction frames were integrated using the SAINT package, and most were corrected for absorption with MULABS.[5,6] The structures were solved by direct methods and refined by the full-matrix method based on F^2 using the SHELXTL software package.[7,8] All non-hydrogen atoms were refined anisotropically, while the positions of all hydrogen atoms were generated with appropriate geometric constraints and allowed to ride on their respective parent atoms with fixed isotropic thermal parameters. The asymmetric unit of a crystal of $\mathbf{1}^{\mathbf{Fc}}$ contains two independent molecules. The asymmetric unit of a crystal of $\mathbf{2}^{\mathbf{Fc}}$ contains two independent complex molecules and a toluene molecule (s.o.f. 0.5) disordered over an inversion centre. Crystallographic data (excluding structure factors) for the structure reported in this paper have been deposited with the Cambridge Crystallographic Data Centre as supplementary publication no CCDC-956709 ($\mathbf{1}^{\mathbf{Fc}}$) and CCDC-956710 ($\mathbf{2}^{\mathbf{Fc}}$). Copies of the data can be obtained free of charge upon application to CCDC, 12 Union Road, Cambridge CB2 1EZ, U.K. [fax (0.44) 1223-336-033; e-mail deposit@ccdc.cam.ac.uk].

	$\mathbf{1}^{Fc}$	$\mathbf{2}^{Fc}$
empirical formula	$C_{15}H_{14}N_2Fe$	$C_{31.75}H_{28}Fe_2MoN_4O_2$
Fw	278.13	705.22
cryst syst	monoclinic	monoclinic
space group	$P2_1/n$	$P2_1/c$
a / Å	11.5135(4)	10.5484(3)
b / Å	9.2502(3)	15.3410(4)
c / Å	23.8167(9)	34.5525(10)
β / deg	100.173(1)	96.912(2)
volume / Å^3	2496.65(15)	5550.8(3)
Z	8	8
density (calcd), Mg m^3	1.480	1.688
absorp coeff, mm^{-1}	1.189	1.514
F(000)	1152.0	2852.0
cryst size, mm^3	0.62×0.21×0.02	0.41 × 0.12 × 0.06
θ range for data collection	2.37 to 35.05	2.35 to 29.19
index ranges	$-18 \le h \le 18$	$-14 \le h \le 14$
	$-14 \le k \le 14$	$-21 \le k \le 21$
	$-37 \le l \le 38$	$-47 \le l \le 47$
no. of reflns collected	133696	136381
no. of indep reflns	11016	15018
R_{int}	0.0661	0.00937
completeness to θ_{max}	99.9	99.9
max. / min transmn	0.9766 / 0.5260	0.9146 / 0.5757
goodness-of-fit on F^2	0.898	0.931
final R indices [$I > 2\sigma(I)$]]	R_1 = 0.0336	R_1 = 0.0336
	wR_2 = 0.0695	wR_2 = 0.0737
R indices (all data)	R_1 = 0.0665	R_1 = 0.0556
	wR_2 = 0.0756	wR_2 = 0.0787
Largest diff peak and hole, e / Å^3	0.550 / –0.391	0.700 / –0.733

DFT calculations were carried out with the *Gaussian09*/DFT[9] series of programs. The B3LYP formulation of DFT was used employing the LANL2DZ basis set set supplemented by d-type polarisation functions[10] on N (ζ = 0.864), O (ζ = 1.154) and P (ζ = 0.340).[9] No symmetry constraints were imposed on the molecules. The presence of energy minima was checked by analytical frequency calculations. The integral-equation-formalism polarisable continuum model (IEFPCM, THF) was employed for solvent modeling. All calculations were performed without explicit counterions and solvent molecules. For NBO calculations NBO Version 3.1 as implemented in Gaussian 03 was used.

Description of the stereochemistry of 2^{Fc} and $3a^{Fc}$

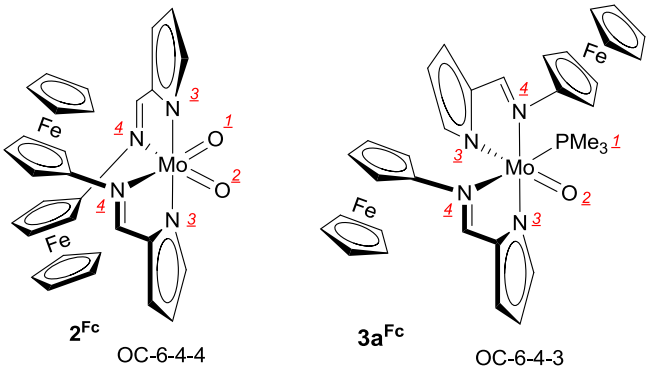

The stereochemistry of the complexes under study will be described by the configuration index according to the Cahn-Ingold-Prelog system[11-14] in an octahedral complex OC-6-x-y with the priority sequence used as follows: PMe_3 > O > $N^{pyrrolato}$ > N^{imine}. The first index x refers to the ligand priority of the ligand *trans* to the ligand of the highest priority (axial ligands) and the second index y refers to the ligand priority *trans* to that ligand of the equatorial plane which has the highest priority of these four equatorial ligands. Thus, molybdenum(VI) complex $\mathbf{2^{Fc}}$ possess OC-6-4-4 stereochemistry, while molybdenum(IV) complex $\mathbf{3a^{Fc}}$ is the OC-6-4-3 stereoisomer as depicted in the above scheme. For the sake of better comparison with previously reported oxido/imido complexes[15] we have enumerated both oxido ligands in $\mathbf{2^{Fc}}$. Correctly, the preferred isomer of $\mathbf{2^{Fc}}$ should be described by OC-6-3-3 as there is no distinguished fourth donor atom present.

[Cartesian coordinates from DFT calculations (p. 19–27) omitted]

1 B. Bildstein, M. Malaun, H. Kopacka, K. Wurst, M. Mitterböck, K.-H. Ongania, G. Opromolla and P. Zanello, *Organometallics* **1999**, *18*, 4325-4336.

2 K. Heinze and M. Schlenker, *Eur. J. Inorg. Chem.* **2004**, 2974-2988.

3 K. A. Rufanov, D. N. Zarubin, N. A. Ustynyuk, D. N. Gourevitch, J. Sundermeyer, A. V. Churakov and J. A. K. Howard, *Polyhedron*, **2001**, *20*, 379-385.

4 S. Stoll and A. Schweiger, *J. Magn. Reson.* **2006**, *178*, 42-55.

5 *SMART Data Collection and SAINT-Plus Data Processing Software for the SMART System*, various versions; Bruker Analytical X-ray Instruments, Inc.: Madison, WI, **2000**.

6 R. H. Blessing, *Acta Crystallogr.* **1995**, *A51*, 33–38.

7 G. M. Sheldrick, *SHELXTL*, version 5.1; Bruker AXS: Madison, WI, **1998**.

8 G. M. Sheldrick, *SHELXL-97*; University of Göttingen: Göttingen, Germany, **1997**.

9 a) M. J. Frisch, G. W. Trucks, H. B. Schlegel, G. E. Scuseria, M. A. Robb, J. R. Cheeseman, G. Scalmani, V. Barone, B. Mennucci, G. A. Petersson, H. Nakatsuji, M.

Caricato, X. Li, H. P. Hratchian, A. F. Izmaylov, J. Bloino, G. Zheng, J. L. Sonnenberg, M. Hada, M. Ehara, K. Toyota, R. Fukuda, J. Hasegawa, M. Ishida, T. Nakajima, Y. Honda, O. Kitao, H. Nakai, T. Vreven, J. A. Montgomery, Jr., J. E. Peralta, F. Ogliaro, M. Bearpark, J. J. Heyd, E. Brothers, K. N. Kudin, V. N. Staroverov, R. Kobayashi, J. Normand, K. Raghavachari, A. Rendell, J. C. Burant, S. S. Iyengar, J. Tomasi, M. Cossi, N. Rega, J. M. Millam, M. Klene, J. E. Knox, J. B. Cross, V. Bakken, C. Adamo, J. Jaramillo, R. Gomperts, R. E. Stratmann, O. Yazyev, A. J. Austin, R. Cammi, C. Pomelli, J. W. Ochterski, R. L. Martin, K. Morokuma, V. G. Zakrzewski, G. A. Voth, P. Salvador, J. J. Dannenberg, S. Dapprich, A. D. Daniels, O. Farkas, J. B. Foresman, J. V. Ortiz, J. Cioslowski and D. J. Fox *Gaussian 09*, revision A.02, Gaussian, Inc.: Wallingford CT, **2009**; b) NBO version 3.1 is incorporated within Gaussian 03 program package: E. D. Glendening, A. E. Reed, J E. Carpenter and F. Weinhold.

10 S. Huzinaga, J. Andzelm, M. Klobukowski, E. Radzio-Andzelm, Y. Sakai and H. Tatewaki, *Gaussian Basis Sets for Molecular Orbital Calculations*, Elsevier, Amsterdam, **1984**.

11 R. S. Cahn, C. K. Ingold and V. Prelog, *Angew. Chem.* **1966**, *78*, 413-447; *Angew. Chem. Int. Ed. Engl.* **1966**, *5*, 385-415.

12 V. Prelog and G. Helmchen, *Angew. Chem.* **1982**, *94*, 614-631; *Angew. Chem. Int. Ed. Engl.* **1982**, *21*, 567-583.

13 B. P. Block, W. H. Powell and W. C. Fernelius, *Inorganic chemical nomenclature :principles and practice*, ACS Professional Reference Book, American Chemical Society, Washington, DC, **1990**.

14 A. von Zelewsky, *Stereochemistry of Coordination Compounds*, John Wiley & Sons Ltd. **1996**.

15 K. Hüttinger, C. Förster, T. Bund, D. Hinderberger and K. Heinze, *Inorg. Chem.* **2012**, *51*, 4180-4192.

16 N. G. Connelly and W. E. Geiger, *Chem. Rev.* **1996**, *96*, 877.

7.4 Coupled oxygen atom transfer and electron transfer in dioxido molybdenum(VI) complexes bearing neutral and oxidized ferrocenyl substituents

Kristina Hanauer, Christoph Förster and Katja Heinze

Supporting Information

Table S1. X-ray data of compounds **3**^{Fc} and **4**^{Fc}.

	3^{Fc}	**4**^{Fc}
empirical formula	$C_{33}H_{35}Fe_2MoN_4OP$	$C_{60}H_{52}Fe_4Mo_2N_8O_3$
Fw	742.28	1348.41
cryst syst	monoclinic	monoclinic
space group	$P2_1/c$	$P2_1/c$
a / Å	12.0750(10)	11.238(4)
b / Å	13.2747(10)	28.979(10)
c / Å	19.6383(16)	10.674(4)
α / deg	90	90
β / deg	103.734(3)	90
γ / deg	90	89.94(1)
volume / Å^3	3057.9(4)	3476(2)
Z	4	2
density (calcd), Mg m^3	1.612	1.564
absorp coeff, mm^{-1}	1.426	1.224
F(000)	1512	1680.0
cryst size, mm^3	0.22×0.05×0.02	0.38 × 0.05 × 0.02
θ range for data collection	1.74 to 28.01	2.29 to 27.86
index ranges	$-15 \le h \le 15$	$-14 \le h \le 14$
	$-17 \le k \le 17$	$-37 \le k \le 38$
	$-25 \le l \le 25$	$-14 \le l \le 13$
no. of reflns collected	62533	37636
no. of indep reflns	7357	8232
R_{int}	0.1374	0.0982
completeness to θ_{max}	99.6	99.3
max. / min transmn	0.9720 / 0.7444	0.9759 / 0.6535
goodness-of-fit on F^2	0.772	0.948
final R indices [$I > 2\sigma(I)$]]	R_1 = 0.0364	R_1 = 0.0481
	wR_2 = 0.0562	wR_2 = 0.0868
R indices (all data)	R_1 = 0.0907	R_1 = 0.0848
	wR_2 = 0.0651	wR_2 = 0.0951
Largest diff peak and hole, e / Å^3	0.561 / –0.489	1.218 / –0.792

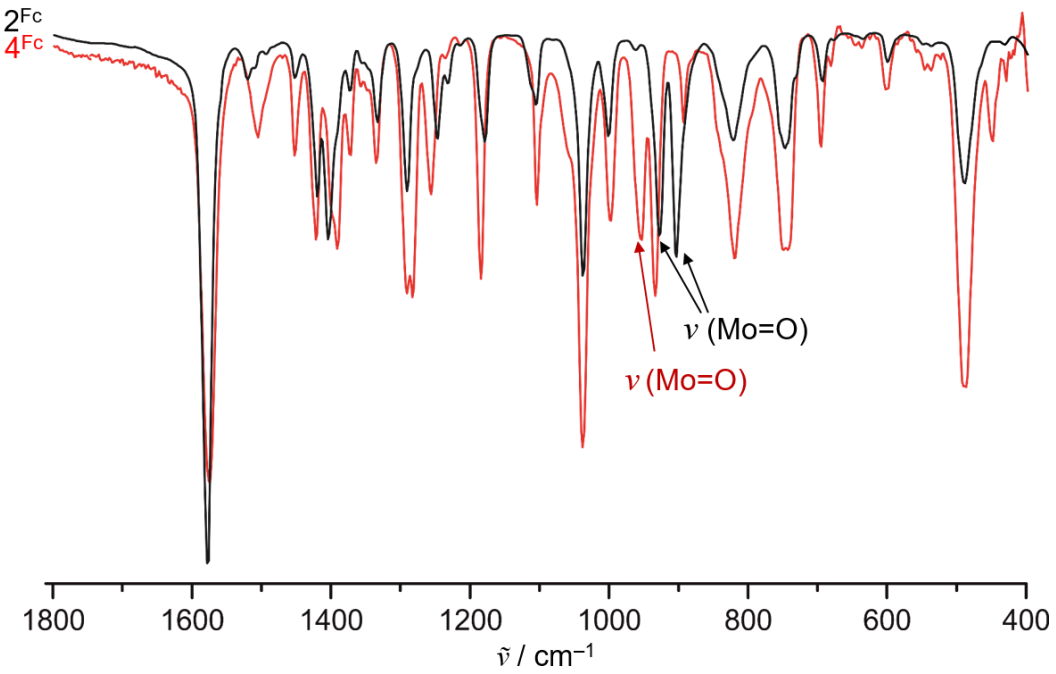

Figure S1. IR spectra of **2**^{Fc} and **4**^{Fc} in CsI.

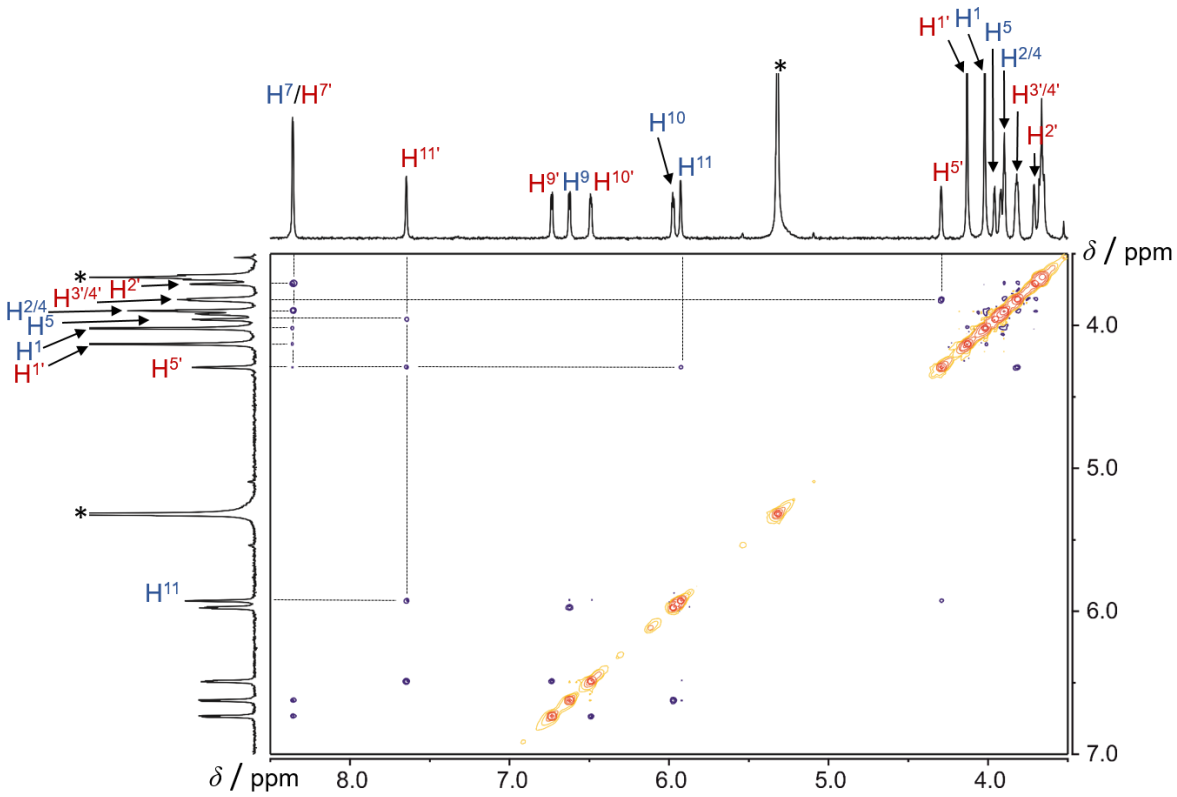

Figure S2. $^{1}H^{1}H$-NOESY spectrum of **4**^{Fc} in CD_2Cl_2.

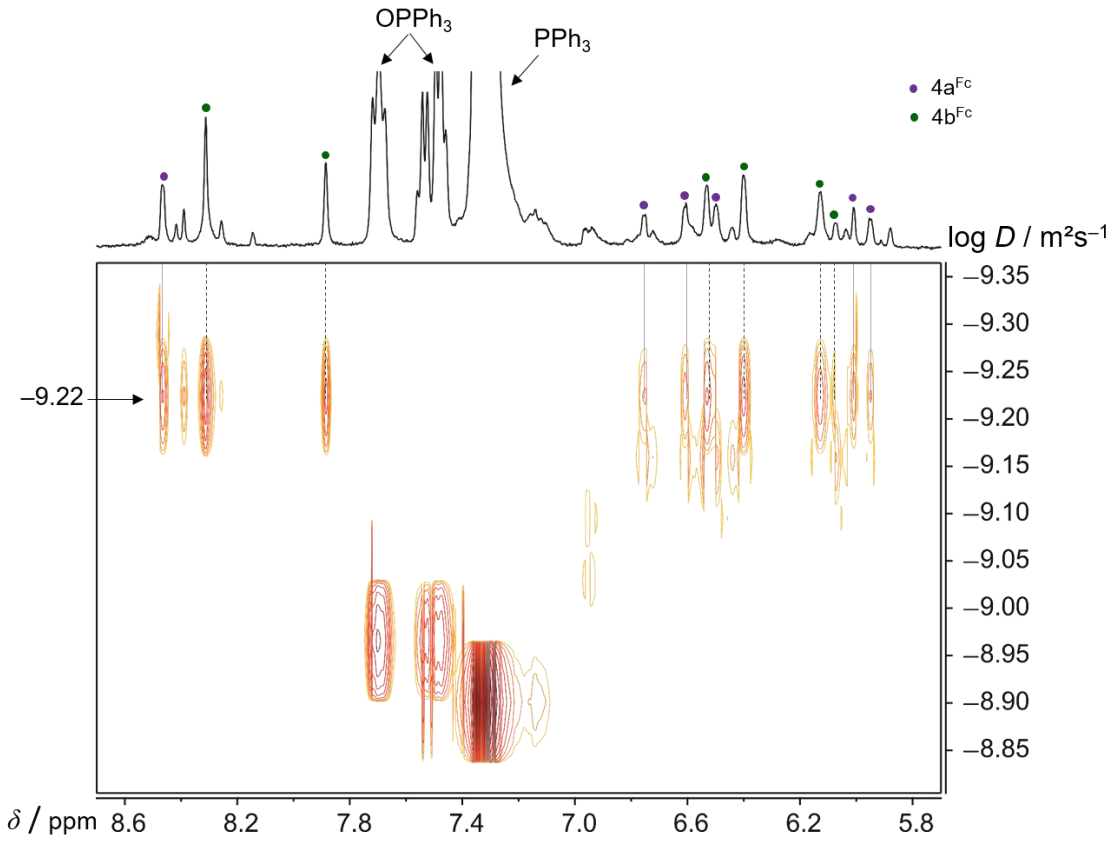

Figure S3. DOSY spectrum of the reaction mixture of **2**^{Fc} with PPh_3 in d_8-THF.

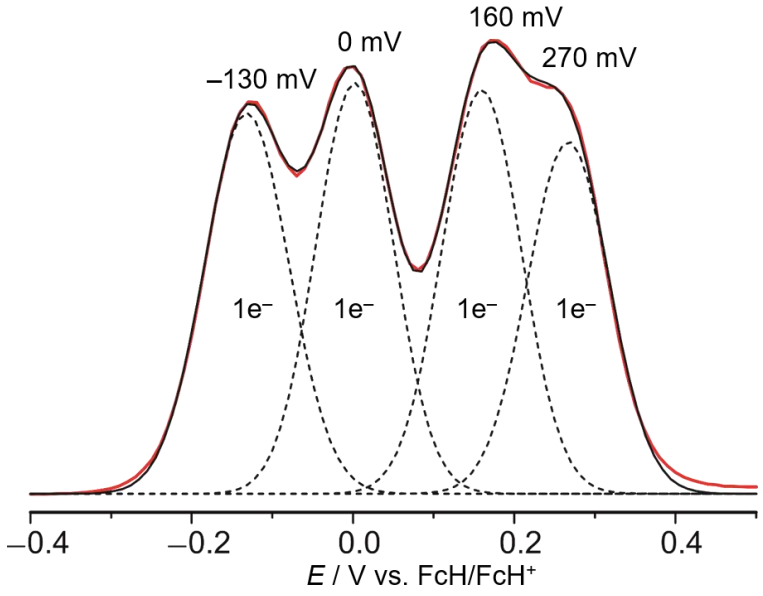

Figure S4. Square wave voltammogram of **4**^{Fc} in CH_2Cl_2 / $[^nBu_4N][B(C_6F_5)_4]$.

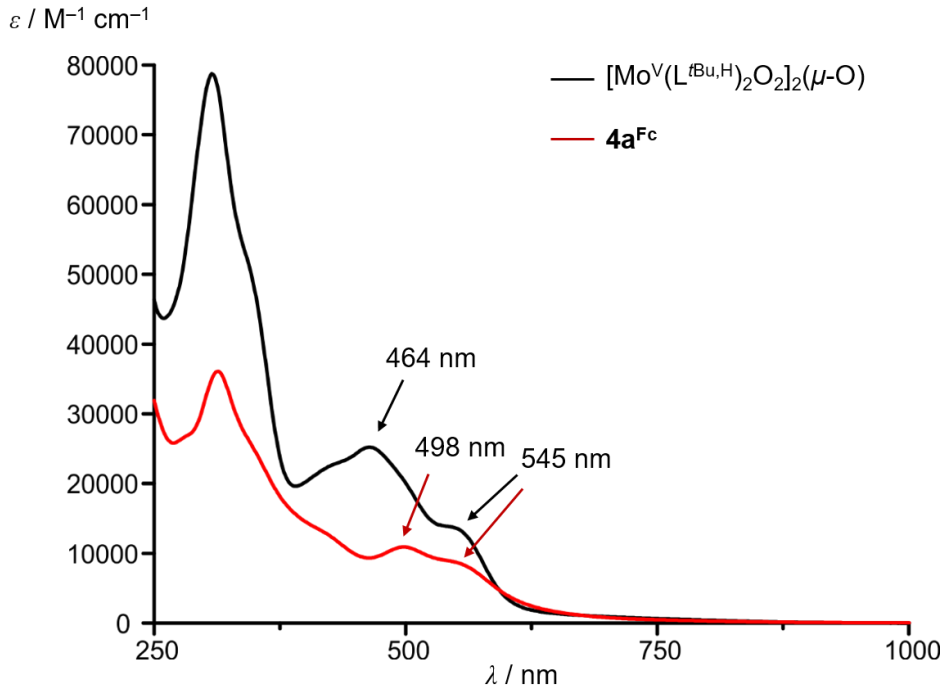

Figure S5. UV-Vis absorption spectra of **4**^{Fc} in CH_2Cl_2 and of $[Mo^V(L^{tBu,H})_2O_2]_2(\mu\text{-O})$ in THF.

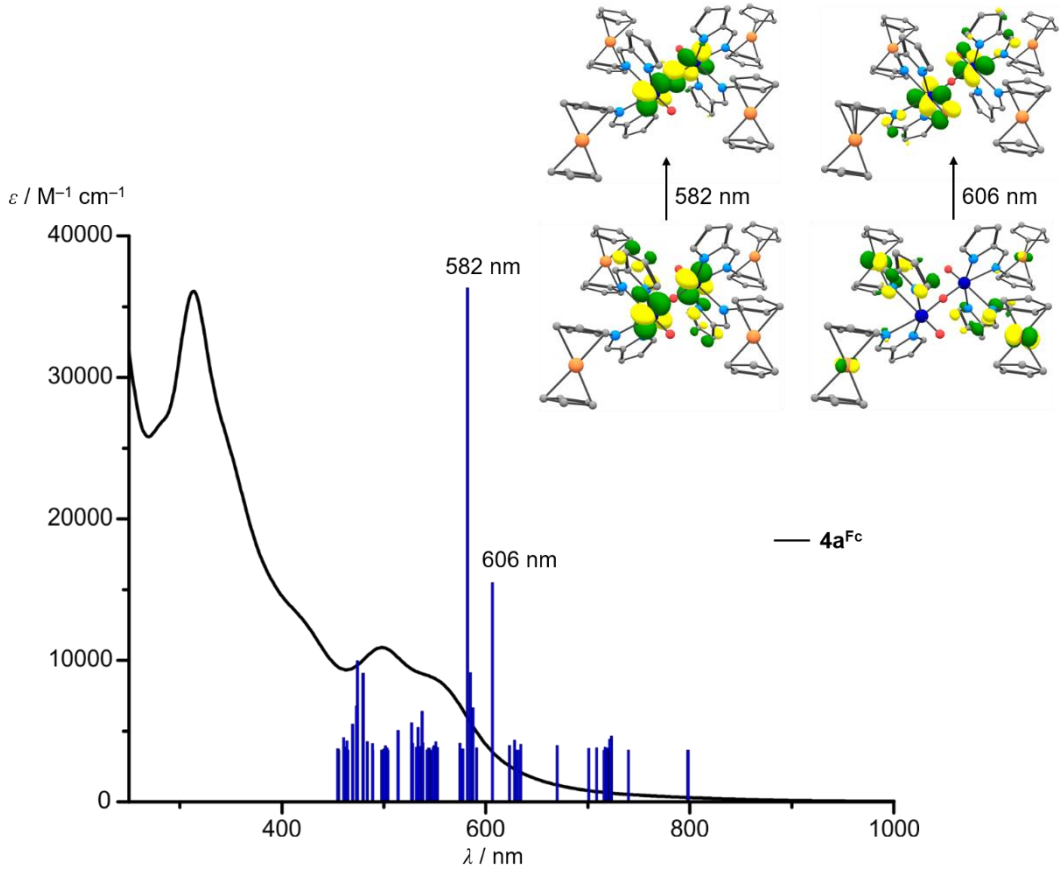

Figure S6. UV-Vis absorption spectrum of **4**^{Fc} in CH_2Cl_2 and TD-DFT-calculated absorption bands.

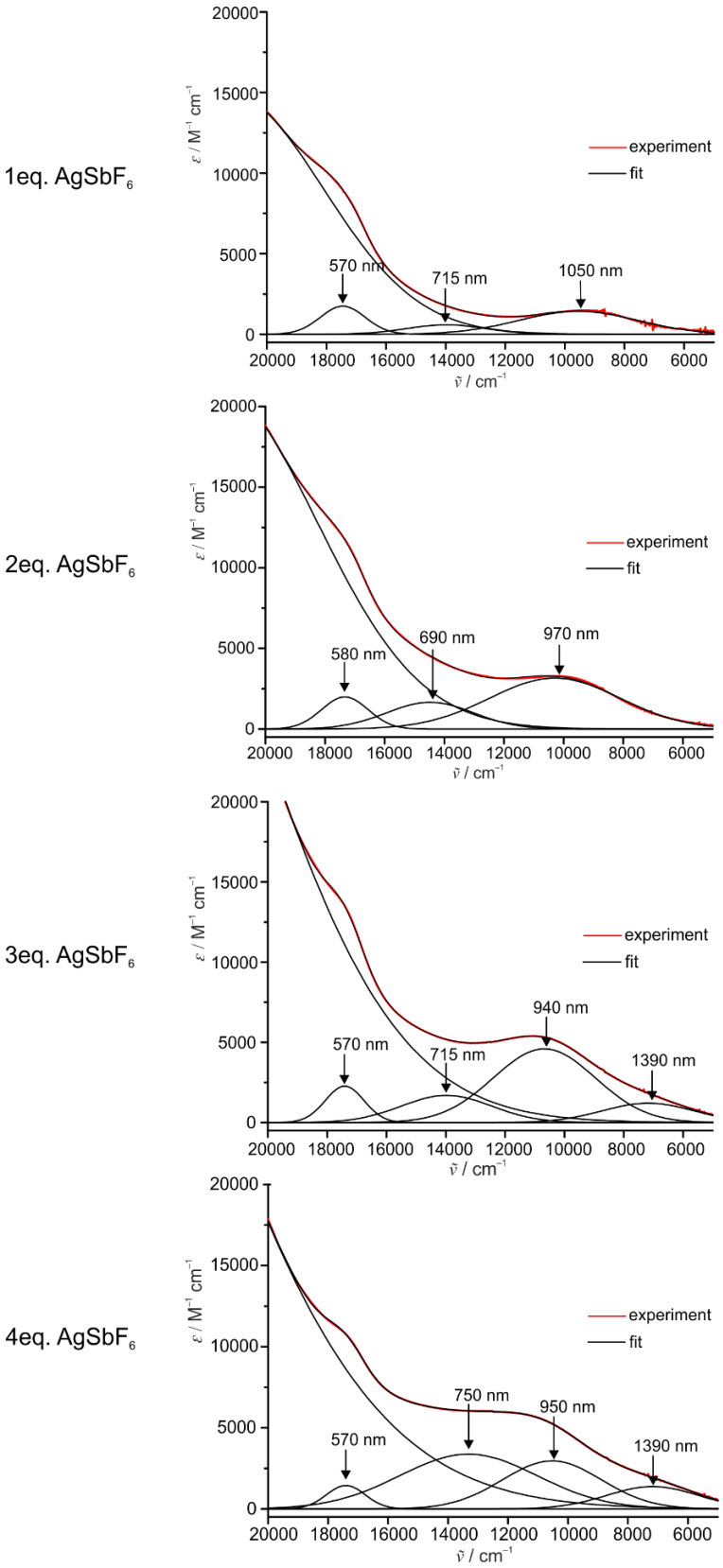

Figure S7. Gaussian band shape analysis of the UV-Vis spectra of $\mathbf{4}^{\mathbf{Fc}}$ after addition of 1-4 eq. of $AgSbF_6$.

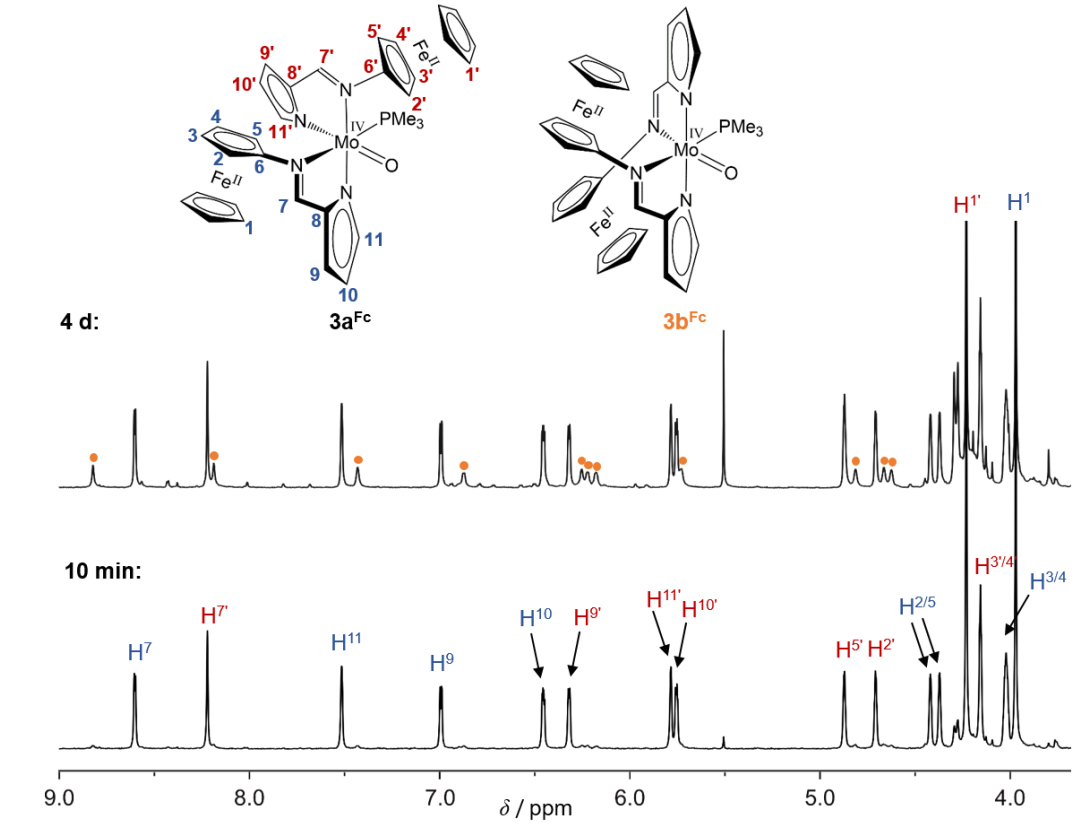

Figure S8. ^{1}H-NMR spectra of crystals of **3a^{Fc}** after dissolution in d_8-THF.

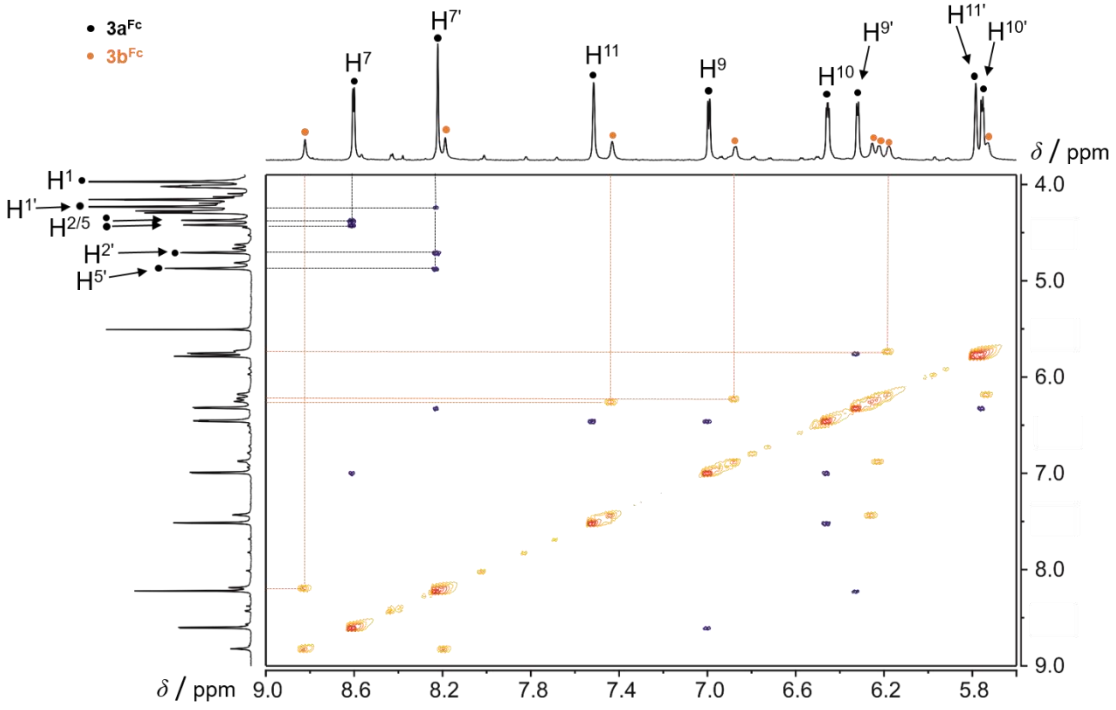

Figure S9. ^{1}H^{1}H NOESY/EXSY spectrum of **3^{Fc}** in d_8-THF.

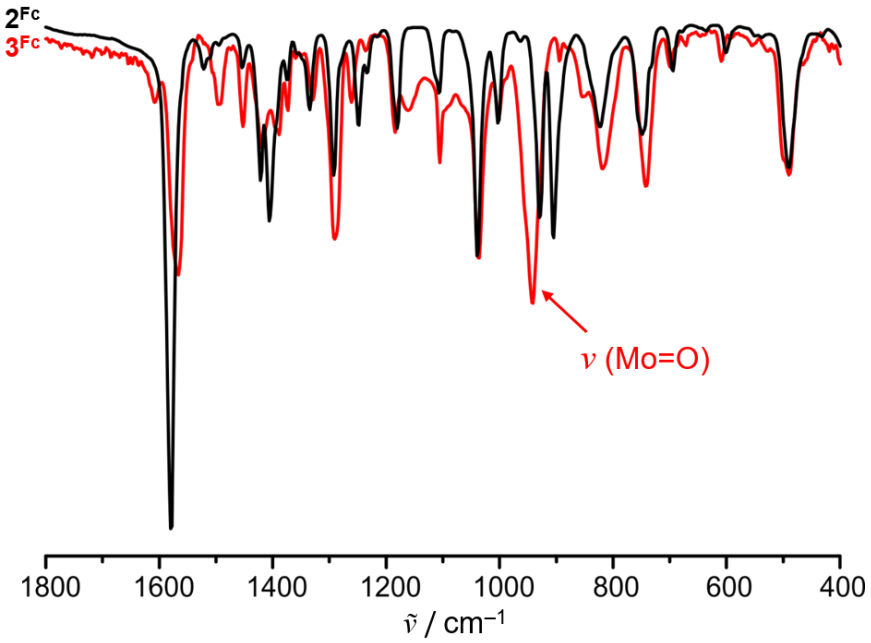

Figure S10. IR spectra of **2**^{Fc} and **3**^{Fc} in CsI.

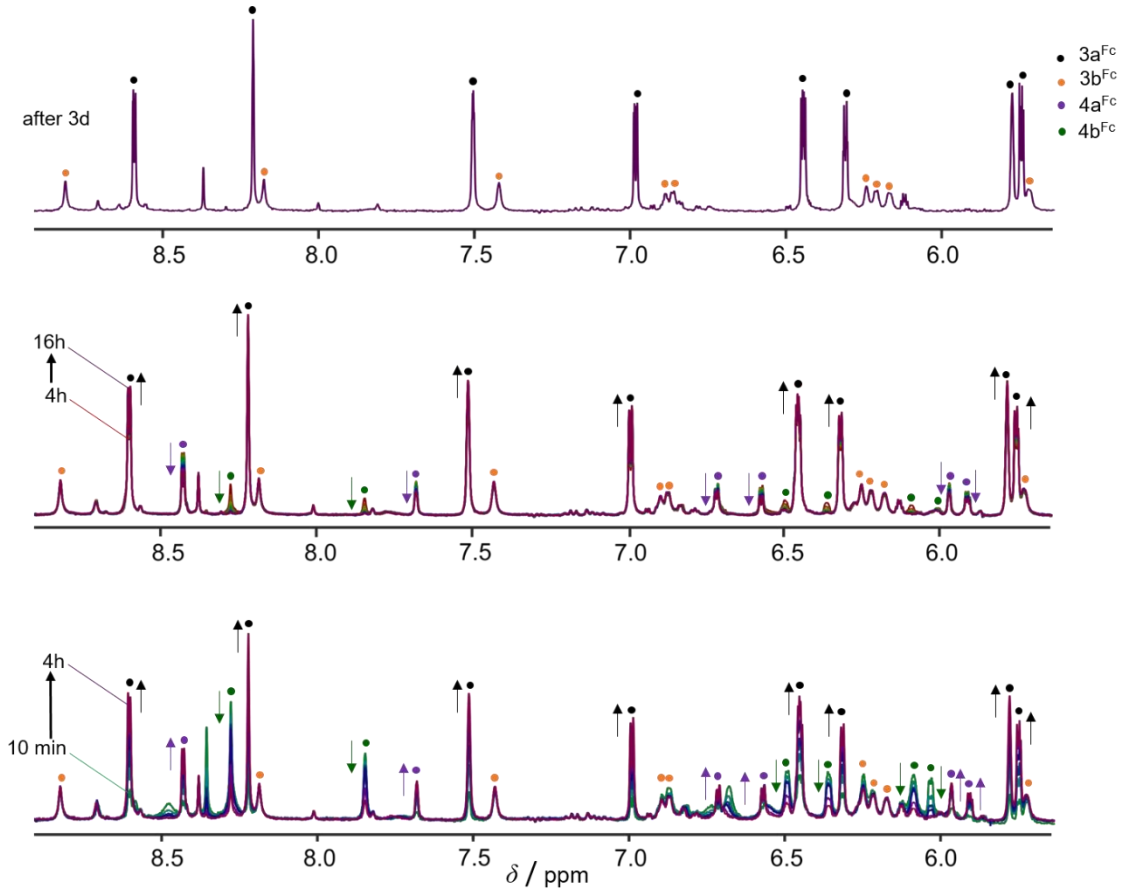

Figure S11. ^{1}H-NMR spectra of the reaction of **2**^{Fc} with 5 eq. PMe_3 in d_8-THF (c = 0.01 mol L^{-1}).

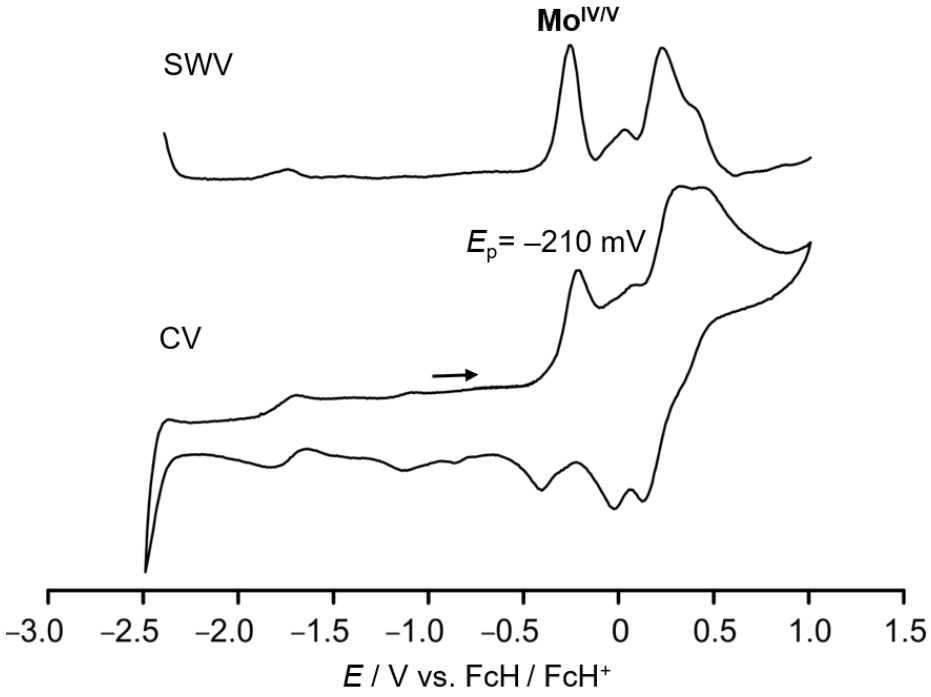

Figure S12. Square wave voltammogram (top) and cyclic voltammogram (bottom) of $\mathbf{3^{Fc}}$ in THF / $[^{n}Bu_4N][B(C_6F_5)_4]$.

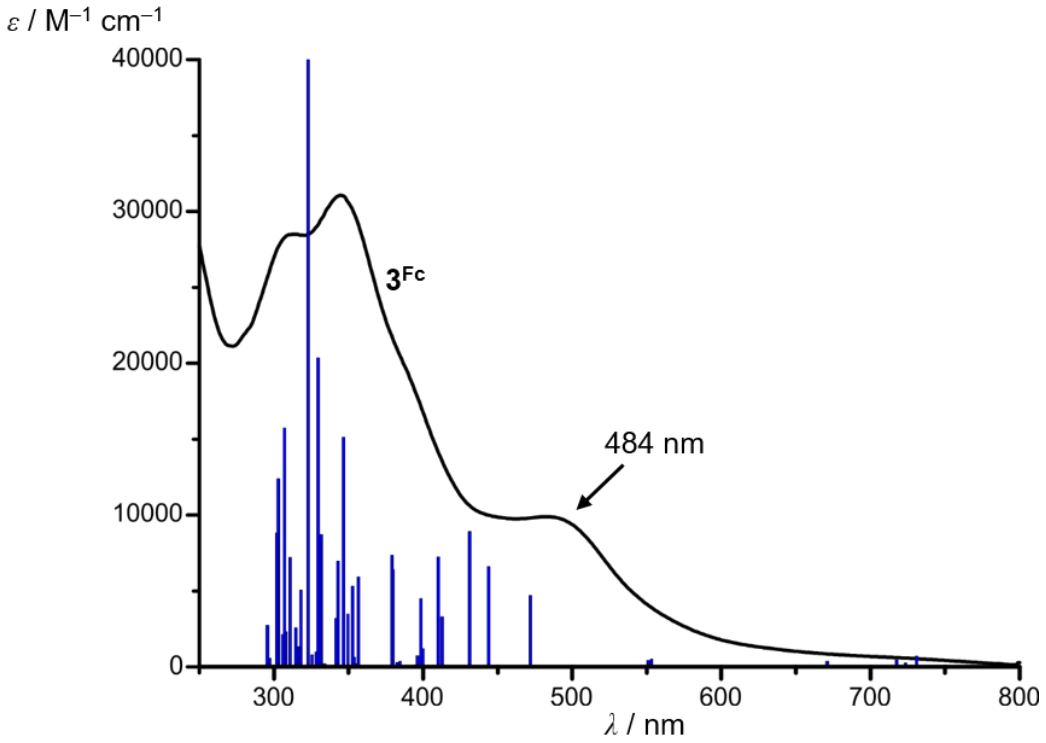

Figure S13. UV-Vis/NIR absorption spectrum of $\mathbf{3^{Fc}}$ in THF and TD-DFT-calculated absorption bands.

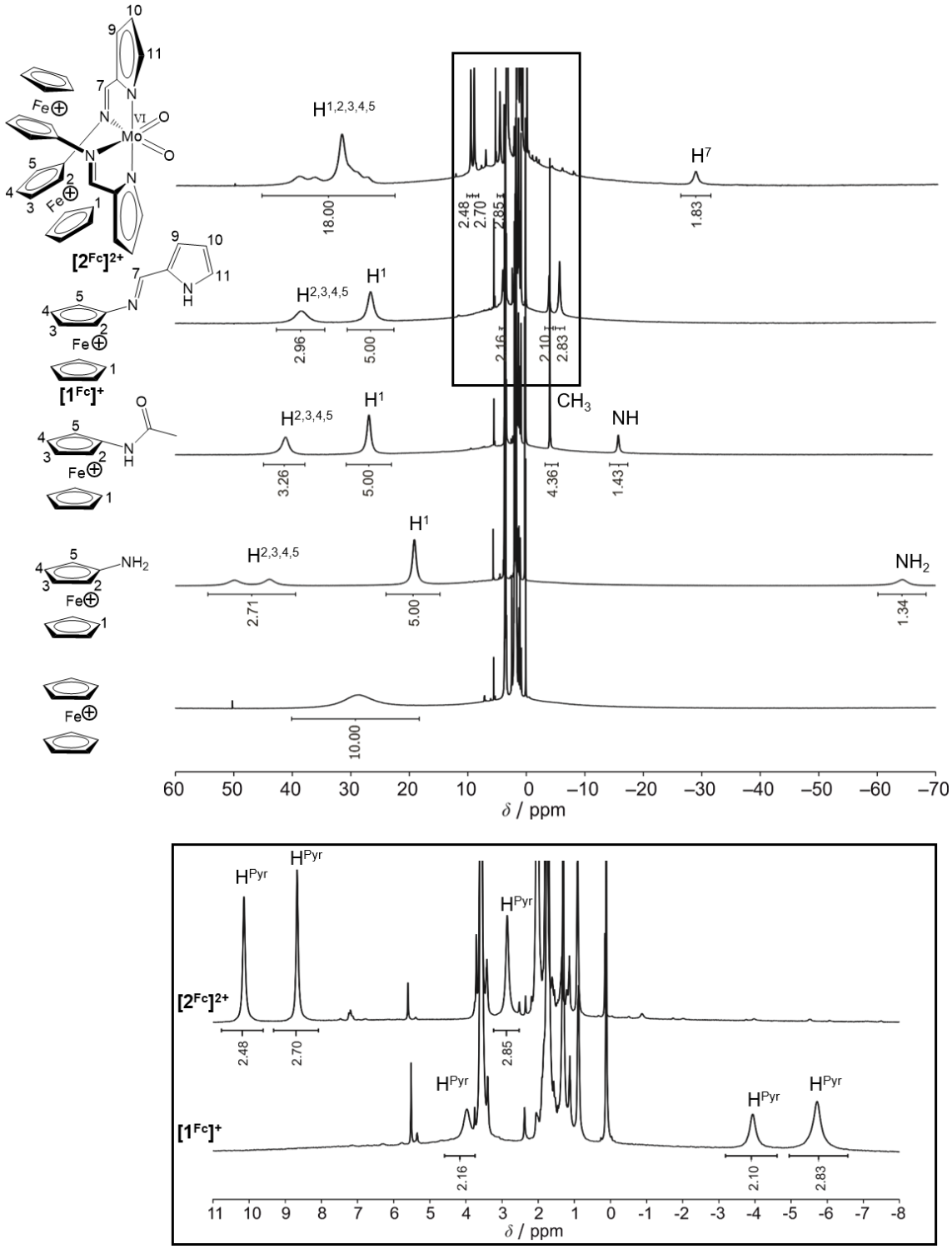

Figure S14. ^{1}H-NMR spectra of **[1^{Fc}]$^{+}$** and **[2^{Fc}]$^{2+}$**, Fc^{+}, $[FcNH_2]^{+}$ and $[FcNHAc]^{+}$ in d_8-THF.

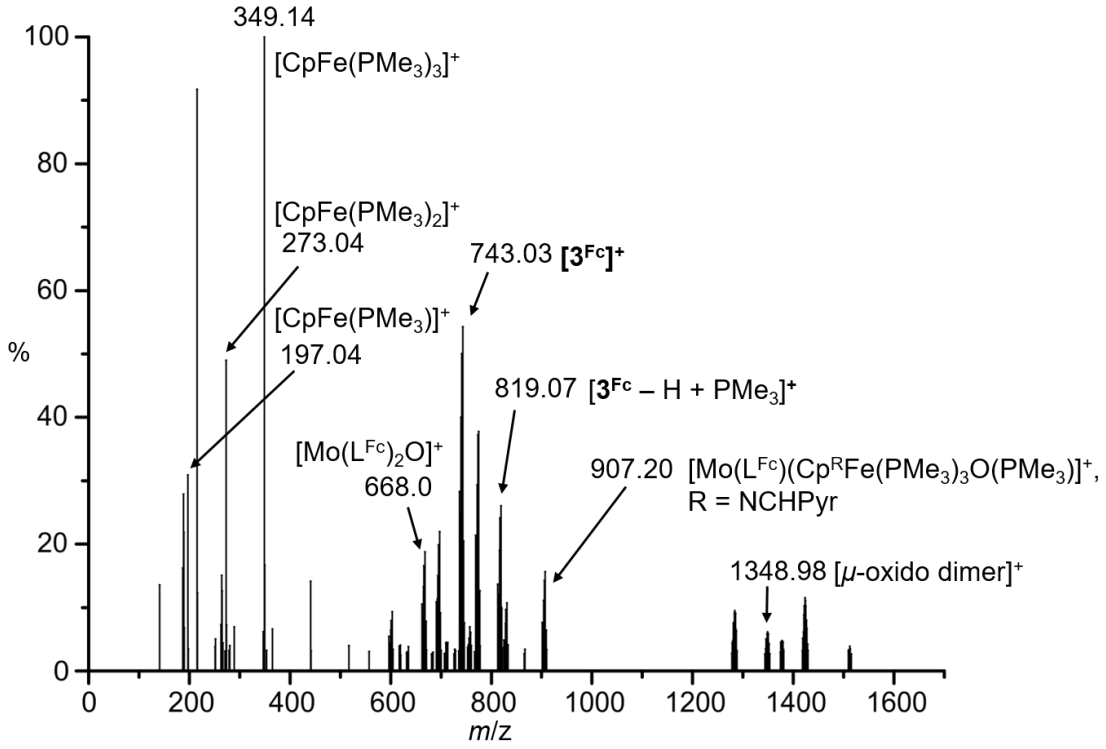

Figure S15. ESI$^+$ mass spectrum of $\mathbf{[2^{Fc}]^{2+}}$ with an excess of PMe_3.

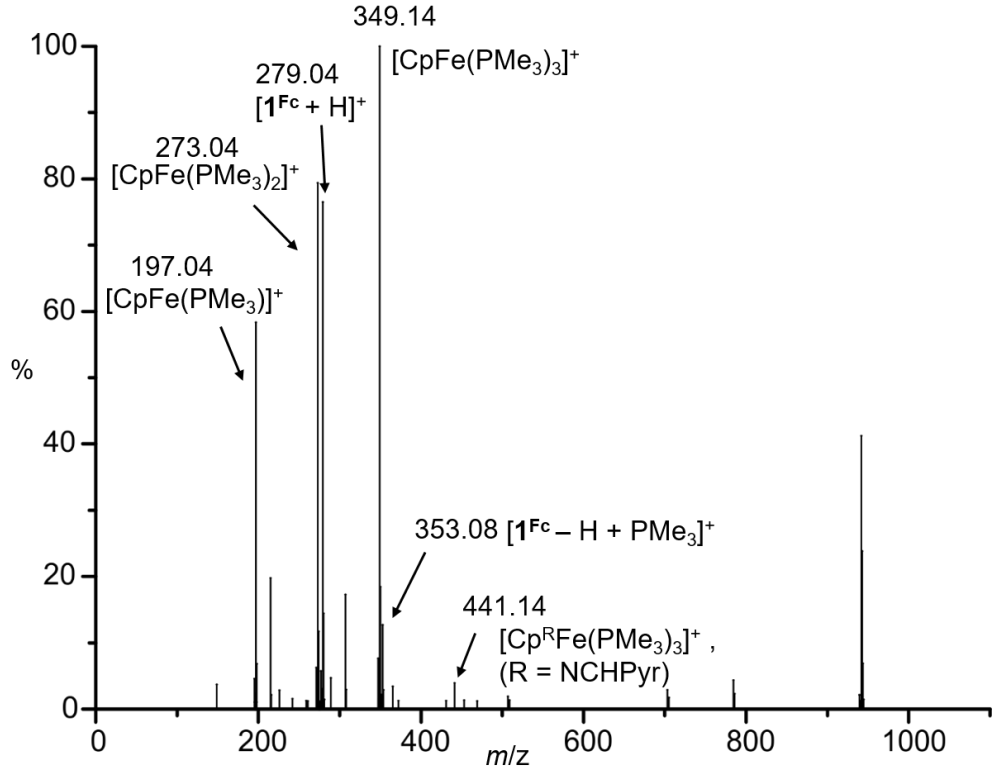

Figure S16. ESI$^+$ mass spectrum of $\mathbf{[1^{Fc}]^+}$ with an excess of PMe_3.

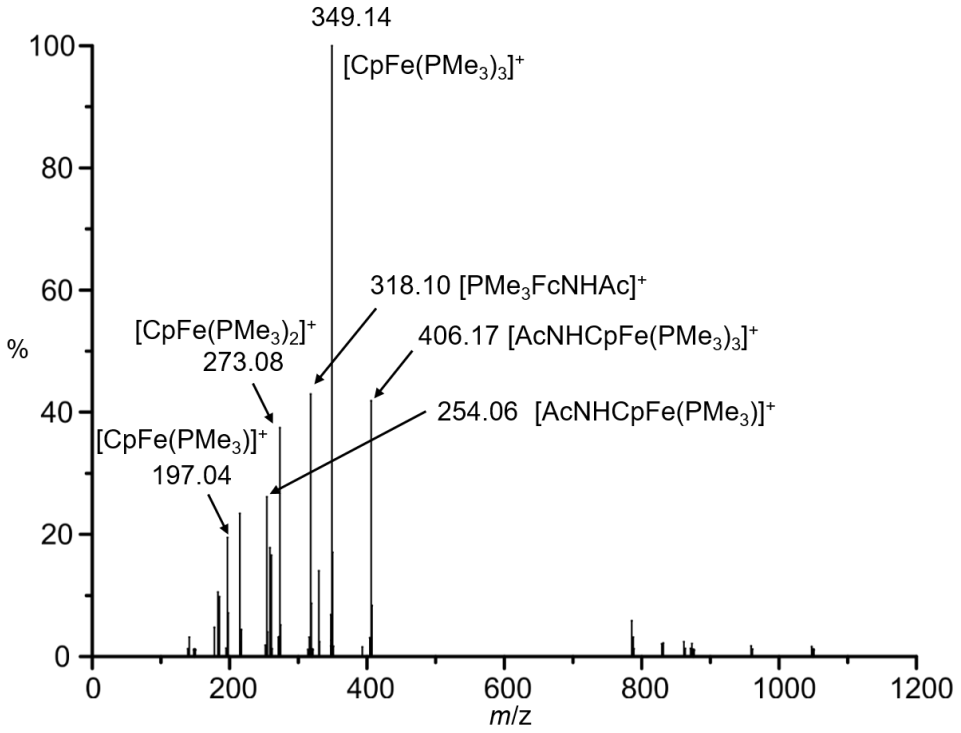

Figure S17. ESI$^+$ mass spectrum of [FcNHAc]$^+$ with an excess of PMe_3.

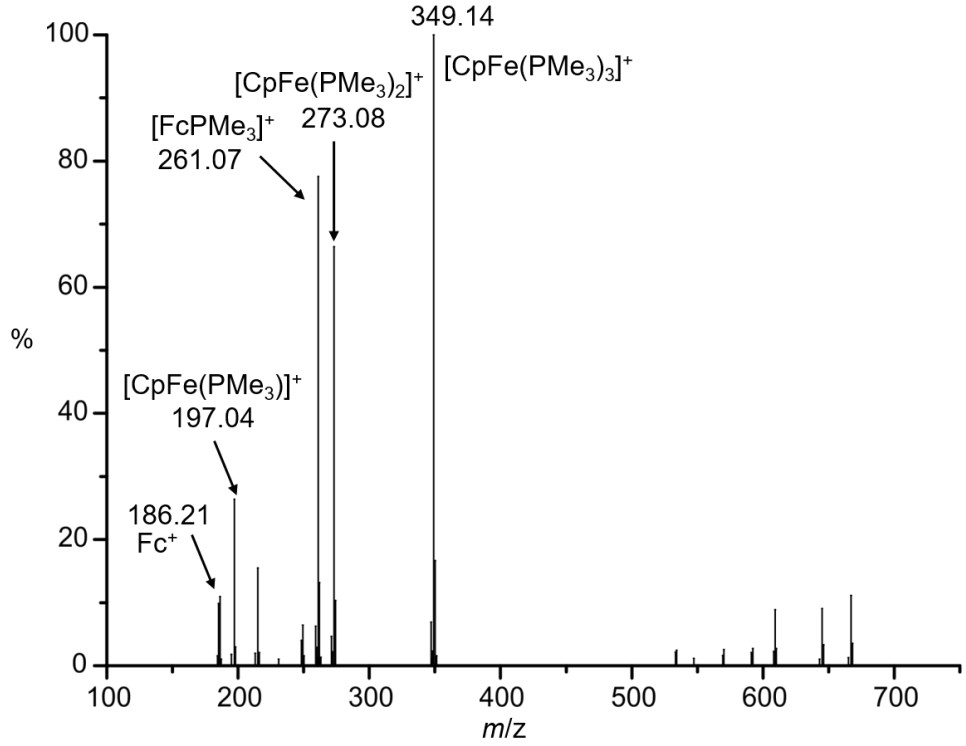

Figure S18. ESI$^+$ mass spectrum of Fc^+ with an excess of PMe_3.

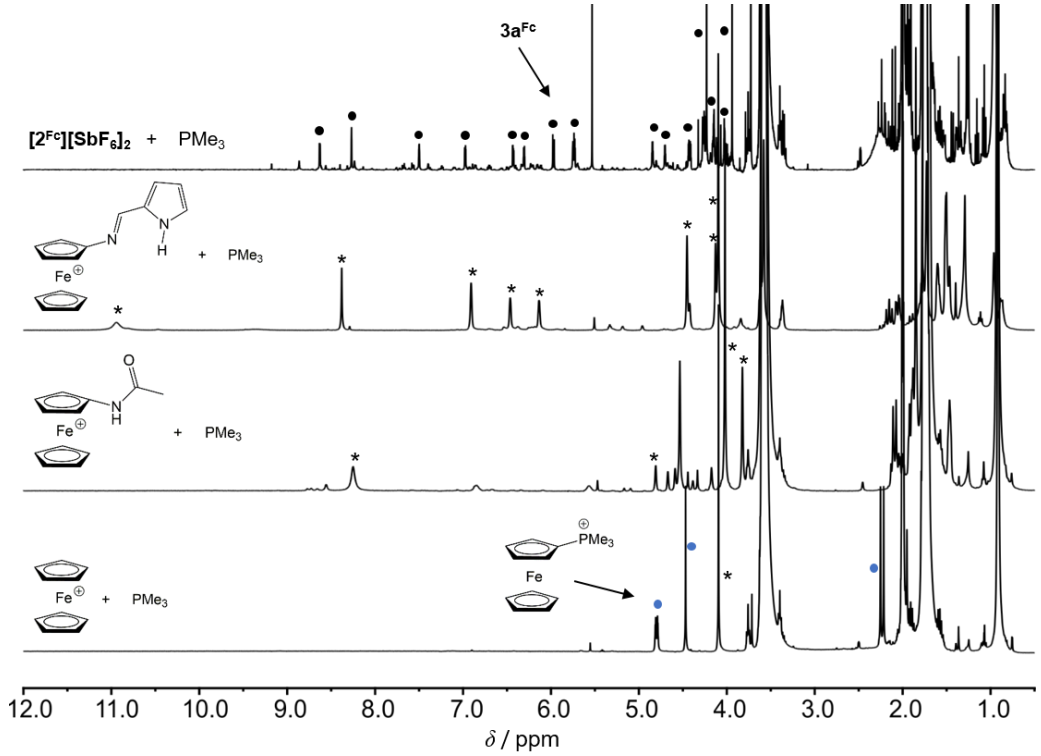

Figure S19. ^{1}H-NMR spectra of $[\mathbf{2^{Fc}}]^{2+}$, $[\mathbf{1^{Fc}}]^{+}$, $[FcNHAc]^{+}$ and Fc^{+} with PMe_3 in d_8-THF and d_8-THF / d_6-acetone in the case of $[\mathbf{2^{Fc}}][\mathbf{SbF_6}]_2$. The proton signals of the neutral compounds are indicated by *.

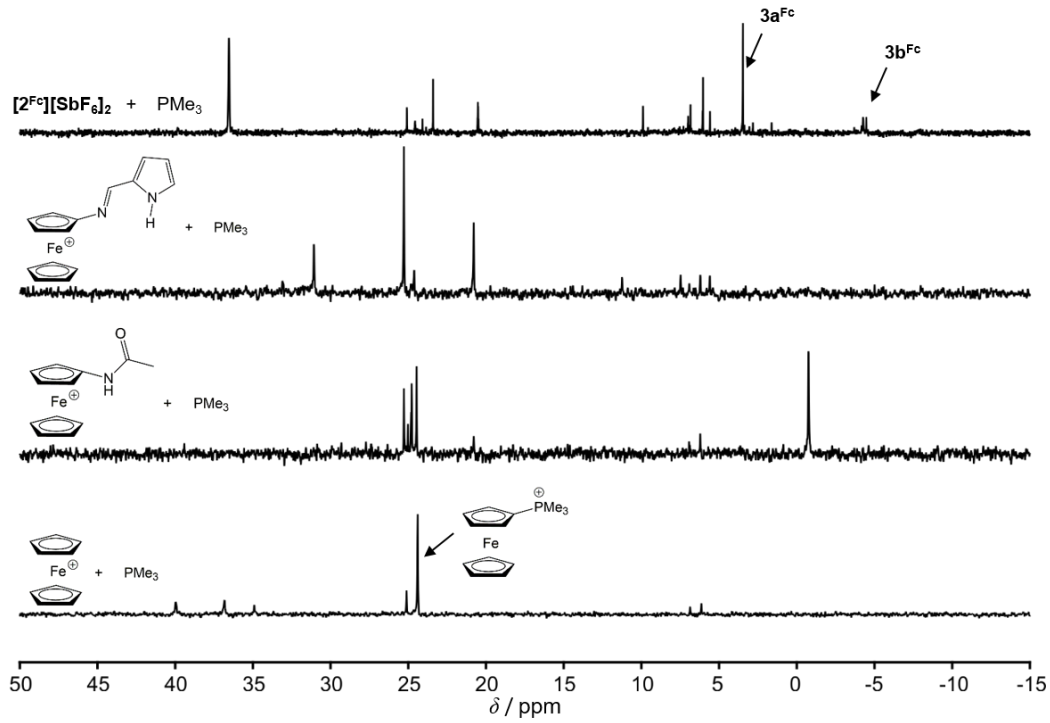

Figure S20. ^{31}P-NMR spectra of $[\mathbf{2^{Fc}}]^{2+}$, $[\mathbf{1^{Fc}}]^{+}$, $[FcNHAc]^{+}$ and Fc^{+} with PMe_3 in d_8-THF and d_8-THF / d_6-acetone in the case of $[\mathbf{2^{Fc}}]^{2+}$.

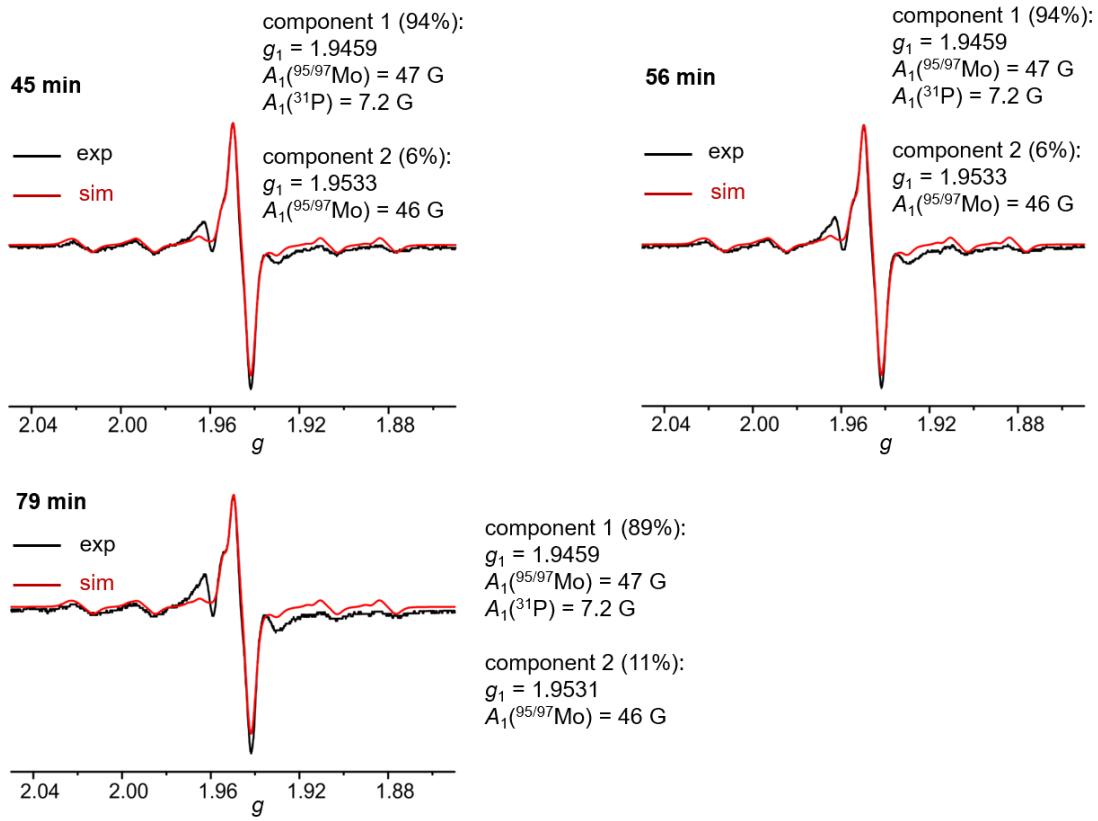

Figure S21. X-Band CW EPR spectra of **[5^{Fc}]$^+$** measured within 80 min, after warming the solution to 295 K in THF (ν = 9.42 GHz, field = 3465.4 G, sweep = 94.74 G, sweep time = 60 s, modulation = 700 mG and MW attenuation = 10 dB, c = 23 mmol L^{-1}). Simulated spectra are presented in red (Gauss pp linewidth = 0.7 MHz, Lorentz pp linewidth = 0.3 MHz).

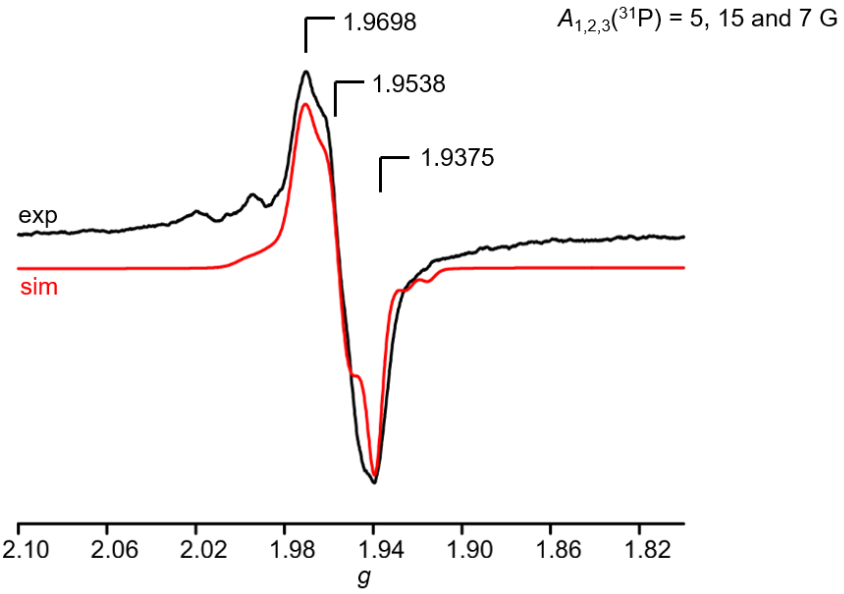

Figure S22. X-Band CW EPR spectrum of **[5^{Fc}]$^+$** in THF at 77 K (ν = 9.42 GHz).

DFT-optimized Cartesian coordinates (in Å)

Fc

Fe	-0.000015	-0.000177	-0.000095
H	1.723775	-2.047763	1.068386
C	-1.728587	1.214782	0.183966
H	-1.722603	2.283817	0.345760
C	-1.728651	0.550380	-1.098261
H	-1.723293	1.034790	-2.064921
C	-1.728871	-0.874494	-0.862724
H	-1.723068	-1.644191	-1.622077
C	-1.728992	-1.090725	0.565114
H	-1.723983	-2.050737	1.062543
C	-1.728530	0.200482	1.211991
H	-1.722920	0.376758	2.278775
C	1.728905	-1.089171	0.568230
C	1.728496	0.203889	1.211458
H	1.722797	0.383164	2.277742
C	1.728646	1.215246	0.180566
H	1.722724	2.284734	0.339351
C	1.728785	0.547228	-1.099756
H	1.723532	1.028897	-2.067787
C	1.728870	-0.876964	-0.860231
H	1.723006	-1.648790	-1.617418

Fc^+ (I)

Fe	-0.000144	-0.001689	-0.002841
H	-1.847414	2.141876	-0.836447
C	1.748405	-0.546058	1.098070
H	1.725267	-1.034338	2.061879
C	1.817176	-1.203394	-0.185707
H	1.832103	-2.271260	-0.353480
C	1.855403	-0.189301	-1.204850
H	1.889136	-0.363495	-2.271572
C	1.806441	1.096177	-0.561908
H	1.810936	2.055326	-1.060677
C	1.742132	0.881817	0.864409
H	1.713877	1.651342	1.622571
C	-1.830211	1.134944	-0.443053
C	-1.761039	0.770989	0.950788
H	-1.744712	1.456101	1.786486
C	-1.737799	-0.673430	1.032137
H	-1.710414	-1.259849	1.939447
C	-1.790175	-1.191772	-0.315745
H	-1.788364	-2.235563	-0.596741
C	-1.849928	-0.073908	-1.220438
H	-1.879102	-0.132608	-2.299831

$CpFeC_5H_4$ (II)

Fe	-0.020671	-0.000167	-0.030115
H	-1.857592	1.353585	1.778477
C	1.723912	-1.169993	-0.333327
H	1.730432	-2.199785	-0.662336
C	1.760663	-0.006243	-1.187801
H	1.800636	-0.011729	-2.268001
C	1.723973	1.166213	-0.345262
H	1.730367	2.192583	-0.684791
C	1.669661	0.727209	1.028973
H	1.631903	1.367733	1.899249
C	1.669585	-0.716990	1.036346
H	1.631779	-1.348605	1.913118
C	-1.806135	0.722865	0.901276
C	-1.806496	-0.722587	0.901323
H	-1.858182	-1.353382	1.778462
C	-1.713568	-1.184315	-0.469841
H	-1.686069	-2.211231	-0.803543
C	-1.658818	0.000015	-1.289104
C	-1.712926	1.184469	-0.469896
H	-1.684938	2.211318	-0.803762

PMe_3

P	-0.000450	-0.000652	-0.612740
C	1.220310	-1.116541	0.283844
H	1.041483	-2.161364	-0.001938
H	2.244161	-0.852084	-0.011455
H	1.128897	-1.024193	1.374506
C	0.358119	1.614505	0.283318
H	1.349669	1.984585	-0.008629
H	-0.386427	2.367985	-0.005271
H	0.332299	1.487152	1.373998
C	-1.577797	-0.497095	0.284228
H	-2.392791	0.178862	-0.006027
H	-1.860099	-1.517246	-0.007384
H	-1.454241	-0.459132	1.374960

$HPMe_3^+$

P	-0.000065	-0.000159	-0.339651
C	-1.732010	-0.175772	0.216342
H	-2.325976	0.660599	-0.165455
H	-2.146278	-1.116709	-0.160076
H	-1.766788	-0.175783	1.310870
C	1.018365	-1.411636	0.216230
H	0.591474	-2.344762	-0.164408
H	2.039387	-1.299280	-0.161550
H	1.037493	-1.440859	1.310832
C	0.713882	1.587566	0.216227
H	1.736714	1.683120	-0.162288
H	0.107265	2.415589	-0.163640
H	0.727021	1.619210	1.310769
H	-0.000759	0.000308	-1.753084

$OPMe_3$

P	-0.000041	0.000095	0.176895
C	-1.115040	-1.274107	-0.557138
H	-0.799722	-2.268249	-0.218435
H	-2.141156	-1.096982	-0.213551
H	-1.091054	-1.242145	-1.652846
C	-0.546643	1.601518	-0.558710
H	-1.564258	1.826427	-0.217691
H	0.121017	2.401705	-0.217796
H	-0.533853	1.563349	-1.654515
C	1.660319	-0.328297	-0.559367
H	2.364328	0.439848	-0.217688
H	2.019119	-1.306965	-0.219027

H	1.621845	-0.319992	-1.655278
O	0.001567	0.000862	1.708088

$FcPMe_3$ (III)

Fe	-1.118484	0.277505	-0.000421
H	-1.951815	-1.534484	-2.214300
C	-0.623893	2.357146	0.717987
H	-1.246825	2.968263	1.358288
C	0.341760	1.391721	1.168475
H	0.594090	1.193581	2.202549
C	1.023692	0.844033	-0.002456
C	0.339615	1.393714	-1.171133
H	0.589616	1.196772	-2.206034
C	-0.625194	2.358458	-0.717352
H	-1.249348	2.970563	-1.355503
C	-2.149133	-1.311823	-1.172225
C	-3.171431	-0.406706	-0.683679
H	-3.834498	0.191595	-1.296862
C	-3.137509	-0.436452	0.744533
H	-3.771734	0.133889	1.412531
C	-2.099108	-1.365526	1.148563
H	-1.857241	-1.633357	2.170407
C	-1.529418	-1.948520	-0.038189
H	-0.769584	-2.720021	-0.072719
P	2.331106	-0.334117	-0.000342
C	4.021149	0.413068	-0.012091
H	4.788708	-0.370072	-0.002733
H	4.138950	1.026899	-0.911699
H	4.141295	1.051393	0.869996
C	2.243803	-1.385080	1.502250
H	3.039817	-2.137243	1.480119
H	2.365517	-0.763939	2.396063
H	1.266583	-1.874517	1.536419
C	2.236438	-1.410161	-1.484843
H	2.301421	-0.797330	-2.390292
H	3.064082	-2.127813	-1.479843
H	1.280333	-1.940779	-1.479346

$[FcPMe_3]^+$ (IV)

Fe	-1.140908	0.201800	-0.000783
H	-1.781204	-1.594886	-2.174953
C	-0.791844	2.182478	0.717933
H	-1.464975	2.741836	1.351638
C	0.239644	1.294606	1.174472
H	0.488611	1.094968	2.206815
C	0.893252	0.733664	0.000529
C	0.242178	1.292078	-1.176171
H	0.494020	1.091806	-2.207714
C	-0.790132	2.181039	-0.723929
H	-1.461461	2.739345	-1.360482
C	-2.036821	-1.340215	-1.156026
C	-3.031535	-0.377309	-0.747554
H	-3.638049	0.228191	-1.406412
C	-3.059277	-0.347843	0.695170
H	-3.689696	0.283857	1.305159
C	-2.081688	-1.292470	1.180295
H	-1.864192	-1.504707	2.217646
C	-1.453185	-1.907008	0.036042
H	-0.693498	-2.675488	0.067588
P	2.364393	-0.290256	-0.000066
C	3.855389	0.773664	-0.097666
H	4.756046	0.150247	-0.097003
H	3.824274	1.367115	-1.016792
H	3.877645	1.448397	0.764161
C	2.456415	-1.268097	1.544405
H	3.367636	-1.875247	1.530161
H	2.492755	-0.598364	2.409406
H	1.583553	-1.921261	1.628338
C	2.359958	-1.414910	-1.445278
H	2.337625	-0.834218	-2.373206
H	3.270022	-2.023753	-1.430252
H	1.484457	-2.068856	-1.406079

$[CpFeC_5H_5PMe_3]^+$

Fe	-1.435534	0.079922	-0.000451
H	0.914593	-1.550995	0.009584
C	-2.836323	-1.399266	0.711159
H	0.420165	-0.048698	2.195797
C	-3.668645	0.673569	0.018221
P	2.916174	-0.216043	-0.000482
H	-3.437796	0.186872	2.199508
C	-3.321608	-0.112717	1.166285
H	-3.457676	0.237058	-2.175541
H	0.414343	-0.079054	-2.198464
H	-2.562562	-2.231665	1.344985
C	3.356901	1.558421	-0.125043
C	0.303188	0.235273	1.157536
C	3.640811	-1.122984	-1.421065
C	3.612098	-0.892816	1.556391
H	-2.574393	-2.200589	-1.383746
C	-0.135074	1.536247	0.710333
C	1.041916	-0.460684	0.000766
H	-0.466480	2.349595	1.341684
C	-3.331895	-0.085856	-1.150501
H	-0.469796	2.330535	-1.375506
C	-0.137049	1.525990	-0.733725
C	0.299541	0.218860	-1.163921
H	-4.054387	1.684424	0.031783
C	-2.841657	-1.382634	-0.728789
H	4.728537	-0.996901	-1.429847
H	3.404178	-2.188967	-1.334931
H	3.227417	-0.736525	-2.358296
H	4.702070	-0.784997	1.555078
H	3.355376	-1.953675	1.646637
H	3.199460	-0.347510	2.411498
H	4.446675	1.665087	-0.087587
H	2.985695	1.969974	-1.068600
H	2.912642	2.110268	0.709061

$[C_5H_6FeCpPMe_3]^+$ (V)

Fe	1.119027	0.254035	-0.007393
H	1.288704	-2.273071	-1.343153
C	2.113978	-1.982287	-0.681791
H	-0.543425	0.986069	-2.265771
C	3.182916	0.016552	0.159630
P	-2.367066	-0.393921	-0.000264

H	3.070683	-0.355729	-2.035563
C	2.726117	-0.615883	-1.041890
H	2.603980	-0.330631	2.315537
H	-0.708175	1.312698	2.131037
H	2.855959	-2.801269	-0.708049
C	-2.294434	-1.547141	-1.419868
C	-0.339827	1.263183	-1.240606
C	-3.939968	0.546758	-0.104205
C	-2.366080	-1.341789	1.566350
H	1.064999	-2.310755	1.363384
C	0.575098	2.285788	-0.816711
C	-0.974427	0.728750	-0.048201
H	1.206784	2.867000	-1.474976
C	2.515157	-0.622929	1.277087
H	1.046943	3.128841	1.215249
C	0.475992	2.439390	0.608185
C	-0.434580	1.461743	1.094877
H	3.848375	0.867605	0.226311
C	1.659588	-1.643310	0.750671
H	-4.791168	-0.140596	-0.053251
H	-3.997173	1.259752	0.724832
H	-3.972804	1.096596	-1.050440
H	-3.226259	-2.019630	1.581202
H	-2.440115	-0.656844	2.416971
H	-1.441456	-1.919784	1.649124
H	-3.166106	-2.209027	-1.392129
H	-2.305608	-0.985263	-2.359563
H	-1.380013	-2.144991	-1.365733

$[C_5H_6FeCpPMe_3]^{2+}$ (VI)

Fe	-1.090271	0.247777	0.107576
H	-2.005522	-1.603067	1.848687
C	-2.682226	-1.528508	0.983968
H	0.751194	1.062603	2.229097
C	-3.180443	0.124062	-0.667868
P	2.505067	-0.449226	0.004112
H	-3.716677	0.489836	1.448341
C	-3.219977	-0.127102	0.710243
H	-2.249174	-1.024680	-2.386187
H	0.832091	1.201171	-2.181355
H	-3.514788	-2.217056	1.209334
C	2.708791	-1.158403	1.675344
C	0.514617	1.289017	1.198642
C	4.021019	0.464051	-0.465699
C	2.216868	-1.778117	-1.220207
H	-1.504002	-2.802703	-0.542439
C	-0.472305	2.231394	0.748229
C	1.104889	0.700324	0.024067
H	-1.081952	2.856031	1.386727
C	-2.449483	-0.966763	-1.324095
H	-0.981800	2.982711	-1.328867
C	-0.388938	2.327441	-0.705934
C	0.562790	1.394303	-1.151241
H	-3.610069	0.976461	-1.178144
C	-2.052797	-1.887567	-0.357388
H	4.874462	-0.221826	-0.430102
H	3.919661	0.858221	-1.482098
H	4.187865	1.290353	0.232007
H	3.097650	-2.428242	-1.251917
H	2.061451	-1.345164	-2.213372
H	1.342023	-2.370268	-0.939353
H	3.506784	-1.908006	1.649528
H	2.986669	-0.371620	2.383435
H	1.778344	-1.633376	1.999664

$Mo(L^{Fc})_2O_2$ (2^{Fc})

Mo	0.002121	-0.015460	2.125037
Fe	-4.247242	-0.090604	-1.202371
Fe	4.245487	0.108470	-1.204094
O	1.372535	-0.014691	3.162029
O	-1.361173	-0.030564	3.171263
N	-0.273190	-2.028619	1.626506
N	1.417866	-0.521254	0.210378
N	0.274178	2.005135	1.655347
N	-1.420430	0.516980	0.224329
C	-1.030793	-3.012246	2.220002
H	-1.657664	-2.796843	3.074986
C	-0.833135	-4.232217	1.549228
H	-1.294909	-5.177213	1.800159
C	0.085036	-3.979633	0.487211
H	0.462235	-4.689738	-0.236867
C	0.411620	-2.612794	0.561349
C	1.289847	-1.765047	-0.178520
H	1.850424	-2.165034	-1.023034
C	2.223913	0.360724	-0.549384
C	2.305034	0.428664	-1.997096
H	1.768799	-0.206635	-2.688431
C	3.169736	1.528464	-2.339917
H	3.420471	1.847403	-3.341842
C	3.636844	2.129600	-1.112809
H	4.307283	2.973617	-1.033002
C	3.060493	1.404762	-0.009784
H	3.213457	1.605248	1.039258
C	5.839829	-0.636068	-0.022116
H	6.019453	-0.374168	1.011329
C	5.022756	-1.730505	-0.488762
H	4.486948	-2.431616	0.136447
C	5.041958	-1.718378	-1.932873
H	4.527691	-2.412888	-2.582935
C	5.871615	-0.615439	-2.358482
H	6.080849	-0.334931	-3.381616
C	6.364777	0.052931	-1.177401
H	7.004244	0.924695	-1.160926
C	1.033388	2.980697	2.259929
H	1.661756	2.754168	3.110941
C	0.835224	4.209237	1.605109
H	1.297966	5.150700	1.867283
C	-0.084950	3.970739	0.541596
H	-0.463019	4.690177	-0.172750
C	-0.412243	2.603258	0.599000
C	-1.292502	1.765347	-0.149653
H	-1.854659	2.175887	-0.988044
C	-2.228506	-0.355885	-0.543809
C	-2.305902	-0.413566	-1.992088
H	-1.765089	0.224213	-2.677553
C	-3.174288	-1.507395	-2.344710
H	-3.423517	-1.818594	-3.349439
C	-3.647257	-2.114895	-1.122985

H	-4.321519	-2.956554	-1.050794
C	-3.071012	-1.399871	-0.013510
H	-3.227311	-1.606735	1.033857
C	-5.019848	1.745885	-0.475916
H	-4.483644	2.440176	0.156493
C	-5.842875	0.651248	-0.020372
H	-6.027186	0.382287	1.010434
C	-6.366414	-0.026992	-1.182613
H	-7.009211	-0.896428	-1.174888
C	-5.866479	0.648257	-2.356922
H	-6.073215	0.376243	-3.382849
C	-5.034081	1.744738	-1.920166
H	-4.514669	2.441987	-2.563171

$[Mo(L^{Fc})_2O_2]^+$ ($[2^{Fc}]^+$)

Mo	0.037832	0.058328	2.045350
Fe	-4.342446	0.049295	-1.114585
Fe	4.377946	-0.125040	-1.165350
O	1.529397	0.118138	2.894644
O	-1.177131	0.102758	3.249354
N	-0.311854	2.054743	1.493432
N	1.323550	0.559577	-0.049186
N	0.277272	-1.973254	1.637436
N	-1.487012	-0.519438	0.274123
C	-1.040669	3.031253	2.108810
H	-1.597051	2.831527	3.015103
C	-0.928849	4.246833	1.390832
H	-1.396631	5.183697	1.657899
C	-0.097114	3.991880	0.277448
H	0.205756	4.690182	-0.491258
C	0.275553	2.625225	0.357964
C	1.109964	1.812269	-0.432535
H	1.583708	2.241583	-1.314383
C	2.120418	-0.252590	-0.840468
C	2.487194	-0.078620	-2.238985
H	2.138843	0.702523	-2.898977
C	3.300500	-1.196715	-2.636931
H	3.670580	-1.384504	-3.634705
C	3.508211	-2.032034	-1.475260
H	4.068145	-2.955574	-1.443701
C	2.816054	-1.429549	-0.368091
H	2.776889	-1.812915	0.639162
C	5.854357	0.394322	0.357748
H	5.792827	0.094941	1.394705
C	5.356952	1.624179	-0.195363
H	4.833610	2.398087	0.349851
C	5.631226	1.623786	-1.606384
H	5.372314	2.408520	-2.303840
C	6.321316	0.397235	-1.930807
H	6.679823	0.109354	-2.909030
C	6.458351	-0.367456	-0.712879
H	6.942176	-1.328903	-0.614544
C	1.051689	-2.937383	2.247031
H	1.724017	-2.688310	3.057266
C	0.797047	-4.187612	1.657378
H	1.255118	-5.126038	1.937221
C	-0.178275	-3.978906	0.636695
H	-0.609926	-4.723069	-0.019163
C	-0.480248	-2.605242	0.650937
C	-1.398915	-1.781819	-0.066790
H	-2.020973	-2.207649	-0.852806
C	-2.323622	0.341919	-0.481824
C	-2.414857	0.393435	-1.929636
H	-1.874359	-0.242535	-2.617182
C	-3.299977	1.475083	-2.276882
H	-3.565751	1.778030	-3.279775
C	-3.767105	2.082069	-1.052862
H	-4.453337	2.913515	-0.977148
C	-3.171735	1.379035	0.053952
H	-3.327172	1.585543	1.101761
C	-5.107488	-1.779504	-0.358968
H	-4.571940	-2.463450	0.285008
C	-5.934877	-0.681538	0.079410
H	-6.121421	-0.397638	1.105772
C	-6.460813	-0.023751	-1.093101
H	-7.106627	0.843378	-1.098870
C	-5.958176	-0.714963	-2.256573
H	-6.166090	-0.459504	-3.286428
C	-5.121795	-1.801170	-1.803090
H	-4.602199	-2.507801	-2.435624

$[Mo(L^{Fc})_2O_2]^{2+}$ ($[2^{Fc}]^{2+}$) triplet

Mo	0.000495	-0.000369	2.038078
Fe	4.522260	0.099019	-1.079436
Fe	-4.522432	-0.098502	-1.078892
O	-1.362888	-0.003174	3.074046
O	1.365058	0.002005	3.072470
N	0.264438	2.000969	1.485448
N	-1.456597	0.477478	0.111310
N	-0.264152	-2.001433	1.484818
N	1.456306	-0.477669	0.110260
C	1.008158	2.999970	2.055911
H	1.613477	2.821219	2.934725
C	0.827117	4.204456	1.340059
H	1.285277	5.154304	1.575741
C	-0.068156	3.925488	0.278632
H	-0.435173	4.615193	-0.469419
C	-0.405662	2.555316	0.386826
C	-1.295558	1.717752	-0.320601
H	-1.862826	2.118767	-1.160299
C	-2.312834	-0.381057	-0.574552
C	-2.572377	-0.428789	-2.001184
H	-2.099153	0.187790	-2.752459
C	-3.482967	-1.514844	-2.256599
H	-3.816541	-1.844452	-3.230182
C	-3.842388	-2.102973	-0.985238
H	-4.503480	-2.944288	-0.834801
C	-3.150013	-1.379723	0.048439
H	-3.217089	-1.564075	1.109419
C	-6.101770	0.730614	0.193955
H	-6.179916	0.564153	1.259309
C	-5.437922	1.835405	-0.440488
H	-4.907862	2.630205	0.066849
C	-5.548016	1.668749	-1.864210
H	-5.148058	2.335849	-2.615162
C	-6.306806	0.465367	-2.117768
H	-6.582394	0.079480	-3.089056
C	-6.648751	-0.117836	-0.840014

H	-7.222376	-1.020429	-0.683949
C	-1.007813	-3.000497	2.055230
H	-1.612654	-2.821987	2.934422
C	-0.827395	-4.204730	1.338779
H	-1.285661	-5.154571	1.574283
C	0.067440	-3.925532	0.277051
H	0.433942	-4.615004	-0.471466
C	0.405281	-2.555468	0.385626
C	1.295008	-1.717818	-0.321908
H	1.861885	-2.118698	-1.161935
C	2.312449	0.380975	-0.575521
C	2.572263	0.428771	-2.002112
H	2.099305	-0.187866	-2.753507
C	3.482594	1.515080	-2.257379
H	3.816182	1.844822	-3.230913
C	3.841663	2.103291	-0.985959
H	4.502479	2.944801	-0.835397
C	3.149311	1.379838	0.047593
H	3.216220	1.564148	1.108581
C	5.436920	-1.835484	-0.441908
H	4.906108	-2.630823	0.063805
C	6.099704	-0.731255	0.194671
H	6.176248	-0.565880	1.260309
C	6.648175	0.118283	-0.837633
H	7.221546	1.020733	-0.679820
C	6.308260	-0.463716	-2.116479
H	6.585290	-0.076853	-3.086969
C	5.549261	-1.667426	-1.865272
H	5.150488	-2.333780	-2.617516

$[Mo(L^{Fc})_2O_2]^{2+}$ ($[2^{Fc}]^{2+}$) open-shell singlet

Mo	0.000604	0.000240	2.038151
Fe	4.522197	0.098617	-1.079508
Fe	-4.522311	-0.098849	-1.078973
O	-1.362427	-0.002348	3.074578
O	1.365524	0.002712	3.072075
N	0.264461	2.001497	1.485141
N	-1.456719	0.477715	0.111535
N	-0.264325	-2.000890	1.485282
N	1.456257	-0.477593	0.110434
C	1.008348	3.000580	2.055239
H	1.613918	2.821957	2.933904
C	0.827129	4.204953	1.339236
H	1.285373	5.154832	1.574632
C	-0.068413	3.925821	0.278080
H	-0.435609	4.615400	-0.469999
C	-0.405899	2.555673	0.386591
C	-1.295948	1.717980	-0.320485
H	-1.863275	2.118787	-1.160242
C	-2.312772	-0.381043	-0.574268
C	-2.572096	-0.429108	-2.000931
H	-2.098850	0.187388	-2.752261
C	-3.482530	-1.515320	-2.256252
H	-3.815947	-1.845137	-3.229819
C	-3.842067	-2.103227	-0.984823
H	-4.503101	-2.944576	-0.834313
C	-3.149906	-1.379699	0.048801
H	-3.217091	-1.563848	1.109806
C	-6.101948	0.730326	0.193444
H	-6.180227	0.564083	1.258821
C	-5.438118	1.835055	-0.441138
H	-4.908223	2.630026	0.066102
C	-5.548018	1.668106	-1.864841
H	-5.148035	2.335095	-2.615876
C	-6.306608	0.464568	-2.118256
H	-6.581987	0.078427	-3.089501
C	-6.648672	-0.118405	-0.840431
H	-7.222200	-1.021040	-0.684251
C	-1.008062	-2.999764	2.055919
H	-1.612845	-2.821014	2.935105
C	-0.827774	-4.204168	1.339723
H	-1.286100	-5.153921	1.575463
C	0.067002	-3.925260	0.277869
H	0.433411	-4.614923	-0.470521
C	0.405013	-2.555216	0.386179
C	1.294854	-1.717816	-0.321498
H	1.861664	-2.118924	-1.161463
C	2.312442	0.380878	-0.575520
C	2.572196	0.428444	-2.002133
H	2.099148	-0.188254	-2.753419
C	3.482624	1.514624	-2.257598
H	3.816204	1.844194	-3.231192
C	3.841807	2.102982	-0.986280
H	4.502720	2.944442	-0.835865
C	3.149432	1.379745	0.047409
H	3.216424	1.564198	1.108371
C	5.436658	-1.835909	-0.441785
H	4.905765	-2.631132	0.064026
C	6.099574	-0.731678	0.194660
H	6.176149	-0.566190	1.260279
C	6.648128	0.117676	-0.837745
H	7.221603	1.020080	-0.680045
C	6.308122	-0.464425	-2.116521
H	6.585182	-0.077705	-3.087059
C	5.548989	-1.668021	-1.865169
H	5.150125	-2.334412	-2.617332

TS1 $Mo(L^{Fc})_2OO\cdots PMe_3$

Mo	-0.426060	1.076662	0.880021
Fe	3.863378	-1.986547	-0.571227
Fe	-4.472263	-1.004667	-0.626153
O	-1.880631	1.871169	1.306696
O	0.879024	2.230882	1.334763
N	-0.474340	1.819146	-1.114389
N	1.132996	-0.253522	-0.481998
N	0.113386	-0.070672	2.583733
N	-1.535896	-1.009994	0.664018
C	-1.157380	2.858605	-1.687286
H	-1.874162	3.437873	-1.119620
C	-0.800402	2.982457	-3.051364
H	-1.193180	3.710695	-3.748432
C	0.159372	1.969900	-3.316420
H	0.655202	1.760904	-4.255642
C	0.345717	1.275844	-2.097842
C	1.157609	0.162589	-1.725281
H	1.785020	-0.318749	-2.476797

C	1.829275	-1.442377	-0.153722
C	1.887498	-2.657099	-0.946237
H	1.417033	-2.802904	-1.908783
C	2.618070	-3.645001	-0.193546
H	2.819232	-4.659607	-0.507953
C	3.027391	-3.041976	1.053417
H	3.598808	-3.522124	1.835292
C	2.548071	-1.683841	1.073606
H	2.677069	-0.970570	1.873129
C	5.523487	-0.679984	-0.383865
H	5.664194	0.034355	0.415518
C	4.843080	-0.432774	-1.632911
H	4.389107	0.501369	-1.933451
C	4.873962	-1.651681	-2.407217
H	4.448658	-1.791954	-3.391526
C	5.573239	-2.652350	-1.635968
H	5.755389	-3.674663	-1.937598
C	5.974703	-2.051626	-0.385642
H	6.508625	-2.545850	0.414278
C	0.888106	0.164436	3.685881
H	1.432489	1.093549	3.795911
C	0.831775	-0.941740	4.563417
H	1.339576	-1.028528	5.514725
C	-0.019983	-1.905481	3.953904
H	-0.292677	-2.879262	4.340018
C	-0.446151	-1.337072	2.733495
C	-1.303793	-1.797661	1.690484
H	-1.742877	-2.791050	1.769111
C	-2.395754	-1.453140	-0.365556
C	-3.193353	-2.670150	-0.407464
H	-3.273429	-3.420349	0.365587
C	-3.853426	-2.725625	-1.686485
H	-4.510480	-3.515635	-2.022833
C	-3.498601	-1.539447	-2.426976
H	-3.841462	-1.280283	-3.418695
C	-2.612539	-0.750842	-1.611647
H	-2.170108	0.194595	-1.880794
C	-5.848878	-0.956009	0.987998
H	-5.859668	-1.646034	1.820641
C	-5.120461	0.288230	0.925627
H	-4.467724	0.688439	1.688589
C	-5.378187	0.891670	-0.360661
H	-4.967406	1.826799	-0.714506
C	-6.269869	0.022594	-1.091650
H	-6.643700	0.191620	-2.092203
C	-6.559269	-1.121495	-0.259353
H	-7.192046	-1.957166	-0.525441
P	1.875174	3.834213	0.241672
C	3.431633	3.696699	1.247317
H	4.096592	2.951307	0.794249
H	3.955007	4.660025	1.296485
H	3.175287	3.367355	2.259611
C	0.957308	5.227914	1.061620
H	1.606338	6.102553	1.198736
H	0.097566	5.513856	0.444247
H	0.590926	4.889312	2.036667
C	2.503907	4.647357	-1.336302
H	3.222631	3.980574	-1.827381
H	1.661743	4.816330	-2.016811
H	2.993250	5.605152	-1.109867

TS1 [Mo(L^{Fc})$_2$OO··· PMe$_3$]$^+$

Mo	-0.325992	1.116468	0.852677
Fe	3.845929	-2.093229	-0.552883
Fe	-4.637093	-0.920135	-0.635930
O	-1.786967	1.915459	1.252993
O	0.973360	2.219296	1.381314
N	-0.324279	1.878820	-1.122639
N	1.183922	-0.253058	-0.476442
N	0.102299	-0.122775	2.546239
N	-1.532371	-0.934484	0.555809
C	-0.949717	2.957107	-1.694950
H	-1.625459	3.581668	-1.125106
C	-0.587026	3.058924	-3.057985
H	-0.934969	3.810157	-3.754080
C	0.315380	1.994578	-3.324102
H	0.800101	1.761584	-4.263213
C	0.464040	1.289951	-2.107711
C	1.229874	0.148704	-1.724850
H	1.845784	-0.361713	-2.465539
C	1.843025	-1.459027	-0.126774
C	1.840457	-2.695930	-0.886718
H	1.356251	-2.847154	-1.841657
C	2.540416	-3.692112	-0.115999
H	2.699370	-4.721153	-0.406218
C	2.991052	-3.073770	1.108729
H	3.555725	-3.555248	1.894487
C	2.569777	-1.696466	1.097212
H	2.749346	-0.966094	1.871044
C	5.554323	-0.845080	-0.417680
H	5.724553	-0.107581	0.354393
C	4.881266	-0.618589	-1.674464
H	4.466996	0.321826	-2.010936
C	4.863383	-1.865750	-2.402603
H	4.432932	-2.025771	-3.381601
C	5.525688	-2.862827	-1.595232
H	5.669061	-3.901697	-1.858573
C	5.952565	-2.231980	-0.368720
H	6.468105	-2.716339	0.449040
C	0.829857	0.043734	3.674279
H	1.403351	0.946394	3.843090
C	0.705638	-1.096882	4.523065
H	1.176825	-1.223160	5.487745
C	-0.141699	-2.003469	3.860753
H	-0.461731	-2.978322	4.203579
C	-0.509697	-1.380265	2.631343
C	-1.348285	-1.776355	1.578204
H	-1.833560	-2.749488	1.623407
C	-2.378792	-1.290613	-0.471885
C	-3.164750	-2.508445	-0.645112
H	-3.166030	-3.373651	0.001549
C	-3.863776	-2.424291	-1.900208
H	-4.470659	-3.204748	-2.336568
C	-3.599166	-1.122932	-2.471042
H	-3.974160	-0.748922	-3.412850
C	-2.729098	-0.414834	-1.572696
H	-2.342024	0.582347	-1.715850
C	-6.126197	-1.224928	0.926599

H	-6.122783	-2.055400	1.618749
C	-5.528108	0.063616	1.149311
H	-4.967994	0.362588	2.024719
C	-5.753146	0.868528	-0.019015
H	-5.410464	1.883673	-0.163308
C	-6.516918	0.087769	-0.964245
H	-6.861691	0.422475	-1.932478
C	-6.749751	-1.211177	-0.378656
H	-7.304363	-2.023519	-0.826637
P	2.062879	3.875672	0.304952
C	3.585141	3.693468	1.355555
H	4.124153	4.645945	1.436769
H	3.291502	3.354642	2.354758
H	4.250644	2.942966	0.912123
C	1.146137	5.272194	1.122349
H	1.803703	6.136760	1.280732
H	0.301826	5.575735	0.492228
H	0.757778	4.929221	2.087597
C	2.741211	4.689143	-1.247037
H	3.456816	4.014109	-1.731010
H	1.918035	4.885675	-1.943192
H	3.244992	5.633383	-0.998275

TS1 [Mo(L^{Fc})$_2$OO··· PMe$_3$]$^{2+}$

Mo	-0.373987	0.966815	0.891216
Fe	4.067348	-1.924447	-0.625011
Fe	-4.775439	-0.825396	-0.617222
O	-1.773120	1.781533	1.429588
O	0.975661	1.974282	1.437722
N	-0.426220	1.846177	-1.037316
N	1.132520	-0.342108	-0.634954
N	0.081664	-0.410011	2.448122
N	-1.635924	-1.036461	0.453524
C	-1.055115	2.961814	-1.500965
H	-1.715135	3.541149	-0.868348
C	-0.724013	3.184290	-2.867092
H	-1.089220	3.994766	-3.482107
C	0.162416	2.156424	-3.244152
H	0.625188	2.004692	-4.210143
C	0.342451	1.341068	-2.091078
C	1.120948	0.192696	-1.852253
H	1.721455	-0.213260	-2.666453
C	1.822661	-1.531336	-0.447914
C	2.148579	-2.546218	-1.438767
H	1.850814	-2.539484	-2.477725
C	2.827331	-3.628810	-0.776150
H	3.134217	-4.557239	-1.236168
C	2.994724	-3.264200	0.612890
H	3.461684	-3.865162	1.379809
C	2.413427	-1.961790	0.801207
H	2.384135	-1.409304	1.726995
C	5.668917	-0.589665	0.029751
H	5.637482	0.009645	0.928969
C	5.258413	-0.168995	-1.281897
H	4.839128	0.794705	-1.536804
C	5.457344	-1.267504	-2.187687
H	5.238384	-1.265937	-3.246480
C	6.008705	-2.372924	-1.439804
H	6.285374	-3.337048	-1.842454
C	6.138552	-1.953511	-0.063455
H	6.531926	-2.546882	0.749656
C	0.846281	-0.341443	3.568104
H	1.436203	0.538223	3.791572
C	0.723159	-1.540412	4.325602
H	1.215237	-1.749525	5.264925
C	-0.164717	-2.378489	3.621127
H	-0.497471	-3.369671	3.899000
C	-0.555437	-1.657260	2.457347
C	-1.444397	-1.949473	1.408086
H	-1.962394	-2.906177	1.408662
C	-2.540973	-1.309968	-0.559800
C	-3.383029	-2.486377	-0.744807
H	-3.403896	-3.372666	-0.128015
C	-4.128966	-2.325047	-1.964186
H	-4.790737	-3.060382	-2.398971
C	-3.826266	-1.018998	-2.502342
H	-4.220582	-0.594929	-3.414487
C	-2.885924	-0.384744	-1.618881
H	-2.464319	0.599582	-1.746573
C	-6.229636	-1.110249	0.984245
H	-6.250709	-1.964588	1.646373
C	-5.552712	0.133813	1.231439
H	-4.953776	0.370048	2.100260
C	-5.768428	0.993147	0.100202
H	-5.376879	1.993757	-0.018641
C	-6.600818	0.289444	-0.847688
H	-6.955837	0.677211	-1.792056
C	-6.887792	-1.016069	-0.299897
H	-7.498228	-1.780725	-0.759076
P	2.077969	3.790538	0.449471
C	3.655091	3.442737	1.372267
H	4.209254	4.368446	1.573048
H	3.412787	2.953280	2.321837
H	4.287239	2.770186	0.779380
C	1.242059	5.073239	1.504836
H	1.924912	5.901524	1.733469
H	0.365558	5.467687	0.977553
H	0.909160	4.608256	2.439198
C	2.680481	4.794130	-1.017343
H	3.349109	4.180254	-1.632568
H	1.822860	5.096626	-1.628653
H	3.220865	5.688952	-0.679829

Mo(L^{Fc})$_2$O(OPMe$_3$) (5^{Fc})

Mo	-0.291809	1.347237	0.673123
Fe	3.688608	-2.291040	-0.352478
Fe	-4.608993	-0.931505	-0.511378
O	-1.445133	2.558238	0.978228
O	1.557301	2.425329	1.039104
N	-0.243054	1.861992	-1.461912
N	1.142434	-0.283008	-0.517048
N	0.078123	0.338786	2.503916
N	-1.631340	-0.409821	0.567080
C	-0.775856	2.876119	-2.190799
H	-1.392266	3.638223	-1.728385
C	-0.432298	2.739545	-3.569634
H	-0.729906	3.406187	-4.368969
C	0.354876	1.572203	-3.672557

H	0.799731	1.147692	-4.563821
C	0.454757	1.051582	-2.348786
C	1.136629	-0.077264	-1.818096
H	1.659856	-0.748883	-2.501842
C	1.716090	-1.481169	-0.034049
C	1.650401	-2.795856	-0.647145
H	1.166452	-3.029428	-1.585360
C	2.279898	-3.738515	0.243825
H	2.373421	-4.802813	0.077457
C	2.756131	-3.010775	1.396824
H	3.277185	-3.432347	2.245030
C	2.418984	-1.621183	1.218486
H	2.618594	-0.818429	1.911649
C	5.483353	-1.162204	-0.329726
H	5.713716	-0.377481	0.377418
C	4.813474	-0.994519	-1.597917
H	4.452901	-0.061887	-2.009352
C	4.700918	-2.293920	-2.218149
H	4.246006	-2.504116	-3.176438
C	5.300642	-3.264629	-1.333185
H	5.368059	-4.329379	-1.509548
C	5.784879	-2.565000	-0.166346
H	6.277048	-3.014342	0.685238
C	0.798540	0.537993	3.641839
H	1.458692	1.389831	3.745674
C	0.538449	-0.498611	4.576532
H	0.972585	-0.592044	5.563351
C	-0.391526	-1.377994	3.964080
H	-0.812651	-2.284046	4.380745
C	-0.661910	-0.830226	2.685682
C	-1.540700	-1.195767	1.629455
H	-2.140566	-2.100634	1.715109
C	-2.470266	-0.805491	-0.503617
C	-2.908483	-2.150217	-0.834911
H	-2.648137	-3.056493	-0.306713
C	-3.701385	-2.075087	-2.035778
H	-4.158587	-2.912757	-2.543787
C	-3.774497	-0.690527	-2.437625
H	-4.300407	-0.304250	-3.299238
C	-3.024068	0.091165	-1.489217
H	-2.866279	1.157643	-1.518589
C	-5.753360	-1.720134	1.090132
H	-5.498895	-2.600501	1.664378
C	-5.354263	-0.365187	1.390162
H	-4.739686	-0.051107	2.222675
C	-5.902305	0.497523	0.370371
H	-5.771818	1.569000	0.308894
C	-6.641184	-0.323798	-0.559636
H	-7.162222	0.024984	-1.440669
C	-6.548773	-1.694940	-0.115674
H	-6.991624	-2.552509	-0.603562
P	2.311615	3.645429	0.415822
C	3.049274	3.300916	-1.226013
H	3.592266	4.182230	-1.587084
H	3.744803	2.459007	-1.139121
H	2.258864	3.040110	-1.936308
C	3.681274	4.105135	1.542040
H	4.246166	4.951849	1.136204
H	3.270054	4.378258	2.519864
H	4.351818	3.247370	1.663445
C	1.222475	5.108097	0.238709
H	0.431023	4.880316	-0.481725
H	0.767792	5.339844	1.208034
H	1.796247	5.973907	-0.111470

$[Mo(L^{Fc})_2O(OPMe_3)]^+$ ($[5^{Fc}]^+$)

Mo	-0.184219	1.524453	0.528533
Fe	3.414599	-2.504966	-0.224699
Fe	-4.527900	-0.927281	-0.417366
O	-1.291343	2.790750	0.734854
O	1.616288	2.473840	0.771176
N	-0.203131	1.806659	-1.571843
N	1.093359	-0.267757	-0.484022
N	0.173964	0.694686	2.414610
N	-1.607328	-0.127588	0.620692
C	-0.740630	2.792020	-2.365867
H	-1.297801	3.615477	-1.938169
C	-0.462749	2.522973	-3.720834
H	-0.768835	3.125121	-4.565185
C	0.281499	1.308350	-3.756835
H	0.660742	0.795798	-4.630931
C	0.426759	0.894785	-2.416217
C	1.076619	-0.212534	-1.794780
H	1.553395	-0.978656	-2.405710
C	1.602283	-1.432950	0.145042
C	1.314781	-2.804880	-0.232378
H	0.703586	-3.111150	-1.070134
C	1.936611	-3.669129	0.736974
H	1.898553	-4.749315	0.738527
C	2.617967	-2.840643	1.703611
H	3.187467	-3.191451	2.552485
C	2.417097	-1.462785	1.335745
H	2.790384	-0.598322	1.863235
C	5.348515	-1.677374	-0.495712
H	5.770157	-0.870132	0.086917
C	4.582900	-1.539677	-1.711745
H	4.336143	-0.609281	-2.204904
C	4.213846	-2.862458	-2.159323
H	3.639416	-3.099485	-3.044282
C	4.752028	-3.816884	-1.219257
H	4.641083	-4.891149	-1.270451
C	5.453134	-3.084697	-0.191619
H	5.957052	-3.514207	0.663105
C	0.961060	0.969287	3.497440
H	1.693624	1.764908	3.473985
C	0.648331	0.084812	4.555508
H	1.111291	0.075787	5.532385
C	-0.379617	-0.776563	4.089433
H	-0.861707	-1.577643	4.633572
C	-0.656477	-0.377927	2.762474
C	-1.574008	-0.794625	1.768694
H	-2.246807	-1.630356	1.944969
C	-2.428191	-0.600175	-0.437842
C	-2.721748	-1.988845	-0.741514
H	-2.362402	-2.848727	-0.194192
C	-3.526314	-2.014891	-1.934060
H	-3.903645	-2.902875	-2.420906
C	-3.739048	-0.653362	-2.363815

H	-4.310021	-0.340390	-3.226182
C	-3.069091	0.221431	-1.438072
H	-3.035196	1.298669	-1.488362
C	-5.592675	-1.783572	1.206034
H	-5.259129	-2.616297	1.809989
C	-5.337666	-0.386365	1.467049
H	-4.772997	0.013924	2.298194
C	-5.965297	0.385285	0.421219
H	-5.949410	1.462362	0.329647
C	-6.609841	-0.534673	-0.485883
H	-7.157792	-0.267453	-1.378857
C	-6.379002	-1.874912	-0.001811
H	-6.728193	-2.786931	-0.465789
P	2.548208	3.620426	0.198712
C	3.983733	3.750835	1.318313
H	4.666928	4.533491	0.970363
H	3.635614	3.996161	2.327249
H	4.512968	2.792462	1.341999
C	1.659009	5.214993	0.168202
H	2.334993	6.013692	-0.158263
H	0.813250	5.154279	-0.523914
H	1.286166	5.443188	1.172200
C	3.133578	3.228313	-1.486107
H	3.691222	2.286190	-1.466924
H	2.279090	3.129102	-2.162932
H	3.788748	4.030498	-1.844859

$[Mo(L^{Fc})_2O(OPMe_3)]^{2+}$ ($[5^{Fc}]^{2+}$)

Mo	-0.148929	1.529120	0.530495
Fe	-4.607840	-0.917816	-0.409238
Fe	3.438965	-2.496869	-0.235746
O	1.599057	2.526901	0.768830
O	-1.328839	2.722881	0.748915
N	-0.200190	1.800262	-1.562492
N	1.135199	-0.242445	-0.478126
N	0.222264	0.682937	2.417346
N	-1.543871	-0.183792	0.622004
C	-0.763498	2.775422	-2.355716
H	-1.322183	3.596013	-1.924537
C	-0.497383	2.503047	-3.711000
H	-0.819225	3.097862	-4.554439
C	0.267278	1.300178	-3.750758
H	0.647057	0.792760	-4.627433
C	0.435298	0.893856	-2.411629
C	1.112598	-0.196800	-1.789593
H	1.602368	-0.957284	-2.396593
C	1.656095	-1.398209	0.160223
C	1.336576	-2.773457	-0.178939
H	0.701070	-3.088539	-0.995369
C	1.974274	-3.625705	0.790567
H	1.924681	-4.705077	0.814756
C	2.692922	-2.787077	1.720617
H	3.283008	-3.128865	2.558938
C	2.501242	-1.414228	1.330294
H	2.908440	-0.545759	1.825332
C	5.383062	-1.712174	-0.552838
H	5.833285	-0.909449	0.014382
C	4.596499	-1.567922	-1.754423
H	4.362246	-0.635784	-2.250888
C	4.191066	-2.886237	-2.183511
H	3.597047	-3.118987	-3.056566
C	4.727540	-3.844081	-1.246261
H	4.593765	-4.916176	-1.286214
C	5.464008	-3.118750	-0.238989
H	5.975552	-3.551852	0.609255
C	0.996852	0.966799	3.494854
H	1.708865	1.781490	3.480038
C	0.711381	0.062642	4.556328
H	1.180018	0.064399	5.530027
C	-0.285527	-0.818296	4.092314
H	-0.743738	-1.636325	4.631416
C	-0.580662	-0.418870	2.758736
C	-1.479913	-0.860838	1.781286
H	-2.134915	-1.708451	1.969807
C	-2.348786	-0.671629	-0.407903
C	-2.758515	-2.045335	-0.625637
H	-2.449403	-2.901631	-0.043271
C	-3.557060	-2.090469	-1.822542
H	-3.959107	-2.983795	-2.278346
C	-3.693602	-0.739475	-2.318429
H	-4.226306	-0.436254	-3.208062
C	-2.978391	0.134287	-1.427572
H	-2.887089	1.204813	-1.527682
C	-5.614835	-0.328227	1.483187
H	-5.105734	0.056646	2.356527
C	-6.121967	0.456143	0.391889
H	-6.079443	1.533424	0.311072
C	-6.695676	-0.444672	-0.580287
H	-7.173762	-0.158953	-1.506561
C	-6.531068	-1.793001	-0.086077
H	-6.868185	-2.696413	-0.574115
C	-5.853345	-1.715953	1.188600
H	-5.584508	-2.554445	1.815784
H	3.685560	2.258227	-1.448050
C	3.149373	3.212087	-1.488974
H	2.299937	3.123407	-2.173455
H	3.825492	3.993784	-1.854159
H	4.505505	2.805051	1.344687
C	3.983618	3.767384	1.317159
H	4.676319	4.545063	0.977286
H	3.626783	4.014967	2.322463
H	2.361097	6.020656	-0.288055
C	1.689396	5.252767	0.112096
H	1.366285	5.540639	1.117765
H	0.812128	5.164576	-0.537026
P	2.560946	3.650853	0.181637

TS2 $Mo(L^{Fc})_2O\cdots OPMe_3$

Mo	0.297464	0.364801	-0.448376
Fe	-4.751438	-1.313265	0.553601
Fe	5.386606	-0.262836	0.417111
O	0.721946	1.588279	-1.539549
O	-2.135498	1.846084	-1.236643
N	0.316140	1.275011	1.511228
N	-1.635432	-0.335316	0.597375
N	0.176987	-1.470865	-1.560106
N	2.192143	-0.589094	-0.055127
C	1.123615	2.127525	2.200253

H	2.016566	2.546919	1.758724
C	0.611541	2.355058	3.506502
H	1.051718	2.997029	4.258297
C	-0.565866	1.578488	3.622141
H	-1.216818	1.486201	4.482319
C	-0.726518	0.929746	2.370390
C	-1.726363	0.066839	1.848373
H	-2.571761	-0.229978	2.468032
C	-2.648087	-1.194253	0.091062
C	-2.987709	-2.504314	0.605619
H	-2.541776	-2.971697	1.473041
C	-3.971258	-3.085743	-0.274055
H	-4.417928	-4.064501	-0.166763
C	-4.252241	-2.129260	-1.319752
H	-4.955009	-2.263391	-2.130444
C	-3.444208	-0.957700	-1.086735
H	-3.397232	-0.050071	-1.669060
C	-6.163262	0.267035	0.673959
H	-6.229122	1.089979	-0.024191
C	-5.366010	0.238211	1.876370
H	-4.741426	1.042896	2.238296
C	-5.554515	-1.047822	2.506321
H	-5.095974	-1.379970	3.427768
C	-6.470545	-1.812588	1.693432
H	-6.809226	-2.819942	1.893210
C	-6.847491	-0.999138	0.561488
H	-7.513545	-1.292482	-0.238315
C	-0.629131	-2.082989	-2.465565
H	-1.544386	-1.623759	-2.811347
C	-0.091710	-3.346267	-2.842024
H	-0.532010	-4.037896	-3.547877
C	1.106910	-3.514324	-2.112997
H	1.780440	-4.361428	-2.134473
C	1.258476	-2.332970	-1.338266
C	2.301285	-1.827543	-0.529765
H	3.196308	-2.414803	-0.334499
C	3.268725	-0.044168	0.698065
C	3.878912	-0.612192	1.879666
H	3.613545	-1.558089	2.331350
C	4.852534	0.330680	2.370888
H	5.469939	0.202568	3.248888
C	4.856412	1.472183	1.486639
H	5.483130	2.347707	1.580993
C	3.886145	1.235073	0.446077
H	3.634584	1.898403	-0.369285
C	6.313820	-2.085722	-0.161807
H	6.015088	-3.074767	0.157530
C	5.835929	-1.387205	-1.332328
H	5.115633	-1.757936	-2.048571
C	6.494281	-0.104075	-1.385543
H	6.343311	0.655904	-2.139655
C	7.381390	-0.009768	-0.250387
H	8.006686	0.836464	-0.001157
C	7.269249	-1.234193	0.506826
H	7.800531	-1.468247	1.419067
P	-2.077886	3.273588	-1.814139
C	-3.753687	4.034273	-1.931323
H	-3.702182	5.043693	-2.356637
H	-4.390759	3.407427	-2.566296
H	-4.195846	4.086710	-0.929578
C	-1.375005	3.347553	-3.514639
H	-1.356358	4.375487	-3.895588
H	-0.356795	2.946216	-3.481633
H	-1.981068	2.725441	-4.183879
C	-1.073850	4.434367	-0.797206
H	-1.492074	4.479515	0.214987
H	-0.050071	4.050684	-0.739926
H	-1.066736	5.441013	-1.232089

TS2 [Mo(L^{Fc})$_2$O···OPMe$_3$]$^+$

Mo	0.332969	0.374826	-0.197531
Fe	-4.877630	-1.221747	0.317886
Fe	5.450056	-0.209007	0.285240
O	0.709548	1.862287	-0.896934
O	-2.175306	1.869584	-0.902645
N	0.417032	0.673222	1.944253
N	-1.597796	-0.605117	0.686159
N	0.221809	-1.089883	-1.760619
N	2.259308	-0.576132	-0.120982
C	1.223936	1.316659	2.815422
H	2.066984	1.906964	2.485924
C	0.793098	1.101178	4.164573
H	1.263319	1.509874	5.048583
C	-0.330120	0.264437	4.103043
H	-0.914103	-0.125771	4.926079
C	-0.559359	0.020014	2.712634
C	-1.570705	-0.658433	2.024960
H	-2.354540	-1.168248	2.584476
C	-2.596825	-1.312948	0.034777
C	-3.185341	-2.582645	0.429169
H	-2.883685	-3.182390	1.276340
C	-4.134982	-2.975194	-0.580265
H	-4.676641	-3.909922	-0.609328
C	-4.205873	-1.910473	-1.558292
H	-4.826625	-1.900226	-2.442965
C	-3.296186	-0.872902	-1.151910
H	-3.118442	0.087181	-1.615491
C	-6.125745	0.561438	0.603354
H	-5.963030	1.506894	0.105278
C	-5.609194	0.187034	1.889423
H	-4.969197	0.793469	2.515735
C	-6.041124	-1.154965	2.173129
H	-5.811992	-1.720955	3.065394
C	-6.854449	-1.608157	1.068207
H	-7.348343	-2.566631	0.992809
C	-6.904788	-0.543765	0.093037
H	-7.440066	-0.563885	-0.845795
C	-0.580097	-1.452047	-2.798766
H	-1.495197	-0.923800	-3.023444
C	-0.020926	-2.551120	-3.505712
H	-0.450791	-3.031923	-4.374026
C	1.191947	-2.879383	-2.858669
H	1.886934	-3.667313	-3.118111
C	1.328104	-1.950391	-1.794210
C	2.384927	-1.640616	-0.908007
H	3.303332	-2.223467	-0.902227
C	3.351526	-0.201465	0.711937
C	4.051642	-1.043382	1.657261

H	3.857067	-2.092559	1.831854
C	5.010728	-0.221726	2.352160
H	5.684743	-0.556171	3.128129
C	4.914072	1.120846	1.830229
H	5.508151	1.968659	2.140795
C	3.896974	1.131600	0.807525
H	3.574293	1.982284	0.224075
C	6.427471	-1.741757	-0.813026
H	6.202955	-2.798154	-0.757441
C	5.832482	-0.790562	-1.722742
H	5.082366	-1.004628	-2.471451
C	6.419542	0.501967	-1.463324
H	6.179695	1.422705	-1.976952
C	7.377643	0.350472	-0.394320
H	7.976430	1.139742	0.038636
C	7.382484	-1.035994	0.008141
H	7.988784	-1.467656	0.792427
P	-2.177462	3.322806	-1.425613
C	-3.888848	3.932836	-1.736208
H	-3.877907	4.961126	-2.116212
H	-4.375568	3.283387	-2.473486
H	-4.460991	3.901695	-0.801657
C	-1.279022	3.530410	-3.018053
H	-1.304035	4.574563	-3.351097
H	-0.241007	3.213573	-2.875612
H	-1.743312	2.897000	-3.783053
C	-1.420589	4.517634	-0.249288
H	-1.956275	4.475001	0.706229
H	-0.376062	4.233275	-0.084337
H	-1.463875	5.539907	-0.643048

TS2 [Mo(L^{Fc})$_2$O···OPMe$_3$]$^{2+}$

Mo	0.341169	0.300791	-0.142928
Fe	5.487970	-0.188596	0.243090
Fe	-4.889895	-1.173373	0.257150
O	-2.160930	1.895789	-1.077822
O	0.760895	1.716572	-0.948443
N	0.338288	0.785597	1.972983
N	-1.624587	-0.555451	0.700963
N	0.224596	-1.254367	-1.616727
N	2.216753	-0.779401	0.090364
C	1.099285	1.487719	2.843121
H	1.940707	2.084195	2.521202
C	0.609734	1.346461	4.179702
H	1.030709	1.815064	5.058558
C	-0.505496	0.497637	4.114700
H	-1.127270	0.156429	4.931498
C	-0.668852	0.171731	2.733598
C	-1.656331	-0.538463	2.038810
H	-2.464967	-1.018025	2.588958
C	-2.613686	-1.274226	0.032578
C	-3.203954	-2.540056	0.426808
H	-2.925355	-3.126142	1.291327
C	-4.131603	-2.943345	-0.599395
H	-4.676322	-3.876244	-0.627730
C	-4.174649	-1.892984	-1.594299
H	-4.773206	-1.893927	-2.494117
C	-3.270457	-0.852146	-1.182407
H	-3.075291	0.100605	-1.656182
C	-6.141437	0.613995	0.485994
H	-5.963602	1.552750	-0.019417
C	-5.659014	0.254365	1.789600
H	-5.038327	0.869488	2.426792
C	-6.101928	-1.082992	2.079233
H	-5.898403	-1.638039	2.984433
C	-6.882545	-1.550239	0.957100
H	-7.374946	-2.509265	0.879614
C	-6.905604	-0.497307	-0.032324
H	-7.415503	-0.528958	-0.984772
C	-0.524874	-1.614224	-2.679708
H	-1.357337	-1.015488	-3.021315
C	-0.040018	-2.832824	-3.256949
H	-0.459375	-3.332157	-4.119298
C	1.064905	-3.234531	-2.493895
H	1.680185	-4.113477	-2.631877
C	1.234517	-2.228578	-1.490468
C	2.254925	-1.952532	-0.580117
H	3.097203	-2.631223	-0.470092
C	3.304053	-0.438827	0.892390
C	4.211207	-1.323919	1.597444
H	4.130338	-2.399607	1.661328
C	5.169625	-0.515394	2.306864
H	5.929217	-0.884730	2.980760
C	4.912187	0.869456	1.982817
H	5.450481	1.725704	2.362734
C	3.793720	0.908151	1.077198
H	3.357857	1.792303	0.634253
C	5.915045	-0.613317	-1.905408
H	5.176584	-0.927463	-2.630591
C	6.255853	0.745566	-1.586994
H	5.835337	1.629732	-2.045517
C	7.259904	0.724987	-0.547975
H	7.733171	1.589654	-0.104570
C	7.527078	-0.656269	-0.218156
H	8.239776	-1.011322	0.512627
C	6.683778	-1.480255	-1.053956
H	6.650525	-2.560856	-1.050934
H	-1.891378	4.396295	0.678818
C	-1.327380	4.473206	-0.258128
H	-0.296811	4.148152	-0.080170
H	-1.328323	5.516786	-0.594525
H	-4.366074	4.019081	-0.932164
C	-3.763729	4.077623	-1.846166
H	-3.692845	5.124876	-2.162386
H	-4.255667	3.496826	-2.635077
H	-1.085766	4.680138	-3.343444
C	-1.130757	3.620029	-3.068767
H	-1.603579	3.057862	-3.882693
H	-0.116633	3.237306	-2.913351
P	-2.092682	3.373807	-1.519731

Mo(L^{Fc})$_2$O

Mo	-0.043032	-0.000126	-0.232385
Fe	-4.922876	0.196817	0.768638
Fe	4.946006	-0.209330	0.758125
O	-0.092037	-0.034286	1.459457
N	-0.031508	-1.887158	-1.203461
N	-2.155863	-0.320573	-0.785788

N	0.010938	1.930430	-1.111956
N	2.097707	0.325500	-0.636454
C	0.859807	-2.883293	-1.488982
H	1.893603	-2.824098	-1.179046
C	0.219694	-3.928468	-2.199230
H	0.687890	-4.839125	-2.547965
C	-1.136427	-3.546642	-2.361789
H	-1.919223	-4.097717	-2.866765
C	-1.266660	-2.286485	-1.730495
C	-2.368222	-1.425807	-1.484401
H	-3.362092	-1.695735	-1.837113
C	-3.241563	0.545948	-0.506611
C	-4.481507	0.687204	-1.247224
H	-4.765780	0.134170	-2.131142
C	-5.244852	1.745013	-0.635134
H	-6.211087	2.098404	-0.966674
C	-4.495427	2.246604	0.492049
H	-4.802030	3.039740	1.158936
C	-3.265697	1.500522	0.578458
H	-2.481630	1.632728	1.309818
C	-4.818883	-0.754905	2.658430
H	-4.042899	-0.586692	3.392250
C	-4.791284	-1.744574	1.607584
H	-3.989918	-2.445512	1.418457
C	-6.011988	-1.620967	0.846098
H	-6.291926	-2.220057	-0.009480
C	-6.794256	-0.554165	1.426260
H	-7.758604	-0.210534	1.078032
C	-6.056776	-0.019829	2.546799
H	-6.369970	0.797197	3.182103
C	-0.857169	2.930436	-1.452260
H	-1.906009	2.879871	-1.197358
C	-0.175615	3.964838	-2.138440
H	-0.620082	4.874666	-2.518913
C	1.183728	3.571870	-2.232252
H	1.993651	4.110205	-2.707315
C	1.273155	2.316025	-1.586514
C	2.353331	1.437634	-1.307756
H	3.365300	1.694756	-1.616713
C	3.154908	-0.572229	-0.344445
C	4.320790	-0.858998	-1.158392
H	4.558743	-0.405656	-2.110418
C	5.070760	-1.900595	-0.502927
H	5.986912	-2.343793	-0.867111
C	4.383520	-2.248791	0.718388
H	4.697111	-2.994138	1.435349
C	3.205032	-1.425819	0.819669
H	2.469332	-1.443026	1.610792
C	6.098058	1.559100	0.563608
H	6.304395	2.072484	-0.365413
C	4.972415	1.798447	1.436329
H	4.180233	2.516344	1.273885
C	5.080291	0.898585	2.559959
H	4.385187	0.827360	3.384828
C	6.272305	0.103212	2.382645
H	6.624672	-0.670640	3.050508
C	6.901526	0.510833	1.148534
H	7.809557	0.098080	0.731001

$[Mo(L^{Fc})_2O]^+$

Mo	-0.063059	-0.090308	0.494328
Fe	-4.716613	-0.040963	-1.004819
Fe	4.722765	0.322549	-0.937136
O	-0.200964	0.081284	-1.181909
N	-0.016779	1.676930	1.683694
N	-2.171185	0.184180	1.125976
N	0.028525	-2.075356	1.216840
N	2.087980	-0.445087	0.728545
C	0.877386	2.610881	2.083485
H	1.898007	2.610105	1.726839
C	0.271320	3.535697	2.989547
H	0.764976	4.377036	3.455453
C	-1.062894	3.132351	3.154335
H	-1.818819	3.589184	3.778983
C	-1.234298	1.979903	2.327730
C	-2.343139	1.188968	2.008619
H	-3.311357	1.405875	2.452285
C	-3.267344	-0.544158	0.703594
C	-4.656492	-0.447341	1.129732
H	-5.052125	0.186789	1.909279
C	-5.420386	-1.438277	0.417379
H	-6.466971	-1.657704	0.573042
C	-4.538621	-2.090877	-0.523055
H	-4.803238	-2.888396	-1.202128
C	-3.232952	-1.504790	-0.382567
H	-2.352975	-1.769454	-0.950029
C	-4.229676	0.809874	-2.965105
H	-3.362844	0.535204	-3.549906
C	-4.302416	1.891149	-2.021960
H	-3.492047	2.558514	-1.762287
C	-5.620014	1.896633	-1.445980
H	-5.983595	2.588065	-0.698640
C	-6.378897	0.825650	-2.053477
H	-7.412820	0.585717	-1.849327
C	-5.515515	0.152631	-2.995566
H	-5.785377	-0.687685	-3.619708
C	-0.827348	-3.091977	1.546407
H	-1.897727	-2.999305	1.426383
C	-0.106312	-4.203145	2.041153
H	-0.531899	-5.139523	2.375097
C	1.266988	-3.845917	2.021042
H	2.107151	-4.446329	2.344482
C	1.323360	-2.530793	1.506865
C	2.388869	-1.634441	1.226856
H	3.420957	-1.934453	1.399252
C	3.122570	0.486117	0.458692
C	4.399161	0.612843	1.136478
H	4.756668	-0.007075	1.946362
C	5.081931	1.752942	0.579962
H	6.054733	2.114518	0.881652
C	4.242457	2.324881	-0.445983
H	4.477485	3.187445	-1.053088
C	3.036504	1.540990	-0.526681
H	2.202364	1.706341	-1.193243
C	5.863663	-1.439201	-1.237366
H	6.208665	-2.101921	-0.455764
C	4.608844	-1.538817	-1.944742
H	3.843543	-2.285464	-1.782164

C	4.548174	-0.457945	-2.899865
H	3.731258	-0.254737	-3.578136
C	5.765685	0.309623	-2.783230
H	6.018661	1.190921	-3.356209
C	6.578626	-0.296291	-1.755305
H	7.548331	0.050097	-1.425524

$[Mo(L^{Fc})_2O]^{2+}$

Mo	-0.001762	-0.646508	0.011408
Fe	4.674981	1.084216	0.179826
Fe	-4.673511	1.078333	-0.222057
O	-0.001485	1.041281	-0.020402
N	0.093414	-1.648474	-1.848341
N	2.168459	-1.042581	-0.267468
N	-0.094058	-1.565878	1.910912
N	-2.170763	-1.039558	0.304568
C	-0.753624	-2.045920	-2.831210
H	-1.811133	-1.820849	-2.802846
C	-0.051238	-2.765409	-3.841847
H	-0.488649	-3.192500	-4.733180
C	1.297249	-2.814642	-3.446601
H	2.117931	-3.293753	-3.963244
C	1.375098	-2.110570	-2.209657
C	2.439358	-1.770988	-1.365005
H	3.452581	-2.071410	-1.618754
C	3.213397	-0.633282	0.550022
C	4.603478	-1.060878	0.541290
H	5.037048	-1.833945	-0.075986
C	5.297495	-0.364878	1.592759
H	6.328015	-0.521796	1.877221
C	4.370443	0.557243	2.207676
H	4.580060	1.219698	3.034932
C	3.104057	0.420533	1.538446
H	2.205234	0.978636	1.758032
C	4.168308	2.982665	-0.758388
H	3.226843	3.496442	-0.623326
C	4.480541	2.054206	-1.810926
H	3.805828	1.730618	-2.591798
C	5.829534	1.597126	-1.619405
H	6.353200	0.884974	-2.242070
C	6.367863	2.257577	-0.453843
H	7.366646	2.135575	-0.059048
C	5.337694	3.116750	0.082251
H	5.428856	3.759163	0.946519
C	0.754333	-1.916324	2.910193
H	1.810968	-1.689082	2.871240
C	0.054698	-2.593022	3.951813
H	0.493799	-2.978157	4.861223
C	-1.293456	-2.665216	3.559253
H	-2.112759	-3.123334	4.096669
C	-1.373759	-2.017052	2.292239
C	-2.438955	-1.719885	1.433562
H	-3.450489	-2.014326	1.700430
C	-3.220281	-0.660877	-0.522128
C	-4.612969	-1.079313	-0.478362
H	-5.044299	-1.818924	0.180031
C	-5.314803	-0.433023	-1.556154
H	-6.349075	-0.598546	-1.821563
C	-4.389896	0.452964	-2.224624
H	-4.605164	1.075762	-3.080802
C	-3.117116	0.342233	-1.563021
H	-2.220627	0.886783	-1.821425
C	-5.710351	1.659635	1.610955
H	-6.142603	0.968156	2.321041
C	-4.383646	2.210896	1.668549
H	-3.634479	1.986130	2.415650
C	-4.210260	3.080459	0.537342
H	-3.313954	3.634516	0.294540
C	-5.441226	3.084969	-0.218981
H	-5.633296	3.656838	-1.115767
C	-6.372540	2.203412	0.446572
H	-7.388775	1.999285	0.140054

$Mo(L^{Fc})_2O(PMe_3)$ OC-6-4-3 ($3a^{Fc}$)

O	-0.153035	0.851677	-2.117732
N	2.032891	0.528336	0.123913
N	-0.095892	1.943744	1.675096
N	1.530589	3.045284	-0.723512
N	-1.207804	-0.159429	0.394096
C	3.035297	1.386913	0.157182
C	2.820904	2.717819	-0.292459
C	3.691366	3.819040	-0.478114
C	2.904178	4.845733	-1.057080
C	1.590612	4.327891	-1.185075
C	-1.375494	-0.090508	1.700452
C	-0.809068	1.003029	2.414036
C	-0.806425	1.355705	3.790190
C	-0.058922	2.555940	3.880349
C	0.355958	2.874684	2.557017
H	4.025904	1.084017	0.495474
H	4.743545	3.857307	-0.226856
H	3.229948	5.834999	-1.349759
H	0.726247	4.826648	-1.603614
H	-1.958202	-0.841463	2.232610
H	-1.275176	0.806283	4.597034
H	0.162656	3.125408	4.774042
H	0.948920	3.720453	2.230405
Mo	0.105059	1.463154	-0.542818
Fe	3.740619	-2.206784	0.102668
Fe	-3.719592	-2.128956	-0.299196
C	-1.723698	-1.297035	-0.281683
C	-2.253941	-1.314137	-1.623185
H	-2.353623	-0.453057	-2.264972
C	-2.557713	-2.679043	-1.971688
H	-2.958567	-3.016213	-2.917286
C	-2.234016	-3.513174	-0.838294
H	-2.343862	-4.587270	-0.783766
C	-1.736369	-2.661472	0.211747
H	-1.372745	-2.983845	1.176962
C	-4.962392	-2.368570	1.404553
H	-4.626226	-2.684098	2.382734
C	-5.040348	-1.006931	0.931804
H	-4.774135	-0.123798	1.495504
C	-5.535677	-1.033474	-0.424459
H	-5.711728	-0.174278	-1.056510
C	-5.764734	-2.411368	-0.789015
H	-6.128154	-2.764038	-1.744477
C	-5.410542	-3.236798	0.341358

H	-5.459696	-4.316363	0.380381
C	2.237259	-0.775451	0.639835
C	3.034203	-1.140895	1.795322
H	3.591316	-0.456745	2.419993
C	2.890758	-2.559723	2.001951
H	3.348900	-3.132776	2.795922
C	2.024180	-3.076022	0.968625
H	1.725313	-4.107277	0.844151
C	1.630834	-1.977186	0.123617
H	0.980614	-2.029858	-0.735969
C	4.960878	-1.423608	-1.443020
H	4.825793	-0.456399	-1.907428
C	4.354292	-2.660405	-1.874589
H	3.687171	-2.779449	-2.717051
C	4.783959	-3.705844	-0.975751
H	4.493107	-4.746143	-1.026185
C	5.655945	-3.115134	0.012224
H	6.137015	-3.636413	0.828459
C	5.765947	-1.704207	-0.277076
H	6.348327	-0.985630	0.283176
C	-2.307297	3.552417	-2.420917
H	-3.181227	4.215136	-2.435650
H	-1.450154	4.073531	-2.862142
H	-2.515043	2.663391	-3.026934
C	-1.795989	4.634228	0.246157
H	-0.919850	5.206111	-0.073194
H	-2.700699	5.230279	0.075180
H	-1.696333	4.420982	1.315413
C	-3.530216	2.360690	-0.073272
H	-3.773828	1.435443	-0.604580
H	-3.447349	2.136225	0.995803
H	-4.329396	3.096303	-0.228281
P	-1.903637	3.026786	-0.681349

Mo(L^{Fc})$_2$O(PMe$_3$) OC-6-4-4 (3b^{Fc})

Mo	0.236248	1.621908	0.428822
Fe	4.481384	-1.109464	-0.356102
Fe	-3.782390	-2.017566	-0.196826
O	1.286490	2.945945	0.615667
N	0.352597	1.815339	-1.761965
N	-1.193376	-0.093112	-0.581035
N	-0.153576	0.867628	2.397920
N	1.553790	-0.181268	0.587337
C	0.974171	2.679309	-2.596935
H	1.611030	3.469940	-2.218024
C	0.663623	2.375439	-3.959202
H	1.032143	2.904798	-4.828530
C	-0.199921	1.261991	-3.934647
H	-0.643674	0.745987	-4.776760
C	-0.378002	0.937779	-2.555700
C	-1.137364	-0.064070	-1.902562
H	-1.673005	-0.800209	-2.504589
C	-1.790263	-1.225569	0.022842
C	-1.761095	-2.590035	-0.475529
H	-1.297051	-2.915015	-1.396231
C	-2.394518	-3.440059	0.500290
H	-2.514638	-4.511814	0.423727
C	-2.835464	-2.608329	1.594432
H	-3.349431	-2.944723	2.483878
C	-2.472403	-1.246891	1.295450
H	-2.645805	-0.391140	1.928480
C	-5.598796	-0.919583	-0.205945
H	-5.849463	-0.119298	0.476460
C	-4.930926	-0.775816	-1.478490
H	-4.589522	0.151232	-1.918340
C	-4.793861	-2.090225	-2.060377
H	-4.333717	-2.319736	-3.011691
C	-5.376667	-3.045851	-1.147982
H	-5.423561	-4.116391	-1.293019
C	-5.874590	-2.321936	-0.002217
H	-6.359587	-2.755038	0.861758
C	-0.856336	1.223962	3.511722
H	-1.492723	2.099419	3.530889
C	-0.603779	0.320474	4.574720
H	-1.027360	0.370989	5.568959
C	0.305112	-0.647054	4.077175
H	0.718185	-1.496258	4.606250
C	0.570687	-0.278854	2.736338
C	1.443735	-0.805879	1.746905
H	2.028246	-1.699024	1.964798
C	2.371216	-0.753131	-0.419194
C	2.662163	-2.161783	-0.618429
H	2.289172	-2.979431	-0.017862
C	3.480265	-2.282776	-1.798114
H	3.850907	-3.207517	-2.217981
C	3.712840	-0.956419	-2.318865
H	4.294797	-0.709029	-3.195425
C	3.037355	-0.014724	-1.464337
H	3.001598	1.055545	-1.591373
C	5.255947	-0.466696	1.509691
H	4.667836	-0.024537	2.302324
C	5.902180	0.248772	0.435200
H	5.884300	1.319255	0.284873
C	6.564829	-0.717201	-0.409316
H	7.129297	-0.496849	-1.304952
C	6.326771	-2.030358	0.142169
H	6.686309	-2.965636	-0.264658
C	5.517632	-1.875350	1.328784
H	5.170496	-2.674966	1.968805
C	-2.346502	3.725342	-1.318767
H	-3.216748	4.387983	-1.234177
H	-1.506671	4.276045	-1.755291
H	-2.586012	2.888239	-1.983184
C	-1.670754	4.631971	1.352662
H	-0.821278	5.205854	0.965913
H	-2.580627	5.241521	1.292076
H	-1.468725	4.383397	2.400306
C	-3.454009	2.354392	0.974290
H	-4.259723	3.091876	0.873903
H	-3.704382	1.462185	0.391950
H	-3.359806	2.069526	2.027048
P	-1.856314	3.074184	0.352517

Mo(L^{Fc})$_2$O(PMe$_3$) OC-6-3-4

N	1.857354	0.452706	0.383372
N	-0.097695	1.943158	2.000627
N	1.649161	3.146736	-0.136119
N	-1.460955	0.222091	0.475186

C	2.936183	1.202431	0.501974
C	2.879178	2.591112	0.208122
C	3.885155	3.601621	0.198504
C	3.232145	4.797473	-0.165483
C	1.856009	4.467655	-0.357452
C	-1.506406	0.023322	1.787495
C	-0.788699	0.905108	2.633282
C	-0.651030	1.026490	4.040624
C	0.145778	2.176914	4.256813
C	0.467339	2.702699	2.974869
H	3.888178	0.776900	0.826720
H	4.933341	3.462021	0.431188
H	3.671225	5.780293	-0.278252
H	1.044472	5.127544	-0.640093
H	-2.112763	-0.774304	2.213805
H	-1.070149	0.365475	4.788369
H	0.455600	2.587942	5.208527
H	1.063038	3.574712	2.736840
Mo	-0.122583	1.884136	-0.127055
Fe	3.156392	-2.540405	0.343122
Fe	-4.322511	-1.082128	-0.249495
C	-2.229735	-0.622438	-0.366092
C	-2.918304	-0.183392	-1.556446
H	-2.968310	0.838518	-1.902389
C	-3.516913	-1.337091	-2.181473
H	-4.094556	-1.334620	-3.094867
C	-3.218296	-2.491154	-1.366473
H	-3.523479	-3.508655	-1.566516
C	-2.434947	-2.051942	-0.237945
H	-2.033495	-2.680107	0.544568
C	-5.358496	-1.500591	1.553079
H	-4.978432	-2.102855	2.366839
C	-5.193198	-0.073669	1.401584
H	-4.663567	0.583492	2.077396
C	-5.851447	0.324037	0.180318
H	-5.898584	1.328808	-0.216146
C	-6.424510	-0.855833	-0.423296
H	-6.973774	-0.890719	-1.354062
C	-6.119898	-1.984060	0.424996
H	-6.405868	-3.010996	0.243657
C	1.905506	-0.866924	0.885634
C	2.672413	-1.342266	2.023326
H	3.347318	-0.746911	2.621752
C	2.316099	-2.717323	2.264923
H	2.706369	-3.343006	3.055507
C	1.348584	-3.108047	1.267285
H	0.888485	-4.081650	1.171776
C	1.105555	-1.972374	0.414585
H	0.419487	-1.941023	-0.415950
C	4.532085	-1.981884	-1.174154
H	4.608666	-1.000259	-1.621054
C	3.701658	-3.067470	-1.640694
H	3.046977	-3.046146	-2.500731
C	3.902280	-4.193892	-0.760309
H	3.416234	-5.156577	-0.839407
C	4.856913	-3.805206	0.250863
H	5.210632	-4.425036	1.063285
C	5.245912	-2.438445	-0.004858
H	5.946345	-1.857832	0.579616
O	-1.185199	3.058284	-0.744501
C	2.196973	1.642692	-3.078566
H	2.962095	1.158886	-2.463427
H	2.349193	1.368167	-4.129694
H	2.298198	2.727125	-2.963825
C	-0.587222	1.909285	-3.792105
H	-0.223842	1.676690	-4.800684
H	-1.613602	1.543900	-3.686291
H	-0.587567	2.994549	-3.644406
P	0.504944	1.116211	-2.508362
C	0.479749	-0.676802	-3.007526
H	1.245618	-1.223491	-2.448037
H	-0.501454	-1.112781	-2.793800
H	0.689467	-0.768432	-4.080636

$Mo(L^{Fc})_2O(PMe_3)$ OC-6-3-3

Fe	4.833655	-1.011040	-0.396532
Fe	-4.611883	-0.952827	-0.855488
C	-3.316950	0.779615	-0.688389
C	-4.718674	1.140524	-0.554303
H	-5.181805	1.628861	0.290835
C	-5.394786	0.770767	-1.772384
H	-6.444761	0.921051	-1.981541
C	-4.432809	0.141592	-2.644004
H	-4.629811	-0.259566	-3.628148
C	-3.159951	0.128646	-1.970517
H	-2.236165	-0.274686	-2.354856
C	-3.992836	-2.970225	-0.632361
H	-3.047364	-3.366365	-0.975441
C	-4.255824	-2.397876	0.666391
C	-5.635821	-1.977793	0.700457
H	-6.138210	-1.509420	1.535726
C	-6.229130	-2.295154	-0.576809
H	-7.250644	-2.096143	-0.870526
C	-5.214098	-2.910789	-1.399190
H	-5.341823	-3.251315	-2.417509
C	3.029398	-0.233818	0.469042
C	4.183858	0.185207	1.236882
H	4.464761	1.208056	1.446724
C	4.851953	-0.999664	1.715657
H	5.737785	-1.019347	2.334823
C	4.126286	-2.150261	1.231000
H	4.378309	-3.185271	1.413756
C	3.009200	-1.677001	0.450251
H	2.272493	-2.281533	-0.058891
C	4.992731	-0.406496	-2.424420
H	4.258246	0.179104	-2.959933
C	5.022063	-1.846561	-2.334615
H	4.310824	-2.524751	-2.785192
C	6.158250	-2.220556	-1.525845
H	6.446617	-3.229062	-1.263249
C	6.831154	-1.010918	-1.114537
H	7.715832	-0.954948	-0.495288
C	6.110681	0.110525	-1.670063
H	6.365913	1.153717	-1.543275
Mo	-0.149597	0.378591	-0.018455
N	0.140447	2.055798	-1.315785
C	-0.616890	2.917111	-2.046043
C	0.204895	3.904980	-2.653433

C	1.536567	3.629043	-2.258869
C	1.467902	2.476521	-1.434196
C	2.442809	1.670792	-0.794872
N	2.044078	0.597180	-0.124972
H	-1.690892	2.806811	-2.119255
H	-0.134445	4.709669	-3.292180
H	2.429932	4.180122	-2.523383
H	3.501769	1.906759	-0.886766
N	-0.113300	1.949266	1.667705
C	0.742047	2.557016	2.527137
C	0.066483	3.546330	3.299860
C	-1.282129	3.533459	2.875018
C	-1.362653	2.531380	1.867938
C	-2.442873	2.080898	1.062402
N	-2.252439	1.099063	0.194002
H	1.793010	2.295152	2.561896
H	0.512502	4.183431	4.052821
H	-2.093961	4.155944	3.229927
H	-3.406339	2.579794	1.143395
O	-0.424522	-1.067787	-0.889870
C	-0.431364	-2.852191	1.876754
H	-0.600590	-3.383619	2.821287
H	-1.259566	-3.052680	1.189518
H	0.490283	-3.223690	1.416001
C	-1.753828	-0.647160	3.244742
H	-1.835794	-1.388636	4.049178
H	-1.633737	0.349440	3.682270
H	-2.670645	-0.649381	2.647384
C	1.092133	-0.929654	3.419573
H	0.845890	-1.556865	4.285779
H	2.031336	-1.274356	2.978629
H	1.213479	0.106578	3.750723
P	-0.280620	-1.016859	2.163966
H	-3.548189	-2.306825	1.475664

$[Mo(L^{Fc})_2O(PMe_3)]^+$ OC-6-4-3 ($[3a^{Fc}]^+$)

O	-0.329123	0.794067	-2.061480
N	2.038816	0.495118	0.018603
N	0.080889	2.025700	1.680216
N	1.505156	2.986687	-0.851976
N	-1.115709	-0.170551	0.618395
C	3.055980	1.337194	-0.043243
C	2.823759	2.658522	-0.507136
C	3.679115	3.756646	-0.761680
C	2.854805	4.781173	-1.290596
C	1.534862	4.267875	-1.323109
C	-1.164638	-0.006125	1.954497
C	-0.570289	1.119999	2.528169
C	-0.453438	1.557269	3.891475
C	0.285768	2.744267	3.850478
C	0.592595	2.988207	2.465071
H	4.061484	1.023698	0.233898
H	4.745754	3.796216	-0.583169
H	3.161476	5.767444	-1.611614
H	0.644771	4.767518	-1.681381
H	-1.672516	-0.723514	2.594533
H	-0.853778	1.053200	4.761265
H	0.581416	3.367236	4.683803
H	1.155978	3.817484	2.054691
Mo	0.095804	1.434595	-0.535085
Fe	3.764823	-2.227848	0.055871
Fe	-3.833406	-2.095124	-0.241339
C	-1.633129	-1.340748	0.103759
C	-1.963953	-1.568421	-1.290161
H	-1.829187	-0.840485	-2.074787
C	-2.338686	-2.945404	-1.461924
H	-2.557828	-3.428204	-2.403620
C	-2.347109	-3.569243	-0.157188
H	-2.565088	-4.605466	0.058807
C	-1.997184	-2.565707	0.812406
H	-1.881432	-2.752837	1.869712
C	-5.576075	-2.101249	1.093771
H	-5.534854	-2.288205	2.157890
C	-5.538050	-0.812168	0.461047
H	-5.435385	0.137813	0.966757
C	-5.612544	-1.009091	-0.959918
H	-5.602297	-0.233223	-1.712776
C	-5.733500	-2.426909	-1.211471
H	-5.836740	-2.893400	-2.181028
C	-5.713980	-3.104405	0.061948
H	-5.796082	-4.170743	0.219248
C	2.254802	-0.798427	0.559643
C	3.051124	-1.128261	1.725493
H	3.604745	-0.423377	2.330191
C	2.919627	-2.542736	1.965965
H	3.384679	-3.093069	2.771696
C	2.057788	-3.092360	0.945910
H	1.771976	-4.129926	0.845860
C	1.655023	-2.017662	0.073442
H	1.018331	-2.097893	-0.795146
C	4.977309	-1.488283	-1.519511
H	4.834542	-0.543082	-2.024942
C	4.387606	-2.748542	-1.902889
H	3.726379	-2.910000	-2.742884
C	4.829496	-3.752317	-0.963775
H	4.553831	-4.797850	-0.974318
C	5.692191	-3.112277	0.000955
H	6.178760	-3.594934	0.837321
C	5.783967	-1.712708	-0.342599
H	6.356884	-0.965653	0.189411
C	-2.304486	3.607605	-2.321337
H	-3.194564	4.248235	-2.315613
H	-1.460934	4.168031	-2.739231
H	-2.484994	2.737127	-2.961644
C	-1.792842	4.602157	0.380311
H	-0.892509	5.160896	0.106850
H	-2.676682	5.223056	0.191329
H	-1.740677	4.362201	1.447193
C	-3.518392	2.316703	-0.026309
H	-3.730232	1.406706	-0.597045
H	-3.445882	2.058576	1.036185
H	-4.332996	3.037249	-0.168708
P	-1.899543	3.028319	-0.600451

$[Mo(L^{Fc})_2O(PMe_3)]^{2+}$ OC-6-4-3 ($[3a^{Fc}]^{2+}$)

O	-0.283354	0.735652	-2.040234
N	2.056681	0.609420	0.133418
N	-0.036962	2.086262	1.666084
N	1.413467	3.040729	-0.850280
N	-1.136709	-0.177442	0.642016
C	3.027949	1.532952	0.094394
C	2.735622	2.799032	-0.429524
C	3.547160	3.937476	-0.709794
C	2.702259	4.875535	-1.326970
C	1.404778	4.284376	-1.387041
C	-1.227281	0.024964	1.970199
C	-0.678635	1.183316	2.525459
C	-0.612005	1.664303	3.876286
C	0.086726	2.875476	3.818032
C	0.420172	3.090182	2.435741
H	4.041519	1.303928	0.419719
H	4.600133	4.043890	-0.485630
H	2.965981	5.859134	-1.689687
H	0.510819	4.721664	-1.811145
H	-1.735175	-0.684925	2.618330
H	-1.020110	1.174396	4.750470
H	0.335860	3.533783	4.639039
H	0.960061	3.930095	2.015853
Mo	0.056719	1.433959	-0.521616
Fe	3.882868	-2.171749	0.067430
Fe	-3.795231	-2.183784	-0.221288
C	-1.625086	-1.371728	0.144546
C	-1.914874	-1.641474	-1.249712
H	-1.782624	-0.931100	-2.050806
C	-2.257949	-3.030450	-1.393839
H	-2.448574	-3.540858	-2.327020
C	-2.280583	-3.621714	-0.074586
H	-2.484358	-4.655972	0.163361
C	-1.971685	-2.586767	0.877141
H	-1.880715	-2.742959	1.941878
C	-5.547090	-2.169679	1.087311
H	-5.514314	-2.288315	2.161369
C	-5.551738	-0.922298	0.374362
H	-5.499259	0.061035	0.819689
C	-5.604230	-1.210475	-1.031718
H	-5.615537	-0.483328	-1.831666
C	-5.666472	-2.643791	-1.195274
H	-5.738579	-3.173589	-2.134603
C	-5.633508	-3.240006	0.118480
H	-5.676747	-4.296901	0.340866
C	2.332623	-0.621383	0.713434
C	3.303838	-0.925284	1.750348
H	3.923179	-0.207608	2.268718
C	3.210367	-2.327735	2.063280
H	3.755748	-2.837531	2.844479
C	2.236620	-2.918523	1.172575
H	1.932478	-3.955216	1.155809
C	1.732025	-1.876642	0.317792
H	1.006945	-1.998760	-0.472101
C	5.097065	-1.582924	-1.701087
H	4.972877	-0.656856	-2.245977
C	4.408199	-2.814250	-1.969329
H	3.695429	-2.981770	-2.764873
C	4.832378	-3.789062	-0.991768
H	4.506362	-4.818194	-0.938139
C	5.779483	-3.148045	-0.109158
H	6.295127	-3.612820	0.719160
C	5.933527	-1.778512	-0.547366
H	6.576763	-1.036595	-0.095265
C	-2.350639	3.450183	-2.456033
H	-3.258200	4.063823	-2.498229
H	-1.510172	4.025669	-2.858952
H	-2.482824	2.558149	-3.077932
C	-1.975650	4.533947	0.236924
H	-1.084770	5.117974	-0.014090
H	-2.870570	5.120028	-0.003673
H	-1.959722	4.322878	1.310894
C	-3.603662	2.172426	-0.170794
H	-3.771275	1.250631	-0.737536
H	-3.555193	1.930697	0.896622
H	-4.435276	2.865284	-0.346879
P	-1.997518	2.934617	-0.705636

***Δ,Λ*-$[Mo(L^{Fc})_2O]_2(\mu$-O) ($4a^{Fc}$)**

Mo	1.855674	-0.269905	0.129149
Fe	7.027918	-1.080644	-0.017184
Fe	1.357557	5.102439	-0.098172
O	0.011695	0.117809	0.038843
O	1.904815	-1.968659	0.127141
N	1.932577	0.340141	2.146642
N	4.061531	0.010645	0.565125
N	2.266292	-0.259909	-1.985464
N	2.222070	2.029906	-0.572120
C	1.034528	0.493246	3.165894
H	-0.022678	0.346672	3.009120
C	1.707287	0.848246	4.357397
H	1.242945	1.027473	5.317484
C	3.090567	0.920119	4.046456
H	3.904245	1.167924	4.715574
C	3.201185	0.596804	2.675694
C	4.299017	0.426889	1.795430
H	5.315574	0.606858	2.139927
C	5.153066	-0.098527	-0.336439
C	5.343092	-1.147163	-1.307824
H	4.690177	-1.993328	-1.454548
C	6.535021	-0.847286	-2.058608
H	6.939514	-1.442154	-2.865175
C	7.095967	0.379082	-1.542887
H	7.990691	0.870284	-1.898809
C	6.250268	0.840657	-0.472120
H	6.379636	1.746796	0.103501
C	8.058137	-1.029486	1.836124
H	8.126879	-0.171999	2.491497
C	7.034394	-2.048015	1.869956
H	6.194939	-2.086832	2.550675
C	7.321011	-3.003549	0.826764
H	6.734145	-3.880437	0.591175
C	8.521798	-2.576729	0.147990
H	8.990009	-3.076462	-0.688862
C	8.977455	-1.356438	0.771046

H	9.849457	-0.784340	0.485435
C	2.364648	-1.255708	-2.912547
H	2.170985	-2.288184	-2.651712
C	2.733186	-0.717152	-4.170386
H	2.875878	-1.277553	-5.084660
C	2.871845	0.682515	-3.990400
H	3.148284	1.420257	-4.732409
C	2.579379	0.933794	-2.627138
C	2.552647	2.120310	-1.839499
H	2.788385	3.079287	-2.301782
C	2.271537	3.194106	0.232267
C	1.357565	3.505906	1.303853
H	0.496140	2.917780	1.579119
C	1.801373	4.723455	1.932249
H	1.324023	5.213144	2.769283
C	2.986442	5.178915	1.243884
H	3.561023	6.063526	1.480780
C	3.274399	4.243343	0.186231
H	4.113787	4.283090	-0.494294
C	0.291262	5.074141	-1.928538
H	0.241445	4.228419	-2.600648
C	-0.614370	5.337808	-0.835939
H	-1.445076	4.711791	-0.541507
C	-0.185395	6.553841	-0.185883
H	-0.651059	7.011743	0.676066
C	0.985622	7.041730	-0.876502
H	1.547013	7.931434	-0.625980
C	1.280431	6.126600	-1.954483
H	2.098310	6.215739	-2.656317
Mo	-1.842230	0.451835	-0.046469
Fe	-7.128932	0.648299	0.256449
Fe	-1.297969	-4.935532	-0.238640
O	-1.945462	2.146612	0.032093
N	-1.904344	-0.025302	-2.102188
N	-4.027655	0.089079	-0.483911
N	-2.251209	0.310063	2.063046
N	-2.126482	-1.900786	0.524670
C	-1.010582	-0.063241	-3.135854
H	0.043474	0.102856	-2.975025
C	-1.681660	-0.342502	-4.348689
H	-1.219641	-0.428169	-5.322698
C	-3.058657	-0.488097	-4.036346
H	-3.868942	-0.710235	-4.718434
C	-3.168332	-0.281778	-2.642960
C	-4.261632	-0.240497	-1.740834
H	-5.272483	-0.457887	-2.080678
C	-5.092076	0.014294	0.452819
C	-5.410760	1.000299	1.454781
H	-4.911299	1.948381	1.583346
C	-6.485749	0.481719	2.261074
H	-6.946305	0.984910	3.099390
C	-6.847501	-0.818714	1.747550
H	-7.620728	-1.465344	2.138031
C	-5.993733	-1.107384	0.624275
H	-5.986827	-2.013182	0.034025
C	-8.305162	0.415422	-1.496219
H	-8.298777	-0.447516	-2.148064
C	-7.464954	1.583736	-1.621777
H	-6.719114	1.756306	-2.385411
C	-7.799745	2.491897	-0.551522
H	-7.341293	3.453824	-0.368761
C	-8.847497	1.886490	0.235914
H	-9.307383	2.313028	1.116689
C	-9.160055	0.603079	-0.347577
H	-9.897833	-0.098312	0.017173
C	-2.414654	1.250299	3.038660
H	-2.303002	2.305827	2.826393
C	-2.717583	0.624542	4.273226
H	-2.890605	1.127493	5.215266
C	-2.746656	-0.771706	4.026799
H	-2.954475	-1.563284	4.734981
C	-2.459600	-0.933887	2.649163
C	-2.398971	-2.074347	1.797122
H	-2.579774	-3.066550	2.212403
C	-2.223785	-3.007698	-0.351998
C	-1.393842	-3.235066	-1.509739
H	-0.558132	-2.621989	-1.808919
C	-1.888665	-4.400791	-2.195366
H	-1.477604	-4.822969	-3.101556
C	-3.020689	-4.910233	-1.457451
H	-3.614465	-5.775377	-1.717891
C	-3.225188	-4.059272	-0.312757
H	-4.010196	-4.154738	0.424582
C	-0.100853	-5.057604	1.506473
H	0.009629	-4.271774	2.240928
C	0.720033	-5.233772	0.332706
H	1.532993	-4.587595	0.033783
C	0.235280	-6.392470	-0.379656
H	0.632110	-6.780175	-1.307970
C	-0.886506	-6.931596	0.353475
H	-1.472689	-7.796256	0.073615
C	-1.093469	-6.106535	1.520646
H	-1.857437	-6.251039	2.272438

Λ,*Λ*-[Mo(L^{Fc})$_2$O]$_2$(*μ*-O) (4b^{Fc})

Mo	-1.845432	-0.333390	0.585730
Fe	-6.953244	-1.351465	0.256074
Fe	-1.904231	4.959114	-0.861025
O	-0.000044	-0.000028	0.540355
O	-1.931087	-1.996554	0.948891
N	-2.018472	-0.805165	-1.501973
N	-2.168375	1.720773	-0.632362
N	-2.051205	0.805400	2.359194
N	-4.076937	-0.010554	0.813600
C	-1.953163	-1.978941	-2.188897
H	-1.771786	-2.916801	-1.680634
C	-2.161542	-1.746529	-3.572732
H	-2.162259	-2.498357	-4.350894
C	-2.363271	-0.351877	-3.726402
H	-2.548709	0.192011	-4.643529
C	-2.267736	0.203501	-2.426674
C	-2.360665	1.528055	-1.918069
H	-2.572343	2.361710	-2.587738
C	-2.387270	3.011251	-0.092062
C	-3.583903	3.813117	-0.257630
H	-4.437184	3.542775	-0.864619
C	-3.450388	4.985241	0.570337
H	-4.183175	5.772901	0.677922

C	-2.167485	4.919240	1.231143
H	-1.764838	5.655481	1.912517
C	-1.508423	3.707537	0.813872
H	-0.532032	3.364034	1.122948
C	-0.066457	5.636696	-1.673120
H	0.908138	5.434712	-1.250699
C	-0.757655	4.823663	-2.645430
H	-0.386987	3.906439	-3.082152
C	-2.028992	5.448835	-2.925573
H	-2.779700	5.086036	-3.614418
C	-2.123388	6.647719	-2.126159
H	-2.960081	7.332445	-2.102517
C	-0.909635	6.763999	-1.352603
H	-0.678917	7.548928	-0.645623
C	-1.215392	1.337256	3.304000
H	-0.141055	1.260135	3.225112
C	-1.965680	1.975481	4.315274
H	-1.561813	2.475036	5.185240
C	-3.334993	1.837220	3.963124
H	-4.194575	2.212257	4.503066
C	-3.357195	1.115616	2.750303
C	-4.399867	0.675559	1.891548
H	-5.439396	0.894093	2.130378
C	-5.092184	-0.365113	-0.111204
C	-6.202593	0.470510	-0.527453
H	-6.411037	1.468414	-0.167274
C	-6.934563	-0.242585	-1.542039
H	-7.810097	0.119504	-2.062461
C	-6.290688	-1.519129	-1.744076
H	-6.603787	-2.286676	-2.437556
C	-5.160091	-1.598370	-0.855810
H	-4.466210	-2.420504	-0.771236
C	-7.113527	-1.882824	2.302860
H	-6.350508	-1.716967	3.051005
C	-7.245488	-3.059568	1.477543
H	-6.597381	-3.924743	1.498215
C	-8.386451	-2.872372	0.612546
H	-8.741177	-3.572244	-0.131496
C	-8.960019	-1.579514	0.903074
H	-9.821830	-1.142906	0.417345
C	-8.173341	-0.967636	1.948432
H	-8.349260	0.004731	2.387884
H	2.572687	-2.361711	-2.587751
C	3.334626	-1.836870	3.963282
C	1.953317	1.978934	-2.189149
C	6.202307	-0.470398	-0.527679
H	4.437126	-3.542645	-0.864562
C	0.066533	-5.636561	-1.673354
H	4.183214	-5.772725	0.678054
C	2.363797	0.351836	-3.726519
H	9.821651	1.140356	0.418384
H	7.809696	-0.119174	-2.062776
H	1.764850	-5.655363	1.912637
Fe	6.953283	1.351282	0.256238
C	3.356947	-1.115379	2.750405
N	2.168220	-1.720765	-0.632474
H	8.743181	3.570362	-0.131740
C	2.360762	-1.528066	-1.918153
C	1.508352	-3.707491	0.813902
H	0.531945	-3.364029	1.122962
Fe	1.904232	-4.959097	-0.860951
H	2.549478	-0.192066	-4.643588
H	8.347598	-0.005247	2.388995
C	1.965266	-1.975145	4.315279
C	6.934256	0.242868	-1.542163
C	8.960082	1.577885	0.903711
H	4.466247	2.420884	-0.770536
C	0.909569	-6.763925	-1.352682
N	2.018517	0.805177	-1.502173
H	1.771849	2.916806	-1.680943
H	2.960106	-7.332526	-2.102210
C	1.215091	-1.336968	3.303903
H	6.603614	2.287232	-2.437124
H	0.140766	-1.259844	3.224896
H	6.599246	3.925331	1.497250
C	0.757965	-4.823582	-2.645545
O	1.931086	1.996591	0.948505
N	4.076807	0.010591	0.813672
C	5.092063	0.365266	-0.111084
C	2.167470	-4.919142	1.231226
C	3.450383	-4.985111	0.570430
C	2.267949	-0.203519	-2.426806
C	2.162023	1.746497	-3.572922
C	8.172610	0.967090	1.949098
H	-0.908136	-5.434530	-1.251126
H	2.780175	-5.086107	-3.614152
H	0.678652	-7.548841	-0.645752
C	2.123468	-6.647740	-2.126018
H	6.410640	-1.468409	-0.167727
C	8.387678	2.871105	0.612509
H	5.439228	-0.893813	2.130635
H	6.350120	1.718399	3.050897
C	5.160020	1.598690	-0.855401
H	0.387444	-3.906326	-3.082324
H	1.561308	-2.474656	5.185229
H	2.162898	2.498306	-4.351101
Mo	1.845289	0.333390	0.585488
N	2.051007	-0.805130	2.359165
C	2.029304	-5.448854	-2.925456
H	4.194153	-2.211869	4.503340
C	3.583852	-3.813011	-0.257572
C	7.246631	3.059605	1.477111
C	2.387175	-3.011201	-0.092062
C	6.290507	1.519542	-1.743805
C	7.113458	1.883301	2.302867
C	4.399701	-0.675409	1.891681

Δ,Λ-[Mo(L^{Fc})$_2$O]$_2$(μ-O) ($4a^{Fc}$) in DCM

Mo	1.842579	-0.250898	0.142014
Fe	7.004731	-1.131640	-0.006500
Fe	1.401412	5.120537	-0.122664
O	0.003686	0.159375	0.049250
O	1.866302	-1.950200	0.151111
N	1.930422	0.372243	2.155130
N	4.052896	0.000950	0.574606
N	2.253493	-0.260290	-1.972508
N	2.237708	2.037614	-0.573669
C	1.035383	0.547435	3.173631

H	-0.024123	0.416053	3.018473
C	1.714196	0.902018	4.361767
H	1.253474	1.096081	5.320730
C	3.098320	0.950677	4.049383
H	3.916110	1.191703	4.715942
C	3.203108	0.614663	2.681330
C	4.297826	0.422936	1.801385
H	5.317105	0.591788	2.143365
C	5.140958	-0.129368	-0.328314
C	5.314960	-1.188698	-1.291020
H	4.651086	-2.027850	-1.428641
C	6.507888	-0.909825	-2.048337
H	6.902622	-1.516504	-2.850944
C	7.085296	0.314157	-1.545137
H	7.984716	0.791440	-1.908077
C	6.248874	0.795247	-0.475654
H	6.390768	1.704679	0.091719
C	8.031519	-1.080721	1.848859
H	8.103414	-0.221796	2.501978
C	7.002315	-2.093712	1.883421
H	6.161395	-2.125980	2.562681
C	7.285977	-3.053666	0.843406
H	6.695084	-3.928192	0.609048
C	8.490461	-2.635106	0.165948
H	8.957668	-3.139624	-0.668598
C	8.951284	-1.415502	0.786586
H	9.826861	-0.848791	0.501170
C	2.338080	-1.262979	-2.893375
H	2.130554	-2.291201	-2.626405
C	2.715019	-0.737470	-4.154305
H	2.850064	-1.305467	-5.065049
C	2.873960	0.661124	-3.982704
H	3.161305	1.390371	-4.728963
C	2.584233	0.924941	-2.621169
C	2.572124	2.116590	-1.840877
H	2.820672	3.069696	-2.308469
C	2.295240	3.205960	0.224056
C	1.377467	3.533060	1.287938
H	0.509064	2.954554	1.561888
C	1.829474	4.749775	1.912288
H	1.351826	5.249287	2.743333
C	3.023178	5.189489	1.228558
H	3.605018	6.069781	1.463820
C	3.308545	4.245000	0.178057
H	4.152006	4.273065	-0.498030
C	0.348236	5.092054	-1.960330
H	0.296467	4.243825	-2.629159
C	-0.562673	5.368090	-0.875033
H	-1.401307	4.751216	-0.583531
C	-0.128724	6.584031	-0.227945
H	-0.596781	7.049955	0.628382
C	1.050865	7.059177	-0.912848
H	1.617688	7.945527	-0.662670
C	1.345924	6.136496	-1.984316
H	2.169968	6.214815	-2.680187
Mo	-1.853410	0.473770	-0.038387
Fe	-7.137830	0.631069	0.269379
Fe	-1.291535	-4.924583	-0.262857
O	-1.976498	2.167468	0.042084
N	-1.911919	-0.000871	-2.094483
N	-4.034679	0.089458	-0.473796
N	-2.255797	0.314120	2.070350
N	-2.109301	-1.887906	0.518327
C	-1.018963	-0.027981	-3.129217
H	0.033492	0.149094	-2.969370
C	-1.688502	-0.312460	-4.341687
H	-1.226944	-0.391734	-5.316469
C	-3.063619	-0.473126	-4.027941
H	-3.872395	-0.702620	-4.709365
C	-3.173859	-0.270038	-2.634171
C	-4.266776	-0.240828	-1.730891
H	-5.275747	-0.467237	-2.070330
C	-5.097893	0.006921	0.463697
C	-5.421037	0.989995	1.467259
H	-4.926711	1.940645	1.596813
C	-6.492929	0.464781	2.273468
H	-6.955821	0.964492	3.112594
C	-6.848234	-0.836821	1.758309
H	-7.617843	-1.488025	2.148331
C	-5.993578	-1.119636	0.634194
H	-5.982636	-2.024521	0.042656
C	-8.316448	0.392866	-1.480940
H	-8.308578	-0.470912	-2.131654
C	-7.479532	1.563249	-1.609344
H	-6.735457	1.736574	-2.374519
C	-7.814941	2.471922	-0.539651
H	-7.358898	3.435376	-0.358855
C	-8.859792	1.864704	0.250318
H	-9.319352	2.291119	1.131331
C	-9.169927	0.579708	-0.331076
H	-9.905174	-0.123212	0.035855
C	-2.427094	1.246409	3.052370
H	-2.329553	2.304540	2.846152
C	-2.717507	0.609379	4.284205
H	-2.893257	1.104407	5.229932
C	-2.730217	-0.785658	4.029198
H	-2.925478	-1.584172	4.733171
C	-2.446246	-0.935934	2.649529
C	-2.376164	-2.071003	1.790672
H	-2.546676	-3.067187	2.200810
C	-2.206299	-2.989711	-0.365020
C	-1.374016	-3.213212	-1.521683
H	-0.534465	-2.602108	-1.814251
C	-1.872921	-4.371399	-2.217201
H	-1.461280	-4.789469	-3.125050
C	-3.009974	-4.879997	-1.486383
H	-3.607383	-5.740229	-1.754650
C	-3.213347	-4.036113	-0.336288
H	-4.000831	-4.132588	0.398272
C	-0.097458	-5.071288	1.483095
H	0.020576	-4.292492	2.223832
C	0.723004	-5.247895	0.309161
H	1.543917	-4.609228	0.015896
C	0.227062	-6.396313	-0.412067
H	0.621015	-6.781586	-1.342620
C	-0.901272	-6.928728	0.315909
H	-1.496430	-7.784893	0.028962
C	-1.101190	-6.109691	1.488512

```
H  -1.867682 -6.251230  2.238279
```

[*Δ*,*Λ*-[Mo(L^{Fc})$_2$O]$_2$(μ-O)]$^+$ ([4a^{Fc}]$^+$) in DCM

```
Mo -1.910990 -0.252927 -0.075993
Fe -7.116360 -0.859203  0.078304
Fe -0.881910  5.146490 -0.017095
O  -0.052140  0.139756  0.036487
O  -1.938688 -1.943707 -0.092294
N  -1.964606  0.381549 -2.083674
N  -4.085081  0.081915 -0.499501
N  -2.334674 -0.196268  2.043668
N  -2.230695  2.149340  0.652533
C  -1.068316  0.507565 -3.109939
H  -0.017240  0.311601 -2.965858
C  -1.736385  0.903312 -4.291355
H  -1.273670  1.069675 -5.254393
C  -3.113267  1.027625 -3.969083
H  -3.921077  1.311102 -4.630771
C  -3.227680  0.693983 -2.601258
C  -4.325247  0.531214 -1.718360
H  -5.341901  0.736471 -2.046756
C  -5.166410 -0.047775  0.414119
C  -5.396527 -1.176980  1.281293
H  -4.807167 -2.081197  1.304916
C  -6.535615 -0.874828  2.108855
H  -6.957815 -1.523098  2.863447
C  -7.022629  0.434745  1.744764
H  -7.868281  0.944392  2.184510
C  -6.184742  0.946597  0.690355
H  -6.266796  1.914458  0.215163
C  -8.348262 -0.519665 -1.617579
H  -8.483602  0.429469 -2.117885
C  -7.346893 -1.512424 -1.931078
H  -6.600926 -1.444655 -2.711002
C  -7.521964 -2.624368 -1.028236
H  -6.923295 -3.524362 -1.005533
C  -8.631901 -2.320470 -0.156691
H  -9.006255 -2.950273  0.638474
C  -9.142823 -1.019990 -0.520701
H  -9.969434 -0.507299 -0.048428
C  -2.489547 -1.178426  2.960027
H  -2.337002 -2.219246  2.705063
C  -2.854558 -0.630507  4.228584
H  -3.032109 -1.195863  5.132868
C  -2.932014  0.760523  4.059465
H  -3.187539  1.506437  4.800224
C  -2.610822  1.013801  2.689641
C  -2.560675  2.201154  1.943665
H  -2.775818  3.142884  2.448519
C  -2.271906  3.316145 -0.084722
C  -1.558725  3.528965 -1.326693
H  -0.924813  2.800722 -1.807022
C  -1.901421  4.825697 -1.844343
H  -1.574011  5.237092 -2.788318
C  -2.773240  5.469414 -0.887610
H  -3.226518  6.445320 -0.987810
C  -2.954904  4.568651  0.220586
H  -3.584803  4.759648  1.077038
C   0.812602  4.963598  1.397196
H   1.039028  4.066349  1.955863
C   1.318960  5.279616  0.090689
H   1.991752  4.659458 -0.483989
C   0.755109  6.542061 -0.318291
H   0.948845  7.051682 -1.251839
C  -0.118061  7.000496  0.736099
H  -0.679946  7.923857  0.742544
C  -0.083778  6.015849  1.797470
H  -0.619611  6.074975  2.734462
Mo  1.801725  0.382539  0.120134
Fe  7.084141  0.474051 -0.168766
Fe  1.121953 -4.994786  0.013422
O   1.981591  2.075634  0.116749
N   1.855145 -0.193644  2.143352
N   3.980858 -0.077970  0.537730
N   2.206631  0.339263 -1.985987
N   2.001800 -1.932916 -0.567960
C   0.954231 -0.250177  3.172517
H  -0.091001 -0.036682  3.014202
C   1.608041 -0.612409  4.370329
H   1.139984 -0.730222  5.338006
C   2.981912 -0.792017  4.054790
H   3.779721 -1.077026  4.727907
C   3.106094 -0.521781  2.675159
C   4.202980 -0.474233  1.776695
H   5.205306 -0.739187  2.107324
C   5.047355 -0.140908 -0.398731
C   5.382385  0.865245 -1.375661
H   4.892770  1.820221 -1.488729
C   6.460527  0.355990 -2.183515
H   6.933007  0.874096 -3.005906
C   6.807651 -0.958264 -1.696320
H   7.579769 -1.601648 -2.094017
C   5.942204 -1.265770 -0.587729
H   5.924843 -2.184524 -0.018351
C   8.242685  0.192524  1.588998
H   8.225620 -0.684011  2.222188
C   7.409436  1.363531  1.733241
H   6.657900  1.523086  2.494239
C   7.760736  2.293526  0.687129
H   7.312519  3.263576  0.522652
C   8.811777  1.698524 -0.103914
H   9.283362  2.141184 -0.970399
C   9.109412  0.400021  0.452898
H   9.845392 -0.298277  0.078865
C   2.387284  1.327233 -2.912725
H   2.302580  2.372127 -2.643531
C   2.672880  0.760357 -4.177394
H   2.855131  1.306706 -5.092983
C   2.674204 -0.648616 -4.003956
H   2.863618 -1.405626 -4.753566
C   2.386770 -0.876953 -2.637550
C   2.286837 -2.056133 -1.843369
H   2.445204 -3.032677 -2.301230
C   2.053002 -3.082918  0.257950
C   1.177936 -3.358418  1.370624
H   0.331956 -2.757037  1.664299
```

C	1.639079	-4.560263	2.016273
H	1.190324	-5.024373	2.883144
C	2.796622	-5.041150	1.299036
H	3.374168	-5.922900	1.538940
C	3.050156	-4.137672	0.206234
H	3.862958	-4.200112	-0.503995
C	-0.015033	-5.033184	-1.776300
H	-0.103727	-4.213989	-2.476523
C	-0.875540	-5.270501	-0.642073
H	-1.704193	-4.646402	-0.338912
C	-0.409651	-6.460876	0.029194
H	-0.836784	-6.895767	0.922426
C	0.738989	-6.959579	-0.690312
H	1.319625	-7.834754	-0.432796
C	0.982638	-6.077188	-1.807257
H	1.772170	-6.182880	-2.538655

[*Δ*,*Λ*-[Mo(L^{Fc})$_2$O]$_2$(μ-O)]$^{2+}$ ([4a^{Fc}]$^{2+}$) in DCM

Mo	1.857825	0.308736	-0.112613
Fe	7.120339	0.500209	0.125220
Fe	0.761039	-5.077701	0.009293
O	-0.000019	-0.000898	-0.000225
O	1.958374	1.999774	-0.147653
N	1.897456	-0.321559	-2.116726
N	4.023137	-0.133471	-0.523162
N	2.273969	0.264477	2.000527
N	2.087813	-2.074627	0.632223
C	0.995916	-0.405683	-3.144720
H	-0.048097	-0.181392	-2.994970
C	1.649771	-0.803255	-4.331469
H	1.181768	-0.944204	-5.295906
C	3.023569	-0.973301	-4.012612
H	3.821186	-1.273330	-4.679143
C	3.149469	-0.664094	-2.641217
C	4.248396	-0.568076	-1.750449
H	5.254833	-0.822260	-2.076153
C	5.099306	-0.132607	0.407177
C	5.426159	0.927199	1.329593
H	4.928389	1.882750	1.395267
C	6.519691	0.476106	2.151102
H	6.993352	1.044043	2.939026
C	6.882360	-0.855989	1.729127
H	7.669238	-1.465147	2.150815
C	6.012837	-1.233424	0.645610
H	6.005335	-2.181668	0.126091
C	8.250037	0.164382	-1.643083
H	8.224765	-0.729667	-2.250965
C	7.415824	1.331754	-1.809111
H	6.654635	1.471079	-2.564575
C	7.784790	2.292006	-0.797151
H	7.340880	3.267504	-0.654997
C	8.847760	1.719455	-0.005798
H	9.333717	2.187044	0.839291
C	9.134814	0.404531	-0.527793
H	9.876179	-0.283007	-0.144795
C	2.456879	1.254852	2.907187
H	2.349732	2.296857	2.633948
C	2.780076	0.709261	4.184521
H	2.970123	1.276675	5.084880
C	2.801291	-0.688595	4.034006
H	3.016495	-1.433126	4.788677
C	2.489546	-0.946708	2.665882
C	2.400369	-2.137900	1.924783
H	2.570828	-3.087350	2.432329
C	2.118539	-3.239576	-0.115156
C	1.366454	-3.460253	-1.331491
H	0.702038	-2.743775	-1.788300
C	1.707407	-4.754338	-1.858063
H	1.349525	-5.174348	-2.787046
C	2.624456	-5.382770	-0.934106
H	3.086986	-6.352557	-1.049624
C	2.838674	-4.474922	0.162127
H	3.505592	-4.650151	0.993956
C	-0.889378	-4.897253	1.469431
H	-1.107209	-3.995521	2.024225
C	-1.430218	-5.233555	0.181762
H	-2.123204	-4.626624	-0.382879
C	-0.865249	-6.494725	-0.228929
H	-1.079393	-7.016916	-1.150962
C	0.042486	-6.932260	0.805081
H	0.614366	-7.849443	0.805070
C	0.028358	-5.936366	1.856091
H	0.590853	-5.979884	2.778172
Mo	-1.857942	-0.309873	0.112182
Fe	-7.120558	-0.497649	-0.125993
Fe	-0.761240	5.077372	-0.007617
O	-1.959331	-2.000882	0.146763
N	-1.897187	0.319900	2.116476
N	-4.022900	0.133396	0.523022
N	-2.273983	-0.265066	-2.000975
N	-2.087008	2.073751	-0.632219
C	-0.995461	0.403140	3.144377
H	0.048458	0.178597	2.994352
C	-1.649018	0.800230	4.331455
H	-1.180838	0.940472	5.295908
C	-3.022786	0.971027	4.012866
H	-3.820176	1.271064	4.679664
C	-3.148988	0.662661	2.641306
C	-4.247990	0.567508	1.750534
H	-5.254334	0.821925	2.076312
C	-5.099075	0.133748	-0.407374
C	-5.426703	-0.925167	-1.330546
H	-4.929712	-1.881080	-1.396800
C	-6.519765	-0.472586	-2.151860
H	-6.993910	-1.039640	-2.940132
C	-6.881390	0.859517	-1.729018
H	-7.667856	1.469527	-2.150244
C	-6.011666	1.235493	-0.645183
H	-6.003533	2.183280	-0.124837
C	-8.250311	-0.162161	1.642365
H	-8.224506	0.731448	2.250868
C	-7.417024	-1.330276	1.807759
H	-6.656051	-1.470744	2.563225
C	-7.786545	-2.289576	0.795089
H	-7.343323	-3.265306	0.652386
C	-8.848944	-1.715694	0.003947

H	-9.335136	-2.182348	-0.841526
C	-9.135087	-0.400907	0.526766
H	-9.875834	0.287477	0.144089
C	-2.457245	-1.255200	-2.907841
H	-2.350772	-2.297302	-2.634722
C	-2.779899	-0.709229	-4.185143
H	-2.970078	-1.276390	-5.085634
C	-2.800290	0.688618	-4.034428
H	-3.014934	1.433383	-4.789027
C	-2.488666	0.946349	-2.666208
C	-2.399139	2.137373	-1.924866
H	-2.569034	3.086997	-2.432280
C	-2.118057	3.238474	0.115469
C	-1.366471	3.458948	1.332150
H	-0.701931	2.742501	1.788850
C	-1.708152	4.752640	1.859197
H	-1.350894	5.172355	2.788552
C	-2.625132	5.381114	0.935169
H	-3.088231	6.350588	1.051035
C	-2.838559	4.473670	-0.161535
H	-3.505139	4.649052	-0.993607
C	0.888672	4.896538	-1.468315
H	1.105783	3.994871	-2.023499
C	1.430086	5.232036	-0.180686
H	2.122882	4.624481	0.383515
C	0.865980	6.493374	0.230668
H	1.080802	7.015148	1.152779
C	-0.041822	6.931830	-0.802909
H	-0.613032	7.849431	-0.802468
C	-0.028564	5.936334	-1.854304
H	-0.591325	5.980508	-2.776192

8 Danksagung (Acknowledgments)

Ich danke Prof. Dr. K. H. dafür, dass sie mir die Doktorarbeit in ihrem Arbeitskreis ermöglicht hat, für das spannende Thema und die gute wissenschaftliche Betreuung.

Dr. C. F. gilt mein Dank für das zuverlässige Lösen der Kristallstrukturen und die intensiven Diskussionen.

Ich möchte den freundlichen Mitarbeitern der analytischen Abteilung herzlich danken, vor allem P. A. für die Massenspektren, R. J.-P. für die röntgenkristallographische Untersuchung meiner Kristalle und Dr. J. L. für die Tieftemperatur-NMR-Spektren. Ein dickes Dankeschön geht an Dr. M. M. für die großartige Unterstützung beim Messen von NMR-Spektren mit dem steten Bemühen um höchste Qualität und die aufschlussreichen Erklärungen.

Ich danke auch meinen engagierten Forschungspraktikanten J. E., S. S., M. K., D. D., O. S., A. A., L. P. und meinem Bacheloranden N. H.

Ganz besonders danke ich allen aktuellen und ehemaligen Mitarbeitern des Arbeitskreises für die Hilfsbereitschaft, die Diskussionen zu allen möglichen Fragestellungen, die Small Talks zwischen den Laborbänken, die schönen gemeinsamen Freizeitaktivitäten und die gute Stimmung. Insbesondere danke ich: Dr. T. K. und O. B. für das Korrekturlesen, M. T. P. für die tolle Unterstützung im Labor (vor allem während der Schwangerschaft), Dr. A. W., Dr. J. L. und O. B. für die Unterstützung und das Miträtseln bei EPR-Simulationen, Dr. A. B. und Dr. C. K. für den DFT-Support sowie Dr. A. N., Dr. T. K. und P. V. für das Zur-Verfügung-Stellen von Edukten.

Von ganzem Herzen danke ich meiner Familie, die das Vorhaben „Doktorarbeit“ so sehr unterstützt hat. Meiner Mutter M. H. und meinen Schwiegereltern K. und M. H. danke ich für das geduldige Babysitten und die stete Hilfsbereitschaft. Meiner Mutter danke ich auch vor allem für das Kümmern und die wertvollen Ratschläge.

Schließlich möchte ich meinen Liebsten danken, meinem Mann M. für die Beratung in theoretischen Fragen, das zur Seite stehen in allen Lebenslagen, die aufbauenden Worte und so vieles mehr und meinen Söhnen M. und N. für jedes wunderbare Lächeln.